SEISMIC RISK ASSESSMENT AND RETROFITTING

GEOTECHNICAL, GEOLOGICAL AND EARTHQUAKE ENGINEERING

Volume 10

For further titles published in this series, go to:
http://www.springer.com/series/6011

Seismic Risk Assessment and Retrofitting

With Special Emphasis on Existing Low-Rise Structures

edited by

ALPER ILKI

Istanbul Technical University, Turkey

FARUK KARADOGAN

Istanbul Technical University, Turkey

SUMRU PALA

Istanbul Technical University, Turkey

and

ERCAN YUKSEL

Istanbul Technical University, Turkey

Springer

Editors
Alper Ilki
Istanbul Technical University
Maslak Campus
Faculty Civil Engineering
34469 Istanbul
Turkey
ailki@itu.edu.tr

Faruk Karadogan
Istanbul Technical University
Maslak Campus
Faculty Civil Engineering
34469 Istanbul
Turkey
karadogan@itu.edu.tr

Sumru Pala
Istanbul Technical University
Maslak Campus
Faculty Civil Engineering
34469 Istanbul
Turkey
pala@itu.edu.tr

Ercan Yuksel
Istanbul Technical University
Maslak Campus
Faculty Civil Engineering
34469 Istanbul
Turkey
yukselerc@itu.edu.tr

ISSN 1573-6059
ISBN 978-90-481-2680-4 e-ISBN 978-90-481-2681-1
DOI 10.1007/978-90-481-2681-1
Springer Dordrecht Heidelberg London New York

Library of Congress Control Number: 2009927328

Printed on acid-free paper

Springer is part of Springer Science+Business Media (www.springer.com)

Foreword

This volume provides insight into many important aspects of earthquake risk assessment and mitigation, with a focus on the conditions existing in Istanbul and with an emphasis on prevention of collapse of existing low-rise buildings. The large collapse potential of Istanbul's low- and mid-rise buildings in case of earthquake is well documented and is acknowledged to be a major threat to the well-being of this great metropolis. The need exists to identify the most vulnerable buildings and to develop simple means and prescriptive rules for seismic upgrading of the vulnerable building stock.

Many of the vulnerable buildings have relatively poorly constructed concrete framing, which in part or fully is infilled with hollow clay or solid bricks. Configurations are often irregular, and the quality of construction is very variable. In many cases it is not clear how inertia forces find their way to reinforced concrete framing and how the forces and moments are transferred into the soil. These problems are common to many urban areas, worldwide, and have become the subject of research in many countries. The international workshop, which resulted in the publications of this volume, provided an excellent opportunity to bring together leading experts to assess and communicate the state of knowledge in risk assessment and mitigation, and equally important, to deliver a strong message to those who are empowered to make decisions that affect implementation of risk mitigation measures. From the writer's perspective, here are the major messages delivered through the workshop discussions.

- Prevention of collapse of buildings and other structures in a major earthquake is a critical issue for the future of Istanbul.
- The question is not if but when will a major earthquake hit Istanbul with full force.
- Many of buildings (and other structures) in Istanbul are of inadequate resistance and will collapse in a major earthquake – unless actions are taken to mitigate the risk of collapse.
- Time is a critical factor because every day without action is a day lost in the effort to prevent collapses and save lives.
- The time factor (and economic considerations) will make it necessary to develop simple and prescriptive retrofit procedures that can be implemented quickly and

effectively for a large portion of the building stock that is being judged to constitute a severe collapse hazard.

- An initial effort is needed to identify buildings that constitute a severe collapse hazard. Simple and prescriptive rules are needed that can be implemented in a short (walk-through) inspection to assess the need for retrofitting and to recommend the type of retrofit that is most effective to reduce the collapse hazard.
- For the most common type of building structures, which has poorly reinforced concrete framing as the primary shear resisting system, the addition of well confined infill walls (with various strengthening techniques as appropriate), and confinement of concrete framing with fiber reinforced polymer wrapping are judged to be effective retrofit techniques.
- Research needs to be continued in order provide a comprehensive knowledge base on which to base the assessment and retrofit actions needed to address collapse prevention. This research requires international collaboration and funding in view of the fact that many major urban areas face problems similar to those of Istanbul.
- An urgent need exists to translate research information into practical rules that can be implemented in an effective manner. This requires thorough synthesis of available information and an understanding of local design and construction practices. This need can be fulfilled by creating, as soon as possible, a small group of leading researchers and practicing engineers who get charged with the development of these rules and can allocate sufficient time to this effort.

Only time will tell whether this volume, and the workshop from which it resulted, will have any effect on seismic safety in Istanbul.

We should be thankful to Professor Faruk Karadogan who initiated and guided the international workshop and the publication of this volume, and to the organizing committee who very ably organized all aspects of the workshop and publication.

Stanford, CA

Helmut Krawinkler
John A. Blume Professor Emeritus of Engineering

Preface

The *International Workshop on Measures for the Prevention of Total Collapse of Existing Low-Rise Structures* offered an opportunity to bring together leading authorities in the field of earthquake engineering from all over world to discuss not only the technically urgent world wide important problems of big cities full of vulnerable buildings but also to convince the administrators and increase public awareness.

Helmut Krawinkler from the John Blume Earthquake Engineering Research Center, Stanford, said:

> Time is a critical factor; every day without action is a day lost in the effort to prevent collapses and save lives.

There are always urgent issues in the agendas of developing countries which push back the retrofitting problems of thousands of existing structures with inadequate resistance against earthquakes. Because of competing priorities and economic constraints disregard of this difficult problem becomes an attractive alternative for decision makers at all levels of responsibility.

Jim Jirsa from University of Texas at Austin thinks that:

> In a country where there are so many buildings with similar details, in-situ testing offers the possibility of meeting a number of objectives of this workshop. Field tests could be used to stimulate interest in engineering community and improve public awareness of the problem and offer opportunities for collaboration among research groups and academic programs with other groups in seismic regions around the world.

Craig Comartin from San Francisco, an expert in retrofitting techniques and consulting engineer says:

> Unsafe housing is a world wide problem. We in the earthquake community have a responsibility to identify these problems and develop effective means of reducing risk. We will increase our credibility and impact if we work together in an international effort. We should focus on what we know right now to take immediate action for collapse prevention.

Yoshiaki Nakano from Tokyo University gives credit to public awareness and continuation of research and development says:

> The education of media through providing correct information and knowledge on a scientific and engineering basis is significantly essential. Providing school children with

opportunities to identify problems and to seek their solutions with their parents could help raise the awareness.

Paolo Negro from ELSA Laboratories says:

In general, strengthening of existing infill walls is an effective and viable way to improve the seismic safety against collapse of existing deficient reinforced concrete frames, also considering the need to reduce disturbance or disruption of occupancy. Simple guidelines for seismic upgrading of existing building should be developed. These should represent a safe and feasible option; however they should not limit the adoption of different or more sophisticated approaches. The problem of the seismic safety of Istanbul is not different from that of many other south European cities. A common solution to the problem should be sought and international cooperation around it should be continued.

The other experts and leading researchers in their own fields of interest such as A. Ansal, M. Celebi, R. Sofronie, E. Mola, S. Tezcan, Z. Celep, G. Toniolo, G. Chavez-Lopez, S. Pampanin, K. Kusunoki, K. Mosalam, P. Labossiere, G. Ozcebe, M. Bas, H. Toutanji, O. Buyukozturk, U. Ersoy, T. Tankut, M. Fardis, and H. Darama all had exceptional contributions for the success of this workshop presenting their articles and participating in valuable discussions.

All in all, this book intends to put together recent experimental and theoretical findings to come up with a complementary body of work for those interested in the prevention of the total collapse of millions of vulnerable low-cost, low-rise buildings in earthquake prone areas. The danger of collapse is especially visible in developing countries where sophisticated building codes are not followed because of non-scientific reasons.

It is clear that new manners should definitely be developed to make the people understand this serious problem. Local authorities and administrators must implement the findings. Otherwise the communities suffering from earthquakes will never get the chance to benefit from this research.

The manuscripts that are part in this publication are based not only on the talks of participants but also on the discussions and on feedback from the reviewers. Partial expansion of the papers presented at the workshop has been accepted by the editors for the sake of completeness. Therefore some of the relatively short presentations have become chapters. Selection, review and expansion of the presentations contributed to this publication which can better be considered as a book rather than a paper collection. Taking this opportunity, the editors would like to express their deepest appreciation to the exceptional researchers who assisted in this process.

Istanbul, Turkey

Faruk Karadogan
On Behalf of the Editors

Contents

Contributors

Emre Akin Department of Civil Eng., Selcuk University, Konya, Turkey, eakin@metu.edu.tr

Ihsan Engin Bal University of Pavia, Pavia, Italy, ibal@roseschool.it

Dionysis Biskinis Department of Civil Engineering, University of Patras, Greece, dbisk@tee.gr

Holley Britton University of Alabama in Huntsville, Huntsville, AL, USA, Holley.Britton@itt.com

Oral Buyukozturk Massachusetts Institute of Technology, Cambridge, MA, USA, obuyuk@mit.edu

Mehmet Çelebi USGS (MS977), 345 Middlefield Rd., Menlo Park, CA, USA 94025, celebi@usgs.gov

Zekai Celep Istanbul Technical University, Istanbul, Turkey, celep@itu.edu.tr

Gabriela Chávez-López EQECAT/ABS Consulting, Paris, France, gchavezlopez@absconsulting.com

Craig D. Comartin CDComartin, Inc., Stockton, CA, USA, ccomartin@comartin.net

Rasit Comlek Balkar Engineering Company, Istanbul, Turkey, rcomlek@balkar.com.tr

Huseyin Darama Arup North America Ltd., Los Angeles, USA, huseyin.darama@arup.com

Gulseren Erol Istanbul Technical University, Istanbul, Turkey, guluse@yahoo.com

Ugur Ersoy Department of Civil Engineering, Bogazici University, Istanbul, Turkey, ugur.ersoy@boun.edu.tr

Michael N. Fardis Department of Civil Engineering, University of Patras, Greece, fardis@upatras.gr

Éric St-Georges Université de Sherbrooke, Sherbrooke, QC, Canada, ericstgeorges@gmail.com

Fatma Gulten Gulay Istanbul Technical University, Istanbul, Turkey, gulayg@itu.edu.tr

M. Han University of Alabama in Huntsville, Huntsville, USA, hanm@uah.edu

Alper Ilki Istanbul Technical University, Istanbul, Turkey, ailki@itu.edu.tr

James O. Jirsa University of Texas at Austin, Austin, TX, USA, jirsa@uts.cc.utexas.edu

Faruk Karadogan Istanbul Technical University, Istanbul, Turkey, karadogan@itu.edu.tr

Helmut Krawinkler Department of Civil and Environmental Engineering, Stanford University, Stanford, CA, USA, krawinkler@stanford.edu

Koichi Kusunoki Yokohama National University, Yokohama, Kanagawa, Japan, kusunoki@ynu.ac.jp

Pierre Labossière Université de Sherbrooke, Sherbrooke, QC, Canada, Pierre.Labossiere@USherbrooke.ca

Dimitrios G. Lignos Department of Civil and Environmental Engineering, Stanford University, Stanford, CA, USA, dlignos@stanford.edu

Elena Mola Politecnico di Milano, Structural Engineering Department, Milano, Italy, elemola@gmail.com, emola@stru.polimi.it

Khalid M. Mosalam Department of Civil & Environmental Engineering, University of California, Berkeley, CA, USA, mosalam@ce.berkeley.edu

Waiel Mowrtage Bogazici University, Istanbul, Turkey, waiel.mowrtage@boun.edu.tr

Paolo Negro ELSA Laboratory, Joint Research Centre, Via E. Fermi, 1, 21020 Ispra, VA, Italy, paolo.negro@jrc.it

Guney Ozcebe Department of Civil Eng., Middle East Technical University, Ankara, Turkey, ozcebe@metu.edu.tr

Sumru Pala Istanbul Technical University, Istanbul, Turkey, pala@itu.edu.tr

Stefano Pampanin University of Canterbury, Christchurch, New Zealand, stefano.pampanin@canterbury.ac.nz

Patrick Paultre Université de Sherbrooke, Sherbrooke, QC, Canada, Patrick.Paultre@Usherbrooke.ca

Jean Proulx Université de Sherbrooke, Sherbrooke, QC, Canada, jproulx@qci.usherb.ca

Nathalie Roy Université de Sherbrooke, Sherbrooke, QC, Canada, Nathalie.Roy@USherbrooke.ca

Hitoshi Shiohara The University of Tokyo, Tokyo, Japan, shiohara@arch.t.u-tokyo.ac.jp

Mohamed M. Talaat Simpson Gumpertz and Heger, Inc. San Francisco, CA, USA, mtalaat@sgh.com

Kivanc Taskin Istanbul Technical University, Istanbul, Turkey, taskinkiv@itu.edu.tr

Masaomi Teshigawara Nagoya University, Nagoya, Aichi, Japan, teshi@corot.nuac.nagoya-u.ac.jp

Pinar Teymur Istanbul Technical University, Istanbul, Turkey, teymurp@itu.edu.tr

Semih S. Tezcan Bogazici University, Istanbul, Turkey, tezokan@gmail.com

Giandomenico Toniolo Politecnico di Milano, Milano, MI, Italy, toniolo@stru.polimi.it

Houssam Toutanji University of Alabama in Huntsville, Huntsville, USA, toutanji@cee.uah.edu

Renjun Wang University of Texas at Austin, Austin, TX, USA

Sharon L. Wood University of Texas at Austin, Austin, TX, USA, swood@mail.utexas.edu

Tzu-Yang Yu Massachusetts Institute of Technology, Cambridge, MA, USA, youngyu@mit.edu

Ercan Yuksel Istanbul Technical University, Istanbul, Turkey, yukselerc@itu.edu.tr

Chapter 1
Seismic Monitoring to Assess Performance of Structures in Near-Real Time: Recent Progress

Mehmet Çelebi

Abstract Earlier papers have described how observed data from classical accelerometers deployed in structures or from differential GPS with high sampling ratios deployed at roofs of tall buildings can be configured to establish seismic health monitoring of structures. In these configurations, drift ratios are the main parametric indicator of damage condition of a structure or component of a structure. Real-time measurement of displacements are acquired either by double integration of accelerometer time-series data, or by directly using GPS. Recorded sensor data is then related to the performance level of a building. Performance-based design method stipulates that for a building the amplitude of relative displacement of the roof of a building (with respect to its base) indicates its performance. Usually, drift ratio is computed using relative displacement between two consecutive floors. When accelerometers are used, determination of displacement is possible by strategically deploying them at a select number of pairs of consecutive floors. For these determinations, software is used to compute displacements and drift ratios in real-time by double integration of accelerometer data. However, GPS-measured relative displacements are limited to being acquired only at the roof with respect to its reference base. Thus, computed drift ratio is the average drift ratio for the whole building. Until recently, the validity of measurements using GPS was limited to long-period structures (T>1 s) because GPS systems readily available were limited to 10–20 samples per seconds (sps) capability. However, presently, up to 50 sps differential GPS systems are available on the market and have been successfully used to monitor drift ratios [1, Panagitou et al. (Seismic Response of ReinForced Concrete Wall Buildings, 2006)], (Restrepo, pers. comm. 2007) – thus enabling future usefulness of GPS to all types of structures. Several levels of threshold drift ratios can be postulated in order to make decisions for inspections and/or occupancy. Experience with data acquired from both accelerometers and GPS deployments indicates that they are reliable and provide pragmatic alternatives to alert the owners and other authorized parties to make informed decisions and select choices for pre-defined

M. Çelebi (✉)
USGS (MS977), 345 Middlefield Rd., Menlo Park, CA, USA 94025
e-mail: celebi@usgs.gov

A. Ilki et al. (eds.), *Seismic Risk Assessment and Retrofitting*, Geotechnical, Geological, and Earthquake Engineering 10, DOI 10.1007/978-90-481-2681-1_1,

actions following significant events. Furthermore, recent adoption of such methods by financial and industrial enterprises is testimony to their viability.

1.1 Introduction

1.1.1 Background and Rationale

Following an earthquake, rapid and accurate assessment of the damage condition or performance of a building is of paramount importance to stakeholders, including owners, leasers, permanent and/or temporary occupants, and city officials and rescue teams that are concerned with safety of those in the building and those that may be affected in nearby buildings and infrastructures. These stakeholders will require answers to key questions such as: (a) is there visible or hidden damage? (b) if damage occurred, what is the extent? (c) does the damage threaten other neighboring structures? (d) can the structure be occupied immediately without compromising life safety or is life safety questionable? As a result, property damage and economic loss due to lack of permit to enter and/or re-occupy a building may be significant.

Until recently, assessments of damage to buildings following an earthquake were essentially carried out through inspections by city-designated engineers following procedures similar to ATC-20 tagging requirement [2]. Tagging usually involves visual inspection only and is implemented by colored tags indicative of potential hazard to occupants: green indicating the building can be occupied – that is, the building does not pose a threat to life safety; yellow indicates limited occupation – that is, hazardous to life safety but not to prevent limited entrance to retrieve possessions; and red indicating entrance prohibited – that is, hazardous to life. However, one of the impediments to accurately assessing the damage level of structures by visual inspection is that some serious damage may not be visible due to the presence of building finishes and fireproofing. In the absence of visible damage to the building frame, most steel or reinforced concrete moment-frame buildings will be tagged based on visual indications of building deformation, such as damage to partitions or glazing. Lack of certainty regarding the actual deformations that the building experienced may typically lead an inspector toward a relatively conservative tag. In such cases, expensive and time-consuming intrusive inspections may be recommended to building owners (e.g., it is known that, following the [M_w=6.7] 1994 Northridge, CA earthquake, approximately 300 buildings ranging in height from 1 to 26 stories were subjected to costly intrusive inspection of connections [3, 4].

This paper describes an alternative to tagging that is now available to owners and their designated engineers by configuring real-time response of a structure instrumented as a health monitoring tool. As Porter and others [5] state, most new methods do not utilize real-time measurements of deformations of a building for assessments of a building's performance during an event with the exception outlined by Çelebi et al. [6, 7]. In these applications, differential GPS [6] with high sampling ratios and classical accelerometer deployed structures [7] are configured to obtain data in real-time and compute drift ratios as the main parametric indicator of damage condition

of a structure or one or more components of a structure. The rationale here is that a building owner and designated engineers are expected to use the response data acquired by a real-time health monitoring system to justify a reduced inspection program as compared to that which would otherwise be required by a city government for a similar non-instrumented building in the same area[1] [8]. It is possible, depending on the deformation pattern and associated damage indicators observed in a building, to direct the initial inspections toward specific locations in the building that experienced large and potentially damage-inducing drifts during an earthquake.

Examples of and data from either type of sensor deployment (GPS or accelerometers) indicate that these methods are reliable and provide requisite information for owners and other parties to make informed decisions and select choices for predefined actions following significant events. Furthermore, recent additional adoptions of such methods by financial and industrial enterprises validate its usefulness.

1.1.2 Requisites

The most relevant parameter to assess performance is the measurement or computation of actual or average story drift ratios. Specifically, the drift ratios can be related to the performance-based force-deformation curve hypothetically represented in Fig. 1.1 [9]. When drift ratios, as computed from relative displacements between consecutive floors, are determined from measured responses of the building, the performance, and as such "damage state", of the building can be estimated as in Fig. 1.1.

Measuring displacements directly is very difficult and, except for tests conducted in a laboratory (e.g., using displacement transducers), has not yet been feasible for a variety of real-life structures. For structures with long-period responses, such as tall buildings, displacement measurements using GPS are measured directly at the roof only; hence, drift ratio then is an average drift ratio for the whole building. Thus, recorded sensor data is related to performance level of a building and hence to performance-based design, which stipulates that for a building the amplitude of relative displacement of the roof of a building with respect to its base indicates its performance. For accelerometer-based systems, the accelerometers must be strategically deployed at specific locations on several floors of a building to facilitate real-time measurement of the actual structural response, which in turn is used to compute displacements and drift ratios as the indicators of damage.

Table 1.1 shows typical ranges of drift ratios that define threshold stages for steel moment resisting framed buildings. The table is developed from [4]. For reinforced concrete framed buildings, the lower figures may be more appropriate to adopt.

[1]The City of San Francisco, California, has developed a "Building Occupancy Resumption Program" (BORP, 2001) whereby a pre-qualified Occupancy decision-making process, as described in this paper, may be proposed to the City as a reduced inspection program and in lieu of detailed inspections by city engineers following a serious earthquake

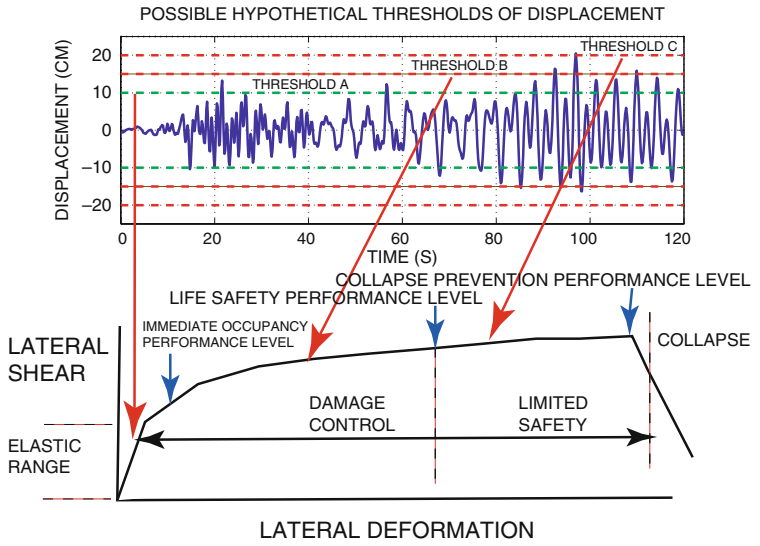

Fig. 1.1 Hypothetical displacement time-history as related to performance [modified from Fig. C2-3 of *FEMA-274* (ATC 1997)] [9]

Table 1.1 Summary of suggested typical threshold stages and ranges of drift ratios

Threshold Stage	1	2	3
Suggested Typical Drift Ratios	0.2–0.3%	0.6–0.8%	1.4–2.2%

1.2 Two Approaches for Measuring Displacements

1.2.1 Use of GPS for Direct Measurements of Displacements

1.2.1.1 Early Pioneering Application of GPS

Until recently, use of GPS was limited to long-period structures (T>1 s) because differential GPS systems readily available were limited to 10–20 sps capability.[2] Currently, the accuracy of 10–20 Hz GPS measurements is ± 1 cm horizontal and ± 2 cm vertical. Furthermore, with GPS deployed on buildings, measurement of displacement is possible only at the roof.

A schematic and photos of a pioneering application using GPS to directly measure displacements is shown in Fig. 1.2 . In this particular case, two GPS units are used in order to capture both the translational and torsional response of the 34-story building in San Francisco, CA [6]. At the same locations as the GPS

[2]Recently, up to 50 sps differential GPS systems are available on the market and have been successfully used ([1], Panagitou et al., 2006, and Restrepo, pers. comm. 2007).

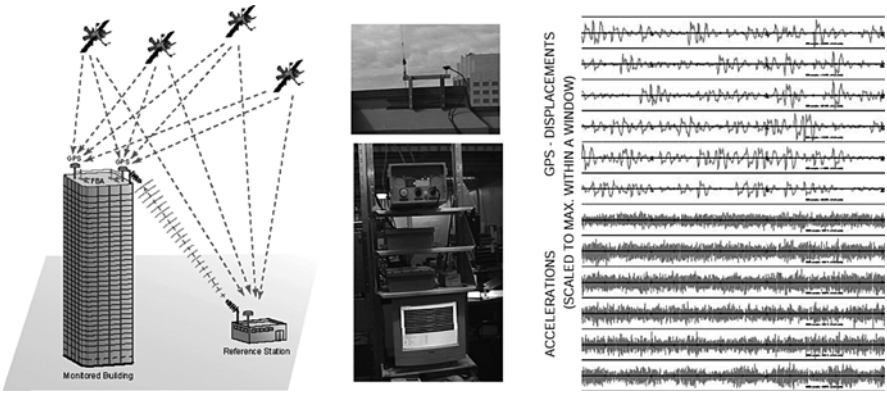

Fig. 1.2 (*Left*)- Schematic of the overall system using GPS and accelerometers (San Francisco, CA.): (*Center*)- GPS and radio modem antenna and the recorders connected to PC, (*Right*)- streaming acceleration and displacement data in real-time

antennas, tri-axial accelerometers are deployed in order to compare the displacements measured by GPS with those obtained by double-integration of the accelerometer records. Both acceleration and displacement data stream into the monitoring system as shown also in Fig. 1.2.

To date, strong shaking data from the deployed system has not been recorded. However, ambient data obtained from both accelerometers and GPS units (Fig. 1.3 a–d) have been analyzed. Sample cross-spectra (Sxy) and coherency and phase angle plots of pairs of parallel records (N-S component of north deployment [N_N] vs. N-S component of south deployment [S_N], from accelerometers are

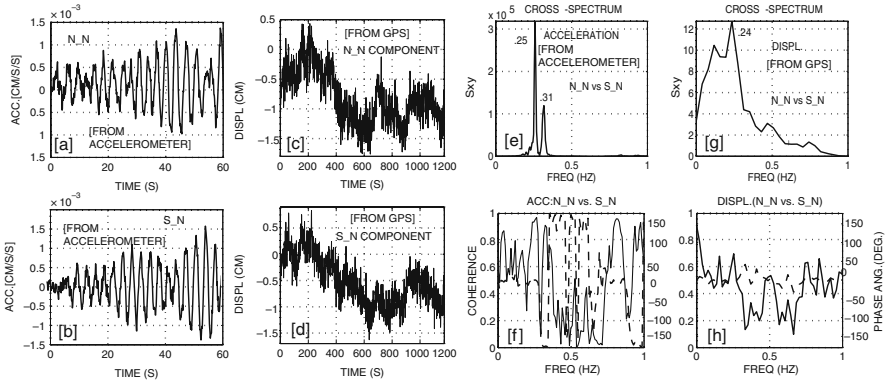

Fig. 1.3 (**a, b**) 60-second windowed accelerations and (**c, d**) 1200 s windowed GPS displacement data in the north-south orientation and at N (North) and S (South) locations (acceleration data sampled at 200 sps and GPS at 10 sps). Cross-spectra (Sxy) and associated coherency and phase angle plots of horizontal, and parallel accelerations (**e, f**) and GPS displacements (**g, h**). [Note: In the coherency-phase angle plots, solid lines are coherency and dashed lines are phase-angle]

shown in Fig. 1.3e–f. The same is repeated for the differential displacement records from GPS units (Fig. 1.3 g–h). The dominant peak in frequency at 0.24–.25 Hz seen in cross-spectra (Sxy) plots from both acceleration and displacement data are compatible with expected fundamental frequency for a 34-story building. A second peak in frequency at 0.31 Hz in the acceleration data belongs to the torsional mode.

At the fundamental frequency at 0.24 Hz, the displacement data exhibits a 0° phase angle; however, the coherencies are low (~0.6–0.7). The fact that the fundamental frequency (0.24 Hz) can be identified from the GPS displacement data (amplitudes of which are within the manufacturer specified error range) and that it can be confirmed by the acceleration data, is an indication of promise of better results when larger displacements can be recorded during strong shaking.

1.2.1.2 Recent Developments with Higher Sampling Rate GPS

Recently, GPS units with higher sampling ratios (50 Hz) have become commercially available. Thus, direct measurements of displacements of low-rise buildings (e.g. 2–10 stories) and other structures with correspondingly shorter fundamental periods are now possible also. Figure 1.4 (left) shows a photo of a 5 story shear wall structure tested at University of California San Diego (UCSD) shake table (Restrepo, pers. comm. 2007). Figure 1.4 (right) shows how well displacement of the actuator of the shake table measured with (linear variable displacement transducer) LVDT compares with that measured with 50 Hz GPS unit. Figure 1.5 shows relative displacement of the roof of the building with respect to the shake table and also the amplitude spectrum of the relative displacement ([1], Restrepo, and Panagiotou, pers. comm. 2007). These successful new test results indicate how promising the application of GPS is in dynamic monitoring of a wide (frequency) range of

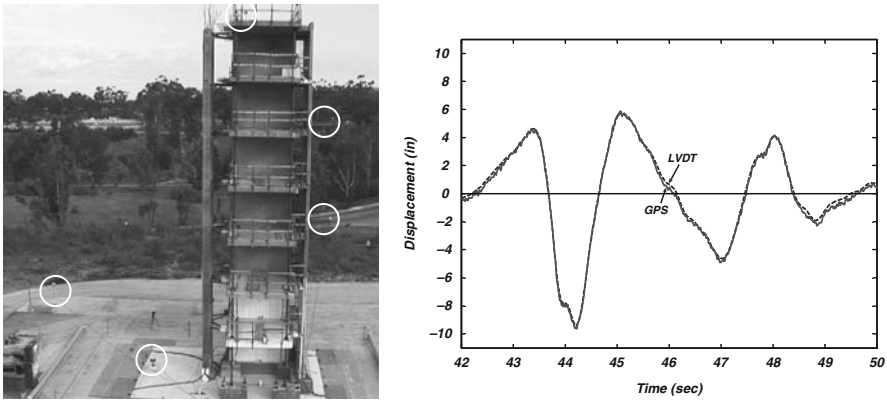

Fig. 1.4 (*Left*) Photo of a 7-story shear wall building tested at the University of California, San Diego (UCSD) Shake Table. 50 Hz-GPS sensors and LVDT's are used. *Circles* show the locations of GPS antennas ([1], Restrepo, pers. comm. 2007). (*Right*) Comparison of displacement time-histories of the shake table actuator obtained from LVDT and 50 Hz GPS

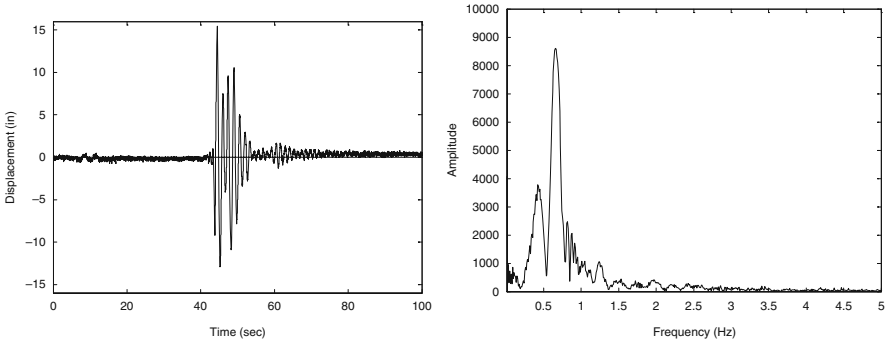

Fig. 1.5 UCSD 50 Hz GPS results: (*left*) Relative displacement of the roof with respect to the shake table platform (for the Northridge earthquake, Sylmar station input). (*Right*) Amplitude spectrum of the relative displacement ([1], Restrepo and Panagiotou, pers. comm. 2007)

structures. Therefore, GPS with higher sampling rates can now be used to monitor low-rise (3–10 stories) buildings which are very common in seismically active regions of the world.

1.2.2 Displacement via Real-Time Double Integration

A general flowchart for an alternative strategy based on computing displacements and drift ratios in real-time from signals of accelerometers strategically deployed throughout a building is depicted in Fig. 1.6 and described by [7]. Although ideal, deploying multiple accelerometers in every direction on every floor level is not a feasible approach, not only because of the installation cost, but also from the point of view of being able to robustly, and in near real-time, (a) stream accelerations, (b) compute and stream displacements and drift ratios after double-integration of accelerations, and (c) visually display threshold exceedances, thus fulfilling the objective of timely assessment of performance level and damage conditions.

A schematic of a recently deployed health monitoring system which utilizes these principles is shown in Fig. 1.7 [7]. The distribution of accelerometers provides data from several pairs of neighboring floors to facilitate drift computations. The system server at the site (a) digitizes continuous analog data, (b) pre-processes the 1000 sps digitized data with low-pass, anti-alias filters (c) decimates the data to 200 sps and streams it locally, (d) monitors and applies server triggering threshold criteria and locally records (with a pre-event memory) when prescribed thresholds are exceeded, and (e) broadcasts the data continuously to remote users by high-speed internet. Data can also be recorded locally on demand to facilitate studies while waiting for strong shaking events.

A "Client Software" remotely acquires acceleration data that can then be used to compute velocity, displacement and drift ratios. Figure 1.8 shows two PC screen

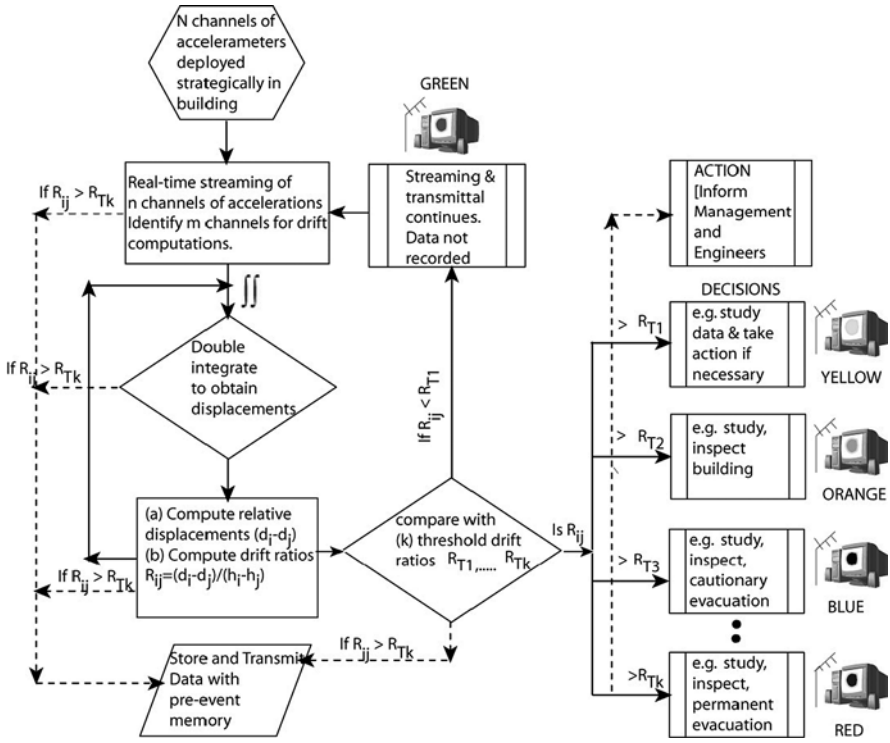

Fig. 1.6 Flow-chart for observation of damage levels based on threshold drift ratios

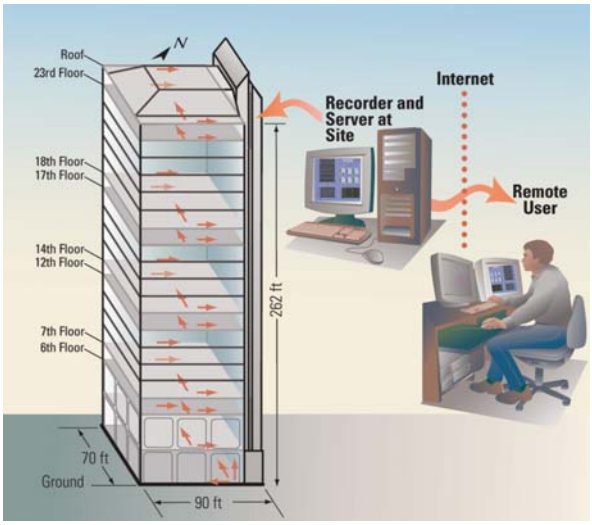

Fig. 1.7 Schematic of real-time seismic monitoring of the building (See also Plate 1 in Color Plate Section on page 453)

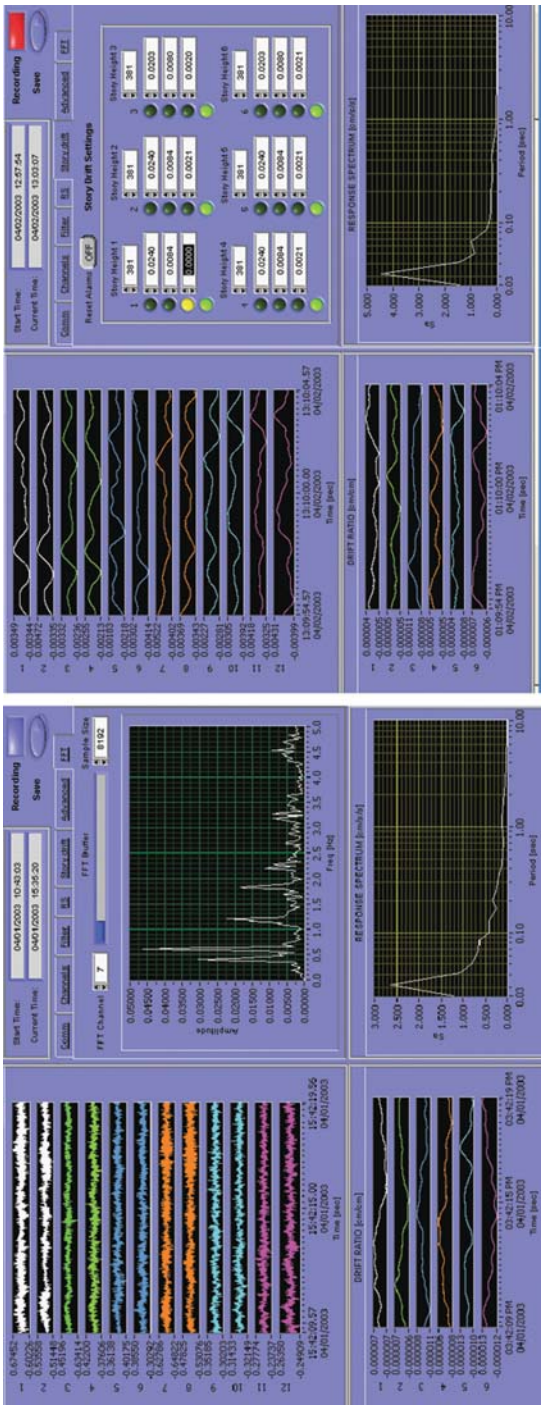

Fig. 1.8 Screen snapshots of sample client software displays: (*left*) acceleration streams and computed amplitude and response spectra, and (*right*) displacement and corresponding drift ratios and alarm systems corresponding to thresholds (See also Plate 2 in Color Plate Section on page 454)

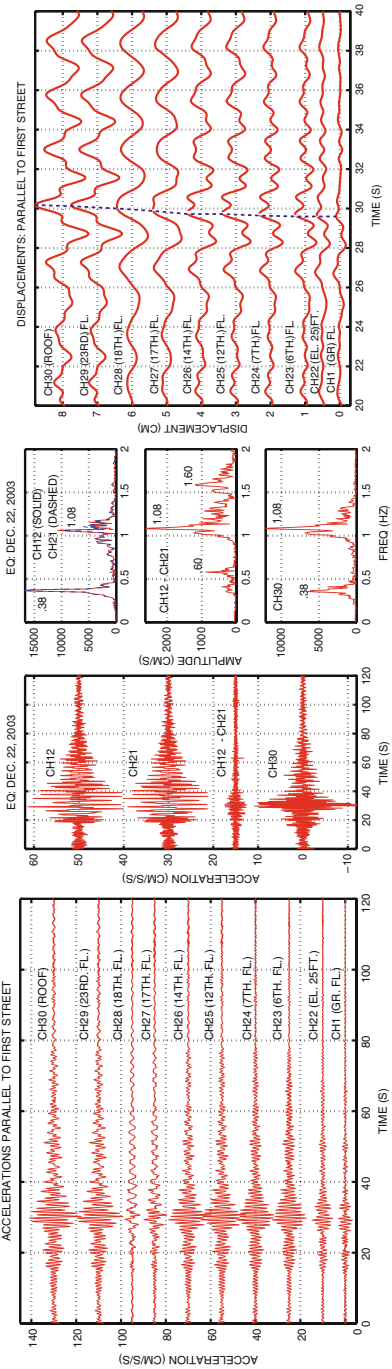

Fig. 1.9 Accelerations (*left*) at each instrumented floor on one side of the building for the San Simeon, CA earthquake of 12/22/2003, (*center*) from parallel channels (CH12, CH21) at the roof, their difference (CH12–CH21), and orthogonal CH30, and corresponding amplitude spectra indicate fundamental frequency at 0.38 Hz. (*right*) A 20-s window starting 20-s into the record of computed displacements shows propagating waves [travel time of ~ 0.5 s – indicated by dashed line] from the ground floor to the roof

snapshots of the client software display configured to stream acceleration or velocity or displacement or drift ratio time series. The amplitude spectrum for one of the selected channels is periodically recomputed and clearly displays several identifiable and distinct frequency peaks. In the lower left, time series of drift ratios are shown.

Corresponding to each drift ratio, there are 4 stages of colored indicators. When only the "green" color indicator is activated, it indicates that the computed drift ratio is below the first of three specific thresholds. The thresholds of drift ratios for selected pairs of data must also be manually entered in the boxes. As drift ratios exceed the designated three thresholds, additional indicators are activated, each with a different color (see Fig. 1.6). The drift ratios are calculated using data from any pair of accelerometer channels oriented in the same direction. The threshold drift ratios for alarming and recording are computed and determined by structural engineers using structural information and are compatible with the performance-based theme, as previously illustrated in Fig. 1.1.

A set of low-amplitude accelerations (largest peak acceleration ~ 1% g) recorded in the building during the December 22, 2003 San Simeon, CA. earthquake (Mw=6.4, epicentral distance 258 km) are exhibited in Fig. 1.9 for one side of the building. Figure 1.9 (center) also shows accelerations at the roof and corresponding amplitude spectra for the (a) two parallel channels (Ch12 and Ch21), (b) their differences (Ch12–Ch21), and (c) orthogonal channel (Ch30). The amplitude spectra depicts the first mode translational and torsional frequencies as 0.38 Hz and 0.60 Hz respectively. The frequency at 1.08 Hz belongs to the second translational mode. At the right of Fig. 1.9, a 20 s window of computed displacements starting 20 s into the record reveals the propagation of waves from the ground floor to the roof. The travel time is about 0.5 s. Since the height of the building is known (262.5 ft [80 m]), travel velocity is computed as 160 m/s. One of the possible approaches for detection of possible damage to structures is by keeping track of significant changes in the travel time, since such travel of waves will be delayed if there are cracks in the structural system [10].

1.3 Monitoring Single Structure vs. Campus Structures

Rather than having only one building monitored, there may be situations where some owners desire to monitor several buildings simultaneously, such as on industrial campus. Figure 1.10 schematically shows a campus-oriented monitoring configuration. Depending on the choice of the owner and consultants, a campus system may have building-specific or central-monitoring systems and as such is highly flexible in configuration. As can be stipulated, potential variations and combinations of alternatives for a campus-wide monitoring system are tremendous. There can be central-controlled monitoring as well as building-specific monitoring or both. A wide variety of data communication methods can be configured to meet the needs (Fig. 1.10).

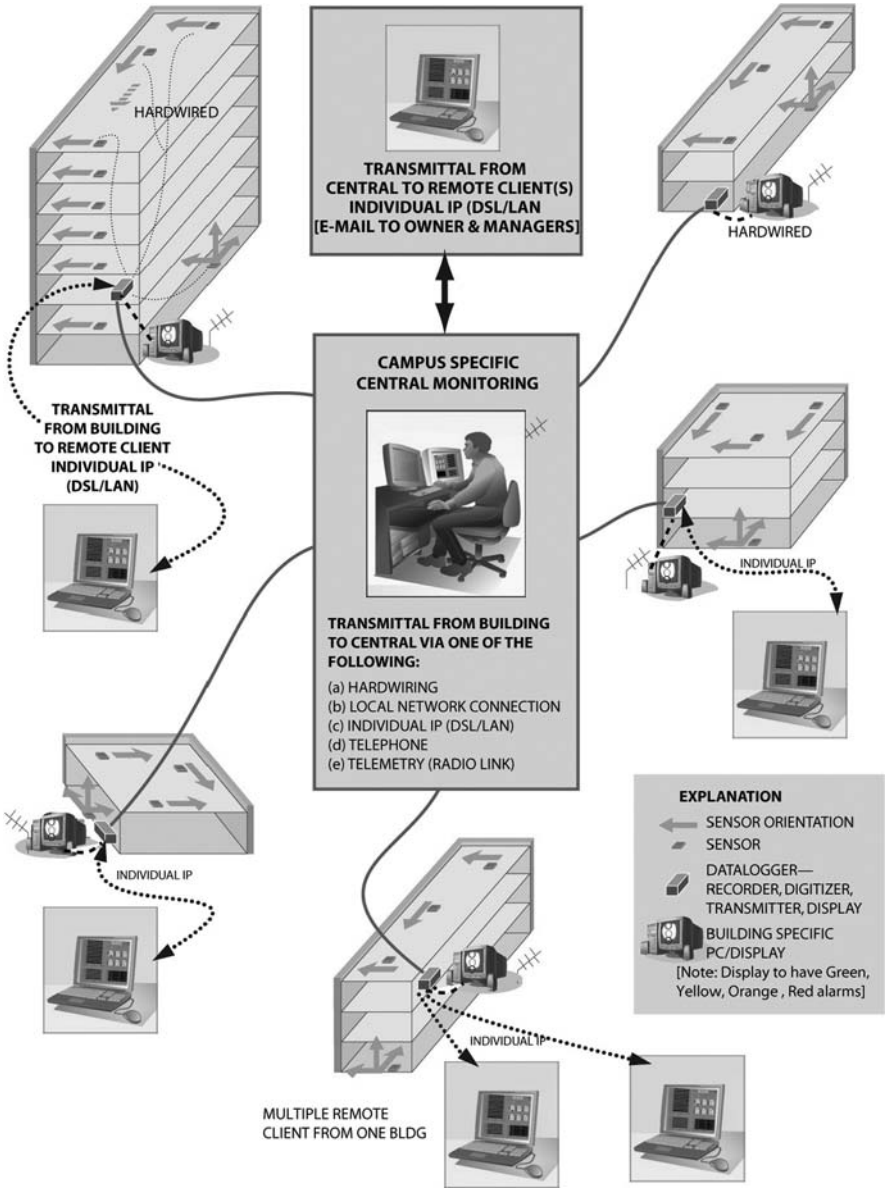

Fig. 1.10 A schematic of campus-oriented monitoring system. Each building within a campus may have its own monitoring system or there may a central monitoring unit

1.4 Conclusions

Capitalizing on advances in global positioning systems (GPS), in computational capabilities and methods, and in data transmission technology, it is now possible to configure and implement a seismic monitoring system for a specific building with the objective of rapidly obtaining and evaluating response data during a strong shaking event in order to help make informed decisions regarding the health and occupancy of that specific building. Displacements, and in turn, drift ratios, can be obtained in real-time or near real-time through use of GPS technology and/or double-integrated acceleration. Drift ratios can be related to damage condition of the structural system by using relevant parameters of the type of connections and story structural characteristics including its geometry. Thus, once observed drift ratios are computed in near real-time, technical assessment of the damage condition of a building can be made by comparing the observed with pre-determined threshold stages. Both GPS and double-integrated acceleration applications can be used for performance evaluation of structures and can be considered as building health-monitoring applications. Although, to date, these systems were not tested during strong shaking events, analyses of data recorded during smaller events or low-amplitude shaking are promising.

Appendix: Review of Seismic Monitoring Issues

Introduction

Seismic monitoring of structural systems constitutes an integral part of the National Earthquake Hazard Reduction Program in the United States and similarly in some other seismically active countries (e.g. Japan, Italy and in a very limited scale, Turkey). Recordings of the acceleration response of structures have served the scientific and engineering community well and have been useful in assessing design/analysis procedures, improving code provisions and in correlating the system response with damage. Unfortunately, there are only a few records from damaged instrumented structures to facilitate studies of the initation and progression of damage during strong shaking (e.g. Imperial County Services Building during the 1979 Imperial Valley earthquake, [11]). In the future, instrumentation programs should consider this deficiency. Jennings [12] summarizes this view as follows: “As more records become available and understood, it seems inevitable that the process of earthquake resistant design will be increasingly, and quite appropriately, based more and more upon records and measured properties of materials, and less and less upon empiricism and qualitative assessments of earthquake performance. This process is well along now in the design of special structures”.

An instrumented structure should provide enough information to (a) reconstruct the response of the structure in sufficient detail to compare with the response predicted by mathematical models and those observed in laboratories, the goal being to improve the models, (b) make it possible to explain the reasons for any damage to

the structure, and (c) facilitate decisions to retrofit/strengthen the structural systems when warranted. In addition, a structural array should include, if physically possible, an associated associated tri-axial accelerograph so that the interaction between soil and structure can be quantified.

Recent trends in development of performance based earthquake resistant design methods and related needs of the engineering community, as well as advances in computation, communication and data transmission capabilities, have prompted development of new approaches for structural monitoring issues and applications. In particular, (a) verification of performance based design methods and (b) needs of owners to rapidly and informedly assess functionality of a building following an event require measurement of displacement rather than or in addition to accelerations as is commonly done. Thus, new avenues in recording or computing displacement in real or near-real time are evolving. Thus, to meet the requirements for timely evaluation of damage condition of a building following an earthquake are leading the development of acquisition systems with special software that can deliver real-time or near real-time acceleration and displacement measurements. This topic was treated in more detail in the main part of this paper.

This appendix describes the past and current status of the structural instrumentation applications and new developments. The scope of the paper includes the following issues: (a) types of current building arrays and responses to be captured, (b) recent developments in instrument technology and implications, and (d) issues for the future. The scope does not include cost considerations (as this varies from one locality to another).

Historical Perspective

In the United States, the largest two structural instrumentation programs are managed and operated by the California Seismic Instrumentation Program (CSMIP) of the California Geologic Survey and the ANSS [13] of the United States Geological Survey (USGS). Until recently, these programs have aimed to facilitate response studies in order to improve our understanding of the behavior and potential for damage to structures under the dynamic loads of earthquakes. The principal objective has been the quantitative measurement of structural response to strong and possibly damaging ground motions for purposes of improving seismic design codes and construction practices. However, to date, it has not been an objective of either instrumentation program to create a health monitoring environment for structures.

To date, the USGS has conducted a cooperative strong ground motion and structural instrumentation program with other federal and state agencies and private owners. Table 1.2 summarizes the current inventory and cooperative affiliations of the USGS Cooperative National Strong-Motion Program (NSMP) and that of CSMIP. Within the USGS program, and unless other factors are considered and/or specific organizational choices are made apriori, the following general parameters have been considered for selecting and ranking structures for instrumentation:

Table 1.2 Two major agencies and inventory of (building) structural instrumentation arrays

Agency	Extensively Instrumented Buildings (>6 channels)
USGS Cooperative Program	~65 (as of 2007)
CSMIP (California State)	~170 [17, 18]

1. Structural parameters: the construction material, structural system, geometry, discontinuity, and
2. Site-related parameters : severity-of-shaking on the basis of closeness to one or more of the main faults within the boundaries of the area considered (e.g. for the San Francisco Bay area, the San Andreas, Hayward, and Calaveras faults are considered).

Detailed procedures and overall description used by the USGS structural instrumentation program are described by Çelebi, [14, 15, 16]. On the other hand, the State of California CSMIP now has over 170 buildings instrumented in accordance to a predefined matrix that aims to cover a wide variety of structural systems, [17, 18].

General Instrumentation Issues

Data Utilization

Ultimately, the types and extent of instrumentation must be tailored to how the data acquired during future earthquakes will be utilized, even though there may be more than one objective for instrumentation of a structure. Table 1.3 summarizes some data utilization objectives with sample references. As a recent example of data utilization, Jennings [12] analyzed data from two buildings within close proximity (<20 km) to the epicenter of the 1994 Northridge, CA earthquake. He calculated the base shear from the records as 8 and 17% of the weights of the buildings and the drift ratios as 0.8 and 1.6% (exceeding code limitations). Jennings [12] concluded: "A difference between code design values and measured earthquake responses of this magnitude – approaching a factor of ten – is not a tenable situation." Thus, recorded responses revealed excessive drift ratios while shear forces remained reasonable.

Code Versus Extensive Instrumentation

The most widely used code in the United States, the Uniform Building Code (UBC-1997 and prior editions), recommends, for seismic zones 3 and 4, a minimum of three accelerographs be placed in every building over six stories with an aggregate floor area of 60,000 square feet or more, and in every building over ten stories regardless of the floor area [19]. The purpose of this requirement by the UBC was

Table 1.3 Sample list of data utilization objectives & sample references

Generic Utilization
Verification of mathematical models (usually routinely performed), [20, 62]
Comparison of design criteria vs. actual response (usually routinely performed)
Verification of new guidelines and code provisions, [21, 62]
Identification of structural characteristics (Period, Damping, Mode Shapes) [63]
Verification of maximum drift ratio [22, 23]
Torsional response/Accidental torsional response, [24, 25]
Identification of repair & retrofit needs & techniques, [26]
Specific Utilization
Identification of damage and/or inelastic behavior, [11]
Soil-Structure Interaction Including Rocking and Radiation Damping, [27–29]
Response of Unsymmetric Structures to Directivity of Ground Motions, [30]
Responses of Structures with Emerging Technologies (base-isolation, visco-elastic dampers, and combination), [31–32, 64]
Structure specific behavior, [33–35]
Development of new methods of instrumentation/hardware, [36–39]
Improvement of site-specific design response spectra and attenuation curves, [40–43, 61]
Associated free-field records (if available) to assess site amplification, SSI and attenuation curves, [44–48]
Verification of Repair/Retrofit Methods, [49, 26]
Identification of Site Frequency from Building Records, [16]
Recent Trends to Advance Utilization
Studies of response of structures to long period motions, [50]
Need for new techniques to acquire/disseminate data, [38, 51, 52, 39]
Verification of Performance Based Design Criteria (future essential instrumentation work)
Near Fault Factor (more free-field stations associated with structures needed)
Comparison of strong vs weak response (Marshall, Phan and Çelebi, [53, 54]
Functionality Çelebi, 2004, Needs additional specific instrumentation planning)
Health Monitoring and other Special Purpose Verification, [55]

to monitor rather than to analyze the complete response modes and characteristics. UBC-code type recommended instrumentation is illustrated in Fig. 1.11a . Following 1971 San Fernando earthquake, in 1982, in Los Angeles, the code-type requirement was reduced to one tri-axial accelerometer at the roof (or top floor) of a building meeting the aforementioned size requirements [56]. In general, code-type instrumentation is naturally being de-emphasized as a result of strong desire by the structural engineering community to gather more data from instrumented structures to perform more detailed structural response studies. Experiences from past earthquakes show that the minimum guidelines established by UBC for three tri-axial accelerographs in a building are not sufficient to perform meaningful model verifications. For example, three horizontal accelerometers are required to define the (two orthogonal translational and a torsional) horizontal motions of a floor. Rojahn and Mathiesen [57] concluded that the predominant response of a high-rise building can be described by the participation of the first four modes of each of the three sets of modes (two translations and torsion); therefore, a minimum of 12 horizontal accelerometers would be necessary to record these modes. Instrumentation needed to provided acceptable documentation of the dominant response of a structure are

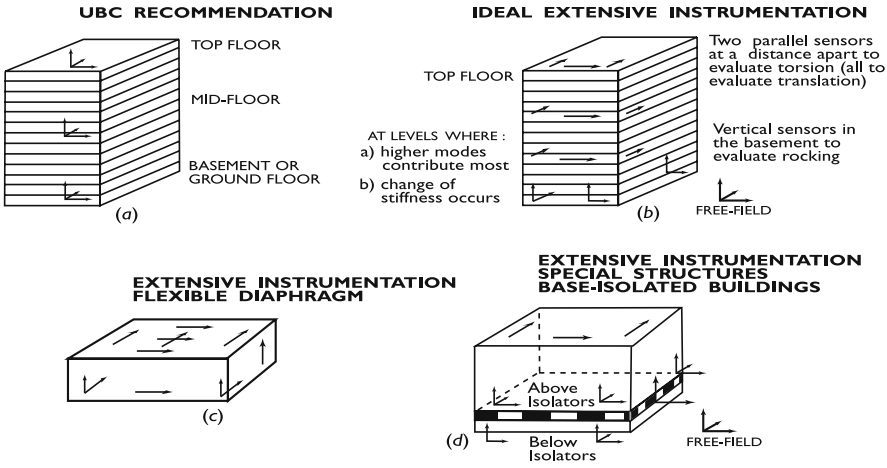

Fig. 1.11 Typical instrumentation schemes

addressed by Hart and Rojahn [58] and Çelebi and others [15]. This type of instrumentation scheme is called the ideal extensive instrumentation scheme as illustrated in Fig. 1.11b.

Specially designed instrumentation arrays are needed to understand and resolve specific response problems. For example, thorough measurements of in-plane diaphragm response requires sensors in the center of the diaphragm (Fig. 1.11c) as well as at boundary locations. Performance of base-isolated systems and effectiveness of the isolators are best captured by measuring tri-axial motions at the top and bottom of the isolators as well as the rest of the superstructure (Fig. 1.11d). In case of base-isolated buildings, the main objective usually is to assess and quantify the effectiveness of isolators. If there is no budgetary constraint, additional sensors can be deployed between the levels above the isolator and roof to capture the behavior of intermediate floors.

Associated Free-Field Instrumentation

More information is required to interpret the motion of the foundation substructure relative to the ground on which it rests. This requires free-field instrumentation associated with a structure (Fig. 1.11b).

However, this is not always possible in an urban environment.[3] Engineers use free-field motions as input at the foundation level, or they obtain the motion at foundation level by convoluting the motion through assumed or determined layers of strata to base rock and deconvoluting the motion back to foundation level.

[3]For example, in San Francisco, California, it is not possible to find a suitable free-field location around the Transamerica building, which is extensively instrumented.

Confirmation of these processes requires downhole instrumentation near or directly beneath a structure. These downhole arrays will yield data on:

1. the characteristics of ground motion at bedrock (or acceptably stiff media) at a defined distance from a source and
2. the amplification of seismic waves in layered strata.

Downhole data from sites in the vicinity of instrumented building or other structures are especially scarce. Two new building monitoring arrays in the United States that include downhole sub-arrays are described later in this part of the manuscript.

Record Synchronization Requirement

High-precision record synchronization must be available within a structure (and with the free-field, if applicable) if the response time histories are to be used together to reconstruct the overall behavior of the structure. Such synchronization has been achieved through extensive cabling from each of the individual sensor to the recorder. Recent technological developments enable decreasing or minimizing, and in certain cases eliminating, the use of extensive cabling. For example, the global positioning systems (GPS) is now widely used to synchronize a building instrumentation with that of a separate recorder system for the free-field; thus, eliminating cable connection between the free-field recorder and recorder within a structure. The issue here is that synchronization must be an integral part of any structure monitoring scheme whether cable or wireless transmission is the means to realize it.

Recording Systems, Constraints and New Developments

Until recently, commercially available recording systems have been limited to a maximum of 12–18 channels (e.g. analog recorder CRA-1,[4] 13 channels; the digital K-2[4], 12 channels; digital Mt. Whitney[4], 18 channels). Although multiple numbers of recording units may be used to accommodate requisite multiple-channel instrumentation systems for a structure, cost restrictions usually limit the number of channels to 12 or 18 (or multiples thereof), unless more channels are needed or special financing is available. Recently, however, with the development of PC-based data acquisition systems that utilize multiple A/D converters, several dozen channels of data can be accommodated. In such systems, the only constraints are the cost of the sensors and data transmission media required. One such system is described later in the paper.

[4]Use of commercial names or trademarks cited herein does not imply endorsement of these products by the U.S. Geological Survey.

Soil-Structure Interaction Array(s)

State-of-the-art practice and analytical approaches require, when warranted, the structure-foundation system to be represented by mathematical models that include the influence of the sub-foundation media. In many cases, under a specific geotechnical environment, certain structures will respond differently than if that structure was built as a fixed based structure on a very stiff (e.g. rock) site condition. This alteration of vibrational characteristics of structures due to soil-structure interaction (SSI) can be both beneficial and detrimental for their performances. To date, the engineering community is not clear about the pros and cons of SSI.

Adverse effects of SSI during the 1985 Michoacan (Mexico) earthquake were addressed by Tarquis and Roesset [59], who showed that, in the lakebed zone of Mexico City, 400 km away from the epicenter, fundamental periods of mid-rise buildings (5–15 stories) lengthened due to SSI. Thus, such buildings were negatively affected due to SSI because the lengthening of their fundamental periods placed them in a resonating environment close to the approximately 2-s resonant period of Mexico City lakebed.

On the other hand, under different circumstances, SSI may be beneficial because it produces an environment whereby the structure escapes the severity of shaking due to shifting of its fundamental frequency. Certainly, in a basin such as that of the Los Angeles area, SSI may cause both beneficial and detrimental effects in the response of structures.

Thus, the identification of the circumstances under which SSI is beneficial or detrimental and the relevant controlling parameters is a necessity. Therefore, measurement of soil-structure interaction effects are required to fully understand the response of a major structure. This is easily accommodated along with the instrumentation schemes of the superstructure. Sensors at critical locations of the foundation are required to capture its relevant motions. Additional sensors may be needed to record the motions of the surrounding geological materials. For example, if vertical motion and rocking are expected to be significant and need to be recorded, at least three vertical accelerometers are required at the basement level (Fig. 1.11b). In some cases; additional instrumentation (e.g. free-field accelerographs on the surface and in boreholes [downhole accelerographs]) may be required. Horizontal and vertical spatial downhole sensors will provide information on how the motions change while traveling through the media and how much it is affected by the building response. Detailed proposals for soil-structure interaction experiments resulting from a workshop are presented in USGS OFR-92-295, [60].

Specialized arrays that will capture SSI effects will further advance the verification of SSI effects that are currently very much limited to theoretical studies.

Two existing SSI arrays are shown in Fig. 1.12 a,b. Each of these arrays have the necessary components of sub-arrays (e.g. superstructure, foundation, surface and downhole free-field sub-arrays). Figure 1.12a depicts Pacific Park Plaza Building array in Emeryville, CA [28] and Figure 1.12b depicts the Atwood Building in Anchorage, AK. Both building monitoring schemes are designed to capture SSI effects in addition to the traditional translational and torsional responses.

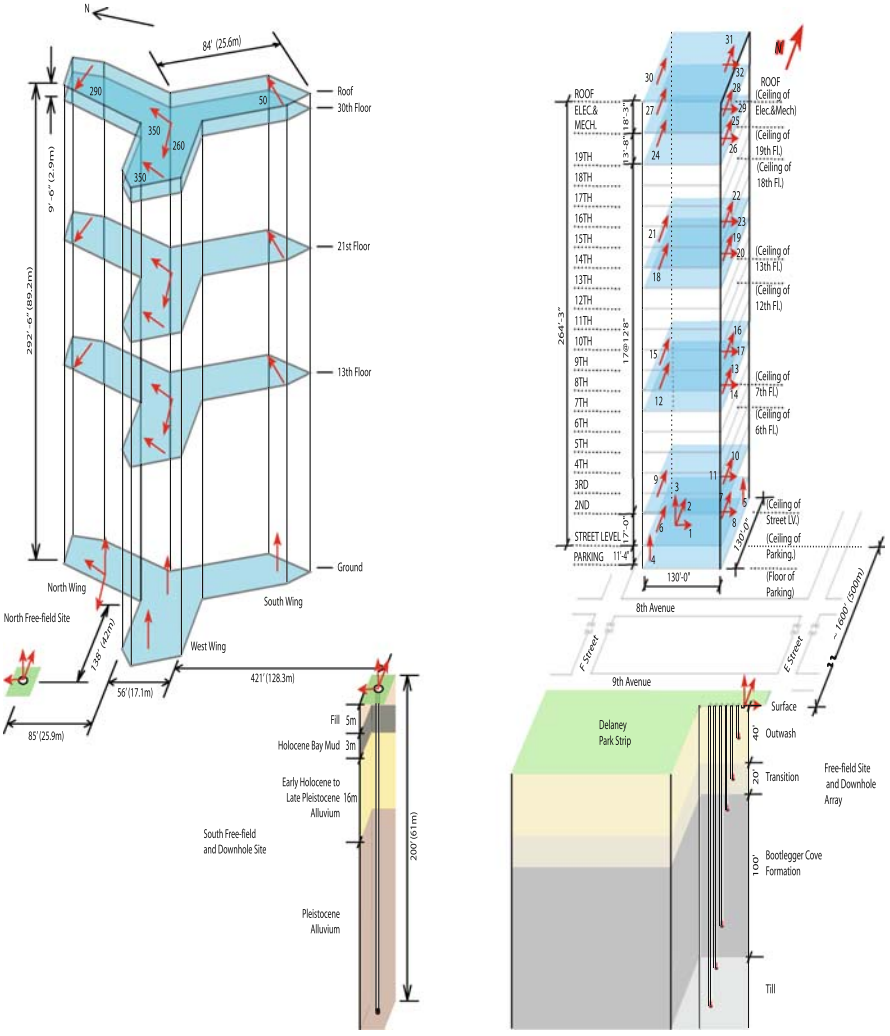

Fig. 1.12 (*Left*) A three-dimensional schematic of the Pacific Park Plaza Building (Emeryville, CA) showing with integrated structure, surface and downhole sub-arrays (Note: The tri-axial downhole accelerograph was added after the 1989 Loma Prieta earthquake). (*Right*) A General three-dimensional schematic of the Atwood Building (Anchorage, AK) showing the general dimensions and locations of accelerometers deployed within the structure and tri-axial downhole accelerometers at free field site

References

1. Panagitou M, Restrepo JI, Conte JP, Englekirk RE (2006) Seismic response of reinforced concrete wall buildings. 8NCEE (1494) San Francisco CA
2. Applied Technology Council (ATC) (1989) Procedures for post-earthquake safety evaluation of buildings, ATC-20, Redwood City, CA.

3. FEMA-352: Recommended post-earthquake evaluation and repair criteria for welded steel moment-frame buildings (SAC 2000)
4. SAC Joint Venture (2000) Recommended post-earthquake evaluation and repair criteria for welded steel moment-frame buildings. Prepared for the Federal Emergency Management Agency FEMA 352 Washington D.C.
5. Porter K, Mitrani-Reiser J, Beck J L, Ching J, (2006) Smarter structures: Real- time loss estimation for instrumented buildings.8NCEE (1236) San Francisco, CA
6. Çelebi M, Sanli A (2002) GPS in pioneering dynamic monitoring of long-period structures. Earthquake Spectra Journal of EERI 18: 47–61
7. Çelebi M, Sanli A, Sinclair M, Gallant S, Radulescu D (2004) Real-time seismic monitoring needs of a building owner and the solution–a cooperative effort. Earthquake Spectra Journal of EERI 19:1–23
8. Building Occupancy Resumption Program (BORP) (2001) City and County of San Francisco Department of Building Inspection Emergency Operation Plan (Rev. 2001). http://seaonc.org/member/committees/des_build.html
9. Applied Technology Council (ATC) (1997) NEHRP Commentary on the guidelines for the seismic rehabilitation of buildings, prepared for the building seismic safety council. Published by the Federal Emergency Management Agency, FEMA 274, Washington, D.C.
10. Safak E (1999) Wave-propagation formulation of seismic response of multistory buildings. ASCE Journal of Structural Engineering 125:426–437
11. Rojahn C, Mork PN (1981) An analysis of strong-motion data from a severely damaged structure, the imperial county services building. El Centro, California. U.S. Geological Survey Open-File Report 81–194
12. Jennings PC (1997) Use if strong-motion data in earthquake resistant design, in Proc.SMIP97 seminar on utilization of strong-motion data. California strong motion instrumentation program, Division of Mines and Geology, California Dept. of Conservation, Sacramento, CA. 1–8
13. An assessment of seismic monitoring in the united states – requirement for an advanced national seismic system (1999) U.S. Geological survey, Circular 1188
14. Çelebi M, Safak E, Brady G, Maley R, Sotoudeh V (1987) Integrated instrumentation plan for assessing the seismic response of structures–a review of the current USGS program, USGS Circular 947
15. Çelebi M (2000) Seismic Instrumentation of buildings. U.S. Geological Survey Open-File Report 00-157
16. Çelebi M (2003) Identification of site frequencies from building records, Journal of EERI, Earthquake Spectra 19(1):1–23
17. Huang MJ, Shakal AF (2001) Proceedings, invited workshop on strong-motion instrumentation of buildings. COSMOS, Emeryville, CA. Cosmos Publication No: CP-2001/04:15–19
18. Shakal AF, Huang MJ, Rojan C, Poland C (2001) Proceedings, Invited Workshop on Strong-motion Instrumentation of Buildings, COSMOS, Emeryville, Ca. November 2001, Cosmos Publication No: CP-2001/04, 5–14
19. Uniform Building Code, International Conference of Building Officials, Whittier, CA, 1970, 1976, 1979, 1982, 1985, 1988, 1991, 1994, 1997 editions
20. Boroschek RL, Mahin SA, Zeris CA (1990) Seismic response and analytical modeling of three instrumented buildings, Proc. 4th U.S. National Conference on Earthquake Engineering, 2: 219–228, Palm Springs, CA
21. Hamburger RO (1997) FEMA-173 Seismic rehabilitation guidelines: The next step–verification, in Proc.SMIP97 seminar on utilization of strong-motion data, California strong motion instrumentation program. Division of Mines and Geology, California Dept. of Conservation, Sacramento, CA. 51–69
22. Astaneh A, Bonowitz D, Chen C (1991) Evaluating design provisions and actual performance of a modern high-rise steel structure, in seminar on seismological and engineering implications of recent strong-motion data: California Department of Conservation, Division of Mines and Geology, 5-1–5-10

23. Çelebi M (1993) Seismic response of eccentrically braced tall building, Journal of Structural Engineering 119(4):1188–1205
24. Chopra A, Goel RK (1991) Evaluation of torsional provisions of seismic codes. Journal of Structural Engineering ASCE, 117(12):3762–3782
25. De La Llera J, Chopra A (1995) Understsanding of inelastic seismic behavior of symmetric-plan buildings. Earthquake Engineering and Structural Dynamics 24:549–572
26. Crosby P, Kelly J, Singh JP (1994) Utilizing visco-elastic dampers in the seismic retrofit of a thirteen story steel framed building. ASCE Structures Congress XII, Atlanta, Ga., 2, 1286–1291
27. Çelebi M (2006) Recorded earthquake responses from the integrated seismic monitoring network of the Atwood Building, Anchorage (AL). Earthquake Spectra 22(4):847–864
28. Çelebi M, Safak E (1992) Seismic response of Pacific Park Plaza-I, data and preliminary analysis: Journal of Structural Engineering 118(6):1547–1565
29. Çelebi M (1997) Response of olive view hospital to Northridge and Whittier earthquakes. American Society of Civil Engineers, Journal of Structural Engineering, April, 123(4): 389–396
30. Porter LD (1996) The influence of earthquake azimuth on structural response due to strong ground shaking. Eleventh World Conference on Earthquake Engineering, Acapulco, Mexico, (No. 1623): Elsevier Science Ltd. (CD-ROM)
31. Çelebi M (1995) Successful Performance of base-isolated hospital building during the 17 January 1994 Northridge earthquake. Journal of the Structural Design of Tall Buildings 5:95–109
32. Kelly JM, Aiken ID, Clark PW (1991) Response of base-isolated structures in recent California earthquakes. Seminar on seismological and engineering implications of recent strong-motion data. Preprints: California Division of Mines and Geology, Strong Motion Instrumentation Program, 12-1–12-10
33. Boroschek RL, Mahin S (1991) An investigation of the seismic response of a lightly-damped torsionally-coupled building. University of California, Berkeley, California, Earthquake Engineering Research Center Report 91/18, 291
34. Çelebi M, Bongiovanni G, Safak E, Brady G (1989) Seismic response of a large-span roof diaphragm: Earthquake Spectra 5(2):337–350
35. Çelebi M (1994) Response study of a flexible building using three earthquake records. Structures Congress XII: Proceedings of papers presented at the structures congress '94, Atlanta, GA, April 24–28, American Society of Civil Engineers, New York, 2:1220–1225
36. Çelebi M, Presscott W, Stein R, Hudnut K, Wilson S (1997) Application of GPS in monitoring tall buildings in seismic areas. 1997a, Abstract, AGU Meeting, San Francisco, CA
37. Çelebi M, Presscott W, Stein R, Hudnut K, Behr J, Wilson S (1999) GPS monitoring of dynamic behavior of long-period structures. Earthquake Spectra 15(1):55–66
38. Celebi M, Sanli A, Sinclair M, Gallant S, Radulescu D (2004) Real-time seismic monitoring needs of a building owner and the solution – a cooperative effort, in print, Journal of EERI, Earthquake Spectra 19(1):1–23
39. Straser E (1997) Toward wireless, modular monitoring systems for civil structures. John A. Blume Earthquake Engineering Center Newsletter, Issue No. 2
40. Abrahamson NA, Silva WJ (1997) Empirical response spectral attenuation relations for shallow crustal earthquakes, Seismological Research Letters 68:94–127
41. Boore DM, Joyner WB, Fumal TE (1997) Equations for estimating horizontal response spectra and peak acceleration from western North American earthquakes: A summary of recent work, Seismological Research Letters 68:128–153
42. Campbell KW (1997) Empirical near-source attenuation relationships for horizontal and vertical components of peak ground acceleration, peak ground velocity, and pseudo-absolute acceleration response spectra. Seismological Research Letters 68:154–179
43. Sadigh K, Chang C-Y, Egan JA, Makdisi F, Youngs RR (1997) Attenuation relationships for shallow crustal earthquakes based on California strong motion data. Seismological Research Letters, 68:180–189

44. Borcherdt, R.D. (1994) Estimates of site-dependent response spectra for design (Methodology and Justification), Earthquake Spectra 10:617–653
45. Borcherdt RD (1993) On the estimation of site-dependent response spectra, Proc., International Workshop on Strong-Motion Data, Menlo Park, CA, Pub. by Port and Harbor Research Institute, Japan, (Preprint of manuscript submitted as "Simplified site classes and empirical amplification factors for site-dependent code provisions", for Proc. NCEER, SEAOC, BSSC Workshop on Site Response during Earthquakes and Seismic Code Provisions, Univ. S. Calif., Los Angeles, CA, November 18–20, (1992), 2: 399–427
46. Borcherdt RD (2002a) Empirical evidence for acceleration-dependent amplification factors, Bulletin of the Seismological Society of America 92:761–782
47. Borcherdt RD (2002b) Empirical evidence for site coefficients in building-code provisions, Earthquake Spectra 18:189–218
48. Crouse CB, McGuire JW (1996) Site response studies for purpose of revising NEHRP seismic provisions. Earthquake Spectra 12:407–439
49. Çelebi M, Liu HP (1996) Before and after retrofit–response of a building during ambient and strong-motions. 8.US. National Conference on Wind Engineering, The John Hopkins Univ.
50. Hall JF, Heaton TH, Halling MW, Wald DJ (1996) Near-source ground motion and its effects on flexible buildings. Earthquake Spectra 11(4):569–605
51. Çelebi M, Sanli A (2002) GPS in pioneering dynamic monitoring of long-period structures. Earthquake Spectra, Journal of EERI 18(1):47–61
52. Çelebi M (1998) Performance of building structures–a summary, in The Loma Prieta, California, earthquake of October 17, 1989–Building Structures. (M Çelebi editor), USGS Proc.,: 1552-C,: c5–c76, January 1998
53. Çelebi M, Phan LT, Marshall RD (1993) Dynamic characteristics of five tall buildings during strong and low-amplitude motions. Journal of Structural Design of Tall Buildings, J. Wiley, 2:1–15
54. Marshall RD, Phan LT, Çelebi M (1992) Measurement of structural response characteristics of full-scale buildings: Comparison of results from strong-motion and ambient vibration records, NISTIR REPORT 4884, National Institute of Standards and Technology, Gaithersburg, Maryland
55. Heo G, Wang ML, Satpathi D (1977) Optimal transducer placement for health monitoring. Soil Dynamics and Earthquake Engineering 16:496–502
56. Darragh R, Cao T, Graizer V, Shakal A, Huang M (1994) Los Angeles code-instrumented building records from the Northridge, California earthquake of January 17, 1994: Processed Release No. 1, Report No. OSMS 94-17, California Strong Motion Instrumentation Program, California Department of Conservation
57. Rojahn C, Matthiesen RB (1977) Earthquake response and instrumentation of buildings. Journal of the Technical Councils, American Society of Civil Engineers, 103, TCI, Proceedings Paper 13393: 1–12
58. Hart G, Rojahn C (1979) A decision-theory methodology for the selection of buildings for strong-motion instrumentation: Earthquake Engineering and Structural Dynamics 7:579–586
59. Tarquis F, Roesset J (1988) Structural response and design response spectra for the 1985 Mexico City earthquake. University of Texas, Austin, Texas, Report No. GD89-1, 208p
60. Çelebi M (compiler), Lysmer J, Luco E (1992) Recommendations for a soil-structure interaction experiment report based on a workshop held at San Francisco, California on February 7, 1992, U.S. Geological Survey Open-File Report 92–295
61. Borcherdt RD (1994) Estimates of site-dependent response spectra for design (methodology and justification), Earthquake Spectra 10: 617–653
62. Çelebi M (2001) Current practice and guidelines for USGS instrumentation of buildings including federal buildings. COSMOS Proceedings, Invited Workshop on Strong-Motion Instrumentation of Buildings, Emeryville, Ca. November 2001, Cosmos Publication No: CP-2001/04.

63. Çelebi M (1996) Comparison of damping in buildings under low-amplitude and strong motions. Journal of Wind Engineering and Industrial Aerodynamics, Elsevier Science, 59:309–323
64. Kelly J (1993) Seismic isolation, passive energy dissipation and active control, Proc. ATC 17-1. Seminar on state of the art and state of the practice of base isolation 1:9–22

Chapter 2
Dance for Modern Times: Insurance, Economic Stability and Building Strength

Gabriela Chávez-López

Abstract A unique feature of natural catastrophe losses is the widespread nature of each event, potentially affecting a large number of insured contracts. The role of the insurance industry to transfer and finance this risk is very important and the demand for it will continue to increase, but unfortunately catastrophe business is becoming very expensive. When a disaster happens, people will look for insurers to recover their losses, but if they are not covered by insurance, they will then turn to their governments for help. However, a catastrophic event can create severe problems to the economy, especially in developing countries, so much that the government can neither recover in a short period of time, nor help their citizens in an efficient way. The 1999 earthquakes in Turkey showed the great financial impact the lack of insurance has when large catastrophic events occur, not only for the individual but also for the country, and in some instances affecting the world economy as well. To deal with this problem, governments have created special government support insurance mechanisms that will protect their citizens in case of a catastrophe and promote the creation of new laws to improve the quality of construction in preparation for the next event. In order to create these mechanisms, we need to understand and identify the risk we are taking. Catastrophe loss calculation models (CAT models) are the tools that help the insurance industry to evaluate these risks and help buy adequate protection.

2.1 Preparing the Stage

According to Swiss Re, in 2006, there were 136 natural catastrophes and 213 man made disasters recorded in the world causing more than 31,000 deaths worldwide of which earthquakes were the ones causing most of the fatalities. Total losses were estimated at about USD 48 bn of which only a third was covered by insurance. Of

G. Chávez-López (✉)
EQECAT/ABS Consulting, Paris, France
e-mail: gchavezlopez@absconsulting.com

A. Ilki et al. (eds.), *Seismic Risk Assessment and Retrofitting*, Geotechnical, Geological, and Earthquake Engineering 10, DOI 10.1007/978-90-481-2681-1_2,

the covered losses, about three quarters were caused by natural catastrophes [1]. In 1999, there were total losses of about USD 100 bn worldwide of which USD 28.6 bn were insured losses and about 85.5% of the covered losses were due to earthquakes and storms [2].

There are enough metropolitan areas in the world with populations of 2 millions or more close to an earthquake zone. If a catastrophic event strikes a national capital or an unstable region, the political and economic repercussions could be felt for a very long time. In any given event, the economic losses do not only represent the property and casualty losses but also the loss in revenue which with globalization can touch not only the country where the event has occurred, but the rest of the world. At the country level, one major city loss can have an important impact on the economy of the country, especially if this city is an economic center. This will weaken the economy and will have negative effects on the financial markets.

The lack of insurance can have great impact on the economy of a country. This was one of the lessons the Turkish earthquakes of 1999 have taught us. According to Bakir and Boduroglu [3] the event had great impact on the economy, society, administration and environment of Turkey.

The area most heavily damaged was the area around Itzmit, the industrial center of Turkey. "The area directly affected by the Marmara earthquake is responsible for 14% of Turkey's total value-added industrial output. The region holds only 4% of Turkey's population but generates 16% of the country's total budget revenues." [5]. There were about 120,000 damaged residential buildings beyond repair with a total of 600,000 people needing housing of which only 14,000 were insured. The rest had to rely on the government. For the government, the reconstruction costs for housing and infrastructure was significant [5]. This prompted the creation of the Turkish Catastrophe Insurance Pool (TCIP), a public sector insurance entity providing catastrophe risk insurance for Turkish homeowners.

2.2 Government Schemes – Insurance

At different levels, citizens, insurers, reinsurers, and governments carry the burden of natural catastrophe losses, and each one must do their part to minimize the losses. To simplify we can say that there are two main rules society is obliged to follow. The first one is the preservation of life and the second one is the preservation of the quality of life.

We see the role of government in both, first on the preservation of life (prevention) by setting up rules that will protect their citizens in case of disaster like construction codes and land use; but also on the preservation of the quality of life after a natural catastrophe (disaster relief) by supplying shelters, first aid, food, and support for reconstruction. And unfortunately governments cannot escape. We can not predict magnitude or location of the next event, but we know that an event of a certain magnitude is likely to occur in a specific zone with a certain frequency.

Therefore, after some major catastrophes, governments have seen that if the disaster is too big, the cost of rebuilding is too high, and it is hard for them to help their citizens in an efficient way. As a result they found a solution by creating specific insurance programs for funding losses from natural catastrophes.

As each country has different priorities and needs, there are a variety of programs. They will depend on the peril being covered, the social and political conditions, the economy, and the insurance penetration. They are intended to "limit the financial burden that earthquakes place on government budgets, ensure risk sharing among its residents, encourage a higher standard for building practices and establish long-term financial resources" [6].

The oldest one is the Switzerland Elementarschadenpool, created in 1939 to cover for damages caused by flooding, storm, hail, avalanche, snow pressure, landslide, rockslide, rock fall and earth slip, or what is know as "elemental perils". It is a pooling of private insurance companies for better distribution of the risk. This scheme allows an affordable flat premium for all policyholders, regardless of which is the risk they are most exposed to.

The Consorcio de Compensación de seguros from Spain was created in 1954 as an extension to the Consorcio de Compensación de Motín, which covered war damages. It covers losses due to earthquakes, tidal waves, floods, volcanic eruptions, cyclone storms, acts of terrorism, rebellion, insurrection, riots, civil commotion, and act or actions of the armed forces in times of peace. It is obligatory and it is included when one purchases a policy that covers damage to property or life insurance.

The Japanese Earthquake Reinsurance Company (JER) was created in 1966 to cover earthquake, tsunami and volcanic damage to residential properties. The system includes a mechanism for pooling all earthquake insurance policies, as well as an aggregate accumulation of funds for earthquake contingency reserves. It is partially funded by the government.

The National Flood Insurance Program (NFIP) form the United States was created in 1968 to cover damage caused by water (flood and its consequences), and any necessary cleaning up of property. In order to benefit from the NFIP, communities must be qualified, that is, the risk has to be assessed, area has to be mapped and risk control measures have to be designated. It is funded by the government and managed by the Federal Emergency Management Agency's Federal Insurance and Mitigation Administration.

The Icelandic Catastrophe Fund created in 1975, according to the Iceland Catastrophe Insurance Act. It automatically covers all property and contents insured against fire against direct losses resulting from earthquakes, volcanic eruptions, snow avalanches, landslides, and floods.

The Norsk Naturskadepool from Norway was created in 1980 and it covers the damages caused by floods, storms, earthquakes, avalanches, volcanic eruptions and tidal waves to personal and commercial property. It is a pooling of private insurance companies for better distribution of the risk.

The Régime d'indemnisation de Catastrophes Naturelles from France was created in 1982 after the floods of 1981 in the south of France. Mandatory insurance

guarantee (with specific premium) attached to property insurance contracts covering insured against direct damages (plus loss of profit) resulting from natural events. All compensation under the 1982 Law is subject to the declaration of the state of natural disaster by interministerial decree. It is a mixed system between the State and the private insurance.

The Florida Hurricane Catastrophe Fund (FHCF) from the United States was created in 1993 after the hurricane Andrew. It covers residential structures against windstorm damage during a hurricane. Only a hurricane declared by the National Hurricane Center can trigger payments from FHCF.

The Earthquake Commission (EQC) from New Zealand was created in 1993 as a replacement of the Earthquake and War Damage Commission of 1945. It covers homes, residential land and personal possessions against earthquakes, tsunami, landslips, volcanic eruption, hydrothermal activity, storm or flood damage and fire following any of these perils. It is reinforced with public awareness campaigns and strict code enforcements.

The California Earthquake Authority (CEA) from the United States was created in 1996 after the Northridge earthquake. It covers earthquake perils for residential personal lines. It covers only the main residence and excludes any other secondary building. It is a publicly managed, largely privately funded entity.

The Turkish Catastrophe Insurance Pool (TCIP) was created after the 1999 earthquakes. It was created by the Turkish government with the cooperation of the World Bank. It covers earthquake damage for residential buildings for all registered habitations, excluding rural areas and unauthorized construction after December 27, 1999. It has not yet passed into final legislation but a large number of people have a TCIP policy [4].

There are newer schemes as the Cat Bond issued in 2006 for the Mexican Government to finance rescue and rebuilding after an earthquake, and the Caribbean Catastrophe Risk Insurance Facility (CCRIF) launched in 2007 and developed with the help of the World Bank. It is based on the TCIP and it is a regional mutual insurance pool to provide immediate funds to Caribbean countries struck by hurricanes and other natural disasters.

By spreading the risk among the citizens, the insurance and the reinsurance industry, the financial markets, and the government, the risk can be managed. But in order to buy adequate protection, we need to understand and identify the risk we are taking and the tools the industry uses for this are the catastrophic loss estimation models, or what we know as CAT models.

2.3 Building Strength

Assessing the vulnerability of buildings is an important part of the evaluation of risk, a complex task as we need to consider the hazard and the building conditions. For a reinsurer or a government, this is a very complicated exercise. As engineers we can evaluate one building, or a group of buildings, knowing all their

inherent characteristics as the construction materials, height, location, etc. However this process still involves uncertainty in the calculation of the loss.

An insurer covers not one but many buildings, some times whole cities and whole countries and a reinsurer covers many insurers. Each contract will involve a variety of structure types, of risks types, construction years, materials, good and bad quality of construction and maintenance, and no effective way to know the detail. Besides, the portfolios are dynamic, for ever changing as policyholders modify their policy or new insureds get covered. Yet we need to know as much as possible to estimate the probable losses in order to accumulate enough reserves to pay in case of a future event, buy extra protection, and avoid bankruptcy.

After hurricane Andrew in 1992, the industry realized that the "old" way of estimating the losses was not the best way to go about it. This was done based mainly on statistical studies of past losses or the experience of the underwriter. But the problem was that there is not enough historical data and standard actuarial techniques of loss estimation were inappropriate for the evaluation of catastrophe losses. The result was that some insurance companies were bankrupt and closed, and others had their assets heavily drained. But besides creating the FHCF, this was the event that pushed the development of CAT Models.

2.4 CAT Models – Do You Want To Dance?

The difficulty one has in imagining all possible causes of an event, or the ways it can occur, often leads to an underestimation of the probability of infrequent events. We tend to imagine only a subset of all possible scenarios; we not only underestimate their probability but also tend to be overconfident in their predictions.

For catastrophic events that occur relatively infrequently, the limited historical records are only a small sample of the entire population of possible events. As we have seen, losses greater than what we expected are possible but since the industry has not experienced such an event, it is likely we are underestimating its likelihood.

A unique feature of natural catastrophe losses is the widespread nature of each event, potentially affecting a number of insured contracts. The challenge any insurer has is to evaluate the natural catastrophe exposures on an individual contract basis in order to make informed business decisions on each account, then "accumulate" all individual contracts to obtain the group accumulated liability.

Catastrophe models are tools that generate different scenarios based on geographic and historical data, and calculate the probability of potential losses. Insurers use them in two ways: to give an idea of what′s at risk and to help them evaluate the exposure following a catastrophe.

The CAT loss estimation models consist of three main parts:

- **Hazard module**
  The hazard module is the event intensity generation tool. It could be earthquakes, hurricanes, typhoons, storms or flood. It uses historical data and the latest scientific knowledge on the peril to create the event set. Since the calculation of

the losses depends on the intensity of the event, this module represents the most important part of the process. Mainly, the resulting events need to be credible, as close as possible to what could really happen.

- **Damage module**
  The damage module is the calculation of the damages to the insured property. They could be for the building, the contents and/or business interruption. A great deal of information is required to obtain reliable damage distributions.
- **Loss calculation module**
  The loss calculation module is the application of the insurance, reinsurance and the retrocession conditions, if any, to the property damages.

As expected, the whole process involves a certain degree of uncertainty that needs to be taken into account when we evaluate the resulting estimations. This uncertainty represents not only the approximation of the earthquake effects, but also the number and types of structures being analyzed and the relationship of structural response to damage.

Much could be said about the Hazard module and the Loss calculation module but I will focus on the damage module because the most interesting part for engineers is the development or creation of the vulnerability curves, the direct loss calculation.

What do we do to get the damage distribution or what we call the vulnerability curves? For insurers and reinsurers this is not an easy task. Engineers can calculate the damage but to calculate the loss we need more information, like the cost of replacement, and specially the cost of repairing the building after a mayor event. We need to know the value of replacement for the contents and the assigned value for the loss of revenue (business interruption). This may imply more costs than normally expected.

As engineers, we know how to calculate the damage for one structure but insurers and/or reinsurers have two main problems. One is the evaluation of loss for all possible events knowing that there are many ways a structure can fail, and the second is the evaluation of loss for several sites for all possible events for a region or a facility whose sites are related. Therefore, the estimation of loss requires multiple calculations that should consider all sets of characteristics for all the buildings, all sources and all locations. This represents a formidable numerical task!

Most of the time we just receive information at the CRESTA[1] level, what we call aggregate information. This means that we only have total insured values or premiums[2] by region.

Not always the information has how much of the insured values represent which line of business (LOB), that is, if the risks covered are residential, commercial,

[1]CRESTA was set up by the insurance industry in 1977 as an independent organization for the technical management of natural hazard coverage. It has established a globally uniform system for the accumulation risk control of natural hazards – particularly earthquakes, storms and floods.

[2]Premium: The sum paid by a policyholder to keep an insurance policy in force. It is not related to the actual insured values.

and/or industrial. Most of the time it is necessary to estimate how much of those insured values are for building, contents, or business interruption. For industrial facilities, we do not get details of the site installation which can have several buildings with different characteristics for different uses, like offices, warehouse, process plant, silos, pipelines, etc. thus to create reliable vulnerability curves is a little complicated.

The first generation CAT models were based on the Applied Technology Council ATC-13 damage curves, developed to estimate the earthquake damage/loss ratios for California in 1985. These were state-of-the-art back then for California and since these first models were made for California earthquake, this was not a real problem; but the difficulties began when we decided that we needed CAT models for other countries and other perils. What happened was that the results from the ATC-13 study were adapted to other countries and similar empirical methods were developed.

We had claims information, what we had paid for past events, but the same problem we have to get information on the covered risk we had it to assign the losses. It is difficult to assign a loss to aggregate information, where we do not really know where the risks are, which were their structural characteristics and condition at the time of the event, which ones were the most damaged, and what damage we were really paying, because after a catastrophic event, damage evaluation for payment may not be that accurate and some times there is none at all. It could happen that a fixed amount was paid regardless of the damage. We have also the recorded measures of the event intensity in different places, but not always where the damage was produced.

Nevertheless, the second generation models had a more engineering approach. Not only the historic losses and the ATC-13 information were used, we start asking engineers and researchers to do analysis to create new damage curves, composite or construction type only, that take into account the different construction techniques of different countries and several seismic codes. These were then calibrated with the losses we had available for different events. We created damage curves specifically by LOB, by peril, and by county which included damage curves for building, contents and business interruption, and we started to evaluate the effects of age and height in some of the models, on the ones we had more information.

These models use Mercalli intensity to estimate the damage ratio. We are now on the third generation CAT models which use peak ground acceleration and spectral acceleration to estimate the damage ratio.

It is important to keep in mind that the building losses are only a small part of the whole picture. Sometimes the losses to a company are bigger than the losses to the buildings because there is damage to the contents and there is loss of revenue while the facilities are being repaired. Sometimes there is no building damage at all but their suppliers are affected by the general disruption of the event or they've suffered damage and are unable to respond. There could be damage to life lines and the facility cannot function. There could be a large amount of human casualties or employees cannot arrive to their work places due to transportation and communication failures. In addition, we need to consider that up to a certain amount of

damage, the structure is considered a complete loss even if it is still standing, and the vulnerability curves should account for this. But once building damages have been estimated, all losses can be calculated.

Even though the models are more sophisticated, we still depend on the data we receive and the results we obtain will depend on how we can translate this information in something we can model.

2.5 Let's Dance – The TCIP

Let's look at the TCIP. Currently 30 local insurance companies sell TCIP policies in Turkey. These policies are sold when a house is sold or bought and in spite of not being formally ratified, there is a majority of newly constructed buildings that are covered by the pool. The TCIP policy only covers earthquake damage to residential buildings with a limit of 110,000 TYL (about 64,000 €) and there is a 2% deductible applied over the sums insured.

The amount of premium charged is determined by three factors:

- The earthquake CRESTA zone where the building is situated
- The construction type of the building
- The area of the building in square meters

There are five risk zones and 15 different tariff rates for each construction type (Table 2.1).

The rates are based on the Turkish Earthquake CRESTA Zone Map prepared by the Ministry of Public Works and Housing.

The determination of insured values is based on price by square meter of construction. These are determined by the Ministry of Reconstruction (Table 2.2).

Table 2.1 Tariff rates per zone and construction type

	Risk zones				
Construction type	Zone 1 ‰	Zone 2 ‰	Zone 3 ‰	Zone 4 ‰	Zone 5 ‰
Steel, reinforced concrete	2.20	1.55	0.83	0.55	0.44
Masonry	3.85	2.75	1.43	0.60	0.50
Others	5.50	3.53	1.76	0.78	0.58

Table 2.2 Insured values per construction type

Construction type	Price by square meter (TL)
Steel, reinforced concrete	450
Masonry	320
Others	170

The amount of premium is then calculated by multiplying the rate by zone, the price by square meter, and the area. Insured values will therefore be calculated by multiplying the area by the square meter unit cost.

Note that the price by square meter may not be what the building actually cost to build nor what it will cost to rebuilt but what the Ministry is setting for reimbursement in case of an event. This represents the minimum coverage for residential buildings.

The total residential buildings in Turkey has been estimated by the government to be about 16 million (2000 census) but some are not covered either because they have not yet purchased the cover or because they are excluded from the policy.

As of today, the TCIP portfolio covers 95.86% of the total insured values (Fig. 2.1.).

The zone with the most insured values is the region of Istanbul (zone 01) followed by the region of Ankara (zone 10).

The values are distributed by zone, as showed in Table 2.3.

The information also includes age and height of the building. Taking into account this, the portfolio is distributed as showed in Tables 2.4 and 2.5.

The goal of the pool is to be able to cover a 1-in-250 year event (which is the reference return period for earthquake losses for the industry, probability of non-exceedance of 99.6%), without becoming insolvent. The pool calculates then its rates based on the results of the probabilistic analysis performed with the CAT models.

In order to show the impact of the quality of construction on the results, an analysis was made with the CAT model developed by EQECAT, Worldcatenterprise® (WCe).

The first assumption was to take the cedant original data, that is, type of construction, age, and height and called this portfolio "Real". For the following analyses height and construction type were still considered but the quality of the construction was modified. One analysis considered that all of the risks were of poor quality

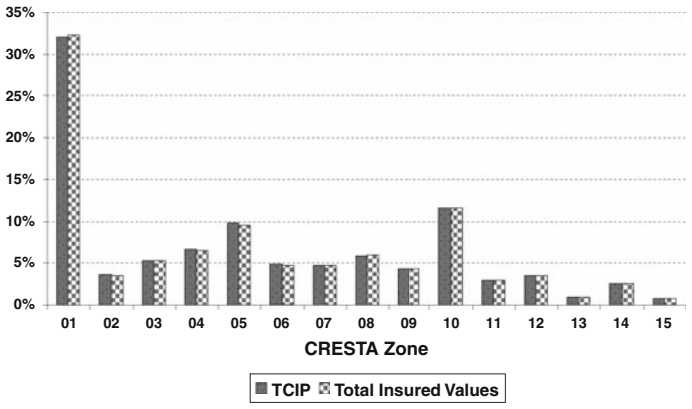

Fig. 2.1 TCIP Insured values by CRESTA Zone

Table 2.3 Construction type by CRESTA Zone

CRESTA Zone	Masonry	Reinforced concrete	Other
1	1.17%	98.68%	0.16%
2	2.64%	97.10%	0.26%
3	1.72%	97.99%	0.28%
4	1.98%	97.65%	0.36%
5	1.84%	97.88%	0.28%
6	6.60%	91.80%	1.60%
7	2.12%	97.69%	0.19%
8	2.48%	97.25%	0.28%
9	10.47%	88.15%	1.38%
10	1.98%	97.68%	0.33%
11	4.06%	94.93%	1.00%
12	4.94%	93.91%	1.15%
13	3.22%	96.08%	0.70%
14	4.55%	94.67%	0.78%
15	7.15%	91.10%	1.75%

Table 2.4 Building height distribution of portfolio

Height	Percentage
> 8 stories	16.45%
< 5 stories	48.90%
Between 5 & 7	34.65%

Table 2.5 Building age distribution of portfolio

Construction age	Percentage
1975 & Before	9.80%
1976 – 1996	40.70%
1997 – 1999	13.51%
2000 & After	35.99%

(Poor), another one considered all of good quality (Good) and a last one where the risks were considered having average quality construction (Average).

By good quality it is implied that the building complies with the seismic code requirements and thus the poor quality implies that it does not comply with code requirements or has not been correctly maintained or repaired.

The comparison was then made using the losses for the Average portfolio. The resulting ratios for building coverage only are shown in Figure 2.2.

And if we applied a 2% deductible the resulting ratios are shown in Figure 2.3.

This means that for a return period of 250 years if we have all structures constructed to code standards we will have in average about 36% less losses than if our portfolio was a mixture of good and bad structures. Subsequently, if our portfolio was formed of only poorly constructed structures, we will have in average

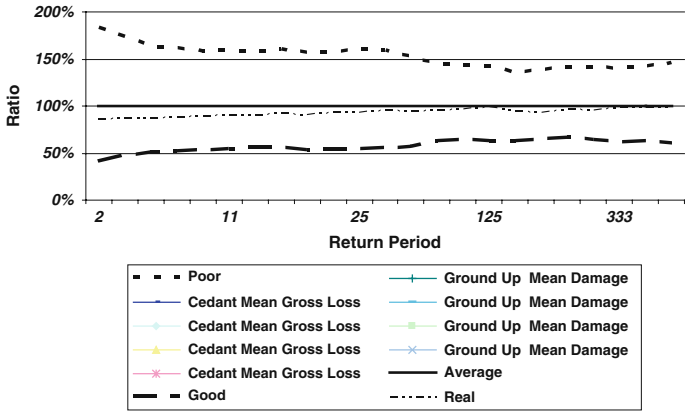

Fig. 2.2 Comparison of ground up losses

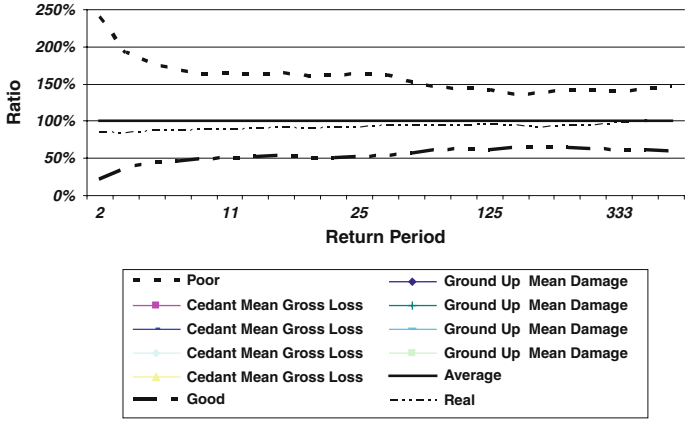

Fig. 2.3 Comparison of gross losses with 2% deductible

about 42% more losses. Usually reality is in between. The more buildings comply with code standards, the less the losses will be. More losses will require to charge a higher rate and fewer losses will reduce it.

2.6 Conclusion

The process of estimating losses after a catastrophic event is a complicated task but a necessary one to prepare for the inevitable. As Peter Bernstein put it "only the foolhardy take risks when the rules are unclear". Decisions are made on the basis of available data and CAT models provide the best estimation we have.

CAT models are sophisticated tools that use information from many sources: from the scientific community, engineers, and the insurance industry. They are dynamic tools that evolve as new knowledge becomes available, as new events happen, and new requirements are needed.

The insurance industry uses CAT models to rate catastrophe exposures, to calculate group accumulations, to estimate reserves, to help the underwriting with a more refined and detailed exposure control, to diversify the portfolio, and to standardize risk control within the market.

Governments need to prepare for the events that may disrupt the economy and the life of their citizens. These Insurance mechanisms stimulate higher standard for building practices and establish long-term financial resources. The use of CAT models allows them to evaluate more realistic schemes and estimate an insurance premium that is affordable and that adequately covers the risk. In the case of the TCIP, a better constructed structure will have less damage, therefore reducing the rate and the premium needed.

Insurance is not the only solution but it helps after a catastrophic event. One important part is the education of the citizens so they can prepare against an event and be part of the solution.

Everyone involved on the risk management chain, that is homeowners, insurance, engineers, developers, and Government officials, can promote mitigation efforts and assist recovery after an event.

Acknowledgments I will like to thank many people at SCOR but specially Mark Buker for sharing his information on the Turkish insurance market, Osman C. Gursoy from AON for sharing his ideas on how to go about presenting the insurer point of view to engineers, and to my brother Dr. Óscar Chávez for checking I was making sense.

References

1. Swiss Reinsurance Company. *Natural catastrophes and man-made disasters in 2006: low insured losses*. Sigma N° 2/2007. Economic Research and Consulting. Zurich, Switzerland. 2007
2. Swiss Reinsurance Company. *Natural catastrophes and man-made disasters in 1999: Storms and earthquakes lead to the second highest losses in insurance history*. Sigma N° 2/2000. Economic Research and Consulting. Zurich, Switzerland. 2000
3. Bakir, Pelin G, and Boduro lu, Hasan M. *Earthquake risk and hazard mitigation in Turkey*. Earthquake Spectra, Volume 18, No. 3, pages 427–447, August 2002
4. Gurenko, Eugene et al. *Earthquake insurance in Turkey: History of the Turkish catastrophe insurance pool*. The World Bank, Washington, DC, 2006
5. Cadirci, Cigdem. *Devastating earthquakes in Turkey call for set-up of a catastrophe insurance pool*. GE Frankona Re. EXPOSURE no. 6. August 2001
6. Bromley, Geoff. *Now we are in control*. Reinsurance. May 2006. http://www.guycarp.com/portal/extranet/pdf/Articles/016_RE_0506.pdf

Further Readings

Statistics Finland – *World in figures* – Tables. 5 October 2007 http://tilastokeskus.fi/tup/maanum/taulukot_en.html
The Swiss Natural Perils Pool. Consumer information. 8 August 2007. http://www.svv.ch
Consorcio de Compensación de Seguros. 8 August 2007. http://www.consorseguros.es/Index.cfm
Fujikura, Masaaki et al. Overview of Japanese earthquake insurance and its characteristics. The institute of actuaries of Japan, Catastrophic Risk Research Group. April 1999. http://www.actuaries.org/ASTIN/Colloquia/Tokyo/Mitsuishi.pdf
FEMA: The National Flood Insurance Program. 8 August 2007. www.fema.gov/business/nfip/
Kelman, Ilan. Iceland catastrophe insurance. 8 August 2007. http://www.islandvulnerability.org/iceland.html#insurance
Norsk Naturskadepool Norwegian Natural Perils Pool. 8 August 2007. http://www.naturskade.no
Les Catastrophes Naturelles en France. Caisse Centrale de Réassurance (CCR). http://www.ccr.fr/fr/pdf/catnat_2007_bd.pdf
FSBA Florida Hurricane Catastrophe Fund. 8 August 2007. http://www.sbafla.com/fhcf/legislation.asp
EQC Earthquake Commission. New Zealand. 8 August 2007. http://www.eqc.govt.nz/home.aspx
California Earthquake Authority. 8 August 2007. http://www.earthquakeauthority.com/
Bernstein, Peter L. *Against the Gods: The remarkable story of risk*, John Wiley & Sons, Inc., 1996
Woo, Gordon. *Mathematics of natural catastrophes*, Imperial College Press, 1999

Chapter 3
A Critical Review of Current Assessment Procedures

Elena Mola and Paolo Negro

Abstract The correct evaluation of seismic vulnerability of the existing building stock is a key issue for every earthquake prone Country; the need for reliable decision making tools for the assessment and retrofitting of the existing building stock is widely recognized. Still, the applicability, effectiveness, accuracy of currently codified seismic assessment procedures strongly vary, depending on the features of the assessed structures, and often also on the engineering judgement and knowledge of the applicator. Moreover, time and costs constraints, to which the assessment procedures are necessarily bound, pose further issues as to the details and immediateness of the implementation of such analyses. In the paper, a critical review of the most widespread currently codified seismic assessment procedures is carried out, with reference to the case study of a plan-wise irregular reinforced concrete (RC) frame structure which underwent extensive pseudo-dynamic testing, both in the "as-built" and in retrofitted configurations, in the framework of the activity of the ELSA Laboratory of the JRC. Some conclusions on the relative performance of such assessment procedures and their possible improvements, with reference, in particular, to the issues posed by torsion, are finally presented.

3.1 Introduction

The correct evaluation of seismic vulnerability of the existing building stock is a key issue for every earthquake prone Country, in Europe and worldwide: given the large number of existing units designed prior to the latest generation of seismic codes and given the economic and practical unfeasibility of fully demolishing and rebuilding those non-compliant with the latest seismic design requirements, the need of decision making tools on the seismic hazardousness of said stock and on rehabilitation strategies has become more and more evident.

E. Mola (✉)
Politecnico di Milano, Structural Engineering Department, Milano, Italy
e-mail: elemola@gmail.com, emola@stru.polimi.it

A. Ilki et al. (eds.), *Seismic Risk Assessment and Retrofitting*, Geotechnical, Geological, and Earthquake Engineering 10, DOI 10.1007/978-90-481-2681-1_3,

Cost- and time-effectiveness, reliability and straightforward implementation are fundamental pre-requisites of seismic assessment tools, which are meant to be applied to huge populations of buildings, by practicing engineers, usually with strict time and budget constraints; they are basically designed to be a screening tool calibrated so as to point out gross inadequacies and intolerable hazards while tolerating minor inadequacies or less-than-modern design approaches when they do not imply immediate risks to the safety of the inhabitants.

In the past decades, a number of different assessment procedures were conceived and codified in all the major codes and normative documents worldwide.

The evolution of the codification of assessment procedures, their upgrading and improvements closely followed that of the design approaches, incorporating the most recent basic concepts of capacity design, performance levels, and acceptance criteria (correlated both to the required performance and to cost-benefit considerations).

Actually, interest in performance-based earthquake engineering concepts found its initial boost in the field of seismic assessment: in fact, after the observation of damage and casualties deriving from earthquake events, it became clear that, in many cases, lack of compliance with the rules of modern seismic codes did not cause an unacceptable performance of buildings, thus not being a compelling reason to upgrade them. On the other hand, it was also evident that particular structural configurations, (for example plan- or height-wise irregularities) brought about difficult issues regarding the seismic hazard of a number of buildings. Recognizing that decision-makers and owners would rather decide to upgrade when a realistic evaluation of future performance could be given, the ATC produced the FEMA-273 [7] report, titled "NEHRP Guidelines for Seismic Rehabilitation of Buildings", in which the first attempts at developing performance-based evaluation and upgrade of building structures were made. The approach was oriented to practice, with a menu for the selection of the appropriate performance objectives for individual designs. The approach was perfected and further developed in the subsequent FEMA-356 Report, "Prestandard and Commentary for the Seismic Rehabilitation of Buildings".

The important innovation brought about by these documents was that a series of standard performance outcomes, called performance levels, were defined. In particular, three different levels were described: the collapse prevention level, the life safety level and the operational level. These performance levels were linked to different seismic excitation levels, thus making it clear that for a performance objective to be defined, the combination of a performance level and of a given seismic hazard level (i.e. a spectrum, with a probability of exceedance) needs to be given.

The FEMA-273 and FEMA-356 procedures had some drawbacks, from the point of view of a fully performance oriented approach to structural assessment. Also, as will be discussed in the following, with reference to a case study, inadequacies from the point of view of structural analysis procedures and methods were present in older drafts; for example, crucial issues like that of torsional effects were not adequately tackled, thus leaving the practicing engineer without clear guidelines on how to correctly estimate possible causes of gross misbehavior.

In Europe, a dedicated chapter of Eurocode 8 was drafted in the meantime: EC8 Part3 – "Design of structures for earthquake resistance, Part 3: Strengthening and repair of buildings". This document went through a number of revisions and subsequent improvements, reflected into the most recent and final draft (2006).

The basic concepts codified in EC8 Part 3 are those of capacity design; still, especially in older versions, the proposed assessment method was a force-based one, rather than a displacement-based, performance-oriented one.

The acceptance criteria and required verifications were expresses in terms of forces, at element level, even if a difference was made between ductile elements and non ductile ones, which had to be verified according to capacity design, i.e. for the actions developing in them when the maximum ductile resources of the elements involved in energy dissipation in the predicted failure mechanism were attained. In the most recent version of EC8 Part 3, though, the evolution towards performance-based assessment methods and the detailed implementation of analysis methods such as the nonlinear static one, as opposed to the extensive use of linear equivalent or modal analysis, clearly stood out. Also, the results of cutting edge research in the field, like those coming out of the SPEAR project's large experimental activity itself, were all incorporated into the new draft of the code, so that many issues previously left unanswered or poorly dealt with became much more clearly detailed (i.e. structural irregularity, joint detail modeling, ductility limits for hinging sections, interaction between shear and flexural actions.).

Another milestone in the development of assessment methods was achieved when the New Zealand National Society for Earthquake Engineering published the well known document named "The Assessment and improvement of the structural performance of earthquake risk buildings", which also underwent two major drafts, one in 2000 and one in 2002, where practical approaches to the assessment of existing buildings were extensively codified and became widely applied worldwide.

In this document, the practice-oriented character of the proposed assessment tools is clearly highlighted, and pursued by leaving large freedom of choice to the engineer, as to the methods to use; in fact, both a force- and a displacement-based assessment methods are codified and clearly detailed on a step-by-step basis.

In each of the two approaches to the assessment, the engineering judgment is largely appealed to, to the point, though, that no clear and fool proof guidance is given on key issues of difficult solution (such as, once again, torsional effects).

Finally, it must acknowledged that Japanese authorities were strongly interested in the development of assessment tools for their Country, which were then used in the South East at large.

In particular, the Japanese Building Disaster Prevention Association first issued a draft of the document named "Standards for seismic capacity evaluation of existing reinforced concrete buildings", as early as in 1977, which then underwent a major revision in 1990.

This document proposed a highly simplified assessment approach, based on a three-tiered evaluation procedure, meant to provide a rough screening of buildings with low computational costs at Level 1, to focus on possibly hazardous ones only at Level 2 and 3 with more refined calculations.

The enforced method was a force-based one, with demand-to capacity ratios computed at storey level and in terms of forces: possibly hazardous structural configurations and/or details were taken into account by a series of empirical "penalisation" coefficients, reducing the computed storey capacity. Also in this case, key issues such as torsional effects were only dealt with in a highly simplified way, and no quantification of additional twist-induced drifts or ductility demands on edge elements could be provided by this method. Moreover, neither a safety margin against failure could be quantified, nor could possibly dangerous local failure mechanisms be detected: these shortcomings were perceived as issues to be overcome in future reviews and updated drafts of the document.

From the very short reviews reported above (for more detailed discussions on the procedures, see [11]), it is evident that the direction in which assessment methods and provisions evolved in the recent past, also thanks to highly improved computational tools, was that of a deeper analysis of the nonlinear range of behavior of the structure, with a focus on the prediction of the failure mechanisms and the quantification of ductility demands in structural, rather than internal actions (i.e. forces). Still, the goal was to be pursued while retaining the simplicity and straightforwardness in the application, and the general practice-oriented spirit inherent to assessment of buildings, where no additional complications have to be added to the process if not strictly necessary to overcome intolerable gaps in knowledge.

In this framework, the attention and efforts dedicated to the development, codification and subsequent improvement of nonlinear static analysis as probably the most powerful assessment tool able to retain both "simplicity" and "accuracy" in results, can be fully understood.

Nonlinear static (commonly called "pushover") analysis has thus become the basic tool enforced in the "second generation" of assessment procedures, and still at present undergoing upgrading, development and improvement by constant feedback between normative bodies and practicing engineers (see the whole ATC-58 project dedicated efforts).

The advantages of pushover analysis as an assessment tool are manifold, as will be discussed in the following with reference to a case study: in fact, FEMA 356 and the NZ Guidelines, which allowed for nonlinear static analysis as an alternative to static equivalent one also in older versions, provided more detailed evaluations of the seismic behavior of the benchmark structure than the other procedures.

From pushover analyses, failure mechanisms can be predicted, based on simplified assumptions as to the nonlinear behavior of supposed plastic hinging areas, which in turn can be easily derived by basic sectional analysis concepts. Also, pushover analysis provides an expedite way to determine the so-called "target displacement" of the building under a given earthquake, thus enabling step-by-step monitoring of the behavior of all the structural elements, in terms of displacements, up to the target displacement, following the development of the failure mechanism. Acceptance criteria and ranges expressed in terms of local rotational ductility of hinges or acceptable deformation limits for contents of non-structural elements can also be taken into account. A more complete picture of the response of the structure to the seismic excitation can thus be gathered.

Still, pushover analysis remains a simplified method, resting on a number of hypothesis and assumptions, among which for example, that of a mainly first-mode-governed seismic response of the structure, rigid in-plan behavior, and structural detail designed according to the basic criteria for seismic resistance (i.e. with a relatively "modern" approach to the provisions for local ductility, such as adequate stirrups, bonding, provisions for stress transfer).

All of these aspects, and more (see for example [3, 18]), make pushover analysis a very powerful tool for screening and evaluation of relatively "regular" buildings, which nonetheless shows its limitations when peculiar structural configuration (i.e. once again plan- or height-wise irregularity) or strongly sub-standard local structural detail (i.e. smooth rebar, almost complete lack of confinement, peculiar bonding or stress transfer mechanisms at sectional level) are present. This clearly came out of the assessment exercise that will be described in the following.

3.2 The SPEAR Project: Framework, Motivation, Methods

The above reported remarks are meant as a framework to more clearly understand part of the motivations and goals of a EU-funded research project, named SPEAR (*S*eismic Performance *A*ssessment and *R*ehabilitation of Existing Reinforced Concrete Buildings) and specifically aimed at assessing and retrofitting of existing buildings, which was carried out in the past few years by a European consortium seeing the participation of the ELSA Laboratory. The activity of the project in turn, makes up the framework in which the presently reported critical review of assessment procedures was carried out. For a complete description of the SPEAR project, see [6]; for the purposes of the present paper, the description will be limited to the parts relevant to the understanding of the assessment exercise.

The SPEAR project was in fact meant to provide a critical review and improvement of current seismic assessment procedures and retrofitting design strategies, by means of a balanced mix of experimental and numerical activities; the former objective was pursued through a "blind" assessment exercise: a benchmark structure (the so-called SPEAR structure) was designed to be representative of older southern European construction prior to the latest generation of seismic codes; the structure thus exhibited a number of sub-standard details, total lacking of lateral resistance provision and plan-wise irregularities adding up to a 10% double eccentricity. The four assessment procedures reviewed above were then applied to the benchmark structure, with the aim of quantifying their relative performance, both in terms of immediateness in the application and of scatter in the results. Finally, the benchmark structure underwent a complete series of full-scale bi-directional pseudo-dynamic tests in its "as-built" configuration: by comparing the experimental data to the predictions of the assessment procedures, it was also possible to assess effectiveness of the latter in highlighting the actual weaknesses and hazards of the benchmark structure. As a final step, improvement to the current approaches were proposed, some of which were actually incorporated in the latest version of EC8 part 3.

In the following, at first a description of the SPEAR structure is provided; after that, the assessment exercise is presented: details of the application of each of the four methods are provided, together with a review of the outcomes of each of them; a short review of the experimental activity and the main experimentally derived features of the response of the mock up is then carried out. The comparative review of the experimental data and the outcomes of the assessment exercise is then carried out, highlighting the shortcomings of the procedures, with a particular focus on the torsional effects on the response.

Based on the lessons derived from the experiments and the assessment exercise, conclusions were then drawn on possible improvement of the methods and a critical review of the most recent version of EC8 Part 3 that, as previously stated, incorporated some of said amelioration is also carried out.

3.3 The SPEAR Structure

As briefly mentioned above, the SPEAR structure is a simplification of an actual three-storey building representative of old constructions in southern European Countries, such as Greece, without specific provisions for earthquake resistance. It was designed for gravity loads alone, using the concrete design code enforced in Greece between 1954 and 1995, with the construction practice and materials typical of the early 70s; the structural configuration and detailing show the lack of consideration of the basic principles of earthquake resistant design.

The materials used for the structures are also those typical of older practice: for concrete a nominal strength $fc = 25$ MPa was assumed in design; smooth rebar steel was used; given the scarcity of the current production, it was only possible to find bars with a characteristic yield strength larger than initially requested ($fy \approx 450$ MPa instead of $fy = 250$ MPa); the end hooks for the steel bars were designed following the minimum requirements of old codes.

The structure is regular in elevation: it is a three-storey building with a storey height of 3 m. The plan configuration is non symmetric in two directions (Fig. 3.1),

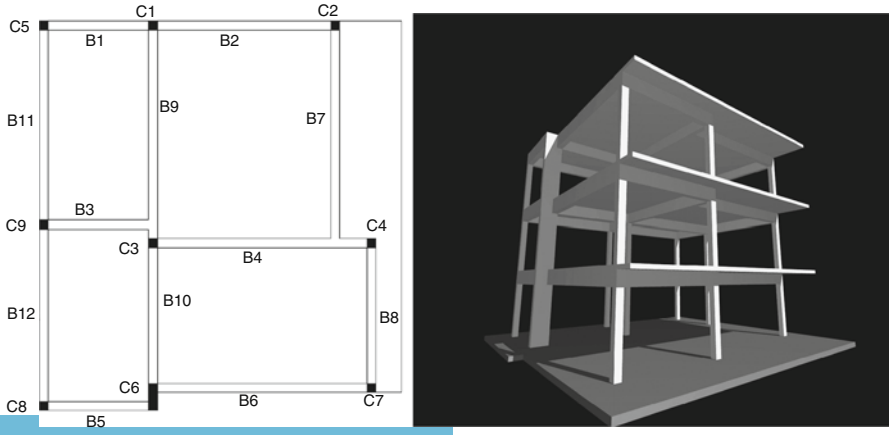

Fig. 3.1 The SPEAR structure: plan and 3D view

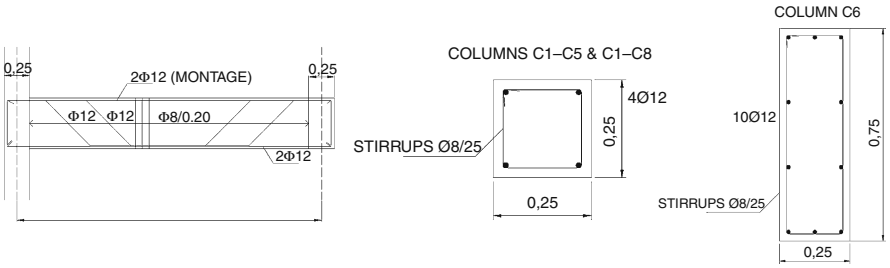

Fig. 3.2 Details of the beam and column rebars

with 2-bay frames spanning from 3 m to 6 m; the presence of a balcony on one side and of a part of the structure 1 m (in the weak direction) or 0.5 m (in the strong one) longer than the rest increases the plan irregularity, shifting the centre of stiffness away from the centre of mass.

The concrete floor slabs are 150 mm thick, with bi-directional 8 mm smooth steel rebars, at 100, 200 or 400 mm spacing.

Details of the rebar of one of the beams are shown in Fig. 3.2. Beam cross-sections are 250 mm wide and 500 mm deep. Beams are reinforced by means of 12 and 20 mm bars, both straight and bent at 45 degrees angles, as typical in older practice; 8 mm smooth steel stirrups have 200 mm spacing. The confinement provided by this arrangement is thus very low.

Eight out of the nine columns have a square 250 by 250 mm cross-section; the ninth one, column C6 in Fig. 3.1, has a cross-section of 250 by 750 mm, which makes it much stiffer and stronger than the others along the Y direction, as defined in Fig. 3.3, which is the strong direction for the whole structure.

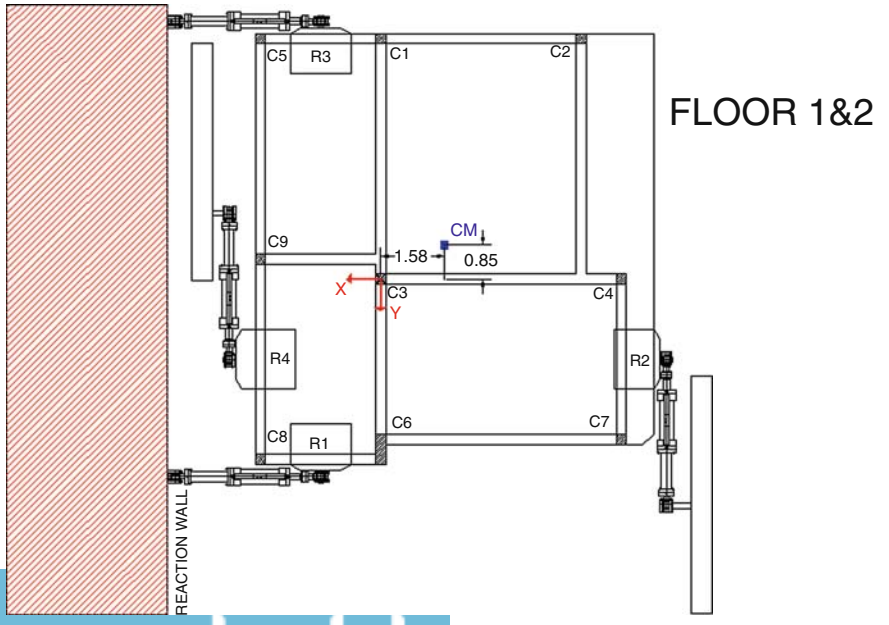

Fig. 3.3 Location of the CM of the structure

As can be seen in Fig. 3.2, all columns have longitudinal reinforcement provided by 12 mm bars (4 in the corners of the square columns, 10 along the perimeter of the rectangular one). Columns' longitudinal bars are lap-spliced over 400 mm at floor level. Column stirrups are 8 mm with a spacing of 250 mm, the same as the column width, meaning that the confinement effect is almost non-existent.

The joints of the structure are one of its weakest points: neither beam nor column stirrups continue into them, so that no confinement at all is provided. Moreover, some of the beams directly intersect other beams, so that beam-to-beam joints without the support of columns originate.

Design gravity loads are 0.5 kN/m^2 for additional dead load and 2 kN/m^2 for live load.

As described above, the structure is regular in elevation and has the same reinforcement in the beams and columns of each storey. The resisting elements in both directions are all of the same kind (frames). All of these features mean that the structure belongs to a special class of multi-storey buildings, the so-called regularly asymmetric multi-story structures, in the sense that the centre of mass (CM), the centre of stiffness (CR) and the centre of strength (CP) of each storey are located along three vertical lines separated by the distances e_r and e_s.

The centre of stiffness (based on column secant-to-yield stiffness) is eccentric with respect to the mass centre by 1.3 m in the X direction (~13% of plan dimension) and by 1.0 m in the Y direction (~9.5% of plan dimension).

The reference system used in the PsD test and the location of the CM of the structure at the first and second floor are shown in Fig. 3.3. The origin of the reference system is in the centreline of column C3. The coordinates of the CM of the first two storeys with respect to this reference system are (–1.58 m, –0.85 m); at the third storey the coordinates of the CM vary slightly, becoming (–1.65 m, –0.94 m).

3.4 Assessment Exercise: Introductory Remarks

The four procedures that were considered in the original review and assessment exercise were:

- Federal Emergency Management Agency (FEMA), **FEMA 356 Report-** "Prestandard and commentary for the seismic rehabilitation of buildings", 2000, [8]
- **New Zealand** National Society for Earthquake Engineering (2002) "The Assessment and improvement of the structural performance of earthquake risk buildings", Draft 06 May 2002, [16]
- **Eurocode 8 (2001)**: "Design of structures for earthquake resistance, **Part 3**: Strengthening and repair of buildings", Doc CEN/TC250/SC8/N293, Draft No 1, [4]
- **Japan** Building Disaster Prevention Association:, "Standards for seismic capacity evaluation of existing reinforced concrete buildings", 1977 revised 1990 (in Japanese), [10]

Each of them was applied following rules, analysis methods and computational approaches as suggested by the documents themselves, in the way a practicing engineer would apply them. One of the objects of the activity was in fact to state how straightforward and "fool proof" the application of each method would be.

In the following, a summary is given of the prescriptions of each procedure for the evaluation of the seismic response of an existing reinforced concrete 3D structure with doubly bi-eccentric plan configuration, the SPEAR structure.

3.4.1 Prescriptions and Methods

3.4.1.1 FEMA 356

The FEMA 356 indications led to implement a numerical model of the structure into a commercial software, SAP2000 NL, [2]; given the plan-wise irregularity of the specimen, the structure was modeled as a 3D assembly of elements, for which the hypothesis of rigid storey diaphragms was adopted (as suggested in the document, [8]). The structural "frame" element in SAP2000 NL, [2], uses a general, three-dimensional, beam-column formulation, which includes the effects of bi axial bending, torsion, axial de formation, and bi axial shear deformations.

Each storey had a joint representing the CM at each floor and the floor masses, both translational and rotational, were lumped there; in this case, in fact, torsional coupling effects were expected.

The initial flexural stiffness of both beams and column was reduced to take into account the non-linearity of behavior in the computation of the modes of vibration of the structures, because an explicit indication on the issue was given in EC8 whereas no explicit rule was given in FEMA 356, following [15].

The non-linear pushover analysis (aimed, as discussed above, to the determination of the target displacement) required modeling of the non-linear behavior, which was made by means of lumped plastic hinges at the ends of both columns and beams. The values of initial elastic stiffness given to the hinges were the same as those of the corresponding columns or beams, the yield moment was calculated based on the actual materials strengths, and then the yield rotation was determined.

The load patterns for the pushover analyses of the SPEAR structure were a load pattern corresponding to the first natural mode of the structure and a pattern corresponding to the uniform distribution of lateral forces.

3.4.1.2 New Zealand Assessment Guidelines (2000 and 2002)

Also in this case both the force-based approach and the displacement-based were adopted. As for the regular structure, also in this case, the target displacement, which must be determined both for the displacement-based and the force-based procedure, was derived from pushover analysis.

The model for pushover analysis was implemented in SAP2000 NL, [2]; it is the same as for FEMA, as for the rotational capacity of the flexural hinges, but the procedure gives also formulations to take into account shear effects, which are not present in FEMA 356.

For this reason the model referred to as FEMA-NZ in the following pictures is the one implemented with the FEMA indications on the ranges of rotation for the hinges and the New Zealand formulations for shear capacity, found also in [17].

The same remarks about the two approaches as for the flat-slab building are valid for the irregular structure. The issue of plan irregularity is taken into account in the pushover curve used to determine the maximum displacement in the force-based approach; in this case, in fact, one derives the curve from a 3D analytical model which includes eccentricity (ies), reproducing the plan-wise asymmetric configuration. As for the displacement-based approach, where the displacement is derived from hypotheses on the failure mechanism that are conceived for regular structures, it is explicitly advised to take into account the additional displacements caused by torsion.

3.4.1.3 Japanese Guidelines

The Japanese Guidelines do not require the implementation of any computer model (see [10]). All three tiers of the procedure were performed on the torsionally unbalanced building too.

The structural modification factor, made up of a number of different coefficients that in the account for irregularity by reducing the capacity of the structure, in the case of the SPEAR structure was made up of coefficients with values ranging from 0.9 to 0.8 because of the presence of plan irregularities.

In particular, the structure was assumed to have a complex irregular shape (not belonging to the L-, T-, or U-shape category), thus earning a first reduction factor of 0.8, decreased by a further coefficient of 0.9 depending on the relatively low ratio between the dimension of the narrowest part of the structure and its global dimension.

The storey shear capacity and the storey shear demand were computed by means of the approximate formulations given by the procedure.

3.4.1.4 EC8 Part 3 (Draft 2001)

The indications of EC8 Part 3 led to the development of an equivalent linear analysis (with the same finite element model developed for the FEMA procedure, [2]) to check the compliance of the structure with the criteria stated by EC8.

For the SPEAR structure the plan irregularity and its effects on the structural response were dealt with according to the indications of EC8. In particular, the structure did not fully comply with the criteria for regularity in plan because for the X direction of analysis the criterion $e_{0y} \leq 0.30 r_y$ (where e_{0y} is the distance between the centre of lateral stiffness and the centre of mass, in projection on the direction perpendicular to the considered X direction and r_y is the square root of the ratio between torsional stiffness and translational stiffness in the X direction) was

not satisfied; in calculating the position of the CR the approximation suggested by the relevant clause of the Code were followed, assuming it to be the centrum of the moments of inertia of the columns.

Even though the structure does not comply with the plan regularity criteria, it falls into the category of structures for which a simplified approximate analysis can be performed, in virtue of the limited height, of the relative rigidity of the floor diaphragms, and of the regularity in elevation.

For this reason the model enforced was a 3D one, but, as in the case of the regular structure, no rotational masses were assigned to the joints and the effects of torsion were considered separately for the two main directions and the worst between these effects were finally added to the internal actions derived from the static loads and from the linear equivalent analysis under an inverted triangular lateral load distribution.

In the case of EC8, the most noticeable issue was the one regarding the assumption of a behaviour factor for the structure, on which the reduction of the modal analysis depends. In fact, if in the case of the regular building the assumption of a ductility class "L" appeared more than justifiable, more problems arose for the SPEAR structure, as it was designed for gravity loads only, with no specific checks for local or global ductility so that a ductility class "L" was assigned as a trial.

In the document it is not clearly stated how to assume a behaviour factor for this particular kind of structures, because the procedure is mainly based on reducing the assessment of existing buildings to the design rules conceived for new buildings, which is not quite an effective approach to the problem; in fact it was impossible to take into account correctly the double feature of this structure, which did not comply with the prescriptions of the Code and therefore lacked a coherent design of lateral load-resisting systems but at the same time is a "frame structure" and an

Table 3.1 Summary of prescriptions and assumptions for the assessment of the SPEAR structure

FEMA 356	NEW ZEALAND		EC8	JAPAN
Pushover Analysis	Pushover Analysis	Substitute Structure Method	Equivalent linear analysis	Simplified calculations
❖3-D assembly of elements ❖Translational and rotational masses lumped at each storey CM joint ❖Reduced initial flexural stiffness ❖Lumped plastic hinges at the ends (flexural) ❖First mode distribution ❖Uniform distribution of lateral forces	❖Same as FEMA including shear hinges	❖Storey sway potential index ❖Likely failure mechanism and equivalent damping ❖Effective stiffness and period ❖Damped displacement spectrum ❖Torsional effects (?)	❖Base shear coefficient and lateral distribution from EC8 ❖Ductility class "L" (?) ❖q_0 factor (?) ❖Plan irregularity dealt with according to EC8 ❖Simplified approximate analysis of torsional effects	❖Reduced structural modification factor (complex plan irregularity) ❖Approximate formulations given for storey shear capacity and storey shear demand

"existing structure", which means that less strict criteria should be adopted for its verification, to take into account the shorter expected remaining life of the building and the higher costs of a retrofitting intervention in comparison to the cost of a new building.

The basic assumptions for the implementation of the different procedures are presented in Table 3.1.

3.4.2 Implementation and Outcomes

The outcomes of the FEMA and New Zealand guidelines are reported together because they are both displacement-based methods, requiring the implementation of pushover models with very similar features.

The EC8 and Japanese Guidelines methods are also discussed together because they are both force-based methods, whose results are given in terms of demand-to-capacity ratios.

3.4.2.1 FEMA and New Zealand Outcomes

In Fig. 3.4, the pushover curves of the FEMA model are represented. Given the structural irregularity, it must be now reminded that two different curves are to be considered for the two main structural directions (X and Y), and that the positive orientation (i.e. load applied in the +X or +Y orientation) differs from the negative one (i.e. load applied in the –X or –Y orientation).

In Fig. 3.4a, the curves for two lateral load patterns and the two principal directions (positive orientation) are reported: the yellow plot refers to the load pattern distribution according to the first mode of vibration (determined by simplified static equivalent analysis), the cyan line to the pushover with uniform acceleration pattern along the Y (strong) direction and the violet line to the pushover along the X (weak) direction. The same plots are reported in Fig. 3.4b, with reference to negative loading (i.e. loads applied with the same patterns and along the same axes but in the opposite orientation).

The hinges rotational properties were modeled according to FEMA 356 prescriptions. The curves are intersected with the EC8 spectrum scaled to 0.25 g PGA (blue

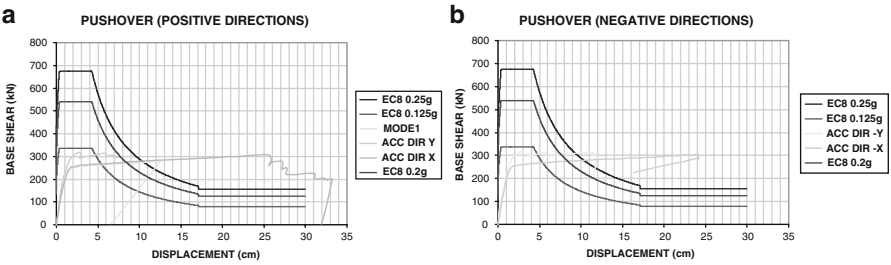

Fig. 3.4 FEMA model pushover

plot), 0.20 g (red plot) and 0.125 g PGA (magenta plot), in order to determine the target displacement at the CM.

From the pictures, it can be observed that the structure exhibits an unsymmetrical behaviour, which leads to different results for the positive and negative X and Y directions, depending on the relative importance of the torsional component of the response with respect to the flexural. The strong direction (±Y) has slightly larger stiffness, due to the presence of the rectangular strong column, and the behaviour in this direction exhibits smaller global displacement. These remarks are valid for the FEMA-NZ model too.

The predicted target displacements are above 55 mm for the 0.15 g spectrum and about 94 mm for the 0.25 g spectrum (in the X positive and negative direction), and of about 50 mm and 85 mm in the Y positive and negative direction.

It can be observed that the intersection with 0.25 g spectrum is not reached by the capacity curve for the acceleration in the positive Y direction, which confirms the scarce ductility of the building in this direction. The New Zealand force-based procedure allows for three different ways to perform the ductility checks for the structure, with an increasing level of difficulty.

The displacement-based approach uses the pushover curve too, but it requires some preliminary steps, such as the calculation of the storey sway potential index, to define the most probable failure mechanism. The sway potential index was above unity for the three storeys in both directions, thus indicating the large probability of column failure that also all the other procedures detected.

It was possible to create the equivalent damped displacement spectrum, following the formulation suggested in the Guidelines, [8], and in [17]; the resulting equivalent damping spectrum has the shape represented in Fig. 3.5: apart for some nonlinearity in the initial part, for very short periods, the curves are quite well represented by straight lines, with displacements linearly increasing with the periods. Since, in reality, such relationship cannot hold true for very long periods, a cut-off at 2 s is suggested and adopted.

To enter the spectrum so derived, it is finally necessary to know the effective period of the structure, which can be determined once the effective stiffness is known. The stiffness was derived from the capacity curve yielded by pushover analysis; from this, the effective period is computed and, with this value, the spectrum plot is intersected and the target displacement is determined.

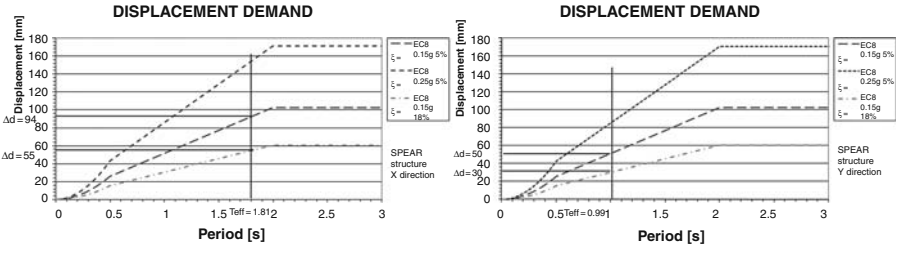

Fig. 3.5 NZ displacement based procedure; demand in X and Y direction

The New Zealand displacement-based procedure confirmed the different behavior of the structure in the two directions; in Fig. 3.5 the capacity side of the application of the procedure is shown. In this case, the only difference with the flat-slab building is that the procedure has to be carried out for both main structural directions, given the plan irregularity of the specimen.

The procedure yielded a response of incompliance for the 0.25 PGA excitation in the Y direction, with a demand to capacity ratio of about 1.28; for the same excitation in the X direction, on the contrary, a positive response came out, as the bare demand-to-capacity (DTC) ratio was of about 0.77.

This result, which could be to a certain extent anticipated, since the displacement-based approach is less conservative than the force-based one, was obtained without taking into account the torsional effects that, as could be learnt from the other procedures, are more relevant in the weak direction.

A drawback of the procedure is the lack of a clearly specified means to account for torsional effects and leads to considering the structure incompliant for the 0.25 PGA excitation because a DTC of about 0.8; when increased to account for torsional effects is too likely to become greater than unity to consider the structure safe. The X direction yielded a result of compliance for the 0.15 g excitation, with a DTC of about 0.5 and, for this excitation, also in the Y direction the evaluation was positive, but with a DTC of about 0.7.

In Figs. 3.6, 3.7, the failure mechanisms coming out of the pushover analyses at the target displacement (as determined above), are reported. The ductility checks are, also in this case, coming out directly of the software: the same color legend as for the regular structure, reported in Table 3.2 for the sake of clarity, defines the level of rotation in each hinge, according to the FEMA performance level classification, used in the implementation. As can be observed from Figs. 3.6, 3.7, the Y direction pushover shows that the central column, (C3), reaches its ultimate curvature first, due to larger axial load, whereas the other columns show a quite uniform and more limited rotation pattern. This is an effect of the presence of the strong column, which spreads the developing hinges all over the three floors.

On the contrary, the X direction corresponds to a more dangerous rotation pattern, developing a mechanism involving above all the first floor columns, thus originating a “soft-storey” mechanism leading to large displacements. The plastic hinges form in the columns, resulting into a weak column-strong beam failure mechanism, which does not comply with the basic seismic capacity design rule enforcing the strong column-weak beam as the fundamental prerequisite for seismically safe structures, [11].

The failure mechanisms derived from the pushover analyses for the SPEAR structure for the Y direction show a smaller ductility and a quite marked descent in the final part, which is produced by the presence of the strong column. The influence of this strong column is clearly proven by the formation of plastic hinges in it only at its base, and only after reducing the development of plastic hinges in the weaker columns during the Y direction pushover. This shows that the final effect of this element might be beneficial. On the contrary, the predictions for the weak direction, in which the difference in capacity and stiffness of the strong column

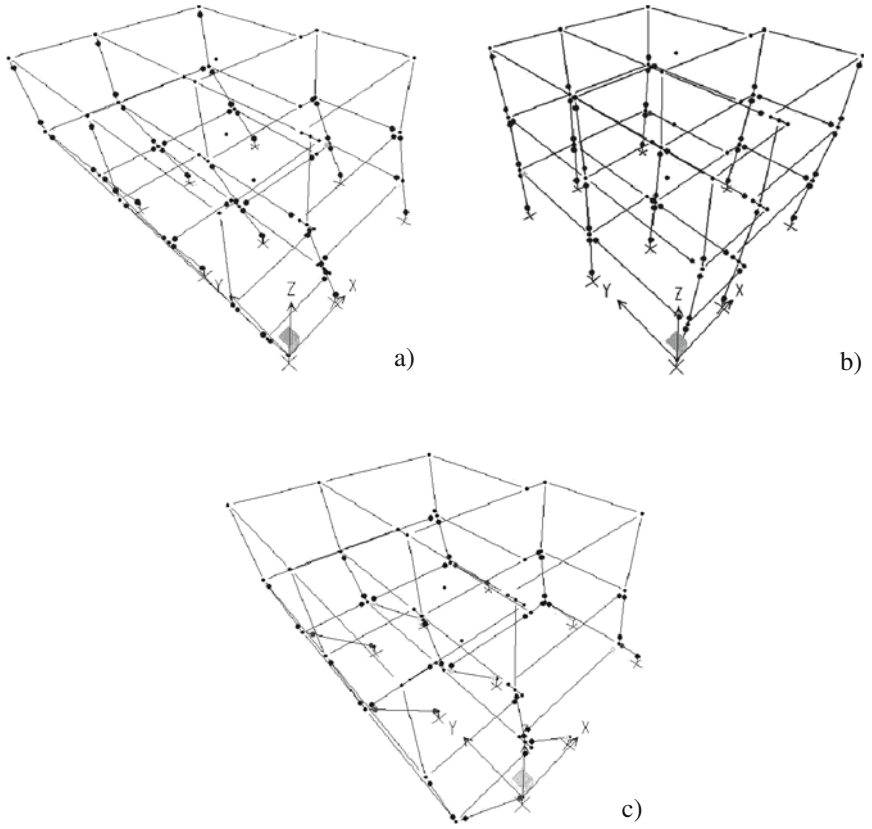

Fig. 3.6 Pushover mechanisms: (**a**) Mode 1 load pattern, (**b**) Acceleration +X load pattern, (**c**) acceleration +Y load pattern

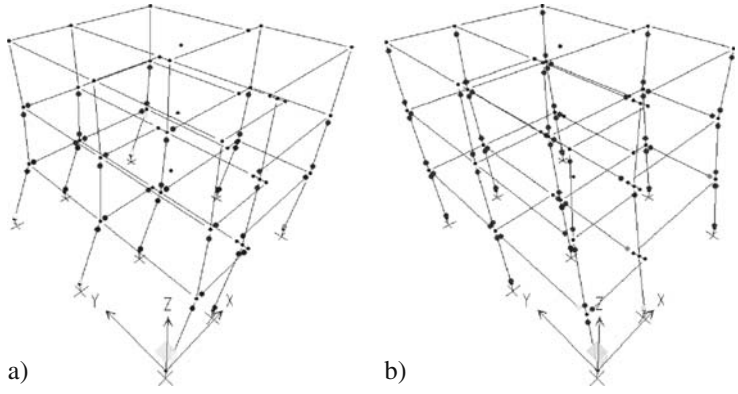

Fig. 3.7 Pushover mechanisms: (**a**) Acceleration –X and (**b**) Acceleration –Y

Table 3.2 Color legend for hinge rotation ranges in pushover analysis

○	YIELDING	○	COLLAPSE
●	IMMEDIATE OCCUPANCY	●	COLLAPSE (REDUCED
○	LIFE SAFETY	●	COLLAPSE (FINAL POINT)
○	COLLAPSE PREVENTION		

with respect to the others is less relevant, led to predict larger rotations, particularly concentrated in the first floor columns, thus leading to larger displacements.

3.4.2.2 Japanese Guidelines and EC8 Procedures Outcomes

The outcomes of the Japanese procedure for the SPEAR structure, being based on force and sectional capacity considerations, led to predict the formation of column hinges in all columns, except for the strong one, in both directions.

The outcomesof the Japanese procedure for the main SPEAR structure are summarized in Table 3.3. In the Table, V_{stor1}, V_{stor2}, V_{stor3} are the storey shear capacities (for each storey) computed according to Level 1 or Level 2 or Level 3 assessment prescriptions, whereas V_i represent the storey shear demand on the storey, computed according to the i_{th} level prescriptions. The comparison was done, and is reported, for different PGA levels, for the three storeys and the two main directions, X and Y.

The outcome was negative at all levels for a PGA value of the spectrum of 0.25 g, as it could easily be anticipated from the results obtained by the pushover analyses

Table 3.3 Outcomes of the Japanese Guidelines assessment procedure

JAPANESE GUIDELINES			Torsionally unbalanced structure		
			EC8 SPECTRUM TYPE 1 PGA=0.25g		
			STOREY 1	STOREY 2	STOREY 3
	LEVEL 1	X DIRECTION	Vstor1/ V1= 556.87/1788.05=0.31	Vstor2/ V2= 556.87/1484.8=0.375	Vstor3/ V3= 556.87/1282.4=0.434
		Y DIRECTION	Vstor1/ V1= 556.87/1788.05=0.31	Vstor2/ V2= 556.87/1484.8=0.375	Vstor3/ V3= 556.87/1282.4=0.434
	LEVEL 2	X DIRECTION	Vstor1/ V1= 698.421/1341.04=0.52	Vstor2/ V2= 582.54/1113.6=0.523	Vstor3/ V3= 473.83/961.80=0.493
		Y DIRECTION	Vstor1/ V1= 889.97/1341.04=0.665	Vstor2/ V2= 695.46/1113.66=0.625	Vstor3/ V3= 685.59/961.80=0.71
	LEVEL 3	X DIRECTION	Vstor1/ V1= 598.646/1149.5=0.52	Vstor2/ V2= 622.11/954.569=0.65	Vstor3/ V3= 438.242/566.77=0.77
		Y DIRECTION	Vstor1/ V1= 677.235/1149.5=0.59	Vstor2/ V2= 616.45/954.569=0.65	Vstor3/ V3= 520.021/566.77=0.91
			EC8 SPECTRUM TYPE 1 PGA=0.15g		
			STOREY 1	STOREY 2	STOREY 3
	LEVEL 1	X DIRECTION	Vstor1/ V1= 556.875/894.02=0.62	Vstor2/ V2= 556.875/742.442=0.75	Vstor3/ V3= 556.87/641.20=0.868
		Y DIRECTION	Vstor1/ V1= 556.875/894.02=0.62	Vstor2/ V2= 556.875/742.442=0.75	Vstor3/ V3= 556.87/641.20=0.868
	LEVEL 2	X DIRECTION	Vstor1/ V1= 698.421/670.52=1.04	Vstor2/ V2= 582.54/556.320=1.046	Vstor3/ V3= 473.83/480.90=0.968
		Y DIRECTION	Vstor1/ V1= 889.972/670.52=1.33	Vstor2/ V2= 695.466/556.320=1.25	Vstor3/ V3= 685.589/480.90=1.42
	LEVEL 3	X DIRECTION	Vstor1/ V1= 598.646/574.73=1.04	Vstor2/ V2= 622.11/477.2845=1.30	Vstor3/ V3= 438.24/283.387=1.54
		Y DIRECTION	Vstor1/ V1= 677.235/574.73=1.18	Vstor2/ V2= 616.45/477.2845=1.30	Vstor3/ V3= 520.021/283.38=1.82

performed for the other procedures; on the other hand, for a PGA value of 0.125 g the response was negative both at Level 1 and at Level 2, and only at Level 3 could a positive evaluation come out. In particular, even if the procedure is exclusively a force based one, therefore lacking the ability to properly highlight local ductility problems, it was able to draw the attention on the formation of plastic hinges almost exclusively in columns.

As for the EC8 procedure, the outcomes are reported in Table 3.4. In this case, the capacity-to-demand ratios (MR/MD) for structural members are given: MD represents the flexural moment derived from numerical analysis (i.e. the demand side), whereas MR represents the flexural moment capacity of the member computed according to EC8 prescriptions; this is reported for the two main directions (X and Y) and the three storeys. It can be observed in Table 3.4 that a large number of members (columns) for which said ratios are less than unity were found (implying tat the demand is larger than the capacity), even for a PGA value of 0.125 g; in particular, the procedure could find out that, in an equivalent elastic analysis, in the stiffer direction (Y) the structure behaves in a less satisfactory way (ductility-wise) than in the soft direction (X).

Table 3.4 Outcomes of the EC8 Part 3 (2001) assessment procedure

EC8 Part 3	*Torsionally unbalanced structure*		
	EC8 SPECTRUM TYPE 1 PGA=0.15g		
	FLEXURAL CAPACITIES		
	Columns		
	Column 1 M_R/M_D=36.59/110.84=0.70 (X) M_R/M_D=36.59/54.00=1.44 (Y)	**Column 1 2P** M_R/M_D=29.12/97.74=0.63 (X) M_R/M_D=29.12/46.52=1.33 (Y)	**Column 1 3P** M_R/M_D=23.13/57.99=0.85 (X) M_R/M_D=23.13/32.67=1.51 (Y)
	Column 2 M_R/M_D=30.18/99.84=0.65 (X) M_R/M_D=30.18/82.40=0.78 (Y)	**Column 2 2P** M_R/M_D=25.73/75.49=0.73 (X) M_R/M_D=25.73/56.85=0.96 (Y)	**Column 2 3P** M_R/M_D=20.61/45.52=0.96 (X) M_R/M_D=20.61/39.98=1.09 (Y)
	Column 3 M_R/M_D=52.61/73.52=1.53 (X) M_R/M_D=52.61/66.03=1.70 (Y)	**Column 3 2P** M_R/M_D=43.25/64.01 =1.44 (X) M_R/M_D=43.25/68.78 =1.34 (Y)	**Column 3 3P** M_R/M_D=30.70/39.05=1.68 (X) M_R/M_D=30.70/46.36=1.41 (Y)
	Column 4 M_R/M_D=36.59/69.92=1.12 (X) M_R/M_D=36.59/98.54=0.79 (Y)	**Column 4 2P** M_R/M_D=29.12/57.66=1.08 (X) M_R/M_D=29.12/77.11=0.80(Y)	**Column 4 3P** M_R/M_D=23.13/36.33=1.36 (X) M_R/M_D=23.13/50.27=0.98(Y)
	Column 5 M_R/M_D=26.69/103.19=0.55 (X) M_R/M_D=26.69/34.97=1.63 (Y)	**Column 5 2P** M_R/M_D=21.35/81.63=0.56 (X) M_R/M_D=21.35/37.06=1.23 (Y)	**Column 5 3P** M_R/M_D=18.22/46.84=0.83 (X) M_R/M_D=18.22/27.20=1.43 (Y)
	Column 6 M_R/M_D=188.4/128.02=3.14 (X) M_R/M_D=188.4/790.99=0.51 (Y)	**Column 6 2P** M_R/M_D=150.00/97.74=3.27 (X) M_R/M_D=150.00/262.81=1.21 (Y)	**Column 6 3P** M_R/M_D=147.7/57.99=5.43 (X) M_R/M_D=147.7/125.64=2.50(Y)
	Column 7 M_R/M_D=27.54/49.88=1.17 (X) M_R/M_D=27.54/95.20=0.62 (Y)	**Column 7 2P** M_R/M_D=23.21/41.67=1.19 (X) M_R/M_D=23.21/70.63=0.70 (Y)	**Column 7 3P** M_R/M_D=19.58/39.05.=1.07 (X) M_R/M_D=19.58/45.95.=0.91 (Y)
	Column 8 M_R/M_D=23.65/50.63=0.99 (X) M_R/M_D=23.65/33.78=1.49 (Y)	**Column 8 2P** M_R/M_D=20.77/44.58=0.99 (X) M_R/M_D=20.77/35.08=1.26 (Y)	**Column 9 3P** M_R/M_D=17.90/27.32=1.4 (X) M_R/M_D=17.90/24.90=1.53 (Y)
	Column 9 M_R/M_D=31.53/71.72=0.94 (X) M_R/M_D=31.53/40.93=1.64 (Y)	**Column 9 2P** M_R/M_D=26.69/59.22=0.96 (X) M_R/M_D=26.69/49.49=1.15 (Y)	**Column 9 3P** M_R/M_D=21.10/35.65=1.26 (X) M_R/M_D=21.10/34.51=1.30 (Y)
	Beams (the most challenged for each floor)		
	Beam 1 (C6-C3 FLOOR 1) M_R/M_D=116/245.83=1.01	**Beam 2 (C6-C3 FLOOR 2)** M_R/M_D=116/263.35=0.94	**Beam 3 (C6-C3 FLOOR 3)** M_R/M_D=116/107.99=2.29

Moreover, the procedure predicted very large flexural actions in the strong column, especially at the first storey; the same results were not derived by the Japanese procedure, which is based on a global storey capacity evaluation. It can be concluded that the approximate analysis by EC8 is less adequate, because the structural behavior is far from being linear and because of the uncertainties on the behavior factor to be assumed, but it was able to predict some important features of the structural response.

Apart from the obvious differences due to the different conceptual perspective of the procedures (some of them are force-based, some are displacement-based, some of them are prescriptive, some attempt a performance-oriented assessment), the focus of the present work is also on the different approach to plan-wise irregularity, within eccentricity values such as those exhibited by the SPEAR structure. In the SPEAR specimen, as was previously mentioned, the eccentricity values in both the main directions are limited to within 10% of the plan dimensions and, for this reason, they are often disregarded or dismissed as "minor" by current assessment approaches.

Whether it is correct to assume that the interaction between the two eccentricities will not adversely affect the response or induce unpredicted higher mode effects, even though, taken separately, the eccentricity values involved are minor, is questionable. In the light of the experimental response more light can be drawn on the matter.

In this framework, it must be said that the procedure that allows more freedom in the investigation of the effects of plan-wise irregularity is probably the NZ one. At the same time, though, it does not give, in the writer's opinion, sufficient guidelines for the practicing engineer to implement a procedure, however simplified, to reliably quantify possible interaction effects.

At this regard, FEMA 356 is more accurate, even if the basic assumption of independence between the torsional effects in the two main structural directions is made. The FEMA procedure has the obvious advantage of explicitly defined performance levels, and corresponding ground motion excitation levels.

The performance-oriented framework that informs the procedure is also very well detailed as for implementation rules: this is an advantage, considering the target users for whom the document is conceived. Practicing engineers need to have a reliable tool to employ for cost- and time- effective assessment: FEMA provides a good balance between expedite application and ability to draw the attention of the evaluator on possible problems of the analyzed structure. This is obtained through an approach that extensively turns to nonlinear static analysis, which proves good in detecting atypical failure modes or concentrations of inelastic deformations, thus screening out problematic structures from the ones that do not exhibit particularly concerning features and are thus easily dealt with. Of course, the limitations of nonlinear static analysis come out, especially when torsion is involved, as will be further discussed in the following Chapter, but attempt are made at giving tools to incorporate irregularity into NSA with reasonable adjustments; in particular, the amplification of the target displacement by means of a displacement multiplier depending on the ratio between the average and the maximum displacement id suggested, in the

cases where the eccentricities are small enough for two 2D analyses to be run in the two main structural directions.

Along the same lines, the EC8 approach states that the values of eccentricities are small enough for two separate 2D static equivalent analyses can be performed. The code explicitly states that pushover analysis can significantly underestimate deformations at the stiff edge of a torsionally flexible structure or when the second mode is predominantly torsional: for such structures, it is said that edge displacements must be increased, but no specific criteria to do that are suggested: the use of an amplification factor based on the results of elastic multi-modal analysis of a spatial model is deemed suitable to overcome the underestimation.

As for the Japanese Guidelines, they enforce the most straightforward way to take into account torsional effects, but also the most simplified one.

Actually, the difference between a mostly force based and a mostly displacement based approach remain in the fact that the latter allows a more detailed assessment of the structural performance, and a more confident measure of the distance between the performance point and the point of failure (i.e. the structural safety), quantified in terns of immediate applicative meaning, such as drifts, rotation, top displacements. The notion put forward in the New Zealand's Guidelines is the one of a larger freedom for the designer or evaluator in dealing with torsional effects and evaluating their influence on the response.

In fact, different procedures are proposed and allowed, with different refinement and a range of computational costs: a rapid evaluation procedure can be used, when no major causes of concern are deemed to exist in the structure, together with a displacement-based procedure and a force-based one.

Both of them are detailed, as for their implementation and the compliance criteria: still, they lack a fool-proof approach to the quantification of torsional effects; in the force-based method, though, for roughly estimate twist-induced additional drifts at the edges are proposed. The idea that the stiff edge, even though, it displaces less, can become the critical one in terms of ductility demands, according to most of the findings revised in the Preamble (and Part A of the Appendix), is also clearly stressed.

The notion of failure mechanisms and is central in the approach of the NZ Guidelines and a range of tools for rough but reliable estimations of the associated displacements and drifts are suggested, even if much is left to sound engineering judgment of the applicator as for the choice of the methods and the eye for hot issues and possible weaknesses of the analyzed structural systems.

3.4.3 Comparison between the Experimental Results and the Assessment Outcomes

3.4.3.1 Maximum Displacements

In Fig. 3.8, the CM drifts are plotted (Y direction drift against X direction one) together with the boundaries of target displacements that were derived from the

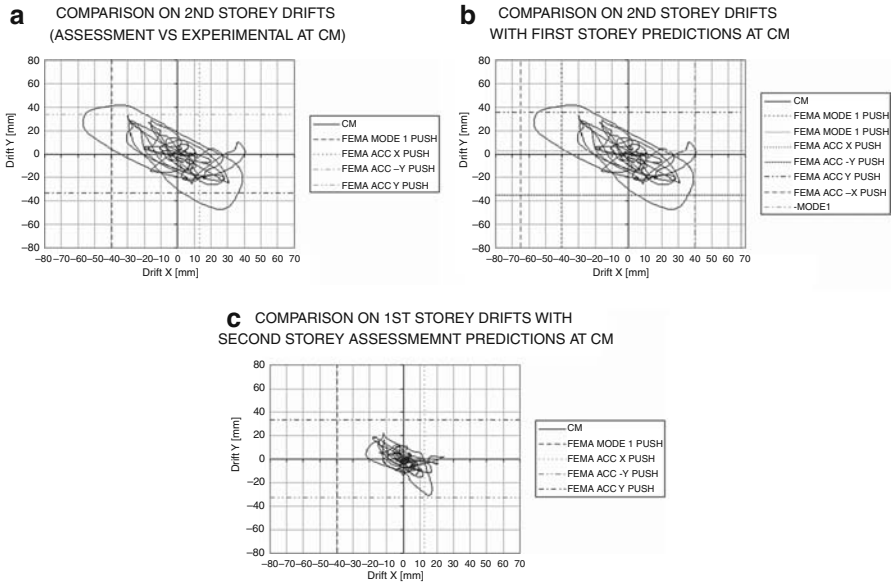

Fig. 3.8 First and second storey drifts at CM compared to the target displacements from the FEMA procedure

FEMA and FEMA-NZ model pushover in terms of interstorey drifts (see Chapter 1 for reference). The CM (centre of mass) is the locus where the storey mass is located, as defined in the Preamble; as a consequence, it is the locus where the resultant of the inertia forces due to earthquake excitation is ideally applied. It is due to the eccentricity between this locus and the CS (centre of stiffness), i.e. the locus where the resultant of the vertical element lateral stiffness is located, that torsional effects arise, as will be discussed in the following; for further details on the above reminded definitions, see the Preamble.

It can be observed that the two procedures and the experimental results did not agree in determining the storey with the largest demands in terms of displacements: the failure mechanism highlighted by the assessment procedures was of the soft-storey kind in the X direction at the first floor; due to the larger axial load that the first storey columns had to sustain, they resulted the least ductile and those who would suffer the most, up to the formation of a storey mechanism leading to large displacements.

The test, though, showed that the floor with the largest drifts was the second one; the second level also absorbed more energy than the other two. This can clearly be observed from Fig. 3.8a, in fact, shows that in the X direction the FEMA procedure considerably underestimated the displacements at the CM of the second storey; the upper bound in the X positive direction, given by the light blue line, is less than half the value reached during the test; in the negative X direction the agreement was better, but still the displacements reached during the test were about 60 mm against 40 mm of the prediction.

The main difference remains with the fact that the storey mechanism took place at the second storey, not at the first one. To better understand the discrepancy, in Fig. 3.8b the experimental second storey CM drifts are plotted together with the FEMA boundaries for the first storey drift in the X direction; from this comparison it can be understood whether the order of magnitude of the estimates was correct but assigned to the wrong storey. From Fig. 3.8b, though, it can be observed that in this case there was a remarkable overestimation of the maximum displacements mainly in the positive X direction when the light green line is considered; in the negative X direction once again there is a better match. Finally, in Fig. 3.8c, the first storey experimental drifts at the CM are compared to the limits obtained by the procedure for the second storey; also in this case from the comparison it can be understood whether the order of magnitude of the predictions was correct. In this case, in the negative X direction a strong overestimation of the displacement is shown, whereas in the positive X direction the underestimation of the displacements is evident: the second storey estimation is still smaller than the first storey experimental drift.

The conclusion that can be drawn is that in the test the second storey took the role that was predicted for the first; the predicted failure mechanism was then wrong and led to an underestimation of the maximum displacements at the second storey and an overestimation of those at the first storey. The different load patterns of the pushover analyses yielded different target displacements: it can be concluded that the load pattern following the first modal shape performed better than the uniform acceleration pattern in the weak direction; it must also be observed that the positive drifts estimates were worse than the negative ones. This latter observation highlights the difficulties in obtaining equally reliable predictions in both fundamental directions, arising from the asymmetry of the structure.

Moreover, it must be taken into account that the drifts at the CM, that were considered in this paragraph, are smaller than the drifts of the individual columns, for which the effects of the rotation at the CM are to be taken into account, as it will be discussed in the following. This means that a further gap between the predictions and the edge column interstorey drifts (those that are to be considered when assessing an irregular structure) came out.

3.4.3.2 Column Drifts

When observing the plots of the single column interstorey drifts together with the plot of the drifts of the CM: the remarkable effects of torsion on the response are evident.

In Figs. 3.9, 3.10, 3.11 the plots of the drifts are arranged along the plan-wise configuration of the structure: this is helpful in understanding how the relative positions of the CM, the centre of stiffness (CR) and of each column, all lead to develop different drift histories and considerably different demands on the individual elements.

First of all, to better understand the motion of the structure, it is necessary to locate the CR of the system. It is known that different definition of this locus can

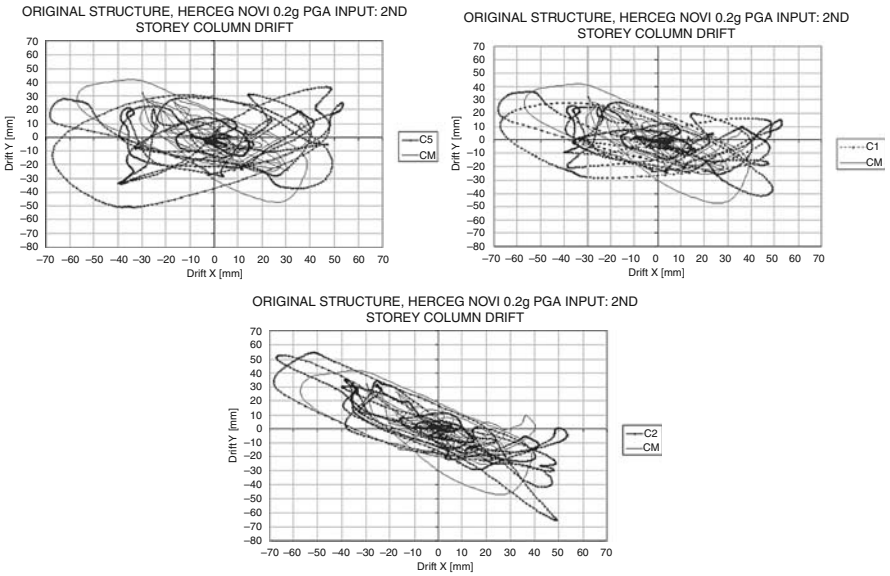

Fig. 3.9 Second storey column drifts compared to that of the CM: columns C5, C1, C2

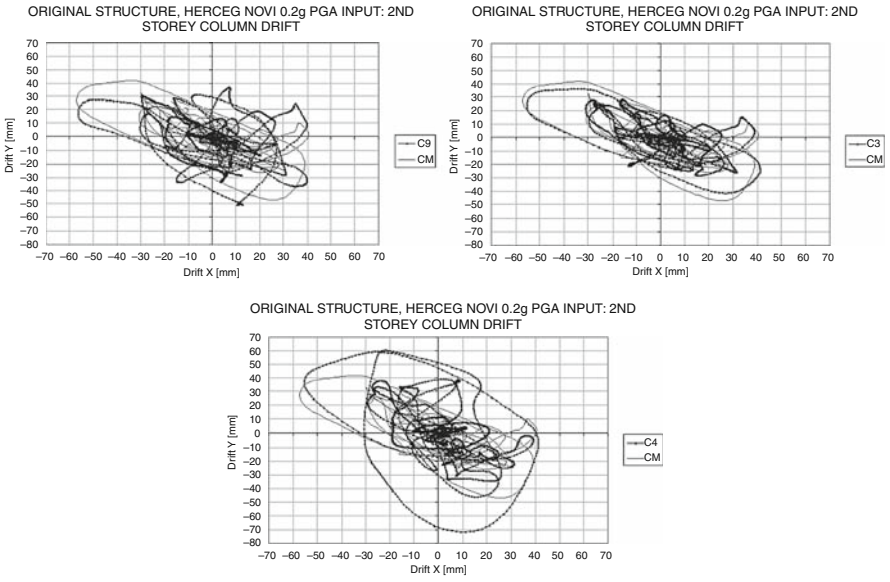

Fig. 3.10 Second storey column drifts compared to that of the CM: columns C9, C3, C4

be adopted: in this case, as stated in previous paragraphs, the location CR of the structure was computed following the prescription of EC8 [4], taking into account only the contribution of the moments of inertia of the columns, and is represented in Fig. 3.12.

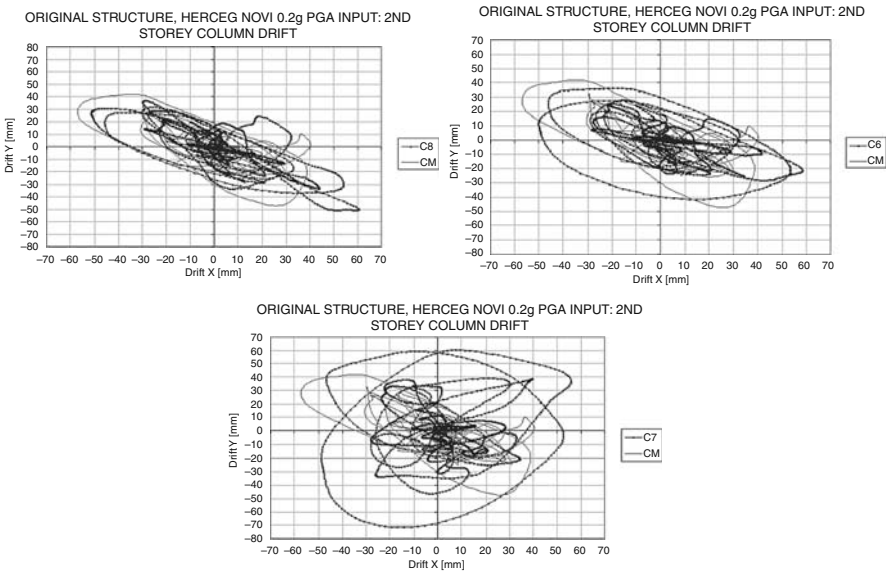

Fig. 3.11 Second storey column drifts compared to the CM: columns C8, C6, C7

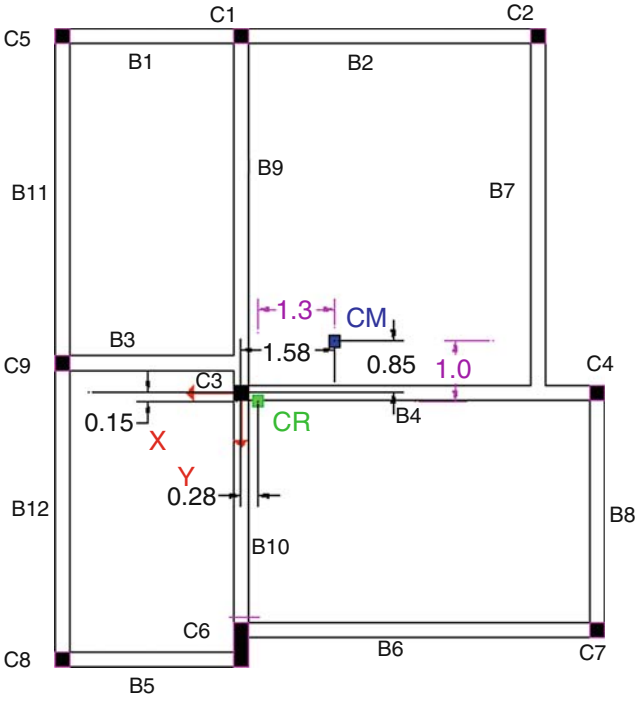

Fig. 3.12 Location of the CM and CR and respective eccentricities

At floors 1 and 2 the CR is eccentric with respect to the CM by 1.3 m in the X direction and 1.0 m in the Y direction, respectively about 13% and 9.5% of the total plan dimensions. At floor 3 a very slight difference in the eccentricity occurs; it becomes 1.34 m and 1.04 m in the X and Y directions respectively.

The CM and the CR are almost perfectly located along the diagonal connecting column C8 and C2; on the other hand, the CM is located along the diagonal connecting C4 and C5, whereas the CR is displaced of about 1.6 m along the opposite diagonal, as can be observed in Fig. 3.12.

The input signal consisted of two components applied along the – X direction and the –Y direction. The structure mainly displaced along a 45° direction (the C4-C5 diagonal), as can be seen from the observation of the CM drifts.

Column C3, which is located very close to the CR, and close to the CM, exhibited the least significant drift increments in both directions, but especially in the X direction, where the eccentricity is smaller. This is in agreement with the reconstruction of the motion of the structure that was drawn from the experimental data.

On the contrary, all the other columns were affected by torsion: the edge columns in the Y direction were affected by torsional effects in their drifts in the X direction, whereas the reverse happened for the X direction edge columns, which were affected in their maximum drifts in the Y directions.

When comparing the relative importance of torsion-effected drift increments for the X and Y edge columns, it can be seen that columns C7 and C5 are the most affected: this means that the Y direction edge columns suffered the most. This is in good agreement with the relative position of CM and CR above analyzed: along the line C1-C4 there is a remarkable distance between CR and CM, the Y eccentricity is larger and the two columns are the farthest from the CR.

Finally, it must be observed that the significant extent of the difference between the drifts at the CM and the edge column drifts is one of the most important outcomes of the test: the torsional effects on the response turned out to be much larger than predicted.

In fact, the test showed that, despite an eccentricity that could be defined not too large (in the order of 10% of the plan dimension), the effects of torsion on the drifts of the edge columns are remarkable in both directions. In the X direction, where the structure is less rigid and the drift at the CM is already quite large, the maximum drift reached at the CM is 55 mm, whereas the maximum drift reached at the edge columns C1, C2 and C5 was about 70 mm, a difference which is not negligible.

In the Y direction the maximum drift reached at the CM was 45 mm, whereas the maximum drift of the edge columns C4 and C7 was above 70 mm, i.e., more than 50% larger.

This result confirmed one of the basic remarks that had been drawn at the end of the assessment exercise with regard to the use of pushover analysis in assessing the displacement capacity of irregular multistory buildings: conventional pushover tends to underestimate the displacements because the pushover curve refers to the CM of the model. The prescription of the procedure to take into account the increases of displacements on the edge elements should thus be more precise and

compelling, because, as was demonstrated in this case, to reach a safe-side estimation of the flexible edge elements drifts, increases as high as 50% of the displacements at the CM can be necessary even for moderate eccentricity.

These large increases are larger than could be expected when considering the values of plan eccentricity of the structure in themselves: an eccentricity of around 10% is defined in all procedures as not likely to have major effects; for example, the structure falls in the EC8 category where the separate analysis in the two main direction is allowed and in the Japanese Guidelines it is in the category with the lowest capacity-reductive factor.

Nevertheless, it was proven by the test that in this case the interaction of the eccentricity in both directions had a role that cannot be neglected in enhancing the torsional effect on the response even if the two eccentricity values were not large.

From Fig. 3.13, it can also be observed that the rotation time-history exhibited its maximum effects in the final range of the response (from 10 s to 15 s); it was in fact observed that the structure moved mainly in its translational modes in the initial part of the excitation, following the first modal shape, which was mainly flexural in the weak (X) direction.

Meanwhile, the values of the total energy absorbed by the rotational mode were smaller in comparison to those absorbed by the translational DoFs, as can be seen in Fig. 3.13; moreover, in the last part of the response, it came out that when the rotation strongly increased and the torsional component became very important, it caused a shifting of the column drifts with respect to that of the CM and the strongest increase in the maximum values of the edge column drifts.

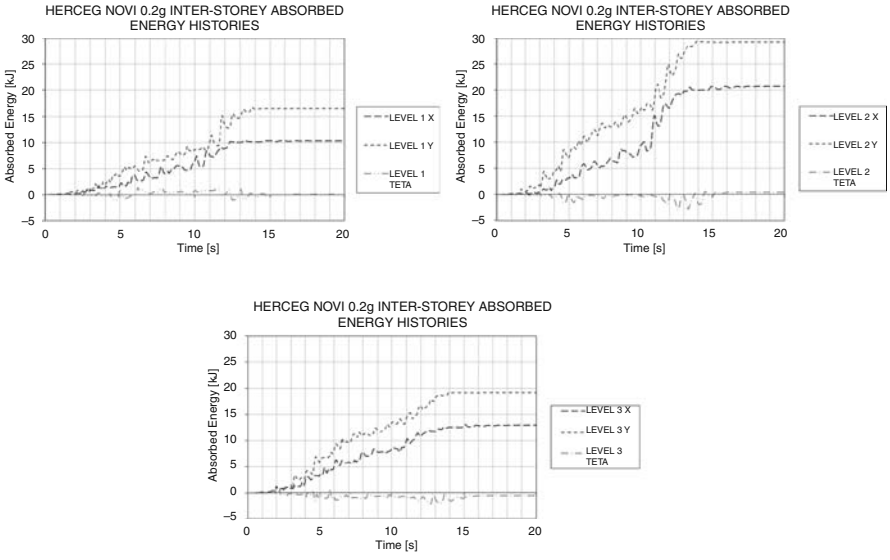

Fig. 3.13 Herceg-Novi 0.2 g input: interstorey total absorbed energy histories

This can also be seen in Fig. 3.13: in the same time range, the energy absorbed by the rotation reaches its maximum (negative, since there is no input energy associated to torsion, therefore the absorbed energy is the opposite of kinetic energy) values. In the PhD test algorithm, in fact, no input energy is associated to the rotational DOF (the input excitation is in the X and Y directions only), so on the whole, the sum of the kinetic and absorbed energy for that DOF have to be zero. Still, kinetic energy is always positive by definition, which means that, to have equilibrium, the absorbed energy (associated to the rotational DOF) results negative. The physical meaning of this fact is that the energy which is input into the specimen by the input excitation according to X and Y DOFs is "transferred" (even if in small quantities) also on the teta DOF, due to the coupling effects between the DOFs due to the plan-wise irregularity of the specimen.

In any case, it must be noted that the absorbed energy in rotation is far less than that absorbed in translation and goes back to values very close to zero at the end of the excitation, which is correct given the zero input rotational energy. The rotational absorbed energy peaks in the last phase of the response, as mentioned before, show the time in which torsional effects were more active in affecting the local (in time) modal vibration pattern of the response, as will also be shown in Chapter 3, with reference to the Karhunen-Loève analysis results.

This behavior highlights one of the widely agreed conclusions drawn from research on the torsional response of asymmetric structures: the effects of higher modes and the dynamic amplification of eccentricity are very important factors in affecting the behavior of multi-storey plan-irregular buildings, Rutenberg [18]. For this reason the drawbacks of the static equivalent approach even corrected with the use of design eccentricity, must not be forgotten and the caution in extending to multi-storey buildings the conclusions drawn from single storey models was justified by the results of the test hereby described.

3.4.3.3 Concluding Remarks

From the comparison between the outcomes of the assessment procedures and the experimental results important drawbacks of the current codified approaches for the assessment of torsionally unbalanced multi-storey buildings were highlighted.

The procedures were correct in assessing the role and behavior of the strong column: even if at first sight this column might appear critical because of its higher stiffness and because it is the largest source of irregularity, its effect turned out to be beneficial in improving the behavior of the structure in the Y direction, without suffering any damage. This was correctly predicted by all assessment procedures, both the force- and the displacement-based ones.

On the other hand, the procedures failed in predicting the global failure mechanism of the structure; in fact, a first-floor soft-storey mechanism was predicted by all the pushover analyses, whereas in the test the second storey was the most affected, with larger drifts and absorbed energy. This confirms that much care should be paid in applying simplified SDOF procedures to multi-storey irregular buildings.

The absolute values of interstorey drifts were not adequate either: the maximum displacements at the CM were underestimated; moreover, it must be noted that the effects of torsion on the individual column drifts were very large even if the eccentricity had been dismissed by many procedures as "minor". This led to a further underestimation of edge displacements and to neglecting the possible interaction of the two plan eccentricities, which during the test corresponded to unpredicted effects.

From the above mentioned remarks, it can be concluded that margins for improvement in current procedures do exist: in particular, the effects of bi-eccentricty, the evaluation of safe-side drifts at the CM, the reliability of the prediction of the failure mechanisms should be further investigated.

3.4.4 Further Developments and Recent Advancements

As mentioned above, long-standing interest in the development of sound and foolproof assessment procedures and decision-making tools has led to a continuous improvement and refinement of codified approaches and guidelines, by means of remarkable dedicated research efforts.

Two of the most outstanding examples are the FEMA 440 and the ATC-58 project in the US, leading to the draft of improved nonlinear analysis (pushover) approaches for the seismic assessment of existing structures, and the revision and finalization of the most recent draft of EC8 part 3 in Europe, which incorporated many of the lessons and outcomes almost directly derived from the SPEAR project, by means of continuous liaisons between the Consortium an the competent normative bodies, since many of the SPEAR partners served as members or convenors of the relevant TGs.

As was made apparent by the detailed discussion of the outcomes of the SPEAR experimental activity, even limited to the "as-built" structure (many more complex issues more strictly related to decision-making strategies for retrofitting would be raised by a detailed discussion of the outcomes of the tests in the two different retrofitted configurations, as can be found in [6]), pushover analysis is a key tool to be employed for assessment; provided it can be correctly detailed and applied, it has to lead to a confident safe-side estimation of top "target" displacement and associated storey drifts; such estimation needs to take into account, where necessary and in a simplified way, twist-induced additional drifts due to structural irregularity; once the displacements and drifts are made available, clearly explicated acceptance criteria for ductile or non ductile, structural or non-structural elements must be provided in order for the engineer to immediately determine critical areas and non-compliant elements.

Ideally, it is clear that the final step to provide a fully consistent decision making tool consists in providing cost-estimates associated to different damage levels based on largely "socially-accepted" values and criteria.

The task strictly pertinent to research is that of tuning in the most effective way the prediction tools, reducing the degree of uncertainties in correlating the damage

pattern and intensity to the input excitation on one side, and on the other, to express the damage in terms of parameter of engineering meaning that can easily transfer to the language and understanding of the end-users.

In this direction, both FEMA 440, ATC-58 and EC8 part 3 2004 represent the most advanced achievements; if specifically applied to the case study of the SPEAR structure, in fact, they would all yield more accurate results, more closely matching the experimental data, with a lessened or at least unchanged effort, as will be shortly highlighted in the following.

Still, it is the Authors' opinion that margins for improvement still exist, especially on the side of simplicity and straightforwardness of application; considering the situation of newly accessed or accessing Countries in Europe, where the bulk of the housing stock consists in under-designed, often irregular and strongly ill-detailed units, the needs for easy and quick scanning and evaluation are impellent.

Moreover, the gap between research and practice still being significant in most countries, nonlinear static analysis implies a number of choices and assumptions that can ill-condition the final results if incorrectly made by practitioners: the sensitivity of the tool to human errors is maybe still to high to indiscriminately count on it as the solution for the matter hereby discussed.

Also, as will be shown in a companion paper, when retrofitting choices are involved, the importance of strictly engineering parameters, such as eccentricities or additional drifts or vertical distribution of hinging at ultimate, yield importance with respect to a number of other variables and constraints of a more "practical" kind that cannot possibly be disregarded, even more so when the aim of optimizing costs and computational time is pursued, [11, 12].

3.4.4.1 FEMA 440 and ATC58

As highlighted above, the application of different computational tools by practicing engineers led to the widespread feeling of the scattering of the results of the predictions: hence in the US the Applied Technology Council (ATC) proposed to the Federal Emergency Management Agency (FEMA) in 2000 that a study be conducted to determine the reasons for differing results and to develop guidance for practicing engineers on improved application of these two methods, the ATC-55 Project.

One of the most important aims of the project was the improved understanding of the inherent assumptions and theoretical underpinnings of existing and proposed updated inelastic analysis procedures, which should be leading to the recognition of the applicability, limitations, and reliability of the various procedures.

The FEMA 440 Report, coming out of the project and summing up many of the outcomes of the project activity, had three specific purposes: (1) to provide guidance directly applicable to the evaluation and design of actual structures by engineering practitioners; (2) to facilitate a basic conceptual understanding of underlying principles as well as the associated capabilities and limitations of the procedures; and (3) to provide additional detailed information used in the development of the document.

The document is thus very precious because it gives a comparative evaluation of the different approaches to nonlinear analysis for assessment and reviews some case studies of practical validity. The same "exercise" that was presented above with reference to the SPEAR structure and to irregularity-induced issues, was thus carried out in a much more extensive way. This proves the interest for an improved knowledge and understanding of the inherent capabilities and limitations of nonlinear static analytical procedures for the assessment of buildings.

The ATC 58 project, on the other hand, aims at building a vision for the next generation of PB seismic codes, focused on expressing performance directly in terms of quantified risks that the building owner or the decision maker will be able to understand: once again the economic and social concern are underlined and play a central role in the conceptual background to PB engineering.

The project is articulated in two phases: the first one focused on the assessment of the seismic vulnerability of existing buildings: in this perspective, verification procedures include rules to model buildings into analysis software and to simulate their seismic response, guidelines to convert these estimations of stresses, deformations and actions into measures of damage experienced by both structural and non-structural components.

3.4.4.2 EC8 Part 3 (2006)

The latest, and final, draft of the EC8 Part 3 document, now titled "Assessment and retrofitting of buildings", actually retained many of the lessons derived from the previously described research and experimental activity.

The document, in its present format, strongly opens he door to performance-based concepts, displacement based assessment (rather than the older, force-based approach) and specifically provides formulations to compute sectional or structural properties and acceptance ranges specifically tailored on the feature of existing buildings, rather than referring to the prescriptions for new one, as was the case in the older version.

Also, along the lines of the other recent documents, the importance of nonlinear static analysis as a specific assessment tool is acknowledged, and much more detailed implementation guidelines are provided, on a step by step basis similar to that detailed in FEMA 356.

As for torsional issues and substandard details, as mentioned above, simplified, semi-empirical formulations are provided in order to determine chord rotations, rotational ductility of sections, shear capacity and a number of other significant parameters, to be implemented into lumped plasticity models for global structural analysis and the determination of pushover curves.

Drift limitation ranges are given, based on three performance states, specifically tailored to existing structures: the first one is the Limit State (LS) of Near Collapse (NC), i.e. The structure is heavily damaged, with low residual lateral strength and stiffness, although vertical elements are still capable of sustaining vertical loads. Most non-structural components have collapsed. Large permanent drifts are present. The structure is near collapse and would probably not survive another

earthquake, even of moderate intensity. The second one is the LS of Significant Damage (SD), i.e. The structure is significantly damaged, with some residual lateral strength and stiffness, and vertical elements are capable of sustaining vertical loads. Non-structural components are damaged, although partitions and infills have not failed out-of-plane. Moderate permanent drifts are present. The structure can sustain after-shocks of moderate intensity. The structure is likely to be uneconomic to repair.

LS of Damage Limitation (DL). The structure is only lightly damaged, with structural elements prevented from significant yielding and retaining their strength and stiffness properties. Non-structural components, such as partitions and infills, may show distributed cracking, but the damage could be economically repaired. Permanent drifts are negligible. The structure does not need any repair measures.

It is explicitly noted in the document that the definition of the Limit State of Collapse given in it is closer to the actual collapse of the building than the one given in EN1998-1: 2004 and corresponds to the fullest exploitation of the deformation capacity of the structural elements. The Limit State associated with the "no collapse" requirement in EN1998-1: 2004 is roughly equivalent to the one that, in Part 3, is defined as Limit State of Significant Damage.

The specifically torsional issues are sill dealt with on the basis of the regularity prescriptions given in EC8 Part 1, but more detailed formulations are given to quantify ductility resources of critical regions, taking into account the effects of older structural detailing design, different construction practice and materials. Some of these empirical formulations came out of the experimental evidence of the SPEAR project, which proved a invaluable opportunity to throw more light to the complex issues inherent to the assessment and retrofitting of existing seismically under designed structures.

Acknowledgments The Project SPEAR was funded by the European Commission under the "Competitive and Sustainable Growth" Programme, Contract N. G6RD-2001-00525. A group of European partners took part in the SPEAR Project together with the ELSA Laboratory: the University of Patras (Greece), the Imperial College of London, the University of Ljubljana (Slovenia), the Universities of Rome and Pavia (Italy), the National Laboratory of Earthquake Engineering (LNEC) of Lisbon, the Higher Technical Institute of Nicosia and EQE International (London). The research team of the University of Naples Federico II took part in the design and execution of the retrofitting interventions. The Authors gratefully acknowledge the professional expertise and friendly attitude of the whole ELSA staff.

References

1. ATC-58 Project-Development of performance-based seismic guidelines–Work Plan, http://www.atcouncil.org/atc-58.shtml
2. Computers and Structures inc. (csi), SAP 2000 NL: statics, dynamics and earthquake engineering finite element analysis and design software for structures and bridges (ver 8-9), Berkeley, Ca, USA, 2002
3. Elnashai AS (2002) Do we really need inelastic dynamic analysis? Journal of Earthquake Enginering, 6 (Special Issue 1): 123–130, Imperial College Press, London

4. Eurocode 8 (2001) Design of structures for earthquake resistance. Part 3: Strengthening and repair of buildings. Doc CEN/TC250/SC8/N293, Draft No 1
5. Eurocode 8 (2005) Eurocode 8: Design of structures for earthquake resistance -Part 3: Assessment and retrofitting of buildings, EN 1998-3
6. Fardis M, Negro P, (editors), (2005) SPEAR: Seismic Performance Assessment and Rehabilitation: Proceedings of the international workshop, Ispra, Italy, EU Publications Office
7. Federal Emergency Management Agency, FEMA 273 Report – NEHRP Guidelines for Seismic Rehabilitation of Buildings
8. Federal Emergency Management Agency, FEMA 356 Report (2000) – Pre-standard and commentary for the seismic rehabilitation of buildings
9. Federal Emergency Management Agency, FEMA 440 Report (2005) – Improvement of nonlinear static seismic analysis procedures
10. Japan Building Disaster Prevention Association: Standards for seismic capacity evaluation of existing reinforced concrete buildings, 1977 revised 1990 (in Japanese)
11. Mola E, "Criteria for the seismic vulnerability reduction of existing irregular reinforced concrete structures", PhD Thesis, École Doctorale Mécanique Conception Géomécanique Matériaux, INPG Grenoble, February 2007
12. Mola E, Negro P, "Post-test analysis and interpretation of the results of PsD testing on a full-size three-storey RC plan-wise irregular frame structure: new perspectives", Proc. of the 1st European Conference on Earthquake Engineering and Seismology, Geneva, 2006
13. Negro P, Mola E (2005) Application of the Karhunen-Loeve method to the analysis of the results of a PsD test on a torsionally unbalanced three-storey building. Proc. of 4th European workshop on the seismic behaviour or irregular and complex structures, Thessaloniki, Greece
14. Mola E, Negro P (2009) The importance of plan-wise irregularity. Seismic Risk Assessment and Retrofitting, Springer
15. Negro P, Colombo A (1998) How reliable are global computer models?, Earthquake Spectra, 14 (3):441–467
16. New Zealand national society for earthquake engineering (2002) The Assessment and improvement of the structural performance of earthquake risk buildings. Draft 06 May 2002
17. Priestley MJN (1997) Displacement-based seismic assessment of reinforced concrete buildings. Journal of Earthquake Enginering, 1(1):157–192
18. Rutenberg A, EAEE Task Group (TG) 8: Behaviour of irregular and complex structures, asymmetric structures–Progress since 1998. Proceeding of 12th European Conference on Earthquake Engineering, Paper N. 832, Elsevier Science Ltd, London, 2002

Chapter 4
Risk Management and a Rapid Scoring Technique for Collapse Vulnerability of RC Buildings

Semih S. Tezcan, Ihsan Engin Bal, and Fatma Gulten Gulay

Abstract It is emphasized that Turkey experiences frequent earthquakes, on the order of one damaging earthquake of magnitude 6.0–7.0 at almost every two years, causing extensive losses to economy, life and limb. Every strong earthquake leaves behind poverty and tens of thousands of homeless people. In order to mitigate the losses due to earthquakes, a number of issues are identified to be studied and managed properly on a national scale. Firstly, the importance of education and research about earthquakes and earthquake preparedness, from cradle to grave, is stressed. Secondly, for a successful solution of the risk mitigation problems, the legislative and financial structures as well as the social and technical organizations are presented. Recommendations are given, concerning the disaster management, dealing with emergency matters during and after the earthquake, and also the risk management, dealing with preparations before the earthquake. Finally, the problems related to inventory of buildings, repair and retrofitting issues, earthquake insurance, supervision of design and construction of buildings are discussed. A reference is made to the project of "zero" loss of life during future strong earthquakes which eliminates the necessity for large scale retrofitting of the existing building stock and saves lives. A rapid scoring technique called "*P25- Assessment Method*" is also introduced for determining the collapse vulnerability of RC buildings.

4.1 Introduction

By virtue of its geographic location, Turkey experiences one damaging earthquake almost every two years. In fact, the number of earthquakes occurred in Turkey, within the last century, with magnitudes greater than $M = 5$, is 122. This is the highest rate of earthquake occurrence in the world.

S.S. Tezcan (✉)
Bogazici University, Istanbul, Turkey
e-mail: tezokan@gmail.com

A. Ilki et al. (eds.), *Seismic Risk Assessment and Retrofitting*, Geotechnical, Geological, and Earthquake Engineering 10, DOI 10.1007/978-90-481-2681-1_4,

Over a period of one hundred years, a total of 120,000 people died, and about 550,000 buildings were heavily damaged. Financially speaking, the direct losses to the economy, on the average, have been approximately 900 million US dollars per year. Unfortunately, the amount of research conducted in Turkey for preventing these losses is not adequate. Even if only five percent of these losses were spent for research in earthquake engineering and risk management, these losses would have been significantly reduced.

During the August 17, 1999 Kocaeli earthquake of M_w=7.4 and also during the November 12, 1999 Bolu-Duzce earthquake of M_w=7.2, a total of 17,500 people died, 45,000 people wounded. Out of 854,000 residential units, 108,400 residential units either collapsed or damaged severely beyond repair, 105,000 suffered moderate damages and 117,000 suffered minor damages. Approximately, half a million people were left homeless. There has been a great awareness in public towards earthquakes and earthquake preparedness.

Considering the high ratio of life losses, the priority of mitigation strategies must be given to saving lives. It is known by experience that the collapsed buildings are the main cause of life losses, thus, methods to identify the "collapse vulnerable" structures must be of prime importance to have a complete mitigation strategy.

4.2 Need for Mitigation Strategies at National Level

A complete mitigation strategy, preferably applied at national level, is the basic feature of the successful applications to decrease the losses. The fight with natural disasters needs a synchronized action where each piece of the chain must perform perfectly, and thus, "just retrofitting buildings and bridges" or "just strengthening search and rescue teams" would not be enough to obtain a fully successful picture following a serious shaking. The mitigation issues must be treated as a complete set of precautions of which every piece must succeed. For the sake of completeness, issues related to a national level mitigation strategy have been given below, within the context of the past and current applications in Turkey. Additionally, basic institutions and activities involved in earthquake risk management in Turkey are shown in Fig. 4.1.

4.2.1 Education and Research

The earthquakes and protective measures against earthquakes, also the ways and means of mitigating earthquake hazards, should be studied at all levels of formal education, from elementary schools to universities. Since, the Civil Engineers and Architects are mostly responsible for the proper and safe design of buildings; aseismic design principles should be an integral and compulsory part of their undergraduate curricula. Unfortunately, in Turkish Universities, earthquake related courses, if at all available, are offered mostly as technical electives.

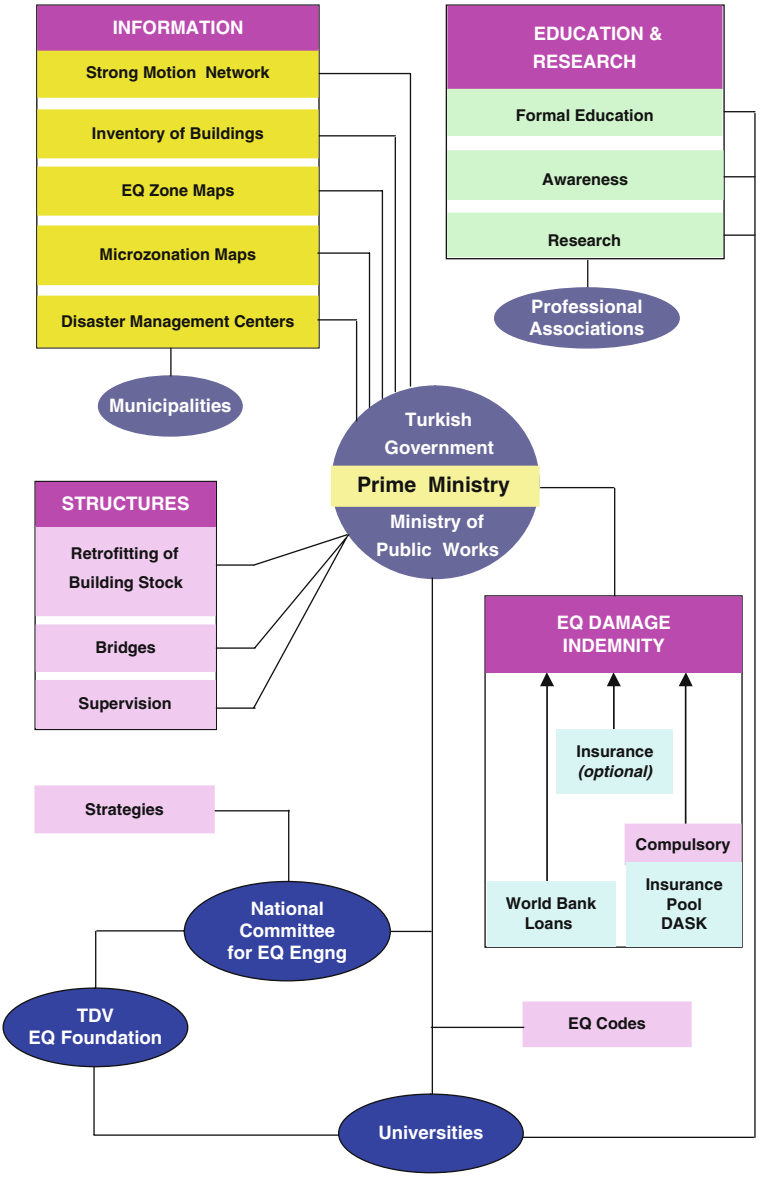

Fig. 4.1 Basic institutions and activities related to earthquake risk management in turkiye (See also Plate 3 in Color Plate Section on page 455)

The engineers and architects already in practice should also be educated as job training, in order to refresh their knowledge, as well as to furnish them with new technological ideas, rules, methods and standards. The areas of earthquake related research are very versatile, encompassing a variety of fields, such as Civil, Structural, Earthquake, Geotechnical, Geological and Geophysical Engineering, City

Planning, Architecture, Social Sciences (economy, administration, civil defense, insurance, financing, etc.). Pre-earthquake activities of research and any spending of resources for the mitigation of hazards, virtually reduce in multifold the possible losses to economy during earthquakes. The professional civil engineering associations in Turkey have already been engaged in these educational activities on regular basis.

Earthquake engineering research is also very important. The volume of experimental as well as theoretical research in earthquake engineering at universities should be increased by obtaining additional financial support from private and public institutions. The financial sources in Turkey, for earthquake related research are TUBITAK (National Scientific and Technical Research Council), Universities, Public Institutions, Private Industry, Earthquake Foundation and international cooperations.

4.2.2 Seismic Network

There is a national strong motion recording instruments network in Turkiye, almost one station at every major city, operated by the Department of Disaster Affairs, within the Ministry of Public Works and Resettlement. The number of stations should be at least doubled if ground motions close to the epicenters of future earthquakes are to be recorded.

Unfortunately, during the Kocaeli Earthquake of August 17, 1999, M_w=7.4, there was no recording station neither at Izmit nor at Golcuk, which are the two heavily populated centers of the Kocaeli Province. Similarly, for the Sultandag-Cay earthquake of February 3, 2002, M_w=6.0, not a single record was available, within a radial distance of 60 kilometres from the epicenter [1]. The absence of ground motion records in a region is a serious deficiency in understanding the earthquake behavior of structures.

A similar seismic network system is operated in Turkiye, by the Kandilli Observatory of Bogazici University, mostly involving velocity-measuring seismograms on a real time basis. Kandilli Observatory also installs and operates strong motion recording systems at various important industrial facilities and infrastructural locations in Turkiye. The number of stations of this type of network should be increased.

4.2.3 Inventory of Buildings and Data Collection

There should be an inventory data bank of buildings for each village, town and city. The data bank should contain information about the owner(s), size, construction materials, structural system, occupancy type, design drawings, city planning alterations, zoning, seismic history, etc. Such information should be made available to researchers and/or administrators upon request. It is indeed a serious problem for Turkiye that more than fifty percent of buildings do possess neither a construction permit nor an occupancy certificate. The design drawings are either not registered at the municipal authorities or do not reflect the real construction conditions.

Some political leaders in Turkiye, before each national election, in order to attract the votes of the inhabitants of such unlawfully built settlements *(gecekondu areas)*, promise amnesties to them before each national election. In fact, after various national elections, the amnesty laws have been accepted by the Turkish National Assembly at more than five occasions in the last twenty years. Therefore, the majority of the unlawful land use and constructions without permit have been legalized. There is however, a strong pressure from the civil and professional organizations and from the public in general to revise the Turkish Constitution so that no political party may propose and pass an amnesty Law in future for the illegal use of land and buildings [2].

Concerning the importance of soil conditions on seismic behavior of buildings, every municipality should also prepare a series of microzoning maps, showing the soft soil conditions, the areas with potential risk of liquefaction, the zones of landslide or slope failure, the possibilities of soil amplification, etc.

Information about soil investigations, bore holes, seismic surveys, microtremor measurements, etc., should be also stored into a data bank and made available to the researchers. The microzoning maps are most essential and should be prepared gradually by each and every municipality of a town or city [3].

In reality, all Provincial Governments and local municipal bodies organized, within the last ten years, very modern and sophisticated Disaster Management Centers and facilities throughout the Country. However, sincere and serious preparations are needed in the area of risk management.

4.2.4 Supervision of New Constructions

The Law No. 4708 enacted on June 6, 2001 by the Turkish National Assembly regulates the supervision of the design and construction of new buildings in Turkiye. The law is for buildings of private sector only and no provisions exist for public construction work. The responsibilities for supervision of design and construction are assigned to *Professional Engineers* and *Professional Architects* with at least 12-years of experience. No construction permit or occupancy certificate may be issued by the municipal authorities unless all necessary work are checked and approved by the pre-appointed "*Professional*" Engineers and Architects.

The consulting engineering company supervising the construction is responsible for the seismic safety of the building for a period of 15 years. The supervising company has also professional liability for the proper functioning of non-structural elements at least for a period of two years. Although, this new law introduces a sound reformist approach to supervision, it needs to be improved. The Law covers only 19 cities of the highest risk zones; however, it should be enforced throughout Turkiye with no city being exempted. Additionally, the fee for supervision is around 3% of the cost of the building and it is not enough for all the stringent activities demanded by the Law.

This fee hardly covers the premiums of the professional liability insurance policies. A premium of 2 per mill in 15- years already makes 3%, which is the

total fee to be received from the owner for the entire supervising work! Furthermore, the certificates of "Professional Engineering" are issued by the Ministry of Public Works but they should rather be issued by the respective Engineering Chambers. Finally, the "Professional Engineering" status is required only for the technical personnel of the supervising company whereas the project manager of the contractor, the designer, the engineers and architects at the central governments and municipal authorities should be also required to possess the "professional" status.

4.2.5 Earthquake Damage Indemnity – The Old System

The Insurance protection against earthquakes in Turkiye, started in *1929* by adapting a practical scheme, in which a separate "Earthquake Clause" is added into the general fire insurance conditions. This practical scheme is interrupted in *1944*, when the State Ministry did no longer allow adding an "Earthquake Clause" into the fire insurance policies. Thus, no earthquake assurances were given until the year 1966, when the scheme of "Earthquake Clause" was reactivated [4].

In *1990*, the State controlled price system for premiums is abandoned, and the insurance companies determined their prices freely on the basis of free market economy. Because of this competition, the rates are reduced significantly to the levels, of 0.44 per thousand. In 1993 however, the State controlled tariff system is reactivated again, resulting in relatively higher premium rates, and declining number of policies.

A total of 4-major damaging earthquakes occurred in Turkiye, between 1992 and 1999, as shown in Fig. 4.2. The Erzincan Earthquake of March 13, 1992, Ms = 6.8 claimed 540 lives, damaged 1,200 residences heavily and 4,600 residences moderately. The direct economic losses were on the order of 0.4 billion $ US. The insurance companies paid only 20 million $ US of compensation after this earthquake. It is seen that 20 million $ US of compensation by the insurance companies beside 400 million $ US economic losses, was so small and did not possess much of a meaning thus, the remaining economic losses were compensated by the State, using long term loans borrowed from the World Bank. In other words, the indemnity was supplied by the State, using the public funds. That means, all tax payers of both today and tomorrow shared the burden.

The total economic losses, during the Adana-Ceyhan earthquake of June 27, 1998, for instance, were 0.9 billion $ US, while the compensations paid out by the insurance companies were only 5.5 million $ US [5]. Similarly, the total economic losses of the Kocaeli earthquake of August 17, 1999 reached to 12.6 billion $ US, while the total compensations paid out by the insurers were only 570 million $ US. The huge difference, between the earthquake indemnities paid out by the insurers and the total economic losses is always compensated by the "*Father State*!"

Historically, all earthquake damages to buildings owned by the private sector have been indemnified always by the State [4]! It is perhaps for this reason that the

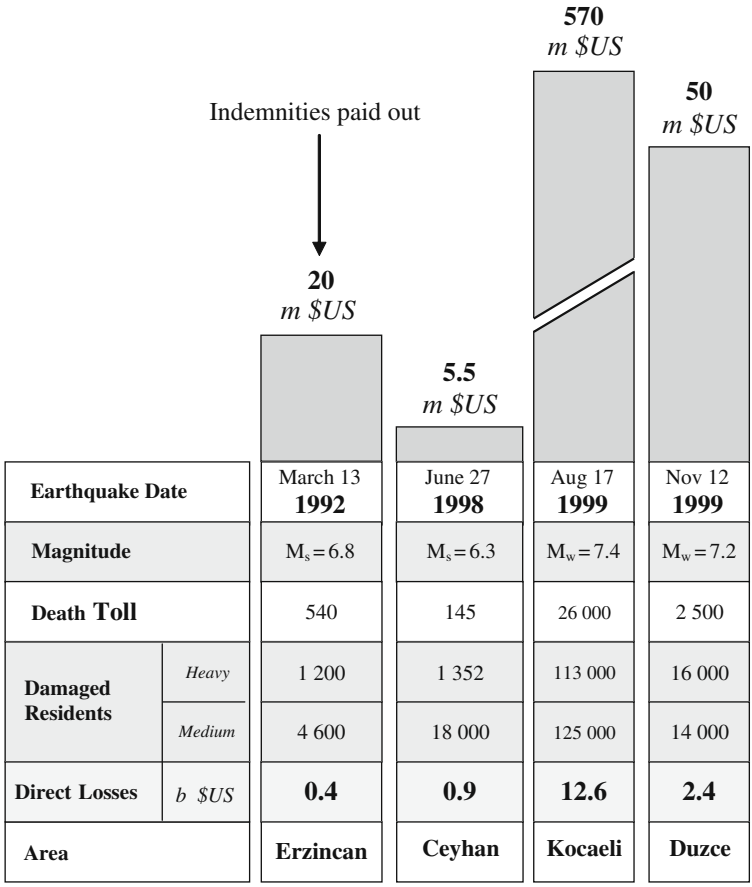

Earthquake Date		March 13 **1992**	June 27 **1998**	Aug 17 **1999**	Nov 12 **1999**
Magnitude		$M_s = 6.8$	$M_s = 6.3$	$M_w = 7.4$	$M_w = 7.2$
Death Toll		540	145	26 000	2 500
Damaged Residents	*Heavy*	1 200	1 352	113 000	16 000
	Medium	4 600	18 000	125 000	14 000
Direct Losses	*b $US*	**0.4**	**0.9**	**12.6**	**2.4**
Area		**Erzincan**	**Ceyhan**	**Kocaeli**	**Duzce**

Fig. 4.2 Earthquake indemnities paid out after the recent 4-Turkish earthquakes

State is called by the people as "Father State" (Devlet Baba). Usually, the funding necessary to compensate for the damages come by way of State Loans from the World Bank. A lump sum cash money is paid by the State to the owner of the building with "minor" damage, on the order of about $US 500 for the purpose of cosmetic repairs, such as plaster, ceramic, painting, etc. In moderately damaged buildings however, since the lateral load carrying structural elements like columns, beams, and shear walls may have been cracked, even to the extent of forming plastic hinges, the "Father State" allocates the necessary funds, usually on the order of $5,000 to $8,000 in order to repair and strengthen the building. Buildings in "severe" damage category on the other hand, are demolished. The "Father State" however, constructs new modern housing and assigns new residential units, to these "severe damage" owners. The cost is reflected to the new owners on the basis of long term loans without interest [4].

4.2.6 Earthquake Damage Indemnity – The DASK System

The damages of any intensity to private buildings during future earthquakes in Turkiye will no longer be indemnified by the State. The "Father State" no longer exists! The premiums of the compulsory earthquake insurance policies accumulated inside a pool called *DASK* (Natural Disasters Insurance Agency) will be utilized to indemnify the damages. The pool *(DASK)* is a semi-public nongovernmental organization, established under the auspices of the Turkish National Treasury. The organization is managed by a 7-member executive board which reports directly to the Treasury of the Turkish Government. The annual premiums are collected by a selected group of insurance companies, on the basis of 12.5% commission, and $50,000 guarantee bond.

Fully commercial or industrial buildings, public properties, rural residences inside villages, and the illegal buildings constructed after Dec 27, 1999 with no proper construction permit are all exempt from the compulsory earthquake insurance. Further, the compulsory earthquake insurance policy provides coverage for building damages only. No indemnity is provided for movable assets, bodily injuries and/or indirect losses.

There are about 18 million householders and retail offices in Turkiye. If all of them purchase a compulsory insurance policy, theoretically 2.1 billion $ US dollars will flow into the DASK pool annually. Combined with the possible funds to be received from the reassures from outside Turkiye, the DASK pool will be able to operate successfully to indemnify all sorts of damages after a new earthquake in Turkiye.

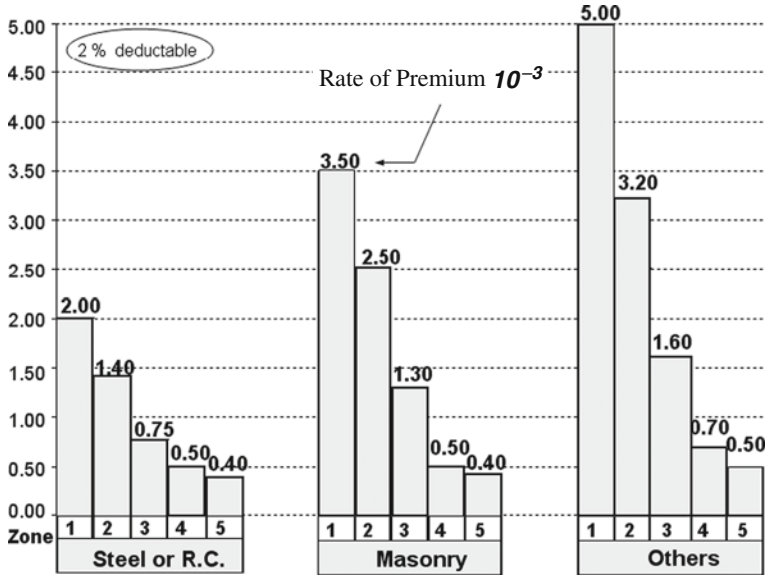

Fig. 4.3 Rates of premiums for compulsory earthquake insurance *(effective 27.09.2008)*

Currently, the number of compulsory earthquake insurance policies did not exceed 2.5 million by the mid-2009. All independent residential units and/or condominiums, or any independent portion of the building used for commercial purposes, old or new must be insured against earthquake damages for a predetermined fixed amount of assurance. The amount of assurance is determined on the basis of the floor area of the unit multiplied by the officially approved market value of the building. The premium rates for the compulsory earthquake insurance policies are shown in Fig. 4.3. The policies contain a deduction clause of 2%.

The maximum amount of assurance for a residential unit of 100 square meter plan area is about USD 20,000. Certainly, additional earthquake assurances may be purchased at the option of the owner. But, premiums of such additional earthquake policies do not go into the DASK pool.

4.3 The Zero Loss of Life Project

As part of the complete mitigation strategies and efforts to decrease the life losses to zero, a conceptual proposal has been introduced hereinafter. So called the project "zero" loss of life has already been proposed in several publications, by the principal author of this article [6]. The proposal suggests concentrating on saving lives and directing the limited resources and time in a way that the collapse vulnerable buildings will be identified primarily and necessary actions will be taken, urgently.

The earthquake design criteria in the national earthquake codes are constantly upgraded and improved with the increase in knowledge about the real behavior of structures during earthquakes. In view of the new design requirements, the old buildings are rendered as "unsafe", thereby in need of retrofitting. The money and time required to retrofit all of the existing buildings are prohibitively high. Therefore, it should not be attempted!

A practical idea exists by realizing that an "unsafe" building in accordance with the national code does not necessarily mean that it will collapse. In fact, only six percent of the building stock collapsed during the August 17, 1999 Kocaeli Earthquake, and there was absolutely no loss of life in the remaining 94% of the buildings [6]. Therefore, as far as the life safety is concerned, only a few percent of the current building stock will have to be retrofitted. Such a clever idea of retrofitting only a few percent of the building stock preliminarily results in a considerable saving of time and money. It is therefore a distinct question as to which buildings are the "candidates" for total collapse.

As explained above, if the buildings in Istanbul are assessed in accordance with the new Turkish Earthquake Code [7], about 94% of them will come out as "unsafe" requiring retrofitting! On the other hand the statistics indicate that the ratio of buildings which may survive the earthquake without total collapse is also on the order of 94%. These buildings, comprising 94% of the overall building stock will most probably not experience total collapse; therefore they do not need to be retrofitted, urgently. There is a dilemma regarding the solution to this problem. Which recommendation to follow? Strengthen 94% of buildings, which are found to be "unsafe" in accordance with the earthquake code. This is an impossible task with available

sources and time constraints, or strengthen only the identified 6% of buildings, which will most likely collapse totally during a severe future earthquake.

The difference between the two recommendations is great. For instance, as will be explained later, for the City of Istanbul, a total of USD 25 billion and 25 years are required to retrofit 94% of buildings. However, only USD 0.8 billion will be required to retrofit only the collapse vulnerable buildings (6%), if they can be identified with a reliable tool. . Then, no retrofitting will be necessary for the remaining 94%, as far as the life safety is concerned. The success for "zero" loss of life is evident as will be explained below and the dilemma will thus be eliminated!

A conceptual approach to overcome the above-mentioned retrofitting dilemma has been proposed earlier [6]. Any and all buildings private or public, residential or retail, hospital, or school will be inspected by a team of experts, including a civil engineer, an architect, and a geophysical engineer. The team members will collect a series of "photographic" data about the building, as will be outlined in Section 4.4. No 3D computer analyses, no insitu testing, no laboratory investigation will be conducted in this initial phase of preliminary assessment process. The basic structural data about the load carrying system will be obtained either from the design drawings, if available, or/and from some simple insitu measurements at ground floor level only.

The possibilities of collapse will be assessed, after the site collected data is recorded and stored into the computer. A series of point grades, as well as indexes are assigned to each building, on the basis of pre-determined damage criteria. The damage criteria used for scoring and indexing purposes, have been calibrated through the real data obtained from the damaged and/or collapsed buildings during the past earthquakes [8–15].

The percentage of buildings to be classified as "candidate" for total collapse is about 5–7% within the Marmara region [16]. These "collapse susceptible" buildings will be either strengthened or vacated, then the possibility of loss of life, during a future severe earthquake, will be theoretically "zero". Hence, it will be a great success and a national pride to arrive at such a happy end, with zero loss of life.

4.4 P25 – Rapid Scoring Technique

The basic features of the *P25 – Rapid scoring technique* will be explained herein. It has been initially proposed by Bal [10] and then developed and calibrated through a research project supported by *TUBITAK* (*Turkish Scientific and Technical Research Council*) [15]. The method is applied to 323 RC buildings with different damage states, located on different soil conditions and subjected to various seismic actions [10, 11, 13–16]. It is called "*The P25-Rapid scoring technique*" utilizing some 25 different structural features, which are either measured or observed visually and then the building performance score is determined by means of simple calculations.

The proposed method is primarily based on calculating of the cross sectional areas and moments of inertias of the structural members and infill walls as well as on observing and listing the most important structural parameters which may affect the seismic response of a building. The basic parameters of the methodology

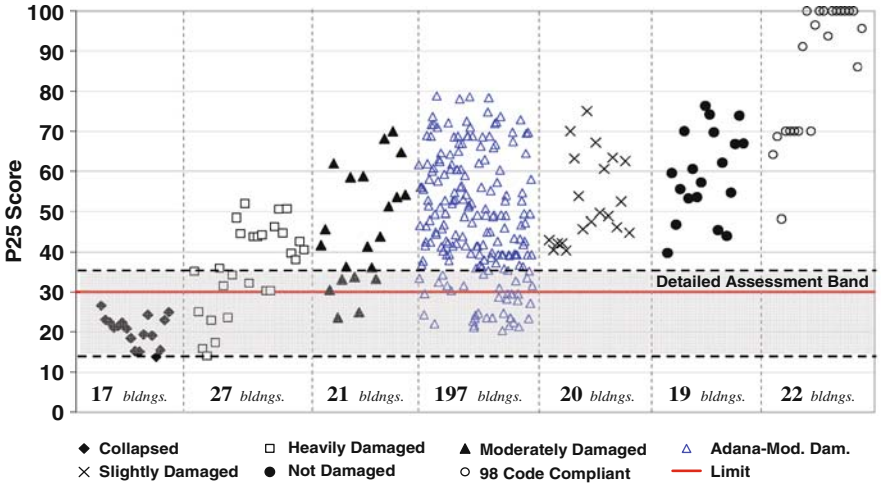

Fig. 4.4 P25 scores for 323 case study buildings experienced wide range of damages

may be listed as (a) cross-sectional dimensions of RC columns, shear walls and infill walls at the critical floor, (b) storey heights, h_i, and the total height of the building, H, (c) outer plan dimensions L_x *and* L_y of ground floor, (d) typical beam dimensions, (e) effective ground acceleration, (f) building importance factor, (g) soil conditions and soil profile, (h) other observational or measurable parameters like material quality, confinement zones of columns, various structural irregularities such as torsion, frame discontinuity, etc.

The method considers seven different failure scores P1 to P7 and their interactions, if any. The final performance score P, of the building is an amalgamation of these seven scores and is graded between 0 and 100, varying from the worst to the best, respectively. Recent studies on some hundreds of buildings [10, 11, 13–16] show that the performance score of 30 may be considered as the safety-limit as shown in Fig. 4.4. Buildings below this score are suggested to be assessed in detail by exact analytical and experimental techniques.

Parameters of the method, as described hereinafter, have been calibrated by employing intensive analytical work related to the real buildings damaged during the past earthquakes. Several case study buildings have been subjected to nonlinear static and dynamic analyses to obtain the average values of the parameters proposed. Details of those calibration analyses, as well as the validation of the method by using detailed assessment methods, as described in the Turkish earthquake code [7], may be found in [15, 16].

4.4.1 Calculation of the Basic Score, P_1

The most collapse vulnerable storey in a building is believed to be the ground floor, which is called as the "*critical storey*" in this particular scoring technique. However, some exceptions to this rule may exist. Thus, to be on the safe side, all possible other

weak storeys should be checked and the storey which results in the smallest score should be accepted as the "*critical storey*". Plan dimensions L_x and L_y are the x and y-sides of the smallest rectangle into which the plan of the critical storey may be inserted. Thus, the buildings with irregular plan dimensions will be penalized in scoring since a relatively larger plan area than the actual will have to be considered.

Eventually, for the *critical storey*, the floor area will be calculated as $A_p = L_x L_y$ and the moments of inertia values of the plan area will be calculated as $I_{px} = L_y L_x^3/12$ and $I_{py} = L_x L_y^3/12$. The sum of the cross-sectional areas and the moments of inertias of columns, shear walls and masonry infill walls will be divided by the overall floor area and moments of inertia, respectively. This operation is applied to both x and y- directions and effective statistical minimum values $C_{A,ef}$ and $C_{I,ef}$ are selected as follows:

$$C_A = 2\,(10^5)\,A_{ef}/A_p \tag{4.1}$$

(calculate in x and y)

$$C_I = 2\,(10^5)\,(I_{ef}/I_p)^{0.2} \tag{4.2}$$

(calculate in x and y)

$$C_{A,ef} = [0.87\ C_{A,min}^2 + 0.50\ C_{A,max}^2]^{0.5} \tag{4.3}$$

$$C_{I,ef} = [0.87\ C_{I,min}^2 + 0.50\ C_{I,max}^2]^{0.5} \tag{4.4}$$

in which,

$$A_{ef} = \sum [A_c + A_s + (E_m/E_c)\,A_m] \tag{4.5}$$

$$I_{ef} = \sum [I_c + I_s + (E_m/E_c)\,I_m] \tag{4.6}$$

The final score $\boldsymbol{P_1}$ is obtained as

$$P_1 = \left(\frac{C_{A,ef} + C_{I,ef}}{h_0}\right) \prod_{i=1}^{14} f_i \tag{4.7}$$

$$h_0 = -0.6H^2 + 39.6H - 13.4 \tag{4.8}$$

In above equations, $E_m$is the modulus of elasticity of masonry infills, E_c is the modulus of elasticity of concrete, A_s, A_c and A_m are the areas of the shear walls, columns and masonry walls, respectively. Finally, I_s, I_c and I_m are the moments of inertia of shear walls, columns and masonry walls, respectively.

The correction factors f_i for various irregularities and weaknesses are listed in Table 4.1. Since, the cross-sectional dimensions of vertical structural elements at ground floor (critical storey) increase with the overall height H of the building; it is also included as a correction parameter h0 in the evaluation of *P1*. As the number of storeys increases, the mass as well as the base shear will also increase. On the other hand, depending on the soil group, the base shear coefficient obtained from the response spectrum gradually decreases as the overall height of the building increases. Therefore, for low and medium rise buildings, the increase

Table 4.1 Correction factors of irregularity (f_i)

Factor	Irregularity	Degree of irregularity		
		High	Medium	None
f_1	Torsional irregularity	0.90	0.95	1.00
f_2	Slab discontinuity	0.90	0.95	1.00
f_3	Vertical discontinuity	0.65–0.70	0.90	1.00
f_4	Distribution of mass	0.75	0.85	1.00
f_5	Corrosion	0.80	0.90	1.00
f_6	Heavy facade elements Mezzanine floor	0.90	0.90	1.00
f_7	*(γ=Mezzanine floor/Full area)*	0.90 $\gamma \geq 0.25$	0.95 $0 < \gamma < 0.25$	1.00 $\gamma = 0$
f_8	Unequal levels of floor	0.80	0.90	1.00
f_9	Concrete quality[a]	$f_9 = (f_c/20)^{0.5}$		
f_{10}	Strong column criterion[b]	$f_{10} = [(I_x + I_y)/2\ I_b]^{0.15} \leq 1.0$		
f_{11}	Lateral tie spacing[c]	$f_{11} = 0.60 \leq (10/s)^{0.25} \leq 1.0$		
f_{12}	Soil type[d]	0.90 (Z_4)	0.95 (Z_3)	1.00 (Z_2, Z_1)
f_{13}	Foundation type	0.80–0.90 (*singular*)	0.95 (*continuous*)	1.00
f_{14}	Depth of foundation	0.90 ($D < 1$ *m*)	0.95 ($1 \leq D \leq 4$ *m*)	1.00 ($D > 4$ *m*)

[a] f_c is the 28th day strength of concrete in MPa.
[b] I_x, I_y are the average column moments of inertia values, whilst I_b is the moment of inertia of a typical beam.
[c] s is the tie spacing within the confinement zone in cm.
[d] Z_1, Z_2, Z_3 and Z_4 soil types in the Turkish Earthquake Code approximately correspond to soil types A, B, C and D, respectively as defined in Eurocode 8.

in height adversely affects the strength parameter *P1*. For taller buildings however, the increase in height has a favourable effect in the calculation of *P1*.

Considering all these variations, a suitable correction factor h_0, is proposed as seen in Eq. 4.8, which represents the effect of building height. This correction factor becomes h_0=*100* for H= 3 m, the single storey building *(nominal value)* and becomes h_0=466 for a 5-storey building with H=15 m. The formula has been obtained by generating around 9-thousand buildings having several different design input values. The change in dimensions of the structural elements depending on H = the total height of the building has been investigated. The final regression analysis yielded the formula given in Eq. 4.8.

4.4.2 Short Column Score, P_2

A short column is relatively shorter than all the others in a given floor thus leading to an increased shear demand and nonductile shear failure during a severe earthquake. There are six different scores for short columns, varying between *20* and *70* as seen in Table 4.2, according to the Short Column Height/Storey Height ratios and the ratio of the number of short columns to the total number of columns at the critical storey (n).

Table 4.2 Short column score, *P2*

	Short column hight/storey height [a]	
n=Ratio of the number of short columns	>2 /3	≤2 /3
A few n < 15 %	70	50
Some 0.15 ≤ n ≤ 0.30	50	30
Very many n > 0.30	45	20

[a]Height of the critical storey where short columns exist.

4.4.3 Soft-Weak Storey Score, P_3

There is a tendency to accommodate commercial functions at ground floors, such as show rooms, shopping centers, banks, etc., resulting in relatively higher storey heights and lack of masonry infill walls. This phenomenon may be reflected in the score P_3 as follows:

$$P_3 = 100\ [r_a r_r\ (h_{i+1}/h_i)^3\ ]^{0.60} \tag{4.9}$$

$$r_a\ = \left(A_{ef,i}/A_{ef,i+1}\right) \leq 1 \tag{4.10}$$

$$r_r\ = \left(I_{ef,i}/I_{ef,i+1}\right) \leq 1 \tag{4.11}$$

in which, r_a and r_r are the total cross-sectional areas and moments of inertias of columns, shear walls and infill walls, respectively as shown in Eqs. 4.5, 4.6. The values r_a and r_r are calculated for both x and y- directions and average of these values are utilized in Eqs. 4.10, 4.11.

4.4.4 Frame Discontinuity Score, P_4

The overhang of the structural floor slabs above the ground floor is one of the most traditional characteristics of the Turkish residential architecture. This particular overhang feature adversely affects the safe earthquake response of reinforced concrete buildings since it changes the mass distribution, plan regularity and frame action. In fact, there are no perimeter beams to connect the lines of perimeter

Table 4.3 Discontinuity of peripheral frame, *P4*

	Location of overhang		
Beams	At single facade	At two facades	At all facades
Existing	90	80	70
None	70	60	50

columns, thus leading to reduction in lateral strength. Bal and Ozdemir [17] studied this issue on a number of buildings and proposed to consider a decrease in strength varying between 4% and 54%. Following this proposal the score P_4 is assumed to vary between 50 and 90 as summarised in Table 4.3.

4.4.5 Pounding Failure Score, P_5

Pounding of any two adjacent buildings may be either eccentric or concentric type [18, 19]. The concentric pounding occurs if the line connecting the centers of the mass of the two adjacent buildings passes through the mid-point of the common sides along the edge where two buildings are expected to hit each other. The other cases are called the eccentric pounding. There are 16 different scores of pounding as shown in Table 4.4, depending on the types of positions of buildings. The most favourable pounding occurs (score of 75) when the two adjacent buildings are of the same height, their slabs are at the same elevations, and they experience concentric pounding.

Table 4.4 Pounding score, *P5*

Type of impact	Concentric impact		Eccentric impact	
	Slabs at equal level	Slabs at different level	Slabs at equal level	Slabs at different level
The last block within a row	60	30	40	25
Two unequal buildings	55	30	35	25
Low-rise next to high-rise	75	40	50	35
Two identical buildings	75	50	65	45

4.4.6 Soil Failure Scores, P_6 and P_7

The liquefaction score, P_6 is given in Table 4.5 to vary between 10 and 60, depending on the level of *GWT*=ground water table and the calculated liquefaction risk potential to be as "low", "medium" or "high" [3]. Soil bearing capacity failure score P_7 is given in Table 4.6 to vary between 10 and 100 depending on the soil type and depth of *GWT*.

Table 4.5 Liquefaction score, *P6*

GWT *(m)*	Calculated liquefaction potential		
	Minor	Medium	High
> 10 m	60	45	30
2.0 m–10.0 m	45	33	20
< 2.0 m	30	20	10

Table 4.6 Soil movements score, *P7*

Soil Type	GWT (m)	P_7
Z_1, Z_2	–	100
Z_3	GWT ≤ 5.0	25
	GWT> 5.0	35
Z_4	GWT ≤ 5.0	10
	GWT> 5.0	20

Z_1, Z_2, Z_3 and Z_4 soil types in the Turkish Earthquake Code approximately correspond to soil types A, B, C and D defined in Eurocode 8.

4.5 Final Score in the P25 – Method

The final score should be adjusted by means of a correction factor, α, defined in accordance with the values of building importance factor, the effective ground acceleration, the level of participation of live loads and the topographic effects, given as follows:

$$\alpha = (1/I)\,(1.4 - A_0)[1/(0.4n + 0.88)]\,t \tag{4.12}$$

The building importance factor, I, is reflected in the correction factor as inverse proportional. The level of effective ground acceleration, A_0, varies between 0.10g and 0.40g for the four different earthquake zones in Turkiye. Normally, the live load participation factor, n =0.30 is used for residential buildings. The correction for topographic effects, t, is assumed as 0.7 if the building is on top of a hill, while t =0.85 if the building is on a steep slope and t=1 for buildings on lower elevations. The increase in earthquake demand due to topographic effects has been based on the two earlier studies [20, 21].

The correction factor, β, is calculated by considering the weighted interaction among the parameters from P_1 to P_7. The minimum of these seven scores is considered as P_{min} and the weight, is assumed as w=4 for this minimum parameter. The weighting factors for other scores are shown in Table 4.7. The weighted score, P_w, is calculated as

$$P_w = \sum (w_i P_i) \Big/ \sum w_i \tag{4.13}$$

The interaction correction factor, β, represents the degree of interaction and the possibility of triggering an interactive failure and is recommended, to be as follows:

Table 4.7 Weighting factors for *P1* to *P7*

Weighting factor	P_1	P_2	P_3	P_4	P_5	P_6	P_7	P_{min}
w	4	1	3	2	1	3	2	4

$$\begin{aligned} &\beta = 0.70 \ \ for \ \ P_w \leq 20 \\ &\beta = 0.55 + 0.0075 P_w \ \ for \ \ 20 \leq P_w \leq 60 \\ &\beta = 1.00 \ \ for \ \ P_w \geq 60 \end{aligned} \tag{4.14}$$

The final score, P, is then calculated by selecting P_{min} which is the smallest score among P_1 to P_7 as follows:

$$P = \alpha \beta P_{\min} \tag{4.15}$$

Application of the *P25- rapid scoring technique* on 323 real buildings shows that the high risk band is between scores of P=15 and P=35 and the performance score of 30 may then be considered as the safety-limit, as shown in Fig. 4.4. Buildings in high risk band are strongly suggested to be assessed in detail by expert engineers, and if they are determined to be collapse vulnerable for sure, they should be evacuated or retrofitted. The method is still in development stage and will be validated and updated as more additional data become available.

4.6 Conclusions

The preparation of appropriate earthquake risk zones, the implementation of risk management strategies, as well as the disaster control preparations in a country are very complex issues and the interdisciplinary activities require expertise, extensive time and money. If however, there is an awareness of the importance of these issues in the minds of politicians, administrators, professionals, researchers and the public in general, the path to success is wide open.

It should be remembered that a dollar spent before the earthquake for any activity to mitigate the possible earthquake losses will be recovered by multifold, at least twenty to fifty times, in the way of savings and reductions in direct and indirect losses due to earthquakes. Therefore, the pre-earthquake risk management activities and projects should be of much higher priority and importance compared to the preparations related to the emergency management operations.

In light of above discussions, the proposed project of "zero loss of life" has been discussed in detail in this paper. The amount of funding necessary for the City of Istanbul to achieve "zero" loss of life, for example including both the rapid scoring and also the exact scientific assessment stages of study is around 800 million USD. If however, the route of strengthening of all "unsafe" buildings was blindly selected, then the cost would have exceeded 25 billion USD, which is more than thirty folds higher.

As part of the efforts of reducing the life losses theoretically to zero, a preliminary assessment method, called the P25-rapid scoring technique has been introduced in this paper. Its application in a metropolitan area will not only save lives, but will also save considerable time and money. The P25 rapid scoring technique to determine the collapse vulnerability of RC buildings as part of the risk management projects outlined above enables the central and/or local governments to reduce the loss of life to a theoretical "zero" value, simply by strengthening only those

buildings, which are assessed as "candidates for total collapse". Such a project should have the highest order of priority in risk management of a country, since it is directly related to public safety.

Acknowledgments The writers gratefully acknowledge the financial support extended by TUBITAK, Turkish Scientific and Technical Research Council, through the Grant No. 106M278.

References

1. Tezcan SS, Ipek M, Aydan O, Ozbek M and Akguzel U (2002) Sultandagi, Afyon depremi inceleme raporu. Turkish Earthquake Foundation (http://www.depremvakfi.org) Istanbul
2. Tankut T (2002) Earthquake risk mitigation strategy for Turkiye. International seminar on seismic risk mitigation 20th Year celebrations of CLSMEE, Bulgarian Academy of Sciences, Sofia, Bulgaria
3. Tezcan SS and Ozdemir Z (2004) Liquefaction risk analysis and mapping techniques. Higher education and research foundation publications, Etiler, ISBN 975-93005-1-6, (www.egitim-arvkfi.org)
4. Tezcan SS (2001) Insurance systems for earthquake damage indemnity in Turkiye. International seminar on natural hazards and insurance systems, Turkish National Reassurance Co., Istanbul, Turkiye, (http://www.millire.com.tr)
5. Tezcan SS, Boduroglu H (1998) A reconnaissance report – The June 27, 1998 Adana-Ceyhan earthquake, Turkiye. Turkish Earthquake Foundation, www.depremvakfi.org, Istanbul
6. Tezcan SS and Gursoy M (2002) 'Zero' loss of life during a future earthquake. Proceedings of the regional workshop on seismic hazard and risk management, Tsakhadzor, Armenia, 24–27
7. Turkish Earthquake Code (2007) Specifications for the buildings to be constructed in earthquake hazardous areas. Ministry of Public Works and Settlement, Ankara, Turkiye
8. Hassan AF and Sozen MA (1997) Seismic vulnerability assessment of low-rise buildings in regions with infrequent earthquakes. ACI Structural Journal 94(1): 31–39
9. Yakut A (2004) Preliminary seismic performance assessment procedure for existing reinforced concrete buildings. Engineering Structures 26:1447–1461
10. Bal IE (2005) Rapid assessment techniques for collapse vulnerability of reinforced concrete structures. Master thesis Faculty of Civil Engineering Istanbul Technical University
11. Bal IE, Tezcan SS and Gulay FG (2006) Advanced applications of the P25 scoring method for the rapid assessment of RC buildings. Proceedings of the 1st ECEES, Geneva
12. Yakut A, Ozcebe G and Yucemen MS (2006) Seismic vulnerability assessment using regional empirical data. Earthquake Engineering and Structural Dynamics 35:1187–1202
13. Bal IE, Tezcan SS and Gulay FG, (2007) P25 rapid screening method to determine the collapse vulnerability of RC buildings. In: Proceedings of 6thNational Conference on Earthquake Engineering, Istanbul, Turkiye, 16–20 October 2007 *(in Turkish)*
14. Bal IE, Gulay FG and Tezcan SS, (2008) A new approach for the preliminary seismic assessment of RC buildings: P25 Scoring Method. In: The 14th World Conference on Earthquake Engineering October 12–17, 2008, Beijing, China
15. Gulay FG, Bal IE, Tezcan SS (2008) Calibration of the P25 Scoring Method developed for the seismic safety of reinforced concrete buildings and its application on a pilot region. TUBITAK (Turkish Scientific and Technical Research Council) Research Project No 106M278, Final Report (in Turkish)
16. Gulay FG, Bal IE and Gokce T (2008) Correlation between detailed and preliminary assessment techniques in the light of real damage states. Journal of Earthquake Engineering 12(1):129–139

17. Bal IE and Ozdemir Z (2006) The adverse effects of perimeter frame discontinuity on earthquake response of RC buildings. Proceedings of the 7th International Congress on Advances in Civil Engineering Yildiz Technical University, Istanbul, Turkiye
18. Athanassiadou CJ, Penelis GG and Kappos AJ (1994) Seismic response of adjacent buildings with similar or different dynamic characteristics. Earthquake Spectra 10(2):293–317
19. Tezcan SS and Ipek M (1996) A reconnaissance report – October 1, 1995 Dinar, Turkiye Earthquake. Engineering Structures 18(12):906–916
20. Sholtis SE and Stewart JP (1999) Topographic effects on seismic ground motions above and below a cut slope in sand. Research Report, University of California, Department of Civil and Environmental Engineering
21. Celebi M (1987) Topographical and geological amplifications determined from strong-motion and aftershock records of the 3 March 1985 Chile Earthquake. Bulletin of Seismological Society of America 77(4):1147–1167

Chapter 5
The Importance of Plan-Wise Irregularity

Paolo Negro and Elena Mola

Abstract In the framework of the experimental activity of the ELSA Laboratory of the JRC, an extensive PsD testing campaign was carried out on a doubly bi-eccentric plan-wise irregular RC frame structure representative of non-seismically designed buildings widespread in Europe. In spite of the torsional irregularity being minor, the torsional response turned out to be quite significant, as a result of the choice of the seismic input. The opportunity was thus taken of experimentally assessing the effects of irregularity on the seismic behaviour and to compare it to the effects of poor structural detailing and lack of basic seismic design requirements. Also, the effectiveness was assessed of two different retrofitting strategies, a ductility-only intervention and a strength-only one, in providing a satisfying seismic response and tackling the structural weaknesses detected by the tests in the unretrofitted configuration. Conclusions are thus drawn on the basic criteria to be taken into account when devising a retrofitting strategy for existing irregular buildings under strict time and budget constraints. Also, it is discussed if whether a reduction of torsional effects is a basic aim to be pursued in retrofitting under above said constraints or if it can be neglected in the decision making process, even though the role of torsional effects in affecting the response is indisputably acknowledged.

5.1 Introduction

The importance of the effects of plan- or height-wise irregularity in the structural arrangements on the global seismic response of structures has long been understood and largely acknowledged, with an ever increasing bulk of research efforts in the field and the ever growing awareness of the complexity of the problem.

A certain degree of irregularity, on the other hand, represents a quite common feature in the existing building stock, given the fact that, until the last decades, no specific investigations or provisions for an optimum seismic behaviour of the

P. Negro (✉)
ELSA Laboratory JRC, Via E. Fermi, 1, 21020 Ispra, VA, Italy
e-mail: paolo.negro@jrc.it

A. Ilki et al. (eds.), *Seismic Risk Assessment and Retrofitting*, Geotechnical, Geological, and Earthquake Engineering 10, DOI 10.1007/978-90-481-2681-1_5,

structural systems were taken in design, so that the possibly hazardous effects of irregularity were not taken into account and, especially in the case of plan-wise irregularity, the opportunity of saving room for staircases or cores, a better internal arrangement of housing units or simple feasibility issues induced designers to quite freely adopt unsymmetrical arrangements of vertical elements, both in terms of location, stiffness and (often unaware) of strength.

It has thus long become clear that, when faced with the problem of assessing the seismic vulnerability of existing structures, the importance of the critical issues related to irregular configuration cannot be disregarded.

Still, irregularity introduces a number of additional issues of inherent complexity in the estimation of the main features of the seismic response, often requiring more refined analysis tools than those practicing engineers are familiar and confident with. Moreover, it is inherent in the assessment process itself that strict and compelling time, budget and computational costs restraints are often present, and that sound decision making tools, based on easily expressed and quantifiable criteria, need to be produced as an outcome of the assessment process, in order to enable the owner/users or the competent bodies to make decisions as to the opportunity of retrofitting, non-retrofitting, or rebuilding and to choose the most effective retrofitting strategy, in terms of costs, downtime and enhanced performance in the event of an earthquake.

Given the above reported remarks, the effective importance of torsional irregularity as a basic design criterion to lead the design of rehabilitation strategies for existing buildings has been investigated, taking advantage of the experimental and analytical activities carried out in the framework of the EC-funded research project named SPEAR.

The present paper thus reviews, under a different light, the motivations and outcomes of the research activity carried out in the recent past at ELSA in the framework of said research project, which was specifically targeted to a comprehensive investigation on the seismic behaviour of existing irregulars structures. The aim is to assess if, given the undisputed importance of torsional effects arising even from moderate eccentricities (as shown by the experimental tests), a valid and even more convenient (from the global point of view of costs, downtime, computational and design time) rehabilitation strategy for the bulk of the building stock can be conceived by-passing irregularity issues and be based on other basic criteria, more familiar to the practicing engineer, in particular local ductility enhancement.

The outcomes of the experimental and numerical activities of the SPEAR project taught very interesting lessons at this regard, leading to conclusions along the above reported lines, as detailed in the present paper.

5.2 The SPEAR Project: Framework, Motivation, Methods

The EU-funded research project named SPEAR (*S*eismic *Pe*rformance *A*ssessment and *R*ehabilitation of Existing Reinforced Concrete Buildings) and specifically aimed at assessing and retrofitting of existing buildings, was carried out in the past

few years by a European consortium with the co-ordination of the ELSA Laboratory. The activity of the project makes up the framework in which the presently reported critical review of the importance of torsional issues as a vulnerability reduction criterion was carried out. A complete description of the SPEAR project, can be found elsewhere [1, 2]; for the purposes of the present paper, the description will be limited to the parts relevant to the understanding of the experimental outcomes and the choice of the retrofitting strategies.

The SPEAR project was meant to provide a critical review and improvement of current seismic assessment procedures and retrofitting design strategies, by means of a balanced mix of experimental and numerical activities; the former objective was pursued through a 'blind' assessment exercise: a benchmark structure (the so-called SPEAR structure) was designed to be representative of older southern European construction prior to the latest generation of seismic codes; the structure thus exhibited a number of sub-standard details, total lacking of lateral resistance provision and plan-wise irregularities adding up to a 10% double eccentricity. Four world-widely used assessment procedures (i.e. FEMA 36, New Zealand Assessment Guidelines, Japanese Assessment Guidelines, EC8 Part 3) were then applied to the benchmark structure, with the aim of quantifying their relative performance, both in terms of immediateness in the application and of scatter in the results. Finally, the benchmark structure underwent a complete series of full-scale bi-directional pseudodynamic tests in its as-built configuration: by comparing the experimental data to the predictions of the assessment procedures, it was also possible to assess effectiveness of the latter in highlighting the actual weaknesses and hazards of the benchmark structure. As a final step, improvement to the current approaches were proposed, some of which were actually incorporated in the latest version of EC8 part 3. The outcomes of the former activity are critically reviewed in a companion paper, [3].

In the following phase, two conceptually different retrofitting strategies were conceived and implemented: the first strategy was a ductility-only intervention, where all the vertical elements, badly lacking confinement in the plastic hinging areas, were provided with such confinement by means of fiber reinforced polymer (FRP) wrapping.

In the case of the second retrofitting strategy, the effectiveness of a design strategy based on more challenging concepts, such as the one of strength re-allocation and torsional mechanisms control was explored.

The designed strategy took the origin from the basic concepts of reducing the torsional components of the seismic response of the specimen, which had been highlighted in the response of the as-built structure, by means of a reduction of the eccentricity of the plastic centre with respect to the centre of mass. The implementation of the strength re-location was made by means of the traditional technique of concrete jacketing, limited to selected elements, based on the balance between the results of numerical analyses and the practical feasibility of the intervention.

In the following, at first a description of the SPEAR structure is provided; after that, the design, implementation and comparative evaluation of the two retrofitting interventions is presented. The comparative review of the experimental data collected in the tests in the as-built and retrofitted configurations will thus be used to

draw conclusions of broader meaning on the relative importance of different possible criteria to be assumed as leading when designing effective retrofitting strategies for existing buildings.

5.3 The SPEAR Structure

As briefly mentioned above, the SPEAR structure is a simplification of an actual three-storey building representative of old constructions in southern European Countries, such as Greece, without specific provisions for earthquake resistance. It was designed for gravity loads alone, using the concrete design code enforced in Greece between 1954 and 1995, with the construction practice and materials typical of the early 70s; the structural configuration and detailing show the lack of consideration of the basic principles of earthquake resistant design.

The materials used for the structures are also those typical of older practice: for concrete a nominal strength $f_c = 25$ MPa was assumed in design; smooth rebar steel was used; given the scarcity of the current production, it was only possible to find bars with a characteristic yield strength larger than initially requested ($f_y \approx 450$ MPa instead of $f_y = 250$ MPa); the end hooks for the steel bars were designed following the minimum requirements of old codes.

The structure is regular in elevation: it is a three-storey building with a storey height of 3 m. The plan configuration is non symmetric in two directions (Fig. 5.1), with 2-bay frames spanning from 3 to 6 m; the presence of a balcony on one side and of a part of the structure 1 m (in the weak direction) or 0.5 m (in the strong one) longer than the rest increases the plan irregularity, shifting the centre of stiffness away from the centre of mass.

The concrete floor slabs are 150 mm thick, with bi-directional 8 mm smooth steel rebars, at 100, 200 or 400 mm spacing.

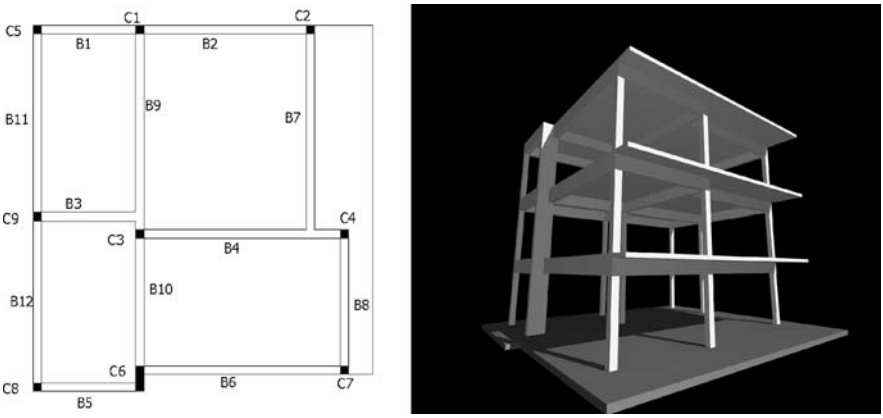

Fig. 5.1 The SPEAR structure: plan and 3D view

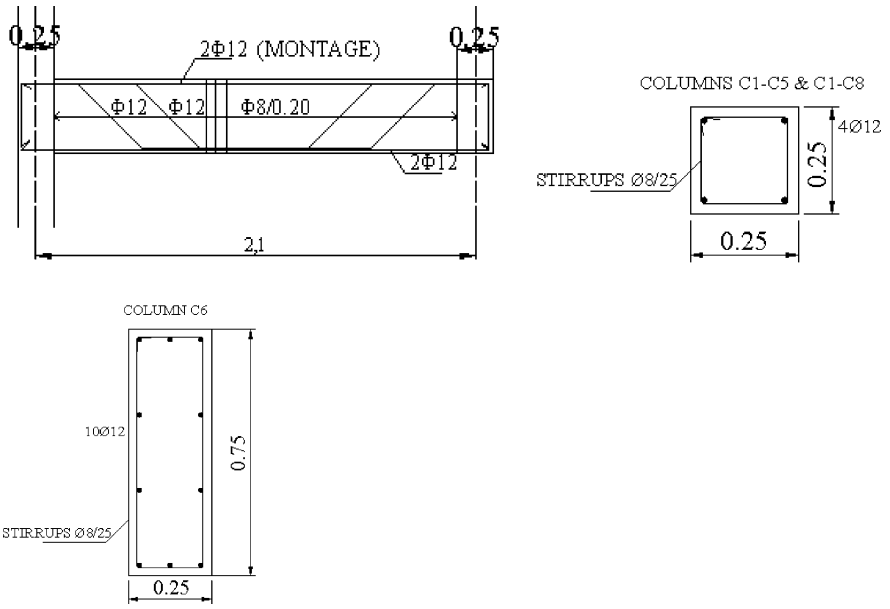

Fig. 5.2 Details of the beam and column rebars

Details of the rebar of one of the beams are shown in Fig. 5.2. Beam cross-sections are 250 mm wide and 500 mm deep. Beams are reinforced by means of 12 and 20 mm bars, both straight and bent at 45° angles, as typical in older practice; 8 mm smooth steel stirrups have 200 mm spacing. The confinement provided by this arrangement is thus very low.

Eight out of the nine columns have a square 250 by 250 mm cross-section; the ninth one, column C6 in Fig. 5.1, has a cross-section of 250 by 750 mm, which makes it much stiffer and stronger than the others along the Y direction, as defined in Fig. 5.3, which is the strong direction for the whole structure.

As can be seen in Fig. 5.2, all columns have longitudinal reinforcement provided by 12 mm bars (4 in the corners of the square columns, 10 along the perimeter of the rectangular one). Columns' longitudinal bars are lap-spliced over 400 mm at floor level. Column stirrups are 8 mm with a spacing of 250 mm, the same as the column width, meaning that the confinement effect is almost non-existent.

The joints of the structure are one of its weakest points: neither beam nor column stirrups continue into them, so that no confinement at all is provided. Moreover, some of the beams directly intersect other beams, so that beam-to-beam joints without the support of columns originate.

Design gravity loads are 0.5 kN/m^2 for additional dead load and 2 kN/m^2 for live load.

As described above, the structure is regular in elevation and has the same reinforcement in the beams and columns of each storey. The resisting elements in both directions are all of the same kind (frames). All of these features mean that the structure belongs to a special class of multi-storey buildings, the so-called regularly

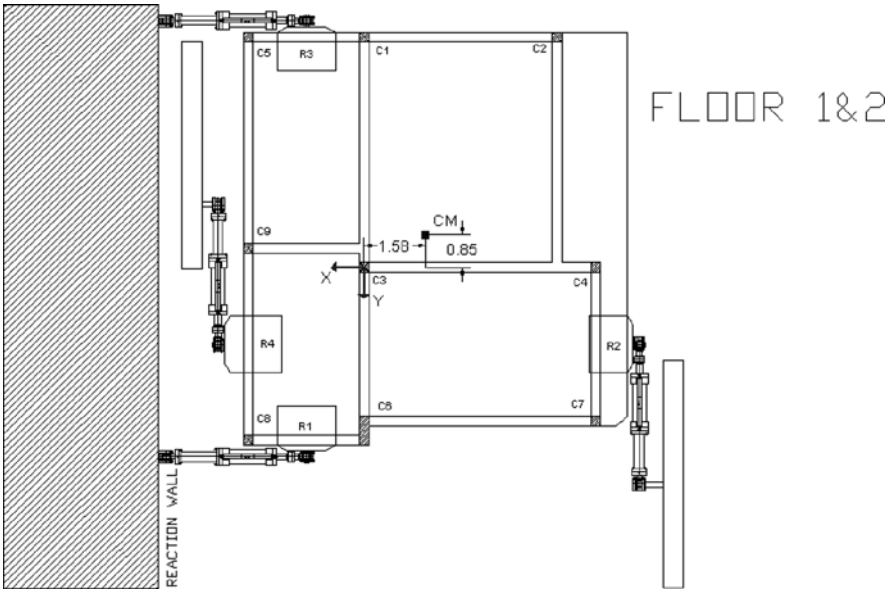

Fig. 5.3 Location of the CM of the structure

asymmetric multi-story structures, in the sense that the centre of mass (CM), the centre of stiffness (CR) and the centre of strength (CP) of each storey are located along three vertical lines separated by the distances $e_r$and e_s.

The centre of stiffness (based on column secant-to-yield stiffness) is eccentric with respect to the mass centre by 1.3 m in the X direction (~13% of plan dimension) and by 1.0 m in the Y direction (~9.5% of plan dimension).

The reference system used in the PsD test and the location of the CM of the structure at the first and second floor are shown in Fig. 5.3. The origin of the reference system is in the centreline of column C3. The coordinates of the CM of the first two storeys with respect to this reference system are (–1.58 m, –0.85 m); at the third storey the coordinates of the CM vary slightly, becoming (–1.65 m, –0.94 m).

5.4 Critical Review of the Experimental Results

5.4.1 As-Built Configuration

A detailed discussion of the outcomes of the experimental activity on the structure in its as-built configuration and of the analysis of the relevant measured data can be found in [2–4]: in the following, the outcomes of the analyses in the as-built configuration are reported as for what is relevant to the understanding of the most remarkable effects of the moderate plan eccentricities on the seismic response.

The most significant features of the seismic response of the SPEAR irregular specimen that came out of the PsD tests in the as-built configuration were also

presented and discussed in detail in [6] and in a companion paper [3], with a focus on an evaluation of the performance of codified assessment procedures in correctly predicting such aspects.

First of all, torsional effects strongly affected the response, in an often unpredictable way: a comparison between the drift measured at the CM and the drifts of the edge columns, the most deformed ones, clearly showed that the effects of torsion on the drifts of the edge columns were remarkable in both directions. In the X direction, where the structure was more flexible and the drift at the CM was already quite large, the maximum drift reached at the CM was 55 mm, whereas the maximum drift reached at the edge columns C1, C2 and C5 was about 70 mm, a difference that is not negligible. In the Y direction the maximum drift reached at the CM was 45 mm, whereas the maximum drift of the edge columns C4 and C7 was above 70 mm, i.e., more than 50% larger.

These large increases are larger than could be expected when considering the values of plan eccentricity of the structure in themselves: an eccentricity of around 10% is defined in all currently codified assessment procedures [2] as not likely to have major effects. Nevertheless, it was proven by the test that in this case the interaction of the eccentricity in both directions had a role that cannot be neglected in enhancing the torsional effect on the response even if the two eccentricity values were not large.

Moreover, the failure mechanism developed by the specimen was of the soft-storey kind but at the second floor and not at the first one, as was reasonably expected due to the higher axial load of first storey columns that would negatively affect the ductility capacity of their cross sections: the effects of higher modes and the dynamic amplification of eccentricity were clearly pointed out by this behaviour, which confirmed that they are very important factors in affecting the behaviour of multi-storey plan-irregular buildings, [8].

5.4.2 Torsional Issues vs Other Critical Issues

The damage pattern was influenced both by torsional effects and by poor local detailing; in fact, damage was expected to develop in the vertical elements at the lower storey, due to their increased axial load, which further reduces ductility resources. Moreover, it was expected to develop at the level of lap splicing, i.e. 400 mm from the bottom of the columns, due to very low confinement and the presence of two hooks in bars (smooth steel rebars were used).

These expectations, based on engineering judgment and confirmed by pre-test numerical analysis, were partly overridden by the experimental results: the damage patter was that corresponding to a soft storey failure mechanism developing at the second storey instead of the first.

This phenomenon, not easily justifiable in the beginning, was later explained (also by means of a piecewise non linear modal analysis method applied to the experimental data series, as fully reported in [4, 5]) with higher mode effects caused by the irregular plan configuration, which affected the relative importance of the rotational and translational components of the response throughout its duration and

produced a twisting mechanism of the second storey columns, which were pressed in-between the first and third floor, whose rotational components of the response were in opposite directions.

As for the location of the damage, the expectations were not fully complied with: most of the damage to the vertical elements was located at their top, instead of at the bottom or lap splicing level; this was another torsion-induced effect.

Still, it became immediately quite obvious that the almost total lack of ductility of the vertical elements (due to the poor structural detailing design) was a key factor in leading to failure and governing the damage development, especially since the drift demand on edge columns was so significantly increased by the rotational component of the response.

In fact, at the top of the elements, heavy spalling of the external layers of concrete was caused by the insufficient presence of stirrups; also, another design inaccuracy, typical of older practice, i.e. that of keeping the cross section and rebar of central columns constant with respect to lateral ones, in spite of heavier axial loading, caused a further reduction of the ductility resources of the central column, which soon exhibited heavy signs of damage and incipient collapse. The transfer of part of the loading to the adjacent ones, due to the exhausted bearing capacity of column C3, soon originated a sort of chain reaction, with damage quickly spreading to the other vertical elements and giving way to a strongly unsafe and non-dissipating failure mechanism. Some of the visible damage exhibited by the structure after the 0.20 g PGA test is reported in Fig. 5.4; it must be reminded that such damage was expected to be significant but not beyond repair, in order to allow the execution of the retrofitting phase.

As mentioned above, in order to further assess the relative importance of torsion with respect to other issues in affecting the seismic behaviour, the two retrofitting strategies that were thus conceived aimed at tackling on one side the shortcomings of the vertical elements in term of ductility supply (FRP wrapping), on the other side at reducing the ductility demand through the reduction of the rotational component of the response (RC jacketing).

Fig. 5.4 Damaged structure after 0.2 g PGA test: (**a**) C3 at 2nd storey; (**b**) C3 at 2nd storey; (**c**) C4 at 2nd storey

5.5 Retrofitting Strategies: Conceptual Design

5.5.1 FRP-Retrofitted Configuration

In this case, the design of the retrofit has then aimed at the local strengthening of structural members in order to prevent undesirable local failures and achieve a more satisfactory seismic behaviour. This can be pursued by means of a light strengthening that, increasing the ductility of columns and boosting the strength of other brittle mechanisms, could allow attaining a more ductile and energy dissipating global performance, [7].

Fiber Reinforced Polymer (FRP) composites represent a sound technique for such light upgrade: they ensure an easy and fast installation, strength and/or ductility increase, high durability, low impact on the use of the structure, almost no increase of mass and geometrical dimensions of the cross-sections. In the majority of the applications Carbon FRP (CFRP) laminates have been used especially when high durability performance are requested or, in general, when the modulus of elasticity of FRP plays a major role (i.e., flexural or shear strengthening).

In cases in which durability does not govern the design (i.e., interior applications in buildings), the use of Glass FRP (GFRP) laminates could represent an interesting and cheaper alternative to CFRP with particular reference to confinement applications. Experimental tests have shown that GFRP confinement of RC columns could allow significant improvements of the column behavior in terms of both strength and ductility, [7]. Based on such considerations, the upgrade of columns by providing them with higher strength and ductility via GFRP confinement was chosen.

The repair/retrofitting intervention was designed to take place in two distinct phases: the first one was the repair phase and the second the retrofitting phase.

The first phase consisted into the strictly necessary interventions needed to repair the damage caused by the test in the "as-built" configuration: detection of cracks, removal of spalled/damaged concrete from columns, reconstruction of the spalled/damaged parts, epoxy injection of all the cracks. This phase was a preliminary work necessary to create the conditions suitable for the application of the fibre wraps, which make up the actual retrofitting intervention.

As for the retrofitting phase, the following designed scheme was adopted: all the columns with square cross-sections (8 per floor at all three storeys) are reinforced by installing two plies of GFRP laminates. The design curvature radius for corner rounding is 20 mm.

Top and bottom of each column are wrapped for 0.60 m from the interface with the joint using MapeWrap G UNI-AX 900/100 laminates characterized by density of 900 gr/m^2, height of 0.60 m, thickness of dry fibers of 0.48 mm/ply, modulus of elasticity of 80.7 GPa and tensile strength of 2560 MPa. Some of the executive drawings of the intervention are reported in Fig. 5.5.

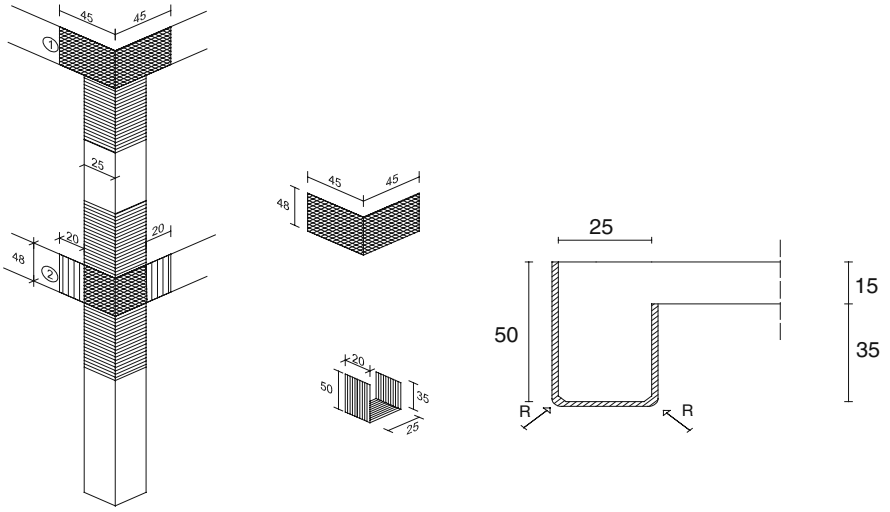

Fig. 5.5 Details of the FRP retrofitting intervention

5.5.2 RC-Jacketed Configuration

The second retrofitting strategy was focused on the improvement of the global response of the structure to the seismic excitation. In this case, the stronger cause of concern in the features of the behaviour exhibited during the tests in the as-built configuration was the excessive increase in the edge column drifts with respect to those of the CM, which was disproportioned to the eccentricities involved. This, together with the unpredicted strong damage developed at the second floor, confirmed the assumption that non negligible interaction effects between the eccentricities in the two directions had arisen, thus amplifying the torsional effects that would have been induced by the same value of eccentricity acting in one direction only.

Moreover, it was deemed interesting to investigate whether torsional effects could be better reduced and somehow controlled operating in the non-linear range of behaviour of the structure, i.e. modifying its lateral strength distribution, rather than acting on the stiffness one, which in fact is only governing the response in the linear range of behaviour, [2–8].

The aim of the second retrofitting intervention was thus to reduce the importance of torsional effects in the response by relocating the centre of strength of each floor of the structure (i.e. the locus where the resultant of the yield moments of the vertical elements is located at each floor), without explicitly tackling stiffness eccentricity.

According to previous research in the field, [8], in fact, in the inelastic range of the response torsional effects are mainly governed by strength eccentricity, rather than stiffness eccentricity.

In view of this, it was the subject of extensive research in previous years how to obtain the optimal location of the CP in plan-wise irregular structures to most effectively reduce the torsional component of the response, as opposed to the reduction of the stiffness eccentricity in design (or re-design, as in the case at hand).

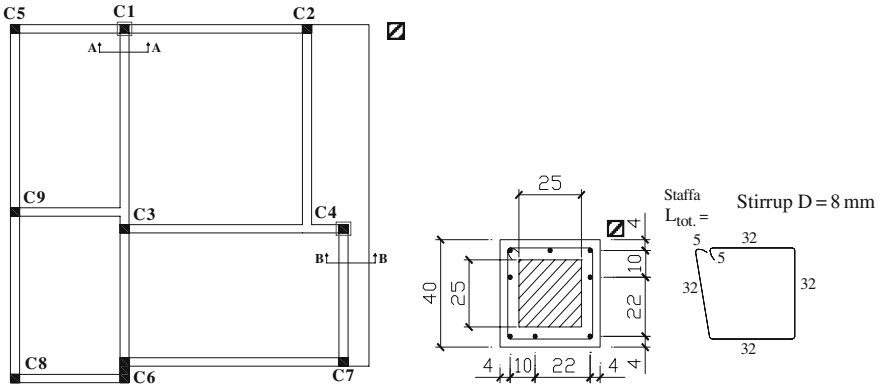

Fig. 5.6 Plan view of the structure with the jacketed columns

The case at hand, offering the possibility of testing a full-scale retrofitting intervention informed by these conceptual principles, thus led to the design of an appropriate retrofitting strategy so to verify the importance on the location of the CP in governing the nonlinear seismic response, and whether the CP location that derives from the application of the rules currently embodied in codes (i.e. the use of the so-called design eccentricity) is actually the most effective on torsional effect.

The designed strategy tackled only selected vertical elements, to guarantee feasibility, easiness and quickness of the intervention, having in mind that, should it be applied to real structures, the shortest possible disruption of use would be required, also in order for this kind of approach to be competitive with the use of FRPs. Two columns were chosen, column C1 and column C4, to undergo concrete jacketing, which, as above mentioned, was mainly aimed at strongly increasing the amount of rebars, with a relatively small increase in the column section dimensions.

The two columns' cross sections were in fact increased from the original 250×250 mm to the jacketed 400×400 mm. New rebars were added: 8 16 mm diameter bars per column were added as longitudinal reinforcement, plus new 8 mm diameter stirrups, with 100 mm spacing at the top and bottom of the columns at each storey (the first 700 mm from the slab) and 150 mm spacing for the remaining length of the columns. Details of the executive drawings are reported in Fig. 5.6.

5.6 Retrofitting Strategies: Comparative Critical Review of the Experimental Results

5.6.1 FRP-Retrofitted Configuration

In Fig. 5.7, the global hysteresis loops (i.e. the base shear vs top displacement lines) for the FRP retrofitted specimen are reported (magenta line), together with those for

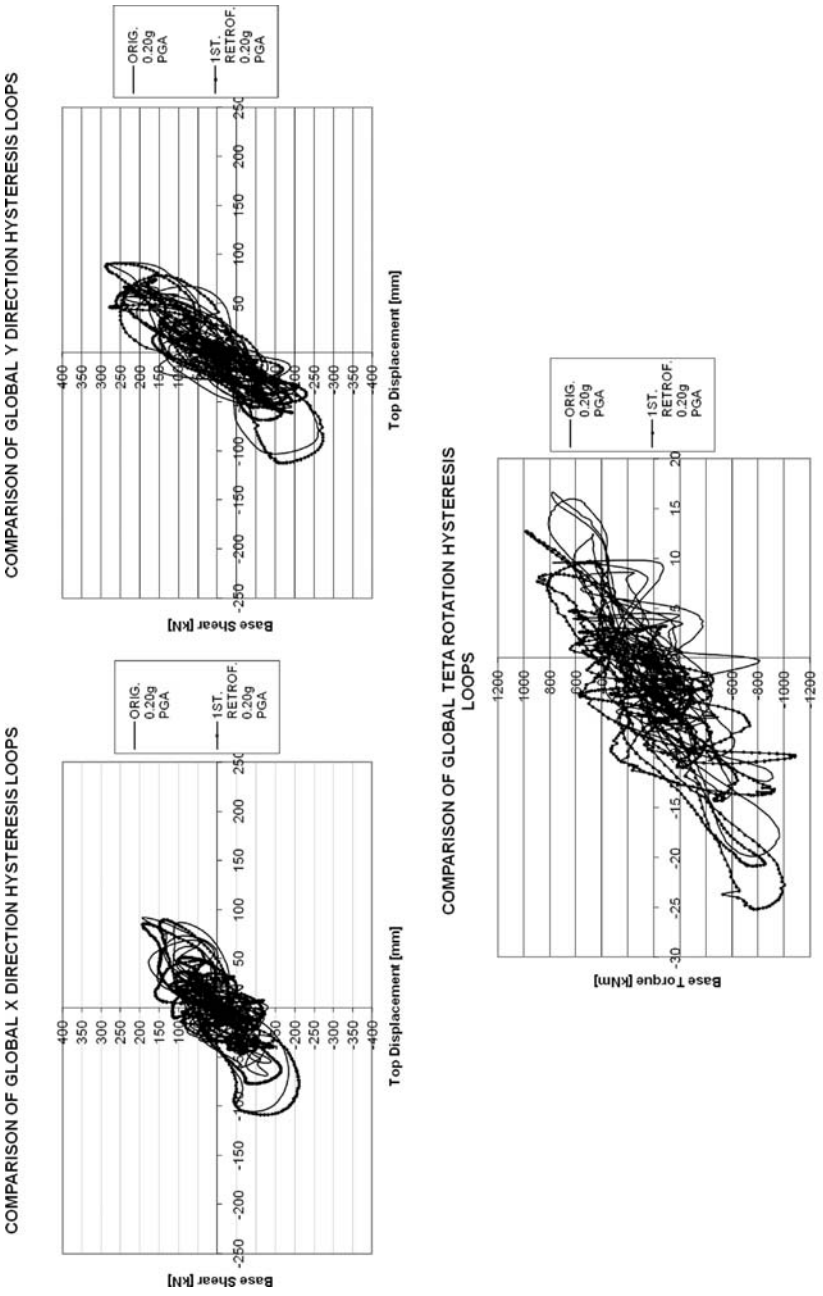

Fig. 5.7 Original structure and FRP retrofitted structure, 0.20 g PGA test: Global hysteresis loops in the X and Y direction and rotation θ

the structure in the as-built configuration (blue line); in both cases the plots refer to the 0.20 g PGA test.

It can be observed that the same displacements were reached in both directions without loss of strength or stiffness; also, the initial slope of the loop remained the same, meaning that, as assumed in design, structural stiffness was not significantly affected by the intervention. Finally, the relative importance of rotational DoFs with respect to translational ones was also unchanged, meaning that no reduction of the torsional effects was effected by the intervention, as, in fact, this was not the aim to be pursued by this approach. In Fig. 5.7c, it can be seen that the maximum absolute values of rotation reached in the FRP-wrapped configuration were even higher than those in the as-built one, for the same values of torque.

After the PsD tests at 0.20 g PGA, the structure did not show any sign of damage, except for diffused fine cracking at the top and bottom of vertical elements. This was expected, given the increased ductility of the vertical elements, due to the presence of the FRP wrapping. The 0.30 g PGA level of intensity was also expected to be withstood by the structure without developing evident damage.

After the end of the test, careful visual inspection of the structure was carried out, which yielded the confirmation that no evident structural damage was present, except for minor cover concrete damage at the top of some columns, especially at the second floor (Fig. 5.8).

Later on, the FRP wraps were removed from the columns and joints, in order to allow the new retrofitting intervention. In this phase, it was possible to see that, under the wrapping, concrete had not cracked extensively at the top and bottom of elements: the effect of confinement yielded by the fibres was very good.

5.6.2 RC-Jacketed Structure

In Fig. 5.9, the global hysteresis loops are represented for the RC-jacketed structure (magenta line), together with those for the as-built structure (blue line), for the 0.20 g

Fig. 5.8 Post-test visual inspection and damage detection after the tests in the FRP-retrofitted configuration

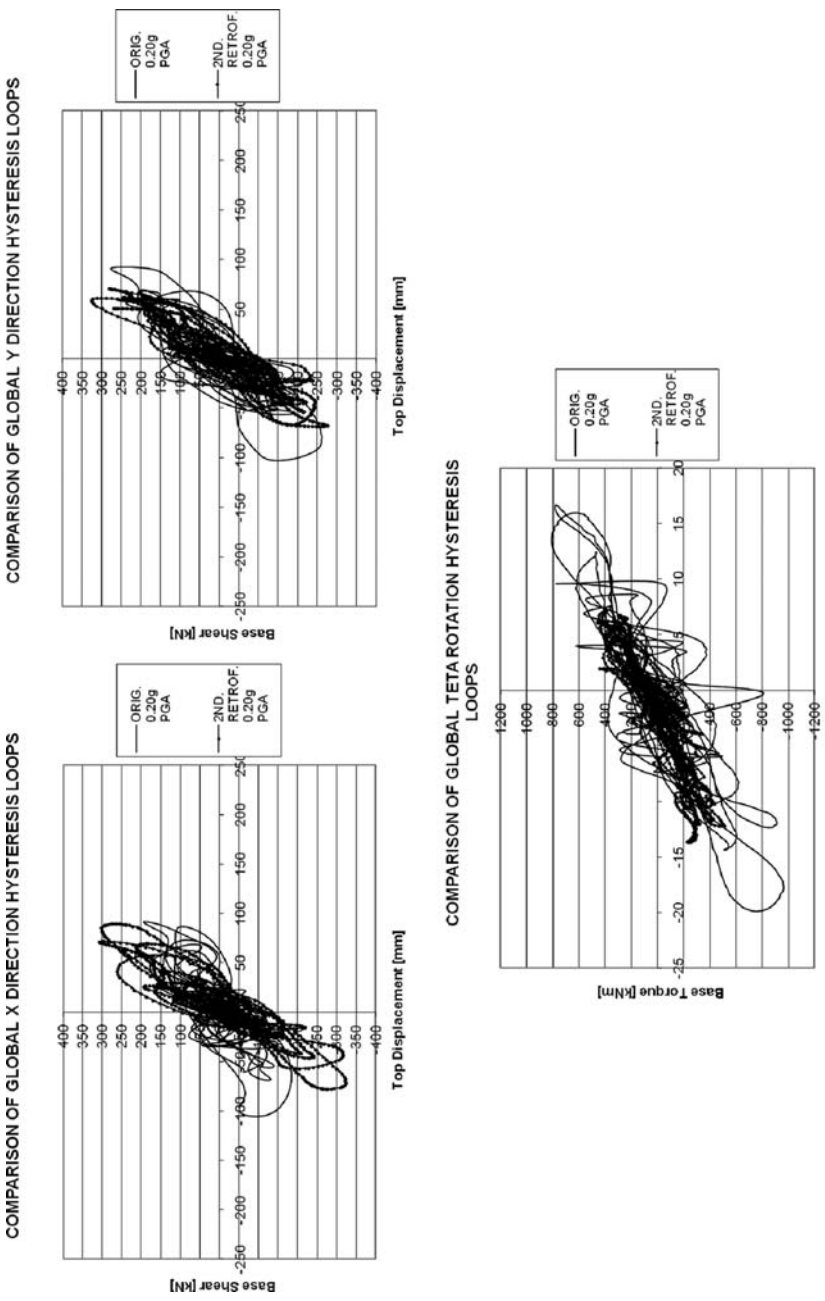

Fig. 5.9 Original structure and RC jacketed structure, 0.20 g PGA test: Global hysteresis loops in the X and Y direction and rotation θ

PGA earthquake. It can be observed that, in this case, the relative importance of the rotational DoF with respect to the translational ones in the energy dissipation process decreased; the attained maximum rotations were also reduced. The initial slope of the loops increased, as the retrofitting intervention modified the global structural stiffness, affecting in particular the X direction, which was originally significantly weaker than the Y direction, thus being more sensitive to the increase in the cross-section of the two retrofitted vertical elements.

The damage developed by the specimen at 0.20 g PGA level was more intense in comparison with that of the structure in the FRP-wrapped configuration.

In fact, after the 0.20 g PGA test, it was already clear that the structure did not have a sufficient ductility supply to meet the displacement demands, however reduced by the retrofitting intervention, which the 0.30 g PGA input would have imposed. In fact, significant damage was detected at the end of this test on the element with the highest axial load ratio, the central column C3: heavy spalling of cover concrete at the top of it at the first storey was visible, with initiation of buckling of the longitudinal rebar. This damage increased in the last test until, in the end, the test had to be stopped after a duration of about 13 s of the accelerogram (the original length was 15 s for the recorded excitation plus 5 s of free vibration to allow the structure to stop oscillating, for a total duration of 20 s) because two vertical elements completely failed, which actually coincided with the global structural failure, making it pointless and even dangerous to continue the test.

The two failed vertical elements were column C3 (the central one) and column C9 (the one nearest to C3) at the first floor. This was due to their high axial load: C3 at the first floor had the highest axial load of all the vertical elements. As a result, the column could not meet the displacement demand during the excitation and completely failed at the top. Cover concrete was completely spalled, and the exposed longitudinal rebars totally buckled with complete dislocation and became inefficient. For this reason, and without the confinement of the transverse reinforcement, even core concrete completely crushed and fell apart, thus making the original cross section practically non-existent. At that moment, the portion of axial load originally competing to C3 mostly migrated to the nearest column, C9, which turned out to be at that moment in an even worse situation than C3: for this reason, shortly after, C9 failed completely in the same way as C3, with even more concrete crushing and dislocation and fracture of longitudinal rebar. Consequently, the data regarding the 0.30 g PGA test were only available up to a time of 12.93 s.

5.7 Critical Evaluation of the Performance of the Interventions

Interesting remarks on the relative performance of the structure in the three different configurations can be made when examining Figs. 5.10, 5.11, 5.12, representing the maximum interstorey drifts at the CM of each storey, measured during the different intensity level tests of each of the three rounds.

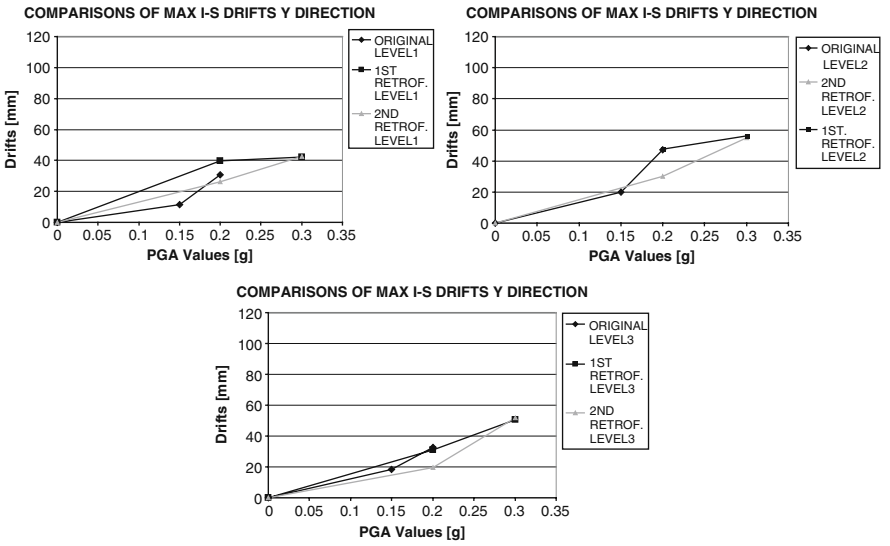

Fig. 5.10 Comparison of maximum interstorey drifts at all storeys for the three different configurations at all the intensities in the Y direction

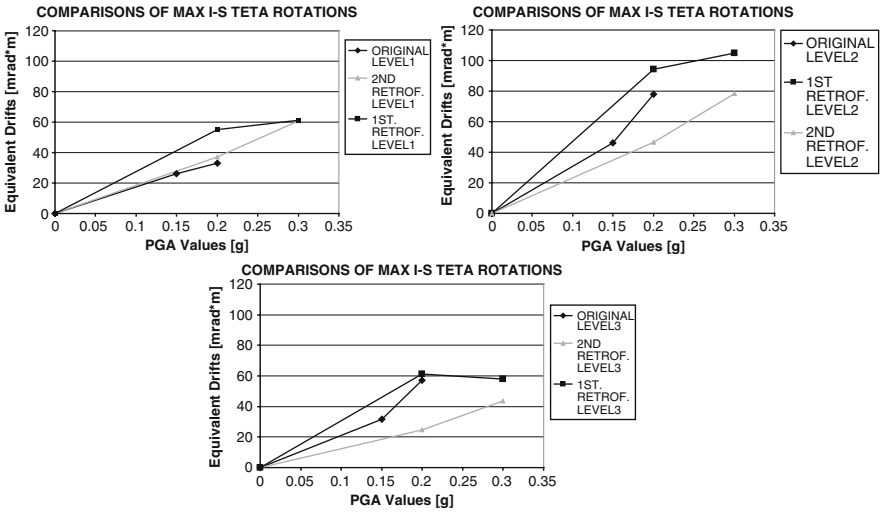

Fig. 5.11 Comparison of maximum interstorey rotations at all storeys for the three different configurations at all the intensities in rotation θ

Such plots can be considered as a sort of pseudo-vulnerability curves, even if built only out of a very small number of points (corresponding to intensity levels) and not explicitly taking into account the effects of the accumulated damage.

It can be observed that the original structure became highly vulnerable between the 0.15 g and 0.20 g intensity levels, especially at the second floor and in the X

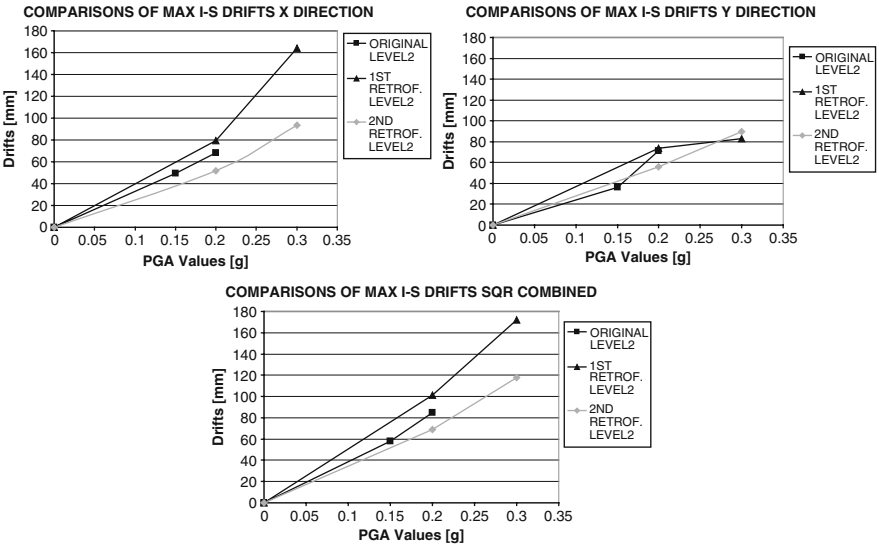

Fig. 5.12 Comparison of maximum interstorey drift at the worst column (level 2) for the three different configurations at all the intensities

direction: the slope of the plot increases sharply. This in fact corresponded to the development of significant damage indicating the vicinity of failure of some of the structural elements during the 0.2 g PGA test. The failure mechanism approached during the test was in fact that of a soft-storey kind mostly in the X direction, as this was the weak direction for the whole structure.

On the contrary, the FRP-retrofitted specimen exhibited similar values to the ones of the original structure up to 0.20 g PGA, but a less steep slope when passing to the 0.30 g PGA level, especially when the Y direction and torsion are considered. It must be noted, though, that the 0.20 g PGA response is for all the DoFs almost the same as that of the original structure: this is what was expected, as the intervention was not intended to increase the stiffness and the strength of the specimen; this fact is further confirmed when noting that the critical direction is still the X one, due to the fact that no balancing of strength and/or stiffness was pursued in this case. The differences in the curves confirms that the FRP retrofitting intervention provided the structure with a sufficient ductility for it to withstand the 0.30 g PGA level without approaching the failure zone.

The intervention proved more effective in improving the response of the structure in the Y direction and in rotation (the slope of the corresponding curves is almost horizontal or even negative between 0.20 g and 0.30 g), whereas, despite the additional ductility, the X direction was still more challenged (positive slope).

It can thus be concluded that the FRP retrofitting intervention thus tackled efficiently the shortcomings of the as-built structure by modifying its global ductility capacity, without modifying the drift demand: the complementary face of the problem was approached with the second intervention, RC jacketing.

When observing the corresponding curves in Figs. 5.10, 5.11, 5.12, it can be noted that the initial slope is less steep than the other two in all cases: this means that the intervention increased the global stiffness of the structure, thus reducing the maximum interstorey drifts at all levels. The drifts where reduced proportionally at all the levels for the X and Y direction, whereas a more significant reduction in the interstorey rotation at the second level can be noted: this suggests that the intervention was effective in reducing the effects of torsion in the development of the failure mechanism at the second floor, thus improving the structural behaviour.

This demonstrates that the second intervention partially reached its design aim too: relocating the centre of strength of the structure reduced the relative importance of the rotational DoF with respect to the translational ones, thus somehow increasing the seismic resistance on the structure affecting the demand side.

The overall performance of the RC-jacketing intervention, though, was not as effective as that of the FRP wrapping, as can be noticed when comparing the two curves: the reduction in drifts was not enough when the 0.30 g intensity level was reached; the structure did not have the necessary ductility (the intervention did not increase the ductility at all) and for this reason it failed, as opposed to the perfectly safe behaviour it had under the same earthquake when the vertical elements were confined with fiber wraps.

The same remarks regarding the trends of seismic behaviour of the specimen hold true when referring to the drifts of the most displaced column at each storey, instead of the drifts at the CM; the difference remains in the fact that in edge columns the drifts are remarkably larger that at the CM, so the vulnerability curves have a steeper slope, meaning an increased sensitivity to increases of the intensity level, and an overall worse behaviour.

When the effects of torsion are somehow incorporated in locally meaningful quantities (in this case the drifts in the two main direction), this must be taken into account when assessing the structure and duly accounted for in the criteria enforced by codified assessment approaches.

5.8 Criteria for the Design of Retrofitting in Plan-Wise Irregular Structures

It came out of the experimental results that acting on the demand side requires a better knowledge of the mechanisms of the response than conceiving an extended element ductility-enhancing intervention. The performance of the RC retrofitted specimen was, in fact, not as satisfying as that of the FRP retrofitted one: the reduction of the strength eccentricity was not enough to overcome the almost total lack of ductility of the columns, which led the structure to premature failure.

The lesson thus learnt from the experimental evidence was that, if strength relocation is to attempted, still, it has to be coupled or subordinated to other measures directed at ductility enhancement: otherwise, the behaviour in terms of global response, such as the maximum level of PGA that can be withstood by the structure,

will not be able to guarantee the same performance as that obtained by means of other strategies directly aiming at ductility.

Moreover, in case strength relocation is attempted, a good knowledge of the state-of-the-art and open issues in the field of the seismic response of irregular structures is a fundamental prerequisite: this kind of knowledge is not yet directly available to the practicing researcher, as a strong gap still remains between the advanced findings of the research community and their implementation into normative documents.

In addition to this, when effecting strength-relocation, care must be taken in a more refined and accurate assessment of the non retrofitted structure, since gross mistakes in the predictions of parameters such as maximum drifts or maximum attainable PGA values would cause wrong dimensioning of the retrofitting intervention and finally lead to the development of a response totally different from the expected one, since many structural properties primarily affecting the seismic behaviour are modified by this kind of intervention.

As a consequence, even if the outcomes of the experimental activity were very promising in showing that working on the demand side and exploiting strength relocation for the reduction of the rotational components of the seismic response of irregular, sesimically under-designed structures is actually possible, still, the main criterion to be taken into account in conceiving retrofitting intervention for this category of structures remains local ductility: when ductility is guaranteed, then a reasonably extended safety margin can be guaranteed against undesirable seismic behaviour.

The other conclusion drawn from the experimental activity is that the fundamental parameters to be considered in the structural response are the local storey drifts: the drift demand at the edge columns, i.e. the worst ones, taking into account torsion-induced added drifts at the edge elements.

Interstorey drifts, rather than displacements and, less obviously, interstorey twists, i.e. the distribution of the rotational components of the response along the height of the building, were the parameters affecting the damage distribution in the strongest way. In fact, the analysis showed, for example, that the failure mechanism developed in the structure at the second storey was caused by heavy twisting effects acting on the storey itself.

Based on the lesson learnt from the case at hand, it can be concluded that an extensive ductility enhancement intervention focused on upgrading of vertical elements for compliance to recent structural detailing standards (be it through innovative techniques such as FRP wrapping or by more traditional interventions) proved to provide the most effective balance between immediateness in the design, straightforwardness in the application, effectiveness in the results and economically rewarding performance.

Moreover, the design of such intervention, responding to basic engineering judgment rather than the implementation of very refined analytical models, responds in the best possible way to the needs of practicing engineers and overcomes the potential risks related to lack of accuracy in the predictions of the

response by providing the structure with abundant ductility resources at reasonable costs.

Acknowledgments The Project SPEAR was funded by the European Commission under the "Competitive and Sustainable Growth" Programme, Contract N. G6RD-2001-00525.

A group of European partners took part in the SPEAR Project together with the ELSA Laboratory: the University of Patras (Greece), the Imperial College of London, the University of Ljubljana (Slovenia), the Universities of Rome and Pavia (Italy), the National Laboratory of Earthquake Engineering (LNEC) of Lisbon, the Higher Technical Institute of Nicosia and EQE International (London). The research team of the University of Naples Federico II took part in the design and execution of the retrofitting interventions.

The PsD tests were a common effort of the whole ELSA staff, whose professional expertise and friendly attitude the authors gratefully acknowledge.

References

1. Fardis M, Negro P, (editors) (2005) SPEAR (Seismic Performance Assessment and Rehabilitation): Proceedings of the International Workshop. Ispra, Italy, EU Publications Office 2005
2. Mola E (2007) Criteria for the seismic vulnerability reduction of existing irregular reinforced concrete structures. PhD Thesis, École Doctorale Mécanique Conception Géomécanique Matériaux, INPG Grenoble
3. Mola E, Negro P (2009) A critical review of current assessment procedures. Seismic Risk Assessment and Retrofitting, Springer
4. Mola E, Negro P (2006) Post-test analysis and interpretation of the results of PsD testing on a full-size three-storey RC plan-wise irregular frame structure: new perspectives. Proceeding of the 1st European Conference on Earthquake Engineering and Seismology, Geneva
5. Negro P, Mola E (2005) Application of the Karhunen-Loeve method to the analysis of the results of a PsD test on a torsionally unbalanced three-storey building. Proceeding of 4th European workshop on the seismic behaviour or irregular and complex structures, Thessaloniki, Greece
6. Negro P, Mola E, Molina FJ, Magonette G (2004) Full-scale PsD testing of a torsionally unbalanced three-storey non-seismic RC frame. Proceeding of 13th World Conference on Earthquake Engineering, 968, Vancouver, Canada
7. Prota A, Nanni A, Manfredi G, Cosenza E (2004) Selective upgrade of underdesigned reinforced concrete beam-column joints using carbon fiber-reinforced polymers. ACI Structural Journal, 101:699–707
8. Rutenberg A (2002) EAEE Task Group (TG) 8: Behaviour of irregular and complex structures, asymmetric structures – Progress since 1998. Proceeding of 12th European Conference on Earthquake Engineering, 832, Elsevier Science Ltd, London

Chapter 6
Advanced Composite Materials and Steel Retrofitting Techniques for Seismic Strengthening of Low-Rise Structures: Review

Houssam Toutanji, Holley Britton, and M. Han

Abstract Low-rise structure collapse can be caused by several different factors including natural disasters, fire, blast, and poor construction. This study focuses on preventing collapse due to earthquakes and it is concerned with the retrofit of structures against future total collapse using innovative materials, such as fiber reinforced polymer (FRP) composites and traditional materials such as steel. A review of recent technology to strengthen low-rise building using FRP composites and steel is presented.

6.1 Introduction

The general categories that describe the causes of building collapse are bad design, faulty construction, foundation failure, extraordinary loads, unexpected failure modes, and a combination of other causes. The extraordinary loads are those caused by natural disasters. The most frequent causes for building collapse are external events, poor construction and bad maintenance. External events include natural disasters and blasts. Natural disasters include hurricanes, flooding, high winds, and earthquakes. Today, due to terrorism, blasts are also of great concern. The focus herein is on the external event such as earthquakes.

Earthquakes are external events that often cause the collapse of low-rise structures. During an earthquake, the ground moves and the buildings have a dynamic response to the movement. The ground movement causes out-of-plane loading in the structure. To withstand an earthquake, the building needs to be able to endure cyclic, axial, and lateral loads. Figure 6.1 shows a graphical representation of how a building reacts during a seismic event, [1].

Earthquakes cost billions of dollars in damages and often result in loss of life due to the collapse of buildings. Many cities across the world are built in heavy seismic

H. Toutanji (✉)
University of Alabama in Huntsville, Huntsville, USA
e-mail: toutanji@cee.uah.edu, toutanji@eng.uah.edu

A. Ilki et al. (eds.), *Seismic Risk Assessment and Retrofitting*, Geotechnical, Geological, and Earthquake Engineering 10, DOI 10.1007/978-90-481-2681-1_6,

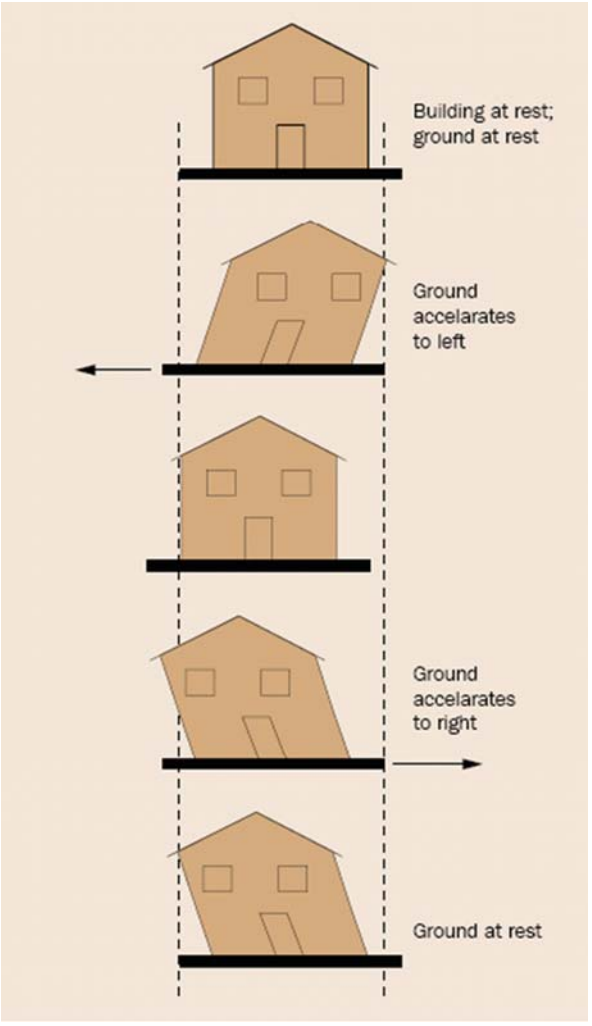

Fig. 6.1 What happens to a building in an earthquake? (See also Plate 4 in Color Plate Section on page 456)

active zones. In many cases, buildings in these old cities were not built up to the seismic design codes of today. An example of such a city is Istanbul, Turkey. Istanbul has lots of buildings that are not properly designed or strengthened for earthquake conditions. Scientists believe Turkey will experience a massive earthquake in the next 30 years, [2]. In order to save lives, it is of utmost importance to retrofit the current low-rise structures to conform with the most recent design codes.

The total collapse of steel-frame buildings appears to be a rare event, even when large earthquakes are involved. Almost all buildings that collapse due to seismic events are low-rise reinforced concrete and heavy masonry buildings. Low-rise

structures are classified as having 1–4 levels. Engineers are constantly trying to strengthen and retrofit buildings against collapse. In past decades, the conventional strengthening methods, such as the addition of shear walls, bracings, and column and beam jacketing were effective retrofitting techniques. These methods have a good record in seismic events. The post-cast shear walls and steel braced frames were the most commonly applied methods because of the associated lower cost and the familiarity with this technique in the construction industry, [3]. Another common strategy for low-rise building seismic retrofitting is to increase building earthquake strength, deformation resistance, and energy dissipation capacity. The strengthening can be accomplished by adding primary resisting elements such as concrete walls or frames, particularly in the lower stories. Another seismic retrofitting technique is to strengthen the existing primary building elements, such as beams, columns, and joints with FRP composites.

FRP composite retrofitting techniques for strengthening different structural elements along with several innovative steel techniques for retrofitting existing low-rise structures against possible future collapse caused by seismic events is presented in this paper.

6.2 Causes of Collapse

To prevent structural collapse, modern earthquake design guidelines use a strong column and weak beam design, story drift limits, and post elastic energy dissipation. Buildings can be designed to avoid collapse during earthquakes by imposing the post-elastic response and by locating and detailing areas in the building where large post elastic deformations are allowed, [4]. Once these areas are determined, they should be detailed to resist the actions. However, in recent earthquakes, several modern buildings that were constructed according to seismic design guidelines have collapsed. It is noted that modern seismic guidelines do not take into account a structure that repeatedly moves into the inelastic range of deformation caused by multiple earthquakes. If the structure continually moves into the inelastic range, there could be accumulated permanent deformations that cause the dominant forces to be gravity forces. This causes lateral instability which results in building collapse, [5].

In order to withstand seismic forces, structures need to be ductile. The steel reinforcement in concrete provides the ductility of the reinforced concrete (RC) structures. Following a seismic event, several patterns have emerged in RC frame construction that can lead to building collapse. These patterns are as follows, [6]:

1. RC columns experience shear failure and concrete crushing.
2. Structural sections without ductile detailing can experience a decrease in stiffness and strength.
3. Design deficiencies such as incomplete load paths and architectural features.
4. Failure of individual members and connections between column and beams.
5. Reinforcement detailing is not adequate.

Fig. 6.2 Shear failure of column (See also Plate 5 in Color Plate Section on page 457)

6. The structure has a soft story. Soft stories occur when the first floor is taller than the other floors or the first floor has a lot of open space.
7. Short column failure caused by high shear stress.

An example of a column failing in shear caused by seismic forces can be seen in Fig. 6.2. Beam and column joints are a source of failure that results in building collapse during an earthquake. Another example of a soft story mechanism and soft story collapse resulting from seismic forces is shown in Fig. 6.3, [6].

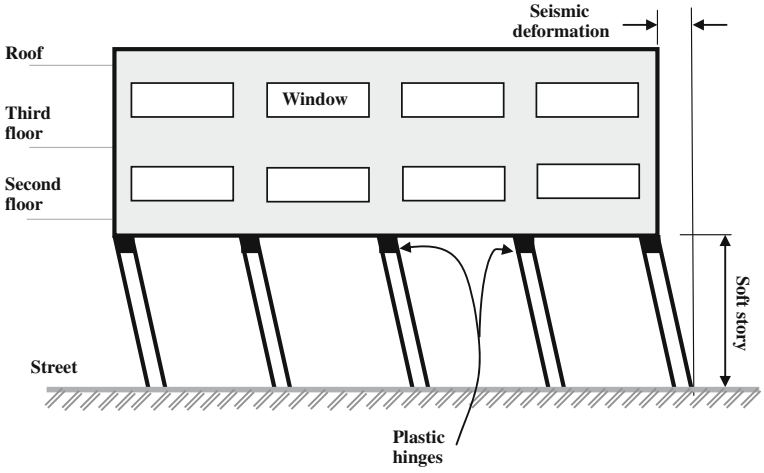

Fig. 6.3 Soft story mechanism

6.3 FRP Retrofitting Techniques for Collapse Prevention

There are a number of retrofitting techniques that can be used to prevent total collapse of low-rise structures. In many cases, the low-rise structures are low cost structures. It is very important to be able to strengthen these existing structures against total collapse in order to save lives and property. One easy method for strengthening low-rise structures against total collapse is to use FRP composites. Wrapping different components of a RC frame with FRP sheet is a feasible method for improving the structure's ability to withstand seismic activity. Columns, beam-column joints, and masonry walls can all be retrofitted with FRP composites.

6.3.1 Strengthening Columns

In many RC structures, columns carry very large loads especially during earthquakes. By wrapping a structural column with FRP composites, the displacement ductility and curvature ductility are increased significantly, [7]. An example of a column retrofitted with FRP against future seismic events can be seen in Fig. 6.4. It is proposed that square RC columns with poor transverse reinforcement can be retrofitted by confining the columns with Carbon FRP (CFRP) or Aramid FRP (AFRP) strips that are pre-stressed. This method increases the strength and ductility of the column. With this method, strips are wrapped around the column and the ends of the strips are clamped together with a crossbar and bolt. The FRP strips are pre-stressed by tightening the bolts in the crossbars, [8]. This confinement method using pre-stressed FRPs increases the strength, ductility and the behavior in the linear elastic zones of the confined column. This method of pre-stressing can be seen in Fig. 6.5, [9]. FRPs can be applied to RC beams to increase shear and flexural capacity. Flexural capacity can also be added to RC slabs with the application of FRP sheets. When FRP sheets are added to slabs or beams, the shear and flexural strengths are increased for both positive and negative moments.

6.3.2 Column-Beam Joints

In buildings, the joints between the columns and the beams are often a source of failure during seismic events. In a structure that experiences lateral loads, if the beam-column joint does not have sufficient shear reinforcement, the joint is the weakest link in the entire system. The bond of the reinforcement bars in the beam and in the column along with the shear deformation of the joint are the joint's controlling factors. Shear stresses are transferred into the joint area when the reinforcing bars are well anchored at the joint. If the reinforcement bars are not well anchored and there is bond slip, there will be less shear stress transferred to the joint, [10]. Load transfer takes place in the beam-column joints and a shear failure in these joints could result

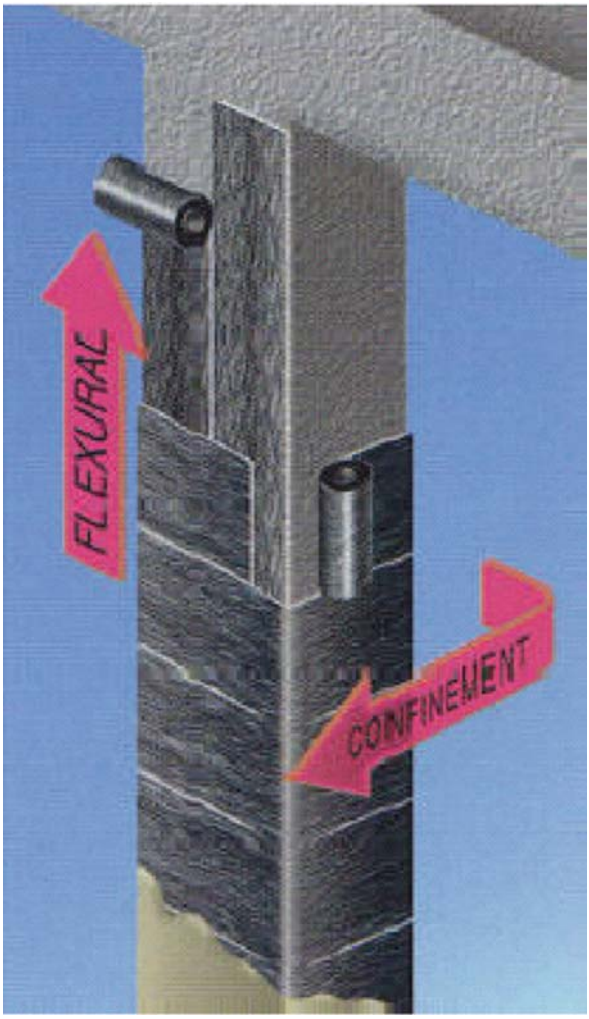

Fig. 6.4 Retrofitting a column with FRP for seismic performance (See also Plate 6 in Color Plate Section on page 458)

in a total collapse of the structure. It would not be possible to replace all structures with weak joints; however, it is possible to retrofit the joints in existing structures.

Seismic retrofitting of joints can be broken down into three areas. First, in order to move the failure region away from the joint, the joint's shear capacity should be improved. The second area involves improving the anchorage of the longitudinal reinforcing bars in the beams by controlling the concrete cracking in the joint core. The third area concentrates on a strong column and weak beam condition. Increasing the flexural strength of the beam ends is of utmost importance if this condition exists. Also, if this condition exists, joint core shear failure should be eliminated as well as failure caused by bond-slip of the longitudinal reinforcement bars, [11].

Fig. 6.5 Method of pre-stressing (See also Plate 7 in Color Plate Section on page 459)

Applying FRP jackets to these joints will rid the structure of brittle failure modes without greatly altering the structural response. These failures include shear failure in the joints and bond slip of the reinforcing bars. Because the FRP strips do not have a lot of effect on the concrete's initial stiffness but do improve the strength, the joint jacketing changes the location of the damage and the damage pattern in the structure.

The application of vertical and horizontal strips on the beam and column improves the joint's strength and stiffness. The application of the corner strips also provides a path for shear stress transfer between the beam and the column even after the joint has deteriorated. Orthogonal strips applied to the beam and column act in tension to aid in preventing the growth of tensile cracks at the join's face. These strips also act in shear, thereby, reducing the joint core's shear distortion, [12].

There are two newly proposed composite retrofitting methods proposed by Wang et al., [11] for beam-column joints. The first involves wrapping the joint in CFRP sheets and adding steel angles, Fig. 6.6. The second involves the use of concrete haunches. Isosceles triangular haunches made of plain concrete are applied to the top and bottom corners of the beam-column joint. The haunch width and column width are equivalent. Instead of detailing the haunches with steel bars, externally bonded CFRP sheets are applied to the haunches. The haunches are confined with two CFRP strips applied to the haunches in the vertical and horizontal directions. The extended ends of the strips are anchored at the column or beam ends of the joint. An example of this retrofit method can be seen in Fig. 6.7. Several conclusions are made regarding these two methods. The failure mode changed to a ductile flexural failure in the beam ends from a brittle shear failure occurring in the joint. The retrofitted joints had improved ductility, strength, and energy dissipation. The CFRP strips and concrete haunch retrofit technique is the most beneficial in improving the ductility and capacity of energy dissipation in the joint.

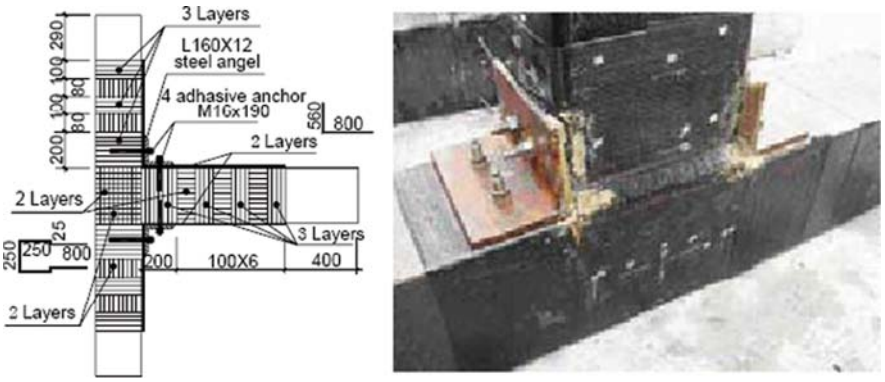

Fig. 6.6 CFRP and steel angle joint retrofit

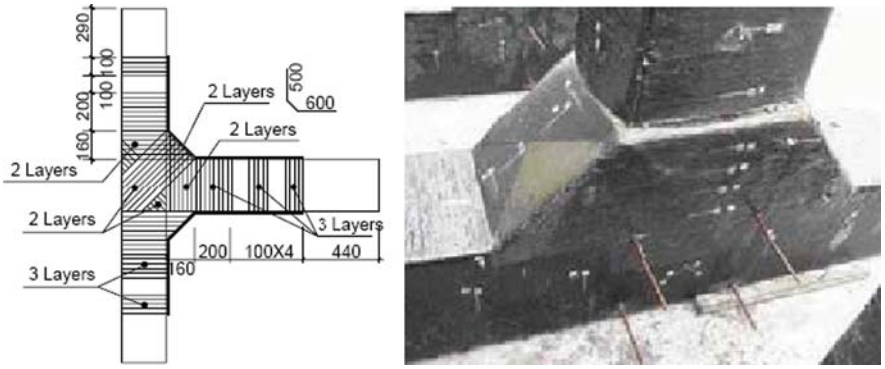

Fig. 6.7 CFRP and concrete haunch retrofitted joint

6.3.3 Concrete Columns Confined with Hybrid Composite Materials

In recent years, retrofitting of existing concrete columns by wrapping and bonding of fiber reinforced polymer (FRP) sheets, straps, or pultruded FRP shells around the existing columns has become increasingly popular. A similar application for new construction is the concrete confined with FRP tubes. Despite their promising results in the laboratory, FRP tubes have yet to be used extensively in the construction industry, due to the high cost of fibers. To achieve more durable and economical structures, new types of structural concrete columns were developed for new construction, [13]. These columns are made of a concrete core encased in PVC tubes reinforced with fiber reinforced polymers (PVC-FRP). The proposed hybrid column, cast in place, consists of a PVC tube reinforced with fiber reinforced polymer (FRP) hoops, which increases the compressive strength and ductility for the concrete columns. The basic structure includes an exterior PVC-FRP shell with a

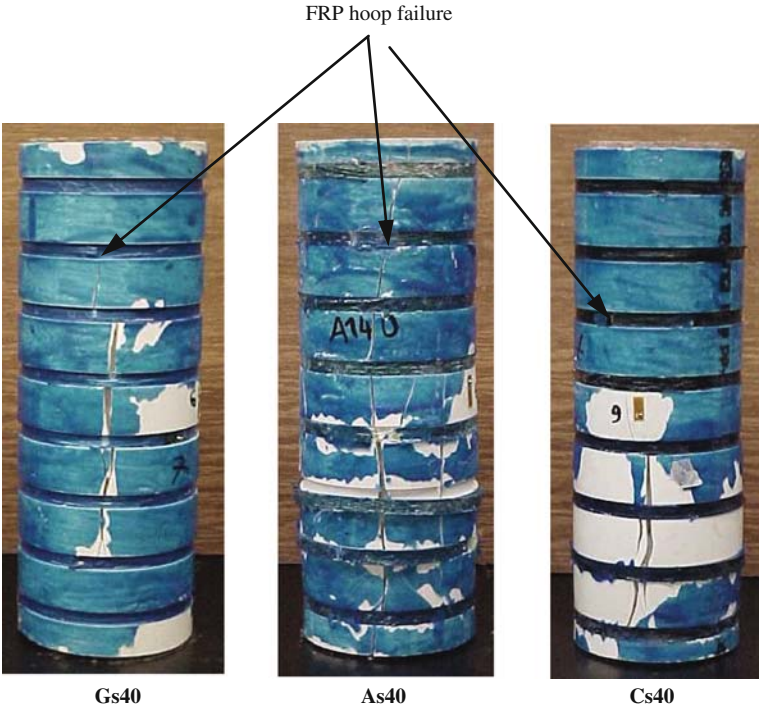

Fig. 6.8 Typical failure mode of PVC-FRP confined concrete specimens (See also Plate 8 in Color Plate Section on page 459)

concrete core. The exterior shell is a commercially available cylindrical PVC pipe externally reinforced with impregnated continuous fibers in the form of hoops at different spacings, which are placed in grooves as shown in Fig. 6.8. The PVC shell acts as formwork and it protects the concrete as well as the internal reinforcement from environmental effects such as chloride and corrosion, while the FRP provides confinement to the concrete. The amount of composite that is required for this concrete reinforcing scheme is very small as compared to the FRP tubes and FRP jacket methods, [14]. In addition, the process by filament winding is fast and can be cost-effective. The spacing of the FRP hoops is dependent on the strength and performance requirements. Significant improvement in the ultimate axial strength, axial strain, and lateral strain of RC columns confined with this hybrid composite system.

6.3.4 Masonry Walls

FRP composites can also be used as a method for strengthening unreinforced masonry infill walls in buildings. By applying FRP sheets directly to the surface of the masonry wall, the overall load capacity of the wall can be increased, [6].

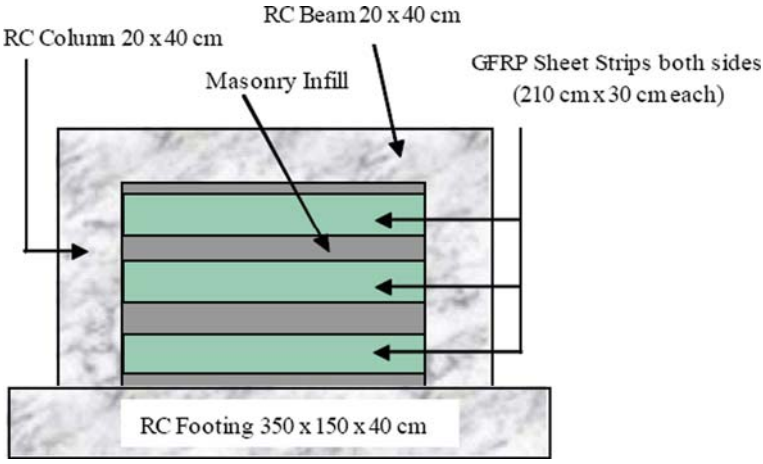

Fig. 6.9 GFRP strips applied to masonry infill wall (See also Plate 9 in Color Plate Section on page 460)

According to Tumialan et al., [15], by applying FRP strips to the surface of the wall along the wall's longitudinal axis, it greatly increases the strength and stiffness of the wall. Depending upon the amount of FRPs used, the nominal masonry capacity can be increased in increments of 4–14 times the initial capacity. The application of the FRPs causes the initial cracking of the wall to be delayed. According to Almusallam et al. [16], glass FRP (GFRP) can also be used to retrofit masonry walls against in-plane seismic loads. Unidirectional GFRP strips can be applied on both sides of the masonry walls as shown in Fig. 6.9 to prevent out-of-plane failure and to increase the overall strength of the wall.

Infill brick walls can be retrofitted with a newly proposed technique by Kobayashi, [17]. This technique is accomplished by drilling small holes at grid points on wall panels. Fiber strand bundles dipped in epoxy are then passed through the holes and then the wall is sewn together in a cross diagonal method. The fiber

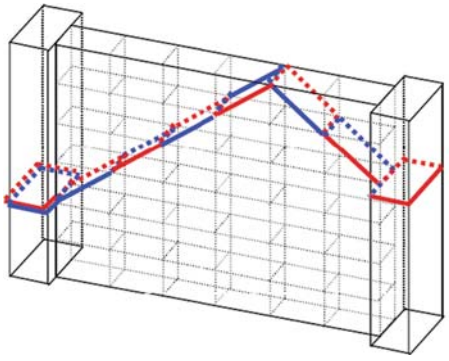

Fig. 6.10 Wall "sewn" together with fiber strands

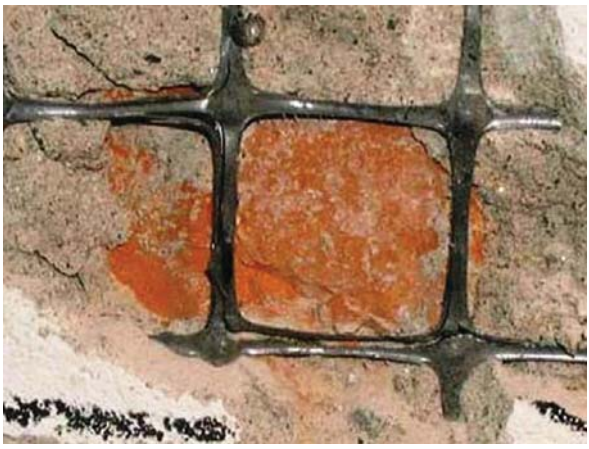

Fig. 6.11 Polymeric grids applied to masonry wall

ends are wrapped around the columns. This anchors the fiber bundles and ties the columns to the walls. An example of this technique can be seen in Fig. 6.10. It is suggested that this method of retrofit improves the deformability of the wall and keeps the wall inside the frame in the case of seismic activity.

Masonry walls can also be retrofitted by applying polymeric grids to the surface of the wall, according to Stoica et al., [18]. The grids are placed only on the perimeters of the external walls. A lime or a lime-cement mortar layer is applied to the wall. The polymeric grid is then inserted into the mortar layer. An example of this technique can be seen in Fig. 6.11. The grids can be removed from the walls at any time without causing damage to the initial wall.

6.3.5 Near Surface Mounted Reinforcement Technique

Taljsten [19] reports that concrete structures can be strengthened with near surface mounted reinforcement (NSMR). Carbon FRP (CFRP) rods are placed in grooves cut into the concrete cover. The rods are held in place with an epoxy or cement bond. This strengthening technique has been around since the 1940s, however, until recently, steel rods were used. Rectangular shaped rods are the most desirable for this technique. The cut grooves have parallel, vertical sides. The bonding agent placed in the groove has a uniform thickness around the rod. Using NSMR rods for strengthening protects the strengthening material against external damage better than the other traditional external strengthening methods. FRP sheets bonded to concrete often experience a de-bonding failure. Using NSMR rods can possibly yield a better bond surface than when FRP sheets are bonded to the surface. By using prestressed rods in the NSMR technique, tests show improvements in flexural behavior. This includes increasing the cracking load of the concrete and the yielding load of the steel.

6.4 Steel Retrofitting Techniques Used to Prevent Collapse

6.4.1 Columns Retrofitted with Steel

The weakness of the RC columns subjected to earthquake forces is usually not the insufficient vertical capacity of the column; instead, it is the inadequate hoop strength and low quantity of transverse reinforcement. Once the integrity of hoops is breached, the vertical reinforcement will lose the protection capability. One simple retrofit is a procedure called grouting. The grouting procedure consists of surrounding the column with a jacket of steel plates that are formed and welded into a single cylinder. The space between the jacket and the column is then filled with concrete, [20].

6.4.2 Existing Frame Retrofitted with Steel Strips

Frame retrofitting schemes include increasing column strength, stiffness, and ductility or the combination of these three factors. It is widely known that increasing stiffness of the frame leads to decreasing ductility. One important reason why old buildings built before the 1960s have bad experience records in recent earthquakes is the insufficient lateral load carrying capacity and limited ductility of the frame. Thus, the major challenge for engineers is to determining the relationship among strength, ductility and stiffness and how these factors play the role of increasing seismic capacity.

Ghobarah et al. [21] studied a case of a 30-year-old low-rise, three-storey RC office building which was retrofitted by 4 different approaches for increasing columns strength, ductility, or stiffness. Evaluation of the damage index and storey drifts show both retrofit strategies of increasing strength and ductility result in a significant reduction in the damage index by 18% and 24.6%. Since increasing the ductility of the columns resulted in a higher story drift (drift increase by 78.5%), the increase in strength is a more effective seismic retrofit strategy.

Later, Mustafa et al. [22, 23] proposed two retrofitting model systems of vertical and diagonal steel strips which give a low-rise RC wall better seismic strength and ductility. The simulated seismic load test of six large scale walls with rectangular cross sections showed the steel strip system prevents development of the rigid body rotation and allows cracks to spread more evenly over the entire wall. It was also suggested to use vertical strips that are attached with through-thickness bolts, stiff steel angles, and anchor bolts to connect the steel strips to the foundation and the top loading beams. In order to provide greater out-of-plane strength and minimize out-of-plane displacement, the proposed strip system should be applied on both sides of the wall, [22].

6.4.3 URM Retrofitting with Steel

There are a large amount of unreinforced masonry walls in the seismically active region in the world. Several retrofitting approaches have been reviewed by

EI-Gawady et al., [24]. Except for steel strips which were mentioned above, confining URM using RC tie columns is another low-rise building retrofitting technique where steel reinforcement is involved. This approach uses a vertical RC or reinforced masonry tie column to confine the walls at all corners and wall intersections as well as at the vertical borders of doors and window openings. In China, such confinement is used in existing buildings as well as new buildings. Unfortunately, this retrofitting approach is actually hard work to apply on the existing buildings. The effective connection between tie columns and tie beams should be done at every floor level.

6.4.4 Energy Dissipation Devices and Damage Control Structure

The concept of structural damage control was introduced in the seismic retrofitting area in late 1980s. The so called damage-control structure is a structure which consists of two parallel structures. One is the primary structure and the other is a damping system, [25]. During the most severe earthquake, damage is allowed to happen in the primary structure without damping system's protection. Thus, the spine of the structure can be saved by the damping system and the structure can be kept from experiencing a total collapse. The damping system is actually an energy dissipation device which is usually made of steel plates joined together by rivets or steel bolts, steel bars, concrete prisms or cubes. Under severe earthquake loads, the primary structure behaves elastically while the damping system responds to the earthquake loads by transferring seismic energy to other forms of energy. This energy transformation or energy dissipation is either through the yielding of mild steel, sliding friction, motion of a piston or a plate within a viscous fluid etc., [26].

Compared to other low-rise building seismic retrofitting approaches, such as base isolation, the damage control structure concept is applicable to new as well as to old existing structures. Damper installation is more cost efficient than other approaches. The following two cases are examples of damper applications on old low-rise masonry buildings, [27]. The Harry Stevens Building, (Fig. 6.12), was built

Fig. 6.12 X-braced friction damper in Harry Stevens Building

Fig. 6.13 Friction dampers in Pump House Building

in 1963. It is a reinforced concrete structure with URM in-fill walls. It has two above ground floors and a basement. The Pump House Building, (Fig. 6.13), has a two-storey reinforced concrete moment frame with interior and exterior brick masonry walls. This building was built in 1924 with additions in 1940 and 1970. Both of these buildings were seismically retrofitted with a friction damper by Public Works and Government Services Canada.

6.5 Conclusions

External events such as earthquakes often cause the collapse of low-rise structures. These structures can be retrofitted to better withstand these external events. The use of FRPs and steel in the retrofitting process has proven successful. It has been shown that FRPs are perfect for strengthening structures to withstand these natural disasters. They are lightweight and do not add much mass to the structure. This is important because any additional mass could increase the chance of failure. The FRPs can be applied directly to the damaged or deficient structure for strengthening. The application of FRPs to the structures' surface is non-invasive and often will not displace the inhabitants of the building during the retrofit procedure. The beauty of using FRPs to retrofit columns is that they are easy to install and they can be made to be aesthetically pleasing.

Compared with FRP application, steel retrofitting techniques are more conventional. Several steel retrofitting techniques, such as steel bracing, steel dampers and exterior shear reinforcement have been widely used for more than 20 years. Most low-rise buildings retrofitted by steel reinforcement have a good record in terms of seismic events. The relatively new steel retrofitting technologies that include columns retrofitted with steel and existing RC frames retrofitted with steel was presented. The last steel retrofitting technique mentioned in this paper was steel friction dampers. Even this technique has been used for 20 years; however, it is still a popular

seismic retrofitting technique worldwide because of the excellent retrofitting effect and minimal interruption to occupants.

Of course, engineers cannot design against every level of external event. However, by retrofitting existing structures with the application of FRPs or by using steel retrofitting techniques, engineers can prevent some of the future building collapse caused by the external events. Preventing any amount of building collapse will save lives.

References

1. CWC, Canadian Wood Council (2003) Wood-frame construction: meeting the challenges of earthquakes. Building Performance Series no. 5, http://www.cwc.ca/NR/rdonlyres/287CDD66-C63C-4B48-8D24-10AD5A4F56E7/0/BP_5earthquakee.pdf, Accessed 12 July 2007
2. Purdue University (2006) Experts urge action to protect Istanbul from earthquake. Science Daily. http://www.sciencedaily.com/releases/2006/01/060108223950.htm, Accessed 30 August 2007
3. IST Group (2004) Methods for seismic retrofitting of structures. http://web.mit.edu/istgroup/ist/documents/earthquake/Part5.pdf, Accessed 11 September 2007
4. King A (1998) Earthquake loads and earthquake resistant design of buildings. Branze Limited. http://www.branz.co.nz/main.php?page=Free20Publications, Accessed 12 July 2007
5. Villaverde R (2007) Methods to assess the seismic collapse capacity of building structures: State of the art. J Struct Eng 133(1): 57–66
6. Yakut A (2004) Reinforced concrete frame construction. World Housing Encyclopedia, Summary Publication
7. Hosseini A, Fadaee S (2004) Behavior of high strength square concrete columns strengthened with carbon fiber reinforced polymers (CFRP). 1st Proc Conference on Application of FRP Composites in Construction and Rehabilitation of Structures, Tehran
8. Yamakawa T, Banazadeh M, Fujikawa S (2005) Emergency retrofit of shear damaged extremely short RC columns using pre-tensioned aramid fiber belts. J Adv Concr Technol 3(1): 95–106
9. Taleie SM, Moghaddam H (2007) Experimental and analytical investigation of square RC columns retrofitted with pre-stressed FRP strips. Proceedings of the FRPRCS-8, Patras, Greece
10. El-Amoury T, Ghobarah A (2005) Retrofit of RC frames using FRP jacketing or steel bracing. JSEE 7(2): 83–94
11. Wang B, Wang P, Liu BQ et al. (2007) Experimental investigation on seismic retrofit methods of RC beam-column joints based on CFRP sheets. Proceedings of the FRPRCS-8, Patras, Greece
13. D'Ayala D, Penford A, Valentini S (2003) Use of FRP fabric for strengthening of reinforced concrete beam-column joints. Proceedings of the 10th International conference on structural faults and repair, London
13. Toutanji H, Saafi M (2001) Durability studies on concrete columns encased in PVC-FRP composite tubes. J Composite Structures 54(1): 27–35
14. Toutanji H, Saafi M (2002) Stress-strain behavior of concrete columns encased in hybrid composite tubes. J Mater Struct 35(250): 338–347
15. Tumialan JG, Galati N, Nanni A (2003) FRP strengthening of URM walls subject to out-of-plane loads. ACI Struc J 100(3): 312–329
16. Almusallam T, Al-Salloum Y, Alsayed S et al. (2007) Seismic response of infill walls strengthened with FRP sheets. Proceedings of the FRPRCS-8, Patras, Greece

17. Kobayashi K (2007) Innovative application of FRPs to seismic retrofit of brick-infilled RC frames. Proceedings of the FRPRCS-8, Patras, Greece
18. Stoica D, Tragakis P, Plumier A et al. (2007) Masonry structures retrofitting with polymeric grids. Proceedings of the FRPRCS-8, Patras, Greece
19. Taljsten B (2004) FRP strengthening of concrete structures: New inventions and applications. Prog Struct Eng Mater 6: 162–172
20. Wikipedia (2006) The free encyclopedia of seismic retrofit. http://en.wikipedia.org/wiki/Seismic_retrofit. Accessed 29 August 2007
21. Ghobarah A, EL-Attar M, Aly NM et al. (1998) Evaluation of retrofit strategies for reinforced concrete columns: A case study. Eng Struct 22 (2000): 490–501
22. Mustafa T, Bruneau M, Saatcioglu M et al. (2000a) Seismic retrofitting of low-rise masonry and concrete walls using steel strips. J Struct Eng 126(9): 1017–1025
23. Mustafa T, Bruneau M, Saatcioglu M et al. (2000b) Analysis and design of low-rise masonry and concrete walls retrofitted using steel strips. J Struct Eng 126(9): 1026–1032
24. EI-Gawady M, Lestuzzi P, Badoux M et al. (2004) A review of conventional seismic retrofitting techniques for URM. 13th International Brick and Block Masonry Conference Amsterdam, The Netherlands
25. Oliveto G, Marletta M (2005) Seismic retrofitting of reinforced concrete buildings using traditional and innovative techniques. ISET J Earthq Technol 42(454): 21–46.
26. Naeim F, Brzev S (2004) Advanced technologies in housing construction. Overview of Advanced Technologies, World Housing Encyclopedia, Summary Publication, EERI
27. Foo S, Naumoski N, Cheung M et al. (2001) Research and application of seismic retrofit technologies in Canada. RPS/AES/Technology Directorate, Public Work & Government Services Canada

Chapter 7
A Novel Structural Assessment Technique to Prevent Damaged FRP-Wrapped Concrete Bridge Piers from Collapse

Oral Buyukozturk and Tzu-Yang Yu

Abstract Repairing deteriorated concrete bridge piers using externally wrapped fiber reinforced polymer (FRP) composites have been proven as an effective approach. This technique has also been applied to low-rise building structures. Failures in FRP-wrapped concrete structures may occur by flexural failures of critical sections or by debonding of FRP plate from the concrete substrate. Debonding in the FRP/adhesive/concrete interface region may cause a significant decrease in member capacity leading to a premature failure of the system. In this chapter, a novel structural assessment technique aiming at inspecting the near-surface FRP debonding and concrete cracking of damaged FRP-wrapped concrete bridge piers to prevent the structures from collapse is presented. In the first part of this chapter, failure mechanisms of FRP-wrapped concrete systems are briefly discussed. The second part of this chapter introduces a novel structural assessment technique in which far-field airborne radar is applied. In this development, emphasis is placed on inspection of debonding in glass FRP (GFRP)-wrapped concrete cylinders, while the technique is also applicable to beams and slabs with bonded GFRP composites. Physical radar measurements on laboratory specimens with structural damages were conducted and used for validating the technique. Processed experimental measurements have shown promising results for the future application of the technique. Finally, research findings and issues are summarized.

7.1 Introduction

Strengthening and repair of concrete structures has become an important issue for public safety and for effective infrastructure management. Engineering technologies are developed and introduced for extending the service life of concrete structures by means of restoring their design capacity for continuous use and/or upgrading them for possible future challenges from the environment. The use of fiber reinforced

O. Buyukozturk (✉)
Massachusetts Institute of Technology, Cambridge, MA, USA
e-mail: obuyuk@mit.edu

A. Ilki et al. (eds.), *Seismic Risk Assessment and Retrofitting*, Geotechnical, Geological, and Earthquake Engineering 10, DOI 10.1007/978-90-481-2681-1_7,

polymer (FRP) composites as an externally bonded element to confine the concrete in order to secure the integrity of concrete structures has been proven, both theoretically and practically, to be an effective strengthening/repair approach. FRP composite jacketing systems have emerged as an alternative to traditional construction, strengthening, and repair of reinforced concrete columns and bridge piers. A large number of projects, both public and private, have used this technology and escalating deployment is expected, especially in seismically active regions. Integration of the new FRP composite with the existing concrete substrate results in the formation of a new structural system. Differences in the material properties of the two structural components (FRP and concrete) pose challenging problems of predicting the behavior of the integrated structural system. Extensive research effort has been devoted to this active field as reported in the literature on structural engineering, and composite materials and construction.

The integration of concrete structures with externally bonded GFRP composites forms a multi-layer composite system. Construction defects and structural/environmental damages may occur within the GFRP-retrofitted concrete structures, and especially, in the vicinity of FRP-concrete interfaces. FRP-concrete interface and concrete conditions cannot be fully revealed until physical removal of the FRP composite layer unless the member has already been subjected to apparent substantive damage. Partial or complete removal of the FRP composite layer for observation of the damage may pose a danger of structural collapse. It has been identified recently that a FRP-retrofitted beam or concrete column could appear safe without showing any sign of substantial damage underneath FRP composites and yet containing a severely deteriorated concrete and debonded FRP composites. Such scenario could happen when the structure has undergone a modest seismic event that has significantly damaged the FRP-concrete system while the system has not reached the failure stage. Failures of damaged FRP-concrete systems are often brittle, involving delamination of the FRP, debonding of concrete layers, and shear collapse, and can occur at load levels lower than the predicted theoretical strength of the retrofit system. Among these failure modes are fracture of concrete along the planes in the vicinity of FRP-adhesive interfaces, debonding or peeling of the FRP from the concrete surface due to the mechanical and environmental effects, and epoxy decohesion. Gradual debonding of the FRP composite under service load conditions may result in premature failures of the retrofitted system, leading to the total collapse of the structure. Thus, there is a need for inspection of debonding in such multi-layer systems using appropriate nondestructive testing (NDT) techniques applicable in field conditions. This is essential for safe applications of FRP strengthening of deteriorated concrete structures in prevention of total collapse.

In this chapter, first the various failure mechanisms of debonding in FRP-wrapped concrete structures are discussed. The chapter then focuses on the NDT techniques for the inspection of FRP-wrapped concrete systems. A novel NDT technique based on the far-field radar measurements developed by the authors is

discussed as a structural assessment tool to prevent damaged GFRP-wrapped concrete structures from total collapse. In this development, emphasis is placed on inspection of debonding in GFRP-wrapped concrete bridge piers. Radar measurements are conducted on laboratory cylinder specimens with structural damages. Measurement results are provided and processed by the image reconstruction algorithm to render images for condition assessment.

7.2 Failure Mechanisms of FRP-Wrapped Concrete Systems

Failures in FRP-wrapped concrete or reinforced concrete systems may occur by flexural failures of critical sections, such as FRP rupture and crushing of compressive concrete, or by debonding of FRP plate from the reinforced concrete (RC) beams, both triggered by the presence of construction defects and structural damages. Construction defects such as trapped air voids or pockets can occur between FRP sheets/plates and concrete substrate during construction. Under mechanical effects stress concentrations would develop around such regions, leading to further development of delamination in the interface region and debonding of FRP from the concrete substrate. Structural damages such as concrete cracking or crumbling inside the FRP wrapping, and/or debonding of the FRP sheet from concrete could occur under various degrees of confinement pressure provided by the FRP wrap. This type of failure has been observed in FRP-wrapped concrete specimens [1], and also FRP-wrapped large scale reinforced concrete structures, [2]. In addition, environmental (moisture) effects have been shown to lead to debonding, [3]. Various approaches on the modeling of debonding have been proposed, such as strength approach, semi-empirical and empirical models, and fracture approach, [4–6]. The presence of these defects and damages can initiate the brittle failure of FRP-strengthened concrete structures.

FRP debonding occurs with a loss in the confinement action between the bonded FRP and the RC member. Experimental results have shown that FRP debonding is a highly complex phenomenon that can involve failure propagation within the concrete substrate, within the adhesive, within the FRP laminate, and the interfaces of these layers [4, 7, 8]. It is possible that high stress concentrations around flexural cracks may promote debonding [9], however, such stress concentrations diminish rapidly with propagation of debonding, resulting in a certain debonded area. Durability of the FRP-strengthened RC system remains a major concern in rehabilitation applications. Behavior of FRP-strengthened RC systems subjected to freeze-thaw, wet-dry, and temperature variation cycles or various aqueous solutions prior to loading have been studied by researchers and varying degrees of strength degradation have been observed, [10–15]. The influence of moisture on the adhesive is believed to play a critical role in the debonding failure of FRP/adhesive/concrete systems. The plasticization effect of moisture enhances the fracture toughness of adhesives due to greater plastic deformation and enhanced crack-tip blunting

mechanisms, [16]. Cohesive strength may, however, be reduced [17, 18] to sufficiently offset the increased toughness. These results show that durability is an important issue in FRP/adhesive/concrete systems.

7.3 Structural Assessment Technique – Far-Field Airborne Radar NDT

In this section, a novel structural assessment technique called FAR (far-field airborne radar) NDT is described for the inspection of GFRP debonding, as the precursor of structural failures, in GFRP-concrete systems. Current NDT techniques are first reviewed. Compared to other NDT techniques such as acoustic NDT, thermal NDT, and radiography NDT, radar (electromagnetic wave) NDT is promising in field applications; the method is less vulnerable to temperature variation, and less constrained in field installation. While most current radar or microwave NDT adopt near-field inspection scheme [19], the developed FAR NDT technique uses far-field inspection scheme allowing inspections from distance for highway and cross-river bridge piers.

7.3.1 Review of Current NDT Techniques

7.3.1.1 Acoustic and Ultrasound NDT

Acoustic and ultrasound NDT are based upon elastic wave propagation in solids. Examples include the techniques of pulse-echo, impact-echo, ultrasonic, acoustic emission, and spectral analysis of surface waves (SASW). Disadvantages of acoustic NDT include the need of intimate contact between the equipment and the subject, the use of sound couplant, as well as the existence of multiple paths through the same subject that make result interpretations difficult, [20].

7.3.1.2 Thermal NDT

Thermal NDT is based on the detection of heat flow in the object in which air gaps resulting from debonding act as insulators blocking out the proper heat flow. Data interpretation is, however, complicated because of varying ambient temperature conditions and surface emissivity variations, which is a function of surface properties, [21]. An attempt was made [22] to quantify subsurface damages of FRP-bonded concrete using infrared thermography.

7.3.1.3 Radiography NDT

Radiography NDT uses high frequency electromagnetic radiation (X-rays and Gamma rays) or particular beams (beta rays and neutron radiation) passing through the subject and exposing it onto a film on the other side of the subject. Limitations

include the need to access both sides of the subject, the need of safety precautions, long exposure, and two-dimensional (2D) images of three-dimensional (3D) subjects, [23].

7.3.1.4 Radar/Microwave NDT

Radar/microwave NDT uses electromagnetic (EM) wave in probing the target structure for inspection. It has been used extensively for site characterization in geotechnical engineering and for evaluating concrete structures, pavements, and bridge decks. Most radar/microwave NDT techniques used in civil engineering applications operate in the range from VHF (very high frequency) (30~300 MHz) to SHF (super high frequency) (3~30 GHz). Radar NDT relies on the reflected signals from the target for ranging and interpretation, while microwave NDT uses reflected as well as transmitted signals for the same purpose. The wave properties of received radar signals, such as velocity and amplitude, depend on the dielectric properties and geometrical properties (scattering effects) of the target structures. Thus, characteristics of the target structure can be revealed from the received signals. Voids, delaminations, rebar, and material characteristics can be detected and interpreted from the reflected waves. Optimization between penetration depths and detection capability, two inversely related parameters that are dependent on the frequencies and bandwidth of the wave, could be a challenge. Conventional radar often makes use of low frequencies to enhance penetration but with sacrificed detectability. With the proper development of wideband, multi-frequency capability and tomographic imaging techniques, along with measurement of dielectric properties of the subject materials, however, radar can be a powerful tool in assessing structural members that consist of hybrid materials.

Several radar NDT techniques for assessing the condition of FRP-retrofitted/wrapped concrete structures have been reported in the literature [24–27]. Most of the reported radar NDT techniques for damage detection in concrete and FRP-concrete structures rely on the near-field measurements in which EM waves are essentially cylindrical or spherical. The near-field approach is inherently sensitive to localized defects and damages of the structure since the probing device is placed in a close distance to the surface of the structure. Strong reflection response can also be expected. Advantages of the near-field approach include (i) finer spatial resolution, (ii) less vulnerability to unwanted edge reflection, (iii) small size of probing devices/radiators (e.g., antenna, waveguide), and (iv) simple calibration scheme, [28]. Disadvantages of the near-field approach include (i) the constraint of short standoff/inspection distance, (ii) complex radiation patterns in the near-field region, and (iii) degradation in measurement sensitivity due to the surface roughness of the specimen.

The far-field approach, on the other hand, is not constrained by the requirement of accessibility to the structure, neither easily hampered by the surface condition of the structure. The proposed FAR (far-field airborne radar) NDT technique remedies coarse resolution problem by the integration of inverse synthetic aperture

radar (ISAR) measurements and tomographic reconstruction methods. Details of this technique will be provided in the following sections.

7.3.2 Overview of the FAR NDT Technique

The FAR NDT technique mainly consists of an airborne horn antenna, a signal generator, a signal modulator, and an analyzer. In principle, radar signals are designed and generated by the signal generator, modulated by the modulator, and transmitted by the horn antenna. The horn antenna is placed beyond the far-field distance from the structure. Hence, the impinging radar signals on the structure will be essentially plane waves whose waveform is mathematically simplified for analysis. The inspection scheme is illustrated in Fig. 7.1 where the radar is positioned at an inclined angle, ϕ, with respect to the horizontal axis (level).

Continuous wave (CW) radar signals in the frequency range of 8–12 GHz and linearly polarized in HH (transverse electric) and VV (transverse magnetic) were used for the relevance of their wavelengths in matching the typical size of FRP debonding. Reflected EM waves or radar signals are collected by the same horn antenna and processed by the analyzer. The radar measurements are collected in ISAR (inverse synthetic aperture radar) mode; in other words, the reflected signals are received at different angles with respect to the structure. Collected far-field ISAR measurements are represented in dBsm (decibel per square meter) for the amplitude

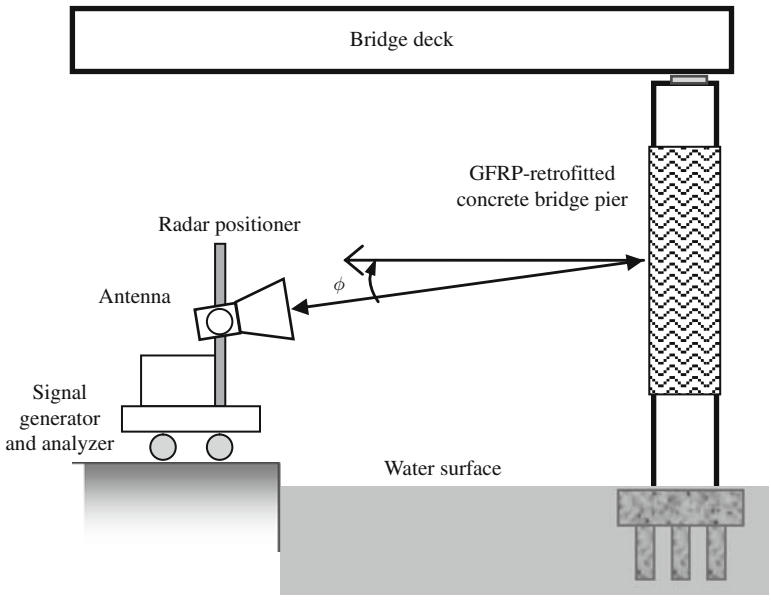

Fig. 7.1 Inspection scheme of the FAR NDT technique

and in radian for the phase. Far-field ISAR radar measurements collected at various angles and frequencies constitute the frequency-angle data for signal processing based on tomographic reconstruction methods. Image reconstruction processing is implemented by fast projection algorithm, [29]. Reconstructed imagery is used as a basis for condition assessment.

7.3.3 Specimen Description and Experimental Measurement

Laboratory GFRP-wrapped concrete cylinders with and without an artificial defect embedded in the interface region between the GFRP layer and the concrete were manufactured and subjected to radar measurements. Two representative GFRP-concrete specimens are shown in Fig. 7.2 . In Fig. 7.2a, the intact concrete cylinder was wrapped with one layer of GFRP after 28 days of curing. The artificial defect made of a cubic-like Styrofoam (3.81 cm-by-3.81 cm-by-2.54 cm) was introduced to the damaged specimen as shown in Fig. 7.2b. The mix ratio of concrete for both specimens was water:cement:sand:aggregate is 0.45:1:2.52:3.21 (by weight). The diameter of concrete cores was 15.2 cm, and the height was 30.4 cm. A unidirectional glass fabric system was used and molded with epoxy resin to form the GFRP-epoxy sheet wrapped on the surface of the concrete core. The volumetric ratio of epoxy:GFRP was 0.645:0.355. The thickness of the GFRP-epoxy sheet was 0.25 cm.

Physical radar measurements of the GFRP-wrapped concrete specimens were performed at the M.I.T. (Massachusetts Institute of Technology) Lincoln Laboratory using the Compact Radar Antenna Range facility capable of achieving high

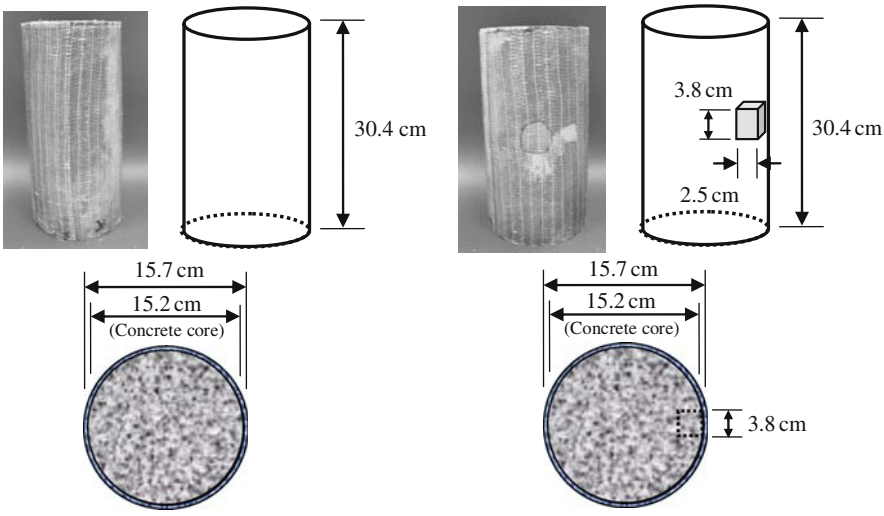

Fig. 7.2 Intact and damaged GFRP-wrapped concrete cylinder specimens

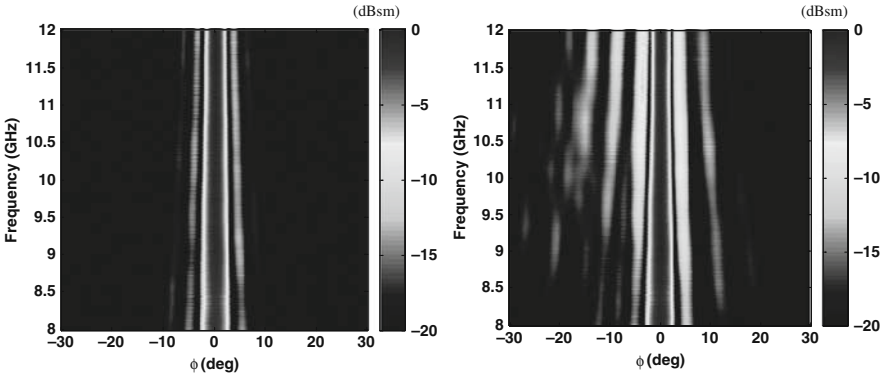

(a) Intact specimen (b) Damaged specimen

Fig. 7.3 Frequency-angle data of the intact and damaged specimens (HH polarization, 8∼12 GHz)

signal-to-noise ratio measurements for a large frequency bandwidth ranging from UHF (0.7 GHz) to 100 GHz and producing a 20 m quiet zone for different antenna radiation patterns and full polarimetric measurements. Collected far-field ISAR measurements from the intact and the damaged specimens in the frequency range of 8–12 GHz is provided in Fig. 7.3 a,b. In Fig. 7.3b, the incident angle of 0-degree corresponds to the center location where the artificial defect is placed. In Fig. 7.3a,b, it is found that the presence of the defect produces more scattering of radar signals in the total reflection response of the damaged specimen than the one of the intact specimen. This is especially significant in the angular region other than normal incidence (0-degree case), as observed in Fig. 7.3b.

7.3.4 Progressive Image Focusing

Image reconstruction is performed through the progressive image focusing in conjunction with the use of far-field ISAR measurements for the intact specimen. In this application, the near-surface artificial defect with characteristic lengths 3.72 cm (range) and 3.76 cm (cross-range) are theoretically detectable beyond a far-field distance 10 m with bandwidth 4 GHz (center frequency 10 GHz) using a horn antenna with aperture size 0.4 m, Fig. 7.4 . The center frequency is shifting with the increasing of bandwidth in Fig. 7.4. It is shown that, in Fig. 7.4, the range and cross-range resolutions of the far-field ISAR measurements are dramatically improved with increasing bandwidth.

The measurements are processed to render the images as shown in Fig. 7.5 . Bandwidth of each image is increased from the upper left image (0.44 GHz) to the lower right image (4 GHz), with frequency band indicated in each image. In Fig. 7.5, the features of the specimen are gradually revealed by the converging of scattering signals in the images. Two scattering signals representing the effect of the two ends of the specimen are identified in the upper middle image with bandwidth 0.88 GHz. This feature becomes clearer in other images with wider bandwidths.

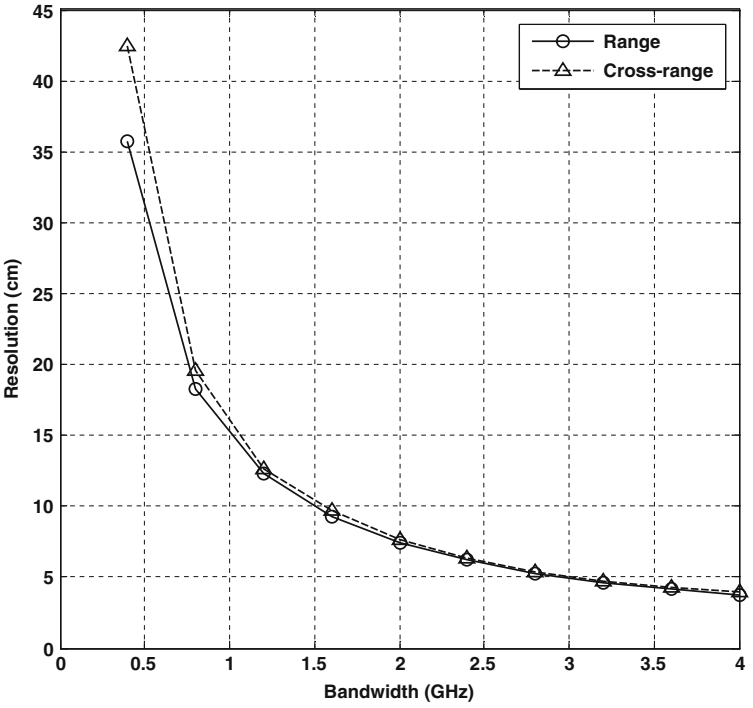

Fig. 7.4 Range and cross-range resolutions versus bandwidth – shifting center frequency

Although 4 GHz bandwidth is presumably suggested, geometric features of the specimen are visually detectable when the bandwidth is only about 1 GHz. This implies that, by taking the advantages of ISAR measurement and fast backprojection algorithm, the ability of the imagery to capture the features of the target structure can be increased if *a priori* knowledge on the shape and size of the target structure is available. This is the case for preliminary inspection where the global features would be first revealed at narrow bandwidths. Therefore, the detection ability of the imagery is believed to be higher than theoretical values as shown in Fig. 7.5. This feature also makes the proposed radar NDT technique promising for in-field applications.

7.3.5 Image Reconstruction for Structural Assessment

7.3.5.1 Damage Detection

Damage detection for the structural assessment of GFRP-wrapped concrete systems is conducted by interpreting scattering signals in the reconstructed

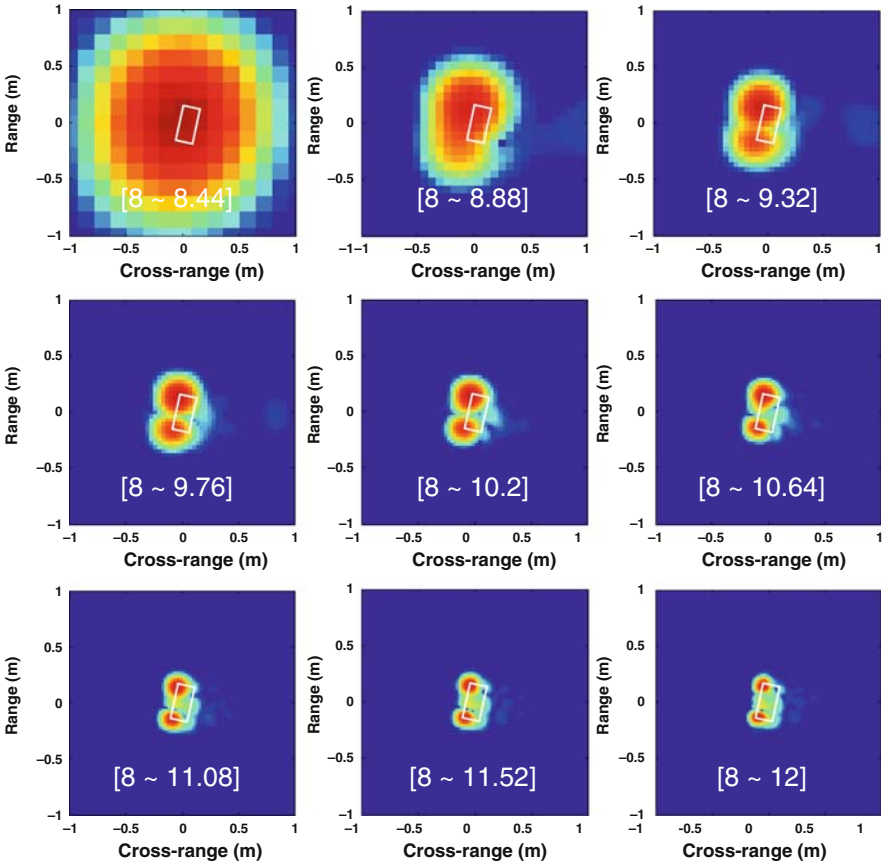

Fig. 7.5 Processed images of the intact specimen with various bandwidths (See also Plate 10 in Color Plate Section on page 460)

images. To demonstrate this, reconstructed images of the intact and the damaged GFRP-wrapped concrete specimens using the far-field ISAR measurements (Fig. 7.3) are rendered and shown in Figs. 7.6 and 7.7, respectively. In these figures, the specimen boundaries are indicated in solid lines. In Fig. 7.6, the reconstructed scattering signals are only due to the edge or surface reflection. On the other hand, in Fig. 7.7, the reconstructed image reveals not only the edge reflections but also the presence of the defect. In other words, the presence of the artificial defect is detected and represented by the scattering signal in the middle of the specimen in Fig. 7.7, ($\phi = 10°$).

Knowing the nature of these scattering signals and the geometry of the structure, image interpretation can be performed for damage detection. Factors such as incident angle, bandwidth, and center frequency are to be discussed for their effects on the performance of image interpretation in the following sections.

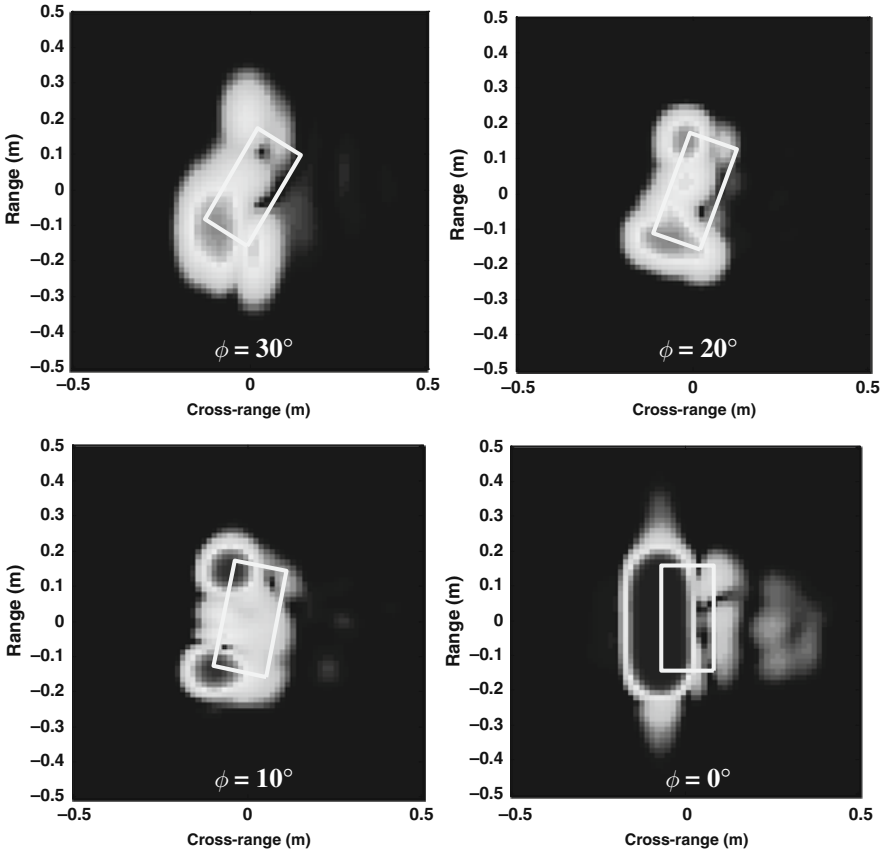

Fig. 7.6 Reconstructed images of the intact GFRP-concrete specimen ($\phi = 30° \sim 0°$)

7.3.5.2 Effectiveness of Incident Angle

In the reconstructed images, significant scattering signals are encountered when reflected signals due to the presence of defects are strong, except in the normal incidence (or specular return) case ($\phi = 0°$). Excluding the scattering signals due to edge reflection and specular return, the stronger the scattering signal is, the more affirmative there is a defect.

Since defects can always be implicitly or explicitly characterized by their orientation, certain ranges of incident angle can be more effective than others in revealing or triggering the scattering signals due to defects. It is shown that, in Fig. 7.7, the defect indication is most obvious when $\phi = 10°$ among other angles.

7.3.5.3 Effects of Bandwidth and Center Frequency

As shown in Fig. 7.5, the increase of bandwidth (B) in image reconstruction processing leads to the improvement of image resolutions. Such increase can be associated

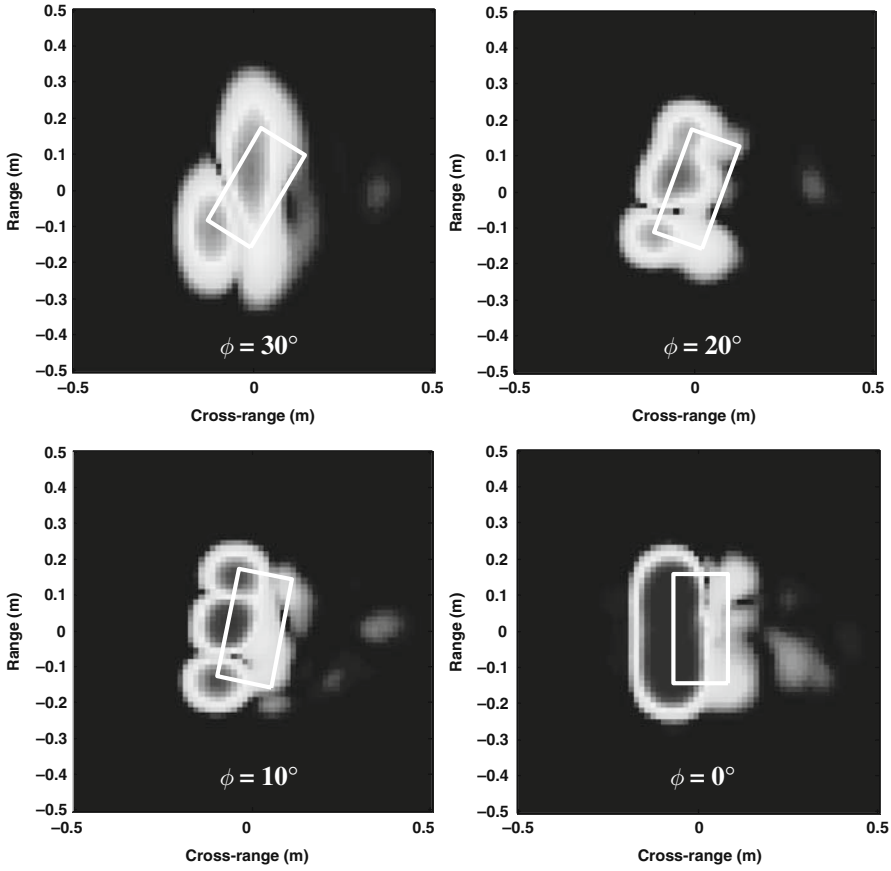

Fig. 7.7 Reconstructed images of the damaged GFRP-concrete specimen ($\phi = 30° \sim 0°$)

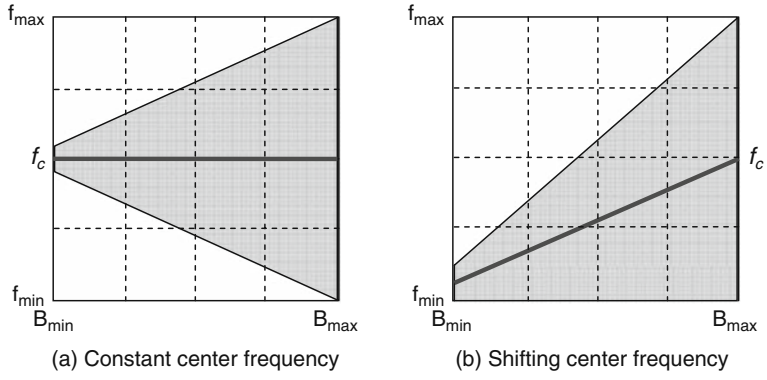

Fig. 7.8 Constant and shifting center frequency schemes

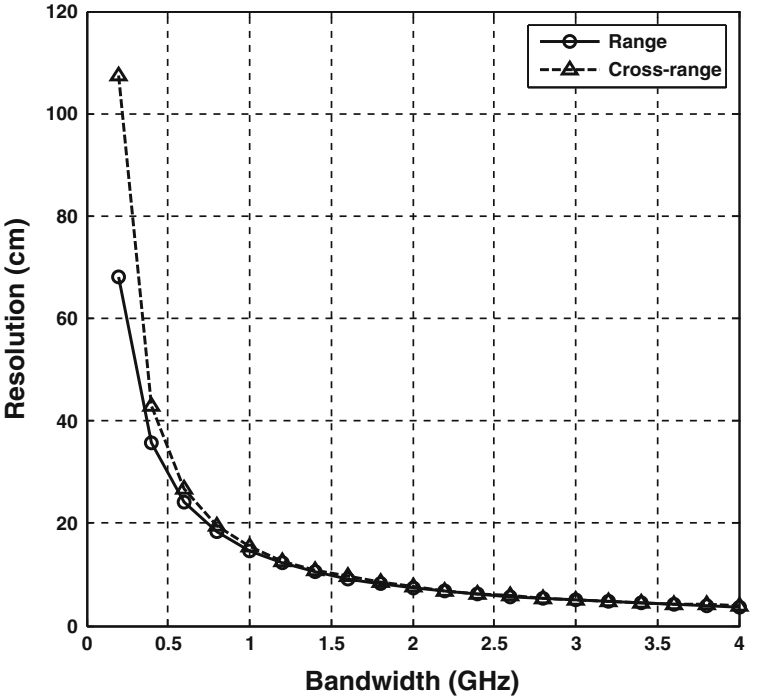

Fig. 7.9 Range and cross-range resolutions versus bandwidth – constant center frequency

with constant center frequency (f_c) or shifting center frequency, Fig. 7.8 . The example in Fig. 7.5 uses shifting center frequency. The use of constant center frequency results in the resolution versus bandwidth relationship as shown in Fig. 7.9 .

Comparison of Fig. 7.5 (shifting center frequency) and Fig. 7.9 (constant center frequency) shows the improvement of the rate of range and cross-range resolutions using shifting center frequency. This is because shifting center frequency scheme has more complete frequency content than the constant scheme. This observation also suggests a continuous exploration in the frequency band and an increasing use of bandwidth for processing.

7.4 Conclusions

The developed FAR NDT technique for the structural assessment of GFRP-wrapped concrete structures mainly consists of two components: (1) far-field ISAR measurements, and (2) image reconstruction algorithm. In this chapter, work is reported on laboratory radar measurements of GFRP-concrete specimens in the far-field region at different angles in the frequency range of 8–12 GHz. The measured frequency-angle data are processed by the imaging algorithm (fast backprojection algorithm)

to reconstruct the range-cross-range imagery of the structure for structural assessments.

The presence of the artificial defect is detected and represented by the scattering signal in reconstructed images, as demonstrated in this chapter. Progressive image focusing based on fast projection algorithm provides a capability for various purposes of inspection in field applications. Image reconstruction using shifting center frequency is proved to be more efficient than using constant center frequency scheme. In the FAR NDT technique, the increase of bandwidth implemented in image reconstruction significantly improves the image resolutions. The detectability of defects is sensitive to the selection of incident angle. Further research is needed to quantitatively define the relationship between the detectability of defects and the incident angle. From the results presented in this chapter, it is believed that the developed FAR NDT capability is applicable for the field inspection of GFRP-wrapped concrete bridge piers in prevention of collapse.

Acknowledgments This work was supported by the National Science Foundation through Grant CMS-0324607, and by the MIT Lincoln Laboratory through Grant ACC-376 (Advanced Concepts Committee). Wide-bandwidth radar measurements were performed at MIT Lincoln Laboratory under the supervision of Dennis Blejer. We gratefully acknowledge his efforts and contributions to the research reported in this chapter. The authors thank Fyfe Co. LLC for supplying the materials used in the experimental work.

References

1. Au C, Buyukozturk O (2005) Effect of fiber orientation and ply mix on fiber reinforced polymer-confined concrete. J Compos Constr 9(5):397–407
2. Sheikh SA, Yau G (2002) Seismic behaviour of concrete columns confined with steel and fibre reinforced polymers. ACI Struct J 99(1):72–80
3. Au C, Buyukozturk O (2006) Peel and shear fracture characterization of debonding in FRP plated concrete affected by moisture. J Compos Constr 10(1):35–47
4. Buyukozturk O, Gunes O, Karaca E (2004) Progress on understanding debonding problems in reinforced concrete and steel members strengthened using FRP composites. Constr Build Mater 18:9–19
5. Teng JG (2006) Debonding failures of RC beams flexurally strengthened with externally bonded FRP reinforcement. Proceedings of Eleventh International Conference and Exhibition of Structural Faults and Repair 2006, University of Edinburgh, Scotland
6. Buyukozturk O, Yu T-Y (2006) Understanding and assessment of debonding failures in FRP-concrete systems. Proceedings of Seventh International Congress on Advances in Civil Engineering. Yildiz Technical University, Istanbul
7. Buyukozturk O, Hearing B, Gunes O (1999) Performance and durability related issues in retrofitting concrete members with FRP. Proceedings of the 13th ASCE Engineering Mechanics Division Conference, June 13–16, The John Hopkins University, Baltimore, MD
8. Smith ST, Teng JG (2001) Interfacial stresses in plated beams. Eng Struct 23(7):857–871
9. Leung CKY (2001) Delamination failure in concrete beams retrofitted with a bonded plate. ASCE J Mater Civil Eng 13(2):106–113
10. Chajes MJ, Thompson TA, Farschman CA (1995) Durability of concrete beams externally reinforced with composite fabrics. Constr Build Mater 9(3):141–148
11. Toutanji H, Gomez W (1997) Durability characteristics of concrete beams externally bonded with FRP composite sheets. Cement Concrete Compos 19(4):351–358

12. Karbhari VM, Zhao L (1998) Issues related to composite plating and environmental exposure effects on composite-concrete interface in external strengthening. Compos Struct 40(3–4):293–304
13. Green MF, Bisby LA, Beaudoin Y, Labossiere P (2000) Effect of freeze-thaw cycles on the bond durability between fibre reinforced polymer plate reinforcement and concrete. Canadian J Civil Eng 27(5):949–959
14. Hamilton HR III (2000) Durability of FRP reinforcements for concrete. Progress Struct Eng Mater 2:139–145
15. Di Tommaso A, Neubauer U, Pantuso A, Rostasy FS (2001) Behavior of adhesively bonded concrete-CFRP joints at low and high temperatures. Mech Compos Mater 37(4):327–338
16. Kinloch AJ (1982) The science of adhesion. J Mater Sci 17(3):617–651
17. Antoon MK, Koenig JL (1980) The structure and moisture stability of the matrix phase in glass- reinforced epoxy composites. J Macromolecul Sci – Rev Macromolecul Chem C19(1):135–173
18. Hutchinson AR (1986) Durability of structural adhesive joints. Ph.D. Thesis, Dundee University, UK
19. Yu T-Y, Buyukozturk (2008) A far-field airborne radar NDT for detecting debonding in GFRP-retrofitted concrete structures, NDT&E International 41:10–24
20. Hillger W (1987) Inspection of concrete by ultrasonic testing. Proceedings of the 4th European Conference on Non-Destructive Testing. London UK, 2:1003–1012
21. De Vekey RC (1990) Non-destructive evaluation of structural concrete: a review of European practice and developments. In: Proceedings of Nondestructive Evaluation of Civil Structures and Materials. Boulder, CO
22. Starnes MA, Carino NJ, Kausel EA (2003) Preliminary thermography studies for quality control of concrete structures strengthened with fiber-reinforced polymer composites. ASCE J Mater Civ Eng 15(3):266–273
23. Malhotra VM, Carino NJ (1991) CRC handbook on nondestructive testing of concrete. CRC Press, Boca Raton, FL
24. Li J, Liu C (2001) Noncontact detection of air voids under glass epoxy jackets using a microwave system. Subsurf Sens Tech Appl 2(4):411–423
25. Feng MQ, De Flaviis F, Kim YJ (2002) Use of microwave for damage detection of fiber reinforced polymer-wrapped concrete structures. J Eng Mech 128(2):172–183
26. Kim YJ, Jofre L, De Flaviis F, Feng MQ (2003) Microwave reflection tomographic array for damage detection of civil structures. IEEE Trans Antennas Prop 51(11):3022–3032
27. Akuthota B, Hughes D, Zoughi R, Myers J, Nanni A (2004) Near-field microwave detection of disband in carbon fiber reinforced polymer composites used for strengthening cement-based structures and disbond repair verification. J Mater Civil Eng 16(6):540–546
28. Zoughi R, Lai J, Munoz K (2001) A brief review of microwave testing of stratified composite structures: A comparison between plane wave and near-field approaches. Mater Eval 60(2):171–177
29. Yegulalp AF (1999) Fast backprojection algorithm for synthetic aperture radar. In: Proceedings of IEEE Radar Conference, 20–22 April:60–65

Chapter 8
Strengthening of Low-Rise Concrete Buildings: Applications After Dinar (1995) and Adana-Ceyhan (1998) Earthquakes

Zekai Celep

Abstract In the rural areas in Turkey masonry buildings are generally constructed without receiving any engineering service, i.e., they are considered to be non-engineered structures. However, although it is much easier to construct one or two stories houses as masonry buildings, they are very often are built as reinforced concrete structures. Reinforced concrete buildings are most common building type in Turkey, since additional stories can be added on them easily without consulting any civil engineer or receiving professional engineering service although it is not a legal way to do it. These buildings have reinforced concrete slabs supported by beams (or tie beams) on the walls and columns (or vertical ties) in some corners of the walls. Generally, neither beams nor columns have adequate cross sectional dimensions and reinforcement detailing. This is also the case for beam-column joints. These columns and beams produce weak concrete frames and the situation is aggravated unreinforced infill walls which behave as a diagonal struts. During the Dinar (1995) and the Adana-Ceyhan (1998) earthquakes, numerous low-rise buildings were damaged to various degrees. In this paper, the post-earthquake strength evaluation, repair, strengthening and upgrading techniques for these low-rise buildings carried out by the team of the Research and Application Center for Structures and Earthquake of the Istanbul Technical University, are presented. It is emphasized that the strengthening of these non-engineered concrete buildings can be done cost effectively by applying the methods used for the masonry buildings.

8.1 Introduction

After the Dinar (1995) and the Adana-Ceyhan (1998) earthquakes, numerous low-rise buildings were damaged. The post-earthquake strength evaluation and repairs, strengthening and upgrading techniques of low-rise buildings were carried out by

Z. Celep (✉)
Istanbul Technical University, Istanbul, Turkey
e-mail: celep@itu.edu.tr

A. Ilki et al. (eds.), *Seismic Risk Assessment and Retrofitting*, Geotechnical, Geological, and Earthquake Engineering 10, DOI 10.1007/978-90-481-2681-1_8,

the several leading centers in Turkey. The objective of this paper is to present a summary of the comprehensive work done and the procedure developed by the team of the Research and Application Center for Structures and Earthquake of the Istanbul Technical University. Furthermore, structural aspects of low-rise buildings in Turkey, their post-earthquake strength evaluations and repair, strengthening and upgrading techniques applied in Dinar and Adana-Ceyhan areas are discussed.

8.2 Turkish Seismic Code Provisions for Masonry Buildings

Unreinforced walls of the masonry buildings are vulnerable to in plane and out of plane loads in the lateral direction. Experiences and observations from past earthquakes as well as research have shown that the performance of masonry buildings can be greatly improved, if the principles below are followed, [1, 2]:

a) Simple plan configuration
b) Avoiding vertical irregularities
c) Regular distribution of structural walls in both directions
d) Parallel wall configuration in each orthogonal direction
e) Avoiding re-entrant corners and recesses
f) Avoiding irregular mass distribution in plan and elevation

Although the Turkish code for the earthquake resistant design essentially focuses on the design of the reinforced concrete and steel structures, it also contains some general specifications for the plain (unreinforced) masonry buildings, [3]. The requirements related to the reinforced concrete and the steel structures are updated considerably in 1998 to reflect the new developments in earthquake resistant design. Minor modifications are done in 2007 regarding the design requirements of the buildings, whereas a new chapter is added for the seismic capacity evaluation of the existing buildings. However, the requirements related to the masonry buildings have undergone only very minor modifications. The code states that all masonry buildings have to comply with the minimum requirements given. The minimum requirements given in the code deal with the restriction on the number of stories of the masonry buildings, the dimensions of the door as well as window openings, the lengths and the thickness of the structural walls, the unsupported lengths of the structural walls, the dimensions of the lintels and the tie beams.

The code provides the minimum requirements for the structural design and construction of the masonry buildings and states that if these minimum provisions are satisfied, an earthquake analysis for masonry buildings is not required. An analysis can be carried out only for a detailed examination of the masonry buildings under earthquake load. When a numerical earthquake analysis is to be performed, the total equivalent earthquake load (the base shear force) is defined as

$$V_t = A_o\, I\, W\, S/R_a \geq 0.10\, A_o\, I\, W \tag{8.1}$$

where A_0 is the effective ground acceleration coefficient that depends on the seismic zone and is between 0.40 (seismic zone 1) and 0.10 (seismic zone 4), I is the building importance coefficient (1.0 for buildings of low occupancy), S is the spectral coefficient (2.5 for masonry buildings), R_a is the earthquake load reduction coefficient (2.0 for masonry buildings), W is the total weight of the building, which includes G_i is the gravity loads and Q_i is the live loads (2.0 kN/m^2 for residential buildings) for each floor. The total weight of the building is calculated by taking into account the coefficient for the contribution of the live load n (0.30 for residential buildings),

$$W = \sum_i W_i = \sum_i (G_i + n\, Q_i) \tag{8.2}$$

In the Turkish Seismic Code the number of stories of the masonry buildings is limited depending on the seismic region. In the first seismic zone where the seismic risk is of the highest degree, the maximum number of stories is limited to two, whereas three stories of masonry buildings can be built in the second and the third seismic zones. In the fourth seismic zone the maximum number of stories is limited to four. However, a masonry building can have additional basement floor and a roof floor having maximum 25% of the normal floor area.

The units used in the masonry walls can be solid and hollow clay or concrete blocks having a maximum pore ratio of 35% and a minimum compressive strength of 5 MPa obtained by considering the total cross section of the unit. Natural stones having a minimum compressive strength of 10 MPa can be used in basement walls. Minimum thickness of the masonry walls depends on the seismic zones as given in the code.

Ratio of the total length of the masonry walls in two directions excluding windows and door openings to the floor area should not be less than 0.20I m/m^2. Masonry walls should be laterally supported at interval not exceeding 5.5 m in the first seismic zone and to 7.5 m in the other seismic zones. When this condition can not be satisfied, then vertical tie beams should be provided maximum in every 4.0 m including the corners along the masonry wall for which the unsupported length can not be longer than 16.0 m in any case.

Window and door openings should not be closer to the corners (to each other) more than 1.5 m (1.0 m) in the first and second seismic zones and 1.0 m (0.8 m) in the third and fourth seismic zones, respectively. When vertical tie beams are provided in each side of the masonry walls, these minimum lengths can be reduced by 20%. These openings should not be closer than 0.5 m to any support of the masonry wall. Lintels above the window and the door openings should have a minimum support length of 0.2 m and 15% of the opening span.

There is an increasing trend within the engineering community today that the rules may be too conservative for buildings that have received engineering service during their construction. However, when the requirements are inspected, it is seen that they are reasonable and they are derived from the lessons learned from the damage observed in the past earthquakes. In addition, the requirements are certainly not conservative, for buildings constructed in the rural areas without acquiring any civil engineering service.

8.3 Low-Rise Buildings: Masonry vs. Reinforced Concrete Frame Buildings?

Traditionally, earthquake resistant design of masonry buildings has been based on the construction of thick, massive walls that relied on their self weight to resist the horizontal loads. Walls are plastered and connected to each other by slabs to improve their stability against horizontal loads. Resistance of masonry buildings subjected to an earthquake is defined by the inter-connectivity between structural components as well as the strength and the stiffness of the individual components. Good connection between the components of the building creates continuous load paths for the gravity and the inertia loads. It is of prime importance to provide connection between walls through good quality bond at corners and construction of horizontal tie beams. Furthermore it is important to provide connections between walls and foundations and to provide connection between the walls and the roof plate.

In Turkey, the masonry buildings are generally built without receiving any engineering service, i.e., they are considered to be non-engineered structures. Very often one or two story houses are built as reinforced concrete, although it is usually much easier to construct them as masonry. However, some people prefer reinforced concrete buildings, because stories can be added to them mostly without consulting any civil engineer or receiving any professional service. However, the low-rise buildings constructed without receiving any professional service have reinforced concrete slabs supported by beams (or tie beams) on the walls and columns (or vertical ties) in corners of buildings. Generally, neither beams nor columns have adequate cross sectional dimensions and reinforcement conforming to the requirements of the code. Mostly they have four longitudinal reinforcements with ties having a spacing of 20~30 cm. The beam-column joints do have not proper detailing. This is a common construction type for low-rise building practice not only in Turkey, but worldwide. There are low-rise buildings having reinforced concrete "frame" with unreinforced infill walls. When the building is subjected to earthquake loads, diagonal braces develop within the infill walls and increase the lateral rigidity and the load bearing capacity of the buildings.

Low-rise reinforced concrete buildings have become a common construction practice in the rural areas and in the outskirts of the metropolitans, although they are constructed without proper professional attention. They are usually built up to 2–3 stories in height. However, depending on the economical conditions of the owner, the buildings are constructed up to 6 stories or more by using common construction practices to support the vertical weight of the structure. As a result, the majority are damaged in earthquakes, as they are not designed to resist lateral forces produced by the seismic excitations.

Some low-rise concrete buildings have large internal openings within the infill walls or unsymmetrical masses at the first or the ground floor level. This may cause severe structural damage and even collapse. A soft or weak storey collapse generally comes into being due to the lack of the infill walls in the ground floor with a higher story height which is often used for commercial purposes. In fact many buildings are prevented from collapse by the presence of the "non-structural" infill walls that act

as shear walls despite not being designed for this purpose. The infill walls are mainly made of brick or concrete block. They are most effective when the construction procedure involves a high degree of bonding between the wall and columns at the corners. This is often achieved during the construction, by building the walls up to first floor level leaving a gap at the column positions, then casting the columns using the walls as shutters.

Large window and door openings severely undermine the ability of the infill walls to act as shear walls. Shear wall behavior is prevented, when these openings are placed too close to the corner columns of the building. Lintels are placed over the openings to prevent the weakness of the wall due to openings. Some seismic codes recommend to extent the lintels over the length of the wall. During seismic loading infill walls experience diagonal shear cracking which extend from the openings to the top and bottom of the solid walls. Generally, the greatest damage occurs in the ground floor level whereas upper stories survive with slight damage.

Considering these all these negative properties of the low-rise buildings, it is very difficult, if not impossible; to consider their structural systems as reinforced concrete frame system. On the other hand, it is often difficult to explain, how these structural systems support their own weight or why they did not collapse during earthquakes without considering the contribution of the walls. These buildings have a behavior in between a reinforced concrete frame system and a masonry building. However, their behavior may be considered to be close to masonry, although they do not satisfy the basic requirements of the code related to the masonry buildings. Since they have a lower structural quality and generally they do not have acceptable level of seismic safety, it is reasonable to improve them seismically by using economical strengthening interventions to prevent the total collapse even if they do not have any damage.

It is not a good idea to strengthen these buildings by jacketing columns and adding shear walls together with enlarging of the existing foundation. These interventions can not be done due to several reasons. Firstly, it is not advisable to add shear walls to low-rise buildings and concentrate the lateral load in some specific location, since the transfer of the lateral force to the shear walls can not be done adequately. Secondly, since almost all columns require jacketing, it is not feasible to do this in economical terms. Thirdly, these buildings do not have proper foundations as concrete frame buildings do. Therefore strengthening of the foundations will be required as well, which is difficult. However, these buildings can be strengthened relatively easily as is done in masonry buildings.

8.4 The Dinar (1995) and the Adana-Ceyhan (1998) Earthquakes

The Dinar (1995) earthquake occurred with a magnitude of 5.9–6.0, on Sunday, October 1, 1995, at 17:57 local time, after a series of foreshocks of various degrees with the last four days. Dinar, being in the first seismic zone is located in the southwestern part of Turkey. The epicenter of the main shock having peak ground

acceleration about 0.30 g was about 5∼10 km away from the city center. The death toll was about 90 and severe structural damage occurred in Dinar and in the surrounding villages having a total population of 91,000 according to the 1990 census. Numerous reinforced concrete and masonry buildings, especially those located on soft soil on the lower basin of Dinar, suffered substantial damage.

The Adana-Ceyhan of magnitude of 5.9 earthquake occurred on June 27, 1998 at 16:56 local time. The depth of the earthquake is given as 13–22 km. On July 4, 1998 at 9:24 local time, the largest aftershock of magnitude 5.1 occurred. The records from Ceyhan, where the largest number of deaths and damage occurred, had peak ground accelerations of 0.22 g (NS), 0.27 g (EW) and 0.087 g (UP). The earthquake caused approximately 150 deaths and injuries to several thousand people.

8.5 Damage in Low-Rise Buildings

Typical construction in the rural area is reinforced low-rise concrete frame building with (brick or hollow-brick) infill walls. There is a significant number of older, stone or brick masonry buildings in Dinar and Adana-Ceyhan area. These buildings suffered considerable levels of damage. However, in many cases, the infill walls within the beam-column frame have increased the strength and stiffness. The presence of infill walls have also improved the performance of the buildings and decreased the damage. It should be stated that there is a significant number of mid-rise and tall buildings which displayed an acceptable seismic performance during the Dinar and The Adana-Ceyhan earthquake, since they generally received engineering service, [4, 5].

Masonry structures are well suited for gravity loads. However due to the low-tensile strength and the brittle properties of bricks, such houses can suffer damage in earthquakes. As in various small towns in Turkey, the low-rise buildings have widespread application in Dinar, Adana and Ceyhan. During the earthquakes, most of these buildings were damaged to various degrees. Some of them collapsed and there was no chance to use them any more. These types of buildings were demolished down in a very short time; the remaining damaged buildings were taken under the loop for closer inspection for decision of rehabilitation, Table 8.1.

In fact, the main causes of different type of damages suffered by low-rise concrete buildings is the weak frame system having a very low moment resisting capacity and the low tensile and shear strength of walls. On the other hand, the main weaknesses constructions are heavy weight and very stiff buildings which attract large seismic inertia forces, very low tensile strength of infill units and poor mortars having low shear strength. Brittle behavior of masonry units in tension and compression causes the buildings to collapse without showing significant plastic behavior. Weak connections between the walls and the roof produce total collapse of the building quickly from a minor damage initiated at one of the weak region of the building. Furthermore, large window and door openings and considerable deviation from symmetry of wall layout cause stress concentration at corners.

Table 8.1 General post-earthquake damage data collection form for low-rise buildings

■	*Building number and address*						
	Number of the independent parts of the building				○		
	Occupancy	○	*residential*	○	*commercial*	○	
	Photo	○	*provided*	○	*layout*	○	*provided*
	Year built	○					
	Owners	○					
■	*Number of stories*	○					
	Story height	○					
	Soil type	○					
	Discontinuities in the load bearing system between floors, percentage of coincidence of the layout of infill walls in each story:			○			
	Materials, thickness and workmanship of masonry walls in each story:						
	Basement	○		○		○	
	First story	○		○		○	
	Second story	○		○		○	
	Third story	○		○		○	
	Type of the slabs, the beams and the lintels (reinforced concrete, wooden):						
	Basement	○		○		○	
	First story	○		○		○	
	Second story	○		○		○	
	Third story	○		○		○	
	Roof and stairs	○		○		○	
■	*Damage evaluation in each story by giving length and thickness of cracks and separations:*						
	Cracks and separation in infill walls			○		○	○
	×cracks in masonry walls			○		○	○
	Cracks and separation in infill walls in corners			○		○	○
	Cracks in corners of windows			○		○	○
	×cracks in between windows and door openings			○		○	○
	Cracks between horizontal tie beams and floor slab			○		○	○
	Damage in stairway and roof structure			○		○	○
■	*Proposal for repair and strengthening:*						
	Cracks and separation in infill walls			○		○	○
	×cracks in masonry walls			○		○	○
	Cracks and separation in infill walls in corners			○		○	○
	Cracks in corners of windows			○		○	○
	×cracks in between windows and door openings			○		○	○
	Cracks between horizontal tie beams and floor slab			○		○	○
	Damage in stairway and roof structure			○		○	○
Date		○	*Inspected by*		○		

The inspection of numerous masonry buildings in Dinar and Adana-Ceyhan revealed that the main causes of damage in earthquakes can be classified as follows:

Use of substandard masonry units and mortar, Figs. 8.1, 8.2, 8.3, 8.4.

a) Poor workmanship and unfilled joints between masonry units, Figs. 8.5, 8.6, 8.7, 8.8, 8.9.
b) Deviation of walls from vertical plane and discontinuities in the load bearing system, Fig. 8.10.
c) Lack of integrity of walls
d) Inadequate connections between walls at corners

Fig. 8.1 Poor material and mortar in the wall

e) Lack of connection between floors, roof plate and walls, Figs. 8.11, 8.12.
f) Absence of rigidity in the roof plane
g) Plan irregularities
h) Alterations and extensions done without paying proper attention to the load bearing system
i) Soft or weak first story
j) Inadequate wall area and poor quality of construction materials, Figs. 8.8 and 8.9.

Large window and door opening, Fig. 8.13.

a) Inadequate coupling of walls
b) Deterioration in structural systems.

Fig. 8.2 Poor material and mortar in the ground floor (the other two stories are added later)

Fig. 8.3 Poor material and mortar in the wall

8.6 Post-Earthquake Evaluation of Damaged Low-Rise Buildings

During the Dinar (1995) and the Adana-Ceyhan (1998) earthquakes, numerous low-rise buildings in this area were damaged. Considering the constraints in time as well as in budget, simple and effective evaluation and strengthening techniques

Fig. 8.4 Poor material and mortar in the wall

Fig. 8.5 Substandard wall units

were developed by the team of the Research and Application Center for Structures and Earthquake of the Istanbul Technical University by following force-based linear analysis. The post-earthquake strength evaluation and repair, strengthening and upgrading techniques of 225 low-rise buildings having one, two and three stories, were carried out. After a preliminary screening by the experts of the Department of Earthquake Research Institute of Turkish Government, rehabilitation of 225 low-rise buildings were entrusted to the Research and Application Center for Structures

Fig. 8.6 Substandard wall units

Fig. 8.7 Substandard plaster

and Earthquake of the Istanbul Technical University. The first inspections revealed that the earthquake damage in 18 buildings was very severe. They were either too close to collapse or their strengthening was not feasible from an economical point of view or their architectural layouts were not worth to rehabilitate. Their demolition is recommended and carried out. These investigations also showed that the damage in two buildings was of minor importance and they did not need any strengthening. However, for twelve buildings, pulling down of upper stories is recommended

Fig. 8.8 Substandard wall units

Fig. 8.9 Substandard wall units

in order to restore a limited seismic strength for the remaining part of the buildings. Examination was carried out in several steps. After detailed assessment study, a rehabilitation program was started for the remaining 205 buildings.

To decide the level of the damage, an examination was carried out in several steps. At first step, a data collection form was developed for collecting general data about the load bearing system of the buildings and earthquake damages. The data

Fig. 8.10 Soft/weak second story

Fig. 8.11 Lack of integrity between walls

collection form includes the number of stories, the type and the thickness of the walls, workmanship of the walls and the type of the staircase.

Most damage patterns in infill walls of low-rise buildings can fit in the following groups:

Fig. 8.12 Damage at the corner part of the wall

Fig. 8.13 Large openings in the walls

a) Separation of walls at corners and T intersections
b) Diagonal cracks starting at wall openings
c) Out-of-plane partial or complete collapse of walls
d) Diagonal and × type of cracks
e) Cracking between the walls and the roof/floor
f) Diagonal cracks between wall openings

Each building was visited twice to investigate its existing condition. In the data collection form, special attention was paid for determining significant discontinuities in the configuration of the structural walls and the geometrical irregularities between the stories. In the form, the presence of an adjacent structure to the building and that of the important visible deterioration of the infill walls were also noted. In this way, major deficiencies in the load carrying system of the low-rise buildings were checked as well. Furthermore, cracks in the load bearing walls, damages in the roof and stairs of the building due to the earthquake loads were also noted in the evaluation form. In a later visit the walls to be strengthened were selected by considering the structural and the architectural layout of the building.

8.7 Strength Evaluation of Low-Rise Buildings

In common masonry, buildings vertical forces due to the dead and the live loads and the lateral forces due to the earthquake are resisted by the structural walls. In masonry buildings, beside the structural walls, partition walls are used for the separation of the rooms having different functional purposes. Since the capacity of these partition walls in the load carrying process is very small in comparison with the structural walls, their capacities are neglected, Structural walls of low-rise buildings are very sensitive to the tensile stresses, and this weakness can be avoided by reinforcing within the masonry units. Although reinforced masonry is very common in various parts of the world, it is used very seldom in Turkey. However, plain unreinforced masonry buildings are constructed very widely in the rural parts of the country.

Because of the multi-axial nature of the ground shaking, infill walls are subjected to simultaneous vertical, out-of-plane and in-plane horizontal loads under seismic forces. While vertical loads come into being as a result of the weight of the building, the inertia mainly yields horizontal forces. The in-plane loads are the results of the resistance of the wall rigidity to the inertia forces from the other parts of the masonry buildings, such as floor masses, whereas the inertia of the wall itself results in out-of-plane loads. Since the masonry buildings are very rigid, their seismic capacities are evaluated by using strength based analysis instead of displacement based analysis. In several cases, strength evaluations of the masonry buildings by using sophisticated methods can be of very controversial nature due to the assumptions in the analysis. Irregularities in the units of infill walls which do not conform to the corresponding standards and deficiencies in the workmanship are very difficult to grasp in the modeling phase. In course of the analytical investigations, three analyses having different degrees of accuracies were carried out. The differences of these analyses were in the modeling of the masonry buildings as well as in the simplification of the analysis by neglecting some of the secondary effects.

The first analysis was carried out by considering all the walls and by taking into account the window and the door openings for very few buildings only. Torsional effect of the seismic forces due to the difference between the centers of the mass and the rigidity was considered in this analysis by using finite element modeling

of the walls. In the second analysis, the procedure was simplified by considering only the solid parts of the walls and by ignoring parts of walls having window and door openings. Finally, in the third analysis, shear stresses due to the lateral seismic forces were calculated in proportion to the wall cross sections only. However, earthquake loads were obtained in three analyses by using the requirements of the code as described in the preceding chapters. Comparison of the results showed that the third analysis yielded quite acceptable results for the interpretation of the behavior of the buildings due to the simple assumptions used and due to irregularities in the walls.

In the analysis, the total base shear due to the seismic loads is obtained according to the requirements of the code and it is distributed over the height of the building in proportion to the floor weight w_i and its height from the ground h_i. The story shear forces F_i are obtained and distributed over the masonry walls in the direction of the shear forces in proportion to the wall section areas A_i.

$$\begin{aligned} F_i &= V_t w_i\, h_i / \sum_{j=1}^{N} w_j h_j \\ V_i &= \sum_{j=i}^{N} F_j \\ \tau_{xi} &= V_i / A_{xi}, \tau_{yi} = V_i / A_{yi} \end{aligned} \tag{8.3}$$

The shear stresses are obtained and compared with the equivalent ultimate shear stresses reduced by a suitable safety factor:

$$\begin{aligned} \text{Concrete block masonry walls:} \quad & \tau_{ult} = 50 kN/m^2 \\ \text{Brick and stone masonry walls:} \quad & \tau_{ult} = 150 kN/m^2 \\ \text{Concrete basement walls:} \quad & \tau_{ult} = 750 kN/m^2 \end{aligned} \tag{8.4}$$

When the shear stresses did not exceed the corresponding allowable shear stress, the building was assumed to have adequate seismic safety. On the other hand, when it was not the case, then it was decided that the building needed some type of strengthening. Although this analysis is used for masonry buildings, it is extended to the low-rise buildings as discussed in the subsequent section.

8.8 Techniques for the Repair and Upgrading of Damaged Low-Rise Buildings

As a rule of thumb for all types of structures, it is much cheaper to design a low-rise building for earthquake resistance in the first place than to carry out repair and strengthening works. Studies have shown that a building designed for seismic resistance is about 10% more expensive only. However, repairs to a non-engineered

building may involve as much as 2–3 times the initial cost of introducing seismic features into a building. If strengthening has to be carried out, this could even be 4–8 times as expensive.

In Dinar and Adana-Ceyhan area, each building was investigated and when the building was found to be moderately damaged or to have inadequate shear capacity, a suitable strengthening technique was chosen to improve the deficient shear capacity of the damaged building.

In the strengthening decision, the following points have to be kept in mind:

a) Sophisticated strengthening techniques should not be considered, due to the inherent uncertainties in the structural system and the poor workmanship in buildings in general.
b) Selected strengthening system should be applicable very easily by using local material and workmanships and it should be cost-effective. Since the number of the buildings is large, a uniform and simple strengthening method should be applied at a reasonable cost.
c) Although the requirements of the code should be followed as much as possible, there are almost no requirements related to the type of the strengthening selected. Generally low-rise buildings are to be transformed to reinforced masonry buildings.
d) The seismic safety level should be in between the levels of the life-safety and the prevention of the total collapse due two reasons: (a) The lateral load capacity of the buildings considered can not be evaluated accurately enough. (b) Due to the economic shortcomings, the method should be cost-effective.

Strengthening techniques which were widely used in Dinar and Adana-Ceyhan consisted of providing additional thickness to the existing walls by applying shotcrete after anchoring steel web reinforcement to the inside and/or outside face of the existing walls. However, the following additional alternatives were considered as well, Table 8.2.

a) Increasing the shear capacity of the existing walls by filling in some door and windows openings with masonry units
b) Improving the shear capacity of the damaged walls by removing the damaged part of the walls and repairing it by using new units and repair mortar.

Considering the weaknesses of the damaged buildings, application of a uniform and simple strengthening method is selected. In the strengthening process, the shear capacity of walls is increased by applying shotcrete, repairing the existing infill walls and providing additional thickness to the existing walls. However, indoor applications of shotcrete caused severe problems due to back spring of the concrete material in a small room. Furthermore, the corners between the walls, the walls and the floors and the ceilings can not be properly done. Due to these difficulties, indoors as well as in some narrow places, ready-made repair mortar was applied instead of shotcrete. In general, before the application of the shotcrete, steel web reinforcement was laid over inside and/or external faces of the existing walls. Steel

Table 8.2 General strengthening plan for earthquake damaged low-rise buildings

Damaged level	*Story*		
	First storey	*Second storey*	*Third storey*
One-story building having medium damage	*Application of shotcrete and web reinforcement to the corners of the building from outside only*		
Two-story building having medium damage	*Application of shotcrete and web reinforcement to the corners of the building from inside and outside*	*Application of shotcrete and web reinforcement to the corners of the building from outside only*	
Three-story building having medium damage	*Application of shotcrete and web reinforcement to the corners of the building from inside and outside*	*Application of shotcrete and web reinforcement to the corners of the building from inside and outside*	*Application of shotcrete and web reinforcement to the corners of the building from outside only*
One-story building having severe damage	*Application of shotcrete and web reinforcement to the corners of the building from inside and outside*		
Two-story building having severe damage	*Application of shotcrete and web reinforcement to the corners of the building from inside and outside*	*Application of shotcrete and web reinforcement to the corners of the building from inside and outside*	
Three-story building having severe damage	*Application of shotcrete and web reinforcement to the corners of the building from inside and outside*	*Application of shotcrete and web reinforcement to the corners of the building from inside and outside*	*Application of shotcrete and web reinforcement to the corners of the building from inside and outside*

webs were anchored by steel bars to integrate the added concrete thickness with the existing walls. These and the other details of the strengthening applications are given in Figs. 8.14, 8.15, 8.16, 8.17, 8.18, 8.19, 8.20, 8.21, 8.22.

The thickness of the added walls was chosen to be 50 mm in one face of the wall in order to obtain a homogenous concrete layer. In fact during the application process it found that 50 mm was a good choose. When larger thickness is used, for their integration and to provide adequate concrete cover to web reinforcement, shotcrete is applied as an additional measure. However, when smaller thickness is applied, it is very difficult to establish integration between the wall and the shotcrete layer. However their lengths as well as the number of stories to be strengthened were determined by checking the results of the strength evaluation. In the distribution of the shear stresses over the infill wall cross sections, the infill wall sections were considered to be a composite one and the ratio of the modulus of elasticity was assumed as follows:

$$E_{concrete\ wall}/E_{concrete\ block\ wall} = 15$$
$$E_{concrete\ wall}/E_{brick\ wall} = E_{concrete\ wall}/E_{stone\ wall} = 5 \tag{8.5}$$

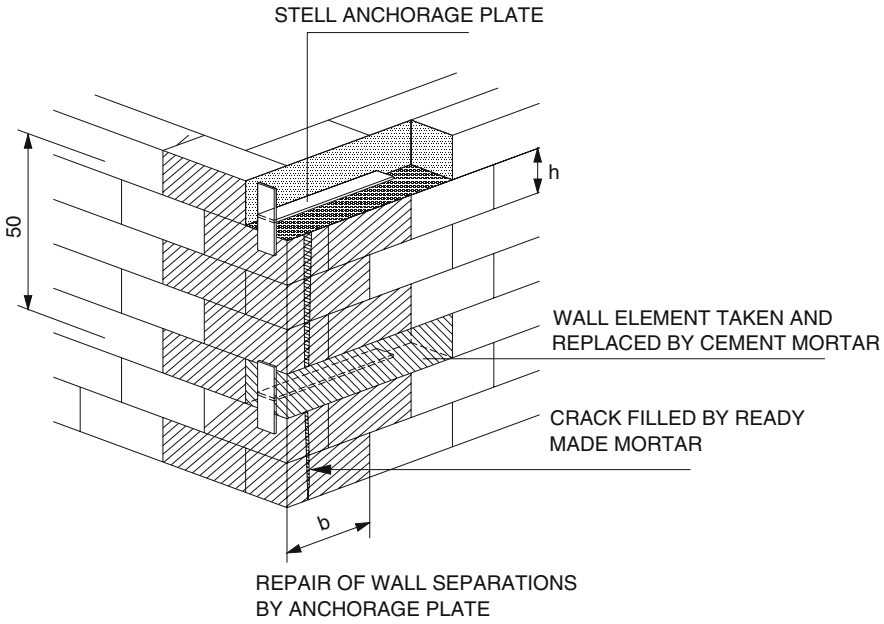

Fig. 8.14 Repair of wall separations by anchorage plate

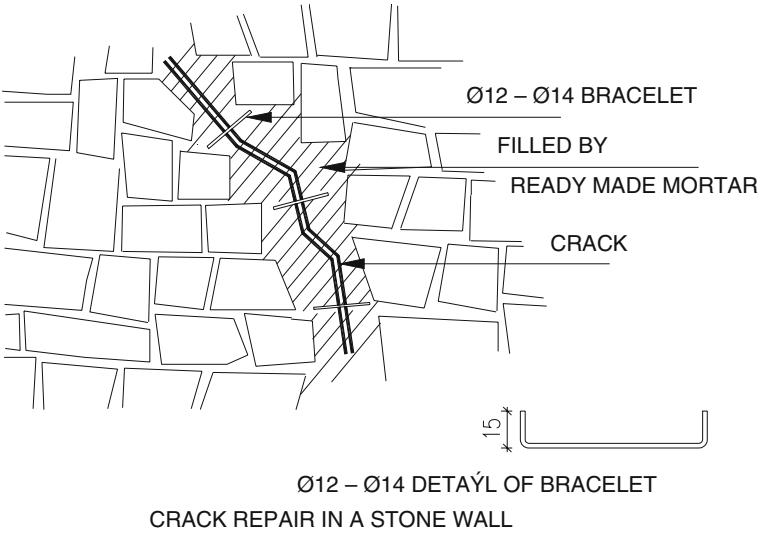

Fig. 8.15 Crack repair in a stone wall

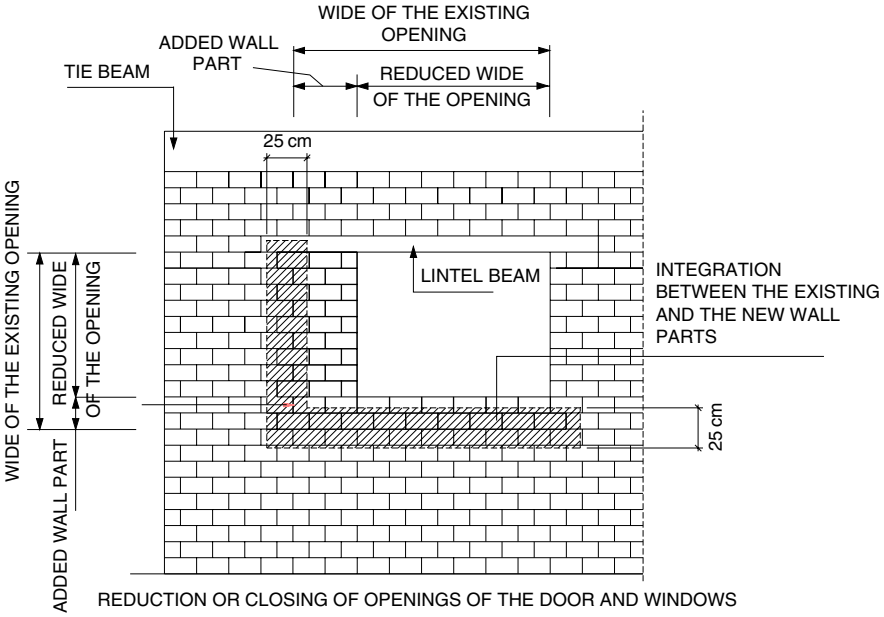

Fig. 8.16 Reduction or closing of openings of doors and windows

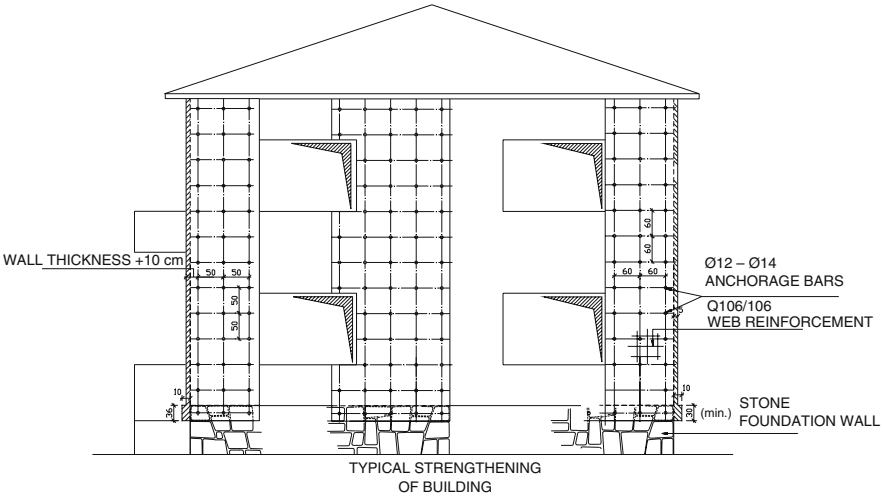

Fig. 8.17 Typical strengthening of a building

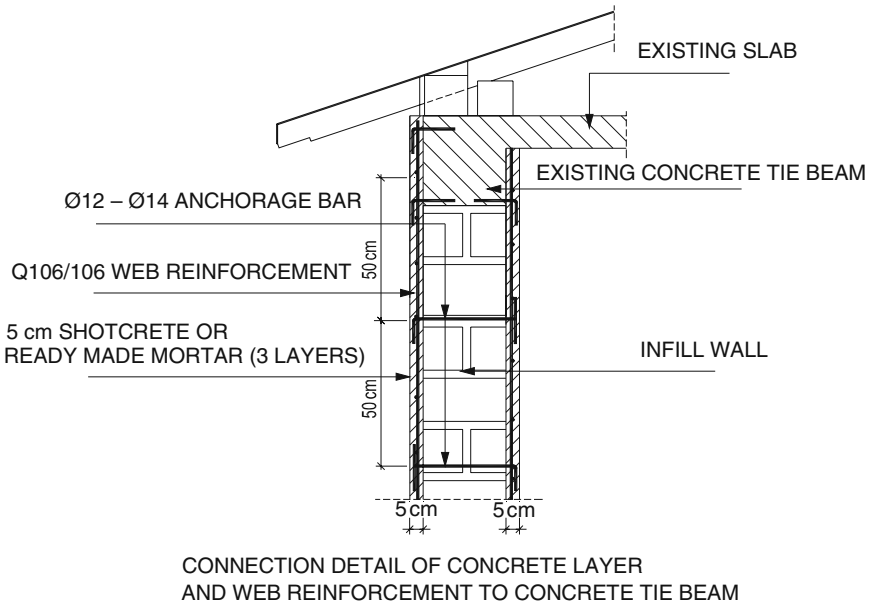

Fig. 8.18 Repair of wall separations by anchorage plate

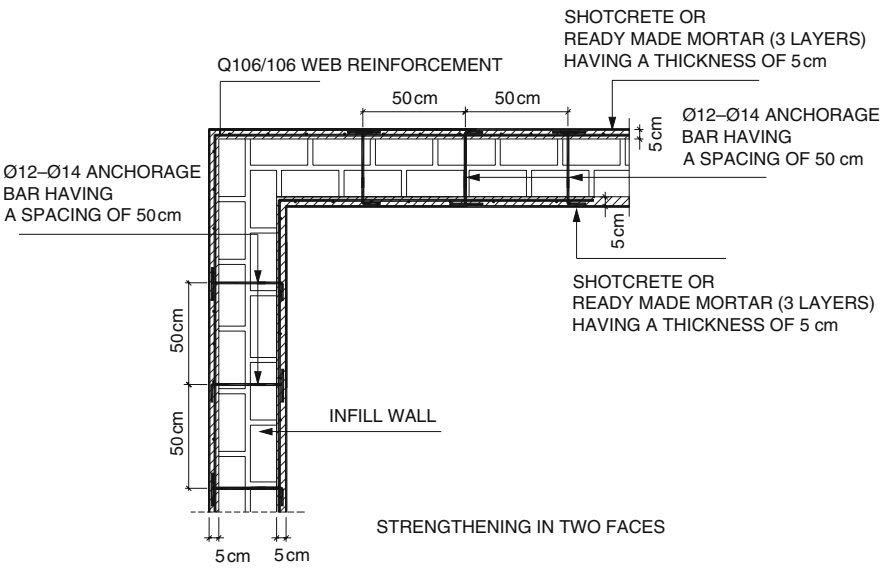

Fig. 8.19 Strengthening in two faces of the wall

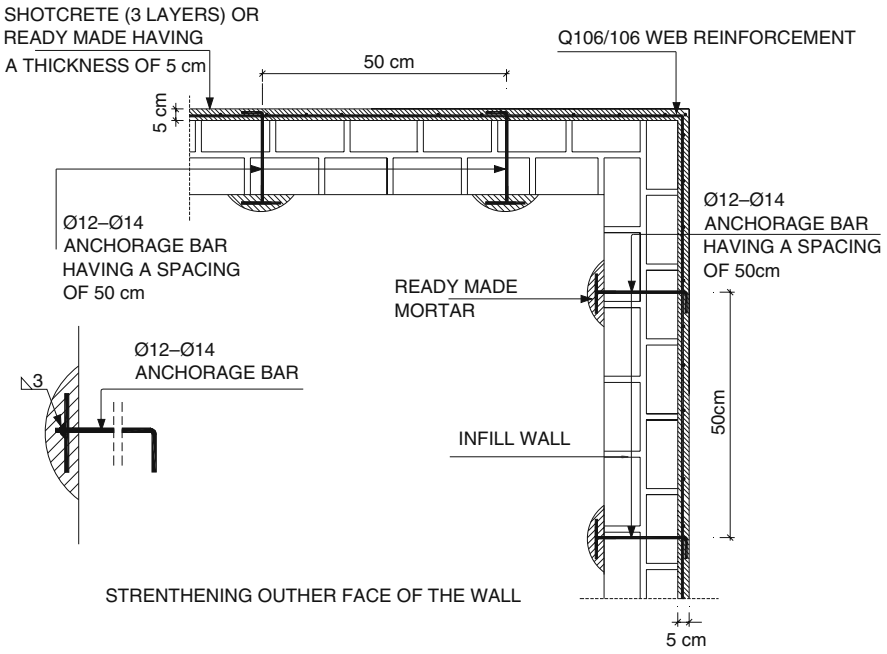

Fig. 8.20 Strengthening of the external face of the wall

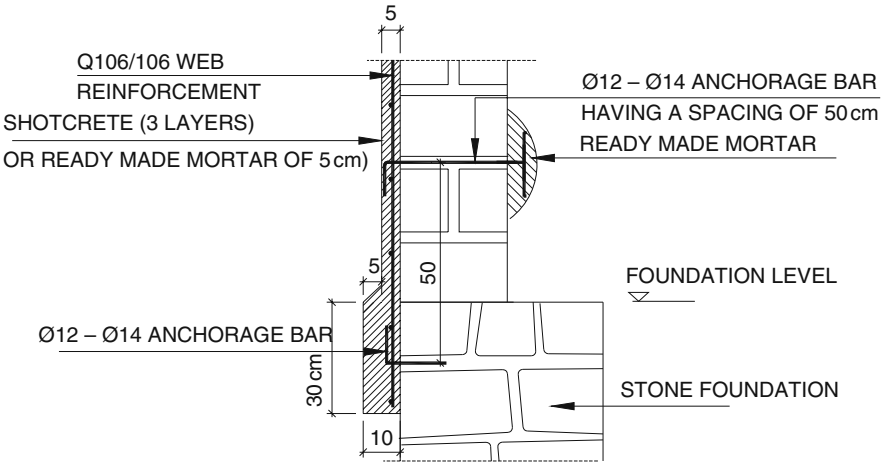

Fig. 8.21 Integration of strengthening layer to stone foundation

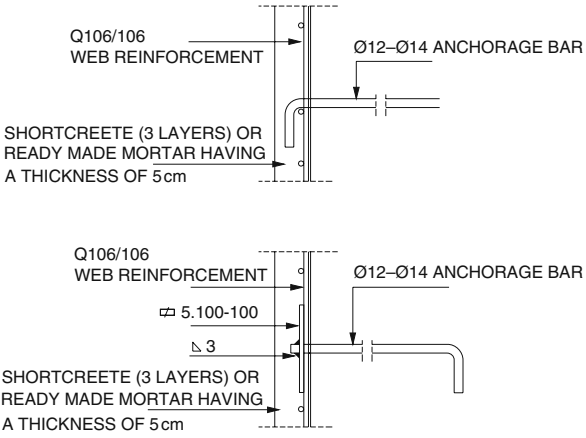

Fig. 8.22 Anchorage elements used for integration of the strengthening layer to the existing wall

Fig. 8.23 Application of web reinforcement

Furthermore, seismic loads were reduced by 1.2 (1.5) for building having strengthened walls with web reinforcement in one (two) face(s), due to the improved ductility of reinforced masonry walls relative to the unreinforced masonry wall.

8.9 Application Details

In order to produce the application details, one has to consider that due to the seismic oscillations, the inertia forces are generated in the existing system where the masses are concentrated. These inertia forces have to be transferred safely to the structural system. The integration of the existing and the added systems has to be provided. General application details used in Dinar and Adana-Ceyhan are given in figures. Figure 8.14 shows the repair of the joint of the two walls. This application establishes a robust integration of the two walls to each other. In this way the lateral load capacity of the walls are increased. Figure 8.15 shows the crack repair in a

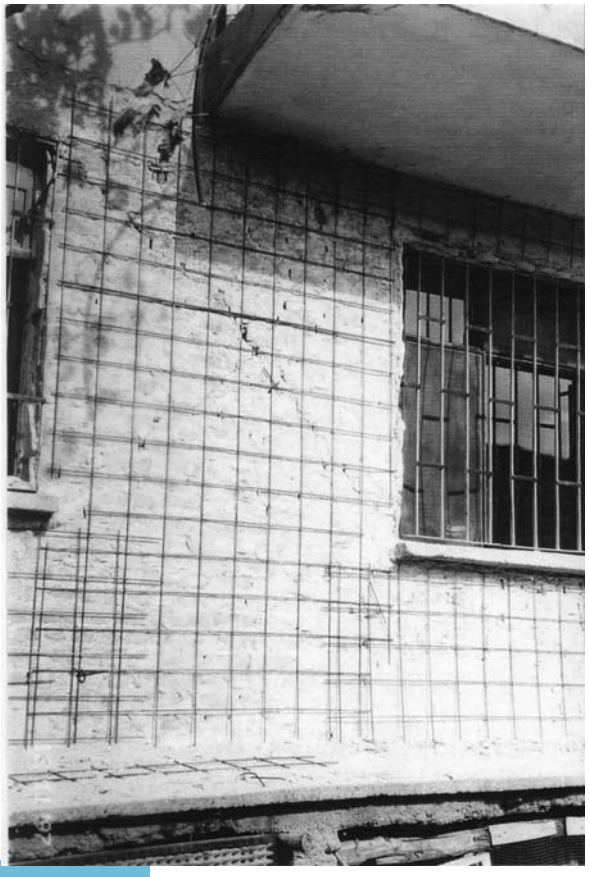

Fig. 8.24 Application of web reinforcement

Fig. 8.25 Application of web reinforcement

Fig. 8.26 Application of shotcrete

stone wall by applying a steel connector and ready made grout. Application details of shotcrete or ready made mortar to walls are given in Figs. 8.16, 8.17, 8.18, 8.19, 8.20, 8.21, 8.22. It is usually recommended that concrete layer should be applied in two faces of the walls and these layers should be connected through the steel connectors to each other to establish a suitable integration with the existing wall. The connections of the layers to the slab through the tie beam and to the foundation are of prime importance as observed in the figures. Some application of web reinforcement and shortcrete are given in Figs. 8.23, 8.24, 8.25, 8.26. In various applications, closing or decreasing the size of the windows or door openings is recommended as shown in Fig. 8.16. In this case, it is of major importance to establish the integration of the added wall part to the existing one.

8.10 Conclusions

It has been suggested that the seismic safety investigation and strengthening of various low-rise buildings in Turkey can be achieved by applying the methods used for masonry buildings, because they are non-engineered structures and the principles used for reinforced frame building can not be applied for these buildings. It is not wise to retrofit these buildings by applying column jacketing, because the beams are very weak and the buildings do not have a proper framing system. Furthermore, these buildings can not be strengthened by adding shear wall, which may require a large foundation. In strengthening low-rise buildings, integration of the added concrete layer to the existing structure is of prime importance. Nevertheless, proper anchorage bars should be used between the added concrete layers and the existing concrete elements such as the tie beams and columns and the foundation beams.

References

1. Celep Z, Kumbasar N (2004) Introduction to earthquake engineering and earthquake resistant design, Beta, Istanbul, Turkey. (in Turkish)
2. Celep Z, Ozer E (1998) Post earthquake rehabilitation of moderately damaged masonry structures, Second Japan-Turkey Workshop on Earthquake Engineering, Istanbul Technical University, 61–72, Istanbul
3. Turkish Code for Earthquake Resistant Design (2007) Ministry of Public Works and Settlement, Ankara, Turkey.
4. UNP/UNIDO (1983) Repair and strengthening of reinforced concrete, stone and brick-masonry buildings, Building Constructions under Seismic Conditions in the Balkan region, Volume 5, Vienna, Austria.
5. Paulay T, Priestley MNJ (1992) Seismic design of reinforced concrete and masonry buildings, John Wiley & Sons, New York, USA.

Chapter 9
Rehabilitation of Precast Industrial Buildings using Cables to Develop Diaphragm Action

Renjun Wang, James O. Jirsa, and Sharon L. Wood

Abstract Precast frame buildings are often used in Turkey for industrial facilities. One-story warehouses are the most common structural configurations. The lateral load resisting system is derived primarily from cantilevered, precast columns. Because the precast structures are flexible and lack redundancy, many were damaged beyond repair during the 1999 earthquakes in Turkey. A rehabilitation scheme is proposed to introduce a structural diaphragm at the roof level by adding diagonal bracing. With diaphragm action, the inertial forces can be distributed more uniformly among the cantilevered columns, and can be transmitted to the vertical diagonal braces around the perimeter of the structure to enhance seismic performance.

9.1 Introduction

One-story industrial buildings represent the most common form of precast construction in northern Turkey [4]. A large portion of these structures (Fig. 9.1) sustained severe damage during the 1999 earthquakes in Kocaeli and Düzce [1, 2] and in previous earthquakes [3]. Deficiencies in this structural system were studied and a practical rehabilitation scheme was developed. The rehabilitation scheme is discussed in this chapter.

The precast concrete industrial buildings are generally rectangular in plan with one to four bays in the transverse direction, and ten to thirty bays in the longitudinal direction (Fig. 9.2). The length of bays ranges from 10 to 25 m in the transverse direction, and 6–8 m in the longitudinal direction. Story height is typically 6–8 m.

During construction, rectangular precast columns were inserted into footings with sockets, and the gaps between the columns and the footings were grouted. The columns provide the lateral support for the entire structure and are assumed to be fixed at the base. Long-span roof girders, typically trapezoidal in shape, span in the

J.O. Jirsa (✉)
University of Texas at Austin, Austin, TX, USA
e-mail: jirsa@uts.cc.utexas.edu

A. Ilki et al. (eds.), *Seismic Risk Assessment and Retrofitting*, Geotechnical, Geological, and Earthquake Engineering 10, DOI 10.1007/978-90-481-2681-1_9,

Fig. 9.1 Collapsed precast industrial building near Adapazarı following the 1999 Kocaeli Earthquake

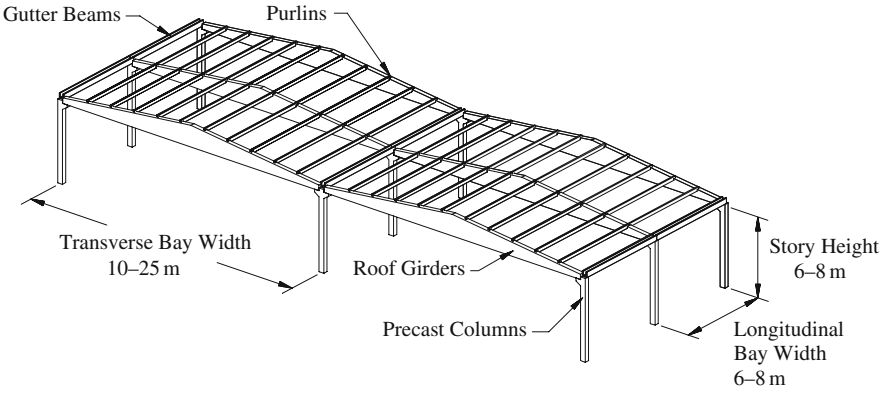

Fig. 9.2 Typical geometry of one-story precast industrial buildings

transverse direction of the building. Purlins and U-shaped gutter beams span in the longitudinal direction. The roof is constructed from lightweight materials, typically metal decking or asbestos panels.

The precast roof girders, gutter beams, and purlins were pinned at both ends. Vertical dowels extended up from the supporting member and the horizontal elements were cast with vertical holes near their ends to accommodate these dowels. The holes were filled with grout in most buildings. In some cases the dowels were threaded, and nuts were installed before grouting.

Fig. 9.3 Flexural hinge at base of cantilevered, precast column

In general, the cantilevered columns provided the lateral strength and stiffness of the buildings. Even when precast wall panels were used for cladding, the connection details were developed such that the wall panels did not contribute to the lateral stiffness of the building.

Two types of structural damage were frequently observed in the precast buildings: flexural hinges at the base of the columns (Fig. 9.3) and relative movement of the precast elements at the roof level (Fig. 9.4). In addition, buildings under construction were susceptible to collapse when the roof girders rotated off their supports (foreground in Fig. 9.1).

The one-story, industrial buildings considered in this investigation had the following features and/or deficiencies:

1. Large open areas with few or no interior partitions.
2. Precast concrete columns, set in sockets in the footings.
3. Weak pinned connections between precast elements.
4. Cantilevered columns provided only resistance to lateral loads.
5. No structural diaphragm at the roof level.
6. Roof girders were vulnerable to overturning.

To correct these deficiencies, a practical rehabilitation scheme is proposed. Diaphragm action is developed by adding tension-only steel braces in a horizontal plane at the roof level. Vertical, tension-only braces were also added around the perimeter of the building.

Fig. 9.4 Relative movement of precast elements at roof level

The objectives of this study were aimed at devising a practical rehabilitation scheme by:

1. Developing a diaphragm that would distribute and transfer the lateral forces to the existing lateral force resisting members and the new vertical braces.
2. Adding lateral force resistance.
3. Strengthening the connections between elements supported at the top of columns. The strengthened connections must prevent the roof members from sliding off the tops of the columns and the roof girders from overturning.
4. Developing an analysis method for assessing the rehabilitation design; including determination of fundamental period, estimation of maximum seismic displacement, and calculation of internal forces.

9.2 Prototype Building

An 80 by 200 m building in Adapazarı (Fig. 9.5), which sustained light damage during the Kocaeli earthquake, was selected as the prototype structure for this study. This building also served as the prototype for earlier studies at the University of Texas [6]. Details of the building (Fig. 9.6) are listed below:

1. Fourteen continuous bays in longitudinal direction, 7.5-m c-c spacing
2. Four continuous bays in transverse direction, 20-m center to center spacing
3. Precast, 7.0-m high columns fixed at grade
4. Trapezoidal roof girders span along the transverse axis of the building

Fig. 9.5 Photographs of prototype building

Fig. 9.6 Structural system in prototype building

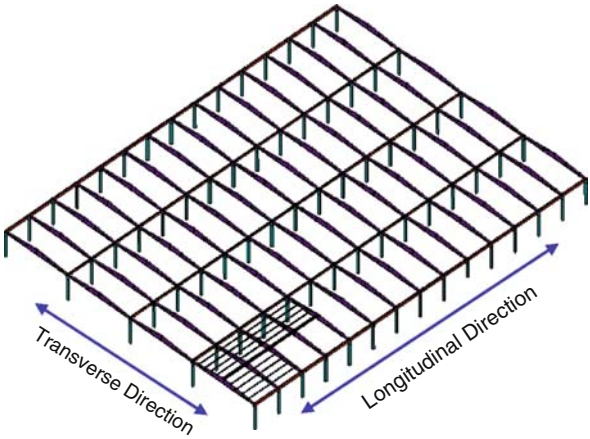

Material properties and member dimensions were taken from the design drawings provided by the precast manufacturer. The dimensions of a typical precast column are shown in Fig. 9.7 and the connections between precast members in the prototype building are shown in Fig. 9.8.

9.3 Ground Motions

Fifteen ground motion records (Table 9.1) were considered in this investigation. Most of the recording stations were within 50 km of the epicenters of the 1999 earthquakes, and all were within 20 km of the surface trace of the faults [2]. The ground motion records were divided into two groups depending on the soil conditions at the recording station. Records from Bolu, Düzce, and Yarimca were used to determine the spectral characteristics for soft soil. Smoothed response spectra for acceleration

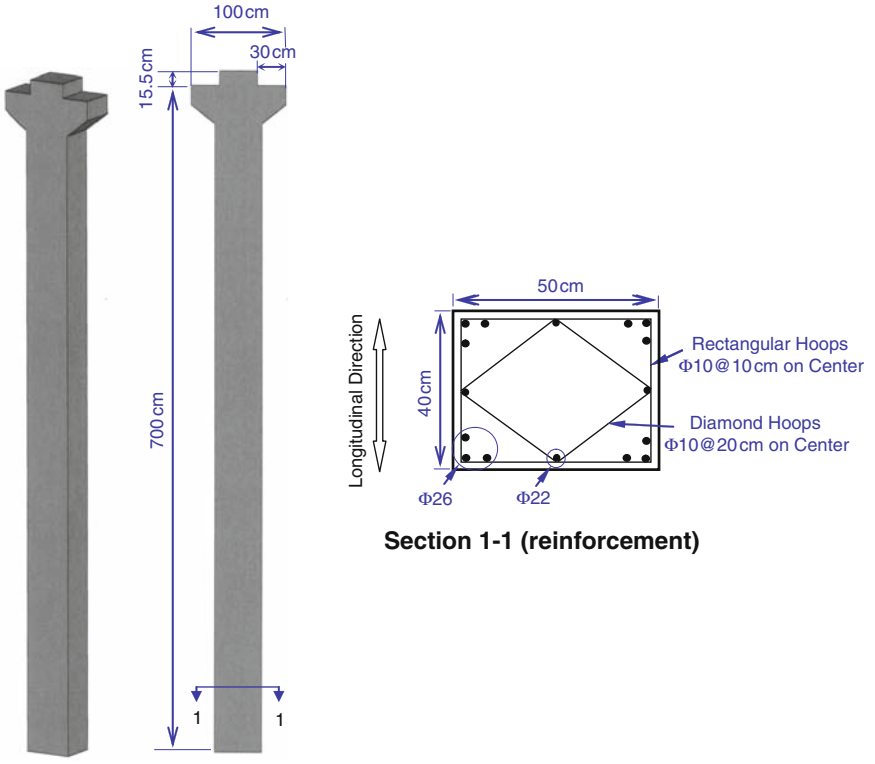

Fig. 9.7 Column in prototype building

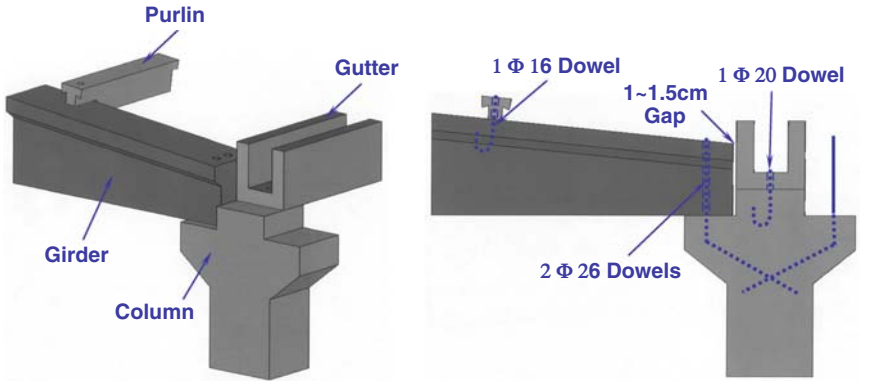

Fig. 9.8 Connections between precast members in prototype building

(Fig. 9.9) and displacement (Fig. 9.10), which were representative of the maximum elastic response at soft soil sites, were used to evaluate the seismic response of the prototype, one-story, precast industrial building.

Table 9.1 Ground motions considered in investigation

Station	Component	Peak Accel. g	Epicentral Distance km	Soil Conditions
Düzce (DZC)	180 270	0.41 0.51	10**	Soft Soil
İzmit (IZT)	090 180	0.23 0.17	12*	Rock
Yarimca (YPT)	240 330	0.30 0.32	22*	Soft Soil
Sakarya (SKR)	090	0.41	35*	Stiff Soil
Bolu (BOL)	000 090	0.74 0.81	42**	Soft Soil
Gebze (GBZ)	000 270	0.27 0.14	50*	Stiff Soil
Arcelik (ARC)	000 090	0.21 0.13	60*	Stiff Soil
Düzce (DZC)	180 270	0.32 0.37	110*	Soft Soil

*Approximate distance to epicenter of Kocaeli earthquake.
**Approximate distance to epicenter of Düzce earthquake.

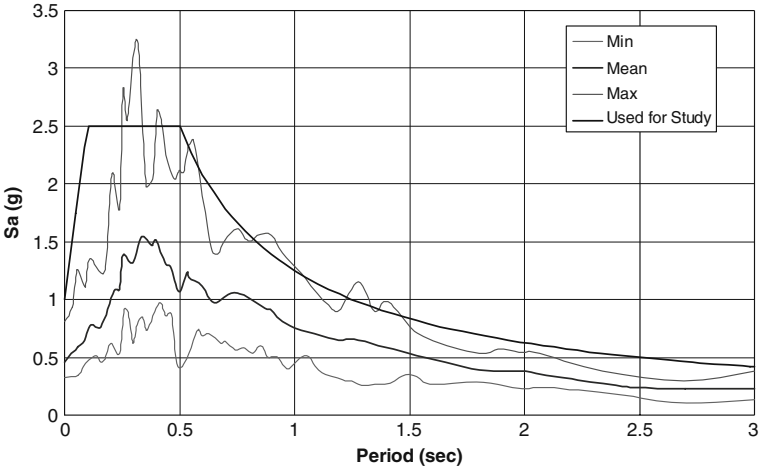

Fig. 9.9 Acceleration response spectra for soft soil sites (damping = 2%)

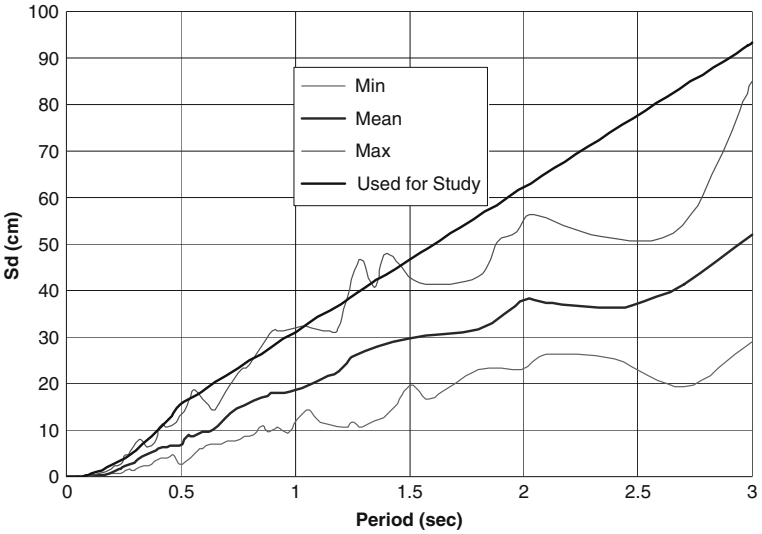

Fig. 9.10 Displacement response spectra for soft soil sites (damping = 2%)

9.4 Overview of Rehabilitation Scheme

During an earthquake, the columns acted as cantilevers with the maximum bending moment occurring at the base. The flexural deformation of the column can be modeled by concentrating inelastic rotation within a plastic hinge at the base and assuming elastic curvature over the height of the column.

Analyses indicate that in both the transverse or longitudinal directions, the columns in the prototype building have little margin against failure under the idealized response spectrum. The proposed rehabilitation scheme includes adding elements to the lateral-force-resisting system and creating a diaphragm at the roof level.

The concept for the rehabilitation scheme can be seen in a simple model of the roof elements (Fig. 9.11). The members in Fig. 9.11a represent the existing roof elements. The roof girders and gutter beams are indicated. Steel pins connect all the elements so that no moment is transferred between elements. Because the girders and gutter beams in the prototype building can carry little tensile force due to the weak connections, the girders and gutter beams were provided with a "slider" to allow extension of the elements under tension loads. However, those elements carried compressive loads by butting against each other at the joints. The restraint was idealized by simple supports at the ends of the braced panels. In the prototype system there is no lateral force transfer system at interior supports. With the diagonal braces, the model can carry external lateral forces in all directions.

The rehabilitation scheme developed for the prototype building includes three parts:

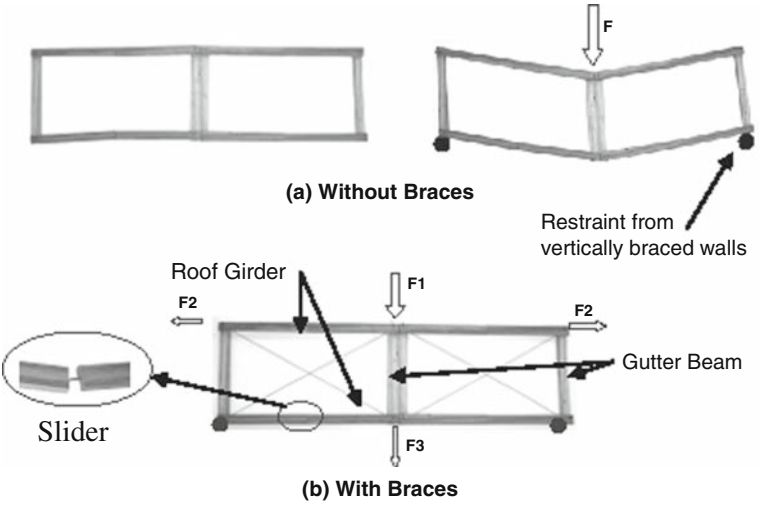

Fig. 9.11 Influence of tension-only braces in roof diaphragm

1. Adding vertical diagonal steel braces around the perimeter of the structure to increase the lateral strength and stiffness (Fig. 9.12).
2. Introducing diagonal braces to the roof frame of the one-story industrial building immediately under the girders forms a diaphragm made up of diagonal steel braces carrying tension and precast concrete members (girders and gutter beams) carrying compression. Forces at the edge of the diaphragm are transferred to the vertical lateral force resisting system that also includes diagonal tension braces. Figure 9.13 shows the top view of the braced prototype building.
3. Installing steel clamps at the top of the columns to hold the vertical and horizontal braces and to connect the elements together to avoid sliding of roof girders and gutter beams on the column supports and to prevent overturning of roof girders.

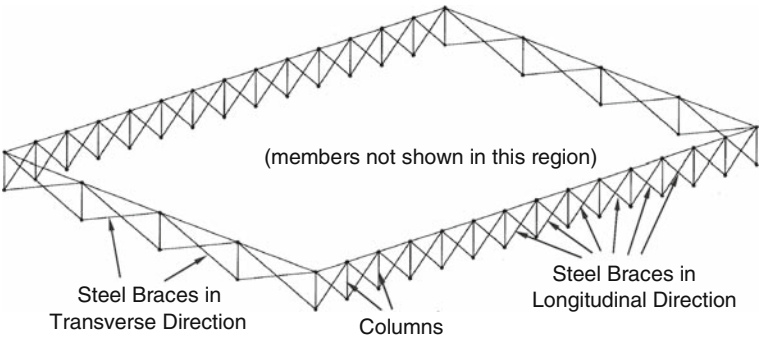

Fig. 9.12 Layout of vertical braces around perimeter of prototype building

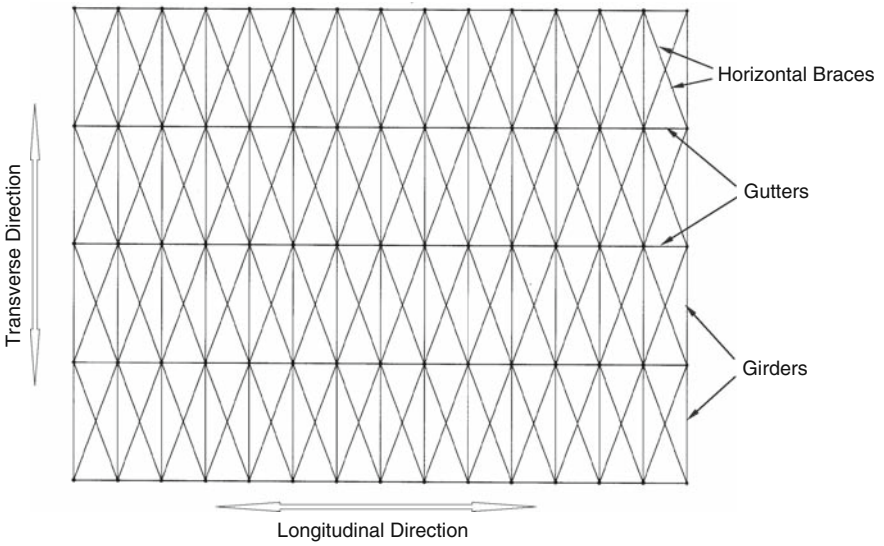

Fig. 9.13 Braces added to form diaphragm at roof level

9.5 Analytical Models

In order to simulate the static and dynamic behavior of the prototype building, two different structural models were created. Both were capable of modeling the inelastic response of the structure. SAP2000 [7] was used for static and modal analyses of the structure. The computational platform OpenSees [5] was used for the inelastic dynamic analyses.

The characteristics of the SAP2000 model for the prototype building are summarized below and in Fig. 9.14.

1. The mass of all structural members was lumped at the ends of the members.
2. All connections were modeled as pins.
3. Girders and gutter beams were idealized as elastic, compression-only truss elements.
4. Columns were modeled as elastic cantilevers with a plastic hinge at the base.
5. Braces were modeled as tension-only truss members.

The OpenSees model was similar to the SAP 2000 model, with the following differences:

1. The hysteretic properties of all members were represented using fiber elements (Fig. 9.15).
2. The inelastic response of the column was distributed along the length and not concentrated at the base.

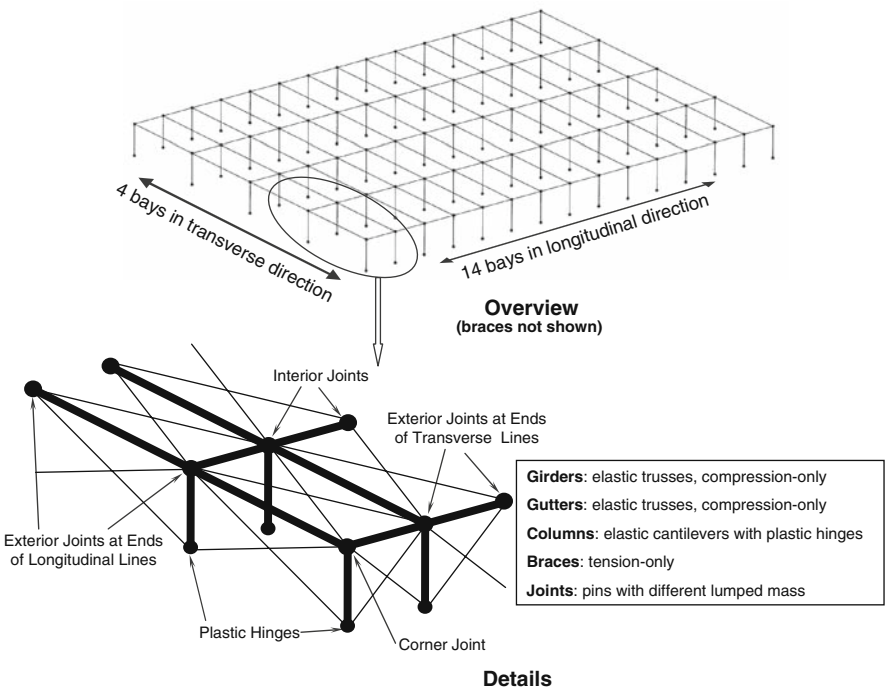

Fig. 9.14 SAP 2000 model of prototype building

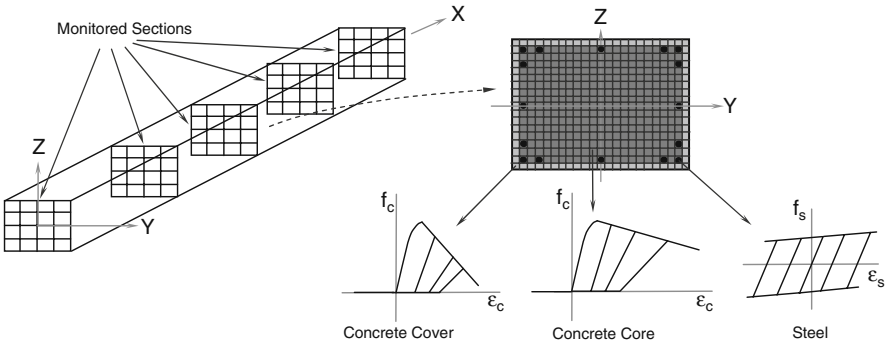

Fig. 9.15 Representation of precast member using fiber elements in OpenSees

Details of the analytical studies are presented in [8]. Static push-over analyses and nonlinear response history analyses were conducted to evaluate the seismic response of the prototype and rehabilitated structures. In addition, a simple model was developed using a tensioned string analogy to estimate the maximum seismic response of the rehabilitated structure.

9.6 Seismic Response of Rehabilitated Building

Using the tensioned string analogy, the sensitivity of the maximum calculated seismic displacements to the brace sizes was determined (Fig. 9.16). After the sizes of the braces were selected, static push-over analyses were conducted using the estimated maximum displacements to determine the forces that must be developed at the connections at the top of the columns.

From the push-over analyses, the following observations were made:

1. All the diaphragm braces remained elastic.
2. Most roof girders and gutter beams were in compression, and the maximum compressive strain was well below levels expected to cause spalling or crushing. Under tension, gaps formed between the members around the perimeter of the building, but the width of the gaps was 1–2 cm.
3. All longitudinal vertical braces yielded but the maximum strains were below levels at which strain hardening would occur.
4. All transverse vertical braces remained elastic.
5. Plastic hinges developed at the base of the interior columns, while the perimeter columns remained elastic.

Overall, the rehabilitated building was expected to perform adequately and survive the earthquake ground motions without severe damage.

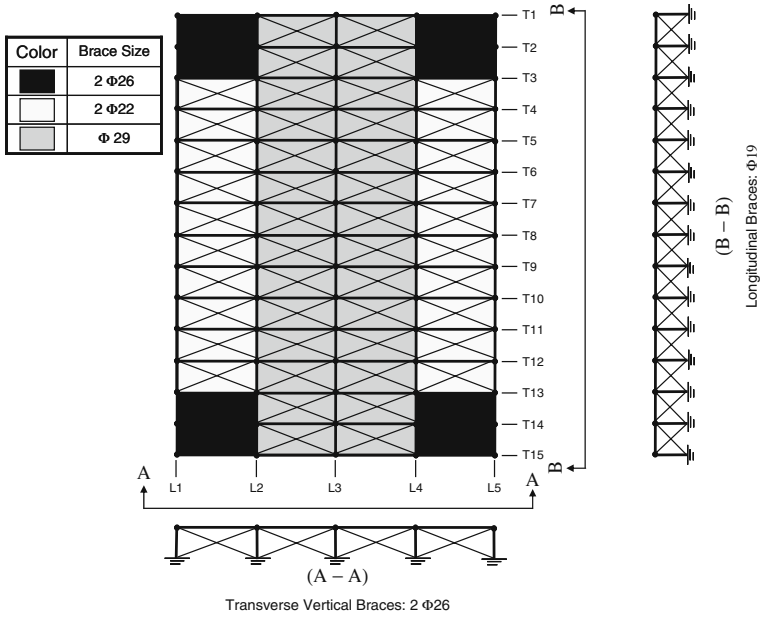

Fig. 9.16 Sizes of braces used to rehabilitate prototype building

9.7 Strengthening of Connections

In the analyses, the connections between precast members were assumed to be pinned. In order to satisfy the performance objectives for the rehabilitated structure, the connections must also accomplish the following:

1. Prevent overturning of roof girders (Fig. 9.17).
2. Prevent roof girders and gutter beams from sliding on their supports at the top of the columns.
3. Transfer large tensile forces from the diaphragm to the vertical braces around the perimeter of the building.
4. Resist differential axial compressive forces in the girders and gutter beams. Axial compressive forces developed in the girders are idealized in Fig. 9.18a, and compressive forces in the gutter beams are idealized in Fig. 9.18b.

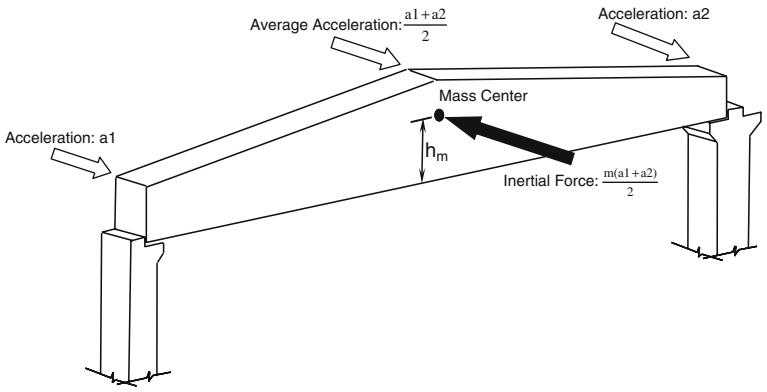

Fig. 9.17 Overturning of roof girders

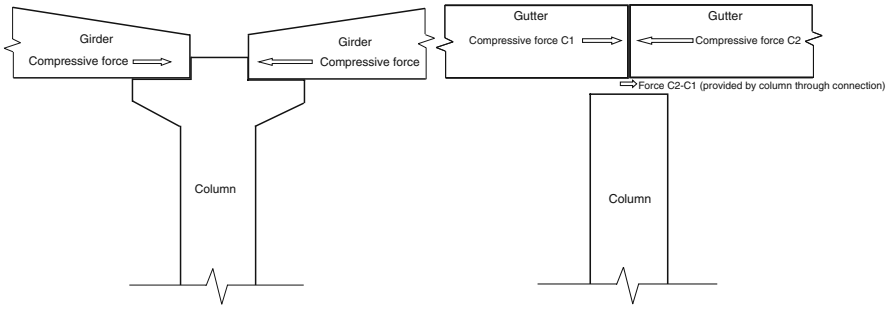

(a) Roof Girders **(b) Gutter Beams**

Fig. 9.18 Compressive forces in roof girders and gutter beams (viewed from side)

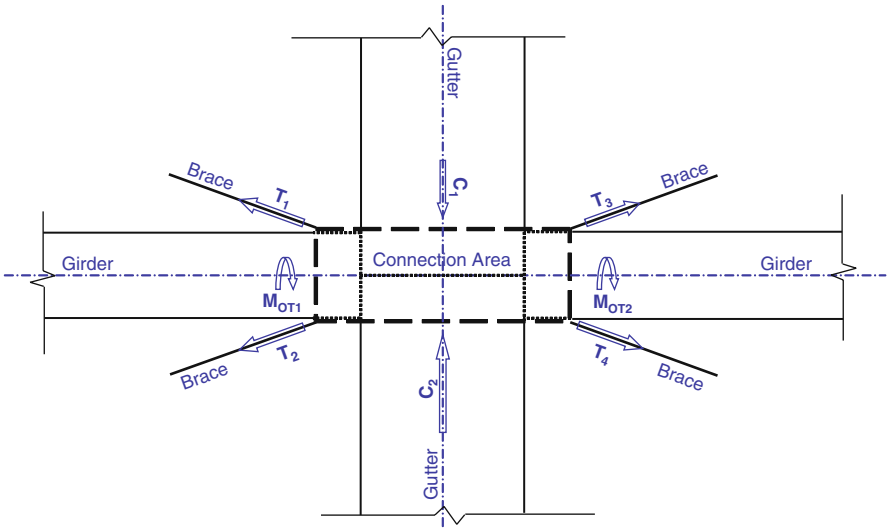

Fig. 9.19 Forces considered for a typical connection

The forces in each of the connections were determined from push-over analyses. Details of the analysis and the criteria for strengthening are discussed in detail in [8]. The key feature of the strengthening scheme was to limit overall lateral deformation levels so that the existing columns would not be damaged and the various elements making up the system were connected at the joints to permit both tension and compression forces to be transferred without developing excessive relative deformations that could cause elements to slide from supports. Forces at a typical interior connection are shown in Fig. 9.19.

The installation of the strengthening elements also needs to be considered. The construction procedure depends on the configuration of the original structure. To make the rehabilitation scheme acceptable, the strengthening operation must be as simple as possible. Strengthening of the connections will be discussed for two cases: interior columns and exterior columns at the ends of the transverse bays. Details of connections at exterior at the ends of longitudinal bays and corner columns are presented in [8].

9.7.1 Interior Connections

There are 39 interior connections in the prototype structure. Considering the requirements discussed above, a proposed strengthening scheme is shown in Fig. 9.20. A clamping device made of steel plates was designed to be installed on the column corbels (Fig. 9.20b). Four vertical plates are used to prevent overturning of roof girders (Fig. 9.21). After the gaps between the roof girders and steel plates are filled using washers, the roof girders and the steel plates are bound together by tightening

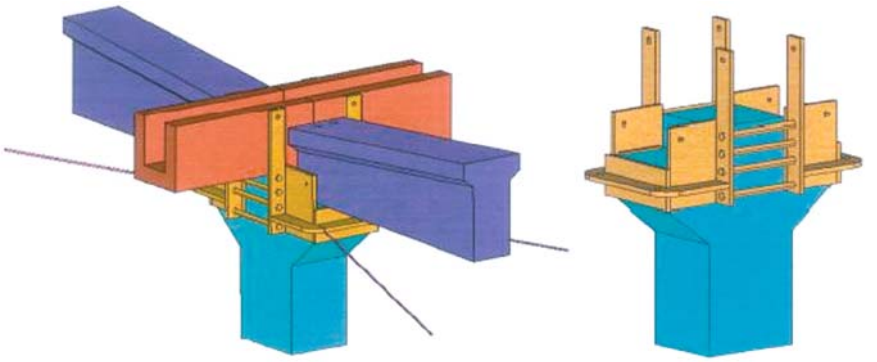

(a) With Roof Girders and Gutter Beams (b) Column and Clamping Device

Fig. 9.20 Details of strengthening scheme for interior connections (See also Plate 11 in Color Plate Section on page 461)

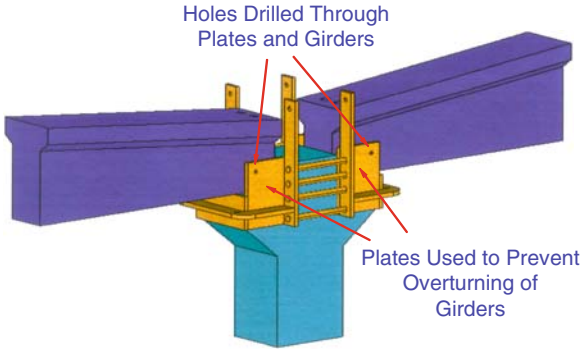

Fig. 9.21 Plates designed to prevent overturning of roof girders supported on interior columns

the bolts. The holes through the roof girders could be grouted to reduce slip between the new plates and the roof girder.

To prevent sliding of the gutter beams, the four steel plates clamped to the column are extended to the top of the gutter beams (Fig. 9.22). Because the gutter beams are used to drain water from the roof, holes should not be drilled in the lower part of the gutter beams and any holes in the gutter beams should be grouted after installation of bolts. The locations of the holes should be selected to avoid cutting reinforcing bars in the precast members.

Horizontal flanges for transfer of tensile forces in the diaphragm braces to the connection are shown in Fig. 9.23. The locations of holes must be carefully determined to avoid additional twisting of the columns. Stress concentrations around the holes need to be considered depending on the way the diaphragm brace is attached.

To make installation of the connection hardware easier, four, 10-mm thick steel tabs are welded to the interior of the clamp to support the clamp on the corbels (Fig. 9.23). Gaps between the roof girders and columns and between adjacent gutter beams should be grouted.

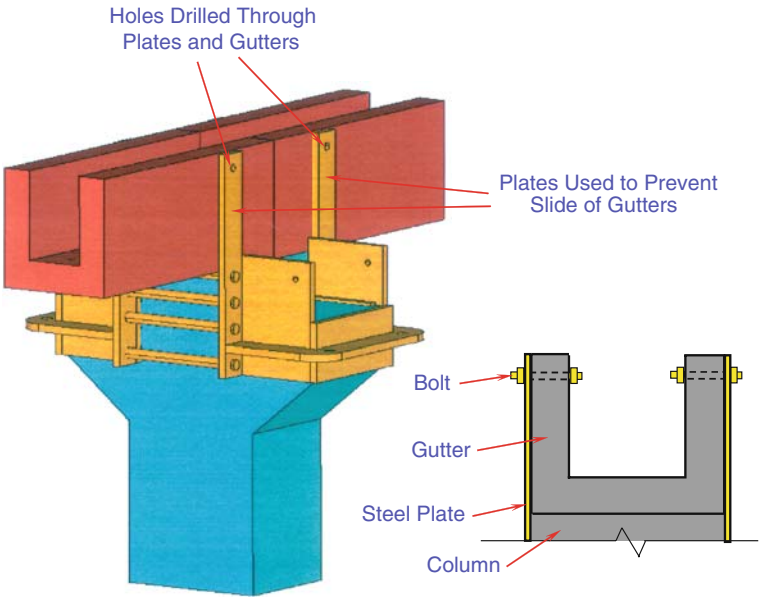

Fig. 9.22 Plates used to prevent sliding of gutter beams at interior column

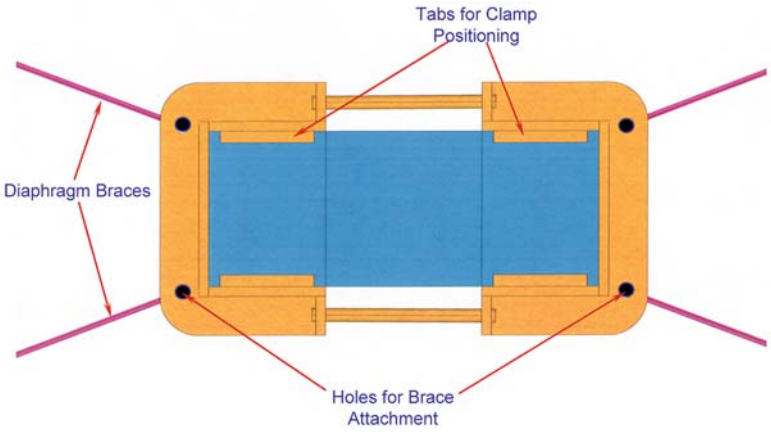

Fig. 9.23 Top view of clamp at top of interior column

9.7.2 Exterior Connections

At an exterior column at the ends of transverse lines T2 through T14, only one girder is supported on the column. However, two vertical braces must be anchored at that location. The clamps are modified as shown in Fig. 9.24.

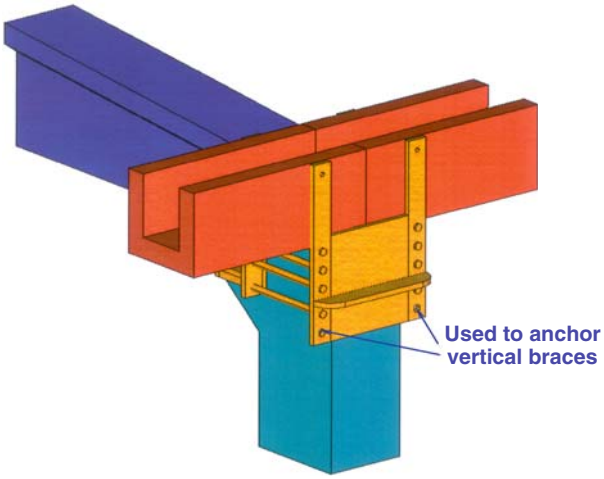

Fig. 9.24 Exterior connection at ends of transverse frames

For the prototype building with the braces shown in Fig. 9.16, the required sizes of the connection clamp plates are shown in Fig. 9.25. The yield stress of the steel material was assumed to be 345 MPa.

The technique of strengthening connections in the precast concrete buildings using steel clamps has been adopted in some buildings in Turkey. Although the proposed strengthening clamps are more complicated, the fact that similar types of clamps have been installed indicates that this rehabilitation scheme is economical and constructible.

9.8 Summary and Conclusions

In this chapter, the seismic performance of typical one-story precast industrial buildings in Turkey was studied. Because the connections between the precast units were not detailed for earthquakes, significant deficiencies in the seismic response of these structures have been identified. Specifically,

1. The lateral force resisting capacity of the buildings was inadequate. All the lateral forces had to be resisted by cantilever columns. There was no redundancy in the system.
2. The roof system could not develop diaphragm action.

The connections were insufficient to keep roof members from separating from the columns. There was little resistance to overturning of the roof girders. From the analyses conducted in this study, the following conclusions can be made:

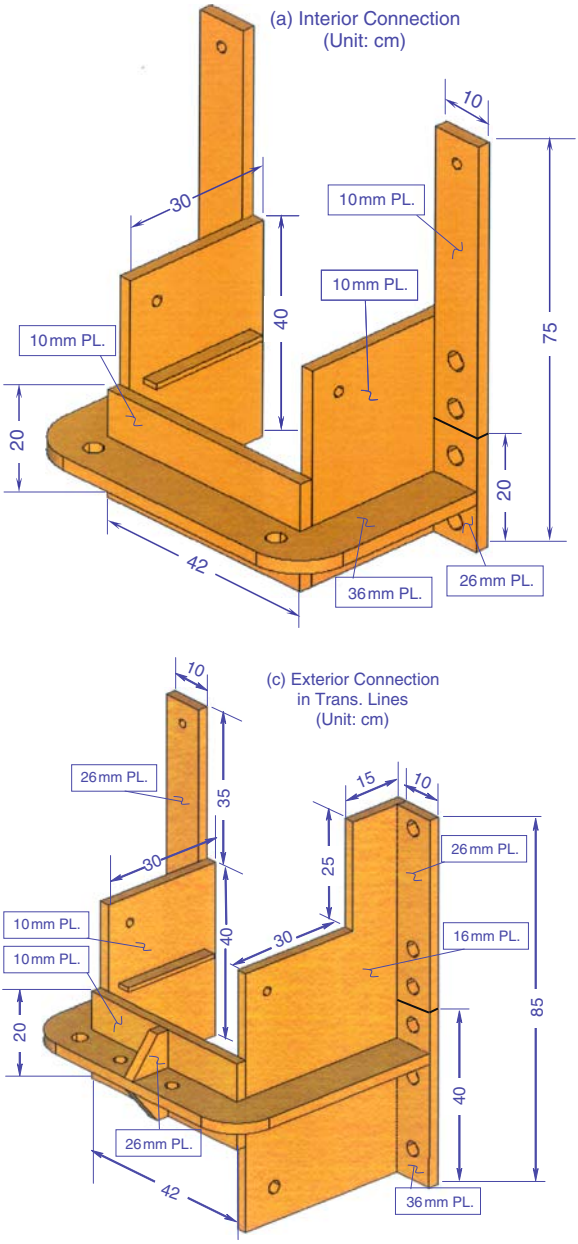

Fig. 9.25 Dimensions of connection clamps

1. The poor performance of existing precast industrial buildings in Turkey can be corrected. The roof drift can be reduced, overturning of the girders can be avoided, and sliding of the roof members from supports can be prevented.
2. A horizontal diaphragm can be provided by adding diagonal steel braces at the roof level. Diaphragm action can be developed by introducing new diagonal braces that act together with the existing roof system, so that the lateral forces can be transferred to lateral force resisting members at the periphery of the building.
3. Existing lateral force resisting systems can be improved by adding vertical diagonal braces on the periphery of the structure.
4. Connections at the tops of columns can be improved. By adding properly designed steel clamping devices, the connections can prevent the roof members from separating from the columns and the roof girders from overturning.

The proposed rehabilitation scheme should have minimal impact on occupancy of the buildings. The strengthening elements are not too large to install and they can be added sequentially to produce a strengthened system.

References

1. Ataköy H (1999) 17 August Marmara Earthquake and the precast concrete structures built by TPCA members.Turkish Precast Concrete Association,Ankara
2. Earthquake Engineering Research Institute (2000) 1999 Kocaeli, Turkey, Earthquake Reconnaissance Report. Earthquake Spectra, Supplement A to Vol. 16
3. Ersoy U, Tankut T, Özcebe G (1999) Damages observed in the precast framed structures in the 1998 Ceyhan Earthquake and their rehabilitation. Department of Civil Engineering, Middle East Technical University, Ankara
4. Karaesmen E (2001) Prefabrication in Turkey: Facts and figures. Department of Civil Engineering, Middle East Technical University, Ankara
5. Open System for Earthquake Engineering Simulation (OpenSees), Pacific Earthquake Engineering Research Center, UC Berkeley (http://opensees.berkeley.edu/OpenSees/home/about.php)
6. Posada M (2001) Performance of precast industrial buildings during the 1999 Earthquakes in Turkey. M.S. Thesis, Department of Civil Engineering, University of Texas, Austin
7. SAP 2000 Integrated Software for Structural Analysis and Design, Computers and Structures, Inc., Berkeley, CA (http://www.csiberkeley.com/productsSAP.html)
8. Wang R (2006) Seismic strengthening by providing a structural diaphragm. Ph.D. Dissertation, Department of Civil, Architectural, and Environmental Engineering, University of Texas, Austin. (http://www.engr.utexas.edu/fsel/)

Chapter 10
Vulnerability Evaluation and Retrofitting of Existing Building Heritage: an Italian Research Programme

Giandomenico Toniolo

Abstract The chapter presents a review of two important national research programmes which received relevant financial support from the Italian Department of civil protection. The first has been devoted to the new definition of the seismic danger over the Italian territory. The research provider has been the National Institute of geophysics and volcanology which involved many university units. The work has been concluded with the delivery of a specific data base containing the map of seismic danger derived from an analytical continuous model, so to allow the definition site by site of the response spectra for a set of return periods. The second research programme refers to the vulnerability evaluation and retrofitting of the existing building heritage and its results should be used to address the national policy of interventions for the upgrading of seismic capacity of constructions. The research provider is the Network of university laboratories of seismic engineering which involves again many university units. The work is in progress and the chapter presents its main objectives. In particular for the research line on precast constructions, which is coordinated by the author, the work can take profit of the results of some previous European projects, adding to them the investigation of some key aspects such as the seismic behaviour of the principal types of connections.

10.1 Introduction

Recently two important projects have been financed by the Italian Department of civil protection. These projects can be defined very large with respect to the ordinary sizes of the national research programmes. The first project refers to the definition of the seismic danger of the Italian territory and now it is concluded, being the results available to public for any pertinent use. The second refers to the vulnerability evaluation and retrofitting of the existing building heritage with respect to earthquake action and it is now in progress, being the conclusion expected within the end of 2008.

G. Toniolo (✉)
Politecnico di Milano, Milano, MI, Italy
e-mail: toniolo@stru.polimi.it

A. Ilki et al. (eds.), *Seismic Risk Assessment and Retrofitting*, Geotechnical, Geological, and Earthquake Engineering 10, DOI 10.1007/978-90-481-2681-1_10,

10.2 Seismic Danger

For the first project (Seismic Danger) the research provider has been the National institute of geophysics and vulcanology which involved the units of many universities. With a budget of about 5 million Euro covering three years work and other different topics, the research has been carried out from 2004 up to 2006, under the general coordination of Massimiliano Stucchi and Michele Calvi. The results have

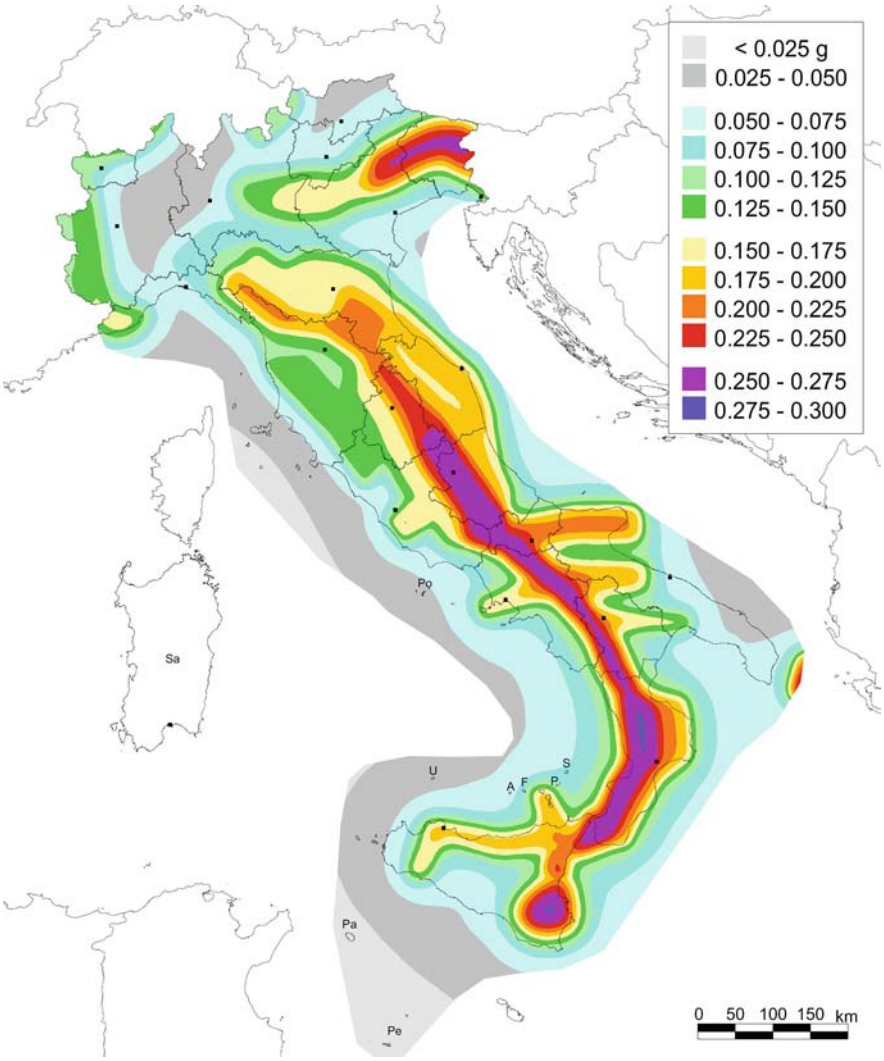

Fig. 10.1 Italian seismic hazard map taken from INGV website (See also Plate 12 in Color Plate Section on page 462)

been delivered in the form of a detailed map of seismic danger covering all the Italian territory.

The definition of seismic danger originates from the large set of data registered during the years all over the territory and has been elaborated through an analytical model simulating the physical propagation, from the main seismogenetic sources, of events with different features corresponding to different return periods. The resulting map has been rendered in a grid of one twentieth of degree, which corresponds to about 5.5 km, by means of sets of specific numerical data available in a dedicated web site.

In Fig. 10.1 the graphic map taken from this site showing the distribution of the peak ground acceleration (mean value) for earthquakes with 475 years of return period can be seen. Except for the isolated Friuli zone at North-east of the country, the main seismic zones develop along the Apennines ridge from Umbria down to Etna volcano in Sicily. Sardinia Island is too far from the seismogenetic sources to be covered by the geophysical model and remains out of the map with a general definition of very low seismicity.

In Fig. 10.2, a sample of five response spectra can be seen. These spectra are taken throughout the territory from low to high seismicity for a rigid rock-like soil type "A" with a peak ground acceleration (mean value) from about 0.05 to about 0.30 of g. The spectra are given by their numerical values corresponding to eleven vibration periods, distributed from T = 0 to T = 2 s. And this description is repeated for three probability fractiles (16%, 50%, 84%), for nine return periods (from 30 to 2475 years) and for the 16921 points of the grid. Globally the data base includes

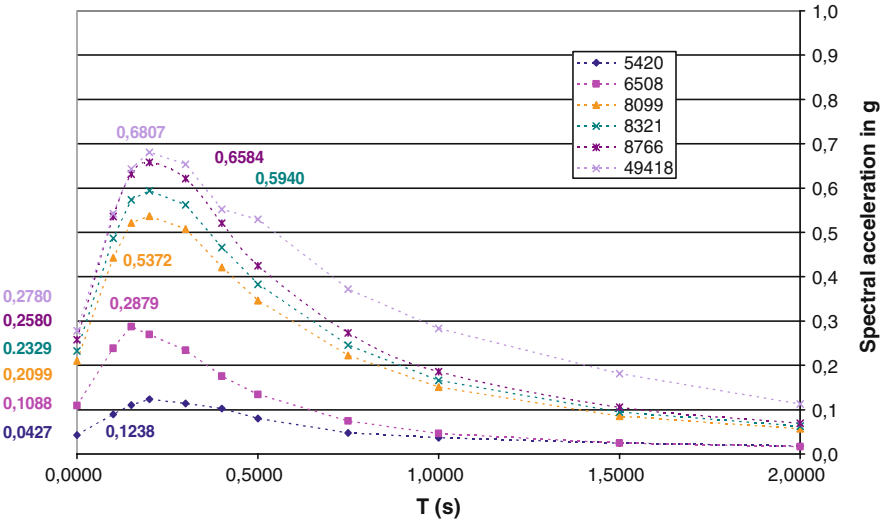

Fig. 10.2 Sample of five response spectra computed for different locations in Italy (See also Plate 13 in Color Plate Section on page 463)

more than 5 million numerical values: exactly 5025537 plus 50753 for the identity code and the geographic coordinates.

10.3 New Design Code

Now the new Italian code for structural design employs these data for the definition site by site of the seismic action and for this purpose it translates the spectra into the model of Eurocode 8 as described in Fig. 10.3.

From the original data base three parameters are computed:

1. the PGA peak ground acceleration mean value for soil "A" a_g;
2. the ratio of maximum amplification of the spectrum $F_0 = S_{max}/a_g$;
3. the limit vibration period of the top plateau of the spectrum T_C.

Figure 10.4 shows an excerpt of the tables given by the code in a special annex, where a reduced number of numerical values are present: exactly 456867 plus 50753 for the identity code and the geographic coordinates.

For the application to a specific construction in a specific site, proper interpolations of the return period and of the geographic coordinates will be necessary. But probably the single regional administrations will provide for data related to any municipal district, avoiding some interpolations.

So the design approach will start from the definition of the return periods to be referred to for ultimate and damage limit states on the base of the importance of the construction. For the specific site of construction the corresponding two groups of base parameters will be taken from the quoted annex. And finally the analytical

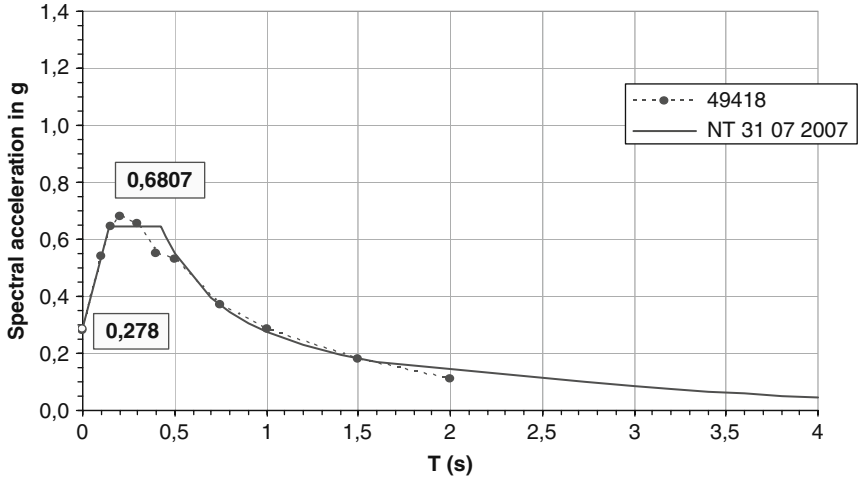

Fig. 10.3 Comparison between the new Italian Code site spectrum and the INGV spectrum

			$T_R = 30$			$T_R = 50$			$T_R = 72$			$T_R = 101$		
ID	LON	LAT	a_g	F_o	T_C^*	a_g	F_o	T_C^*	a_g	F_o	T_C^*	a_g	F_o	T_C^*
13111	6,5448	45,134	0,263	2,50	0,18	0,340	2,51	0,21	0,394	2,55	0,22	0,469	2,49	0,24
13333	6,5506	45,085	0,264	2,49	0,18	0,341	2,51	0,21	0,395	2,55	0,22	0,469	2,49	0,24
13555	6,5564	45,035	0,264	2,50	0,18	0,340	2,51	0,20	0,393	2,55	0,22	0,466	2,50	0,24
13777	6,5621	44,985	0,263	2,50	0,18	0,338	2,52	0,20	0,391	2,55	0,22	0,462	2,51	0,24
12890	6,6096	45,188	0,284	2,46	0,19	0,364	2,51	0,21	0,431	2,50	0,22	0,509	2,48	0,24
13112	6,6153	45,139	0,286	2,46	0,19	0,366	2,51	0,21	0,433	2,50	0,22	0,511	2,48	0,24
13334	6,621	45,089	0,288	2,46	0,19	0,367	2,51	0,21	0,434	2,50	0,22	0,511	2,49	0,24
13556	6,6268	45,039	0,288	2,46	0,19	0,367	2,51	0,21	0,433	2,51	0,22	0,510	2,49	0,24
13778	6,6325	44,989	0,288	2,46	0,19	0,366	2,52	0,21	0,430	2,51	0,22	0,507	2,50	0,24
14000	6,6383	44,939	0,286	2,47	0,19	0,363	2,52	0,21	0,426	2,52	0,22	0,502	2,50	0,24
14222	6,6439	44,889	0,284	2,47	0,19	0,360	2,53	0,21	0,421	2,53	0,22	0,497	2,50	0,24

Fig. 10.4 Excerpt of Annex 1 to the Italian Seismic Code: definition of spectral parameters according to location (ID number of grid, longitude and latitude) for different return periods

equations, adapted for the specific subsoil (type A, B, C, D or E as in Eurocode 8), can be defined for the evaluation of the seismic action. From here the design procedure is equal to the one of Eurocode 8.

This new national code is officially published to be applied starting from January 2008.

10.4 Seismic Vulnerability

The Italian Department of civil protection aims to provide a survey of the existing building heritage so to support the government choices for possible state interventions of strengthening. A classification of the different categories of buildings, with respect to their degree of seismic vulnerability, will allow a preventive aimed policy over the territory, with optimisation of the resources.

A budget of 15 million Euro has been allocated for three years work of research. The research provider is the Network of university laboratories of seismic engineering which involved many Italian university units. The principal coordinators are Edoardo Cosenza and Mauro Dolce, but several other colleagues are involved in the general management of the project.

The work, which seems to be a very large and exacting one, has been organised on ten lines (see Fig. 10.5):

line 1 – devoted to masonry buildings;
line 2 – devoted to concrete buildings;
line 3 – devoted to bridges;
line 4 – devoted to displacement based design;
line 5 – devoted to steel and composite buildings;
line 6 – devoted to retaining works and slopes;
line 7 – devoted to seismic isolation techniques;
line 8 – devoted to innovative materials;

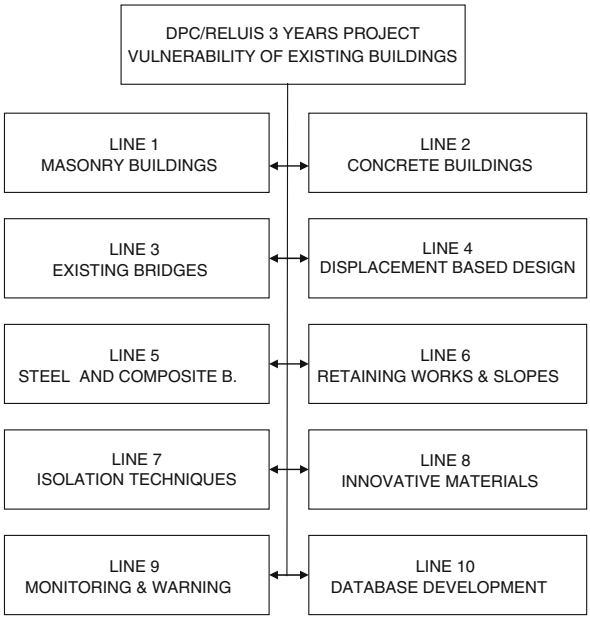

Fig. 10.5 Workpackages (lines) of the RELUISS research project

line 9 – devoted to monitoring and warning;
line 10 – devoted to the development of data base.

Of course it is impossible to deal with all these subjects. The presentation is limited to line 2 and to one of its specific subjects, where the author is directly involved. Figure 10.6 gives the composition of line 2 Concrete buildings with its nine tasks:

task 1 – deals with non destructive methods;
task 2 – deals with reliability factors;
task 3 – deals with non regular buildings;
task 4 – deals with hybrid buildings;
task 5 – deals with cladding effects;
task 6 – deals with staircase role;
task 7 – deals with joint behaviour;
task 8 – deals with biaxial action;
task 9 – deals with precast buildings.

The last task on precast buildings is carried out by four units:

- Politecnico di Milano (which is the coordinator)
- University of Bologna
- University of Molise
- First University of Naples.

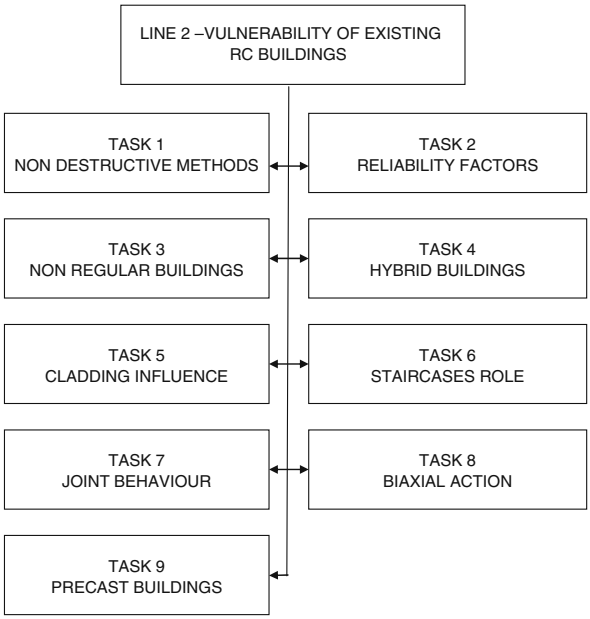

Fig. 10.6 Line 2 (Concrete Buildings) Sub-Tasks

10.5 Previous Researches

The present research follows some previous researches supported by the national industrial associations and by the European Commission.

The initial research, called "Assobeton 1", has been performed during the years 1994–1996 with a co-normative purpose in order to assist the works of finalisation of the previous ENV edition of Eurocode 8 for what concerns prefabrication.

The second research, called "Assobeton 2", has been carried out in the subsequent years 1998–2001 again with a co-normative purpose in order to assist the works of revision of the previous ENV edition of Eurocode 8 for its conversion into the final EN edition.

The third research, called "Ecoleader", has been carried out on the years 2002–2003 with the purpose to investigate the experimental behaviour of complete structural assemblies.

Finally the last research, called "Growth", has been performed on the years 2003–2007 with the purpose to cover the whole panorama of seismic behaviour of precast one-storey buildings.

10.5.1 Assobeton 1

Figure 10.7 shows the set-up of the tests performed at Ispra ELSA laboratory for the first research. In the very first draft of ENV Eurocode 8 precast structures were

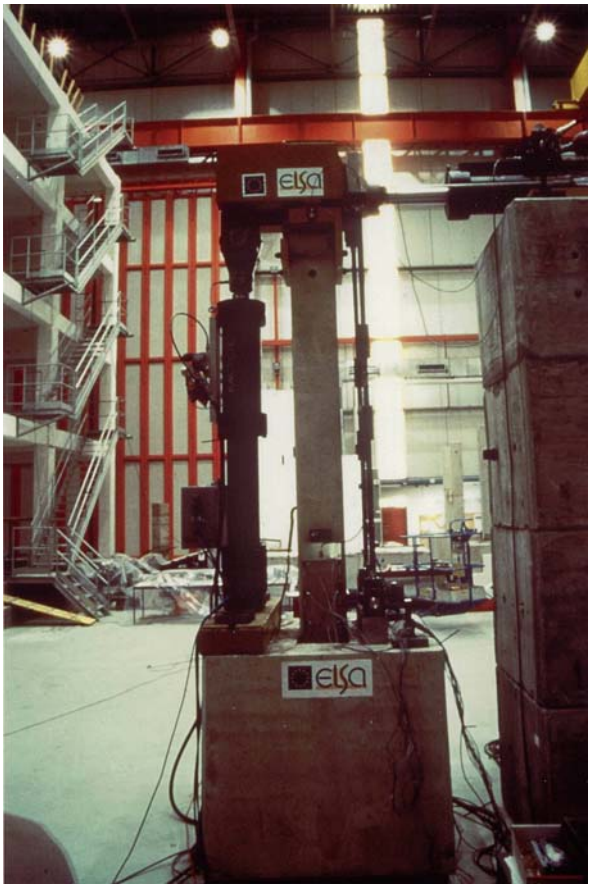

Fig. 10.7 Test set-up for cyclic test on precast columns

heavily penalised with a general presumption of low ductility, [1–3]. So the Italian association of precast producers Assobeton supported this campaign of experimental tests, with the scientific advice of Politecnico di Milano, in order to verify the performances of precast columns, following a specific request of Prof. Tassios.

A large number of cyclic tests and some pseudodynamic tests have been performed with different reinforcement features and different axial loads. A number of results has been obtained, the first of which confirmed the obvious evidence that precast columns with pocket foundations behave exactly like the cast-in-situ corresponding ones, [4].

Over the range of axial actions expected for one-storey precast buildings, not greater than 0.25 of the ultimate axial strength, a good local flexural ductility has been found, quantified in

$\mu_\phi \cong 6$ for a stirrup spacing 5 times the bar diameter;
$\mu_\phi \cong 8$ for a stirrup spacing 3,5 times the bar diameter.

The lower ductility found for the larger spacing of stirrups was caused by the early buckling of longitudinal bars. These values lead to traslatory ductility equal

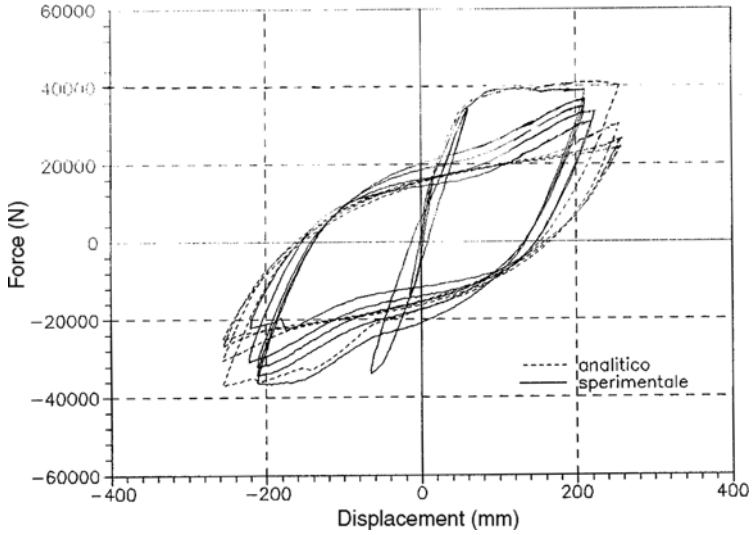

Fig. 10.8 Experimental cyclic loops recorded during "Assobeton 1" tests on precast columns

respectively to 3,5 and 4,5 and this does not confirm, both for precast and cast-in-situ columns, the too permissive detailing provisions of Eurocode 8 for concrete structures.

With the smaller spacing diagrams of cyclic dissipation of energy like the one shown in the Fig. 10.8 were obtained, with values of about 0.4 the energy dissipated by the perfect elastic-plastic cycle (see Fig. 10.9). And this is a good result for concrete columns.

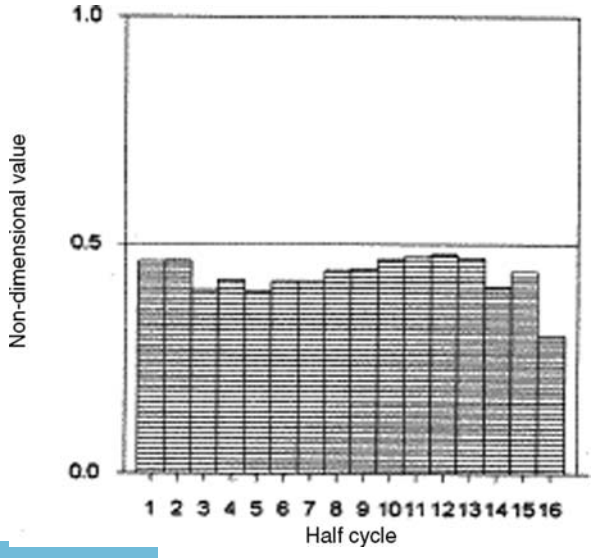

Fig. 10.9 Cyclic dissipation of energy-specific values

Following this research the penalising rules of ENV Eurocode 8 were attenuated in its final draft but, since there were no available experimental evidences on the seismic behaviour of complete assemblies, precast structures kept a behaviour factor lower than what acknowledged to cast-in-situ structures, [5, 6].

10.5.2 Assobeton 2

To investigate the behaviour of complete structures Assobeton supported a new research which was ordered to Politecnico di Milano and consisted on a number of numerical simulations of the dynamic response of complete structures to earthquake action. The idea was that the same amount of energy, dissipated by a cast-in-situ monolithic frame in its numerous critical sections, can be dissipated by a precast hinged frame, designed for the same horizontal force, in its fewer and larger critical sections, dimensioned as they are for a double bending moment (see Fig. 10.10).

To demonstrate this idea many non-linear dynamic analyses have been performed using a special analytic model of degrading stiffness. This model had been calibrated with respect to the pseudodynamic tests performed on some column prototypes in the preceding research. A full probabilistic Monte Carlo approach has been applied using large sets of recorded and artificial accelerograms and evaluating any time the ultimate capacity of the structure through an incremental process taken up to failure.

Figure 10.11 shows the histogram deduced from 1000 numerical simulations elaborated with as many artificial accelerograms applied both to the cast-in-situ and the precast frames. The diagonal corresponds to the perfect equality between the ultimate capacities of cast-in-situ and precast frames. As can be seen by the regression line, the correspondence is really very close and allows to acknowledge the same behaviour factor to both the frames.

These results have been taken to CEN Subcommittee 8 of CEN/TC250 in Vienna meeting on 2002 where, under the presidency of Prof. Fardis, the resolution of full equalisation between monolithic cast-in-situ frames and precast hinged frames was taken, under specific conditions for the connection design, [7–10].

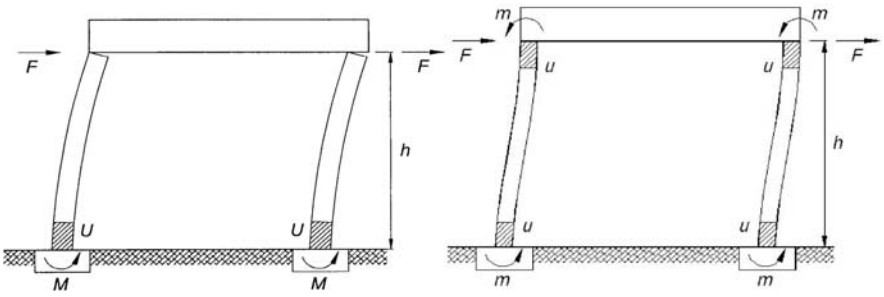

Fig. 10.10 Comparison between the response to lateral loading of a cast-in-situ (2) and a precast (1) frame

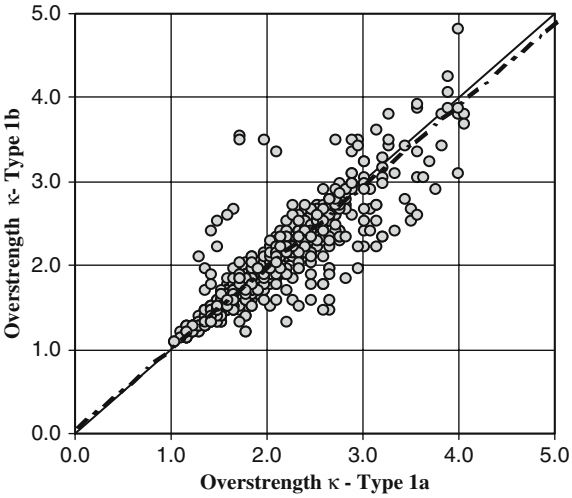

Fig. 10.11 Comparison between the ultimate capacities of cast-in-situ vs. precast frames derived from a fully probabilistic Monte Carlo approach

10.5.3 Ecoleader

An experimental confirmation of these results was still missing and the opportunity to fill this gap arrived with an European Ecoleader funding which covered the costs of the pseudodynamic tests performed at Elsa laboratory in Ispra.

Figure 10.12 shows the full scale precast prototype prepared for the experimentation. And Fig. 10.13 shows the full scale cast-in-situ prototype designed for the same horizontal force.

The costs of the prototypes and of the scientific advice have been supported by the three Italian association AITEC, ASSOBETON and ATECAP (respectively for cement, prefabrication and ready mix concrete industries) joined in ULISSE Project, by the Spanish ANDECE and the Portuguese ANIPC precast concrete associations. Politecnico di Milano coordinated the works.

The results of the tests confirmed those of the numerical simulations: the two structures, cast-in-situ and precast, behaved in a very similar way. In Fig. 10.14 one can see, for both the structures, the vibration curves calculated by the numerical model superimposed to the curves registered during the pseudodynamic tests under the same accelerogram at a level of about 0.7 g of peak ground acceleration. The correspondence is very close and this confirms the reliability of the numerical model together with the numerous results obtained with it.

Actually this type of structures, because of their high natural vibration periods (around 1 s), develops a very high seismic capacity, due to the strong attenuation of the motion. Both the prototypes, through three incremental steps of testing, arrived close to 1 g before showing sign of incipient failure, as expected on the base of Eurocode 8 rules. The damage limit state, applied with the limitation of the interstorey drift, is often the one which governs the dimensioning of the structure [11, 12].

Fig. 10.12 Precast mock up for pseudodynamic testing designed and built for the "Ecoleader" research project

Fig. 10.13 Cast-in-situ mock up for pseudodynamic testing designed and built for the "Ecoleader" research project

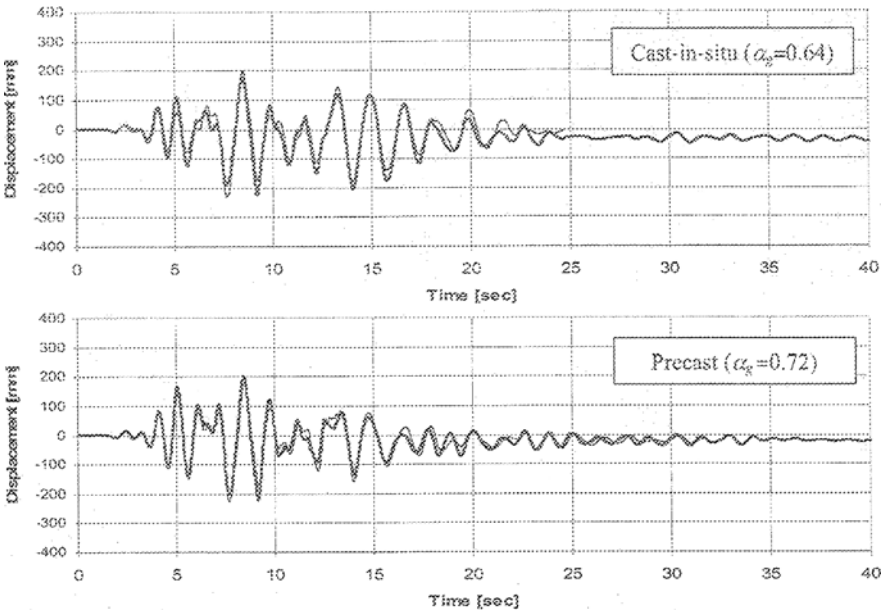

Fig. 10.14 Comparison between experimentally derived and numerically simulated response for cast-in-situ and precast mock ups

10.5.4 Growth

Finally the big project financed by the European Commission within a Growth programme (total cost about 1 million €). The consortium joined ten partners:

1. Politecnico di Milano in the capacity of coordinator (with G. Toniolo);
2. Larco Astori (now Magnetti Building), Italian manufacturer;
3. Gecofin Prefabbricati, Italian manufacturer;
4. Laboratorio national de engeharia civil of Lisbon (with E. Cohelo);
5. Civibral, Portuguese manufacturer;
6. National technical university of Athens (with P. Carydis);
7. Proet, Greec manufacturer;
8. University of Ljubljana (with Matej Fischinger);
9. European Joint Research Center of Ispra (with P. Negro),
10. Tongji university of Shanghai (with Xilin Lu).

It is not possible to present all the numerous results obtained in the three European experimentation centres and in the Chinese one. In the following only some image are presented to show the size of the experimentation.

Figure 10.15 shows one of the full scale prototypes subjected to pseudodynamic tests at Elsa Laboratory of Ispra. In addition to the main features of the seismic

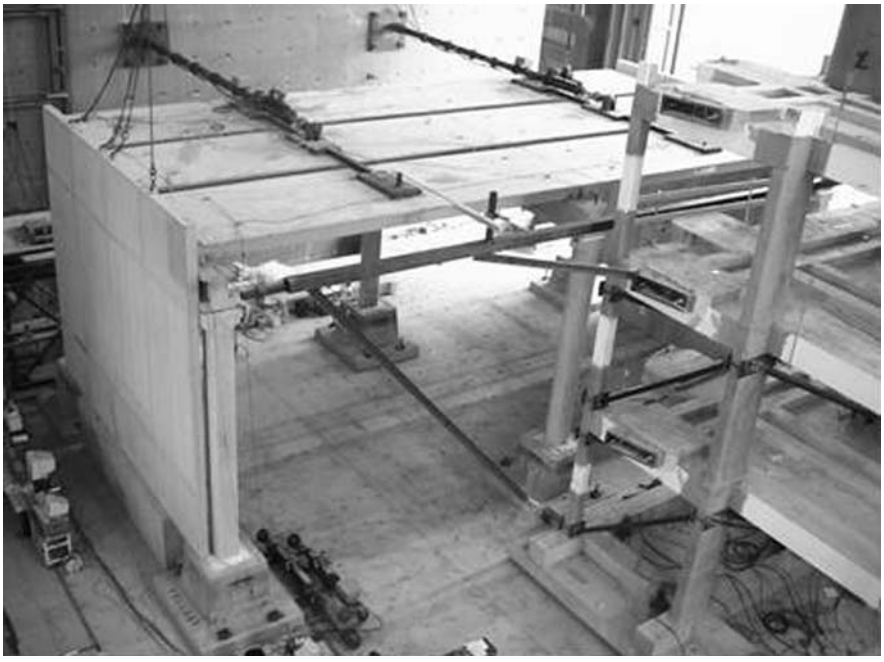

Fig. 10.15 Full scale prototype of a one-storey precast industrial building designed and built for pseudodynamic testing in the "Growth-PRECAST EC8" research project

response, special attention has been addressed to diaphragm action and cladding effects, [13–16].

Figure 10.16 shows the reduced scale two storey structure tested at LNEC Laboratory on its shaking table. In particular the multi-modal response of this type of structure has been investigated, together with the behaviour of some types of connections.

Figure 10.17 shows the reduced scale prototype of a one-storey structure tested at NTUA Laboratory on its shaking table. Again the behaviour of different types of connections has been investigated to quantify their influence on the structural response.

10.5.5 Precast Structures

And finally the research project which is addressed to in the title of the present chapter. Actually the investigation on seismic vulnerability of existing precast buildings obviously will take profit of the quoted previous researches. The work packages are here listed in their development order.

The first stage has been the survey of existing buildings.

Now the identification tests the different types of connections are in progress.

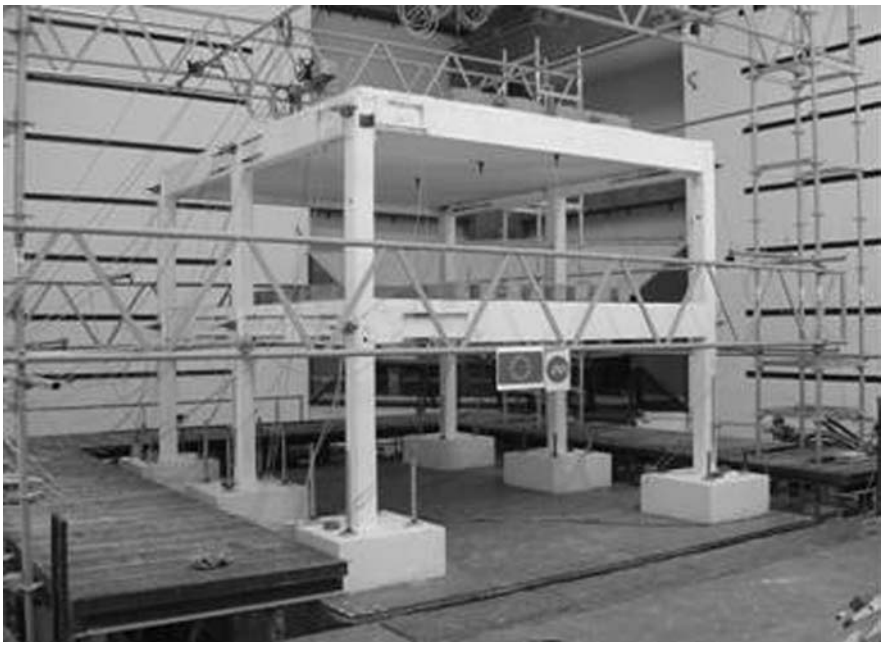

Fig. 10.16 Reduced-scale mock up of a precast building designed and built for shaking table testing at LNEC for the "Growth-PRECAST EC8" research project

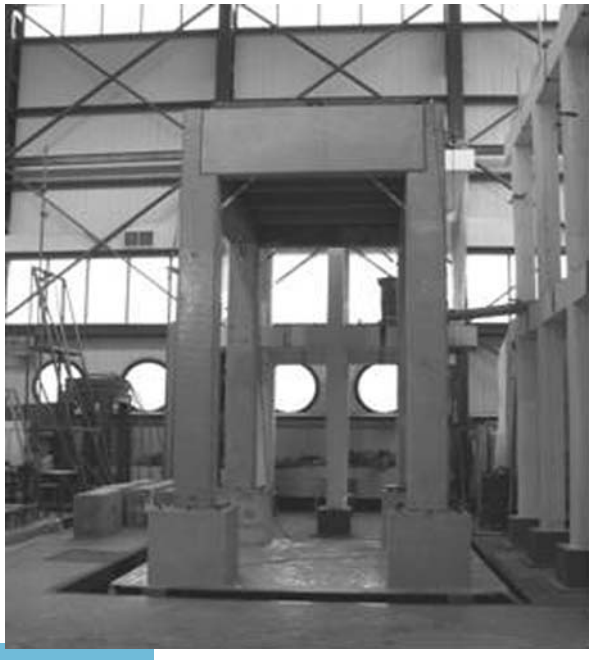

Fig. 10.17 Reduced scale prototype of an one-storey precast structure built and tested at NTUA Laboratory on its shaking table for the "Growth-PRECAST EC8" research project

The third stage will be the definition of the representative type structures.

These type structures will be then analysed to define their seismic capacity.

And finally some possible retrofitting interventions will be identified for defective types.

For the survey of existing precast buildings, with the help of the national association of precast industry, 12 manufacturers have been involved. Each of them provided the design documentation of a number of buildings chosen for different types and different times. Some 150 projects have been collected and this allowed to make a classification of the different types.

The survey covers the years between 1970 up to now and the different zones with different degrees of seismicity as codified at the time of construction. Mainly one-storey industrial buildings have been surveyed, as the precast solution represents more than the 80% of that category of buildings. But also multistorey commercial buildings have been surveyed, as their precast solution is more and more employed in recent times.

With the integrative intervention of some historical memories taken from the old bibliography for what not covered by the survey, a catalogue of building types has been drafted. The following list gives the different chapters of the catalogue dealing with as many types of buildings titled with the name of their more representative element: shed beams, segmental beams, and so on.

1. Shed beams
2. Segmental beams
3. Plane roof (I beams)
4. Plane roof (L beams)
5. Double gridwork
6. Roof elements
7. Skylight frames
8. Trusswork roofs
9. Any other
10. Multistorey

Any type has a number of different completion elements which characterize as many subtypes of structures. And for any subtype, in addition to a graphic representation, the indication of the relative diffusion over the territory and along the years is indicated, together with some comments on its structural capacities.

Figure 10.18 shows the subtype “1a” which refers to one-storey buildings with shed beams and ribbed roof elements. Figure 10.19 shows the subtype “3c” which refers to one-storey buildings with plane roof (I-beams) and special long span roof elements (thin walled folded plates). Finally Fig. 10.20 represents the subtype “10b” of multistorey buildings with a precast structure fixed to a bracing cast in situ element.

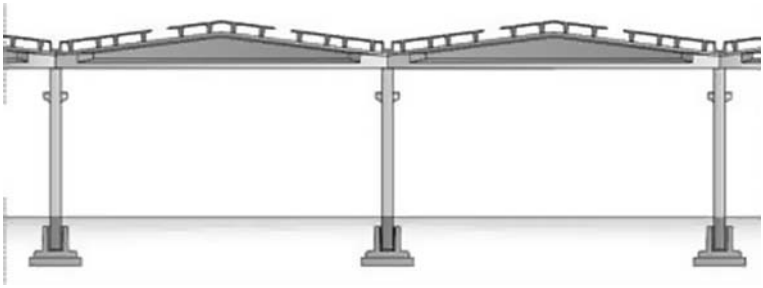

Fig. 10.18 Subtype "1a": one storey buildings with shed beams and ribbed roof elements

Fig. 10.19 Subtype "3c": one storey buildings I-beams of and special long span roof elements

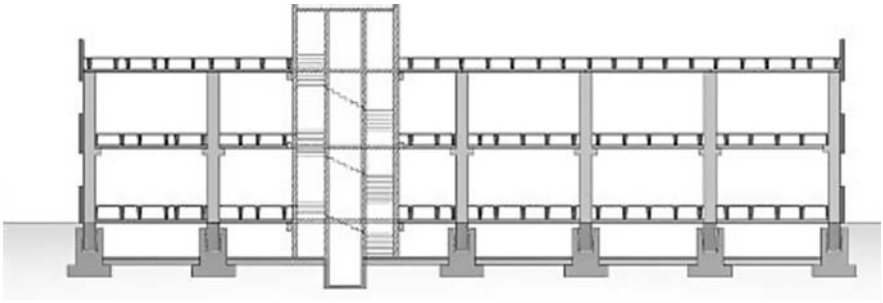

Fig. 10.20 Subtype "10c": multi-storey buildings with a precast structure fixed to a bracing cast-in-situ element

10.5.6 Connections

The second work package, which is in progress, deals with connections for their identification in terms of the mechanical parameters related to seismic behaviour.

The first category refers to the reciprocal connections between adjacent floor (or roof) elements. In the seismic behaviour of the structure, these connections affect

the diaphragm action of the floor which distributes the inertia forces, ensuring in the same time an uniform and coherent overall response.

The second category refers to connections between the floor elements and the supporting beams. These connections provide the peripheral restraints of the floor diaphragm in its behaviour under seismic action.

The third category refers to connections between columns and beams. These connections are typically made by pairs of steel bars passing through the joint or other devices able to guarantee a hinge behaviour in the vertical plane of the beam and a fixed behaviour in the vertical plane orthogonal to the beam.

A fourth category refers to connections between segments of columns, made with protruding bars grouted in hollow sleeves or other mechanical devices. Also connections between columns and foundations are included.

Finally the fifth category refers to connections between the cladding panels and the structure made with special channel bars, steel angles, inserts and fasteners. They shall provide the stability of the panels, allowing the large drifts expected under earthquake condition.

For any single type of the five categories the seismic behaviour will be characterized with cyclic tests on prototypes representative of the local structural arrangement. The characterization will be made in terms of strength, decay, ductility, energy dissipation and deformation following a standard testing protocol.

The experimentation started few months ago and for the moment there are no relevant results to be presented. The following paragraphs present the test set-up of one of the first series referring to a type of connection of the second category (joint between roof element and supporting beam). It consists of two steel angles connected by fasteners to the beam and a dowel passing through the web of the supported element.

The initial type testing has been performed on the reduced mock-up that you can see in Figs. 10.21 and 10.22. Figure 10.23 shows the diagram force-displacement obtained by the test for the subsequent groups of three hysteretical cycles. An indication of a non negligible dissipation capacity can be deduced, although no clear sign of yielding is noticeable.

Failure has been reached in a brittle mode with the spalling of the concrete edge, at a force level largely higher than what expected in actual earthquake condition (see Fig. 10.24).

This is the usual situation of the connections of this type of precast structures: both the supported and supporting concrete edges are brittle and weak; the intermediate steel connector is very strong with some possible ductility resources, [17, 18]. The behaviour of the structural chain of the joint remains brittle. No problem: with a proper capacity design ($F=\gamma_R M_{Rd}/h$ see Fig. 10.25) one can easily overproportion the joint, concentrating the energy dissipation in the ductile critical zones at the base of the columns. This is the usual way to design one storey precast industrial buildings.

One could try to invert the capacity scale of the joint, designing strong concrete edges and special weak ductile steel connectors. This could allow to have a ductile behaviour of the structural chain of the joint. So, considering that ductility

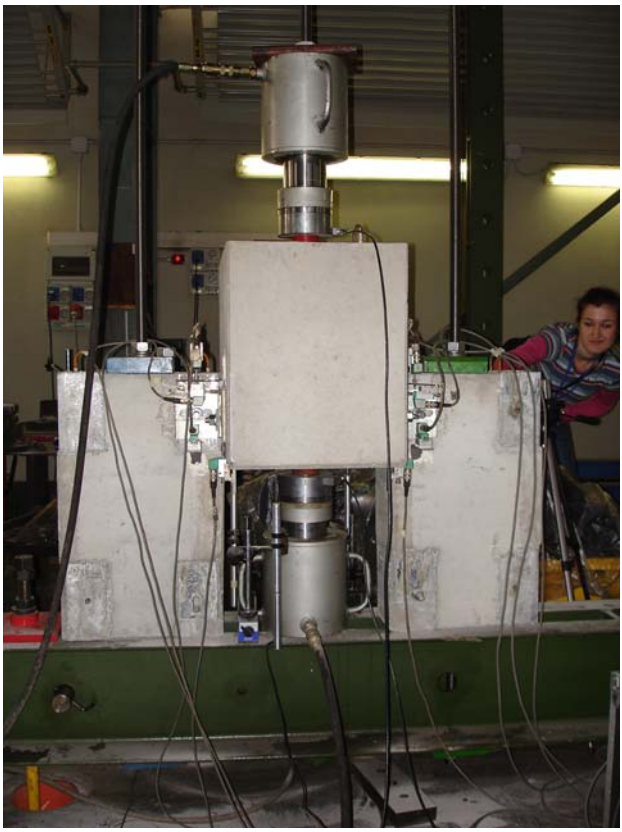

Fig. 10.21 Reduced-size mock up for cycling tests on connections designed and built at Politecnico di Milano

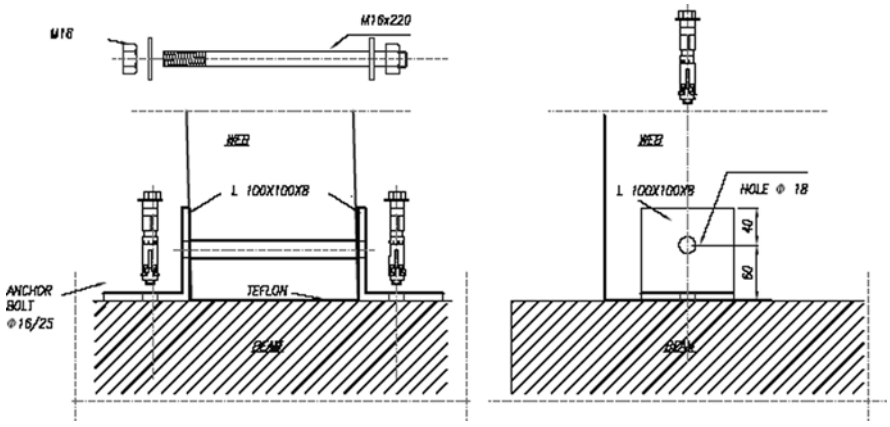

Fig. 10.22 Executive drawings for the connection between a ribbed element and the supporting beam

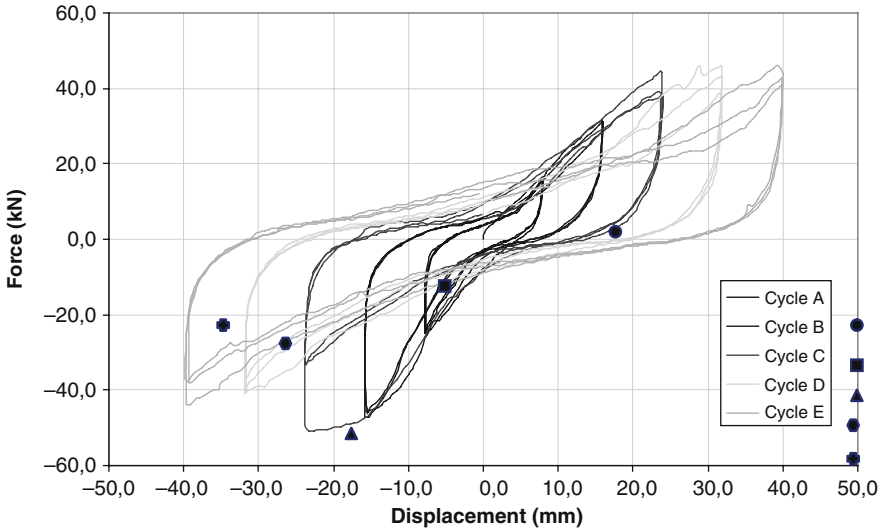

Fig. 10.23 Force-displacement hysteresis loops obtained during subsequent groups of cyclic tests

resources plus cyclic displacements lead to energy dissipation, can one propose a new approach for the design of precast structures based on "floating floors on dissipative joints"?

Fascinating perspective but with a lot of problems to be solved! First how can we design weak steel connectors used in a ductile mode? How can we limit the joint drift within the bearing length having high dissipation? How can we share dissipation between columns and joints in an effective ratio?

I hope to be able to give the answers to these questions at next occasion.

Fig. 10.24 Failure mechanism of the specimen (spalling of cover concrete)

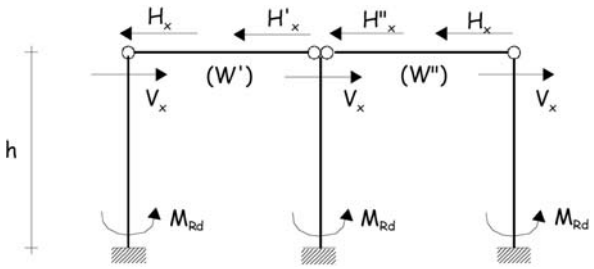

Fig. 10.25 Capacity design concept for the dimensioning of precast frame joints

Acknowledgments The research activities quoted in the text have been performed in the scope of ECOLEADER (JRC-Contract n. HPRI-CT-1999-00059), GROWTH (Contract N. PRECAST – G6RD – CT – 2002 – 00857), RELUISS (2005-09) research projects.

References

1. Englekirk RE (2003) Seismic design of reinforced and precast concrete buildings, Wiley, New York
2. fib Bulletin n. 27 (2004) Seismic design of precast concrete building structures-state of art report
3. Wood SL, Stanton JF, Hawkins NM (2000) New seismic design provisions for diaphragms in precast concrete parking structures. PCI Journal, Jan/Feb
4. Saisi A, Toniolo G (1998) Precast r.c. columns under cyclic loading: an experimental programme oriented to EC8. Studies and Researches 19
5. Fleischman RB, Naito C, Restrepo J, Sause R, Ghosh SK (2005) Seismic design methodology for precast concrete diaphragms, Part. 1: Design Framework. PCI Journal 50(5)
6. Priestley MJN (2003) Myths and fallacies in earthquake engineering, revisited. IUSS Press, Pavia
7. Biondini F, Toniolo G (2004) Validation of seismic design criteria for r.c. frames based on Monte Carlo simulation and psuedodynamic tests. Proc. 13th WCEE, Vancouver
8. Biondini F, Toniolo G (2000) Comparative analysis of seismic response of precast and cast-in-situ frames. Studies and Researches 22
9. Biondini F, Toniolo G (2003) Seismic behaviour of concrete frames: experimental and analytical verification of EC8 design rules. fib Symposium, Athens
10. Biondini F, Toniolo G (2006) Probabilistic calibration of behaviour factor for concrete frames. 2nd International fib Congress, Napoli
11. Biondini F, Ferrara L, Negro P, Toniolo G (2004) Results of pseudodynamic test on a prototype of precast r.c. frame. Proc. ICACS Int. Conference, Xuzou
12. Takeda T, Sozen MA, Nielsen MN (1970) Reinforced concrete response to simulated earthquakes. ASCE Journal of Structural Division, 96
13. Fleishman RB, Sause R, Pessiki S, Rhodes AB (1998) Seismic behaviour of precast parking structure diaphragms. PCI Journal, Jan/Feb
14. Moustafa SE (1981) Effectiveness of shear-friction reinforcement in shear diaphragm capacity of hollow-core slabs. PCI Journal, Jan/Feb
15. Davis G, Elliot KS, Omar W (1990) Horizontal diaphragm action in precast concrete floors. The Structural Engineer

16. Clough DP (1982) Considerations in the design and construction of precast concrete diaphragms or earthquake loads. PCI Journal, Mar/Apr
17. Pincheira JA, Oliva MG, Kusumo-Rahardio FI (1998) Tests on double-tee flange connectors subjected to monotonic and cyclic loading. PCI Journal, May/June
18. Shaikh AF, Feile EP (2004) Load testing of a precast double-tee flange connector. PCI Journal, May–June

Chapter 11
Soft-Landing Base-Isolation System

Koichi Kusunoki and Masaomi Teshigawara

Abstract The authors are developing a new retrofitting method for low seismic performance buildings, especially for soft-first-story buildings. The concept of the method is that the new column, which has the base-isolation system at its middle height, is attached to the existing column by the compression force with PC bars. The existing column will fail in shear during an earthquake, and then the building becomes to be base-isolated. One of the big advantages of this method is that the retrofitting cost can be low compared to the conventional base-isolation retrofitting technique, since the existing columns do not have to be cut prior to an earthquake, which costs a lot. The paper will present the outline of the system and the results of experimental tests which includes shaking table test and static loading tests.

11.1 Introduction

The base-isolation system is one of the retrofitting techniques for existing buildings especially for the building that has very low capacity. The system is very suitable especially for the soft-first-story buildings, because the damage tend to concentrate on the first story as shown in Fig. 11.1. The building, however, needs to be lifted up to install the base-isolation system to the existing building. It costs too much. Therefore, the soft-landing base-isolation system was proposed, which is low cost base-isolation system for existing buildings. The concept of the system is shown in Fig. 11.2. New pre-cast columns, which have base-isolation devices at their middle height, are attached to the existing column on the first floor ((a) and (b) in the figure). The existing column fails in shear during an earthquake ((c) in the figure), then the vertical and lateral loads are carried by the new column and the building becomes to be base-isolated. In order to achieve this system, following items were studied.

K. Kusunoki (✉)
Yokohama National University, Yokohama, Kanagawa, Japan
e-mail: kusunoki@ynu.ac.jp

A. Ilki et al. (eds.), *Seismic Risk Assessment and Retrofitting*, Geotechnical, Geological, and Earthquake Engineering 10, DOI 10.1007/978-90-481-2681-1_11,

Fig. 11.1 Damages of soft-first-story buildings during Kobe earthquake (See also Plate 14 in Color Plate Section on page 463)

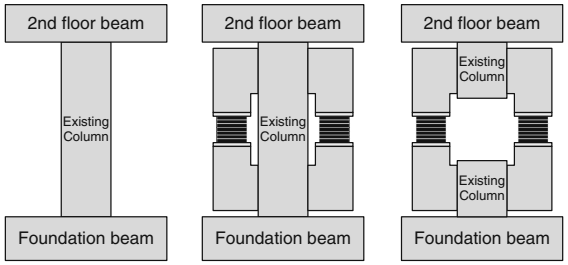

Fig. 11.2 Concept of the soft-landing base-isolation system

(a) Before retrofitting (b) Retrofitted (c) After an earthquake

1. Preliminary shaking table test: In order to verify the ability of the system, a shaking table test was conducted with very simple one story structure.
2. Failure mode control of the existing column: The failure mode of the existing must be controlled to achieve the system.
3. The evaluation method for the capacity of the existing and new column connection.

The vertical and lateral forces are transferred through the connection surface. The vertical force is transferred by the direct shear through the surface, and the lateral force is transferred by the twisting moment through the surface. The evaluation method for the capacity of the connection, however, has not been established yet.

The results of above three series of experimental tests are introduced and discussed in this chapter.

11.2 Outline of the Soft-Landing Base-Isolation System

The concept of the soft landing retrofitting method is shown schematically in Fig. 11.3. There are two ways to attach the new columns to the structure, to the existing column as shown in Fig. 11.3a and to the existing beams as shown in Fig. 11.3b.

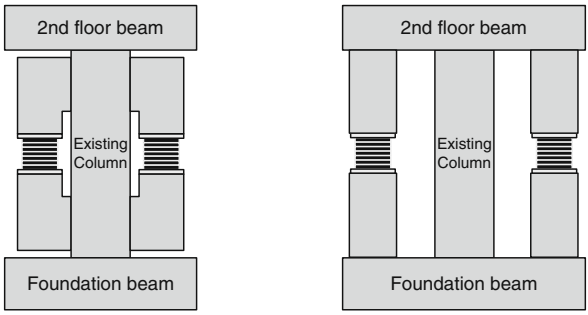

Fig. 11.3 The ways to attach the new column

(a) attached to the existing column

(b) attached to the beams

Figure 11.4 shows the moment distribution of beams and vertical force in the columns due to vertical load. Figure 11.5 shows the moment distribution and vertical force due to vertical load after an earthquake. As shown Fig. 11.5a, no moment except P-delta effect occurs after shear failure of existing column. On the other hand, Fig. 11.5b shows that large moment occurs in the beam at the top of the new columns due to vertical load. It requires strengthening the beams, which cannot be accepted. Therefore, the way shown in Fig. 11.3a is applied for the system.

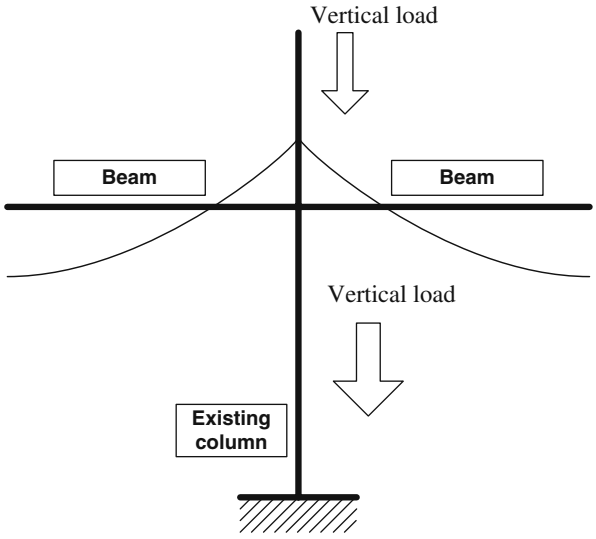

Fig. 11.4 Bending moment and axial force due to vertical load

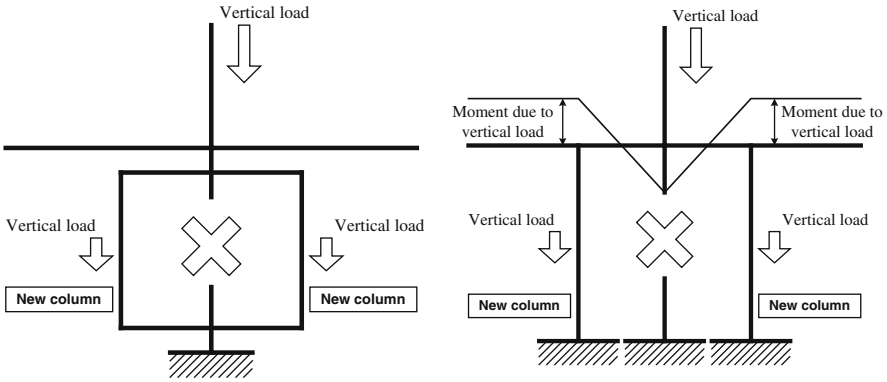

Fig. 11.5 Moment distribution and vertical force due to vertical load after shear failure of existing column

11.3 Shaking Table Test

As the first step to develop the system, a shaking table test with very simple 1-span-1-bay single story specimen was conducted. The photo of the specimen is shown in Fig. 11.6. The specimen is shown in Fig. 11.7. The natural frequency of the first mode was designed to be 2.7 Hz in the real scale from the prototype 10-story structure. The column size was then scaled down by 1/14.7. The mass of 8.8 ton was used. Due to the scale effect, the time axis was also scaled down by 14.7.

The dimension of the column was 75 mm by 75 mm and the height was 300 mm. The column had 4 steel re-bars, of which diameter was 6 mm but no hoops. As shown in Fig. 11.7, three dimensional load cells were attached on the columns to measure the lateral and vertical force carried by each column. Near the columns,

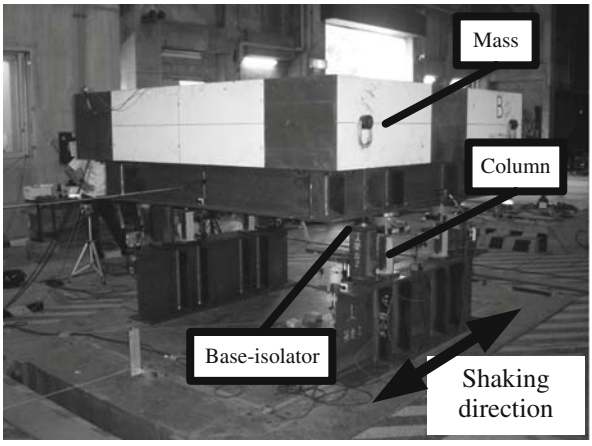

Fig. 11.6 Photo of the specimen

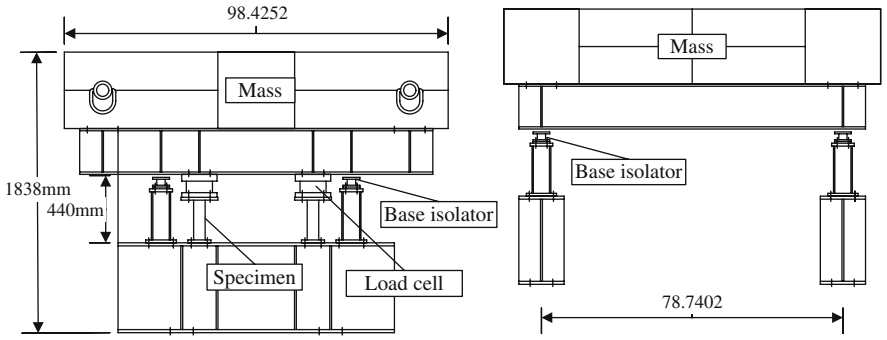

(a) North-south direction (b) East-west direction

Fig. 11.7 Dimension of the specimen

steel columns with base-isolator on its top were placed. They were not attached to the mass and there was a gap of 35 mm. The dimension of the base-isolator is shown in Fig. 11.8. The LRB isolator with 10 rubber layers was applied.

The predominant frequency of the specimen was measured as 9.0 Hz. The table was shaken 9 times as shown in Table 11.1. During RUN 6, shear crack occurs in all columns, and then during RUN7, all columns were failed in shear and the mass landed on the base-isolators as shown in Fig. 11.9. Figure 11.10 shows the relative response displacement (mass to the table) during RUN7. The residual displacement of about 2 mm occurred due to the shear failure. The relative response displacements during RUN 5 and RUN 9 were decomposed with the wavelet transform technique to study the frequency characteristics. Figure 11.11 shows the decomposed component of rank 5 of which Nyquist frequency is 7.81 Hz (close to the initial predominant frequency). Figure 11.12 shows the decomposed component of rank 7 of which Nyquist frequency is 1.95 Hz. The components were divided by the maximum response displacement to normalize them. It can be said from the figures that the response of RUN 5 had the predominant response in G_5. On the other hand, that of RUN9 had the predominant response in G_7, which has longer period. It shows that the specimen was successfully isolated during RUN 9.

11.4 Failure Mode Control of Existing Column

11.4.1 Necessity of Controlling the Failure Mode of Existing Columns

The new columns are attached to the existing column as shown in Fig. 11.2. The shear span ratio of the existing column is changed due to the attachment. It can change the failure mode of the column. The objectives in this test are to verify the possibility of controlling the failure mode by changing the shear span of a column, and to estimate the strength.

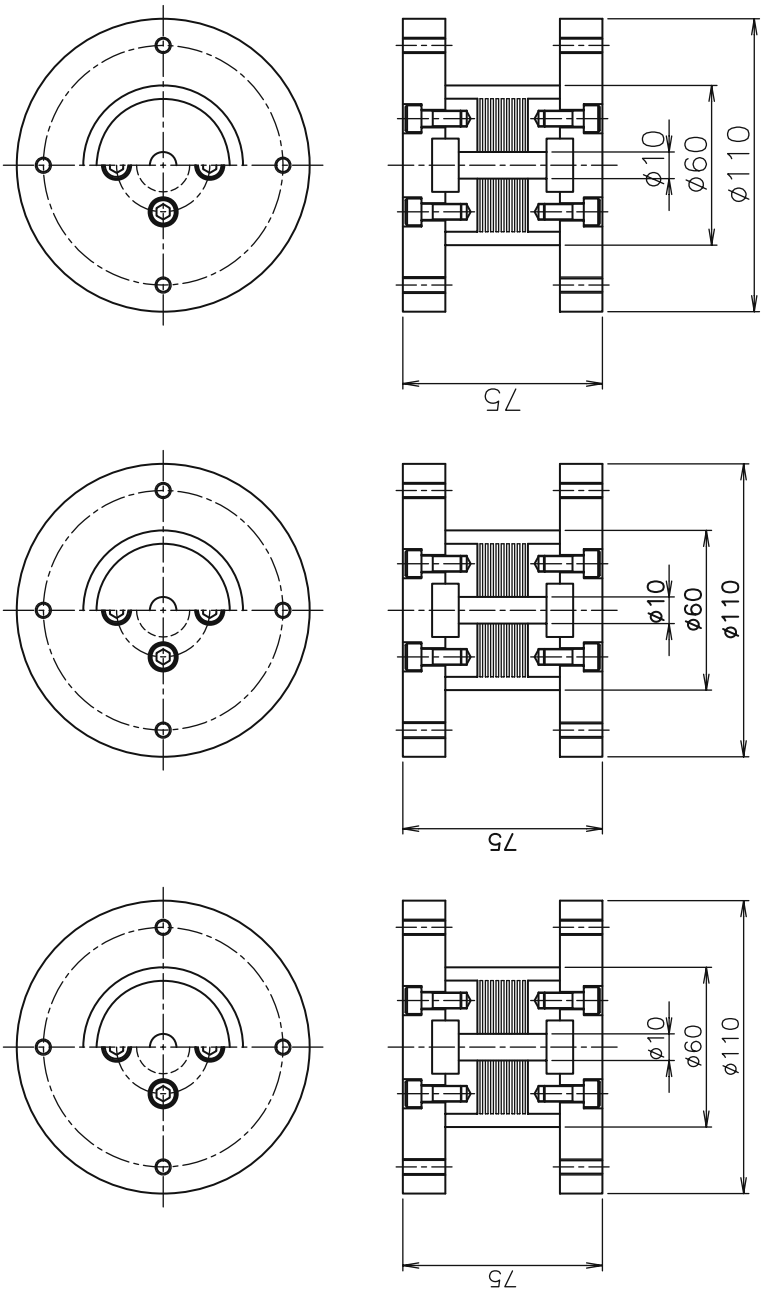

Fig. 11.8 Applied base-isolator

Table 11.1 Shaking test results

Run	Response Acceleration Input Direction (cm/s^2)	Relative Displacement (cm)	Table Acceleration (cm/s^2)	Note
1	116.7	0.2	52.4	
2	279.2	0.8	129.2	
3	330.6	1.1	216.7	
4	459.0	1.7	369.5	
5	508.0	2.4	462.1	
6	584.7	3.2	648.1	Crack
7	541.8	5.3	815.0	Collapse
8	329.6	7.0	973.0	Isolated
9	326.0	7.6	1125.5	Isolated

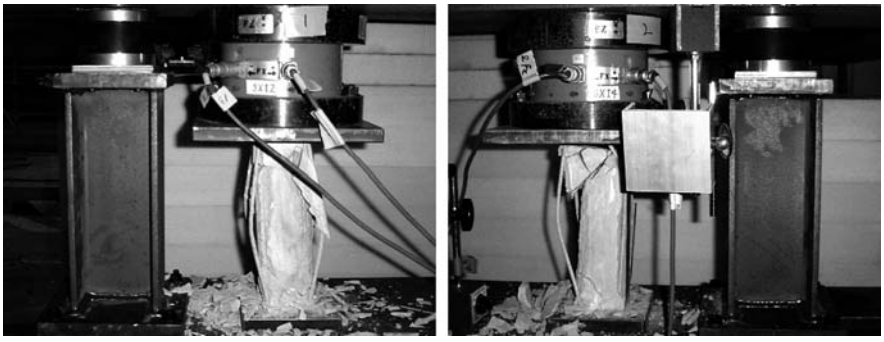

Fig. 11.9 Column damage during Run 7

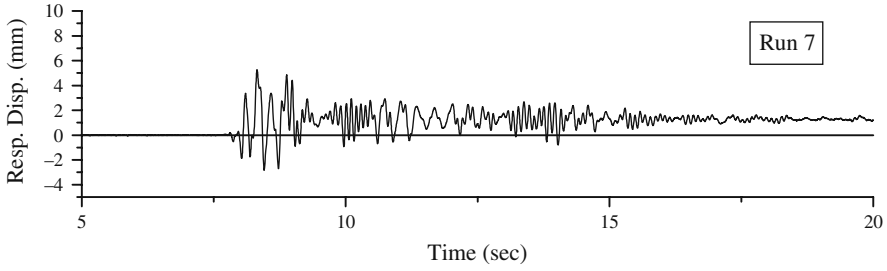

Fig. 11.10 Response displacement during Run 7

11.4.2 Test Specimens

The test specimen was modelled from the column of the first floor inner column of the prototype 7-story RC building with soft-first-story. The prototype column was scaled down by 1/3. Section and common parameters of the test specimen is listed in Fig. 11.13 and Table 11.2. The other parameters of test specimens, such as

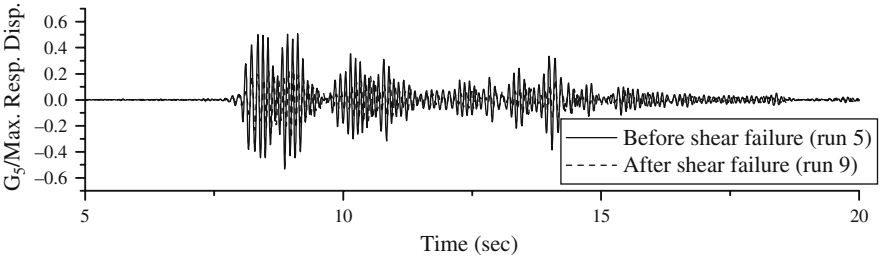

Fig. 11.11 Decomposed G_5 component divided by the maximum response displacement

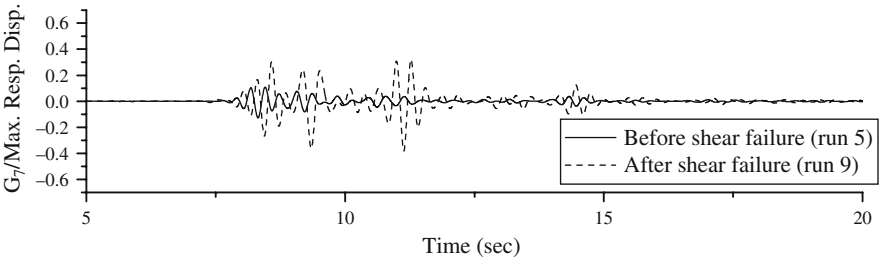

Fig. 11.12 Decomposed G_7 component divided by the maximum response displacement

Fig. 11.13 Section of test specimen

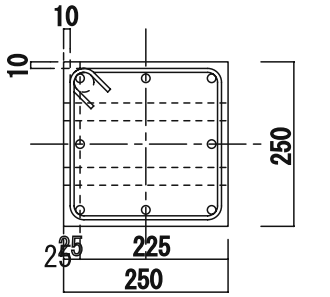

shear span ratios (0.75, 1.0, 1.5), and a height of column, are listed in Table 11.3. Elevations of specimens are shown in Fig. 11.14.

In this chapter, the specimens with shear span ratio of 0.75, 1.0, 1.5, are distinguished by the mark of specimen-S, -M, -L, respectively. There were two specimens with shear span ratio of 1.0 those are marked as M1 and M2. The specimens of M1 and M2 have the different vertical gap between the upper and lower parts of the new supporting column.

Table 11.2 Material properties and common parameters of test specimen

Tensile re-bars ratio pt	0.68 (%)
Hoop pw	0.26 (%)
Compressive strength of concrete fc	19.38 (N/mm2)
Yield strength of longitudinal re-bars	387 (SD345) (N/mm2)
Yield strain of longitudinal re-bars	2166×10–6 (mm/mm)
Yield strength of shear re-bars	350 (SD295) (N/mm2)
Yield strain of shear re-bars	1836×10–6 (mm/mm)
Axial load	187 (kN)

Table 11.3 List of specimens

Specimen	H0 (mm)	h0 (mm)	hbox (mm)	M/QD	dv (mm)
L	1250	750	250	1.5	25
M1	1000	500	250	1.0	25
M2					2
S	1000	500	312.5	0.75	5

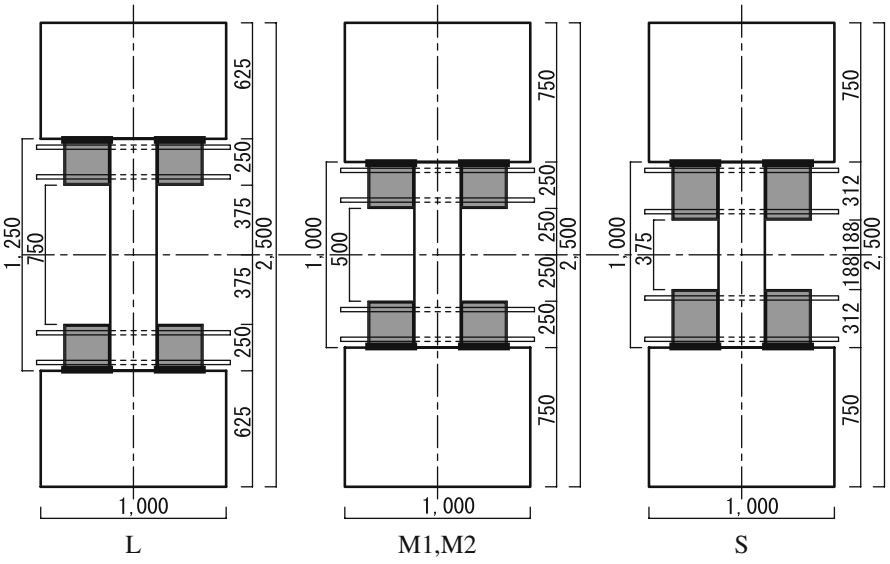

Fig. 11.14 Elevation of the specimens

Four steel boxes were attached to the capital and foot of RC column by four PC bars (4-ϕ23). Clear height of column was changed to 750 mm for specimen-L, 500 mm for specimen-M, and 350 mm for specimen-S, Fig. 11.13.

In the test, new steel supporting columns with sliding devices, which represents base-isolators, were installed in right and left sides of an RC column specimen as shown in Fig. 11.5, instead of a supporting column shown in Fig. 11.2.

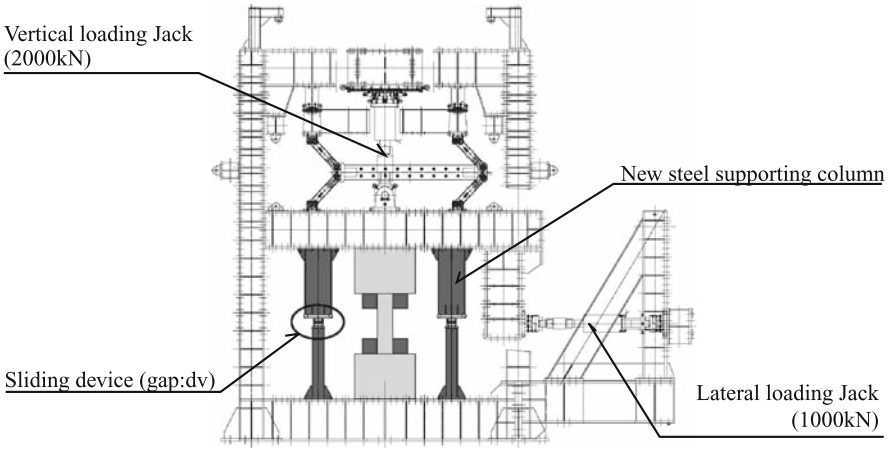

Fig. 11.15 Loading setup

Sliding device used in this test was Teflon and was installed in the mid-height of the supporting steel column. There was a gap between the slider device and the supporting steel column at the start point of the experiment. The distance of a gap was designed to be about 2 mm for the specimen-M2, about 5 mm for the specimen-S, and about 25 mm for the specimen-T and -M1. The axial load borne by the new steel support column was measured by the strain gauges attached to lower part steel frame column.

11.4.3 Loading

Test setup and loading apparatus is shown in Fig. 11.15. Constant axial load of 180 kN was applied by the vertical jack, and shear force was cyclically applied by the lateral jack in push and pull direction. Experiment was controlled by the drift angle in term of clear height of RC column that is one cycle in the drift of 1/400 rad., two cycles in the drift of 1/200 rad., 2-1/100, 2-3/200, 2-1/50, 2-1/40. When a test specimen failed and lost the axial load bearing capacity, axial load was carried by the new supporting column. After that, lateral displacement was forced cyclically within the lateral displacement of $\pm$ 50 mm.

11.4.4 Test Results

The relationship between the shear force and the drift is shown in Fig. 11.16. In all four cases, damage in the top and the bottom portion were prevented, and shear cracks in central part extended and failed in shear as shown in Fig. 11.17. The relationship between the axial displacement and the drift is shown in Fig. 11.18. Test results are listed in Table 11.4.

Specimens-M, and -L reached their strength at the drift angle of about 1% while the specimen-S reached its strength at the drift angle of about 0.5%. After that,

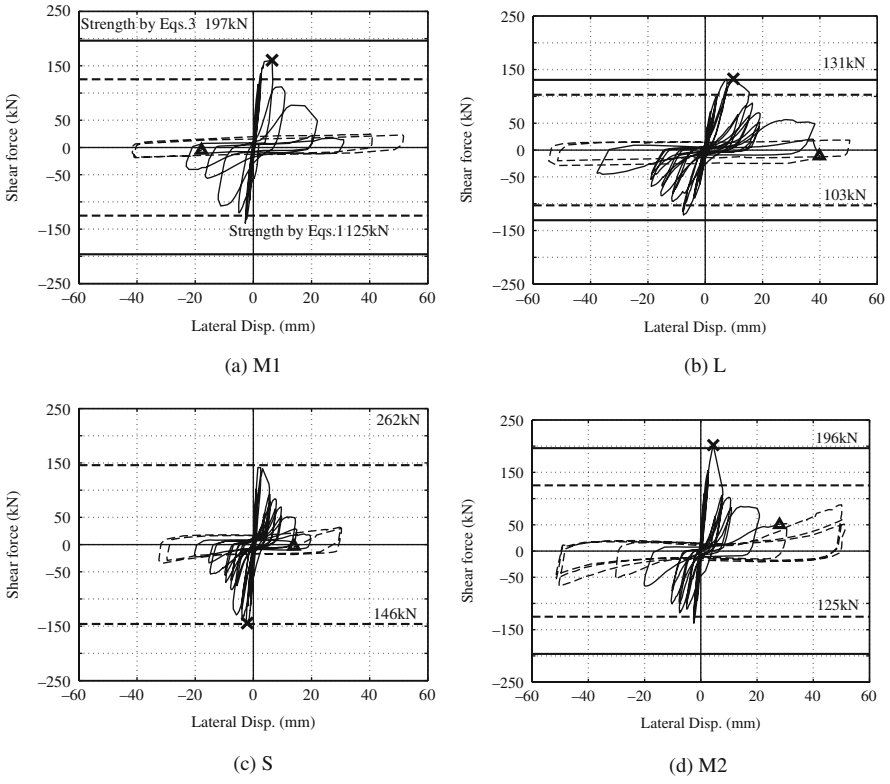

Fig. 11.16 Relationship between shear force and drift

lateral resisting force descended according to the cyclic loading and increasing the drift. All specimens, however, were able to sustain the required axial load up to the drift angle of 5%.

In the specimen-M2 that has the 2 mm gap between the slider device and the new support column, longitudinal reinforcing bars worked as the tension brace, and additional axial force acted on the new support column.

11.4.5 Strength

Strength obtained by the test is shown in Fig. 11.19 and listed in Table 11.5 with the calculated ones. Strength obtained by the test is larger than that of the calculated flexural strength of the specimen with M/QD = 2.0. Strength at the test is lower than that of the flexural strength in case of the clear height h0, and larger than that of the shear strength estimated by Eqs. 11.1 and 11.2. In case of Eq. 11.1, limitation of M/Qd is not applied.

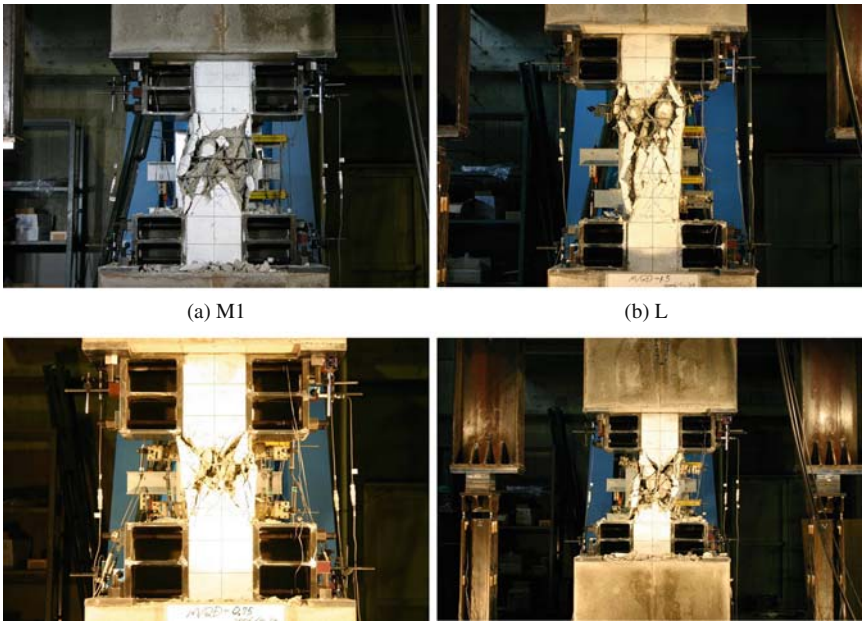

(a) M1 (b) L

(c) S (d) M2

Fig. 11.17 Photos of failure states

11.4.6 Axial Load Carrying Capacity

Yield strength of the longitudinal re-bars in the RC column is larger than working axial load on it. It is one reason why axial load can be sustained up to the large drift while the lateral load resisting capacity descended at small drift angle. Especially, in the case of specimen-M2 whose gap is small as 2 mm that means maximum vertical displacement of the specimen is allowed to be 2 mm, additional axial force is added on the new support column due to the tension brace action of the longitudinal re-bars in the column.

Equation 11.1 (Arakawa)

$$Q_u = \left\{ \frac{0.052 p_t^{0.23} (18 + \sigma_B)}{M/(Qd) + 0.012} + 0.85\sqrt{p_w \sigma_{wy}} \right\} bj, \tag{11.1}$$

p_t: Tensile bar ratio, σ_B: Concrete strength, p_w: Hoop ratio, σ_{wy}: Hoop strength

Equation 11.2 (AIJ)

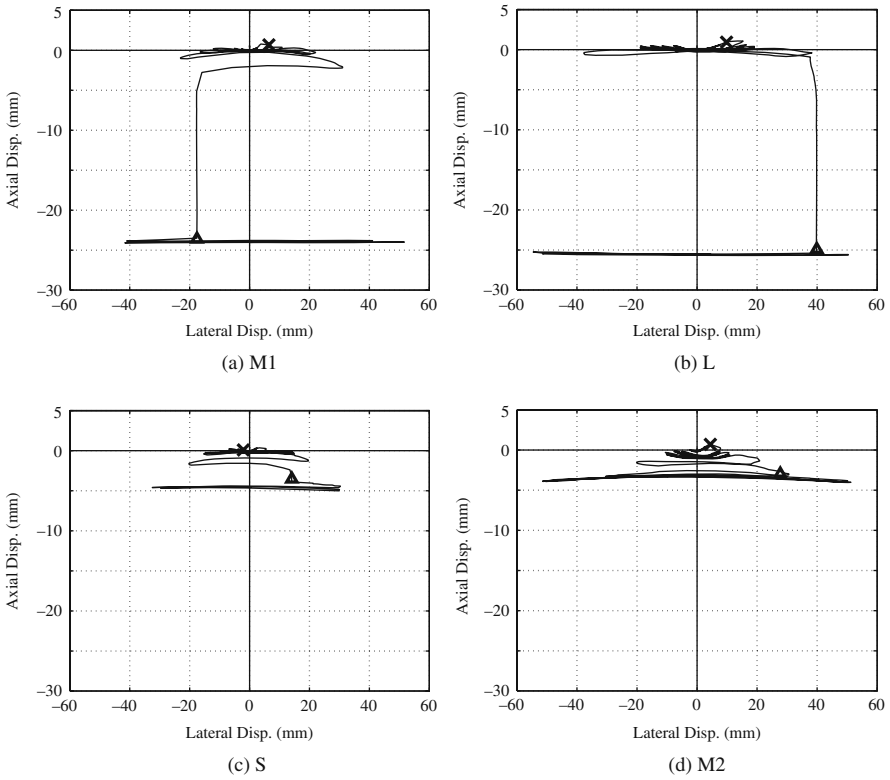

Fig. 11.18 Relationship between axial displacement and lateral displacement

$$
\begin{aligned}
V_u &= \{V_{u1}\ V_{u2}\ V_{u3}\}_{\min} \\
V_{u1} &= \mu \cdot P_{we} \cdot \sigma_{wy} \cdot b_e \cdot j_e + \left(v \cdot \sigma_B - \frac{5P_{we} \cdot \sigma_{wy}}{\lambda} \right) \frac{b \cdot D}{2} \tan\theta \\
V_{u2} &= \frac{\lambda \cdot v \cdot \sigma_B + P_{we} \cdot \sigma_{wy}}{3} \cdot b_e \cdot j_e \\
V_{u3} &= \frac{\lambda \cdot v \cdot \sigma_B}{2} \cdot b_e \cdot j_e
\end{aligned}
\tag{11.2}
$$

Where:

b and D	Width and depth of the column [mm]
j_e	Effective depth for truss action [mm]
b_e	Effective width for truss action [mm]
σ_{wy}	Yield strength of hoop [N/mm^2]
a_w	Hoop area [mm^2]
s	Hoop pitch [mm]

P_{we} $= \dfrac{a_w}{b_e \cdot s}$

μ $= 2 - 20R_P$

R_P Rotational angle at hinge area

σ_B Concrete strength [N/mm^2]

v $= (1 - 20R_P) \cdot v_0$

v_0 $= \dfrac{\sigma_B}{200}$

λ $= \left(1 - \dfrac{s}{2j_e}\right) \cdot \left(1 - \dfrac{b_s}{4j_e}\right)$

b_s $= \dfrac{b_e}{N_s + 1}$

N_s Number of inner hoops in the section

$$\tan\theta = \begin{cases} 0.9\dfrac{D}{2L} & \dfrac{L}{D} \geq 1.5 \\ \dfrac{\sqrt{L^2 + D^2} - L}{D} & \dfrac{L}{D} < 1.5 \end{cases}$$

L Clear height of the column

Equation 11.3 (Flexural shear force)

$$Q_m u = {}^{2M_u}\!/_{h0},\ M_u \tag{11.3}$$

Ultimate flexural strength, $h0$: clear height

11.5 Existing and New Column Connection

In the proposed soft-landing system, the existing column fails in shear during an earthquake, then the vertical and lateral loads are carried by the new column and the building becomes to be base-isolated. The vertical and lateral forces are transferred through the connection surface. The vertical force is transferred by the direct shear through the surface, and the lateral force is transferred by the twisting moment through the surface. The evaluation method for the capacity of the connection, however, has not been established yet. Therefore, a series of experimental tests was conducted to study the behavior at the connection between the new pre-cast column and the existing column.

11.5.1 Specimens

The specimen consists of existing column, new pre-cast columns, and base-isolation devices. The concrete strength for the existing column was 18 N/mm^2, and 36 N/mm^2 for the new column. The base-isolation device was replaced by the two-directional pin connection. The lower half portion of the soft-landing system was tested (Fig. 11.20), since the system is symmetric vertically as shown in Fig. 11.2.

Table 11.4 Test results

Specimen	Axial load	Max. shear force			Status at drift of 1/50 rad.			Status at the axial load sustaining limit			
	kN	Shear force (kN)	Drift (mm)	Drift angle (rad.)	Shear force (kN)	Ratio to max. shear force (%)	Disp. (mm)	Axial force (kN)	Vertical disp (mm)	Vertical disp (mm)	Residual axial force (kN)
L	162	132.8	9.83	1.3	87.6	65.9	16.43	313	–4.2	–0.6	30.8
M1	169	160.2	6.45	1.3	111.5	69.6	9.72	156	–2.55	–0.5	33.2
M2	186	202.0	4.42	0.9	102.5	50.7	9.99	170	–3.01	–0.6	87.3
S	166	144.2	–2.08	–0.6	84.1	58.3	7.38	169	–1.97	–0.5	60.7

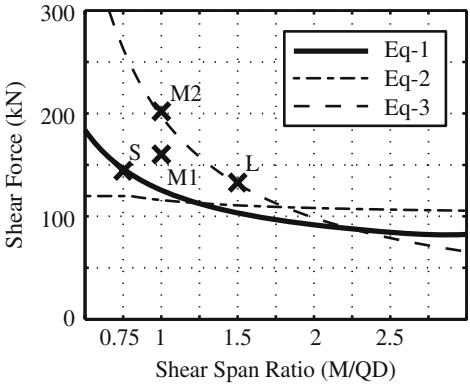

Fig. 11.19 Strength from test and calculation

Table 11.5 Estimated strengths

Specimen	Shear span ratio (M/QD)	Strength by Eq. 11.1 (kN)	Strength by Eq. 11.2 (kN)	Strength by Eq. 11.3 (kN)
L	1.5	103.3	110.7	131.5
M1, M2	1.0	125.4	115.8	197.2
S	0.75	146.1	119.7	262.9

Two new columns were connected to the surfaces parallel to the loading axis. The specimens were scaled down by 1/3.

Dimensions and bar arrangement of the specimens are shown in Table 11.6. Five specimens were tested. The constant vertical force, V_u of 55 kN and 82 kN were applied for No.2 and No.4, respectively. V_u of 156 kN was applied for No.5, of which compression force at the connection was higher than the others. No.1 was loaded only vertically, and No.3 was loaded only laterally without vertical load. All specimens were loaded only vertically to measure the ultimate vertical strength, V_0, after loading laterally.

11.5.2 Capacity of the Connections

The AIJ standard [1] proposes Eq. 11.4 to evaluate the capacity of the column-slab connection of the flat-slab system. Where, V_u is the vertical load, M_u is the twisting moment strength at the vertical load of V_u, V_0 is the ultimate vertical strength under only vertical load, and M_0 is the ultimate twisting moment strength without vertical load. The perfect yielding twisting moment strength is applied for M_0.

$$\left(\frac{V_u}{V_0}\right) + \left(\frac{M_u}{M_0}\right) \leq 1 \tag{11.4}$$

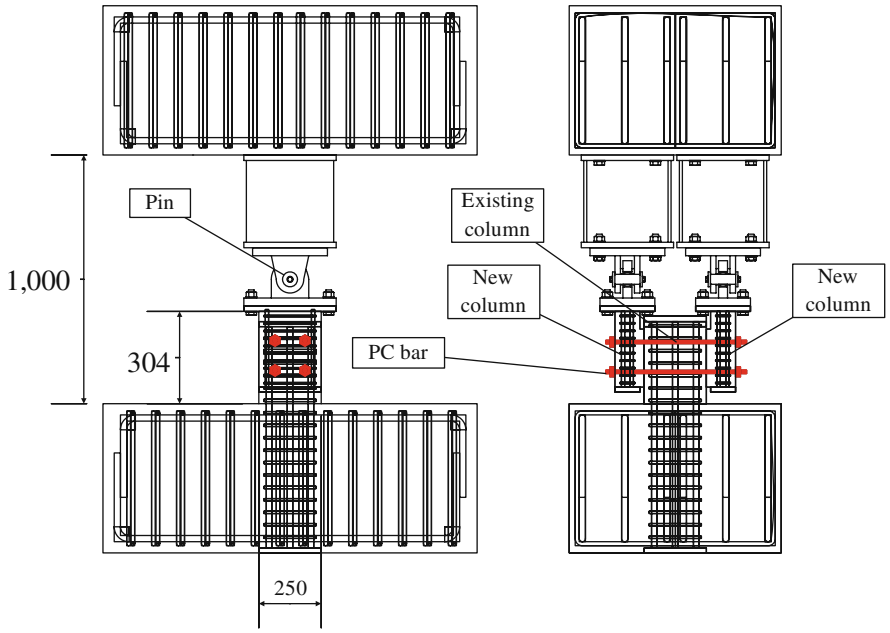

Fig. 11.20 Specimens (See also Plate 15 in Color Plate Section on page 464)

The resistance mechanism of the connection is different from that of the flat-slab system, since the flat-slap system is monolithic, while the new column with the base-isolation system is pre-cast member and no reinforcement bar but un-bonded PC bars go through the connection. Therefore, the force transfer mechanism of the connection can be only the friction at the connection for the vertical force and twisting moment for the lateral force.

The perfect plastic twisting moment is applied for M_0 calculated with Eq. 11.5,

$$M_0 = \frac{a^2}{2}\left(b - \frac{a}{3}\right)\tau_u \alpha \tag{11.5}$$

where a and b are the edge lengths of the connection ($a < b$), τ_u is the ultimate shear stress. The ultimate shear stress magnification factor α of 6 is recommended by AIJ for the flat-slab.

Table 11.6 Dimensions and bar arrangement of the specimen

	b × D (mm)	H (mm)	Main bar (σ_y = 345 N/mm^2)	Hoop (σ_y = 345 N/mm^2)
Existing column	250 × 250	308	Deformed 13	Deformed 6
New column	100 × 250	304.3	Deformed 22	Deformed 13

The ultimate vertical strength of the connection is calculated with Eq. 11.6,

$$V_0 = \tau_u D b \tag{11.6}$$

where D and b are the depth and width of the connection, respectively. Both M_0 and V_0 depend on τ_u and dimension of the section.

M_u and V_u are demand moment and vertical load combination at the design. They are calculated as follows in real scale with a seven-story prototype structure of which base-shear coefficient was assumed as 0.2.

$$V_{ud} = 843.5\,kN$$
$$M_{ud} = V_{ud} \times 0.2 \times 1.12 = 188.9\,kN \cdot m$$

The required ultimate shear stress at the connection, τ, is calculated as 1.86 N/mm^2 by substituting the values of M_u and V_u to Eq. 11.4. The values of V_0 and M_0 are calculated as 976.5 kN and 1401.7 kNm in real scale, respectively.

The compression stress by the PC bars, σ_0, is calculated as 1.86 N/mm^2 with the friction coefficient, μ, of 1.0 and Eq. 11.7. The compression force due to PC bar is calculated as 108.5 kN.

$$\tau_u = \mu \sigma_0 \tag{11.7}$$

The compression force of 108.5 kN was applied specimens No.1 to No.4, and the force of 236.5 kN was applied for specimen No.5 to investigate the effect of the compression force. The combination of M_u and V_u for each specimen is as follows; $M_u = 0.0$ and $V_u = V_0$ for No.1, $M_u = M_0$ and $V_u = 0.0$ for No.1, No.3, $M_u = M_{ud}$ and $V_u = V_{ud}$ for No.2, $M_u = 0.5M_{ud}$ for No.4, and $M_u = 2{\times}1.3M_{ud}$ for No.5. V_u for No.4 and No.5 were calculated with Eq. 11.4 and applied M_u No.1 was loaded only vertical to measure V_0. No.2 to No.5 were loaded laterally to measure M_u under the constant vertical load of V_u. The combination of vertical load and lateral strength, and applied force for PC bars are shown in Table 11.7.

Firstly, No.1 was loaded to obtain τ_u. Secondly No.3 was loaded to obtain a. It will be mentioned later in detail, but obtained τ_u and a were different from the assumed values during the design. Therefore, the combination of vertical and lateral load, and applied force for PC bars are modified as shown in Table 11.8.

Table 11.7 Calculated vertical and lateral strengths and applied force for PC bars

Specimen	Applied force N (kN)	Vertical load (kN)	Lateral load (kN)
No.1	108.5	217.0	0.0
No.2	108.5	187.4	37.9
No.3	108.5	0.0	278.1
No.4	108.5	202.4	18.8
No.5	236.5	205.2	98.5

Table 11.8 Actually applied vertical and lateral strengths and applied force for PC bars

Specimen	Applied force N (kN)	Vertical load (kN)	Lateral load (kN)
No.1	108.5	Loaded	0.0 (const.)
No.2	108.5	55.0 (const.)	Loaded
No.3	108.5	0.0 (const.)	Loaded
No.4	108.5	82.0 (const.)	Loaded
No.5	270.96	156.0 (const.)	Loaded

Loaded: the direction of which strength was investigated by loading, const.: the load was loaded constantly.

11.5.3 Loading and Measuring System

Loading system is shown in Fig. 11.21. The lateral force was applied at the mid-height of the specimen in order to keep the reflection point at the mid-height of the specimen. Two hydraulic jacks (A in the figure) were used for the lateral loading. Other two hydraulic jacks (B and C in the figure) were used to maintain the loading beam parallel to the ground and to apply vertical force. The lateral and vertical loadings were controlled by force until the maximum strength and after reaching the maximum strength, controlled by lateral displacement.

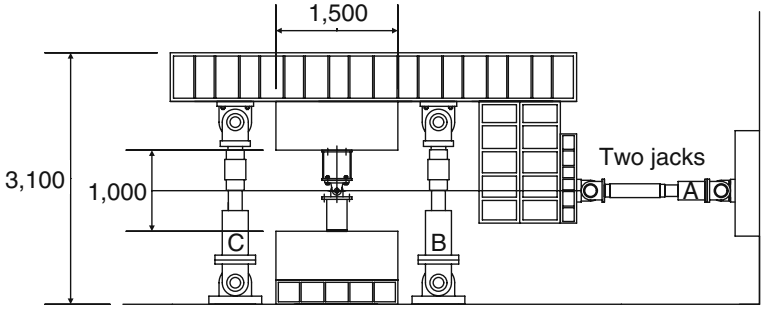

Fig. 11.21 Loading system

Lateral and vertical forces applied to the specimen, vertical and lateral deformations of the specimen, vertical and lateral relative displacement of the new column to the existing column, and strains of steel bars and PC bars were measured during the test.

11.5.4 Experimental Test Results

11.5.4.1 Vertical Load Carrying Capacity

Figure 11.22a and b show the relationship between relative vertical displacement (between existing and new columns) and vertical force at one connection surface of

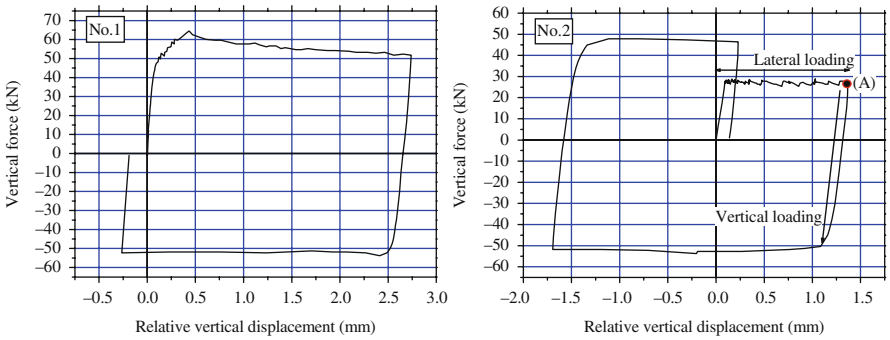

(a) No.1 (b) No.2

Fig. 11.22 Relationship between relative vertical displacement and vertical force (one connection)

No.1 and No.2. As for No.2, vertical force of 27.5 (=55.0/2) was loaded constantly during the lateral loading (until point (A) on Fig. 11.22b). After finishing the lateral loading, the vertical force was increased to investigate the vertical strength. It can be said that the vertical behavior of the connection was stable even after reaching the maximum vertical strength. The results of No.3 to No.5 also showed stable behaviors.

The column (5) in Table 11.9, V_0 shows the vertical maximum strength of the two connection surface. Since the vertical loadings without lateral load of No.2 to No.5 are conducted after lateral loading, the results can contain some error. Because of that, the strengths of No.1 to No.4 are not constant but almost the same. No.5, however, showed much higher strength although the concrete strength of all specimens was the same. It can be said that the vertical strength of the connection depends not on the concrete strength but on the applied compression force by the PC bars.

Table 11.9 Vertical strength and friction coefficient

	(1)	(2)	(3)	(4)	(5)	(6)	(7)
	Applied force for PC bars (kN)				V_0	τ_u	μ
	Initial	Lateral	Vertical	End	(kN)	(N/mm^2)	
No.1	110.61	92.65	92.65	82.23	107.47	0.95	0.58
No.2	109.39	97.09	90.31	85.85	95.75	0.84	0.53
No.3	113.71	96.82	86.21	82.69	96.72	0.85	0.56
No.4	109.62	97.90	93.70	91.94	113.33	1.00	0.60
No.5	270.96	270.96	236.15	230.32	447.46	3.95	0.95

(1) to (4) Applied force for PC bars initially, before lateral loading, before vertical loading, and after vertical loading respectively. (5) vertical strength of two connection surface, (6) ultimate shear stress (=V_0/area/2), and (7) friction coefficient (=(5)/(3)/2).

The column (7) of Table 11.9 shows the measured friction coefficient of the connection surface. The friction coefficients of No.1 to No.4 were almost the same (0.53–0.60), while the value for No.5 was much higher than others (0.95). It can be said that the friction coefficient depended also on the applied compression force by the PC bars.

11.5.4.2 Lateral Load-Relative Rotational Angle Relationship

The relationships between lateral load and relative rotational angle of the new column to the existing column of No.2 and No.5 are shown in Fig. 11.23. The behavior under the lateral load was stable even after the twisting moment reached its strength and started to slip at the connection. No.3 and No.4 also showed stable behavior.

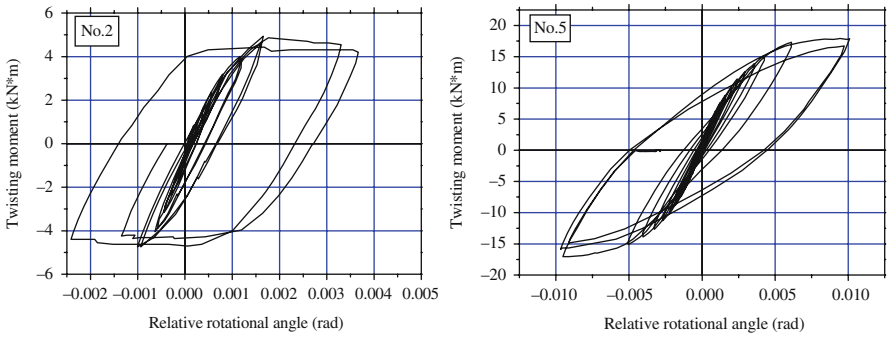

(a) No.2 (b) No.5

Fig. 11.23 Relationship between relative rotational angle and twisting moment

Figure 11.24 shows the relationships between the relative lateral displacement and relative rotational angle of the new column to the existing column of No.2 to No.5. It can be seen that the lateral displacement became relatively larger than the rotational angle when the lateral relative displacement exceed certain levels. In other words, lateral slipping tends to occur more easily than the rotational slip under the relatively large displacement. It is also obvious that the lateral displacement level when the lateral displacement ratio to the rotational angle became larger depends on the compression force applied to the connection by the PC bars.

11.5.4.3 Relationship between Vertical and Lateral Load Carrying Capacity

In this section, the validity of the design criteria of Eq. 11.4 is evaluated. Test results are shown in Table 11.10. V_0 needs to be calculated from the τ_u for the actual design procedure. In this study, however, the vertical strength without lateral load, V_0, and the ultimate shear stress, τ_u, were measured directly from the loading test. The combination of the vertical force and twisting moment, V_u and M_u, are given for the actual design procedure. In this study, on the other hand, V_u was given and applied

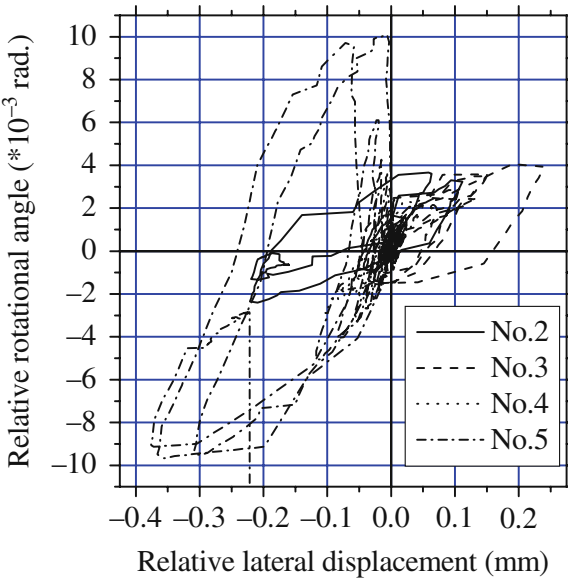

Fig. 11.24 Relationship between relative lateral displacement and relative rotational angle

to the specimen as the constant vertical load, and the twisting moment strength, M_u, was measured from the test. If the test results satisfy the condition shown in Eq. 11.8, it can be said that Eq. 11.4 can be used to evaluate the vertical and lateral load carrying capacity at the connection surface.

$$\left(\frac{V_u}{V_0}\right) + \left(\frac{M_u}{M_0}\right) \geq 1 \tag{11.8}$$

Table 11.10 Test results and from the result

	(1)	(2)	(3)	(4)	(5)	(6)	(7)	(8)	(9)	(10)
	V_0 (kN)	τ_u (N/mm^2)	V_u (kN)	τ_v (N/mm^2)	Q_u (kN)	M_u (kNm)	α	M_0 (α=1.54) (kNm)	V_u/V_0	M_u/M_0 (α=1.54)
No.1	107.47	0.95	–	–	–	–	–	13.71	1.00	0.00
No.2	95.75	0.84	55.00	0.49	30.01	9.48	1.20	12.21	0.57	0.78
No.3	96.72	0.85	0.00	0.00	39.04	12.34	1.54	12.34	0.00	1.00
No.4	113.33	1.00	81.00	0.71	25.62	8.10	0.86	14.45	0.71	0.56
No.5	447.46	3.95	157.30	1.39	107.85	34.08	0.92	57.07	0.35	0.60

(1) vertical strength without lateral force for two connection sufaces, (2) ultimate shear stress (=(1)/total connection area), (3) vertical constant force for lateral loading, (4) shear stress under the vertical load (=(3)/total connection area), (5) lateral strength under the constant vertical load, (6) twisting moment strength for two connection surfaces (=(5)/2×0.316), (7) αcalculated from Equation (2), (2), and (6), (8) the perfect plastic twisting moment with α of 1.54, (9) V_u/V_0 = (3)/(1), and (10) M_u/M_0 = (6)/(8).

The twisting moment strength without vertical load, M_u, is calculated with Eq. 11.5. In the equation, a, b, and τ_u are given from the dimension of the specimen and the test result. The ultimate shear stress magnification factor, α is given as 6.0 in the AIJ standard [1]. The relationships between M_u/M_0 and V_u/V_0 are shown in Fig. 11.25b as the rectangular points. They do not satisfy the Eq. 11.8. Therefore, the Eq. 11.4 cannot be used as the design criteria with the α of 6.0.

Equation 11.5 is the theoretical function to calculate the perfect plastic twisting moment strength regardless of vertical load. Since M_u varied according to the vertical load, α should be variable according to the vertical load. In other words, the shear stress for Eq. 11.5, $\tau_{tu} = \alpha\tau_u$, varies according to the vertical shear stress, τ_v. The column (7) of Table 11.10 shows α calculated from Eq. 11.9. Figure 11.25a shows the relationship between α and τ_v. From the figure, it can be said that Eq. 11.10 can estimate the criteria of the combination of the calculated α and the measured τ_v. Since τ_u for No.1 to No.4 are almost the same and it is possible to consider τ_u as constant, Eq. 11.10 can be transferred as Eq. 11.11 with α of 1.54. The relationships between M_u/M_0 and V_u/V_0 are shown in Fig. 11.25b as the triangular points. The Eq. 11.4 (Eq. 11.11) with α of 1.54 can evaluate the vertical and lateral load carrying capacity at the connection surface of the specimens reasonably.

$$M_u = \frac{a^2}{2}\left(b - \frac{a}{3}\right)\tau_u\alpha \tag{11.9}$$

$$\frac{1}{0.95}\tau_v + \frac{1}{1.54}\alpha \le 1 \tag{11.10}$$

$$\Leftrightarrow \frac{a \cdot b}{a \cdot b}\frac{\tau_v}{0.95} + \frac{\frac{a_2}{2}\left(b - \frac{a}{3}\right)\tau_u}{\frac{a_2}{2}\left(b - \frac{a}{3}\right)\tau_u}\frac{\alpha}{1.54} \le 1$$

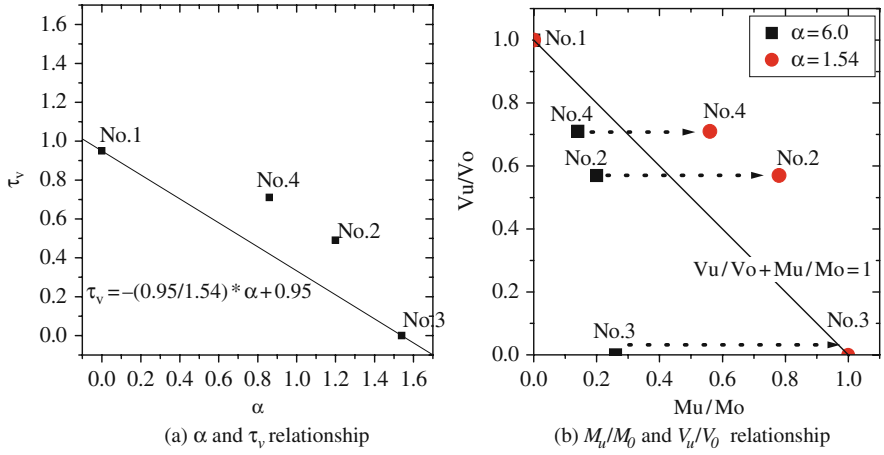

Fig. 11.25 Evaluation of the vertical and lateral load carrying capacity

$$\Leftrightarrow \frac{V_u}{V_0} + \frac{M_u}{M_0} \leq 1 \tag{11.11}$$

11.6 Concluding Remarks

From the preliminary shaking table test, the possibility of the proposed soft-landing retrofitting system is evaluated.

Results obtained from the experimental test on the failure mode control can be summarized as follows:

1. Failure mode is controllable by changing shear span. Shear span is controlled by setting steel boxes at the top and the bottom part of the column in this test.
2. Bending moment capacity at the critical section of the column increases by the setting the steel boxes.
3. RC column in this test failed in shear mode and its lateral load resisting descended suddenly, but its axial load bearing capacity is kept up to relatively large drift.

Results obtained from the experimental test on the new and existing column connection can be summarized as follows:

1. The vertical behavior of the connection was stable even after reaching the maximum vertical strength.
2. The vertical strength and friction coefficient at the connection surface depend on the applied compression force by the PC bars.
3. The behavior of the connection under the lateral load was also stable even after reaching the maximum twisting strength.
4. The lateral displacement level when the lateral displacement ratio to the rotational angle becomes larger depends on the compression force applied to the connection by the PC bars.
5. Equation 11.1 with α of 6.0 cannot estimate the vertical and lateral load carrying capacity at the connection surface.
6. Equation 11.1 with α of 1.54 can estimate the vertical and lateral load carrying capacity at the connection surface of the specimens.

11.7 Future Studies

In order to achieve the proposed system, following study topics are planned to be conducted in this and next year.

1. Shaking table test to study the effect of torsional response due to the difference of the strengths of columns
2. Static loading test to study the effect of the new column on the bending strength increasing of existing column
3. Full scale loading test to study the validity of the system.

Acknowledgments This research is conducted as a part of the grant in the project of research and development for leading technologies related to the house / building (Ministry of Land, Infrastructure and Transport), "The research and development of a soft landing type seismic retrofitting for apartment type housing" (H17FY-H19FY).

Reference

1. Architectural Institute of Japan (1999) AIJ standard for structural calculation of reinforced concrete structures – based on allowable stress concept

Chapter 12
Development of a New Precast Concrete Panel Wall System Incorporated with Energy Dissipative Dowel Connectors

Huseyin Darama and Hitoshi Shiohara

Abstract Conventional methods of earthquake resistant design rely on the ductile behavior of the structural member for energy dissipation. It is required that the structure yields and experiences damage without collapse under a catastrophic event. For newly built structures, ductility requirement can be achieved by providing special detailing where inelastic deformation expected. However, the situation is not straightforward and complex for the existing or poorly detailed structures. In most case, rehabilitation becomes impossible due to insufficient techniques, high costs and long down-time. As a response to these shortcomings, a new Precast Concrete Panel Wall (PCPW) system with dowel connectors is introduced herein. In a moderate event, proposed system relies on the energy dissipated by the dowel connectors at panel attachments. The hysteretic energy dissipation will be concentrated on specially designed connectors and this will reduce the inelastic demand on existing elements. However, under the action of a major event, panels will intact with the frame and contribute stiffness by a diagonal strut action. This will prevent from total collapse of the structure. The dual response mechanisms of PCPW systems inspire us considering them as an alternative passive control system that would be used in strengthening works.

12.1 Introduction

Panel and connector elements are the individual components of a typical PCPW system. Panel is a rigid-block type structural system that its response controlled by rocking motion due to floor accelerations and imposed inter-story drifts. Connectors are the link elements at the interface between panel and frame members. Due to story drift, initially connectors will start bearing (and/or slipping), increase resistance and dissipate energy at small drift values (<1.0% rad.). Then, the distance between the panel and frame will eventually decrease. When it is reached above lager drift levels

H. Darama (✉)
Arup North America Ltd., Los Angeles, USA
e-mail: huseyin.darama@arup.com

A. Ilki et al. (eds.), *Seismic Risk Assessment and Retrofitting*, Geotechnical, Geological, and Earthquake Engineering 10, DOI 10.1007/978-90-481-2681-1_12,

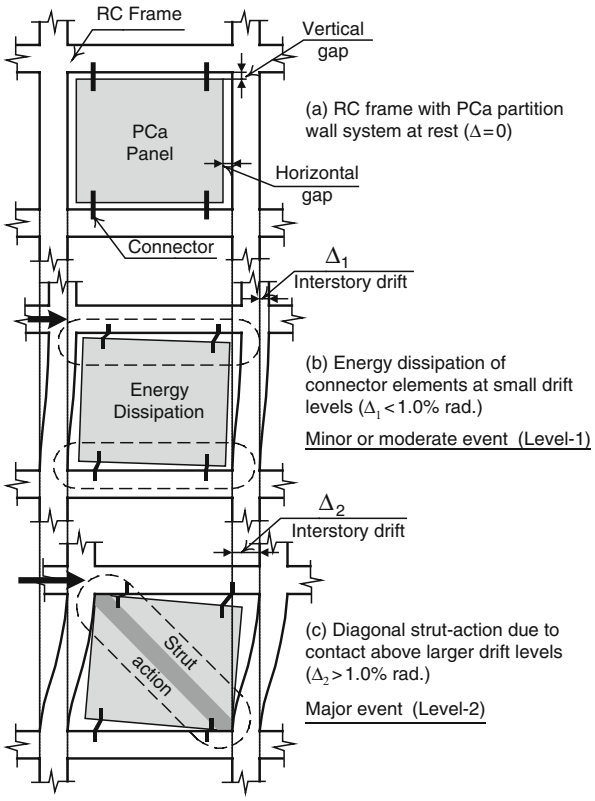

Fig. 12.1 Dual response behaviour of a PC panel wall under seismic excitation

(>1.0% rad.), panel will be intact with frame and start to withstand imposed drift by contributing stiffness via diagonal strut action (Fig. 12.1).

These dual response mechanisms of PCa elements inspire us considering them as an alternative passive control system that would be used in new building and/or even strengthening works. In this chapter, only the energy dissipation mechanisms at small drift levels are interested. Initially, an experimental program is introduced so as to build up a proper knowledge for the nonlinear dowel modeling. Factors influence connector response is discussed. Finally, effects of connectors on the response of a prototype RC building are quantified in terms of shear resistance and supplementary viscous damping ratio.

12.2 Cyclic Panel Tests

Dowel behavior is difficult to predict by analytical methods due to existing highly complex interaction phenomena of concern and the dependency to the parameters involved. Test program were a cooperative work with Shimizu Co. Ltd. and

performed at the Shimizu Institute of Technology Laboratories from June to July, 2005. Specimens were selected frame 6 and 8-story RC residential building used in Japanese practice (koudan jutaku). Loading frame has pin joints at each ends. Specimens and loading frame are all full scaled.

12.2.1 Test Parameters

Total 7 specimens were tested with being A, B and C series. The following items are the parameters of the test program:

1. Panel size (A and B series vs. C series)
2. Attachment configurations of connectors (A1 vs. B1, and C1 vs. C2)
3. Gap distances (B1 vs. B4)
4. Unbounded conditions on deformed bar type connectors (B1 vs. B3)
5. Connector material (B2 vs. B1)

Schematic illustration about the proposed test specimens, and related parameters regarding to materials and connectors are shown in Fig. 12.2.

B series has 4 specimens named as B1, B2, B3 and B4. The panel dimensions for all of the B series is 2000 (height) × 1200 (width) × 120 (thickness) in mm. Total 4 connectors used in each, being 2 at the top and 2 at the bottom.

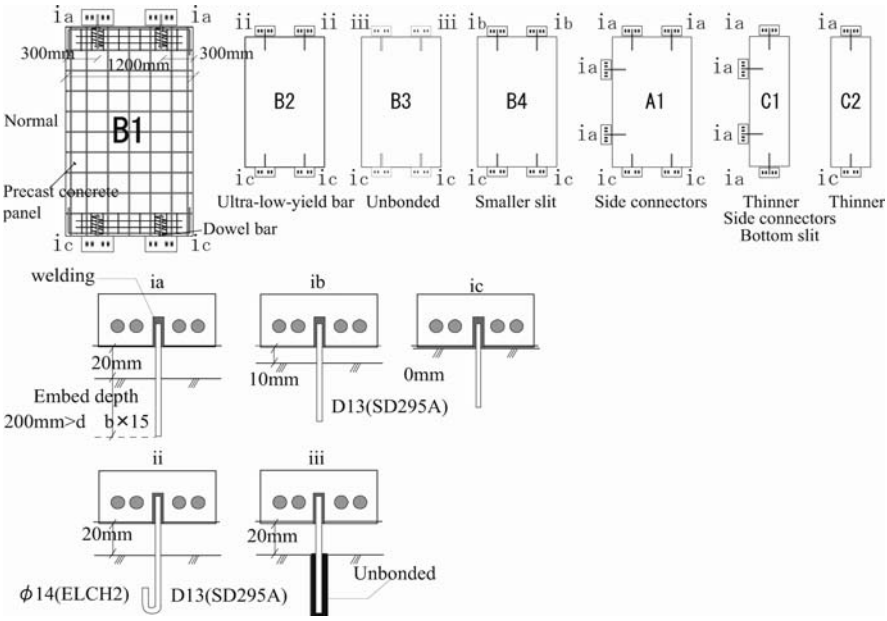

Fig. 12.2 Panel specimens and their connector configurations

A1 is the only specimen in A series and the panel dimensions is exactly the same as B series. The only difference between B1 and A1 is the existence of side connectors in later case. The gap distance value that was left for top and side connections of all specimens is 20 mm except specimen B4. In the case of specimen B4, 10 mm gap distance used for evaluating this effect. The difference between connectors of B1 and B3 is introducing unbonded conditions for later case to see the force coupling (tension and shear) effects on deformed type dowel bars. Only in B2, a special type bar so called "ultra-mild high-elongation plain bar" is used to see the difference in performance from commonly used deformed bar.

The panel size in C series is 2000(Height) × 600(Width) × 120 (Thickness) in mm, which is half width of A and B. For specimen C2, total 2 connectors used, being 1 at the top, 1 at the bottom. For specimen C1, total 4 connectors used, being 1 at the top, 1 at the bottom and 2 at single side of the panel. No gap distances left for bottom connectors at each specimen except C1. In C1, 20 mm gap is used to see the effects. Out of plane effects and contact action have not included in the scope of the experiment at this time yet.

Detailed information about the proposed test specimens, related parameters regarding to materials and connectors are shown in Table 12.1 below.

Table 12.1 Test specimen parameters

	Mark	Connector Type	Connector Quantity			Panel Size	Gap Distances			Concrete Design Strength	Connector Material	Connector Size
			Side	Top	Bot.		Side	Top	Bot.			
1	A1	Deformed bar	2	2	2	2000×1200×120	20	20	0	24 MPa	SD295A	D13
2	B1	Deformed bar	–	2	2	2000×1200×120	–	20	0	24 MPa	SD295A	D13
3	B2	Plain Bar	–	2	2	2000×1200×120	–	20	0	24 MPa	ELCH2	f14
4	B3	Unbonded Deformed bar	–	2	2	2000×1200×120	–	20	0	24 MPa	SD295A	D13
5	B4	Deformed bar	–	2	2	2000×1200×120	–	10	0	24 MPa	SD295A	D13
6	C1	Deformed bar	2	1	1	2000×600×120	20	20	20	24 MPa	SD295A	D13
7	C2	Deformed bar	–	1	1	2000×600×120	–	20	0	24 MPa	SD295A	D13

ELCH2 (4C5412): F_y= 193 MPa, Low yield strength steel
(KOBELCO) F_u= 307 MPa
Elongation= 31%

SD295A: F_y=295 MPa (Nominal Strengt)

12.2.2 Loading History

Early loading history will be force controlled and applied only one full cycle until the elastic limits of connectors. The reason is just the difficulty of controlling and targeting desired peaks at very small drift ranges. When the story drift reaches 0.1% drift (2 mm) the rest of the loading history will be displacement controlled (as shown in Fig. 12.3).

The force will be applied with the increments of 2.5 kN until the 10 kN level, the cycling will start and steps of increment will be change after that to 5 kN. For the specimens B3 and C series, the loading directly applied from displacement

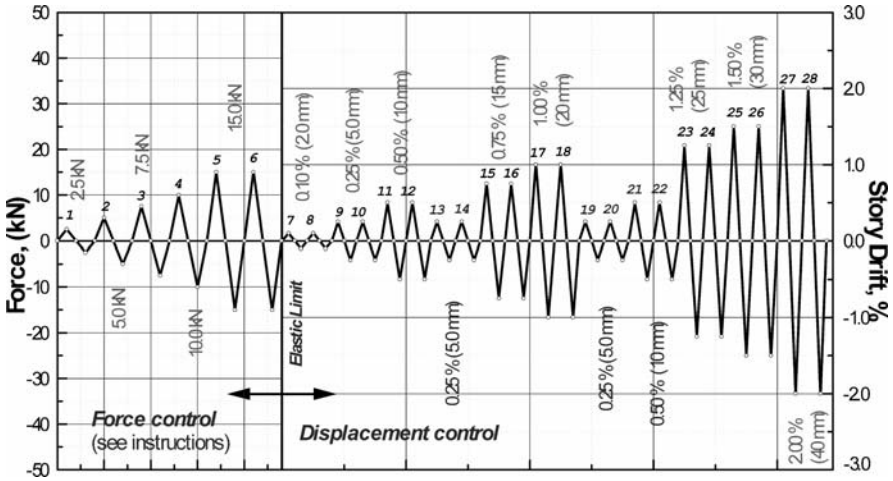

Fig. 12.3 Loading cycles used in the test program

control stages at displacement control stages; two full cycles are applied for each and every corresponding drift levels. The input drift cycles will gradually increase up to a major event level (1.00%) then previous minor events will be repeated (0.25–0.50%). Again the progressive cycles will gradually increase up expected damage state (2.0%). The reason for these smaller cycles (minor event) after a major event is to evaluate how much changes occurred in capacity and hysteretic characteristics of test response.

12.2.3 Loading Frame Setup

Loading frame setup consist of 4 separate H type steel beams connected each other by frictionless pin joints. Selection of profile size and dimensions were done for providing enough strength to keep them remain elastic in all possible load conditions due to connectors. Bottom beam is 4000 mm and fixed to the base. Side frames has the same height of 2300 mm. Upper beam is the loading beam and a little longer than the bottom one with having 4632 mm length. The vertical distance between the pins is fixed with a value of 2000 mm. In the case of horizontal distance between the pin joints is assigned to a value of 3000 mm. This was large enough to test most common panel size seen in practice. 9 mm stiffener plates were used at mid and pin joint location of the each frame member. In addition to that, the holes were opened during the manufacturing at the flange plates of each profile where the joint beams coincide. Figure 12.4 shows the loading frame setup of the experimental program.

Establishing frictionless pin joints is an important concern. There are total 4 pairs of pin joints used on the test frame and they are all same futures and size. Pins were established by 5 different plates. The bottom plate has a size of 280 × 448 × 25. It

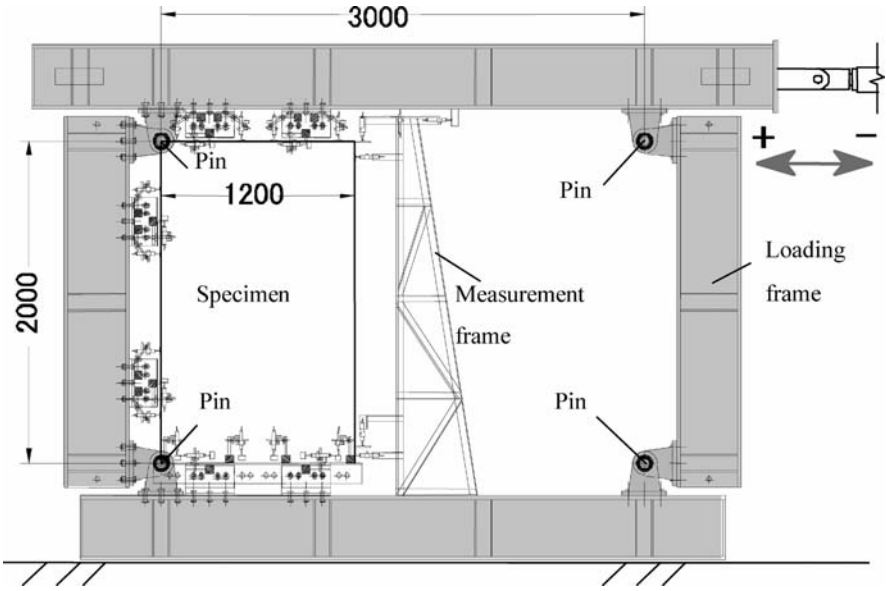

Fig. 12.4 Loading frame setup

is welded to 2 pairs of 19 mm thick vertical plates with a 272 mm distance between them. Each vertical plate has a circular shape at top and a 75 mm hole at the center of this circle.

The distance from the pin center to the bottom plate is 200 mm and total height is 250 mm. The pairs of assembled pin joints connected each other through the pin holes by the frictionless 75 mm circular solid bar. Each bottom plate has 6 holes (26 mm) for providing bolted connection to the corresponding loading frames.

12.2.4 Measurement System

Measuring systems are one of the most important parts of the experimental process that plays crucial role determining the reliability for evaluation of the results. In here, CDPs are used for measuring corner displacements of the panel specimens, relative displacements on each connector elements, and measuring imposed drift (Fig. 12.5). In the panel test, one of the major interest is to record total shear resistance of panel elements by the attached connectors. For this purpose, a load cell is used and corresponding cyclic data recorded. In order to obtain major force components generated on individual connector joints 5 equally spaced tri-axial gages attached on each joint elements (Fig. 12.6). Tri-axial rosette gages used in the experiments were manufactured by Tokyo Sokki Kenkyujo with FRA-10-11 series. For this product, a gage factor of 2.12 was given by the manufacturer. For each gage 3 channels is assigned at data logger. That means total 15 channels of data are stored for each connector.

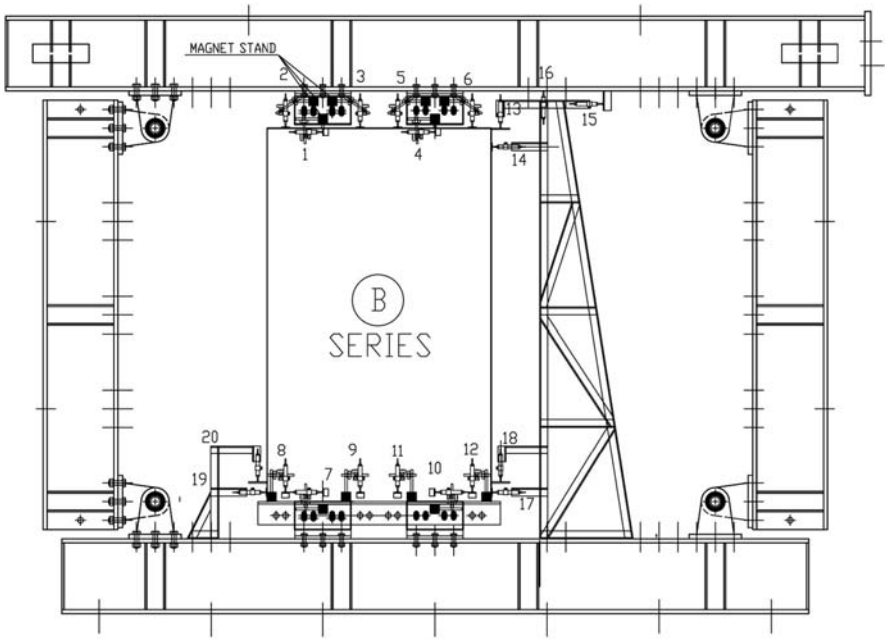

Fig. 12.5 CDP locations and channel numbering assigned for specimens of B series

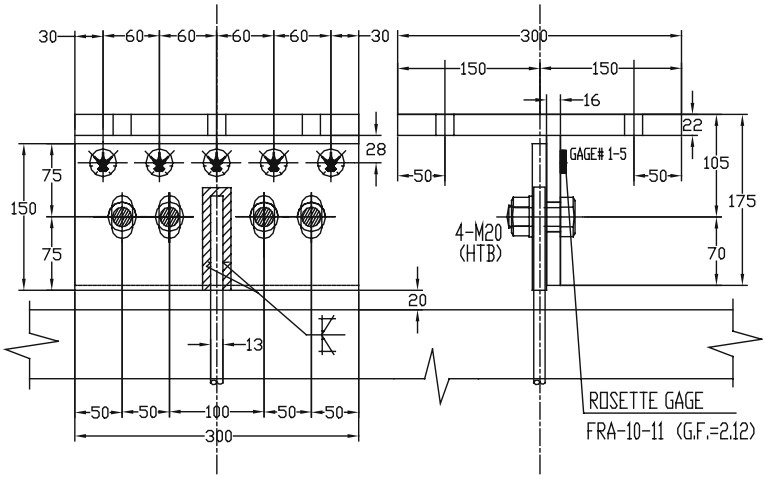

Fig. 12.6 Tri-axial strain attached on joint elements

12.3 Test Results: Measured Force-Displacement Plots

The hysteretic response curves recorded for specimens are shown in Figs. 12.7 and 12.8.

The main test results are summarized at Table 12.2 in terms of peak and failure strengths, shear resistance at certain drift levels, deformation and initial stiffness. The failure process is in the order of sequence of bar yielding, damage to concrete around the bar and fatigue/fracture of bar. Peak strengths and initial stiffness values are different for each specimen. The values for negative cycle are smaller. Possible reason can be attributed to the cumulative damage state following after previous positive cycle done. The strength degradation on recorded hysteretic curves starts when the concrete cracks develop. It is mostly at around 0.25% for all B series except B3 (due to performance shift 0.50%).

12.3.1 Comparison About the Cyclic Envelope and Remarks

For the aim of comparison, the following hysteretic envelope curves were obtained at Fig. 12.9.

Following items are the observations made from cyclic force-displacement and envelope curves.

1. In general, at all specimens, connectors show significant energy dissipation with increase in story drifts,
2. Upper connectors prone to higher energy resistance and energy dissipation (fat loop) relative to bottom ones due to rocking response mode of the panel,
3. Failure mode of dowel bars at all specimens was similar fatigue type at the top plate joint,
4. Due to yielding at small displacement levels, it can be said that connectors are effective at small drift range (<1.00%),
5. Specimens B1 and B4 (deformed bar) reaches failure state before a major event (<1.0% drift). This could be a significant safety risk to the human life,
6. Highest strength and cumulative energy was recorded for specimen A1 due to existence of side connector. Both capacity and deformability improved.
7. Unbounded bars (Specimen B3) allow a shift in performance for larger drift values (no force coupling),
8. The strength degradation started when the concrete cracks develop at around 0.25% for all B and A series except B3 (due to unbonded),
9. Introducing smaller gap distance (B4) causes a significant increase in initial stiffness and strength (34%), however no effects seen at cyclic energy dissipation,
10. Ultra mild-high elongation plain bars (B2) increase the deformability and level of failure state approximately two times compare to the normal deformed bars,
11. Both specimen C1 and C2 (slim panels) remained stable until high drift values, but their resistance contributions are low due to less amount of connector
12. No bottom connector failed for all tested specimens

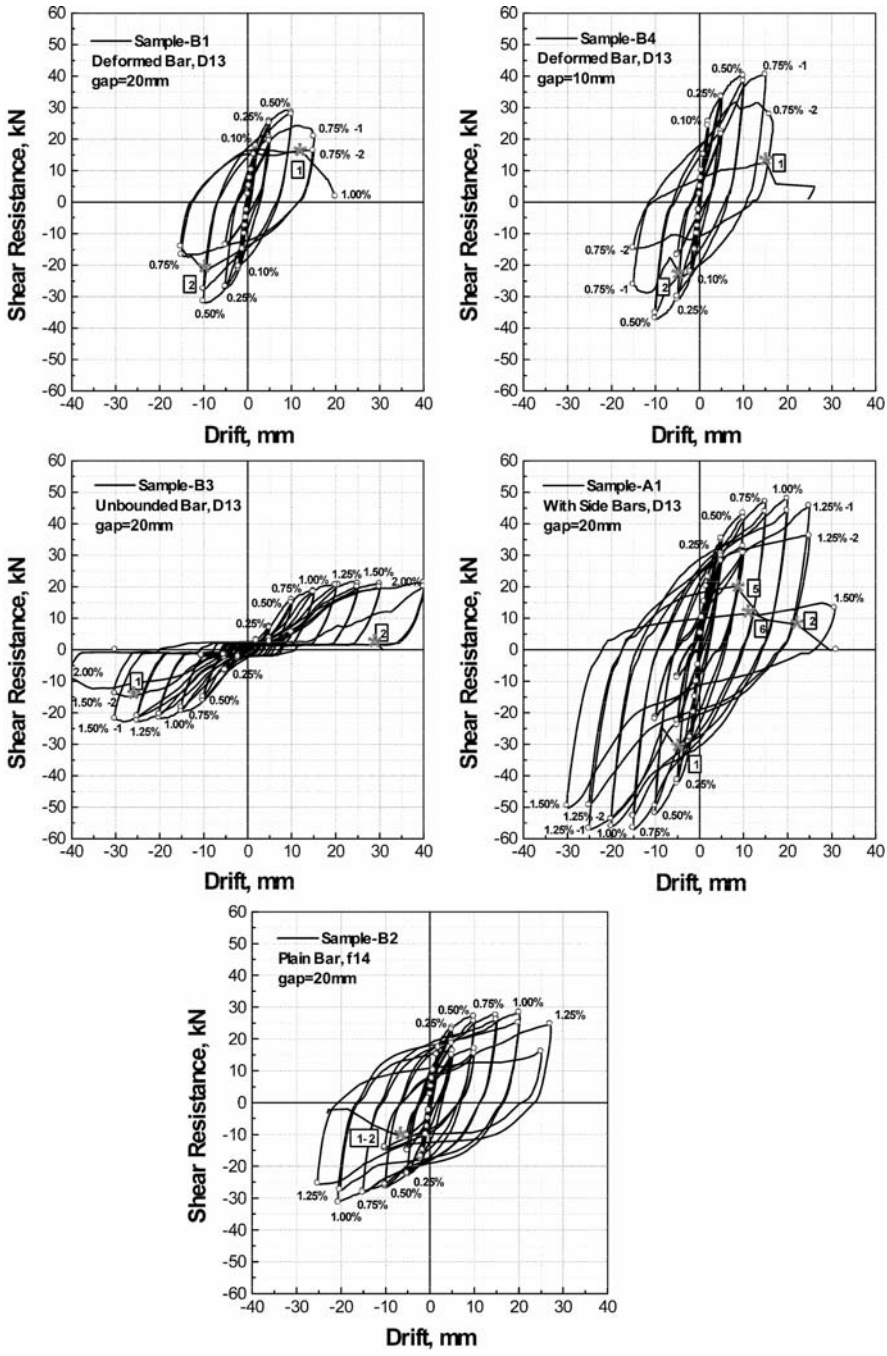

Fig. 12.7 Recorded force-displacement plots for specimens of A and B series

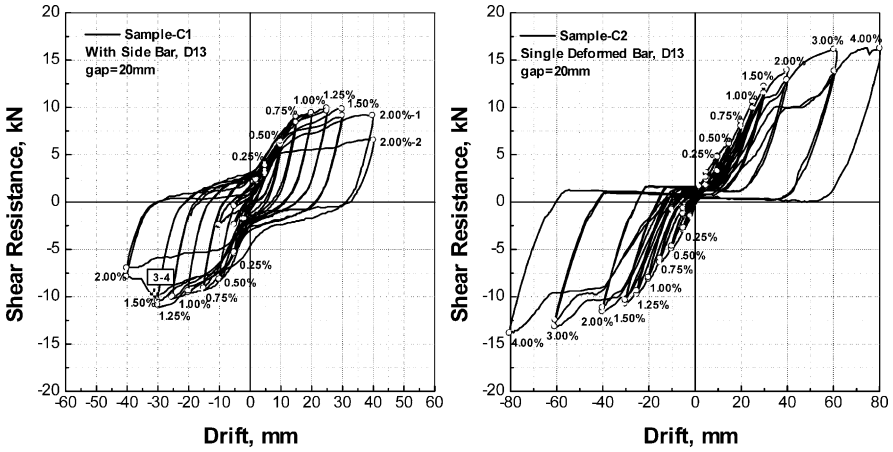

Fig. 12.8 Recorded force-displacement plots for specimens of C series

Table 12.2 Summary of the test results; Peak and failure strength, deformation and stiffness

		Max. Shear strength, kN		Shear at dowel failure, kN		Shear at design levels, kN		Concrete crack	Initial Stiffness
Specimen	Cycle	Q(kN)	D(%)	Q(kN)	D(%)	D=0.50%	D=1.00%	D(%)	S(kN/mm)
B1	+	28.5	0.50	Top	Top	28.5	–	0.25	11.34
	–	–31.5	–0.50	–16.7	–0.75	–31.5	–		15.73
B2	+	28.2	1.00	Top	Top	27.0	28.2	0.25	9.57
	–	–31.4	–1.00	24.7	1.25	–26.5	–31.4		10.39
B3	+	21.0	1.25	Top	Top	15.7	20.6	0.50	1.46
	–	–22.5	–1.25	–13.9	–1.50	–16.0	–21.6		1.34
B4	+	40.4	0.75	Top	Top	40.1	–	0.25	18.42
	–	–36.9	–0.50	–14.6	–0.75	–36.9	–		18.35
A1	+	47.9	1.00	Top	Top	43.3	47.9	0.50	13.68
	–	–56.6	–0.75	–53.8	–1.00	–52.0	–56.1		16.11
C1	+	9.9	1.25	Side failure	Side failure	6.0	9.4	1.25	1.10
	–	–10.9	–1.50	–7.0	2.00	–8.3	–9.6		0.76
C2	+	16.2	4.00	No failure	No failure	4.8	8.5	2.00	0.43
	–	–13.9	–4.00		4.00	–5.0	–8.2		0.42

12.3.2 Calculated Response Energy by the Connectors

One of the most important response characteristics of hysteretic curves is cyclic energy and equivalent damping ratio. This is important for the evaluation of deformability of a structural member and damage state that is involved in. Two factors are determines and directly related to total cyclic response energy. First one is strength amplitude and the second is amount of deformability. In this study, energy (area under the closed hysteretic loop) calculations were performed and evaluated

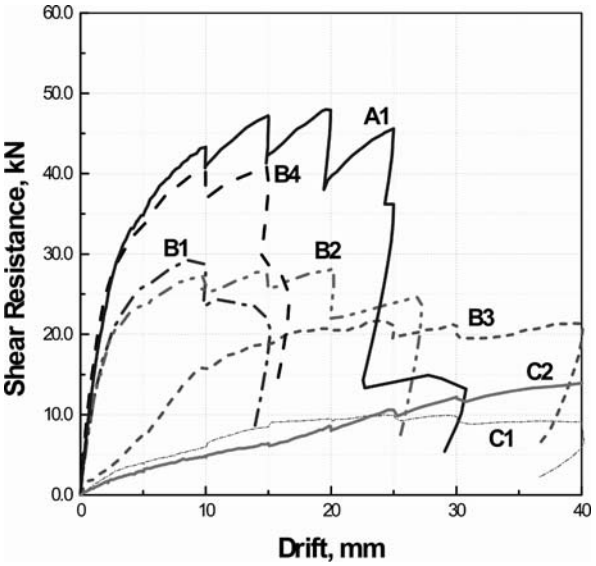

Fig. 12.9 Comparison of hysteretic envelope curves among tested specimens

for all samples. Figure 12.10 shows the comparisons of cumulative cyclic energy among the tested specimens.

Table 12.3 shows the summary of the energy calculation for each specimen at certain drift levels.

The following remarks were made from the cyclic energy calculations;

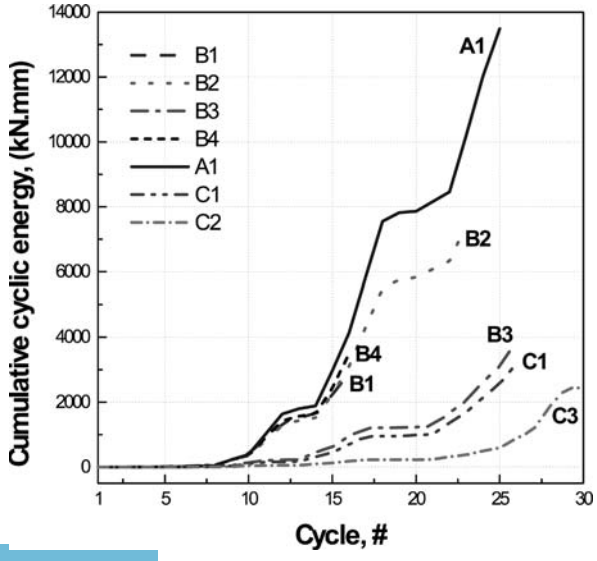

Fig. 12.10 Comparison of cumulative cyclic energy among the tested specimens

Table 12.3 Cyclic energy calculation at certain drift levels

Specimen	Dissipated energy at each drift level, kN.mm				
	0.10%	0.25%	0.50%	0.75%	1.00%
A1	13.2	163.2	461.6	1126.3	1706.7
B1	22.4	139.1	496.5	634.9	–
B2	17.6	199.7	460.5	792.7	1194.5
B3	5.0	14.9	48.3	192.6	295.2
B4	19.3	131	533.8	396.6	–
C1	1.4	9.8	47.0	136.6	247.6
C2	1.5	4.1	10.7	33.9	49.4

1. In general, at all specimens, connectors show significant energy dissipation with increase in story drift.
2. Specimen A1 has the highest resistance and cumulative cyclic energy capacity among all test specimens.
3. Unlike its insignificant shear resistance (1/2 of A1), Specimen B2, has the highest equivalent damping ratio (%31) and relatively good cumulative cyclic energy capacity (deformable ultra mild plain bar).
4. Gap distance makes a significant effect (%34) on shear resistance but no effects seen on cumulative dissipated energy and equivalent damping ratio (B1 vs. B4).
5. Due to bounding conditions and panel size effects, B3 and C series show resistance and dissipate energy at higher drift values relative to rest of B and A series.
6. Even the specimens B4 and A1 has not much capacity difference in shear resistance, however, cumulative dissipated energy for A1 is 5 times higher.

12.4 Failure Criteria for Connectors

One of the important things is to detect the failure state for connectors. CDP measurements installed for each connector can be easily used to for this purpose. Schematic illustration for the CDP installment and the calculation concept for connector strains are shown in Figs. 12.11 and 12.12. In order to search a criterion for connector failure, strain can be an alternative index to determine.

Shear, γ, and axial strains, ε, are obtained by using simple equations indicated at Eqs. 12.1 and 12.2.

$$\varepsilon = (dy_2 + dy_3)/2e \tag{12.1}$$

$$\gamma = dx_1/e \tag{12.2}$$

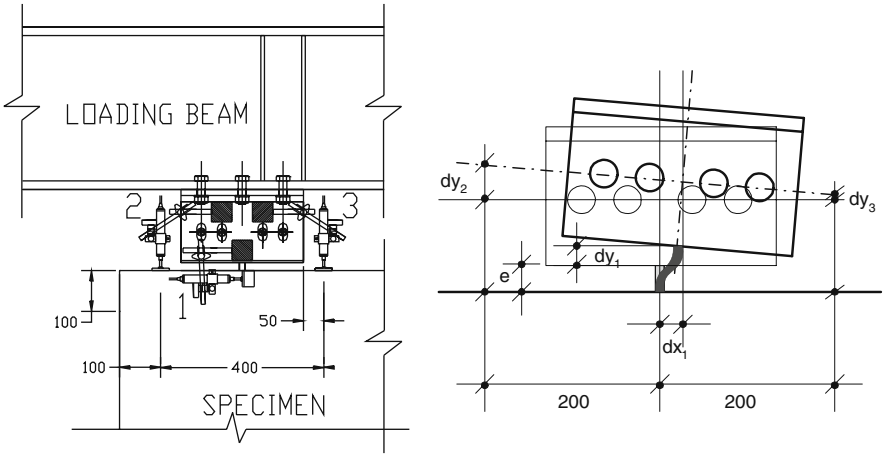

Fig. 12.11 Connector displacements from CDP measurements

where, *e* is the axial strain. In addition to the failure strain values, other parameters such as maximum strain reached before the failure, maximum relative displacements, cycle number and drift values at failure state, were also interested and recorded for further use in correlation study A typical axial strain vs. shear strain plots are shown in Fig. 12.13 (specimen B1). In these figures, different line and symbols are used for better understanding. The dot lines represent the full response, whereas the solid lines for the response up to fail. This is important, since the CDPs continue to measure even after the respective connector fails. The symbol "∗" shows the failure stage. The stage where the connectors fail was determined by the remarks made during the experimental progress. These remarks were done by the staff during the experiment if a failure sound heard or any immediate change occur at the online response figure on the test computer. If there was a failure, then it was immediately cross checked by observing each connector location. Picture was taken and

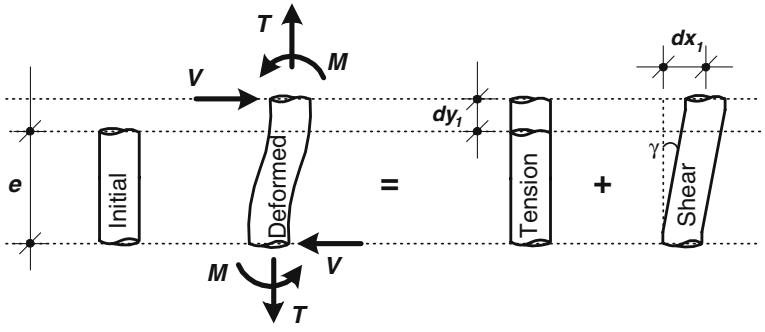

Fig. 12.12 Connector strain components

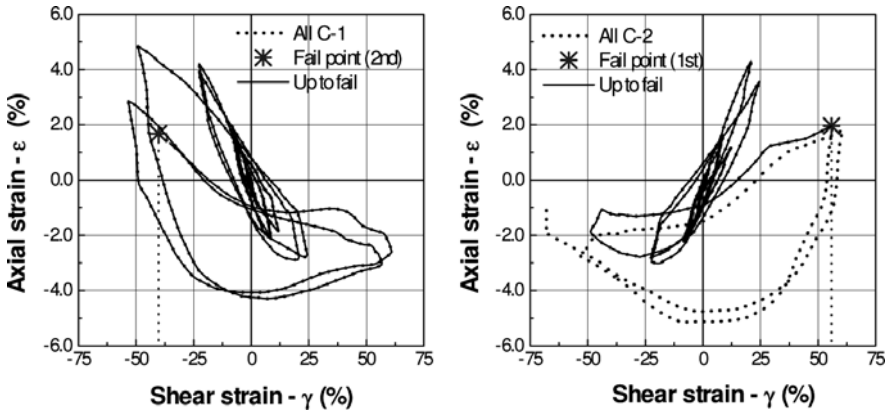

Fig. 12.13 Axial strain vs. shear strain relationships for specimen B1

step number was noted. Summary of the results obtained from each specimen are shown together in Table 12.4.

In here, it is worth to mention that the dowel length kept constant in the calculation with being respective gap distance. This is true if no additional bonding failure occurs or no significant concrete damage generated around the dowel which may increase the level arm.

If they are valid, both factors may cause difference in interpretation of results. The full restrained conditioned at the column face will not be correct. However, due to the limitation on the measuring system, these factors were not included in the calculation. Obviously, it is possible to measure the axial strain due to bonding if any gage installed on dowel bar itself. However, in the scope of this preliminary study, it was not fulfilled.

Table 12.4 Strain measurements on failed connectors of tested specimens

		Maximum displacements and strains reached before failure state (+ and - cycles)								Failure state					
Specimen	Connector	dx (mm) +	dx (mm) −	dy (mm) +	dy (mm) −	ε (%) axial +	ε (%) axial −	γ (%) shear +	γ (%) shear −	dx (mm)	dy (mm)	ε (%) axial	γ (%) shear	Failure Cycle #	Failure Drift %
B1	1	12.1	–9.8	–0.52	0.94	2.6	4.7	60.5	49	–8.03	0.34	1.7	40.2	+17	+1.00
	2	–9.68	11.18	–0.36	0.39	1.8	2	48.4	55.9	11.18	0.39	2	55.9	–15	–0.75
B2	1	13.3	7.89	4.24	0.32	21.2	1.6	66.5	39.5	13.3	4.24	21.2	66.5	+23	+1.25
	2	–11.9	12.16	1.1	3.78	5.5	18.90	59.5	60.8	9.71	1.94	9.7	48.6	–24	–1.25
B3	1	18.90	–12.53	2.03	10.29	0	0	94.5	62.7	–4.93	14	0	24.67	+22	+2.00
	2	–11.64	19.18	2.53	8.98	0	0	58.2	95.8	19.18	8.98	0	95.8	–21	–2.00
B4	1	6.44	–8.24	0.63	2.02	6.3	20.2	64.4	82.4	7.29	1.24	12.4	72.9	+17	+1.00
	2	–5.63	6.39	–0.32	1.34	3.2	13.4	56.3	63.9	6.39	1.343	13.4	63.9	–15	–0.75
A1	1	9.97	–10.49	–0.16	5.01	0.8	25	49.85	52.45	4.98	3.57	17.85	24.9	+24	+1.50
	2	–3.10	7.50	–0.10	3.05	0.5	15.25	15.0	37.5	7.50	3.05	15.25	37.5	–15	–1.00
	5	7.20	–2.23	4.68	1.13	23.4	5.65	23.4	11.15	7.20	4.68	23.4	36	–22	–1.25
	6	7.8	–2.09	0.69	1.3	3.45	6.5	39	10.45	7.8	0.69	3.45	39	–22	–1.25

In the following Fig. 12.14, the comparison of maximum strain and displacement values before and at failure stage were shown for each specimen.

Following remarks were made from the Fig. 12.14

1. For the notice, all specimens were failed from either their top and/or side connectors. Initially failed connectors show their maximum probable strain performance. However the remaining connector fails with less strain capacity (not matching with max. performance). There might be several reasons, but one of them is that fatigue failure due to damage accumulate from the previous cycle (cyclic effects)
2. For the connectors of Specimen B1, failure was occurred at the values around 50% shear strain rate. At this failure stage the axial strain was less then 5%.
3. For the connectors of Specimen B2 and B4, failure was occurred the shear strain values between 50% and 75%. At this failure stage the axial strain was around 20%. One of the reasons for having higher axial strain capacity for specimen B4 is that the gap distance (10 mm) is half of the ordinary specimen. In the case of specimen B2, the difference in performance mainly comes from the high elongation material capacity of steel connector used specifically for this specimen.

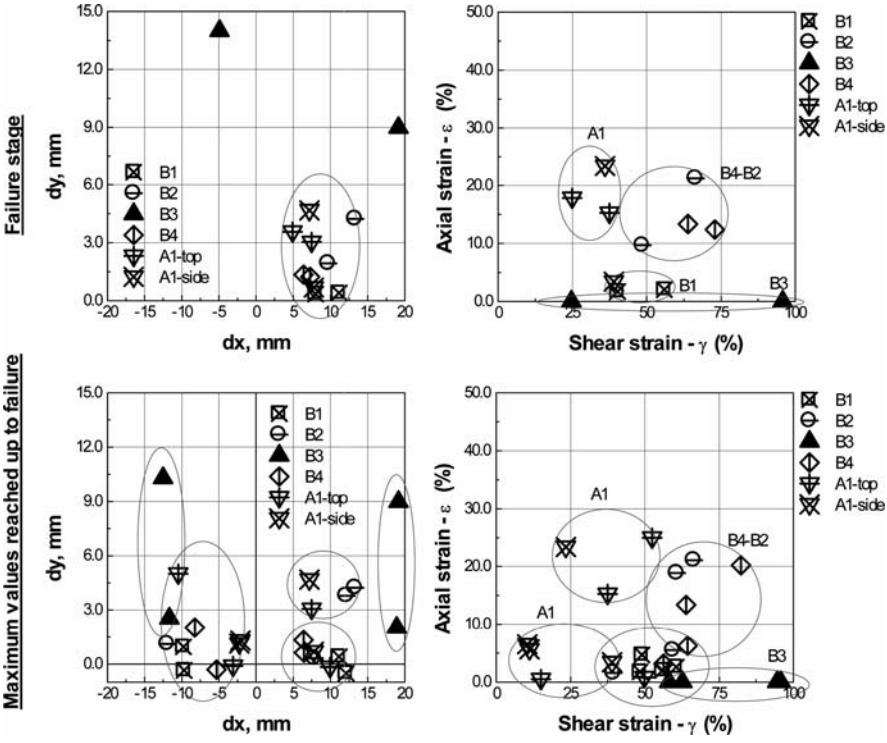

Fig. 12.14 Comparisons of max strain and displacement values before and at failure stage

4. Due to lack of bonding, specimen B3 gone higher shear strain values up to 95%. It is because of the no axial strain generated on the connectors of this specimen. For the notice, even if the measurements show non-zero displacement values on figures, actually there was no stress generated on these connectors (because of the unbounded conditions).
5. Relative displacement at failure stage for all specimens generally accumulate; (a) between 5 mm and 12 mm for transverse, and (b) between 0 mm and 5 mm for longitudinal.
6. For the specimen A1 general tendency is different from the others. Even not having ultra mild special connector or smaller gap distance, the axial strain rates were quite high (up to 25%). This is because of the existence of side connectors.
7. General tendency for the normal deformed bars with certain gap distances is that higher the axial strain rates on connectors cause smaller the shear strain capacity at failure stage. This is mostly due to interaction effects between shear and tension. This can be easily observed at the connectors of specimen A1. Such as for the top connectors of specimen A1, the failure occurred by coupling when the shear strain is around 25–37%, and axial strain is from 15% to 18%. Under the same conditions the difference between a normal deformed bar (B1) and a high elongation bar (B2) is that; (a) normal deformed bar mainly failed by shear with %50 strain (only 2% axial strain). (b) However, a high elongation bar fails by the couples of shear (%65) and tension (21%), which is a much better performance.
8. In order to search for an approximate relationship between shear and axial strains at failure stage, a fitting study performed. Even if it is not totally adequate for representing the behavior with such a small number of data, however, it is necessary to know general tendency. Fitting function of exponential decay looks appropriate for representing these general tendencies. The resultant fitting curve and scatter failure data of specimens were plotted together at Fig. 12.15.

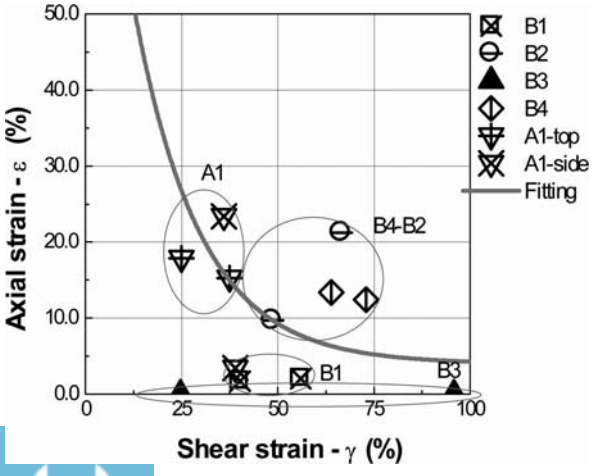

Fig. 12.15 Approximate relationship between axial and shear strains at failure stage

12.5 Simplified Tri-Linear Curves for Connectors

Earlier panel test were performed using certain connector type, diameter size, material strengths and boundary conditions. Not all of but some factors that are affecting individual connector behavior can be obtained from these tests.

The individual connector response curves show three similar distinct regions. One is pre yielding, second is post-yielding and third is descending branches. Strength degradation is significant after the peak. Most appropriate model for simulating such kind of hysteretic behavior is tri-linear model. The proposed simplified curves for deformed bar D13, plotted together with test results at Fig. 12.16.

Parameters describing the backbone curves are the initial stiffness, k_0, secondary or post yielding stiffness, k_1, and descending stiffness, k_2, after peak. Other parameters are, the load at yielding, V_o, load at maximum deflection, d_{max}, which defines the maximum load, V_{max}, and starting of the descending branch, and finally residual load, V_u, at ultimate deflection, d_u. Table 12.5 shows the parameters derived.

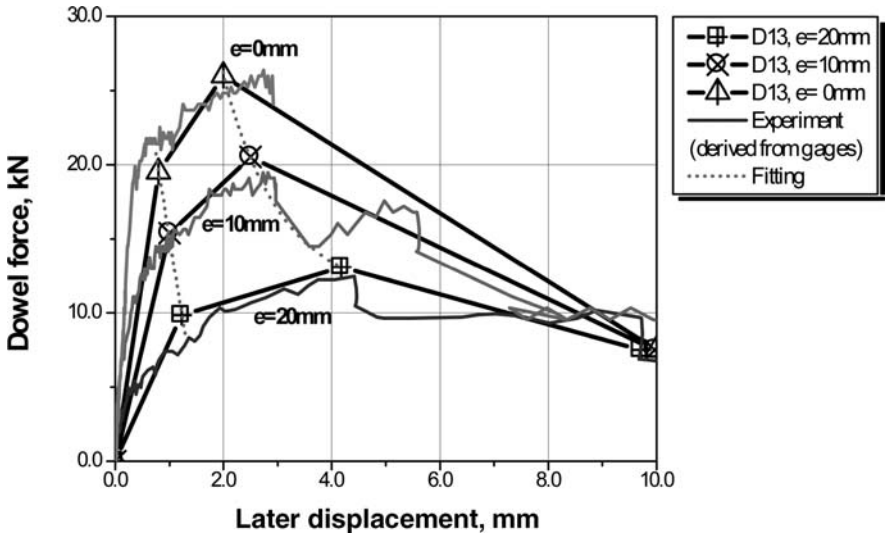

Fig. 12.16 Simplified curves obtained from the tests for change in gap distance

Table 12.5 Proposed control parameters for D13 bar

Gap, mm	Displacement, mm			Dowel force, kN			Stiffness, kN/mm			Ratio	
e	d_y	d_{max}	d_u	V_o	V_{max}	V_u	k_o	k_1	k_2	k_1/k_o	k_2/k_o
0	0.80	2.03	9.3	19.5	26	8	24.4	5.28	−2.47	0.22	−0.10
10	1.00	2.52	9.6	15.4	20.5	7.5	15.4	3.42	−1.75	0.22	−0.11
20	1.23	4.18	10.2	9.83	13.1	7.5	8.0	1.11	−1.01	0.14	−0.13

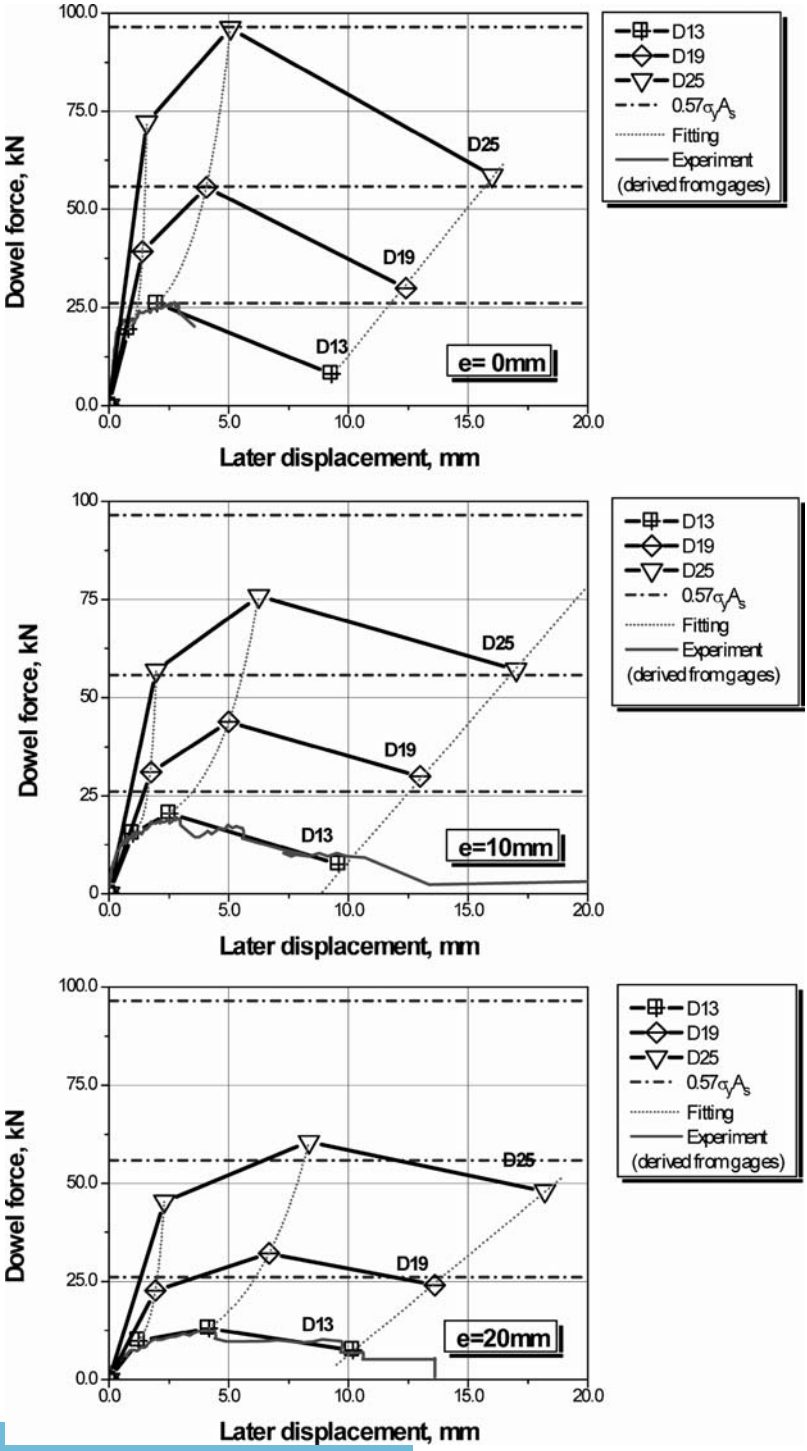

Fig. 12.17 Proposed connector response curves for respective bar diameters (D13, D19, D25) in certain interface conditions ($e = 0$ mm, 10 mm, 20 mm)

Table 12.6 Proposed control parameters of tri-linear response envelope with respect to different bar size and gap distance

	Bar, mm	Displacement, mm			Dowel force, kN			Stiffness, kN/mm			Ratio	
	d_b	d_y	d_{max}	d_u	V_o	V_{max}	V_u	k_o	k_1	k_2	k_1/k_o	k_2/k_o
e= 0 mm	13	0.80	2.03	9.3	19.5	26	8	24.4	5.28	–2.47	0.22	–0.10
	19	1.40	4.06	12.4	39.26	55.4	29.9	29.71	6.12	–3.07	0.21	–0.10
	25	1.58	5.08	16.1	72.12	96.15	58.5	48.08	6.89	–3.44	0.14	–0.07
e= 10 mm	13	1.00	2.52	9.6	15.4	20.5	7.5	15.4	3.42	–1.75	0.22	–0.11
	19	1.75	5.10	13	31	43.8	29.9	18.77	3.95	–1.74	0.18	–0.09
	25	1.98	6.25	16.9	56.9	75	57.13	28.8	4.44	–1.75	0.15	–0.06
e= 20 mm	13	1.23	4.18	10.2	9.83	13.1	7.5	8.0	1.11	–1.01	0.14	–0.13
	19	1.93	6.69	13.6	22.74	32.17	24	12.50	1.985	–1.18	0.15	–0.09
	25	2.31	8.36	18.2	45.43	60.57	48	19.66	2.50	–1.28	0.12	–0.07

As a next step one may think about the conditions in the case where different size of dowel bar used. Unfortunately, there are no existing test results specifically for other bar size (except D13). At this point, theoretical formulas used together to predict the simplified tri-linear curves under respective boundary conditions. So, at Fig. 12.17, the proposed response curves for respective bar diameter are plotted together. Change in control parameters of tri-linear response envelope are also shown in Table 12.6 ($f_c = 30\,\text{MPa}, f_y = 300\,\text{MPa}$).

Next think that has to clarify is the conditions where different concrete strength considered. Again, theoretical formulas used together to predict the simplified tri-linear curves under respective boundary conditions. Three concrete strength parameter of 30, 50 and 70 MPa are mostly used in design practice. Change in control parameters of tri-linear response envelope are also shown in Table 12.7 below ($e = 10\,\text{mm}, f_y = 300\,\text{MPa}$).

Table 12.7 Change in control parameters of tri-linear response envelope with respect to concrete strength and bar diameter

	Bar, mm	Displacement, mm			Dowel force, kN			Stiffness, kN/mm			Ratio	
	d_b	d_y	d_{max}	d_u	V_o	V_{max}	V_u	k_o	k_1	k_2	k_1/k_o	k_2/k_o
f_c= 30 MPa	13	1.00	2.52	9.6	15.4	20.5	7.5	15.4	3.42	–1.75	0.22	–0.11
	19	1.75	5.10	13	31	43.8	29.9	18.77	3.95	–1.74	0.18	–0.09
	25	1.98	6.25	16.9	56.9	75	57.13	28.8	4.44	–1.75	0.15	–0.06
f_c= 50 MPa	13	0.81	2.01	9	19.87	26.5	11	24.53	5.53	–2.21	0.23	–0.09
	19	1.42	4.02	11.75	40	56.6	39.5	28.2	6.38	–2.22	0.23	–0.08
	25	1.6	5.03	15.36	73.48	98	67.87	45.9	7.16	–2.92	0.16	–0.06
f_c= 70 MPa	13	0.6	1.61	8	23.52	31.35	15	39.2	7.72	–2.56	0.20	–0.07
	19	1.05	3.23	10.44	47.35	66.97	47.8	45.09	9	–2.65	0.17	–0.06
	25	1.2	4.03	13.65	86.9	115.9	82.3	74.66	10.17	–3.5	0.14	–0.05

12.6 Quantifying the Effects of Connectors on Building Response

In the scope of this study, supplementary damping and resistance contribution by the connectors to the building response are investigated. It is obvious that introducing additional viscous damping to the structural system is the major interest. Since it causes a reduction on demand (response amplitude) and resulted with a decrease in imposed forces on building.

12.6.1 Supplementary Equivalent Viscous Damping by the Connectors

In order to calculate additional viscous damping due to connectors, a case study performed. In here, the prototype model was a 6-story residential RC building taken from Japanese practice (Koudan Jutaku). The prototype building model and details are shown in Fig. 12.18.

In here, PCPWs are used as partition elements and denoted with hatched areas in elevation plan. Typical floor height is 2850 mm and spanning six bays with a grid of 5600 mm. Typical column size at 1st floor is 1000 × 800 mm, and total 14D32 is used in the section. Beams are same through the floors with the size of 750 × 550 mm, and total 12D30 + 2D16 is used in the section. Total floor area is 454.06 m2. Floor weights for the first two floors are around 7614 kN., and weight for the typical floors (3rd to 5th) is 7090 kN. Finally, the value of the weight for the roof is 6806 kN. The concrete design strength is 30 MPa. Reinforcement materials are SD295A for D10 ∼ D16, SD345 for D19 ∼ D25, and SD390 for ∼D32. The building was designed according to Japanese Building Code regulations with a structure

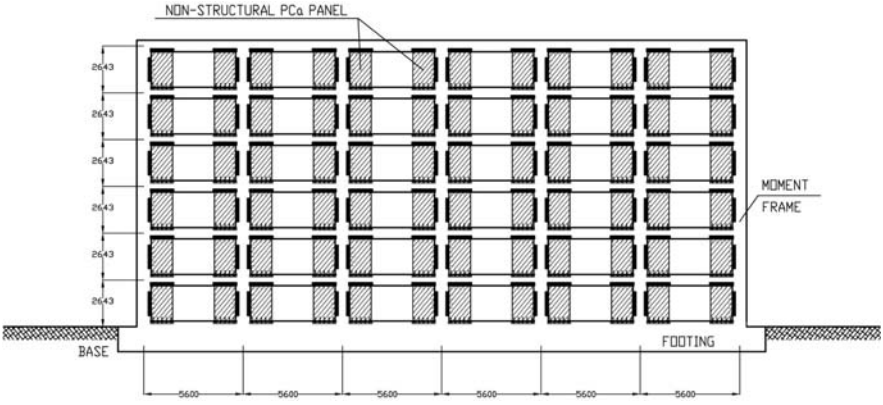

Fig. 12.18 Proposed connector response curves by change in concrete strength (30, 50, 70 MPa) and for respective bar diameters (db = 13 mm, 19 mm, 25 mm)

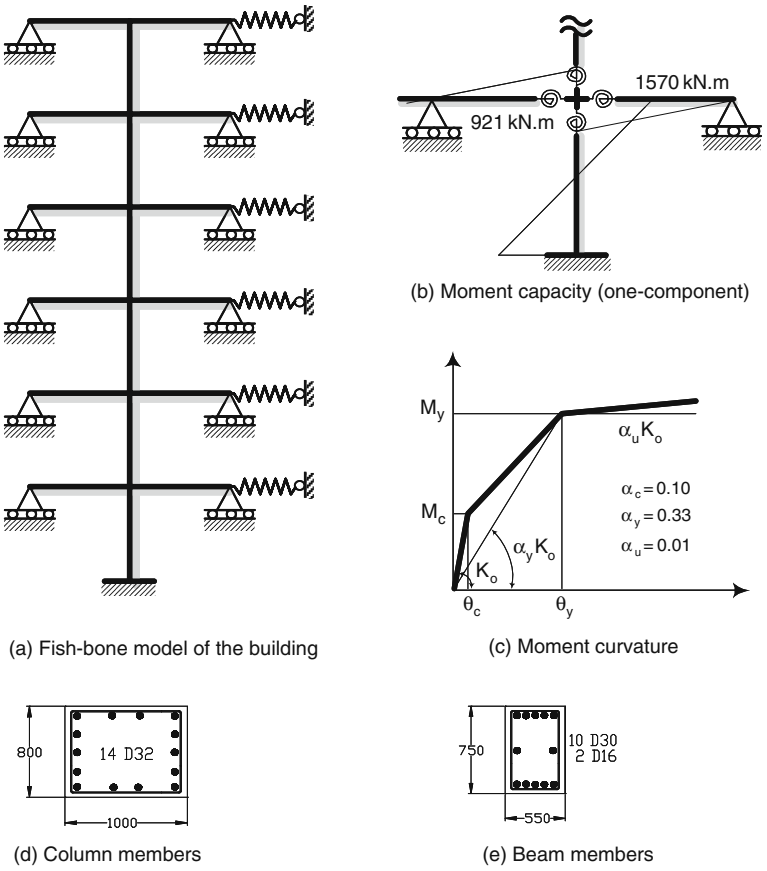

Fig. 12.19 Modeling concept of the building analyzed

factor of Ds = 0.30. For better understanding, Ds can be also called as total seismic weight (or floor weight) to total base-shear (or story shear) ratio at yielding.

A fish-bone model of the building and parameters of the nonlinear moment curvature are shown in Fig. 12.19. In here, for the frame members, nonlinear one-component model with Takeda and Takeda-slip hysteretic behavior was employed according to provisions of Architectural Institute of Japan (AIJ).

In most case, dowel response is effective between 0.25% and 0.5% where a well design building capacity curve at elastic or concrete cracking part. The dowel resistance mostly diminishes at 1% drift levels where a building structure starts to show maximum performance with yielding. Since the maximum performance of connector and bare frame response don't coincide each other, there shouldn't be an over demand on columns. Ultimate response definitely will not be affected at all. Just the maximum performance of two system occur at different levels are combined to form a better shear resistance system.

Pushover curves of the building were calculated for each floor. Then the hysteretic response curves of tested panel specimens were combined together with these pushover curves. For the pushover curve, beam yielding mechanisms assumed with column moment capacity 1.4 times larger than capacity of beams. Floor diaphragms are assumed rigid and each column at the same story will displace with same drift value. The shear force vs. story drift relationships for a single column through the stories is shown in Fig. 12.20.

After calculating the pushover curves for each floor, they later combined with response curves that were obtained from the earlier panel experiments. The calculation concept for equivalent viscous damping ratios of specimen h_{eq} is shown in Fig. 12.21.

In here, it was supposed that each column was attached to a single specimen and each panel specimen was investigated separately. However, it is worth to mention that there could be more attachments according to architectural layout. Most cases in general practice two panels were used for each column at least. The equivalent viscous damping ratio is calculated by the formula indicated at Eq. 12.3

$$h_{eq} = \frac{1}{4\pi} \cdot \left(\frac{\Delta W}{W_e} \right) \tag{12.3}$$

Where, ΔW is the hysteretic energy of cyclic loops of combined system, and W_e is equivalent potential energy which is expressed by the Eq. 12.4.

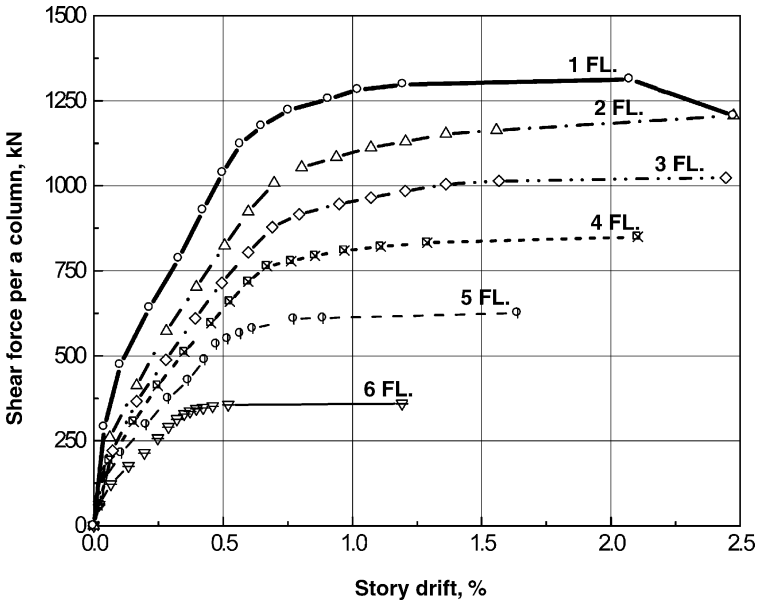

Fig. 12.20 Pushover curve of the prototype 6 story RC moment frame building

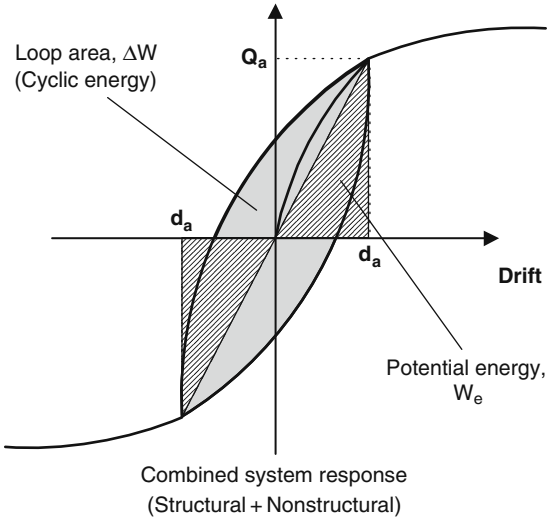

Fig. 12.21 Calculation concept of equivalent viscous damping ratio h_{eq} due to connectors

$$W_e = \frac{1}{2} \cdot Q_a.d_a \tag{12.4}$$

where, Q_a is the story shear force, and notation d_a is denoted to the certain story drift.

As an example, equivalent viscous damping ratios for the 3rd floor of the building are shown in Fig. 12.22.

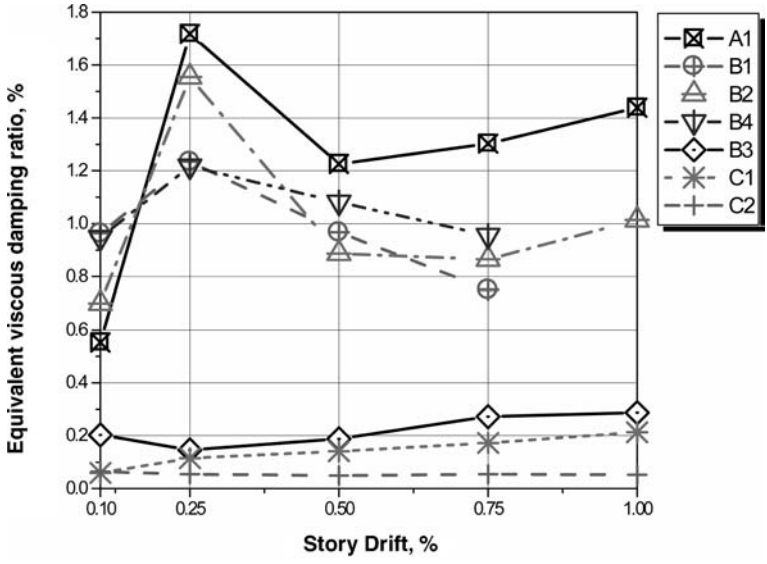

Fig. 12.22 Additional equivalent viscous damping ratio at 3rd floor due to single panel attached at each column

Figures 12.23 and 12.24 show the change in equivalent viscous damping ratios along the building due to different panel attachments.

The following observations were made from the damping analysis;

1. For the specimens A1, B1, B2 and B4 have the peak at the story drift level of 0.25%, and the maximum value among the four was 1.71 (Specimen A1). At such a smaller drift, the value of h_{eq} increases with size of the hysteretic loops.
2. Due to bounding conditions and panel size effects, maximum equivalent viscous values for specimen B3 and C series are under 0.4, which is less than half of the four largest specimens. However, even if their damping contribution is low, no failure observed until very large drift levels.
3. Unlike its insignificant shear resistance (1/2 of A1), Specimen B2, has the second highest equivalent damping ratio (1.6%) and relatively good cumulative cyclic energy capacity (deformable ultra mild plain bar)
4. Gap distance makes a significant effect (34%) on shear resistance but no effects seen on cumulative dissipated energy and equivalent damping ratio (B1 vs. B4)
5. Even the specimens B4 and A1 has not much capacity difference in shear resistance, however, equivalent damping ratio for A1 is 1.42 times higher at 0.25% drift
6. In a major event (at 1.0% drift), the values of h_{eq} for specimens with larger deformability, (specimen A1, B2 and B3), had a reserve strengths and damping capability, such as 1.44 for specimen A1, and 1.01 for specimen B2.
7. By comparing the amplification of equivalent damping ratio at upper floors relative to 1st floor, there is a clear amplification. Trend is similar for all type of specimen.
8. Amplification is 3 times at the 6th floor for specimen A1, with a damping value of 3.7% at the peak.
9. For the specimens B4 and A1, maximum damping ratio at 6th floor of the building model was slightly different. The difference for these specimens is that the highest damping occurred at 1% drift, unlike the peaks at 0.25% for the lower floors.
10. For the C series, even if the attachment at the 6th floor of the building, maximum damping can be reached by is smaller than 0.5%.

As a result, specimen A1 and B2 have seismic energy dissipation to some extent. If we attach one specimen to one column, the value of the equivalent viscous damping ratio (General remarks);

1. h_{eq} is between 1.6 and 1.7 at the seismic drift level of 0.25% (minor event)
2. h_{eq} is between 1.0% and 1.4% at the seismic drift level of 1.0% (major event)
3. It will be greater if we attach the specimen on the upper floor
4. If we increase the number of attachment.
5. It becomes about 3.0% when each column is attached by two specimen walls (it is in general most cases)

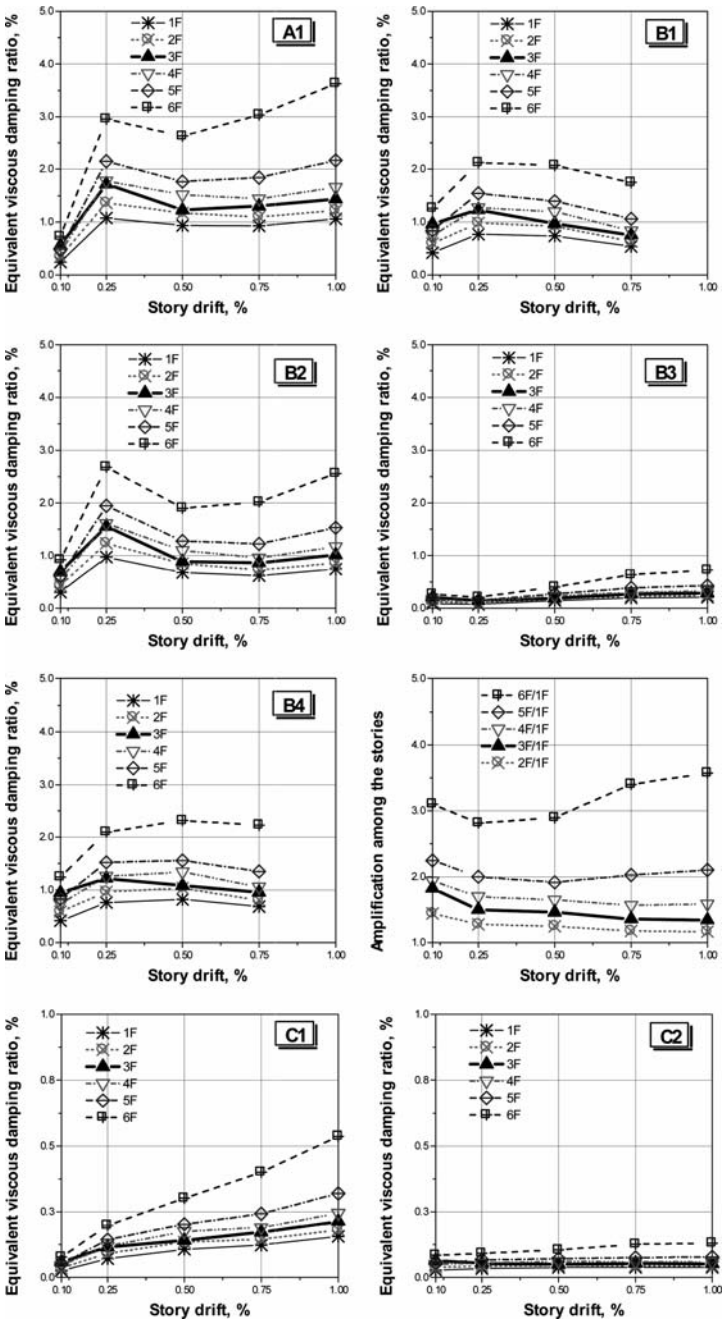

Fig. 12.23 Change in additional equivalent viscous damping ratio along the floors due different type of panel connector (a single panel for each column in case **A, B** and **C** type *panels*)

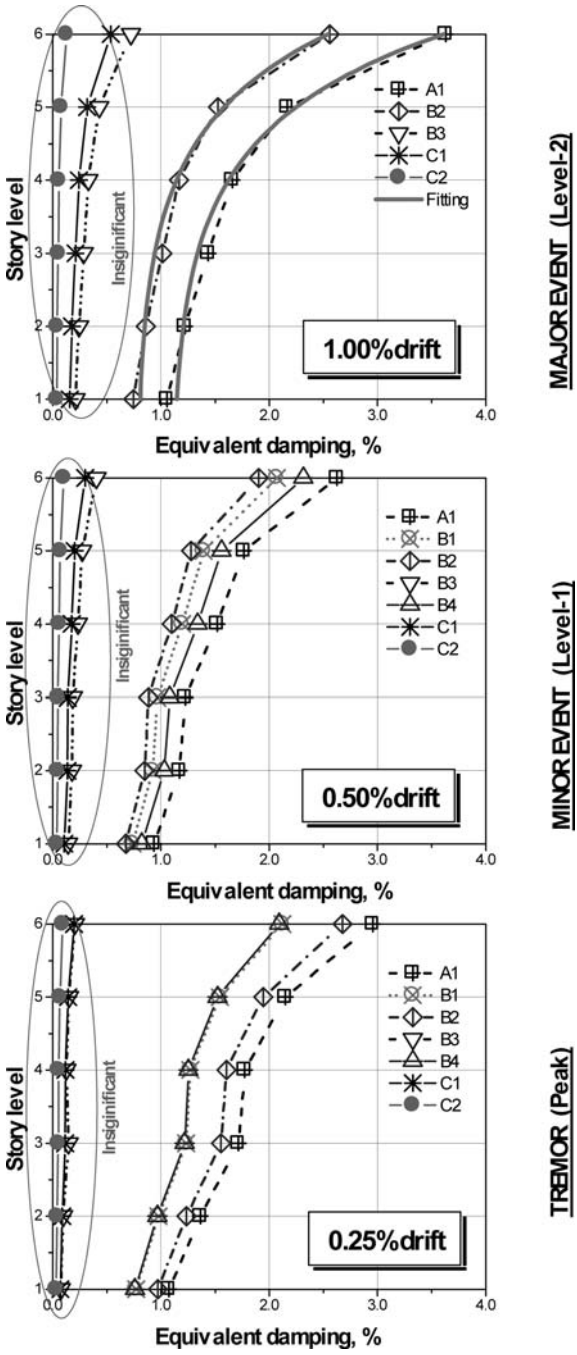

Fig. 12.24 Change in additional equivalent viscous damping ratio along the floors at target seismic demand (a single panel for each column in case **A, B** and **C** type *panels*)

12.6.2 Resistance Contribution by the Connectors

The results of quantifying resistance effects by the non-structural walls are shown in Figs. 12.25 and 12.26 for different type of panel attachments.

The difference of pushover curve for bare frame and frame with non-structural walls plotted together. Even for these minimum connector configurations, and for

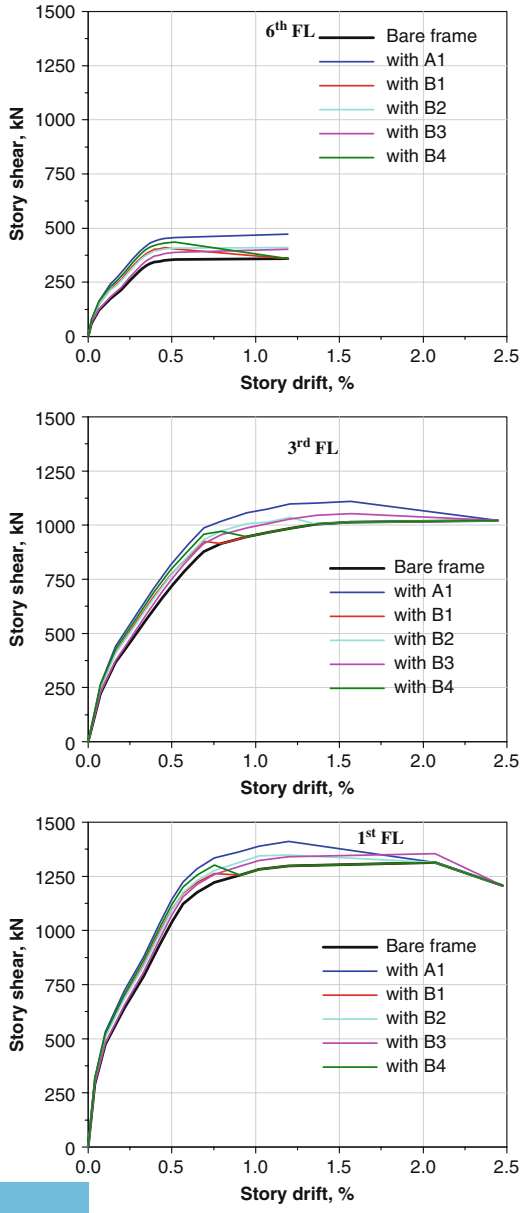

Fig. 12.25 Resistance contribution of connectors on pushover curve (1st 3rd and 6th floor) (See also Plate 16 in Color Plate Section on page 465)

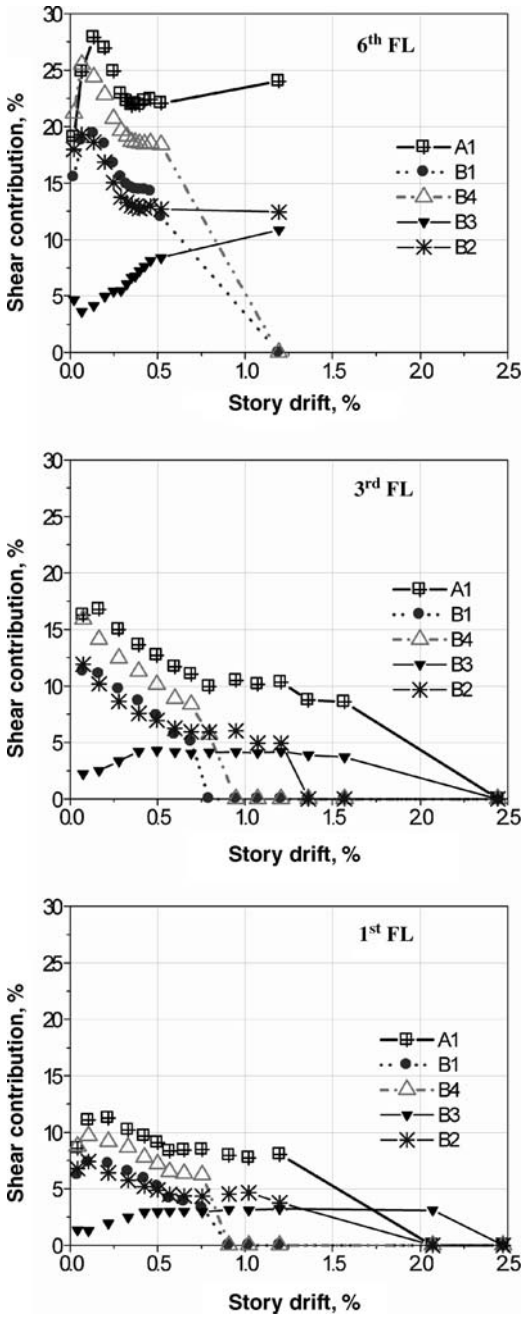

Fig. 12.26 Shear resistance contribution by the connectors, %

the 1st story of the building, a PCa panel with side connectors may contribute the resistance around 10% at 1.0% drift. The contribution is higher (up to 30%) at upper stories.

12.7 Concluding Remarks

Results of this study have shown that PC panel walls can dissipate energy by their dowel connectors at the attachment locations. Due to having low yielding capacity, they are mostly effective at small drift levels (moderate event). Under the action of a major event; panels will intact with the frame and contribute stiffness by a diagonal strut action. This will prevent the structure from total collapse

These dual response mechanisms of PC elements inspire us considering them as an alternative passive control system that would be used in new building design and/or even strengthening works. The real merit is the ability of high energy dissipation of connector elements at even minor events. By providing a comprehensive guideline, it may be possible to design the connector elements as a passive control device even from the beginning of design process. By this way, it may be possible to calculate minimum connector number and size to reach the target equivalent viscous damping ratio. It is obvious that, this target performance will require different connector configuration for each story level of interest in buildings.

With an ordinary reinforcing bar (size) and connector configurations (number of attachments), ultimate response of building will not be affected. The dowel resistance mostly diminishes at 1% drift levels where a building structure starts to show maximum performance with yielding. Since the maximum performance of connector and bare frame response don't coincide each other, there shouldn't be an over demand on columns. The point is that the maximum performance of two system occur at different levels are combined to form a better shear resistance system for the seismic safety of buildings.

From the perspective of connector material, a much higher energy dissipation capacity and deformability can be reached by choosing low yield high-elongation capacity bars (plain), instead of normal deformed bars. The good thing about this type of bar (B2) is that the significant equivalent viscous damping can be reached without a change in stiffness (B1). Increasing damping without any change in stiffness is very important. Because it could be possible to reach higher performance without increasing dowel size or number which may cause extra seismic demand on frame members. Unlike deformed bars, high elongation bars will also prevent the possibility of early failure and eliminate the safety risk to the human occupants before a major event occurrence (B1, B4).

Even if we have always referred to an RC moment frame for the host structure, however, the proposed PCPW jointed wall system could be easily applicable to Steel Structures as well. Especially, the panel joints can be practically assembled even much easier compared to RC frame. It is also worth to mention that a steel moment frame structure (not EBF or CBS systems) is much flexible and generally not rigid

compared to RC systems. In most case the deflections are the control parameter for design. That is why; the stiffness contribution could be much higher and can be forced to attract much higher forces than RC system. In addition to that, even the distribution of panels on the building plan should be carefully considered in order to avoid a major shift between the distance of center of rigidity and center of mass of the floor and among the stories. Irregular distribution of panel connectors could cause a predominant rotation mode for a Steel structure easily.

Chapter 13
Alternative Performance-Based Retrofit Strategies and Solutions for Existing RC Buildings

Stefano Pampanin

Abstract The need for simple and cost-effective retrofit solutions for existing reinforced concrete buildings, particularly those designed before the 1970s, thus prior to the introduction of modern seismic code provisions and capacity design principles, is no longer "just" an academic or scientific research statement, but it is eventually being recognized as a critical socio-political priority at international level. Similarly to what pursued for the design of new structures, a performance-based approach should be adopted when assessing the vulnerability and defining the retrofit strategy for existing buildings. In this latter case, the target limit states or performance levels have to be more realistically adjusted to account for the difficulties encountered in the assessment phase, as well as for the several issues associated to costs, feasibility and invasiveness of the proposed strengthening/retrofit solution. In this contribution, the concept of a partial retrofit strategy, capable of achieving an intermediate but critical objective as the collapse prevention, and based on practical solutions able to be almost "standardized", is proposed as a more realistic whilst effective upgrading strategy, particularly when planning a wide intervention at territorial scale. An overview of alternative retrofit strategies and technical solutions developed and/or further refined in the past few years as part of a multi-year research project on-going at the University of Canterbury on the seismic retrofit of existing reinforced concrete buildings is given. The feasibility and efficiency, in the contest of a performance-based retrofit approach, of adopting and/or combining different solutions such as Fiber Reinforced Polymers, low-invasive low-cost metallic diagonal haunches, post-tensioning wall systems or selective weakening techniques, is also discussed, based on numerical and experimental evidences.

S. Pampanin (✉)
University of Canterbury, Christchurch, New Zealand
e-mail: stefano.pampanin@canterbury.ac.nz

A. Ilki et al. (eds.), *Seismic Risk Assessment and Retrofitting*, Geotechnical, Geological, and Earthquake Engineering 10, DOI 10.1007/978-90-481-2681-1_13,

13.1 Introduction

In the relatively recent past, the crucial need for strengthening or retrofitting existing modern structures designed with substandard details, in order to withstand seismic loads without collapsing or with relatively moderate damage, has been further emphasized by the catastrophic effects of earthquake events (e.g. Turkey, Colombia and Taiwan, 1999, India 2001, China 2008, Italy 2009).

Alternative seismic retrofit and strengthening solutions have been studied and adopted in practical applications ranging from conventional techniques, which utilize braces, jacketing or infills [1–3], to more recent approaches including base isolation, supplemental damping devices or advanced materials (e.g. Fiber Reinforced Polymers, FRP, [4]; Shape Memory Alloys, SMA, [5]). Most of these retrofit techniques have evolved in viable upgrades; however, issues of costs, invasiveness, and practical implementation still remain the most challenging aspects of any intervention, in particular when looking at a larger (urban, region, country) scale and not at an individual building. Even prior to selecting the most appropriate retrofit strategy, a proper assessment of the seismic vulnerability of the structure represents a crucial and delicate step.

Based on recent lessons learned from past earthquakes and on extensive experimental and analytical investigations carried out in the past, it is becoming more and more evident that major and sometimes controversial issues can arise when, for example:

(a) deciding whether the retrofit is actually needed and, if so, in what proportions and to what extent;
(b) assessing and predicting the expected seismic response pre- and post-intervention by relying upon alternative analytical/numerical tools and methods;
(c) evaluating the effects of the presence of infills, partitions or in general "non-structural" elements on the seismic response of the overall structure, which is more typically and improperly evaluated considering only the "skeleton";
(d) deciding, counter-intuitively, to "weaken" one of more structural components in order to "strengthen" the whole structure;
(e) adopt a selective upgrading to independently modify strength, stiffness or ductility capacity;
(f) relying upon the deformation capacity of an under-designed member to comply with the displacement compatibility issues imposed by the overall structure;
(g) defining a desired or acceptable level of damage that the retrofit structure should sustain after a given seismic event, i.e. targeting a specific performance level after the retrofit.

Due to improper assumptions or approaches during either the assessment or the retrofit strategy phases, dramatic consequences could occur. In the worst case scenario, an improper retrofit intervention could in fact condemn the structure to an avoidable collapse which would not have occurred without strengthening.

As if this was not enough, the mentioned considerations on cost-effectiveness, invasiveness, and architectural aesthetics further complicate such a complex decision-making process, along with issues related to the socio-economical consequences of excessive damage and/or downtime due to a limited or interrupted functionality of the structures after the earthquake.

In this contribution, an overview of alternative retrofit strategies and technical solutions developed in the last decade and/or further refined in the last few years as part of a multi-year research project carried out at the University of Canterbury on the seismic retrofit of existing reinforced concrete buildings will be given. The feasibility and efficiency, in the contest of a performance-based retrofit approach, of adopting and, possibly, combining different solutions as Fiber Reinforced Polymers, low-invasive low-cost metallic diagonal haunches, post-tensioning wall systems or selective weakening techniques, will be discussed, based on numerical and experimental evidences.

13.2 Moving Towards a Performance-Based Retrofit Approach

Recognizing the crucial need to design, construct and maintain more resilient earthquake-proof structural facilities, capable of sustaining a limited level of damage following a major earthquake event within "acceptable" socio-economical consequences, an unprecedented effort has been dedicated in the last decade to the preparation of a platform for ad-hoc performance-based design guidelines involving the whole building process, from the concept and design to the construction aspects. Similarly, it should thus be expected that advanced performance-based seismic retrofit approaches of existing buildings shall be defined and implemented following the same philosophy proposed for the design of new structures.

Referring to the concept of Performance Design Objective Matrix (Fig. 13.1), developed as part of the SEAOC Vision 2000 Performance Based Seismic Engineering (PBSE) guidelines [6], expected or desired performance levels are coupled with levels of seismic hazard by performance design objectives. The performance levels are themselves expression of the maximum desired (acceptable) extent of damage under a given level of seismic ground motion, thus representing losses and repair costs due to both structural and non-structural damage.

According to the Basic Objective presented in this performance matrix, and associated to residential/commercial construction, a Life Safety damage level would be considered acceptable under a design level earthquake (traditionally taken as a 500 years return period event). This would imply that extensive damage, often beyond the reparability threshold, is to be considered as an accepted/proposed target, at least within the engineering community. It would not come as a surprise if users, residents, clients, owners/stakeholders of the building facility as well as the territorial authorities had a remarkably different opinion. This is likely to depend on a clearly different understanding of the significance of, and expectation from, the behaviour of an "earthquake-proof" building: life safety and collapse prevention

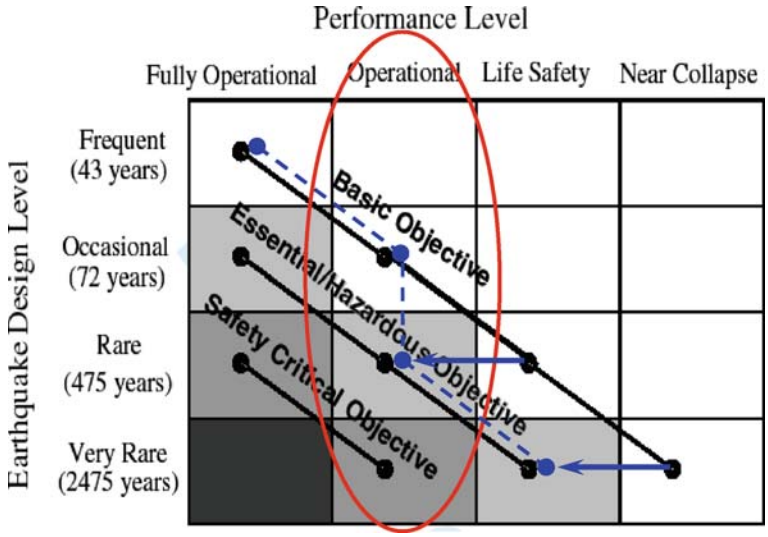

Fig. 13.1 Seismic performance design objective matrix as defined by SEAOC Vision 2000 PBSE Guidelines [6] and proposed modification of the basic-objective curve towards a damage-control (*dashed blue line*) (See also Plate 17 in Color Plate Section on page 466)

would be considered as "granted", and only a minimum level of damage, requiring minimum repairing costs and disruption of the daily activities, would be expected or better accepted.

As a further confirmation of this lack of basic understanding between the engineering community and the more general public, the level of (extensive) damage is, very often, for a design level earthquake, associated to the damage of the structural "skeleton", with the implicit acceptance that most of the non-structural elements such as partitions, claddings, glazing would, most likely, be severely damaged, requiring full replacements even under a lower earthquake intensity (i.e. corresponding, in probabilistic terms, to a more "frequent" event with lower return period). Recent earthquake events have confirmed that, even when the structural skeleton is relatively sound, the direct repairing costs of non-structural elements and the associated indirect costs due to the downtime and business interruption can represent a major component of the overall "losses".

In order to resolve this major perception gap and dangerous misunderstanding, a twofold approach is required:

1. increase the level of communication between academia, practitioner engineers, territorial authorities, industry representatives and/or, generally speaking, end-users. Define, set together and disclose to the wide public the accepted/targeted performance levels built in (and often hidden behind formulas and technical requirements) a Building Act or a design code, including the not-written considerations and accepted compromise between socio-economical consequences,

on one hand, and technical limitations and costs, on the other. It shall be clear that these are to be considered "minimum" not "maximum" standards, with the possibility (implicitly suggested) of achieving better performance if required/desired;
2. significantly "raise the bar" within the engineering community, by shifting the targeted performance goals from the typically accepted Collapse Prevention or Life-Safety level, to a more appropriate and needed Damage-Control level. This could be represented within the Performance Objective Matrix by a tangible shift of the Objective Curves to the left, hence towards higher performance levels or equivalently lower acceptable damage levels (Fig. 13.1). More importantly, as anticipated, the focus should not be limited, in practical applications, to the structural skeleton of the building, but should address the whole "system" performance.

13.3 Seismic Vulnerability Assessment Phase: The Fundamental and Delicate Role of an Appropriate Diagnosis

Prior to and irrespective of the technical solution adopted, the efficiency of a retrofit strategy on a reinforced concrete building strongly depends on a proper assessment of the internal hierarchy of strength as well as of the expected sequence of events (damage mechanisms) within a frame (i.e. shear damage and failure in the joint region, flexural hinging or shear failure in beam and column elements) or a wall (sliding, flexural or shear failure, uplifting etc.). The effects of the expected local damage mechanism on the global response should be adequately considered. As per any diagnosis phase, a simple but reliable analysis procedure should be used to provide useful preliminary information as a support to the retrofit intervention. This seismic upgrading could be either a permanent (ideally still reversible) or a temporary solution, depending on the urgency of the intervention, and/or to the lack of detailed knowledge, technology or funds as well as to the anticipation of possible future variations of loads, boundary conditions or state of the structure.

Recent extensive experimental and analytical investigations on the seismic performance of existing reinforced concrete frame buildings, mainly (when not only) designed for gravity loads, as typically found in most seismic-prone countries before the introduction of adequate seismic design code provisions in the early-mid 1970s [7–13], have confirmed the expected inherent weaknesses of these systems observed in past earthquake events (Fig. 13.2).

As a consequence of poor reinforcement detailing, lack of transverse reinforcement in the joint region, as well as the absence of capacity design principles, brittle failure mechanisms are expected either at a local level (e.g. shear failure in the joints, columns or beams) or a global level (e.g. soft storey mechanism). In particular, a significant vulnerability of exterior beam-column joints has been recognized due to the intrinsic lack of alternative and reliable sources of shear transfer mechanism within the panel zone region after cracking. Moreover, the presence of infills (e.g. typically un-reinforced masonry) can lead to unexpected and controversial effects due to the interaction with the bare frame [14–21].

Fig. 13.2 *Left*: observed damage in a pre-1970s existing reinforced concrete frame buildings with masonry infills (Izmit-Kocaeli earthquake, 1999, courtesy of EERC Library, Berkeley, NISEE Image Collection). *Right*: typical section elevation of a RC frame building designed in Italy in the late 1950s (after [22])

Figure 13.2 (left/hand side) provides a quite unique and unfortunate example of several potential local failure mechanisms likely to occur in a pre-1970s frame building as: incipient soft-storey collapse, shear failure in corner beam-column joints, in beams and columns, in-plane and out-of-plane damage and collapse of infills.

13.3.1 Understanding the Weaknesses of Beam-Column Joints: The Devil is in the Details

The complexity and importance of the behaviour of beam-column joints has always been well recognised in the past as confirmed by the major effort, dedicated in the past thirty-forty years to the development of improved structural details and appropriate assessment and design guidelines. After capacity design principles were intro-

duced in seismic design philosophy in the 1970s, the concept of protecting "the weakest link of the chain" has naturally promoted a higher sensibility towards the detailing and design of this inherently delicate part of a frame structure. However, when dealing with an older structure, the lack of information on the structural detailing, on the material properties and on the original design could be crucial for a correct assessment of its vulnerability under a seismic event and thus for the subsequent definition of an adequate retrofit strategy.

Minor deficiencies in the structural details of the joint could result into a degraded behaviour under seismic loading, significantly enough to lead to a marginal survival, when not to a sudden collapse, of the whole structure. Different damage or failure modes are in fact expected to occur in beam-column joints depending on the typology (exterior or interior joint) and on the adopted structural details (i.e. total lack or presence of a minimum amount of transverse reinforcement in the joint; use of plain round or deformed bars; alternative bar anchorage solutions), as shown in Fig. 13.3d for exterior joints with no transverse reinforcement, mostly typical of older construction.

After diagonal cracking, the shear transfer mechanism in the joint region has to basically rely on a compression strut mechanism, whose efficiency is critically related to the anchorage solution adopted for the longitudinal beam reinforcement. When the beam bars are bent into the joint (Fig. 13.3a,b), they can provide a limited resistance against the horizontally expansion of the joint, until the hook opens under the combined action of the diagonal strut and the pulling tension force in the beam reinforcement, leading to a rapid joint degradation. When the beam bars are bent away from the joint (Fig. 13.3c), as more typical of the older construction practice in New Zealand and Japan, no effective node point is provided for the development of an efficient compression strut mechanism, unless a significant amount of transverse column hoops is placed immediately above the joint core. A rapid joint strength degradation after joint diagonal cracking is expected. The worst scenario is however provided by the solution shown in Fig. 13.3d, typical of the Mediterranean construction practice, where plain round bars with end-hook anchorages were commonly used. As recently shown by a series of experimental tests on exterior

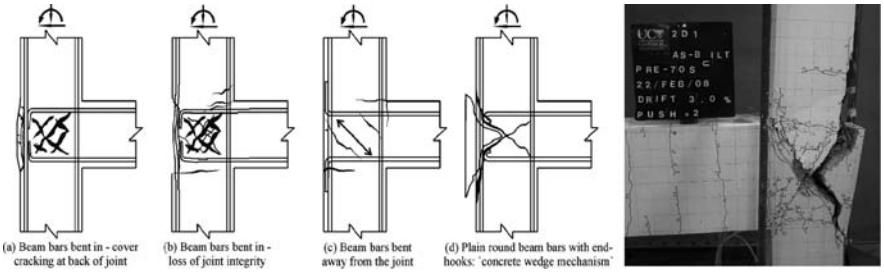

Fig. 13.3 Alternative damage mechanisms expected in exterior joints depending on the structural detailing. *Left* (**a,b**) beam bars bent inside the joint region; (**c**) beam bars bent outside the joint region; (**d**) plain round beam bars with end-hooks. *Right*: observed "concrete wedge" mechanism in an exterior joint subassembly subjected to laboratory simulated seismic loading [24]

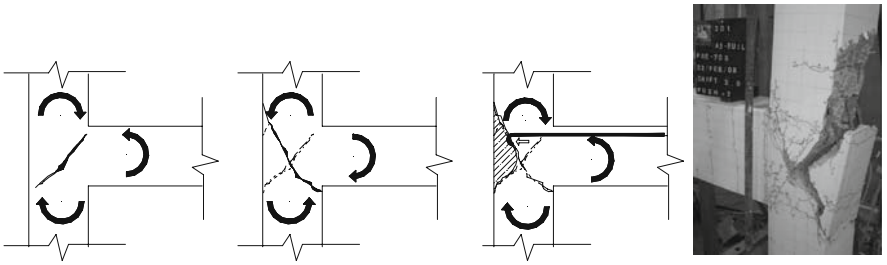

Fig. 13.4 Activation of a "concrete wedge" mechanism in exterior joints with no or limited transverse reinforcement, plain round bars and end hook [23, 27]

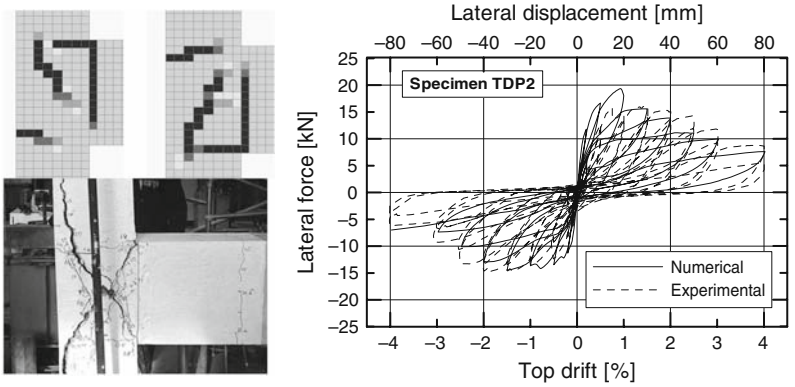

Fig. 13.5 FEM numerical vs. experimentally observed failure modes of exterior b-c joints with plain round bars and end-hooks (after [26])

beam-column joint specimens and a three storey frame system [11, 23, 25] and confirmed by detailed FEM parametric analyses based on a micro-plane concrete models [26], (Fig. 13.5), the combination of an inefficient diagonal strut action and of a concentrated compression force (punching action) at the end-hook anchorage, due to slippage of the longitudinal beam bars, can lead to the expulsion of a "concrete wedge" (Figs. 13.3d and 13.4), with rapid loss of bearing-load capacity.

13.3.2 Hierarchy of Strength and Sequence of Events: A Dangerous Equivalence

The concept of hierarchy of strength is often and improperly mistaken for the actual sequence of events. This apparently subtle difference can actually lead to major consequences in the evaluation of the expected seismic performance of the structure and selection of the most appropriate retrofit/upgrading intervention.

The hierarchy of strength within a frame system, beam-column joint, or structural element is fundamentally and, in principle, solely represented by capacity curves, thus being independent of the demand. The actual sequence of events, instead, defines the order of occurrence of damage and/or failure mechanisms (typically with reference to an increased level of deformation/displacement or stresses/forces) and shall be thus evaluated by considering the correct demand.

As a general example, a set of beam-column joint subassemblies, having the same geometric and mechanical properties but located at different floor levels or within different frame configurations, would have same capacity curves (i.e. inherent hierarchy of strength) while the sequence of events might be substantially different, due to the differences in the demand curves.

13.3.2.1 Importance of Accounting for the Variation of Axial Load

Appropriate demand curves for beam-column joint systems (as well as column-to-foundation connections) shall account for the variation of axial load due to the effects of lateral loads on a frame system, for either opening or closing of the joint, as shown in Fig. 13.6. An incorrect assessment of the sequence of events can otherwise result, possibly leading to an inadequate, and not necessarily conservative, design of the retrofit intervention.

However, most of the experimental cyclic tests on joint subassemblies (as well as column-to-foundation connections) available in literature were carried out, and still are for simplicity, under a constant axial load regime in the column. Whilst this simplified testing procedure is not expected to substantially affect the behaviour of well designed specimens, in the case of poorly detailed subassemblies, the effects on damage level and mechanisms could be significant.

As part of a simple procedure to compare the internal hierarchy of strength within a beam-column-joint, the evaluation of the expected sequence of events can be

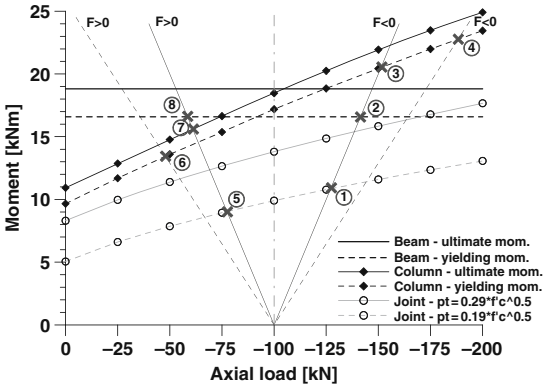

Specimen T1 (as–built)			
Type of lateral force	N°	Event	Lateral force [kN]
Open joint F<0	1	Joint cracking and deterioration starting $p_t = 0.19\sqrt{f'_c}$	−10.94
	2	Beam yielding	−16.59
	3	Upper column yielding	−20.50
	4	Lower column yielding	−22.75
Close joint F>0	5	Joint failure	9.37
	6	Lower column yielding	13.50
	7	Upper column yielding	14.50
	8	Beam yielding	16.59

Fig. 13.6 Evaluation of hierarchy of strengths and sequence of events: Moment-axial Load, *M-N*, performance-domain for an exterior beam-column joint in as-built configuration, (after [11])

carried out through comparison of capacity and demand curves within a *M-N* (moment-axial load) performance-domain [11]. Figure 13.6 shows, as an example, the *M-N* performance domain adopted to predict the sequence of events and the level of damage in the joint panel zone of a 2D exterior beam-column joint subassembly. The capacities of beam, column and joint are referred to given limit states (e.g. for the joints: cracking, equivalent "yielding" or extensive damage and collapse are associated to increased levels of principle tensile or compression stresses) and evaluated in terms of equivalent moment in the column at that stage, based on equilibrium considerations within the b-c joint specimen.

In the case of the as built exterior joint specimen taken herein as example (namely specimen T1 [11]), a shear hinge mechanism, with extensive damage of the joint, prior to any hinging of beams or columns, was in fact expected and predicted, using a proper demand curve (Table in Fig. 13.6) and later confirmed by the experimental tests. However, the order and "distance" of the events strongly depends on the assumption on the demand curve. If a constant axial load curve was used (in this case $N = -100$ kN as shown in Fig. 13.6), mostly typical of experimental tests and analytical assessment methodology suggested in the literature, only a minor increase in the column strength (in addition to the joint strengthening) would appear necessary for the retrofit intervention. In reality, such a strengthening solution would lead to the formation of a column hinging before any beam hinging, thus, possibly, resulting into the development of a soft storey mechanism, in spite of the (possibly quite expensive and invasive) retrofit intervention already implemented.

13.3.3 Effects of Bi-Directional Cyclic Loading

Furthermore, most of the studies available in literature on the seismic assessment and retrofit of existing poorly detailed frame building have concentrated on the 2-dimensional response, thus subjecting the specimen or subassemblies to unidirectional cyclic loading testing protocols. Even when the 3D response under combined bi-directional loading has been taken into account in experimental testing, the attention has been typically given to interior (fully or partially confined) joints. A particularly limited information on the response of existing 3D exterior (corner) joints is available, in spite of their intrinsically higher vulnerability under lateral cyclic loading) due to the lack of reliable joint shear transfer mechanisms, as confirmed in past earthquake events (i.e. Fig. 13.2).

As part of a more extensive research program on seismic retrofit solutions for reinforced concrete buildings, the effects of bi-directional loading, more representative of the actual seismic response of a building structure, on the assessment and design of the retrofit intervention have been investigated [25, 27].

The results confirmed that the bi-directional cyclic loading can significantly affect the response of poorly detailed beam-column joints. If overlooking such effects, the efficiency of a retrofit intervention can be critically impaired. As per the variation of axial load, a controversial outcome could be that an inappropriately

selected retrofit intervention may actually lead to a global failure mechanism (i.e. due to the formation of a soft-storey), which would not have occurred in the as-built (pre-retrofit) configuration.

Similarly to what accepted when evaluating the flexural capacity of columns under bi-directional loading, it can be suggested that the shear capacity of a joint panel zone is represented by a 3D interaction surface (M_y-M_z-P *or* V_y-V_x-P) accounting for the demand in the two orthogonal directions (Fig. 13.7). A remarkable reduction in the joint shear strength capacity would thus occur due to the simultaneous loading in the two orthogonal directions, as well as due to the aforementioned reduction of axial load in a corner joint during the frame sway mechanism.

A series of quasi-static tests under uni- and bi-directional loading has been carried out in the Structural Laboratory of the University of Canterbury on exterior 2D and 3D (corner) beam-column joint subassemblies, 2/3 scaled and representative of pre-1970s construction practice with different structural detailing (i.e. plain round with end hook anchorage or deformed bars, deep beams or shallow/wide beams, minimum or total lack of transverse reinforcement in the joint) [25, 27].

Regardless of the joint structural details adopted, the tests confirmed a significantly lower performance of exterior joints subjected to a bi-directional loading protocol (consisting of a four cloves displacement-control regime) when compared to their 2D counterparts subjected to more typically adopted uni-directional testing loading protocol.

Figures 13.8 and 13.9 show an example of the observed damage and a comparison of the subassemblies hysteresis loops. In both 2D and 3D specimens a shear hinge mechanism developed in the joint region, providing the main source of the observed inelastic deformation and behaviour. The 3D specimen, however, exhibited a more complex three-dimensional concrete wedge mechanism (Fig. 13.8), well

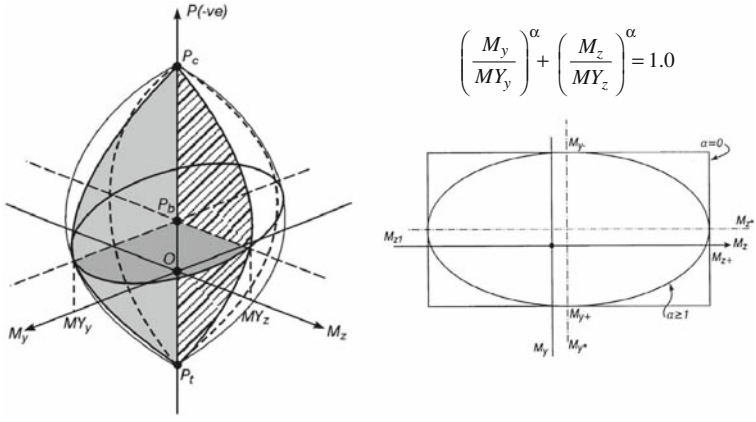

Fig. 13.7 Conceptual shear-axial load (Vy-Vz-P) interaction surface for a RC beam-column joint subjected to bi-axially loading

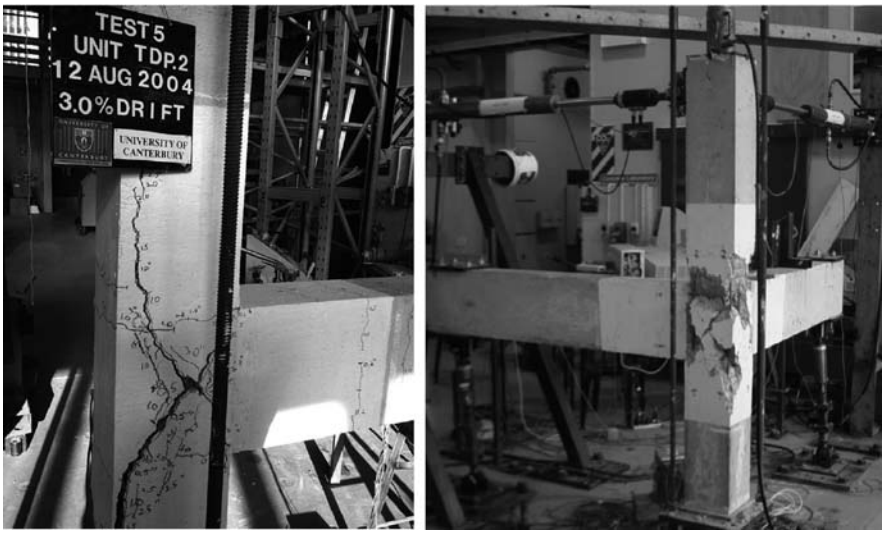

Fig. 13.8 Damage observation in the as-built exterior beam-column joint specimens 2D and 3D subjected to uni- and bi-directional loading, respectively (after [25, 27])

in line with the damage observed in recent earthquake events (e.g. see Fig. 13.2, damaged building after the Izmit-Kocaeli earthquake, Turkey, 1999).

A critical level of joint damage and a more rapid strength degradation were observed when compared to the 2D equivalent counterpart (Fig. 13.9), in spite of the partial confinement effects provided by the orthogonal beam. A reduction of the overall lateral load capacity of approximately 33% and 15%, in the positive and

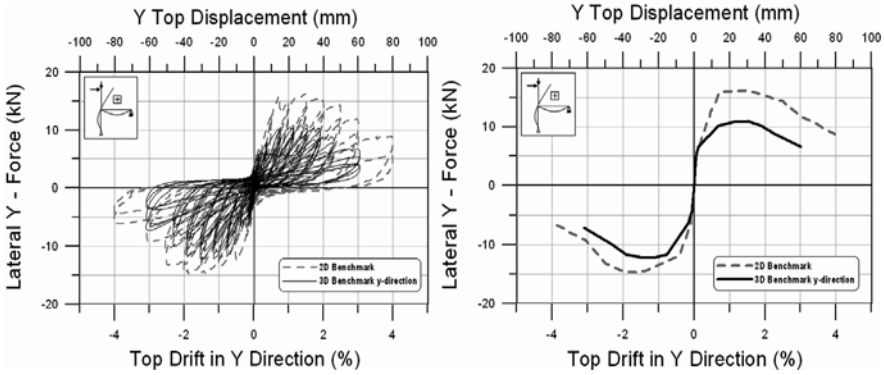

Fig. 13.9 Experimental hysteresis and envelope curves for two exterior 2D and 3D exterior joint subassemblies subjected to uni-directional and bi-directional loading regime, respectively (after [27])

negative direction, respectively (corresponding to decreasing and increasing of the axial load) was recorded.

13.3.4 The Controversial Effects of Masonry Infills on the Seismic Response: An Open Debate

As previously mentioned, the concept of damage has been in the past typically associated to that of the structural skeleton, whilst accepting, for a design level earthquake, a substantial damage to the "dress" of that skeleton, more technically referred to non-structural elements (partitions/infi1lls/claddings/glazing/services).

More recently, following the recognition that the high direct costs associated to the repairing and replacement of non-structural elements, as well as the indirect costs due to downtime and business interruption, can represent a major (in some cases predominant) component of the overall losses after an earthquake events, an increased attention is being paid to the seismic behaviour of non-structural components. More urgently, when dealing with existing reinforced concrete frame buildings with masonry infills, the evaluation of their expected seismic response may not, in general, be safely carried out by referring only to the behaviour of the structural skeleton (bare frame). The consequences of neglecting their interaction with the bare frame can possibly go well beyond a simple underestimation of the expected earthquake costs.

The effects of infills on the response of the overall structure still represents an open and delicate topic, with a critical need of further investigations for the seismic vulnerability assessment of extensive classes of existing buildings. Controversial effects on the global inelastic mechanism can be expected depending on the infills properties (mechanical characteristic and distribution) and on their interaction with the bare frame [15–18]. On one hand, the presence of infills can guarantee higher stiffness and strength, reducing the inter-storey drift demand, while increasing the maximum floor accelerations. A further positive influence of the infills can be recognised in the reduction of column interstorey shear contribution as well as in the possible delay of a soft-storey mechanism which might instead develop in a bare frame solution.

On the other hand, the interaction between the un-reinforced masonry infills and the RC frame can lead to unexpected and peculiar effects when compared with the response of the bare frame, either at a local level (e.g. shear failure in columns; damage to joint region) or on the global seismic response (e.g. soft storey mechanism) as shown in Fig. 13.10. Moreover, the sudden reduction of storey stiffness due to the damage of the infills can lead to the formation of a soft-storey mechanism, independently by the regular or irregular distribution of the infills along the elevation. Similarly, when investigating the response of 3-D frames under either unidirectional or bi-directional earthquake input excitation, inelastic torsion mechanisms can occur due to the irregular distribution of damage to the infills.

a) b) c)

Fig. 13.10 Observed effects of interaction between infills and bare frame: (**a**) shear failure of column and (**b**) exterior joint shear damage (Bonefro, Molise 2002); (**c**) global collapse for soft storey mechanism (Izmit, 1999, NISEE image collection)

13.4 Multi-Level Retrofit Strategy: A Rational Compromise with the Reality

An ideal retrofit strategy for existing frame would not only protect the beam-to-column joints identified as major deficiency in these systems, but would further upgrade the structure to exhibit the desired weak-beam strong-column behaviour which is at the basis of the design of new seismic resistant RC frames. However, due to the disproportionate flexural capacity of the beams when compared to the columns, resulting from gravity-load-only (or -mainly) design, a total inversion of the hierarchy of strength between beam and column can be difficult to achieve in all cases and for all beam-to-column connections without major interventions. This is especially true for interior beam-to-column connections where the moment imposed on interior columns from the two framing beams is significantly larger than for exterior columns. Considering that interior joints are less vulnerable than exterior joints and can exhibit a much more stable hysteretic behaviour with hardening after first cracking, it is thus conceivable, in a bid to protect the interior columns from excessive curvature demand, to tolerate some interior joint damage prior to the columns hinging.

According to a multi-level retrofit strategy approach, alternative objectives can thus be targeted in terms of hierarchy of strength within the beam-column-joint system, depending on the joint typology (interior or exterior) and on the structural details adopted [11, 28].

Two levels of retrofit can for example be considered, depending on whether or not the interior joints can be (or is worth being) fully upgraded. A complete retrofit would thus consist of a full upgrade, by protecting all joint panel zones and developing plastic hinges in the beams while the columns are protected according to capacity design principles. A partial retrofit would, instead, consist of protecting only the exterior joints, forming plastic hinges in the beams framing into exterior columns, while permitting hinging in the interior columns or limited damage to the interior

joints, where a full reversal of the strength hierarchy is not possible. It is in fact important to recognize that, as long as flexural plastic hinges develop in the beams and a sufficient deformation/rotation capacity (not necessarily ductility) is guaranteed within the critical elements and overall system, the formation of a soft-storey mechanism can be critically prevented.

The viability of such a partial retrofit strategy must ultimately be investigated on a case-by-case basis to assure that localized damage in other regions of the structures would not severely degrade the overall response or jeopardize the ability of safely carrying gravity loads.

13.4.1 Implementation of a Multi-Level Retrofit Strategy using Alternative Solutions

In principle, several and different technical solutions can be adopted to implement the aforementioned partial retrofit approach, thus targeting the inversion of hierarchy of strength only in the exterior beam-column joints, with the development of plastic hinges in the beams framing into the exterior columns.

The feasibility and efficiency of two alternative retrofit technical solutions, following this proposed multi-level retrofit strategy approach, has been recently presented in the literature, based on the use of FRP composite materials and of a diagonal metallic "haunch" connection [11, 27, 28]. Experimental and analytical investigations were carried out on a set of as-built and retrofitted 2-D and 3-D beam-column joint subassemblies as well as on two three storey frame systems, representative of older construction practice. Both the selected interventions succeeded in protecting the panel zone region, avoiding the extensive joint shear damage observed in the as-built configuration. More desirable hierarchy of strength and sequence of events were achieved, by developing a plastic hinge in the beam (relocated at a certain distance from the interface with the column) and thus leading to a more ductile and dissipating hysteresis behaviour (Figs. 13.11 and 13.12).

Both solutions have been conceived to be relatively low-invasive, of practical application and simple design, for a broad and extensive (while cost-efficient, as discussed in the next paragraph) application at a large scale.

By implementing such a partial retrofit solution, which aims at developing a sort of partial beam sway mechanism, the main declared target performance, namely life safety and collapse prevention under a design level earthquake, can be achieved with sufficient confidence.

The evaluation of the hierarchy of strength and sequence of events prior and after the retrofit interventions has been carried out, in both cases, using the *M-N* interaction performance domain previously mentioned (Fig. 13.6).

In the FRP solution, uni-directional glass fiber laminates were adopted as shown in Fig. 13.11 (bottom right). One vertical FRP layer is used on each of the two external faces of the column (supposed to be accessible in a real building without

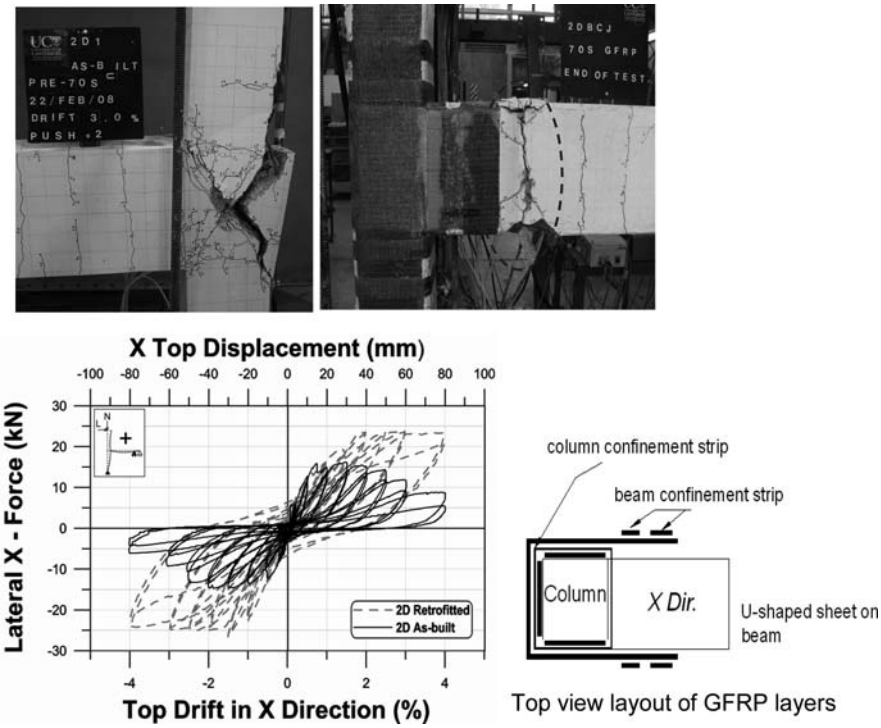

Fig. 13.11 Retrofit of exterior beam-column joint using fiber reinforced polymers. Protection of the joint panel zone and inversion of the hierarchy of strength with plastic hinge in the beam (after [27])

excessive disruption of the internal activities) in order to increase the column flexural capacity as well as the joint shear strength. In addition, one U-shape horizontal laminate, wrapped around the exterior face of the specimen at the joint level, is used to increase the joint shear strength as well as to prevent the expulsion of the concrete wedge observed in both the 2D and 3D as-built configuration.

The enhancement of the flexural strength of the beam and column critical sections and of the joint shear strength (in terms of principle tensile strength) has been evaluated according to the aforementioned procedure presented in [11]. Additional smaller strips were used to provide better anchorage to the main FRP laminates in the beam and column.

In the haunch retrofit solution, a diagonal metallic element (in the form of a cylinder, tube, plate or bracket) referred to as "haunch", is installed locally at the beam-column joint connection level to protect the panel zone from extensive damage and brittle shear mechanism, while inverting the hierarchy of strength within the beam-column subassemblies and forming a plastic hinge in the beam (Fig. 13.12). The conceptual mechanism is relatively straightforward: when haunch type elements are introduced at a distance *L'* from the beam-column interface and connected at an

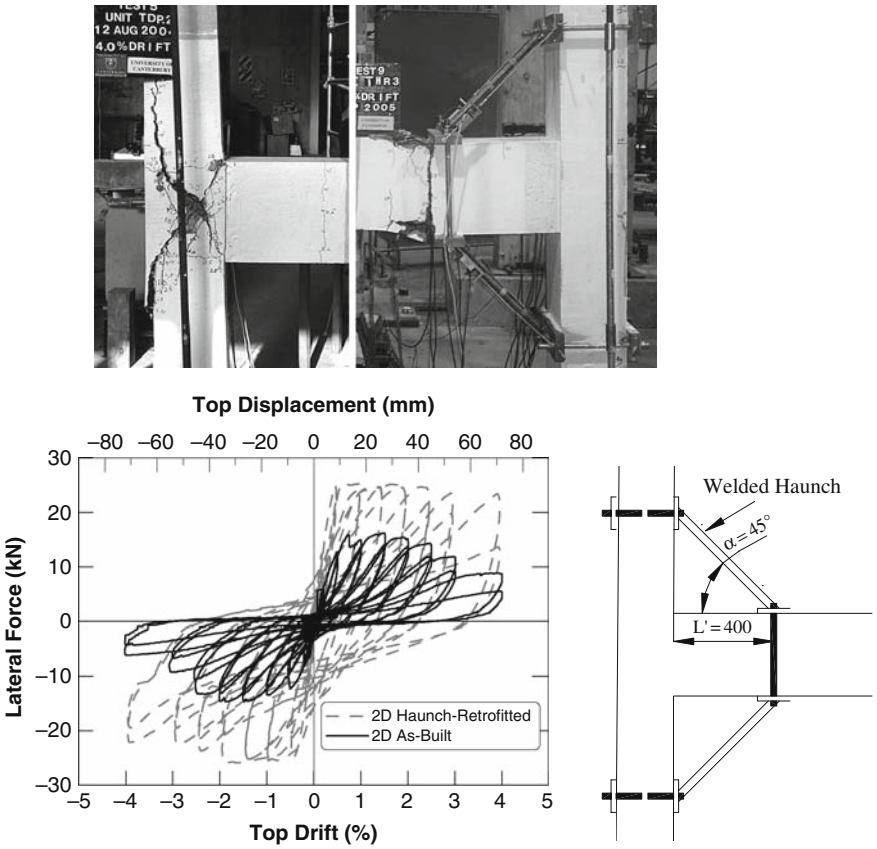

Fig. 13.12 Retrofit of exterior beam-column joint using a metallic diagonal haunch. Protection of the joint panel zone and inversion of the hierarchy of strength with the development of a plastic hinge in the beam (after [28])

angle α above and below the beam, the internal forces of the beam-column assembly are significantly altered (see Fig. 13.13). The beam and column moment demand at the joint panel zone interface is drastically reduced, and with them the joint shear demand. The maximum moment in the beam and in the column is instead relocated away from the original critical sections to the points where the haunches are connected. Simple design considerations, always respecting capacity design principle to avoid brittle mechanisms, can be adopted to force a plastic hinge in the beam.

It is worth noting that the increase of the global strength of the previously shown retrofitting beam-column joint subassemblies is more due to the development of an improved and more favourable inelastic mechanism, through a change of the load path (particularly clear in the haunch solution, see Fig. 13.11) rather than to an actual "strengthening" intervention.

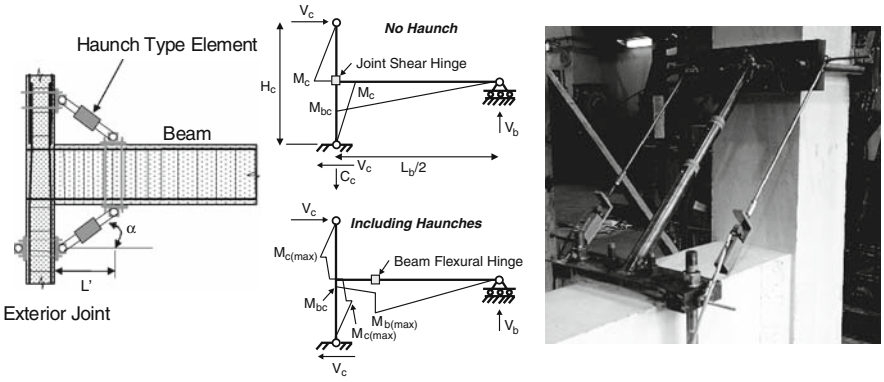

Fig. 13.13 Modification of internal force diagrams and stress flow in an exterior joint retrofitted with the proposed diagonal haunch solution (after [28])

13.5 Suggestions for Advanced Retrofit Solutions

13.5.1 Emerging Trends in Low-Damage Seismic Resisting Systems

Major advances have been observed in the last decade in seismic engineering with further refinements of performance-based seismic design philosophies and definition of the corresponding compliance criteria. Following the worldwide recognized expectation and ideal aim to provide a modern society with high (seismic) performance structures able to sustain a design level earthquake with limited or negligible damage, emerging solutions have been developed for high-performance, still cost-effective, seismic resisting systems, based on an adequate combination of traditional materials and available technology.

In particular, recent technological solutions for precast/prestresssed concrete buildings, originally developed under the PRESSS Program (Fig. 13.14) and further refined [29–31], rely on the use of unbonded post-tensioned tendons with re-centering capability (negligible residual displacements) and are capable of significantly reducing the expected damage after a moderate-to-strong earthquake event.

In these dry jointed ductile solutions, opposite to wet and strong connection solutions, precast elements are jointed together through unbonded post-tensioning tendons/strands or bars. The inelastic demand is accommodated within the connection itself (beam-column, column to foundation or wall-to-foundation critical interface), through the opening and closing of an existing gap (rocking motion), while a reduced level of damage, when compared to equivalent cast-in-place solutions, is expected in the structural precast elements, which are basically maintained in the elastic range. Moreover, the self-centering contribution due to the unbonded tendons can lead to negligible residual deformations/displacements, which should be

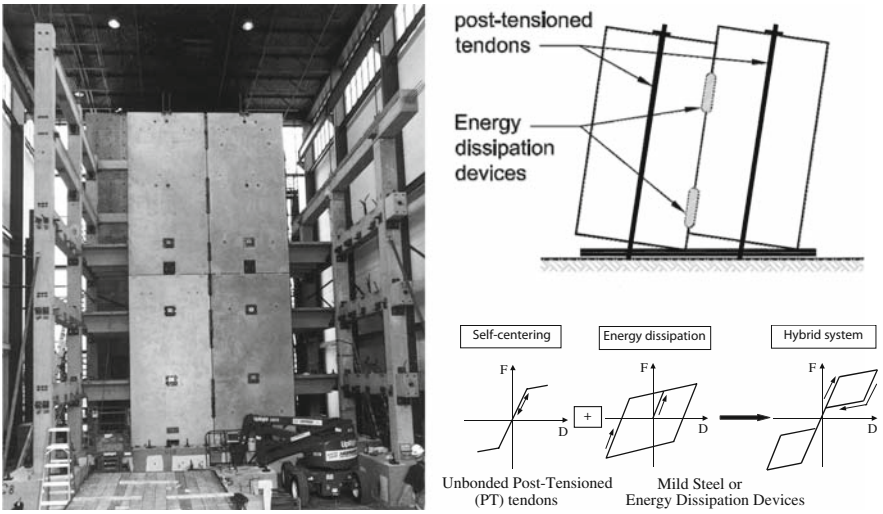

Fig. 13.14 Jointed precast "hybrid" frame and wall connections developed in the US PRESSS-Program ([29, 30, 35,36])

adequately considered as a complementary damage indicator within a performance-based design or assessment procedure [32, 33].

Additional energy dissipation capacity can be provided by non-prestressed (mild) steel or additional external devices. In such a hybrid system [29, 34], a sort of "controlled rocking" motion of the beam or wall panel occurs, while the relative ratio of moment contribution between post-tensioning and mild steel governs the so-called "flag-shape" hysteresis behaviour (Fig. 13.14 bottom right).

The recent emphasis given to the re-centering capability (negligible residual deformations) as well as to the limitation for the structural damage, both achievable by the aforementioned controlled rocking systems, could suggest the development and proposal of advanced seismic retrofit strategies and technologies able to provide a higher performance with limited level of damage and negligible permanent deflections. A couple of options are shown in the following paragraphs.

13.5.2 Use of Precast Post-Tensioned Rocking/Dissipative Shear Walls

Adding internal or external walls is well recognized as being a valuable and widely adopted option for the retrofit of under-designed existing frame buildings. The introduction of a wall has the advantages of increasing the stiffness and strength of the original bare frame. Furthermore, the frame-wall coupling effects, typical of a dual system, can better distribute the deformation demand along the elevation, preventing the occurrence of soft-storey mechanisms. As a result, in addition to an adequate

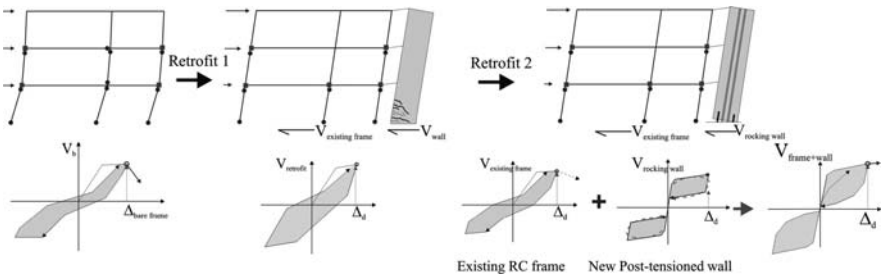

Fig. 13.15 Retrofit solutions using a typical external cast-in-situ walls or a rocking/dissipative post-tensioned wall (modified after [37])

protection against collapse, a reduced level of damage is expected in the frame, when compared to the pre-retrofit configuration. However, depending on the system ductility demand, non-negligible physical damage and residual (permanent) deformations can occur in the retrofitting wall, as typical of a ductile monolithic system. High costs associated to the strengthening intervention on the existing foundation to accommodate the capacity of the new wall are also often required.

An improved retrofit solution can be obtained by using an unbonded post-tensioned rocking wall (more likely but not necessarily composed of precast panels), as shown in Fig. 13.15. If designed according to a displacement-based retrofit approach, the targeted maximum displacement and interstorey drift of the retrofitted building can be selected, for a given seismic intensity, in order to control the local deformation in joints, structural elements and infills, minimizing the damage in the existing building [36]. No structural damage is expected in the rocking wall, nor residual deformations in the overall building, thanks to the re-centering contribution of the post-tensioned wall. Furthermore, a more slender post-tensioned wall would be required when compared to a monolithic option and capacity design considerations can be used to limit the overturning moment per unit/length to the capacity of the existing foundations, thus drastically reducing the need for strengthening.

Moreover, alternative dissipation techniques can be applied to the rocking wall by combining velocity-proportional (viscous) dampers with more traditional displacement-proportional (hysteretic) devices. This solution, referred to as Advanced Flag Shape System, has been proven to be particularly robust and efficient in counteracting the effects of both near field and far field events for either the design of new structures or the retrofit of existing ones [37, 38]. Figure 13.16 shows two prototypes of this advanced post-tensioned wall system, with alternative configurations of external replaceable dissipation devices are implemented, constructed either in precast concrete and in timber (Laminated Veneer Lumber) and subjected to a series of shake table tests [39].

13.5.2.1 Selective Weakening as a Basis for Seismic Retrofit

The concepts of strengthening and retrofit are too often associated, although sometimes improperly. According to advanced retrofit techniques proposed by [40] and

Fig. 13.16 Prototypes of post-tensioned rocking/dissipative concrete and timber walls under shake table tests (after [39])

implemented in the *fib* guidelines for Seismic Assessment and Retrofit of Existing Reinforced Concrete Buildings [1], an upgrading intervention based on stiffness-only, strength-only or ductility-only can be achieved on a single-element as part of a selective retrofit approach. The seismic upgrading or retrofit of the structure can thus be achieved without necessarily implementing any "strengthening" intervention.

By further developing the concept of hybrid or controlled rocking systems and exploiting their significant advantages, in terms of limited level of damage and control of the stress level acting as a fuse, it could be argued that a "weakening", instead of a strengthening approach could be a more valuable, though somehow counter-intuitive, approach to protect an existing structure from an expected earthquake ground motion.

The concept of a selective weakening retrofit approach has been recently presented in literature [41] and implemented with experimental validation on shear wall systems [42]. The basic concept for wall systems is explained in Fig. 13.17: by saw cutting the longitudinal bottom reinforcement of a gravity load dominated beam or of a shear-dominated wall, a better control of the overall mechanism can be achieved, according to hierarchy of strength principles. A flexure-dominated rocking mechanism can be activated, guaranteeing limited level of damage in the structural member as well as control of the maximum level of stress directed to the beam-column joint panel zone or to the existing foundation. The weakest links of the building are thus protected by designing a fuse action (uplifting/yielding of the wall). Moreover, existing shear walls with low aspect ratio (shear-prone) can be split into two adjacent rocking (and coupled, if desired/required) walls. This would

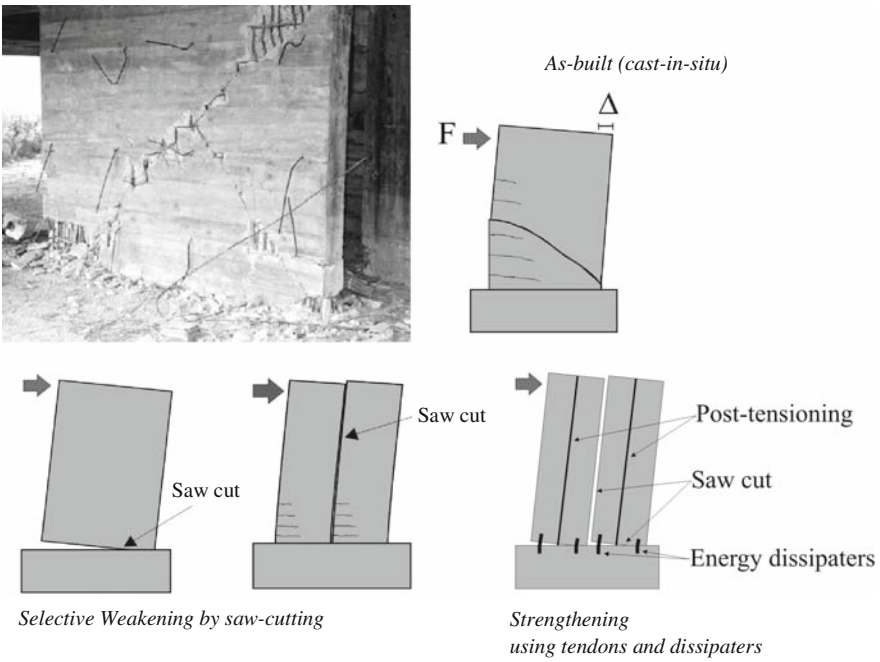

Fig. 13.17 Typical shear failure mechanism in an existing under-designed RC wall and conceptual application of the proposed selective weakening technique (modified after [42])

result into a protection of the shear modes as well as a limitation of the overturning moment demand (per unit length) to the foundation.

Figure 13.18 shows the experimental results of quasi-static cyclic tests on an existing shear-prone walls before and after being retrofitted using the proposed selective weakening intervention. After saw cutting the wall at the base section level to induce a rocking motion (flexural dominated mode), external replaceable dissipaters (mild steel fuses yielding in tension and compression) are added along with vertical unbonded post-tensioning. Further protection of the edge compression toes is obtained with steel angles. Enhanced strength, dependable dissipation and hysteretic behaviour, increased ductility and full-recentering capacity are obtained. Negligible damage is observed up to the design level of drift (2.5%) when compared to the monolithic counterpart.

As previously mentioned in the case of post-tensioned external walls used as a retrofit option, further enhancements of this improved behaviour could be achieved by using advanced energy dissipation devices (e.g. viscous, friction, SMA, combined in advanced flag-shaped systems [38]).

The broader concept of selective weakening, herein presented for wall systems only, has been actually proposed to be extended, in its general form of structural disconnection, and experimentally validated on beam-column joint connections [43]. Furthermore, acknowledging that monolithic behaviour might imply (if a result of

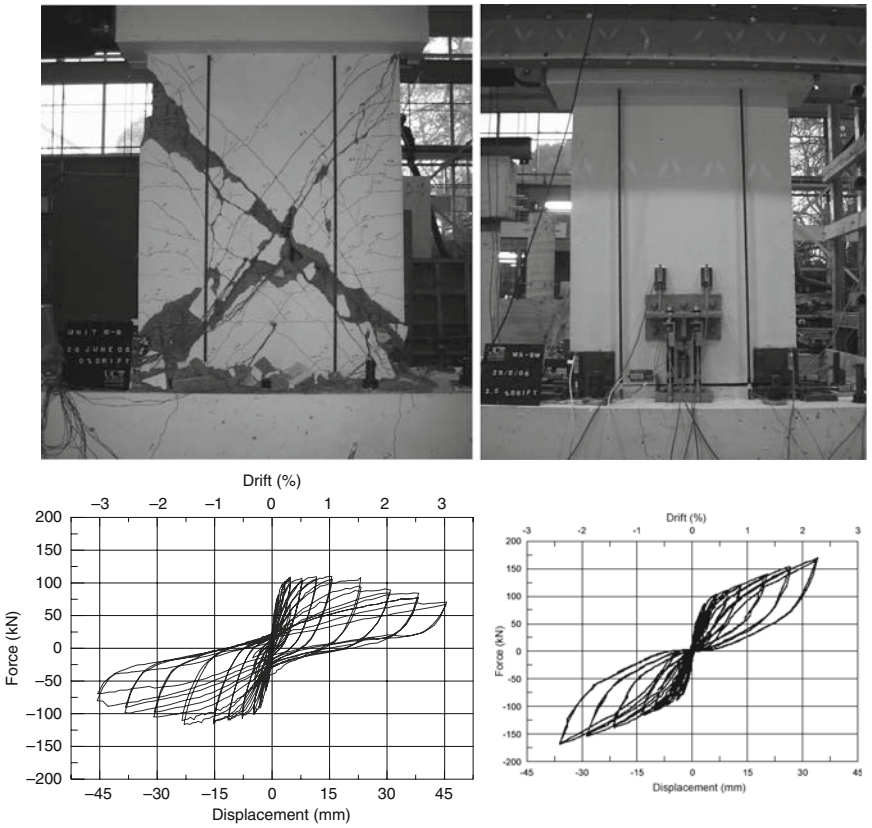

Fig. 13.18 Typical shear failure mechanism in an existing under-designed RC wall and conceptual application of the proposed selective weakening technique (modified after [42])

a cast-in-situ technique) concentration of damage, a low-damage retrofit or new design approach for floor-diaphragm systems can also be achieved by appropriately disconnecting and "isolating" the floor from the lateral load resisting (frame or wall) systems [44]. So doing, not only displacement incompatibility issues can be controlled and reduced, but also undesirable higher mode effects due to the interaction between the floor and the seismic resisting frames could be controlled by the fuse action of lateral shear collector, e.g. dissipating mechanical couplers.

13.6 Remembering the "Bigger Picture": Seismic Risk Analysis and Management as a Decision-Making Tool for the Retrofit Intervention at Territorial Scale

The selection of the most appropriate retrofit solution to be implemented is typically accomplished by targeting, on a case-by-case basis, an acceptable weighted balance

between the benefits due to the improved seismic performance and the direct (and sometimes indirect) costs associated to the intervention. The aforementioned recent developments of viable and low-cost retrofit solutions according to a multi-level retrofit approach, suggest the possibility to implement "standardised" solutions at an urban or territorial scale.

However, when expanding the scale of the intervention (and analysis) to a territorial level (city, region, country), more complex criteria and intervention strategies should be considered and evaluated to define the most effective action plan to minimise the overall risk. In particular, the actual limits of available resources, including budget, material, human and technical resources, logistics and supporting infrastructures, can represent the critical constraints for a large scale intervention. Damage scenarios and seismic risk analysis, devoted to the evaluation of the expected losses for a specific earthquake event or the possible losses in a time period, and the representations of their results in a GIS environment are receiving an increasing attention as helpful tools to support decision making, e.g. planning and prioritizing of retrofit or seismic intervention programs at large scale as well as implementing alternative non structural mitigation strategies and risk transferring through insurance/reinsurance industry.

The efficiency of alternative structural mitigation strategies has been under investigation within the framework of a seismic risk analysis approach [45–46]. In Fig. 13.19 the benefits of different retrofit solutions on the performance of a specific class of existing frames can be appreciated in terms of fragility curves, describing the probability of exceed or equal pre-defined levels of damage.

The effectiveness of targeting a partial or total retrofit intervention (thus aiming at different targeted performance) as part of a territorial scale retrofit strategy (via the adoption of standardized multi-level retrofit strategies) has been investigated and confirmed [45].

A virtual implementation of alternative retrofit strategy and mitigation analyses, consisting on a traditional cost-benefit analysis as well as on a more refined multi-criteria decision approach, has been carried out on a case study region identified with Western Liguria, Italy. A multi-level performance-based retrofit strategy has been implemented with reference to alternative retrofit techniques, i.e. FRP or diagonal haunch (Fig. 13.20). In particular, two levels of upgrading plus a "do nothing" option were considered in this contribution: No Action-As Built condition (AB), Partial Retrofit (PR), Total Retrofit (TR).

Based on the results of these damage scenario analyses pre- and post-retrofit intervention (Fig. 13.21), it was confirmed that a quick implementation in critical sub-areas or regions of "partial" retrofit strategies could be an efficient approach to drastically reduce to a manageable level the consequences of the seismic event, more so when, due to resources constraints, a massive global intervention would not be feasible.

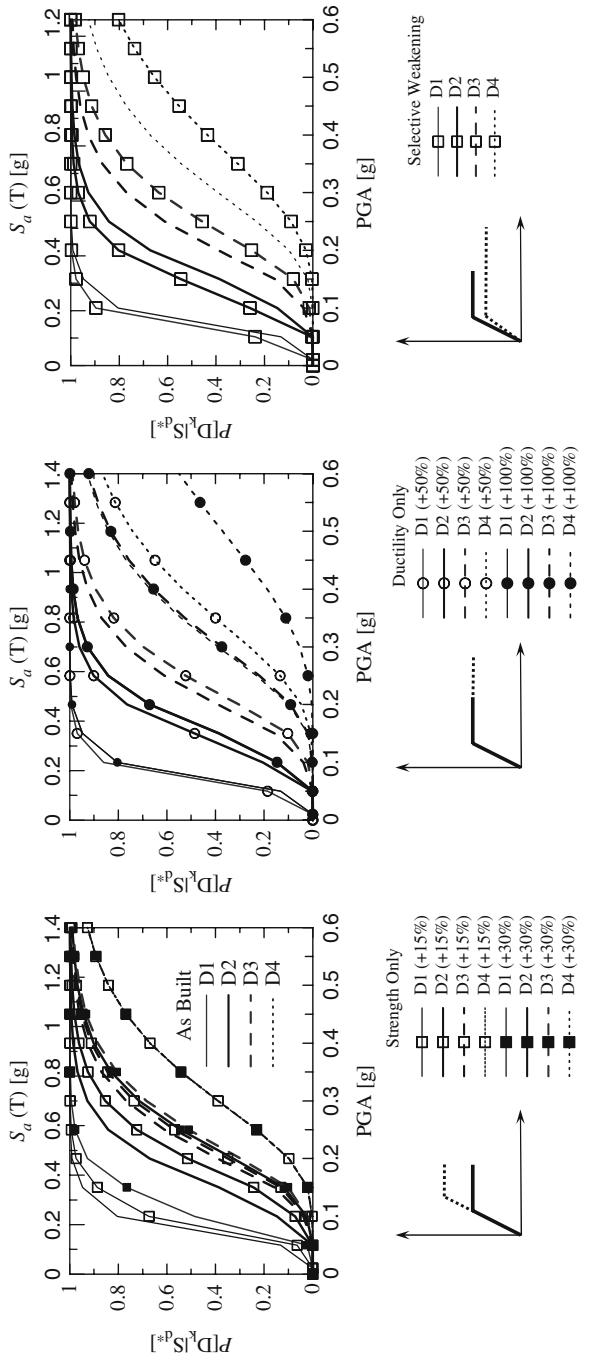

Fig. 13.19 Efficiency of alternative retrofit solutions (strength-only, ductility-only, selective weakening) in terms of fragility curves (after [45])

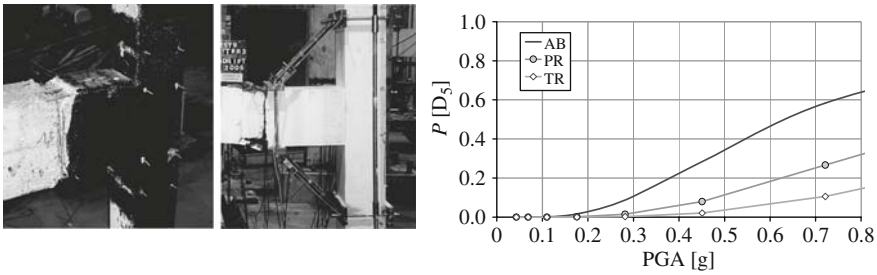

Fig. 13.20 Fragility curves representing the effects of general multi-level performance-based retrofit strategies (using FRP or haunch solution) on a frame system based on two levels of structural upgrading

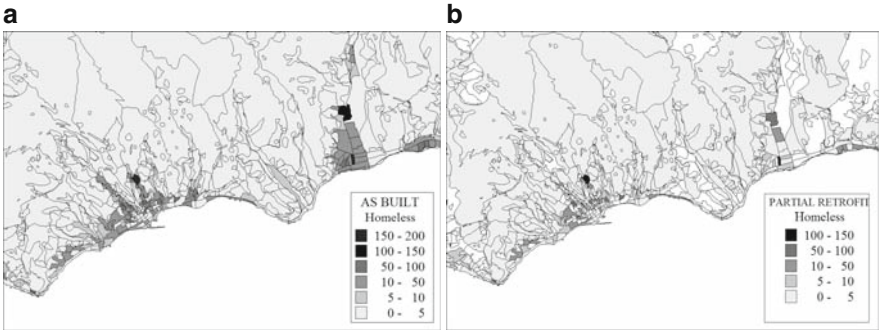

Fig. 13.21 Effects of a controlled (partial) retrofit intervention at a territorial scale (Case Study: Western Liguria, Italy). Homeless people: (**a**) as built conditions, (**b**) after a partial retrofit intervention [46]

13.7 Conclusive Remarks: Time for Some Action

An overview of alternative retrofit strategies and technical solutions developed and/or further refined in the past few years, as part of a multi-year research project on the seismic retrofit of existing reinforced concrete buildings has been given. The feasibility and efficiency, in the contest of a performance-based retrofit approach, of adopting and/or combining different solutions such as Fiber Reinforced Polymers, low-invasive low-cost metallic diagonal haunches, post-tensioning wall systems or selective weakening techniques, have been discussed, based on numerical and experimental evidences.

Emphasis has been given to the crucial need to move, in general terms, towards a performance-based retrofit approach, while accepting due compromises and adjustments of the targeted limit states and performance levels to account for: (a) the health status of the existing "patient", (b) the difficulties to develop an accurate diagnosis as well as (c) the several issues/including, but not limited to, costs, lack of resources, feasibility, invasiveness, related to the actual implementation of an ade-

quate strengthening/retrofit solution. The concept of a partial retrofit strategy, capable of achieving an intermediate approach as collapse prevention, when compared to a total retrofit strategy, has been proposed as a more realistic and valuable solution, when, particularly at territorial scale, an ideal full retrofit strategy is impaired by technical and financial limits.

The complexity of the problem, in particular when considering its scale, is without any doubt exceptional, as is the challenge to the scientific/technical/regulatory community, often perceived as going well beyond the practical feasibility. On the positive side, as noted and demonstrated once again within this contribution, extensive effort and resources (both human and financial) have been dedicated and invested in the past few years to the study of (a) the seismic hazard, (b) the vulnerability of the building inventory, (c) the development of valuable strengthening/retrofit techniques as well as to (d) the estimation through seismic risk analyses of the socio-economical impact (losses) in major seismic prone cities and region, when subjected to an historical or artificially created earthquake scenario. The level of technical knowledge achieved appears to be thus more than sufficient to take some action or "do something".

On the negative side, in spite of the disastrous consequences predicted in some cases, the actual implementation of seismic upgrading intervention at a large scale is still an exceptional event rather than a top priority in the to-do list at either national or international higher levels. The actual lack of immediate financial resources to complete the whole task is too often perceived and blamed as the main obstacle to justify a no action or a "do nothing" strategy.

Certainly, and from a different perspective, the implementation, at such higher levels, of *ad-hoc* regulations and incentives capable of enforcing while favouring such actions, along with the development a realistic prioritization strategy within a long-term multi-year intervention plan, justified on the basis of a robust financial scheme and business case, would help to agree to get started and take some action.

Acknowledgments The financial support provided by the NZ Foundation for Research, Science and Technology (FRST) through the Research Program "Retrofit Solutions for NZ" is gratefully acknowledged.

References

1. fib (2003) Seismic assessment and retrofit of reinforced concrete buildings: state-of-the-art report. International Federation for Structural Concrete (fib), Lausanne
2. FEMA-547 (2006) Techniques for the seismic rehabilitation of existing buildings. Federal Emergency Management Agency, Washington, DC
3. ASCE-41 (2007) Seismic rehabilitation of existing buildings. American Society of Civil Engineers, Reston, VA
4. fib (2001) Externally bonded FRP reinforcement for R.C. structures. International Federation for Structural Concrete, Bulletin n.14, Lausanne
5. Dolce M, Cardone D, Marnetto R (2000) Implementation and testing of passive control devices based on shape memory alloys. Earthquake Engineering & Structural Dynamics Journal, 29(7):945–968

6. SEAOC Vision 2000 Committee (1995) Performance-based seismic engineering. Structural Engineers Association of California, Sacramento, CA
7. Aycardi LE, Mander JB, Reinhorn AM (1994) Seismic resistance of R.C. frame structures designed only for gravity loads: Experimental performance of subassemblages. ACI Structural Journal, 91(5):552–563
8. Beres A, Pessiki S, White R, Gergely P (1996) Implications of experimental on the seismic behaviour of gravity load designed R.C. beam-column connections. Earthquake Spectra, 12(2):185–198
9. Hakuto S, Park R, Tanaka H (2000) Seismic load tests on interior and exterior beam-column joints with substandard reinforcing details. ACI Structural Journal, 97(1):11–25
10. Park R (2002) A summary of results of simulated seismic load tests on reinforced concrete beam-column joints, beams and columns with substandard reinforcing details. Journal of Earthquake Engineering, 6(2):1–27
11. Pampanin S, Bolognini D, Pavese (2007) Performance-based seismic retrofit strategy for existing reinforced concrete frame systems using FRP composites. ASCE Composites for Construction Journal, 11(2):211–226
12. Bing L, Yiming W, Tso-Chien P (2002) Seismic behavior of non-seismically detailed interior beam-wide column joints. Part I: Experimental results and observed behavior. ACI Structural Journal, 99(6)
13. Calvi G M, Magenes G, Pampanin S (2002) Relevance of beam-column damage and collapse in R.C. frame assessment. Journal of Earthquake Engineering, 6(1):75–100
14. Mainstone RJ (1974) Supplementary note on the stiffness and strength of infilled frames. Current paper CP13/74, Buildings Research Establishment, London
15. Klingner RE, Bertero VV (1978) Earthquake resistance of infilled frames. ASCE Journal of the Structural Division, 104(6):973–989
16. Zarnic R, Tomazevic M (1984) An experimentally obtained method for evaluation of the behaviour of masonry infilled R/C frames. Proc. 9th World Conference on Earthquake Engineering, San Francisco
17. Panagiotakos TB, Fardis MN (1996) Seismic response of infilled R.C. frames structures. Proc. 11th World Conference on Earthquake Engineering, Acapulco
18. Dolsek M, Fajfar P (2001) Soft storey effects in uniformly infilled reinforced concrete frames, Journal of Earthquake Engineering, 5(1):1–12
19. Shing PB, Mehrabi AB (2002) Behaviour and analysis of masonry infilled frames. Progress in Structural Engineering and Materials, 4:320–331
20. Magenes G, Pampanin S (2004) Seismic response of gravity-load designed frame systems with masonry infills. Proc. 12th World Conference on Earthquake Engineering, Vancouver
21. Galli M (2007). Evaluation of the seismic response of existing R.C. frame buildings with masonry infills. M.E.E., Istituto Universitario di Studi Superiori, Pavia
22. Santarella L (1957) Il cemento armato. 2, Milan (In Italian)
23. Pampanin S, Moratti M, Calvi GM (2002) Seismic behaviour of R.C. beam-column joints designed for gravity loads, Proc. 12th European Conference on Earthquake Engineering, London
24. Pampanin S, Magenes G, Carr A (2003) Modelling of shear hinge mechanism in poorly detailed R.C. beam-column joints. fib Symposium on Concrete Structures in Seismic Regions, Athens
25. Hertanto (2006) Seismic assessment of pre-1970s reinforced concrete beam-column joint subassemblies. M.E. Dissertation, Dept. of Civil Eng. University of Canterbury, Christchurch
26. Eligehausen R, Genesio G, Ožbolt J, Pampanin S (2008) 3D analysis of seismic response of R.C. beam-column exterior joints before and after retrofit. Proc. ICCRRR2008, Cape Town
27. Akguzel U, Pampanin S (2008) Effects of variation of axial load and bi-directional loading on the FRP Retrofit of existing B-C joints. Proc. 14th World Conference in Earthquake Engineering, Beijing

28. Pampanin S, Christopoulos, Chen T-H (2006) Development and validation of a haunch metallic seismic retrofit solution for existing under-designed R.C. frame buildings. Earthquake Engineering and Structural Dynamics, 35(14):1739–1766
29. Priestley MJN (1996) The PRESSS program current status and proposed plans for Phase III. PCI Journal, 41(2):22–40
30. Priestley MJN, Sritharan S, Conley JR, Pampanin S (1999) Preliminary results and conclusions from the PRESSS five-storey precast concrete test building, PCI Journal, 44(6):42–67
31. Pampanin S (2005) Emerging solutions for high seismic performance of precast/prestressed concrete buildings. Journal of Advanced Concrete Technology (ACT), Invited paper for Special Issue on High Performance Systems, 3(2):202–222
32. Pampanin S, Christopoulos C, Priestley MJN (2002) Residual deformations in the performance-based seismic assessment of frame systems. ROSE Research Report 2002/02, European School on Advanced Studies on Reduction of Seismic Risk, Pavia
33. Christopoulos C, Pampanin S (2004) Towards a performance-based seismic design of MODF structures with explicit consideration of residual deformations. Invited Paper, ISET Journal of Earthquake Technology, 41(1):53–73
34. Stanton JF, Stone WC, Cheok GS (1997) A hybrid reinforced precast frame for seismic regions, PCI Journal, 42(2):20–32
35. fib (2003) Seismic design of precast concrete building structures. International Federation for Structural Concrete, Bulletin 27, Lausanne
36. NZS3101 Standards New Zealand (2006) Appendix B: special provisions for the seismic design of ductile jointed precast concrete structural systems.
37. Marriott D, Pampanin S, Bull DK, Palermo A (2007) Improving the seismic performance of existing reinforced concrete buildings using advanced rocking wall solutions. Proc. NZSEE Conference, Palmerston North
38. Kam WY, Pampanin S, Palermo A, Carr A (2008) Implementation of advanced flag-shape (AFS) systems for moment-resisting frame structures. Proc. 14th World Conference in Earthquake Engineering, Beijing
39. Marriott D, Pampanin S, Bull D, Palermo A (2008) Dynamic testing of precast, post-tensioned rocking wall systems with alternative dissipating solutions. Bulletin of the NZ Society for Earthquake Engineering, 41(2):90–103
40. Elnashai AS, Pinho R (1998) Repair and retrofitting of R.C. walls using selective techniques. Journal of Earthquake Engineering, 2(4):525–568
41. Pampanin S (2006) Controversial aspects in seismic assessment and retrofit of structures in modern times: Understanding and implementing lessons from ancient heritage. Bulletin of NZ Society of Earthquake Engineering, 39(2):120–133
42. Ireland MG, Pampanin S, Bull DK (2007) Experimental investigations of a selective weakening approach for the seismic retrofit of R.C. walls. NZSEE Conference 2007, Palmerston North
43. Kam WY, Pampanin S (2008) Selective weakening techniques for retrofit of existing reinforced concrete structures. Proc. 14th World Conference in Earthquake Engineering, Beijing
44. Jensen J, Bull DK, Pampanin S (2007) Experimental investigation of existing hollowcore seating connection seismic behaviour pre and post retrofit intervention. Proc. NZSEE Conference, Palmerston North
45. Giovinazzi S, Pampanin S, Lagomarsino S (2006) Vulnerability models and damage scenarios for Pre-1970 R.C. buildings before and after alternative retrofit strategies. Proc. 1st ECEES, Geneva
46. Giovinazzi S, Pampanin S (2007) Multi-criteria approaches for regional earthquake retrofit strategies. Proc. 8th Pacific Conference on Earthquake Engineering, Singapore

Chapter 14
FRP Wrapping of RC Structures Submitted to Seismic Loads

Nathalie Roy, Pierre Labossière, Jean Proulx, Éric St-Georges, and Patrick Paultre

Abstract An ongoing research project at the Université de Sherbrooke has shown that fiber reinforced polymers (FRPs) enhance ductility, flexural capacity and shear resistance of RC columns wrapped with such products. A recent experimental program was completed on 2.15-meter-height column specimens which were tested under combinations of axial and cyclic lateral loads. The initial objective of the experimental project was to test a variety of FRP wrapping configurations for reinforced-concrete bridge columns. The tested columns were subjected to cyclic lateral loads combined to sustained axial loads. The selected loads were representative of service conditions for bridges and building, respectively. Two wrapping configurations were selected for the columns: the first one was based on a "conventional" design method while the second one was the outcome of a displacement-based design procedure. Although the original intent of the research program was to develop applicable solutions for bridge piers submitted to seismic load conditions, the results can be useful for low-rise structures in general. The analysis presented in this chapter covers the following topics: (i) an evaluation of the extent of seismic-related damages in the retrofitted columns; (ii) a comparison of the resistance and ductility of columns before and after the FRP retrofit; and (iii) a comparison of the efficiency of two wrapping configurations. The main characteristics of the specimens, rehabilitation techniques, testing apparatus and a selection of result highlights are presented and discussed here.

14.1 Introduction

The study reported here is part of a seismic retrofit project currently underway at the Earthquake Engineering and Structural Dynamics Research Centre (also known as the CRGP: Centre de recherche en génie parasismique) of the Université de

N. Roy (✉)
Université de Sherbrooke, Sherbrooke, QC, Canada
e-mail: Nathalie.Roy@USherbrooke.ca

A. Ilki et al. (eds.), *Seismic Risk Assessment and Retrofitting*, Geotechnical, Geological, and Earthquake Engineering 10, DOI 10.1007/978-90-481-2681-1_14,

Sherbrooke. The main objectives of the project were (1) to optimize a retrofitting method consisting of externally strengthening reinforced concrete columns with carbon fiber reinforced polymers and (2) to evaluate, by means of reverse-cyclic testing, the anticipated behavior improvement of those columns in a potential seismic event.

14.2 Experimental Program

Cyclic tests were performed on large-scale circular columns with properties defined to be representative of typical piers belonging to short-span bridge structures located in Eastern Canada. The 2.15-m high columns have a 300-mm diameter and are embedded in a massive stub that was anchored to a strong floor for the tests. The columns were cast vertically with a 30-MPa compressive strength concrete. This low concrete strength was chosen to be representative of old structures showing signs of relatively severe damages. The specified steel yield strength for the longitudinal reinforcement and the transverse reinforcement is 400 MPa. The longitudinal reinforcement volumetric ratio of ρ_l=2.5%, and the transverse reinforcement volumetric ratio of ρ_h=0.8% are typical of columns that were designed and constructed before the most recent modifications to the code requirements for a minimum amount of transverse reinforcement. The columns are thus expected to dissipate only very little energy during seismic events.

The sustained axial force (corresponding to $0.1A_g f_c'$ and $0.35A_g f_c'$) was applied to the columns by means of two hydraulic actuators, as shown on the test setup illustrated in Fig. 14.1. A photograph of a typical column prepared for testing is

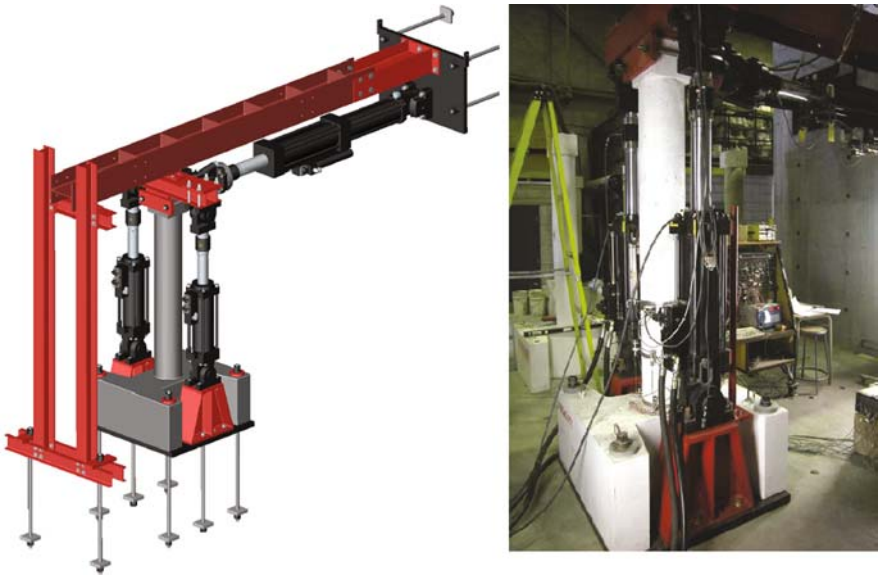

Fig. 14.1 Test setup (See also Plate 18 in Color Plate Section on page 466)

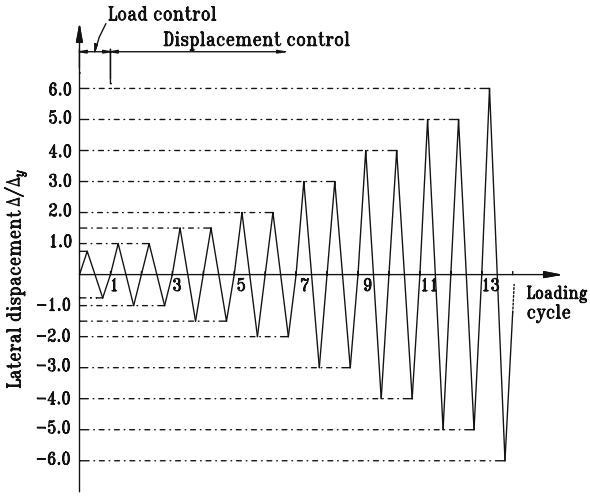

Fig. 14.2 Loading sequence

also shown in the same figure. The axial load was kept constant during the test. Prescribed displacement histories were imposed on the column by means of a 500 kN double-acting displacement-controlled dynamic-rated servo-hydraulic actuator reacting on a large-capacity vertical reaction wall. The purpose of the first cycle was to crack the column and to identify its initial elastic characteristics. In this cycle, the maximum horizontal load was set to reach 75% of the expected yield load. During the second cycle, the yield load was attained and the corresponding yield displacement was identified. Each subsequent cycle was repeated twice with a maximum displacement equal to 1.5, 2, 3, . . . n times the measured yield displacement up to failure. The loading sequence is shown in Fig. 14.2.

The columns were fully instrumented with strain gauges. One set of four linear variable displacement transducers (LVDTs) and two sets of four potentiometers were placed in the plastic hinge region on steel rings at respectively 25 mm, 325 mm and 625 mm from the bottom of the column.

14.3 Performance Based vs. Conventional Confinement

In the field of bridge engineering, the 1971 San Fernando earthquake was a turning point: it provided the impetus to incorporate significant modifications to American structural design standards. After this event, the consequences of other major earthquakes (e.g. Loma Prieta (1989), Northridge (1994) and Kobe (1995)) made owners, managers and design engineers aware of the potential benefits of designing and retrofitting structures according to performance objectives. In addition to better safeguarding human lives, it was shown that the adoption of performance objectives would reduce both the physical damages and the inherent cost of repair that follows earthquakes of intermediate intensity. The fundamental differences of this new

Table 14.1 Performance objectives of the CHBDC 2006

	Bridge classification		
Return period	Lifeline bridge	Emergency-route bridge	Other bridge
Design earthquake (475 years)	Open to all traffic	Open for security/defense purpose	Repairable damages
Large earthquake (1000 years)	Open for security/defense purpose	Repairable damages	No collapse

seismic design approaches were thus related to the following aspects: (i) the setting of performance objectives and, (ii) the definition of acceptable displacement criteria in order to meet the performance objectives.

Nowadays, many bridge codes have adopted the performance approach. For instance, the 2006 edition of the Canadian Highway Bridge Design Code (CHBDC) [1] used the performance approach that had already been adopted in its previous edition of year 2000. This approach is also recommended in the ATC-32 Improved Seismic Design Criteria for California Bridges: Provisional Recommendations [2] and the MCEER/ATC-49 Recommended LFRD guidelines for the seismic design of highway bridges [3]. In the CHBDC, the performance objectives listed in Table 14.1 are implemented for all new bridges. The performance objectives clearly depend on the intended use of the bridges following an earthquake with the potential return period identified in the table.

In the planning phases of the project reported in the present chapter, it was decided to select wrapping configurations for the columns according to two methodologies: the first one would be based on a "conventional" design method while the second one would be the outcome of a performance-based design procedure.

The performance-based retrofitting methodology used to optimize the confinement of RC columns with CFRP was proposed by Tian and Chaturvedi [4]. This method is based on the establishment of the following performance criterion: the retrofitted structure has to meet prescribed ductility and drift requirements for three levels of seismic events, each event corresponding to an exceedance level of either low (1/2500 p.a.), medium (1/1000 p.a.) or high (1/475 p.a.) probability. The conceptual performance matrix associated with this approach is illustrated in Fig. 14.3. The capacity spectrum method was utilized to calculate the applied loads for this performance-based approach and the non-linear structural response of the columns was accounted for.

The alternate conventional methodology was based on the establishment of a simplified relationship between ductility capacity and column aspect ratio. This method was proposed by Priestley et al. [5] and was shown to be suitable for force-based design of simple structures. In this case, the ductility capacity in displacement $\mu_{\Delta u}$ of the bridge structure is defined as $\mu_{\Delta u}=\Delta_u/\Delta_y$ where Δ_u is the ultimate top lateral

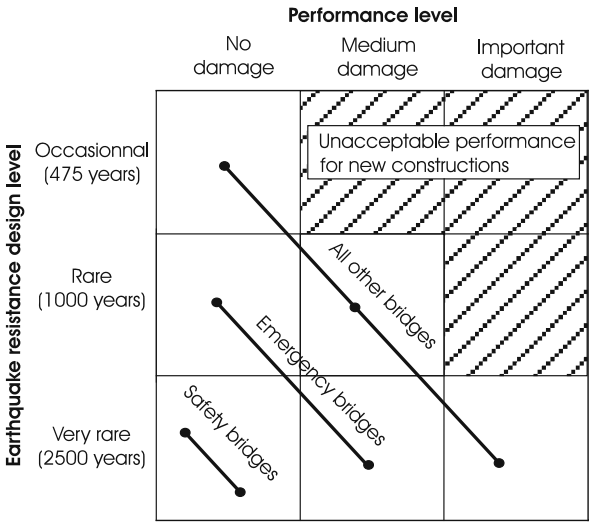

Fig. 14.3 Performance matrix

displacement and Δ_y is the yield top displacement of the column. The calculations to meet the required ductility level in each case led to two levels of confinement that correspond, considering the material chosen for the confinement (specified tensile strength of FRP f_{fu}=849 MPa, elastic modulus E_f =70552 MPa and thickness t_f =1.016 mm), to: (a) 2 layers of CFRP for the performance-based approach ($\mu_{\Delta u}$=3.5), and (b) 4 layers of CFRP for the conventional approach ($\mu_{\Delta u}$=5.0). The FRP-confined area of the columns was limited to the lower 635-mm length. This corresponds to approximately twice the distance to the anticipated location of the plastic hinge length.

14.4 Test Results

The appearance of three specimens at the end of the cyclic loading test is shown in Fig. 14.4. For the unconfined column S1, the concrete cover broke locally during the 3rd load cycle; column failure followed longitudinal buckling of a rebar during the 4th cycle. For the confined columns S2 and S3, horizontal cracks were observed above the CFRP layers and at the juncture between the CFRP-confined column area and the massive concrete stub. For S2, confined with two layers of CFRP, this crack became wider but did not appear to be associated with other damage events. At failure, a narrow band of CFRP broke almost simultaneously with a rupture of one longitudinal rebar anchored in the stub. For S3, confined with four layers of CFRP, the crack between the column and the stub developed soon during the 1st cycle. This crack remained stable through the following cycles until it started to open wider from the 4th cycle onwards. At the 7th cycle, it had reached a width of 35 mm. Finally, at the 9th cycle, failure of a rebar at the bottom of the column led to the interruption of the test.

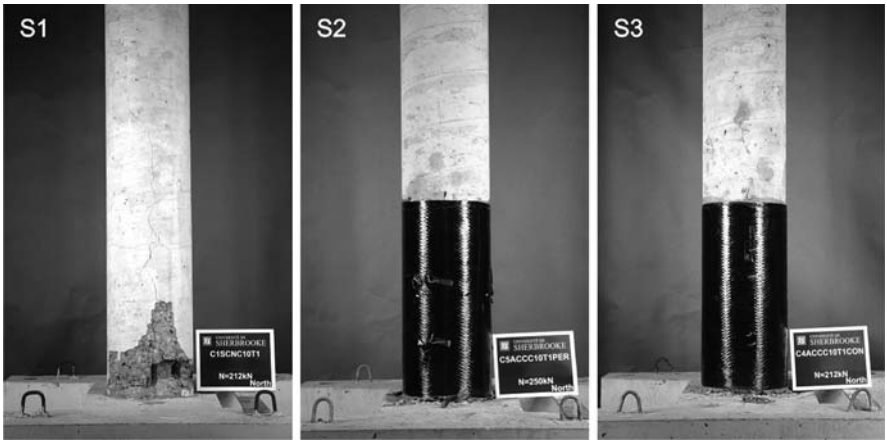

Fig. 14.4 Specimens S1, S2 and S3 after testing

The lateral load-tip deflection response of columns S1, S2 and S3 is shown in Figs. 14.5, 14.6 and 14.7, respectively. All three specimens were subjected to a constant axial load P equal to $10\%A_g f_c'$. Although it does not appear that there are significant differences in the value of the lateral load F that can be sustained by a confined column compared to an unconfined column with similar concrete properties and identical internal reinforcement, the increase in ductility caused by the external CFRP confinement is relatively obvious and can actually be estimated.

For instance, Paultre et al. [6] reported seismic response indicators quantified by structural ductility and by energy-dissipation capacity. The intrinsic interest of a structural ductility indicator is that it can somewhat be directly related to the seismic force reduction factor used in most design codes to calculate the seismic base shear. However, it has also been shown that energy-dissipation capacity is a better parameter to use in the design of short-period structures and structures subjected to long-duration earthquakes. The indicators that can generally be calculated using the

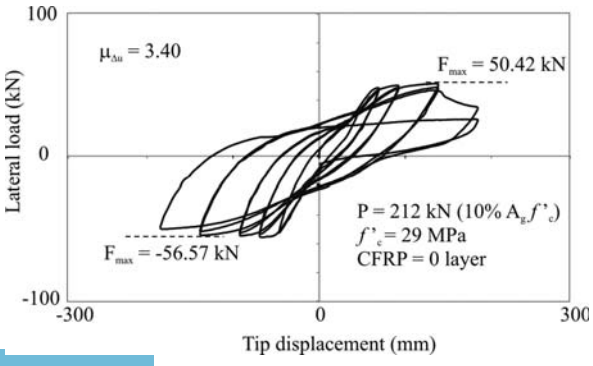

Fig. 14.5 Lateral load vs. tip displacement for column S1 (axial load corresponding to $10\%A_g f_c'$ and 0 layer of CFRP)

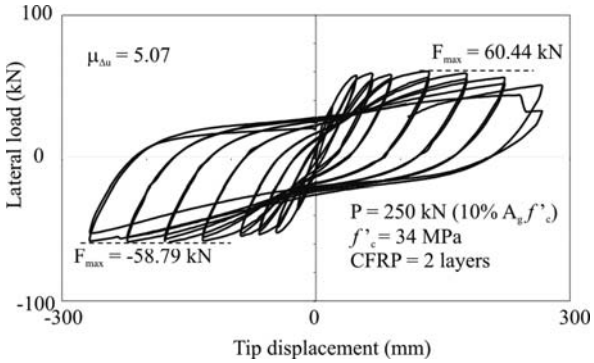

Fig. 14.6 Lateral load vs tip displacement for column S2 (axial load corresponding to $10\%A_g f_c'$ and 2 layers of CFRP)

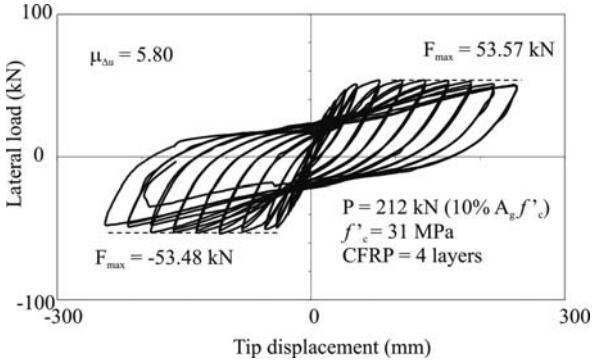

Fig. 14.7 Lateral load vs tip displacement for column S3 (axial load corresponding to $10\%A_g f_c'$ and 4 layers of CFRP)

cyclic lateral load-tip deflection curves such as the one shown in Figs. 14.5 to 14.7 are the ultimate displacement ductility $\mu_{\Delta u}$, Eq. 14.1, the ultimate sectional ductility $\mu_{\varphi u}$, Eq. 14.2, the maximum drift ratio $\delta_{\theta u}$, Eq. 14.3, the normalized dissipated energy E_N, Eq. 14.4, and the work index I_w, Eq. 14.5. The latter had been proposed by Gosain et al. [7].

$$\mu_{\Delta u} = \frac{\Delta_u}{\Delta_y} \tag{14.1}$$

$$\mu_{\varphi u} = \frac{\varphi_u}{\varphi_y} \tag{14.2}$$

$$\delta_{\theta u} = \frac{\Delta_u}{l} \tag{14.3}$$

$$E_N = \frac{1}{F_{\max}\Delta_{yI}} \sum_{i=1}^{n} E_i \tag{14.4}$$

$$I_w = \sum_{i=1}^{n} \frac{F_i \Delta_i}{F_{\max}\Delta_{yI}} \tag{14.5}$$

Table 14.2 Summary of results

Specimen	Axial load ($\%A_g f'_c$)	# layers of CFRP	$\mu_{\Delta u}$	$\mu_{\varphi u}$	$\delta_{\theta u}$ (%)	E_N	I_w
S1	10	0	3.5	7.7[a]	8.89	13.56	11.90
S2	10	2	5.1	8.0	12.88	34.18	25.05
S3	10	4	5.8	7.6	11.72	37.69	31.98

[a]calculated at 325 mm from column's base

The values calculated for the indicators presented above are presented in Table 14.2 in order to enable a rational comparison between the columns tested. The results show that structural ductility criteria were exceeded in both the performance-based and the conventional design. A good comparison between the unconfined and the confined columns can be observed with the normalized dissipated energy factors and work indexes. It can be observed that the values of the sectional ductility $\mu_{\varphi u}$ listed in Table 14.2 are almost the same for the three columns. It had been anticipated that these values would increase with the confinement level but, apparently, this is not the case. We explain this discrepancy by an unexpected movement between the steel rings holding the potentiometers and the confined concrete section. Another explanation of this behavior might be the accumulation of deformations out of the FRP retrofitted area.

A significant increase in structural ductility and energy dissipation for the confined columns is observed and this behavior is more pronounced between the columns having 0 and 2 layers of CFRP. The lower increase between the 2 and 4 layers of CFRP confined columns and the observation of the latter column after the test indicates that over-confinement can induce additional damage in regions close to the confined zone and highlights the fact that capacity design principles must be carefully considered in any seismic retrofit scheme.

14.5 Conclusion

Large-scale reinforced concrete circular columns were tested under combined axial and lateral cyclic loading. The confinement with CFRP varied from 0 to 2 and 4 layers of CFRP. The columns were subjected to a combination of a sustained axial load corresponding to 10 or 35% of the columns' axial load capacity and of a cyclic bending moment. It is shown here that, at sustained level of axial compression equal to 10% of the column capacity, the confinement influences the flexural behavior of the columns and significantly improves its seismic behavior in terms of structural ductility and energy dissipation. Structural ductility criteria were exceeded in both performance-based and conventional design. It is worthwhile to mention that the effect of the first 2 layers of CFRP confinement was more pronounced than the effect of the additional 2 layers. From the results of three typical columns presented here, there are indications that over-confinement may induce more damages to the

unconfined portions of the repaired column and that this effect must be properly accounted for.

Acknowledgments The authors would like to acknowledge the financial support of ISIS Canada, the Natural Sciences and Engineering Research Council of Canada (NSERC), the Fonds québécois pour la recherche sur la nature et les technologies (FQRNT) and Sika-Canada. They would also like to thank Marc Demers, Claude Aubé, Sébastien Gauthier and Laurent Thibodeau at the Université de Sherbrooke for their assistance in the laboratory.

References

1. Canadian Standard Association (2006) Canadian highway bridge design code CAN/CSA S6-06. Toronto, Ontario
2. Applied Technology Council (1996) Improved seismic design criteria for California bridges: Provisional Recommendations ATC-32, Redwood City, California
3. Applied Technology Council and Multidisciplinary Center for Earthquake Engineering Research (2003) Recommended LFRD guidelines for the seismic design of highway bridges. MCEER/ATC-49 Redwood City, California
4. Tian Y, Chaturvedi SK (2004) A seismic retrofit design methodology for R/C bridge columns using fiber composites. Earthquake Spectra, 20(2):483–502
5. Priestley MJN, Seible F, Calvi GM (1996) Seismic design and retrofit of bridges. John Wiley & Sons, New York
6. Paultre P, Légeron F, Mongeau D (2001) Influence of concrete strength and transverse reinforcement yield strength on behavior of high-strength concrete columns. ACI Structural Journal, 98(4):490–501
7. Gosain NK, Brown RH, Jirsa JO (1977) Shear requirements for load reversals on R.C. members. Journal of the Structural Division, Proceedings of the ASCE, 103(7):1461–1475

Chapter 15
Upgrading of Resistance and Cyclic Deformation Capacity of Deficient Concrete Columns

Dionysis Biskinis and Michael N. Fardis

Abstract Rules and expressions are presented for the calculation of the flexural and shear strength, the secant stiffness to yield point and the cyclic deformation capacity of concrete members retrofitted with fiber reinforced polymer (FRP) or concrete jackets, including the case of lap splicing of the longitudinal bars of the original member within the plastic hinge region. They are developed/calibrated on the basis of test results for retrofitted members, including pre-damaged ones. They represent an advancement over rules proposed earlier by the same authors and adopted in Annex A of Part 3 of Eurocode 8 for the retrofitting of concrete members.

15.1 Introduction

Columns are the most critical elements of existing low-rise concrete buildings. Their deficient deformation capacity is often aggravated by short lap-splicing of their vertical bars at floor levels, i.e., where plastic hinges form. The most widely used retrofitting technique for such columns is jacketing of their full storey height with reinforced concrete, while wrapping of their ends with fibre-reinforced polymers (FRPs), is coming up as an overall cost-effective technique. Design of the retrofitting requires knowledge of important properties of the retrofitted members, such as their cyclic lateral strength, secant stiffness to yield point and cyclic deformation capacity, as a function of the parameters of the retrofitting.

On the basis of a large database of cyclic tests carried out at the Structures Laboratory of the University of Patras or elsewhere rules and expressions are developed for the calculation of the flexural and cyclic shear strength, the secant stiffness to yield point and the flexure-controlled cyclic deformation capacity of reinforced concrete (RC) members retrofitted with FRP or concrete jackets, including as a special case the effect of lap-splicing of vertical bars of the original column within the plastic hinge region. These rules combine satisfactory accuracy with simplicity and practicality for everyday retrofit design by the average structural engineer.

M.N. Fardis (✉)
Department of Civil Engineering, University of Patras, Greece
e-mail: fardis@upatras.gr

A. Ilki et al. (eds.), *Seismic Risk Assessment and Retrofitting*, Geotechnical, Geological, and Earthquake Engineering 10, DOI 10.1007/978-90-481-2681-1_15,

15.2 RC-Jacketing of Columns

Jacketing a column is the most cost-effective way to enhance at the same time:

1. its flexural resistance (even converting a weak-column/strong-beam frame into a strong-column/weak-beam one),
2. its lateral stiffness,
3. its shear strength,
4. its deformation capacity and
5. anchorage and continuity of reinforcement in anchorage or splicing zones.

Enhancement of lateral stiffness and flexural resistance is made possible by the increased cross-sectional dimensions and the added longitudinal reinforcement, which – very importantly and in contrast to other retrofit techniques of individual members – can easily extend beyond the member end into and through joint regions. The main contributor to shear strength, deformation capacity and anchorage and splicing of reinforcement is the added transverse reinforcement (acting both against shear and as confining and antibuckling agent).

The multiple effectiveness of concrete jackets is what mainly differentiates them from other techniques of seismic retrofitting individual concrete members, such as wrapping by FRPs, that cannot readily extend beyond the member end and into joint regions. Such techniques are used mainly to enhance some or all of the properties 2–5 above, but normally not the flexural strength (item 1).

Being a composite member of two different concretes and two distinct cages of reinforcement with different detailing and often different types of steel, a jacketed member seems fairly complex and difficult to tackle in everyday retrofit design. The uncertain behaviour of the interface between the old member and the jacket adds to this difficulty. To reduce this problem to a level of simplicity consistent with the popularity of concrete jackets as an easy and low cost retrofitting technique, simple rules are developed for the estimation of the yield moment, the yield drift, the secant stiffness at incipient yielding and the flexure-controlled cyclic deformation capacity of jacketed members. To this end data from 57 monotonic or cyclic tests (55 on columns and two on walls) of members jacketed with concrete employing various bonding measures at the interface between the old and the new concrete, have been used to express the properties of the jacketed column in terms of the corresponding property of an "equivalent" monolithic member.

15.2.1 Strength, Stiffness and Deformation Capacity of Monolithic Concrete Members with Continuous Reinforcement

The yield moment, the secant stiffness at apparent yielding and the cyclic deformation capacity of the jacketed member are calculated here as a multiple or a fraction of the corresponding quantities of a monolithic member, as appropriate.

The chord rotation at member ends (angle between the normal to the end section and the chord between the ends) θ is the member deformation measure.

Apparent yielding is identified with the corner of a bilinear approximation of the monotonic force-deflection curve or of the envelope of loops in cyclic loading up to peak resistance. The effective flexural stiffness to yielding may be taken as:

$$EI_{\text{eff}} = M_{\text{y}} L_{\text{s}} / (3\theta_{\text{y}}) \tag{15.1}$$

where L_{s} is the shear span (moment-to-shear-ratio) at the end of the member, M_{y} is the moment at the corner of the bilinear envelope of the force-deflection curve, taken as the yield moment, and θ_{y} is the chord rotation at that corner point; θ_{y} can be estimated from the following expression fitted to test results [1, 2]:

- for beams or columns:

$$\theta_y = \varphi_y \frac{L_s + \alpha_v Z}{3} + 0.0014 \left(1 + 1.5 \frac{h}{L_s}\right) + a_{sl} \frac{\varphi_y d_{bL} f_y}{8\sqrt{f_c}} (f_{\text{y}}, f_{\text{c}} \text{ in MPa}) \tag{15.2a}$$

- for walls:

$$\theta_y = \varphi_y \frac{L_s + \alpha_v Z}{3} + 0.0013 + a_{sl} \frac{\varphi_y d_{bL} f_y}{8\sqrt{f_c}} (f_{\text{y}}, f_{\text{c}} \text{ in MPa}) \tag{15.2b}$$

where:

- φ_{y} is the yield curvature of the end section; the value of φ_{y} may taken equal to that computed from first principles for linear elastic $\sigma - \varepsilon$ behaviour with the following yield criteria (whichever is met first) [9]:
  - yielding of the extreme tension reinforcement, at a yield stress f_y,
  - a compression strain equal to $0.9f_{\text{c}}/E_{\text{c}}$ at the extreme compression fibers (with f_{c} and E_{c} denoting the strength and the Elastic Modulus of concrete);
    for better agreement with the test results of over 1850 beams or columns and of 110 rectangular walls, the so-computed value of φ_{y} should be multiplied by a calibration factor of 1.025 in beams and columns or of 1.03 in walls;
- $\alpha_v Z$ in the 1st (flexural) term is the tension shift of the moment diagram, with:
  - $z =$ internal lever arm (distance of tension to compression reinforcement),
  - $a_{\text{V}} = 1$ if shear cracking precedes flexural yielding of the end section, i.e. if the $M_{\text{y}}/L_{\text{s}}$ exceeds the shear resistance without shear reinforcement, $V_{\text{R,c}}$;
  - $a_{\text{V}} = 0$ if $M_{\text{y}} < L_{\text{s}} V_{\text{R,c}}$.
- h is the depth of the cross-section,
- d_{bL} is the diameter of longitudinal bars,
- a_{sl} in the 3rd term (expressing the fixed-end rotation due to slippage of longitudinal bars from their anchorage zone beyond the member end) is taken equal to:

– $a_{sl} = 1$ if bar slippage from the anchorage past the member end is possible,
– $a_{sl} = 0$ otherwise.

The flexure-controlled deformation capacity of the monolithic or of the jacketed member is expressed here in terms of the ultimate chord rotation. The ultimate chord rotation at the end of the member, θ_u (conventionally taken to coincide with the post-ultimate-strength deformation beyond which the lateral force resistance cannot increase above 80% of the ultimate strength when the imposed deformation increases); θ_u is taken as the sum of the chord rotation at yielding, θ_y, and of the plastic part of θ_u, denoted as ${\theta_u}^{pl}$. An empirical expression has been developed in [1, 2] (and adopted in [5]) for the value of ${\theta_u}^{pl}$ of members with rectangular compression zone and web, detailing for earthquake resistance and continuous longitudinal bars in the plastic hinge zone:

$$\theta_u^{pl} = d_{sl}^{pl}(1-0.52a_{cy})\left(1+\frac{a_{sl}}{1.6}\right)(1-0.44a_{wall})\cdot(0.25)^{\nu} \left(\frac{\max(0.01;\omega_2)}{\max(0.01;\omega_1)}\right)^{0.3} f_c^{0.2}\left(\min\left(9;\frac{L_s}{h}\right)\right)^{0.35} 25^{\left(\alpha_s\rho_s\frac{f_{yw}}{f_c}\right)} 1.275^{100\rho_d} \quad (f_c \text{ in MPa}) \tag{15.3}$$

where:

– $a^{\,pl}{}_{st} = 0.0185$ for ductile hot-rolled or heat-treated (Tempcore) steel; $a^{\,pl}{}_{st} = 0.009$ for cold-worked steel,
– $a_{cy} = 0$ for monotonic loading and $a_{cy} = 1.0$ for cyclic,
– $a_{wall} = 0$ for beams or columns and $a_{wall} = 1.0$ for walls,
– $\nu = N/bhf_c$ (with b being the width of the compression zone and the axial force N considered positive for compression),
– $\omega_1 = \rho_1 f_y/f_c$, mechanical reinforcement ratio of tension longitudinal reinforcement (including any longitudinal reinforcement between the two flanges),
– $\omega_2 = \rho_2 f_y/f_c$, mechanical reinforcement ratio of compression, reinforcement,
– $\rho_s = A_s/b_w s$, transverse steel ratio parallel in the direction of loading,
– ρ_d: ratio of diagonal reinforcement in each diagonal direction,
– f_{yw}: yield stress of transverse reinforcement,
– α_s: confinement effectiveness factor of transverse reinforcement [10, 5]:

$$a_s = \left(1-\frac{s}{2b_{xo}}\right)\left(1-\frac{s}{2b_{yo}}\right)\left(1-\frac{\sum b_i^2/6}{b_{xo}b_{yo}}\right) \tag{15.4}$$

where s denotes the centreline spacing of stirrups and b_{xo}, b_{yo} the dimensions of the confined core to the centerline of the perimeter stirrup; the sum in the last term refers to the longitudinal bars (indexed by i, with b_i denoting their spacing along the perimeter) which are engaged by a corner or hook of a tie.

Equation 15.3 applies for the deformation capacity of the member as this is governed by flexure. It is well known, however, that a member that has previously

yielded in bending may reach ultimate conditions in shear (by diagonal tension or diagonal compression) before it attains its flexure-controlled ultimate chord rotation (i.e., the value given by Eq. 15.3), because the shear resistance of a flexural plastic hinge decreases with increasing inelastic cyclic displacements and may drop below the shear force M_y/L_s corresponding to flexural yielding of the end section.

The shear resistance against diagonal tension failure decreases with cyclic displacements after flexural yielding. With $\mu_\theta{}^{pl} = \mu_\theta\text{-}1$ denoting the plastic part of the ductility factor of the chord rotation at the member end, $\mu_\theta = \theta/\theta_y$, with θ_y from Eq. 15.2a,b, the axial force N taken positive for compression and zero for tension and for units MN and m, the following expression may be used [3, 5]:

$$V_R = \frac{h-x}{2L_s}\min\left(N;\, 0.55A_c f_c\right) + \left(1 - 0.05\min\left(5;\, \mu_\theta^{pl}\right)\right) \left[0.16\max\left(0.5;\, 100\rho_{tot}\right)\left(1 - 0.16\min\left(5; \frac{L_s}{h}\right)\right)\sqrt{f_c}A_c + V_w\right] \tag{15.5}$$

where:

- x is the neutral axis depth,
- $A_c = b_w d$ is the area of a section with web of width b_w and effective depth d,
- ρ_{tot} is the total longitudinal reinforcement ratio,
- $V_w = \rho_s b_w z f_{yw}$ is the contribution of transverse reinforcement to the shear resistance against diagonal tension according to a 45°-truss analogy.

Equation 15.5 applies for the shear resistance against diagonal tension failure. Squat columns or walls may alternatively fail under cyclic loading by web crushing (diagonal compression) at a shear force less than that of Eq. 15.5 and a chord rotation smaller than that of Eq. 15.3 for flexure-controlled failure.

The cyclic shear resistance of *walls* against diagonal compression failure decreases with increasing ductility demand, $\mu^{pl}{}_\theta$, according to the expression [3, 5]:

$$V_{R,max} = 0.85\left(1 - 0.06\min\left(5;\, \mu_\theta^{pl}\right)\right)\left(1 + 1.8\min\left(0.15; \frac{N}{A_c f_c}\right)\right)\cdot \left(1 + 0.25\max\left(1.75;\, 100\rho_{tot}\right)\right)\left(1 - 0.2\min\left(2; \frac{L_s}{h}\right)\right) \sqrt{\min\left(100\,MPa; f_c\right)}\, b_w z \tag{15.6}$$

Equation 15.6 with $\mu^{pl}{}_\theta = 0$ gives also the cyclic shear resistance in diagonal compression (web crushing) of a wall before it yields in flexure.

A similar expression applies for squat (short) columns with shear span ratio, L_s/h, less than or equal to 2, that fail under cyclic loading after flexural yielding by web crushing along the diagonal of the column, which is at an angle $\delta = \arctan(0.5h/L_s)$ to the column axis [3, 5]:

$$V_{\mathrm{R,max}} = \frac{4}{7}\left(1 - 0.02\min\left(5;\mu_{\theta}^{\mathrm{pl}}\right)\right)\left(1 + 1.35\frac{N}{A_{\mathrm{c}}f_{\mathrm{c}}}\right)\cdot \\ (1 + 0.45(100\rho_{\mathrm{tot}}))\sqrt{\min\left(40\,MPa;f_{\mathrm{c}}\right)}b_{\mathrm{w}}z\sin 2\delta \tag{15.7}$$

15.2.2 Simple Rules for the Strength, the Stiffness and the Deformation Capacity of Jacketed Members

The rules proposed here on the basis of the tests in the database use modification factors on the properties of an "equivalent" monolithic member. The strength, the stiffness and the deformation capacity of the "equivalent" monolithic member are determined according to the rules above and to the additional considerations listed in Table 15.1 [4]. The idea behind assumptions A.3 and A.4 in this Table is that, for common ratios of jacket thickness to depth of the jacketed section, it is mainly the jacket that carries the full axial load at the critical end section and in the plastic hinge of the column. Also, it is the jacket that mainly controls the shear resistance and the bond along the longitudinal reinforcement of the jacket.

In the following, an asterisk is used to denote a calculated value for the jacketed member, as, e.g., in $M_{\mathrm{y}}{}^{*}$, $\theta_{\mathrm{y}}{}^{*}$, $\theta_{\mathrm{u}}{}^{*}$. No asterisk is used (as, e.g., in M_{y}, θ_{y}, $\theta_{\mathrm{u}}{}^{\mathrm{pl}}$) for values calculated for the monolithic member according to the assumptions in Table 15.1 and Eqs. 15.1, 15.2a,b, 15.3, and 15.4. Ratios of experimental values of M_{y}, θ_{y} and θ_{u} for the 57 jacketed members in the database to the values of M_{y}, θ_{y} and θ_{u} calculated for the monolithic member according to the assumptions in Table 15.1 and Eqs. 15.1, 15.2a,b, 15.3 and 15.4 are shown in Fig. 15.1 . Note that in Fig. 15.1 (bottom) $\theta_{\mathrm{u,cal}}$ is taken equal to $\theta_{\mathrm{y}}{}^{*}+\theta_{\mathrm{u}}{}^{\mathrm{pl}}{}_{\mathrm{Eq.15.3}}$, with $\theta_{\mathrm{y}}{}^{*} = 1.05\theta_{\mathrm{y,\,Eq.15.2a,\,b}}$ being the overall best estimate of the chord rotation at yielding for the jacketed member (with θ_{y} from Eq. 15.2a,b). With so defined $\theta_{\mathrm{y}}{}^{*}$, in Fig. 15.1 (3rd figure from the top) the effective stiffness to yield point of the jacketed member is defined as: $EI^{*}_{\mathrm{eff}} = M_{\mathrm{y,cal}}L_{\mathrm{s}}/3\theta_{\mathrm{y}}{}^{*}$. The ratios $M_{\mathrm{y,exp}}/M_{\mathrm{y,calc}}$, $\theta_{\mathrm{y,exp}}/\theta_{\mathrm{y,\,Eq.\,15.2a,\,b}}$, $EI_{\mathrm{exp}}/EI^{*}_{\mathrm{eff}}$ and $\theta_{\mathrm{u,exp}}/\theta_{\mathrm{u,cal}}$ are given from top to bottom of Fig. 15.1 separately for different ways of connecting the jacket to the old member and separately for those members which had been damaged by testing before they were jacketed. Specimens in which the longitudinal reinforcement of the jacket did not continue beyond the member end, or specimens with lap-spliced reinforcement in the original member, are identified in Fig. 15.1 but otherwise lumped together with those tests where the vertical bars in the original member were continuous. For tests that did not reach ultimate conditions and for the two walls that failed in the unstrengthened part of their height, an arrow pointing up signifies an experimental-to-predicted ratio greater than the plotted value.

The average value and ± standard-deviation estimates of the mean test-to-prediction ratios are shown in Fig. 15.1 separately for the various groups of specimens representing different types of jacket-to-old-member connection, with or without damage in the original column. Note that, the distance of the sample average

Table 15.1 Assumptions for the properties of a monolithic member considered as "equivalent" to the jacketed one

I. Flexural resistance and deformation capacity, deformations at flexural yielding	
Case A: Jacket longitudinal bars are anchored beyond the member end sections:	
A1: Dimensions	External dimensions of the section are those of the jacket.
A2: Longitudinal reinforcement	The tension and compression reinforcement are those of the jacket. Longitudinal bars of the old member are considered at their actual location between the tension and compression bars of the jacket: they may supplement longitudinal bars of the jacket between the tension and compression reinforcement and be included in a uniform "web" reinforcement ratio between the tension and compression bars in walls the tension and compression reinforcement of the jacketed member may include old vertical bars at the edges, as appropriate. Lap splices in the intermediate old reinforcement may be neglected. Differences in yield stress between the new and old longitudinal reinforcement should be taken into account, in all cases.
A3: Concrete strength	The f_c value of the jacket applies over the full section of the monolithic member; in the 3rd term of Eq. 15.2a,b, the f_c value of the concrete into which the longitudinal bars are anchored beyond the end section is used.
A4: Axial load	The full axial load is taken to act on the jacketed column as a whole, although it was originally applied to the old column alone.
A5: Transverse reinforcement	Only the transverse reinforcement in the jacket is taken into account for confinement.
Case B. Jacket longitudinal reinforcement stops at the end section:	
B1: Dimensions, longitudinal reinforcement, concrete strength	M_y and φ_y (also in the 1st and 3rd term of Eq. 15.2a,b) are calculated using the cross-sectional dimensions, the longitudinal reinforcement and the f_c value of the old member, neglecting any contribution from the jacket. The effect of lap splicing of the old bars is taken into account as in [1, 2]. The section depth h in the 2nd term of Eq. 15.2a,b is that of the jacket.

Table 15.1 (continued)

B2: Transverse reinforcement	The deformation capacity, θu, is calculated on the basis of the old column alone, with the old column taken as confined by the jacket and its transverse steel. The value of $\rho_s = A_s/b_w s$ for Eq. 15.3 is determined using the value of A_s/s in the jacket and taking as b_w the width of the old column. The confinement effectiveness factor may be taken $\alpha_s = 1.0$.
II. Shear resistance	
Shear resistance (including that without shear reinforcement, $V_{R,c}$, for the determination of the value of α_V in the 1st term of Eq. 15.2a,b) and anything that has to do with shear is calculated on the basis of the external dimensions and the transverse reinforcement of the jacket. The contribution of the old transverse reinforcement may be considered only in walls, provided it is well anchored into the (new) boundary elements.	

from a certain reference value (e.g. 1.0), normalised by the standard-deviation of the mean is a criterion on whether the value of the property of the jacketed member may be taken equal to that calculated for the monolithic member according to the assumptions in Table 15.1 and Eqs. 15.1, 15.2a,b, 15.3 and 15.4 times that reference value.

Figure 15.1 supports the following rules for calculating the yield moment, the chord rotation at the yield point and the ultimate chord rotation, $M_y{}^*$, $\theta_y{}^*$, $\theta_u{}^*$, respectively, of the jacketed member, in terms of the values M_y, θ_y, $\theta_u{}^{pl}$ calculated for the monolithic member according to Table 15.1 and Eqs. 15.1, 15.2a,b, 15.3 and 15.4:

1. For M_y* :

$$M_y* = M_{y,calc} \tag{15.8}$$

2. For $\theta_y{}^*$ (the main target being the stiffness at yield point, $EI^*{}_{eff} = M_{y,cal}L_s/3\theta_y{}^*$ with $M_y{}^* = M_{y,calc}$), irrespective of any pre-damage in the original column:

$$\theta_y^* = 1.05\theta_{y,Eq.15.2a,b} \tag{15.9}$$

(In [5] this rule has been adopted only for a roughened interface of the jacket to the old concrete, with or without dowels, but the more conservative rule: $\theta_y{}^* = 1.2\theta_{y,\ Eq.\ 15.2a,\ b}$ has been adopted [5] for no treatment of the interface, or dowels alone, or jacket bars connected to the old ones via welded U-bars).

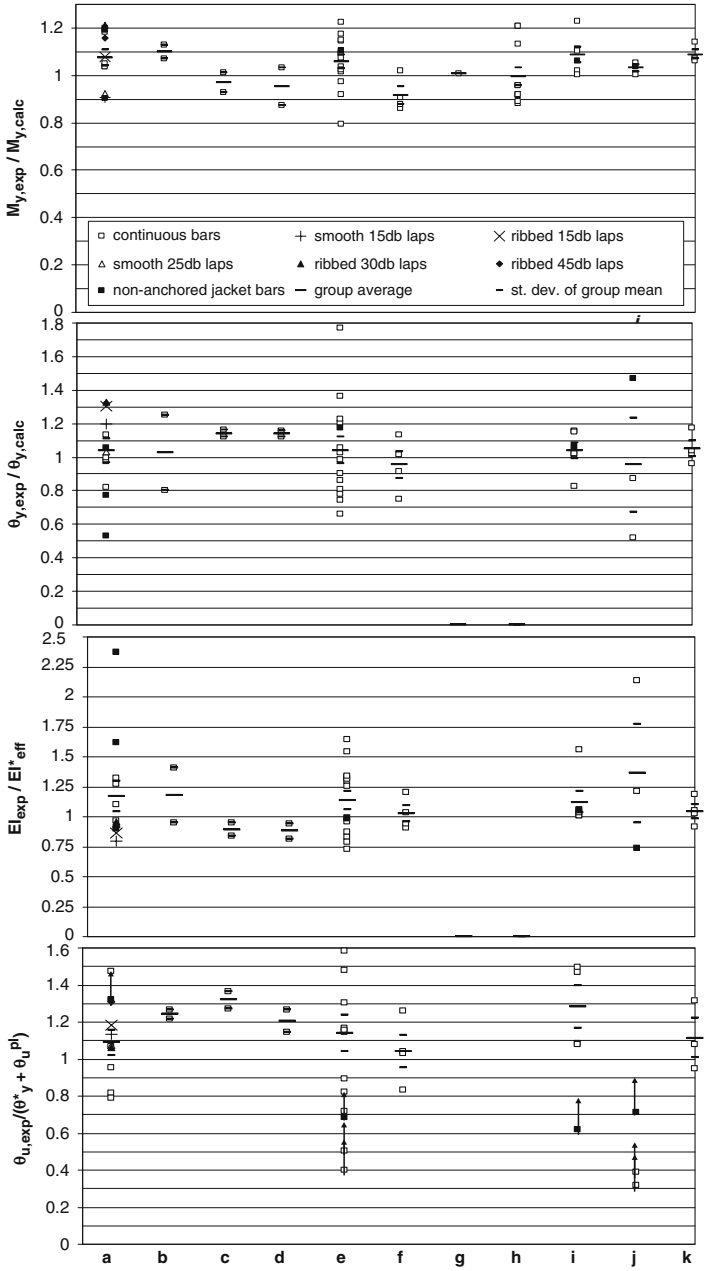

Legend:
a: no treatment of interface,
b: no treatment, predamaged member,
c: welded U-bars,
d: dowels,
e: roughened interface,
f: roughened interface, member pre-damaged,
g: U-bars and roughened interface,
h: U-bars and roughened interface, member pre-damaged,
i: dowels and roughened interface,
j: dowels and roughened interface, member pre-damaged,
k: monolithic member

Fig. 15.1 Experimental value for the RC-jacketed member divided to value calculated for the monolithic member according to Table 15.1

3. For θ_u*:

$$\theta_{\mathrm{u}}^{*} = \theta_{\mathrm{y}}^{*} + \theta_{\mathrm{u}}^{\mathrm{pl}}{}_{\mathrm{Eq.15.3}} \tag{15.10}$$

Rules 1–3, supplemented with assumptions B1 and B2 in Table 15.1, apply also if the jacket longitudinal bars stop at the end section of the member.

If no differentiation is made for the measure taken to enhance the shear transfer at the interface of the old and the new concrete, the ratio of the experimental value to the prediction from rules 1–3 above has overall median value and coefficient-of-variation equal to 1.035 and 10.7%, 0.99 and 23.5%, 1.005 and 30.5%, and 1.145 and 19% for M_{y}, θ_{y}, EI_{eff} and θ_{u}, respectively.

Bonding measures at the interface of the jacket and the old member seem to have a statistically significant effect only on the ultimate chord rotation, θ_{u}. The proposed rules underestimate on average the measured ultimate chord rotation, $\theta_{\mathrm{u,exp}}$, for roughening and/or dowels at the interface or for U-bars welded to the new and the old longitudinal bars. Even when no measure is taken to improve the interface between the old and the new concrete or connect the two materials there, the predictions undershoot the ultimate chord rotation of the jacketed member, but by less. So, it is safe-sided for the ultimate chord rotation, θ_{u}, to neglect the favourable effect of positive connection measures at the interface of the old and the new concrete, underestimating its measured value by 14.5% on average. No systematic positive effect of any connection measures on the yield moment, M_{y}, and the effective stiffness, EI_{eff}, has been found.

The coefficient-of-variation of the ratio of experimental M_{y}, θ_{y}, EI_{eff} and θ_{u} of monolithic members to those computed from 1st principles or Eqs. 15.1, 15.2a,b and 15.3 has been quantified in [1, 2]. It exceeds that of the jacketed members in Fig. 15.1.

The values of M_{y}, θ_{y}, EI_{eff} and θ_{u} predicted for the 57 jacketed specimens in the database as M_{y}*, θ_{y}*, EI *$_{\mathrm{eff}}$ or θ_{u}* above according to rules 1–3 above do not show a systematic bias with respect to any of the following:

- the ratio of f_{c} of the jacket to that of the old member;
- the ratio of the cross-sectional area of the jacket to that of the old member;
- the ratio of the yield stress times the longitudinal reinforcement ratio in the jacket, to the same product in the old member;
- the axial load, normalised to either the product of the full cross-sectional area of the jacketed section and of f_{c} of the jacket, or to the actual compressive strength of the jacketed section; and
- the ratio of the neutral axis depth at yielding to the thickness of the jacket.

The data do support assumptions A3 and A4 in Table 15.1, even when the compression zone extends beyond the jacket, into the section of the old column.

The 57 jacketed specimens in the database did not show any shear distress at failure. This is consistent with the fact that in all tests the shear resistance from Eqs. 15.5, 15.6 and 15.7 was higher by at least 30% than the maximum applied shear force.

15.3 FRP-Jacketing of Columns

15.3.1 Seismic Retrofitting with FRPs

Externally bonded Fibre Reinforced Polymers (FRPs) are used in seismic retrofitting in order to enhance or improve:

- the deformation capacity of flexural plastic hinges (with the fibres along the perimeter of the section and FRP wrapping all-along the plastic hinge);
- deficient lap splices (with the fibres as in 1 above and the FRP applied over at least the full lap length); and
- the shear resistance (with the fibres in the transverse direction where enhancement of shear strength is pursued).

FRPs do not lend themselves for enhancement of the flexural resistance of members against seismic actions even when their fibres are in the longitudinal direction of the member, as they cannot easily be continued into the joint beyond the member end section, where the seismic bending moment is maximum.

Despite their high cost-to-weight ratio, externally bonded FRPs are becoming the material of choice in seismic retrofitting applications, owing to their:

- high strength-to-weight ratio,
- satisfactory resistance to adverse environmental effects,
- easy handling and application (reducing labour costs and minimising disruption of use during installation) and
- very small thickness (minimising losses in premium floor plan area, when applied to vertical members).

15.3.2 FRP-Wrapped Columns with Continuous Vertical Bars

15.3.2.1 Yield Moment and Effective Stiffness to Yield Point

Equations 15.1 and 15.2a,b can be applied also to members with FRP-wrapping of their end regions, but with the following modifications:

In the calculation of the values of φ_y and M_y of FRP-wrapped columns on the basis of 1st principles, the unconfined concrete strength, f_c, is replaced by the value $f_c{}^*$ increased due to FRP confinement according to [6, 7]:

$$\frac{f_c^*}{f_c} = 1 + 3.3 \left(\frac{\min\left(b_x;\, b_y\right)}{\max\left(b_x;\, b_y\right)} \right)^2 a_f \frac{\rho_f f_{u,f}}{f_c} \tag{15.11}$$

where:

- b_x and b_y are the cross-sectional dimensions of the section,
- ρ_f is the geometric ratio of the FRP parallel to the direction of bending,

- a_f is the effectiveness factor for confinement by FRP of a rectangular section having its corners rounded to a radius R to apply the FRP:

$$a_f = 1 - \frac{(b_x - 2R)^2 + (b_y - 2R)^2}{3b_x b_y} \tag{15.12}$$

- $f_{u,f}$ is the effective strength of the FRP, taken according to [6, 7] as equal to:

$$f_{u,f} = E_f(k_{eff}\varepsilon_{u,f}) \tag{15.13}$$

where:

– E_f and $\varepsilon_{u,f}$ are the FRP's Elastic modulus and failure strain, respectively,
– k_{eff} is an FRP effectiveness factor, taken according to [6, 7] as equal to $k_{eff} = 0.6$ for Carbon FRP (CFRP) or Glass FRP (GFRP); for Aramid FRP (AFRP) and FRPs with polyacetal fibres the value of k_{eff} is taken here the same as for CFRP and GFRP ($k_{eff} = 0.85$ has been proposed in [6, 7] for AFRP on the basis of few test results).

The increase of concrete strength according to Eq. (15.11) is not sufficient to capture the enhancement of yield moment due to the confinement by FRP: as shown in Fig. 15.2 a and at the 1st row of statistics in Table 15.2 , the value of M_y computed on the basis of first principles is, on average, 6.5% less than the experimental value. So, when Eq. 15.2a,b is applied to members with FRP-wrapped ends using a value of θ_y from 1st principles, a coefficient of 1.065 should be applied on the 1st (flexural) term. The so-computed value of θ_y is compared in Fig. 15.2b to test results for not-pre-damaged columns wrapped with FRP.

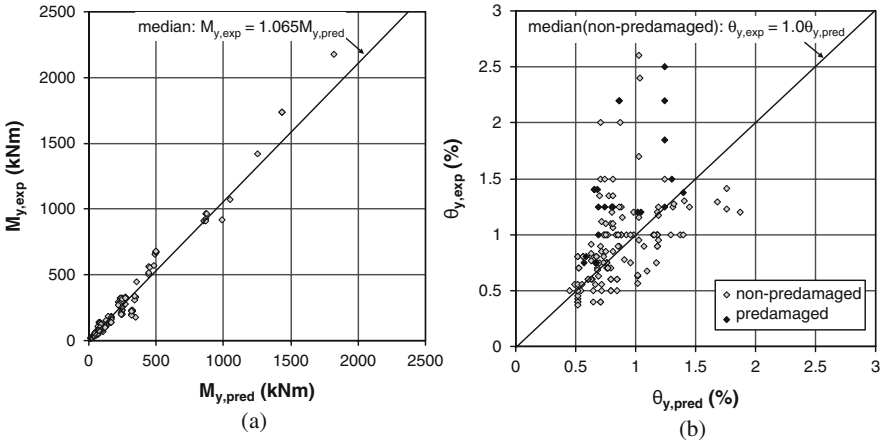

Fig. 15.2 FRP-wrapped *rectangular columns* with *continuous bars*: (**a**) experimental yield moment v prediction from 1st principles and Eq. 15.11 and 15.12; (**b**) experimental chord rotation at yielding v prediction of Eq. 15.2a,b

Table 15.2 Mean[a], median[a] and Coefficient of Variation (C.o.V.) of test-to-prediction ratios for FRP-wrapped rectangular columns with continuous or lap-spliced vertical bars

Row	Quantity	No tests	Mean[a]	Median[a]	CoV (%)
1	$M_{y,exp}/M_{y,pred.\text{-}1st\text{-}principles}$ continuous bars	180	1.065	1.065	19.6
2	$M_{y,exp}/M_{y,pred.\text{-}1st\text{-}principles}$ lap-spliced bars	31	1.06	1.06	11.4
3	$\theta_{y,exp}/\theta_{y,\ Eq.15.2a,\ b}$ no pre-damage, continuous bars	136	1.105	0.995	37.8
4	$\theta_{y,exp}/\theta_{y,\ Eq.15.2a,\ b}$ pre-damaged members, continuous bars	20	1.555	1.475	28.9
5	$\theta_{y,exp}/\theta_{y,\ Eq.15.2a,\ b}$ no pre-damage, lap-spliced bars	31	1.09	1.085	16.6
6	$(M_yL_s/3\theta_y)_{exp}/(EI_{eff})_{Eqs.\ 15.1,\ 15.2a,\ b}$ no pre-damage, continuous bars	136	1.085	1.055	28.7
7	$(M_yL_s/3\theta_y)_{exp}/(EI_{eff})_{Eqs.15.1,\ 15.2a,\ b}$ pre-damage, continuous bars	20	0.73	0.68	22.1
8	$(M_yL_s/3\theta_y)_{exp}/(EI_{eff})_{Eqs.\ 15.1,\ 15.2a,\ b}$ no pre-damage, lap-spliced bars	31	0.995	1.005	18.2
9	$\varphi_{u,exp}/\varphi_{u,\ Eqs.\ 15.11,\ 15.12,\ 15.13,\ 15.15,\ 15.16a,\ b}$ continuous bars	33	1.04	1.01	27.5
10	$\theta_{u,exp}/\theta_{u,Eqs.\ 15.2a,\ b,\ 15.11,\ 15.12,\ 15.13,\ 15.14,\ 15.15,\ 15.16a,\ b,\ 15.17,\ 15.18,\ 15.19}$ no pre-damage, continuous bars	94	1.095	0.995	34.6
11	$\theta_{u,exp}/\theta_{u,Eqs.15.2a,\ b,\ 15.3,\ 15.20}$ no pre-damage, continuous bars	94	1.135	1.095	31.8
12	$\theta_{u,exp}/\theta_{u,\ Eqs.\ 15.2a,\ b,\ 15.3,\ 15.21}$ no pre-damage, continuous bars	94	1.075	1.05	31.4
13	$\theta_{u,exp}/\theta_{u,\ Eqs.\ 15.2a,\ b,\ 15.3,\ 15.22}$ no pre-damage, continuous bars	94	1.07	1.03	31.4
14	$\theta_{u,exp}/\theta_{u,\ Eqs.\ 15.2a,\ b,\ 15.11,\ 15.12,\ 15.13,\ 15.14,\ 15.15,\ 15.16a,\ b,\ 15.17,\ 15.18,\ 15.19}$ pre-damaged continuous bars	18	0.995	0.985	23.1
15	$\theta_{u,exp}/\theta_{u,\ Eqs.\ 15.2a,\ b,\ 15.3,\ 15.20}$ pre-damaged continuous bars	18	0.96	0.93	23.1
16	$\theta_{u,exp}/\theta_{u,\ Eqs.\ 15.2a,\ b,\ 15.3,\ 15.21}$ pre-damaged continuous bars	18	0.945	0.925	23.2
17	$\theta_{u,exp}/\theta_{u,\ Eqs.\ 15.2a,\ b,\ 15.3,\ 15.22}$ pre-damaged continuous bars	18	0.93	0.945	25.4
18	$\theta_{u,exp}/\theta_{u,\ Eqs.\ 15.2a,\ b,\ 15.11,\ 15.12,\ 15.13,\ 15.14,\ 15.15,\ 15.16a,\ b,\ 15.17,\ 15.18,\ 15.19}$ continuous bars, all	112	1.075	0.995	33.4
19	$\theta_{u,exp}/\theta_{u,\ Eqs.\ 15.2a,\ b,\ 15.3,\ 15.20}$ continuous bars, all	112	1.105	1.085	31.4
20	$\theta_{u,exp}/\theta_{u,\ Eqs.\ 15.2a,\ b,\ 15.3,\ 15.21}$ continuous bars, all	112	1.055	1.035	30.8
21	$\theta_{u,exp}/\theta_{u,\ Eqs.\ 15.2a,\ b,\ 15.3,\ 15.22}$ continuous bars, all	112	1.045	1.025	31.1
22	$\theta_{u,exp}/\theta_{u,\ Eqs.\ 15.2a,\ b,\ 15.3,\ 15.20,\ 15.23\text{–}15.25}$ no pre-damage, lap-spliced bars	30	0.98	0.965	26.6

Table 15.2 (continued)

Row	Quantity	No tests	Mean[a]	Median[a]	CoV (%)
23	$\theta_{u,exp}/\theta_{u,\text{ Eqs. 15.2a, b, 15.3, 15.21, 15.23, 15.24, 15.26}}$ no pre-damage, spliced bars	30	0.945	0.925	28.4
24	$\theta_{u,exp}/\theta_{u,\text{ Eqs. 15.2a, b, 15.3, 15.22, 15.23, 15.24, 15.26}}$ no pre-damage, spliced bars	30	0.95	0.98	30.6
25	$V_{R,exp}/V_{R,\text{ Eqs. 15.5, 15.27}}$ diagonal tension failure	10	1.01	1.045	12.9
26	$V_{R,exp}/V_{R,\text{ Eqs. 15.5, 15.28}}$ diagonal tension failure	10	0.99	1.025	14.1
27	$V_{R,exp}/V_{R,\text{ Eqs. 15.7}}$ diagonal compression failure	4	1.15	1.17	9.7

[a] For large sample size the median reflects better the average trend than the mean.

The effective stiffness from Eq. 15.1 using the value of M_y from 1st principles and that of θ_y from Eq. 15.2a,b, with the 1st term incorporating the factor 1.065 of the paragraph above, is compared in Fig. 15.3 to experimental values. Table 15.2 gives also the statistics of the test-to-prediction ratio for the effective stiffness at yielding for FRP-wrapped columns.

Figure 15.2b and Table 15.2 show also the effect of serious previous damage (from yielding to exceedance of ultimate deformation) before repair, FRP-wrapping and re-testing. Such columns have also been included in the comparisons in Fig. 15.2a and in the 1st row of statistics in Table 15.2, showing that repair of the damage and FRP-wrapping fully re-instates the yield moment. However, Figs. 15.2b and

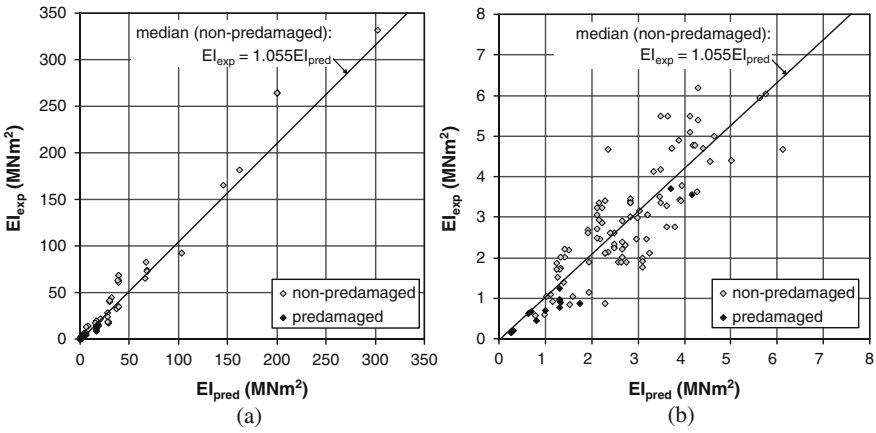

Fig. 15.3 (**a**) Experimental stiffness to yield point of FRP-wrapped *rectangular columns* with continuous bars, v effective stiffness from Eq. 15.1 with M_y from first principles and θ_y from Eq. 15.2a,b; (**b**) detail of (**a**)

15.3, as well as the 4th and 8th rows of statistics in Table 15.2, suggest that, despite the repair and the FRP-wrapping, previous damage markedly reduces the effective flexural stiffness to the yield point.

15.3.2.2 Flexure-Controlled Deformation Capacity

As in Section 15.2, the ultimate chord rotation, θ_u, can be expressed as the chord rotation at yielding, θ_y, computed as in Section 15.3.2.1, plus a plastic part, $\theta_u{}^{pl}$.

Two alternative types of model are proposed here for $\theta_u{}^{pl}$. In the first one, $\theta_u{}^{pl}$ is taken equal to the plastic component of the ultimate curvature, φ_u-φ_y, times a plastic-hinge length, L_{pl}, plus a fixed-end rotation due to bar pull-out from the anchorage zone past the member end. A large volume of data on flexure-controlled ultimate curvatures and chord rotations of rectangular members without FRP-wrapping suggest a fixed-end rotation equal on average to a yield penetration depth of 10 bar-diameters times the average of φ_y and φ_u (corresponding to linear strain hardening of the bar along the yield penetration depth):

$$\theta_u^{pl} = a_{sl}\frac{(\varphi_u + \varphi_y)}{2}10d_{bL} + (\varphi_u - \varphi_y)L_{pl}\left(1 - \frac{L_{pl}}{2L_s}\right) \tag{15.14}$$

Empirical expressions for L_{pl} depend on the models used for φ_y and φ_u. The model used here for φ_y is the one used for Eq. 15.2a,b, based on plane-section analysis and a strength of FRP-confined concrete, $f_c{}^*$, from Eq. 15.11. The model for φ_u is also based on plane-section analysis. For flexural failure in cyclic loading due to rupture of the extreme tension bars it uses a limit strain, ε_{su}, equal to 3/8 the steel uniform elongation at ultimate strength [1]. The concrete $\sigma - \varepsilon$ law is taken as parabolic-trapezoidal with ultimate strength from Eqs. 15.11, 15.12 and 15.13 [6, 7]. If the ultimate strain, $\varepsilon_{cu}{}^*$, is also taken according to [6, 7], the flexure-controlled ultimate curvature and chord rotation of rectangular FRP-wrapped members is considerably under-estimated. So, a different ultimate strain value has been fitted to these data:

$$\varepsilon_{cu}^* = 0.0035 + \left(\frac{10}{h}\right)^2 + 0.4a_f \min\left[0.5;\ \frac{\rho_f f_{u,f}}{f_c^*}\right] a_{eff,j} \tag{15.15}$$

Equation 15.15 is a modification/extension of Eq. 15.18, which has been fitted to a very large database of non-wrapped members failing in flexure under cyclic loading. In Eq. 15.15 the section depth, h , is in mm and ρ_f, a_f, $f_{u,f}$ were defined above via, or in conjunction with, Eqs. 15.11, 15.12 and 15.13. The additional parameter is another effectiveness factor for the FRP jacket, expressing that its effectiveness is not proportional to the geometric ratio and stiffness of the FRP:

$$a_{eff,j} = 0.5\left(1 - \min\left[0.5;\ \frac{\rho_f f_{u,f}}{f_c^*}\right]\right) \text{ for CFRP, GFRP,} \tag{15.16a}$$

$$a_{eff,j} = 0.3\left(1 - \min\left[0.5; \frac{\rho_f f_{u,f}}{f_c^*}\right]\right) \text{ for } \quad \text{AFRP} \tag{15.16b}$$

Note that, if the FRP provides relatively light confinement compared to the transverse reinforcement, the end section may survive rupture of the FRP jacket and attain later a larger ultimate curvature controlled by the confined concrete core inside the stirrups. That ultimate curvature can again be computed on the basis of first principles, but using a parabolic-rectangular $\sigma - \varepsilon$ law for confined concrete, with a confined concrete strength according to [5, 8], first attained at a strain, $\varepsilon_{co}{}^*$, exceeding the corresponding value of unconfined concrete, $\varepsilon_{co} = 0.002$:

$$\frac{f_c^*}{f_c} = 1 + \left(\frac{a_s \rho_s f_{yw}}{f_c}\right)^{0.86}, \frac{\varepsilon_{co}^*}{\varepsilon_{co}} = 1 + 5\left(\frac{a_s \rho_s f_{yw}}{f_c}\right)^{0.86} \tag{15.17}$$

The ultimate strain of the confined concrete core, $\varepsilon_{cu}{}^*$, has been fitted in [1] to data on flexure-controlled ultimate curvatures and chord rotations of rectangular RC members without FRP-wrapping:

$$\varepsilon_{cu}^* = 0.0035 + \left(\frac{10}{h_c}\right)^2 + 0.4\frac{a_s \rho_s f_{yw}}{f_c^*} \tag{15.18}$$

In Eqs. 15.17 and 15.18 ρ_s is the geometric ratio of the transverse reinforcement in the loading direction and α_s its confinement effectiveness factor given by Eq. 15.4. In Eq. 15.18 h_c is the depth of the confined core in mm.

The following empirical expression for the plastic hinge length, L_{pl}, has been fitted to 1300 test results on flexure-controlled cyclic ultimate chord rotations of beams and columns without FRP-wrapping:

$$L_{pl} = 0.2\,h\left[1 + \frac{1}{3}\min\left(9; \frac{L_s}{h}\right)\right] \tag{15.19}$$

It has been proposed in [1, 2] and adopted in [5] to extend the empirical model for $\theta_u{}^{pl}$, Eq. 15.3, to members with FRP wrapping by including in the exponent of the 2nd term from the end the effect of confinement by the FRP, adding to it the term $a_f \rho_f f_{f,e}$, where ρ_f and a_f were defined above via, or in conjunction with, Eqs. 15.11 and 15.12, and $f_{f,e}$, is the effective stress of the FRP:

$$f_{f,e} = \min\left(f_{fu,nom}; \varepsilon_{u,f} E_f\right)\left(1 - \min\left[0.5; 0.7\min\left(f_{fu,nom}; \varepsilon_{u,f} E_f\right)\frac{\rho_f}{f_c}\right]\right) \tag{15.20}$$

with $f_{fu,nom}$ denoting the nominal strength of the FRP and $\varepsilon_{u,f}$ being a limit strain:

- $\varepsilon_{u,f} = 0.015$ for CFRP or AFRP;
- $\varepsilon_{u,f} = 0.02$ for GFRP.

It is proposed here to improve the extension of Eq. 15.3 by adding to the exponent of the 2nd term from the end of Eq. 15.3 a term for the FRP symbolized by the left-hand-side of the following expression and given by its right-hand-side:

$$\left(\frac{a\rho f_u}{f_c}\right)_{f,eff} = a_f \min\left[1.0; \min\left(f_{fu,nom}; \varepsilon_{u,f} E_f\right) \frac{\rho_f}{f_c}\right] \left(1 - 0.4 \min\left[1.0; \min\left(f_{fu,nom}; \varepsilon_{u,f} E_f\right) \frac{\rho_f}{f_c}\right]\right) \tag{15.21}$$

with the limit strain always equal to $\varepsilon_{u,f} = 0.015$. About the same fit to the tests is achieved if the FRP-confinement term added to the exponent of the 2nd term from the end of Eq. 15.3 is based on the effective FRP strength in Eq. 15.13. This alternative, which is more consistent with the confinement model in [6, 7], is:

$$\left(\frac{a\rho f_u}{f_c}\right)_{f,eff} = a_f c_f \min\left[0.4; \frac{\rho_f f_{u,f}}{f_c}\right] \left(1 - 0.5 \min\left[0.4; \frac{\rho_f f_{u,f}}{f_c}\right]\right) \tag{15.22}$$

where $c_f = 1.8$ for CFRP and $c_f = 0.8$ for GFRP or AFRP.

The last term in each one of Eqs. 15.16a,b, 15.20, 15.21 and 15.22 reflects the experimentally documented reduced effectiveness of larger amounts of FRP wrapping.

Figures 15.4 and 15.5 compare the predictions of the models for θ_u (Eqs. 15.2a,b, 15.11, 15.12, 15.13, 15.14, 15.15, 15.16a,b, 15.17, 15.18 and 15.19, or Eqs. 15.2a,b, 15.3 with Eqs. 15.20, 15.21, or 15.22) to the test results for FRP-wrapped columns to which the models were fitted. Rows 10–13 in Table 15.2 refer to the test-to-

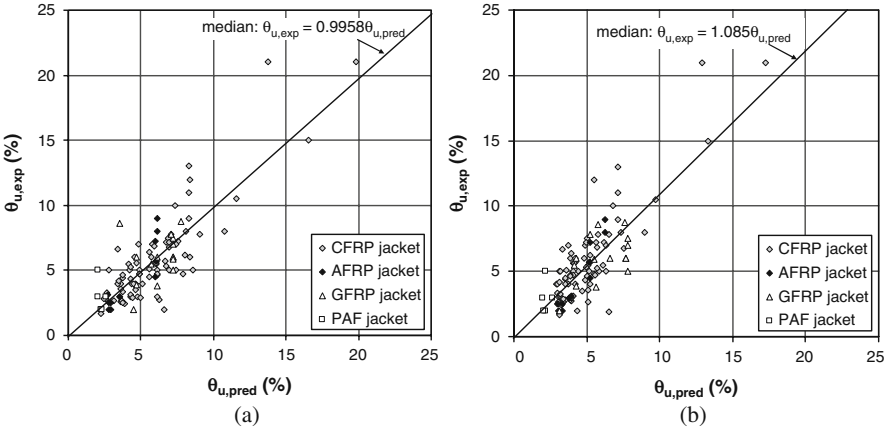

Fig. 15.4 Experimental ultimate chord rotation of FRP-wrapped *rectangular columns* with *continuous bars* v predictions: (**a**) of model based on plastic hinge length, Eqs. 15.11, 15.12, 15.13, 15.14, 15.15, 15.16a,b, 15.17, 15.18, 15.19 and 15.2a,b; (**b**) of empirical model, Eqs. 15.2a,b, 15.3 and 15.20

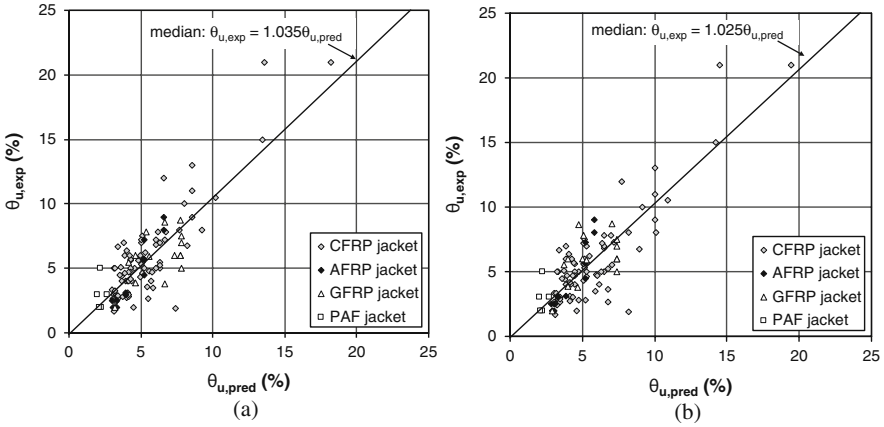

Fig. 15.5 Experimental ultimate chord rotation of FRP-wrapped *columns* with *continuous bars* v predictions of empirical model of Eqs. 15.2a,b, 15.3 and (**a**) 15.21; (**b**) 15.22

prediction ratios of θ_u for specimens without pre-damage, rows 14–17 for pre-damaged ones and rows 18–21 to all specimens, regardless of pre-damage. The results of Eqs. 15.2a,b, 15.11, 15.12, 15.13, 15.14, 15.15, 15.16a,b, 15.17, 15.18 and 15.19 show no evidence of an effect of pre-damage on ultimate chord rotation. Equations 15.20, 15.21, or 15.22, by contrast, do suggest a reduction of θ_u of about 10% due to pre-damage.

15.3.3 FRP-Wrapped Columns with Ribbed (Deformed) Vertical Bars Lap-Spliced in the Plastic Hinge Region

All rules proposed in the present section have been developed and calibrated on the basis of members with FRP wrapping applied over a length exceeding that of the lap. Accordingly, they should be applied only when such wrapping extends over a length from the end of the member at least, e.g., 125% of the lapping.

The available tests on rectangular RC members with ribbed (deformed) longitudinal bars lapped starting at the section of maximum moment show that, in the calculation of the yield curvature, φ_y, (used in the 1st and the 3rd term in Eq. 15.2a,b for θ_y), as well as of the yield moment, M_y, and of the plastic part of the flexure-controlled ultimate chord rotation, θ_u^{pl}, both bars in a pair of lapped compressed bars should count in the compression reinforcement ratio. Moreover, if the straight lap length, l_o, is less than a minimum value $l_{oy,min}$, then φ_y and M_y should be calculated using as yield stress of the tension reinforcement the value of f_y multiplied by $l_o/l_{oy,min}$, while the 2nd term of the right-hand-side of Eq. 15.2a,b should be multiplied by the ratio of the value of M_y as modified for the effect of lapping, to its value without it. If the length of the member where the lap splicing takes place is fully wrapped by FRP, which in the presence for FRP, the value of $l_{oy,min}$ is:

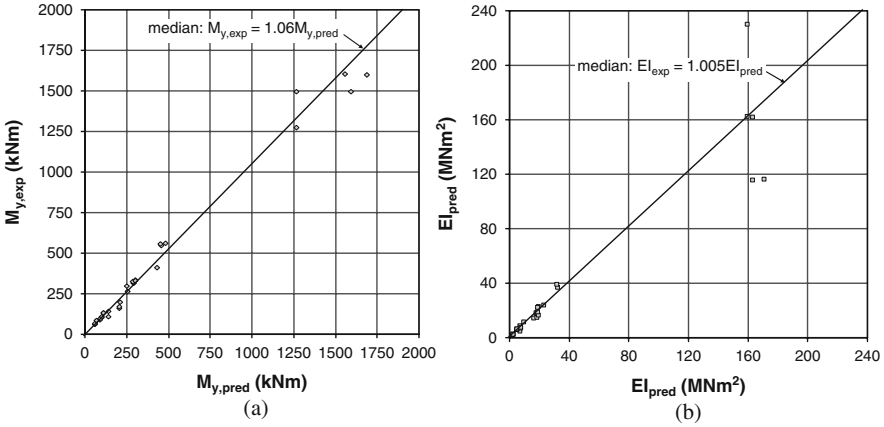

Fig. 15.6 Experimental: (**a**) yield moment and (**b**) effective stiffness of FRP-wrapped rectangular columns with lap-spliced *bars* , compared to predictions from first principles and Eq. 15.1, accounting for bar lap-splicing according to Section 15.3.3

$$l_{\text{oy,min}} = 0.2 d_{\text{bL}} f_{\text{y}} / \sqrt{f_c} (f_{\text{y}}, f_{\text{c}} \text{ in MPa}) \tag{15.23}$$

This rule is a modification of one derived from over one-hundred members with lap-spliced bars but no FRP wrapping. Experimental values of M_{y} and of the effective stiffness from Eq. 15.1 for FRP-wrapped columns with lap splices are compared in Fig. 15.6 to predictions with the effect of bar lapping taken into account according to the above rule. Rows 2, 5 and 8 in Table 15.2 refer to the test-to-prediction ratio of M_{y}, θ_{y} and effective stiffness of such columns.

Regarding the ultimate chord rotation of members with FRP wrapping of their lap-splice length, it has been proposed in [1] and adopted in [5] to extend a rule fitted to a large number of test results on rectangular columns with lap splices confined by the transverse reinforcement alone. According to this proposal the value of $\theta_{\text{u}}^{\text{pl}}$ from Eqs. 15.3, 15.20 is modified as follows, with $l_{\text{ou,min}}$ from Eq. 15.25:

$$\theta_{\text{u}}^{\text{pl}} = (l_{\text{o}} / l_{\text{ou,min}}) \theta_{\text{u}}^{\text{pl}}{}_{\text{Eqs.15.3,15.20}} \text{ if } l_{\text{o}} < l_{\text{ou,min}} \tag{15.24}$$

At the same time, if l_{o} is shorter than the value, $l_{\text{oy,min}}$, from Eq. 15.23, the first paragraph of the present section is applied for the effect of bar splicing on θ_{y}, to be added to $\theta_{\text{u}}^{\text{pl}}$ from Eq. 15.24.

In [1] and [5] the minimum lap length beyond which the lapping does not adversely affect the flexure-controlled ultimate deformation is:

$$l_{ou,\,\min} = \frac{d_{bL} f_{yL}}{\left(1.05 + 14.5 \frac{4}{n_{tot}} a_f \frac{\rho_f f_{f,e}}{f_c}\right) \sqrt{f_c}} (f_{\text{yL}}, f_{\text{f,e}}, f_{\text{c}} \text{ in MPa}) \tag{15.25}$$

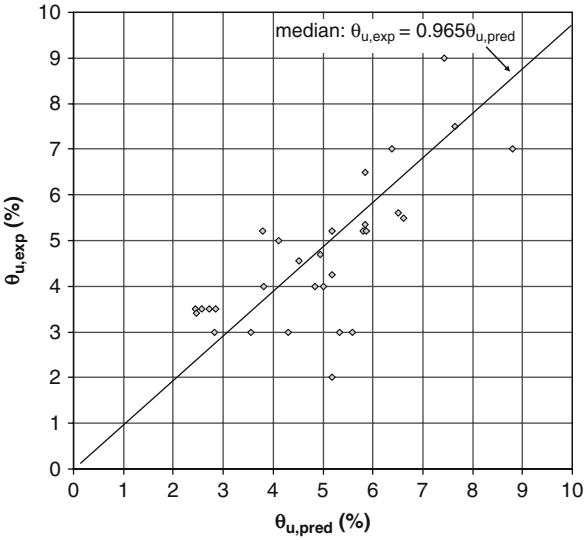

Fig. 15.7 Experimental ultimate chord rotation of FRP-wrapped *rectangular columns* with lap-spliced *bars*, compared to predictions from Eqs. 15.3, 15.24 and 15.25

where ρ_f, a_f and $f_{f,e}$ were defined in conjunction with Eqs. 15.11, 15.12, 15.20 and n_{tot} is the total number of lapped longitudinal bars along the cross-section perimeter (the term $4/n_{tot}$ is the fraction of the total number of lap splices confined by the FRP, as in rectangular columns only the four corner bars, are confined by the FRP wrapped around the corner). Figure 15.7 compares predictions with test results.

The natural extension of the improvement of the approach in [1, 5] by using Eq. 15.21 for the FRP-confinement term is to modify Eq. 15.25 as follows:

$$l_{ou,\min} = \frac{d_{bL} f_{yL}}{\left(1.05 + 14.5 \frac{4}{n_{tot}} \left(a \frac{\rho f_u}{f_c}\right)_{f,eff}\right) \sqrt{f_c}} (f_{yL}, f_{f,u}, E_f, f_c \text{ in MPa}) \qquad (15.26)$$

with $(a\rho f_u/f_c)_{f,eff}$ from Eq. 15.21. Another option is to use in the FRP-confinement term the effective FRP strength $f_{u,f}$ from Eq. 15.13 [6, 7]. This modification uses Eq. 15.22 for the FRP-confinement term in the calculation of $\theta_u{}^{pl}$ for members with continuous bars and FRP wrapping. It is extended to members with lap-spliced bars by using in Eq. 15.26 the value of $(a\rho f_u/f_c)_{f,eff}$ from Eq. 15.22.

The statistics in rows 22–23 of Table 15.2 suggest that, although the modifications of the approach in [1, 5] adding the term of Eqs. 15.21 or 15.22 to the exponent of the 2nd term from the end of Eq. 15.3, instead of using Eq. 15.20, improve the accuracy of the prediction of θ_u for members with continuous bars and FRP wrapping, do not do so if the bars inside the wrapping are lap-spliced. The predictions of Eq. 15.25 [1, 5], which seems to remain the best alternative, are compared in Fig. 15.7 to the experimental results.

Note that for the value of $\theta_u{}^{pl}$ before its reduction due to the lap splice the exponent of the 2nd term from the end reflects confinement by the ties as well as by the FRP (i.e., term $a_f \rho_f f_{f,e}$ is added when Eqs. 15.20 and 15.25 are used, or term

$(a\rho f_u/f_c)_{f,eff}$ from Eqs. 15.21, 15.22 instead if Eqs. 15.21 and 15.26 are applied), but confinement of lapped bars by the FRP alone is considered in Eqs. 15.25 and 15.26.

15.3.4 Cyclic Shear Resistance of FRP-Wrapped Columns

It has been proposed in [1] and adopted in [5] to modify Eq. 15.5 for the contribution of FRP wrapping to the cyclic shear resistance of the plastic hinge, as:

$$V_{R,FRP} = \frac{h-x}{2L_s}\min\left(N;\ 0.55A_c f_c\right) + \left(1 - 0.05\min\left(5;\ \mu_\theta^{pl}\right)\right)\cdot \left[0.16\max\left(0.5;100\rho_{tot}\right)\left(1 - 0.16\min\left(5;\frac{L_s}{h}\right)\right)\sqrt{f_c}A_c + V_w\right] + 0.5\rho_f b_w z E_f \varepsilon_{u,f} \tag{15.27}$$

where E_f and $\varepsilon_{u,f}$ are the FRP's Elastic modulus and nominal failure strain and the factor 0.5 accounts for the linear reduction of the FRP stress over the section depth, from its full failure value of $E_f\varepsilon_{u,f}$ at the extreme tension fibre to zero at the neutral axis. For 10 tests of FRP-wrapped columns that failed by diagonal tension under cyclic loading after flexural yielding, Fig. 15.8 depicts the test-to-prediction ratio for Eq. 15.27, as a function of the chord rotation ductility factor, $\mu_\theta = \theta/\theta_y$. Row 25 in Table 15.2 gives statistics of the ratio of experimental-to-predicted resistance in diagonal tension, V_R. For consistency with Eq. 15.13 and the effective, average strength of the FRP all around the column, $f_{u,f} = E_f(k_{eff}\varepsilon_{u,f})$ [6,7], as well as owing to a slight downwards tendency of the data in Fig. 15.8, the following alternative is depicted in Fig. 15.9:

$$V_{R,FRP} = \frac{h-x}{2L_s}\min\left(N;\ 0.55A_c f_c\right) + \left(1 - 0.05\min\left(5;\ \mu_\theta^{pl}\right)\right)\cdot \left[0.16\max\left(0.5;100\rho_{tot}\right)\left(1 - 0.16\min\left(5;\frac{L_s}{h}\right)\right)\sqrt{f_c}A_c + V_w + 0.5\rho_f b_w z f_{u,f}\right] \tag{15.28}$$

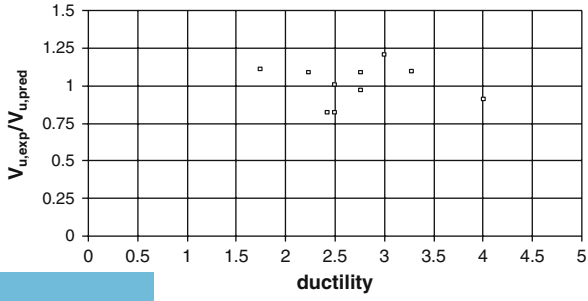

Fig. 15.8 Ratio of experimental shear resistance of FRP-wrapped columns failing by diagonal tension after flexural yielding, to V_R from Eq. 15.27

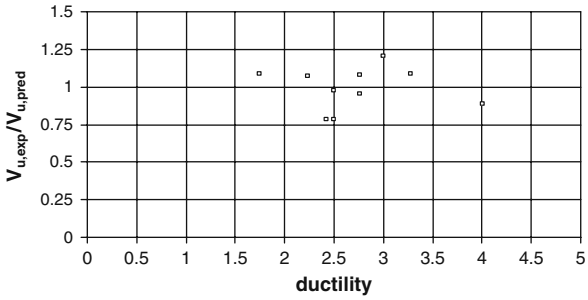

Fig. 15.9 Ratio of experimental shear resistance of FRP-wrapped columns failing by diagonal tension after flexural yielding to V_R from Eq. 15.28

It is clear from Fig. 15.9 and the statistics at the 2nd row from the bottom of Table 15.2, that the improvement effected by Eq. 15.28 is not significant. Equation 15.7, which was empirically fitted in [3] to cyclic tests of squat columns without FRP failing by diagonal compression after flexural yielding, is conservative for FRP-wrapped squat columns failing by diagonal compression after flexural yielding. This is suggested by the statistics at the bottom row of Table 15.2.

References

1. Biskinis DE (2007) Resistance and deformation capacity of concrete members with or without retrofitting. Thesis submitted to the Civil Engineering Department of the University of Patras, in partial fulfilment of the requirements for the Doctoral Degree, University of Patras, Greece
2. Biskinis DE, Fardis MN (2004) Cyclic strength and deformation capacity of RC members, including members retrofitted for earthquake resistance. *5th International Ph.D Symposium in Civil Engineering*, Delft (NL), Balkema, pp 1125–1133
3. Biskinis DE, Roupakias, G, Fardis MN (2004) Degradation of shear strength of RC members with inelastic cyclic displacements. ACI Structural Journal, 101(6):773–783
4. Bousias SN, Biskinis DE, Fardis MN, Spathis L-A (2007) Strength, stiffness and cyclic deformation capacity of concrete jacketed members. ACI Structural Journal, 103(4):521–531
5. CEN (2005) European Standard EN 1998–3:2005. Eurocode 8: Design of structures for earthquake resistance. Part 3: Assessment and retrofitting of buildings. Comite Europeen de Normalisation, Brussels
6. Lam L, Teng JG (2003) Design-oriented stress-strain model for FRP-confined concrete. Construction and Building Materials, 17(6&7):471–489
7. Lam L, Teng JG (2003) Design-oriented stress-strain model for FRP-confined concrete in rectangular columns. Journal of Reinforcing Plastics and Composites, 22(13):1149–1186
8. Newman K, Newman JB (1971) Failure theories and design criteria for plain concrete. In Structure, Solid Mechanics and Engineering Design (Te'eni, ed.), J Willey-Interscience, New York
9. Panagiotakos TB, Fardis MN (2001) Deformations of reinforced concrete members at yielding and ultimate. ACI Structural Journal, 98(2):135–148
10. Sheikh SA, Uzumeri SM (1982) Analytical model for concrete confinement in tied columns. Journal of Structural Division, ASCE, 108(ST12):2703–2722

Chapter 16
Supplemental Vertical Support as a Means for Seismic Retrofit of Buildings

Craig D. Comartin

Abstract A large number of concrete buildings in seismically active areas throughout the world exhibit a common deficiency. Weak columns, in one or more stories, lose vertical load-carrying capacity as a result of lateral distortion. This chapter presents a conceptual strategy for retrofit comprising the installation of supplemental vertical supports to prevent collapse. This procedure utilizes a risk-based perspective based on recent research on the realistic capacity of concrete columns, dynamic instability, and the effects of in-cycle degradation of strength in building systems and components. An example building is used to illustrate the application of the concept.

16.1 Introduction and Background

Buildings subject to earthquake shaking have a potential to reach a point of dynamic instability at which they collapse due to theoretically unlimited lateral displacement. Many buildings, however, lose the ability to support vertical loads and collapse at smaller levels of shaking intensity than that which would otherwise cause lateral dynamic instability (see Fig. 16.1). The procedures proposed here are intended to identify buildings prone to preemptive vertical load collapse and improve their safety by the installation of supplemental vertical supports. Maintaining the capability to support vertical loads changes the critical collapse mechanism to lateral dynamic stability which occurs at larger and less probable lateral displacements (see Fig. 16.2).

Experience in past earthquakes around the world indicates that concrete frames infilled with unreinforced masonry (URM) have been particularly prone to collapse [1]. This most often is due to a weak first story caused by the omission of all or a substantial portion of the infill to allow for retail, parking, or other uses conducive to

C.D. Comartin (✉)
CDComartin, Inc., Stockton, CA, USA
email: ccomartin@comartin.net

A. Ilki et al. (eds.), *Seismic Risk Assessment and Retrofitting*, Geotechnical, Geological, and Earthquake Engineering 10, DOI 10.1007/978-90-481-2681-1_16,

Fig. 16.1 Story collapse vertically downward without significant lateral movement (note vertical alignment with adjacent uncollapsed wing) (See also Plate 19 in Color Plate Section on page 467)

Fig. 16.2 Side sway mechanism with incipient collapse (See also Plate 20 in Color Plate Section on page 467)

open spaces. The infill in upper stories restrains frame action and forces the flexible lower floor to absorb most of the energy demand and drift.

There are several alternatives for retrofit strategy that have been implemented in the past:

1. The infill on upper floors could be removed and replaced with less stiff and less strong materials.
2. The infill on upper floors could be isolated from the structure by installing joints with gaps to prevent interaction with the frame.

3. The lower floor, or floors, could be strengthened with new structural walls. These measures (Items 1, 2, and 3) are effective in reducing the ductility demand in the weak story or stories. However, all of them are costly and intrusive. In the US, it is not unusual for the costs of these types of retrofit to exceed half of the replacement value of the building.
4. Wrap the columns in the weak story with jackets of steel, concrete, fiberglass, or carbon fiber.

The fourth option can increase both the strength and ductility of the columns enough to reduce the collapse risk for most buildings. The cost is somewhat less than for the first three alternatives; however the overall performance would also be less with more damage focused in the weak floor. Column jacketing is popular in the US, but the costs can still be high. In developing countries, the advanced technologies for some types of jackets may not be readily available.

The procedure proposed here incorporates another alternative that has been used in the US to reduce collapse risk. This strategy is to provide supplemental vertical supports designed to prevent preemptive vertical load collapse (see Fig. 16.3). These are intended to support loads that are transferred from shear critical columns as they are damaged and begin to fail. The supplemental supports are typically steel shapes, pipe shoring, or timber shores. They are often installed near individual columns, but

Fig. 16.3 Steel column "pre-shoring" examples from Stanford University and University of California, Berkeley (See also Plate 21 in Color Plate Section on page 468)

also can be placed beneath capable horizontal framing. This technique is effective in reducing collapse risk by avoiding the preemptive vertical collapse mode. The intensity of shaking required for lateral dynamic instability is generally higher and less likely to occur. The installation of supplemental vertical supports is relatively inexpensive. The functional use of the spaces may be affected by the installation, but often this is minor compared to other alternatives. Installations in the US have been made for a very small percentage of the replacement costs for the building.

The following Section 16.2 of this chapter presents the conceptual procedure for determining the benefits of supplemental vertical supports based on recent research. The proposed procedure is illustrated with an example application in Section 16.3. The chapter concludes with a summary Section 16.4 and list of references cited in Section 16.5.

16.2 Conceptual Procedure and Background

Assessment of the potential for vertical load collapse in buildings with weak stories and the effectiveness of supplemental vertical supports can accomplished with the steps outline in this section.

16.2.1 Horizontal and Vertical Load Characteristics of Weak Story Components

Engineers in seismically active areas of the US are using FEMA 356 [2] increasingly for the evaluation and retrofit of existing buildings. In 2006 this document was adapted as a national standard ASCE 41 [3]. Over the past decade important research relating to the inelastic behavior of reinforced concrete has been produced at the Pacific Earthquake Engineering Research Center (PEER). The Earthquake Engineering Research Institute (EERI) in conjunction with PEER presented a seminar summarizing the practical implications of this work for engineers [4]. These implications included the prospect of significant improvement of acceptability criteria for several types of concrete components in FEMA 356 and ASCE 41. Consequently, a supplement to ASCE 41 was proposed and accepted [5]. FEMA 356/ASCE 41 provisions are suitable to determine the post elastic horizontal and vertical behavior characteristics of the weak story components as long as they are properly applied in accordance with the recent supplement.

Column components are characterized by the force and displacement relationship depicted in Fig. 16.4. In the figure, the parameter “a” is the plastic rotation at which horizontal force resistance capacity diminishes significantly to a level defined by parameter “c.” The column fails for vertical loads at a plastic rotation represented by parameter “b.” In FEMA 356/ASCE 41 and Supplement, the assignment of these parameters depends first upon the mode of inelastic behavior for the column

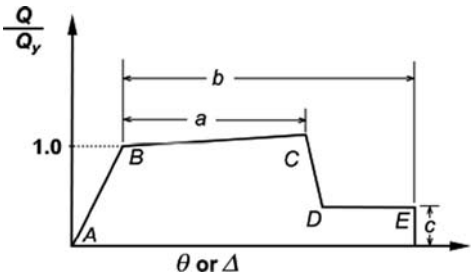

Fig. 16.4 Force and displacement relationship for concrete columns from FEMA 356/ASCE 41

(i.e. flexure, flexure-shear, and shear). Columns are classified in accordance with Table 16.1 depending on the detail of transverse reinforcing. For each "condition" parametric limits are tabulated based on ultimate shear stress, transverse reinforcement ratio, and axial load intensity. The Supplement provides improved parametric limits as illustrated in Fig. 16.5 for flexurally control columns classified as "condition ii."

Recent research [6] demonstrates that the force-displacement relationship for degrading components and systems is a capacity surface which cannot be transgressed during analysis or experiment. It is different than the hysteretic envelope (often termed a "backbone") resulting from a dynamic analysis or experiment. The hysteretic envelope is dependent on loading protocol, whereas the force-displacement capacity boundary is not. This distinction is critically important when determining the inelastic properties of components. The mistaken use of a hysteretic envelope in place of a capacity boundary can result in under-prediction of vertical load capacity and dynamic instability.

Table 16.1 Classification of columns by mode of inelastic behavior and transverse reinforcing details

	Transverse reinforcement details		
Inelastic behavior mode	ACI conforming details with 135° hooks	Closed hoops with 90° hooks	Other (including lap-spliced transverse reinforcement)
Flexure $V_p/(V_n/k) \leq 0.6$	i[a]	ii	ii
Flexure-Shear $1.0 \geq V_p/(V_n/k) > 0.6$	ii	ii	iii
Shear $V_p/(V_n/k) > 1.0$	iii	iii	iii

[a] To qualify for condition i, columns must have p" $\geq$0.002 and s/d $\leq$ 0.5 within the flexural plastic hinge region. Otherwise column shall be considered as condition ii.

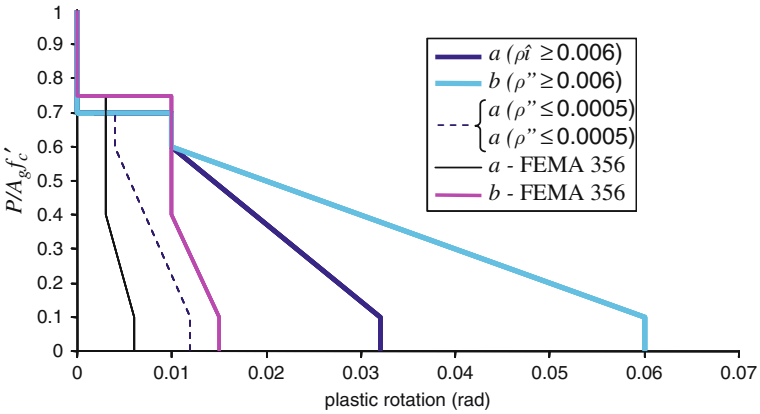

Fig. 16.5 Comparison of modeling parameters for Condition ii and previous *FEMA 356* parameters for columns "controlled by flexure" with nonconforming transverse reinforcement and $v \leq (f_c')^{1/3}$ (See also Plate 22 in Color Plate Section on page 468)

16.2.2 System Capacity Boundary (Pushover)

Figure 16.6 depicts a conceptual analytic model that can be used to determine the probability of vertical load collapse and lateral dynamic instability. In this case, the first-floor is the weakest of the floors and the inelastic response of the structure is assumed to occur at that level. The upper floors are rigid compared with the columns of the first-floor. Consequently the model represents the upper floors as completely rigid. As for most relatively rigid buildings, the flexibility of the foundation is an important factor in its dynamic behavior. The model assumes that the foundation and supporting soils deform elastically imparting a rigid body rotation to the response of the structural model. The rotational stiffness of the foundation should be adjusted to account for the fact that much of the inertial lateral load is applied above the 1st level resulting in larger overturning moments. The response of this model to ground motions represents an approximation of actual response based on a single-degree-of-freedom (first floor drift, θ_{1st}) oscillator. When considering the distortion imparted to the first floor, it is important to account for the rigid body foundation rotation as shown in Fig. 16.6b.

The component capacity boundaries for the weak story, generated as discussed in the previous section, can be assembled using nonlinear static procedures (pushover) to generate a global representation of the force-displacement capacity boundary of the system (see Fig. 16.7).

16.2.3 Simplified Dynamic Analysis

The next step in the process is to determine the intensities of shaking at which vertical load collapse and lateral dynamic instability occur. An incremental dynamic analysis (IDA) is a type of response history analysis which involves subjecting

Fig. 16.6 Analytical model

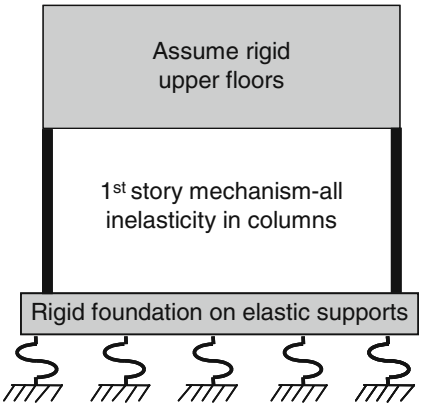

(a) Assumptions

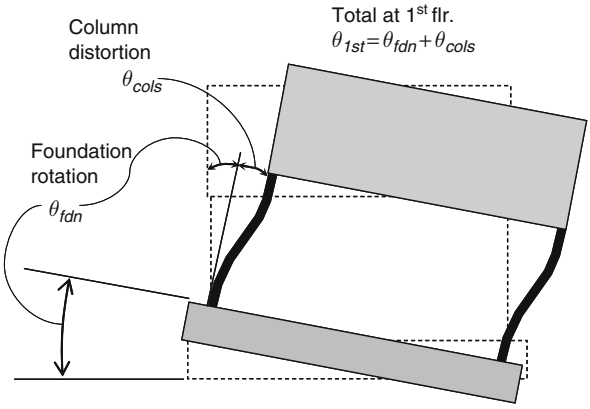

(b) Rotational displacements

a system to a ground motion record successively scaled to increasing levels of intensity, as measured by an intensity measure IM (e.g. spectral acceleration at the fundamental period of the system, S_{aT}), until global dynamic instability is observed [7].

Dynamic instability appears as a rapid, nearly infinite increase in the response of the system, measured by the engineering demand parameter (e.g. rotation at the weak floor, θ_{1st}), for a small increment in intensity. Essentially this means that the model cannot withstand any more increase in the applied intensity and thus responds with infinitely large displacements, indicative of collapse due to dynamic instability. The procedure is normally done with a number of ground motions to gain probabilistic perspective of the potential for collapse as illustrated in Fig. 16.8. In the figure, the force parameter is the spectral acceleration at the period of the SDOF system, normalized by the spectral acceleration at the yield point of the system, $R=S_{aT}/S_{ay}$. The displacement is represented by the ductility demand, $\theta_{1st}/\theta_{yield}$.

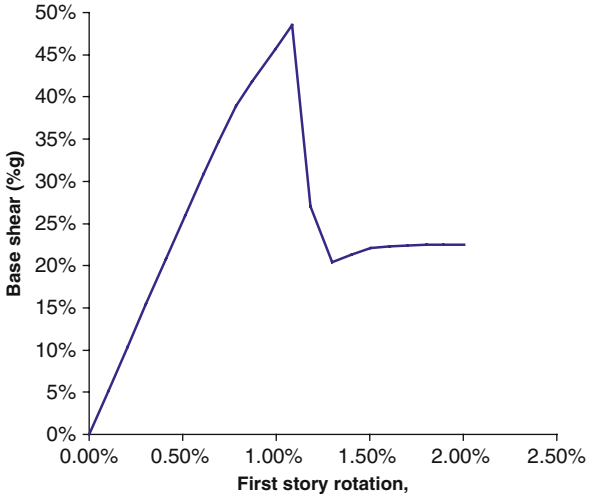

Fig. 16.7 Force displacement capacity boundary from nonlinear static pushover analysis

In Fig. 16.8b, lateral dynamic stability is defined by the intensity and ductility at which the IDA curves reach horizontal. The capacity for vertical load is determined by plotting the ductility at which collapse is expected and finding the associated intensity by intersecting the IDA curves.

16.2.4 Collapse Mode Risks

The information from the simplified dynamic analysis defines the probability of collapse due to each mode conditioned on intensity as shown in Fig. 16.9. The combined probability of collapse due to either mode is expressed by Eq. 16.1 [8]. The combined risk of collapse is expressed in Eq. 16.2.

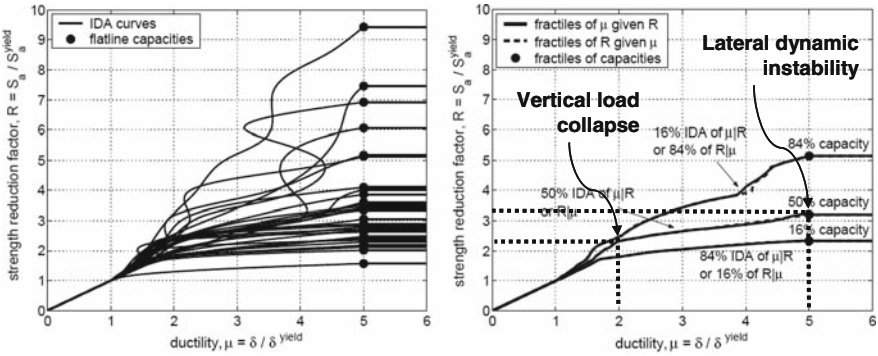

(a) Thirty IDA curves and flatline capacities

(b) Summarization into fractile IDAs, given R or μ

Fig. 16.8 Incremental dynamic analysis

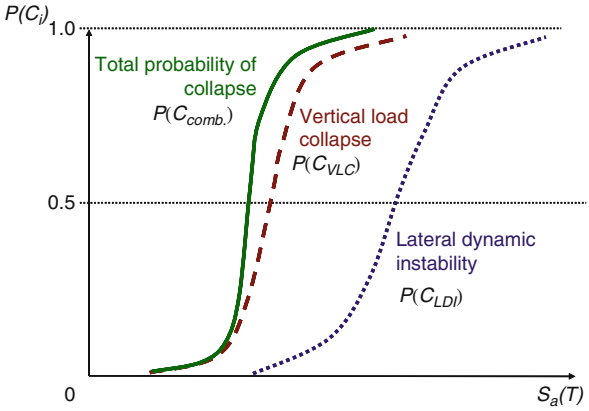

Fig. 16.9 The combined probability of collapse, $P(C_{comb.})$, due to vertical load collapse, $P(C_{VLC.})$, and lateral dynamic instability, $P(C_{LDI.})$

$$P\left(C_{comb.}\right) = P\left(C_{VLC}\right) + P\left(C_{LDI}\right) - P\left(C_{VLC}\right) P\left(C_{LDI}\right) \tag{16.1}$$

$$\lambda_c = \int_{S_a} P(C_{comb.}) \left| d\lambda_{S_a} \right| = \lambda_{S_a}(S_aT) \exp\left(\frac{1}{2} k^2 \beta^2\right) \tag{16.2}$$

The benefit of supplemental vertical supports is measured as the reduction in the risk of collapse that they would provide. To quantify the benefit, the following steps are taken:

1. Assess the probability of each mode of collapse using the procedure outlined in the previous section.
2. Determine the combined risk of prior to the installation of supplemental supports using Eqs. 16.1 and 16.2.
3. Reassess the probability of vertical load collapse after the installation of the supplemental supports.
4. Determine the combined risk after installation using Eqs. 16.1 and 16.2.

In many cases, these procedures can be simplified by assuming that the supplemental supports eliminate the probability of vertical load collapse. Also, a seismic hazard curve can be used to estimate the integration in Eq. 16.2. This is illustrated in the example which follows.

16.3 Example Application

This section demonstrates the application of the procedure to quantify the benefits of supplemental vertical supports to a typical five story concrete frame residential building with unreinforced masonry in-fill partitions in the upper stories and a

Fig. 16.10 Example five story concrete frame building with unreinforced masonry infill

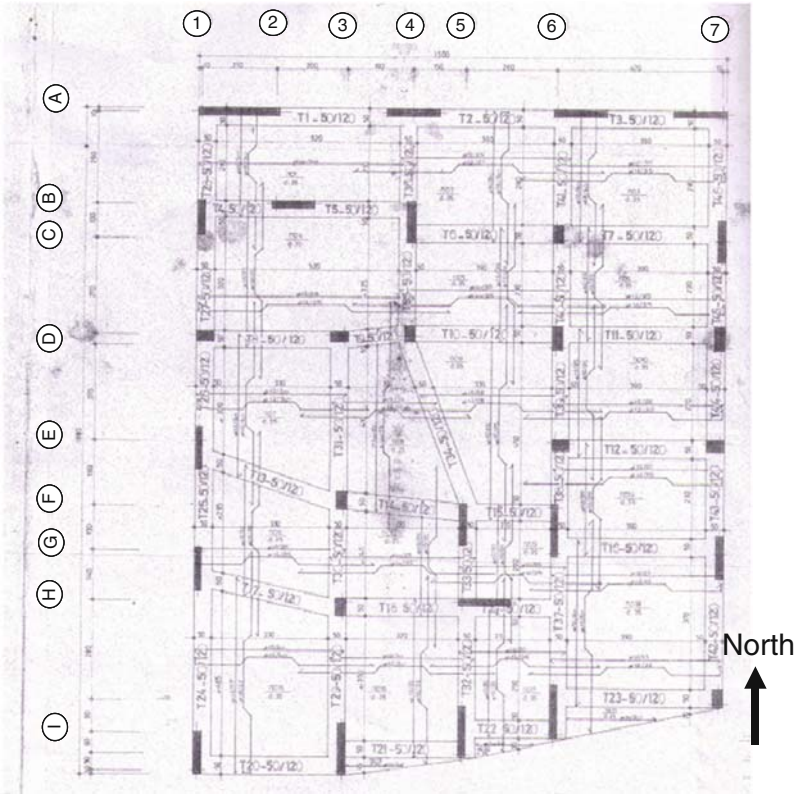

Fig. 16.11 Example building plan

weak open first-floor (see Fig. 16.10). This building is quite typical of construction in Turkey for multi-unit residential construction. Building and many others like it were subject to extensive damage and collapse during the Kocaeli earthquake in 1999. This building was investigated by a team from the Applied Technology Council including the author. The investigation team obtained design drawings from the owner. Although it did not collapse, the building was severely damaged. The most severe damage was found in the columns of the lower floor which had few unreinforced masonry partitions compared to the upper floors.

The columns in the lower floor of the example building are shown in Fig. 16.11. Transverse reinforcing is very light resulting in many shear and flexure-shear critical column components. Component capacity boundaries were generated using the FEMA 356/ASCE 41 procedures outlined in Section 16.2.1. The global capacity boundary for SDOF model of the building generated by a nonlinear static pushover is shown in Fig. 16.12. The data in the FEMA 356/ASCE 41 Supplement lead to a vertical load collapse limit controlled by horizontal distortion within the first floor. This limit translates to a total 1st story rotation including foundation flexibility of approximately 1%. The Supplement limits were developed to produce reliability against collapse of 85%. In this example, the vertical load collapse rotation was increased to 1.2% as an estimate of the median value.

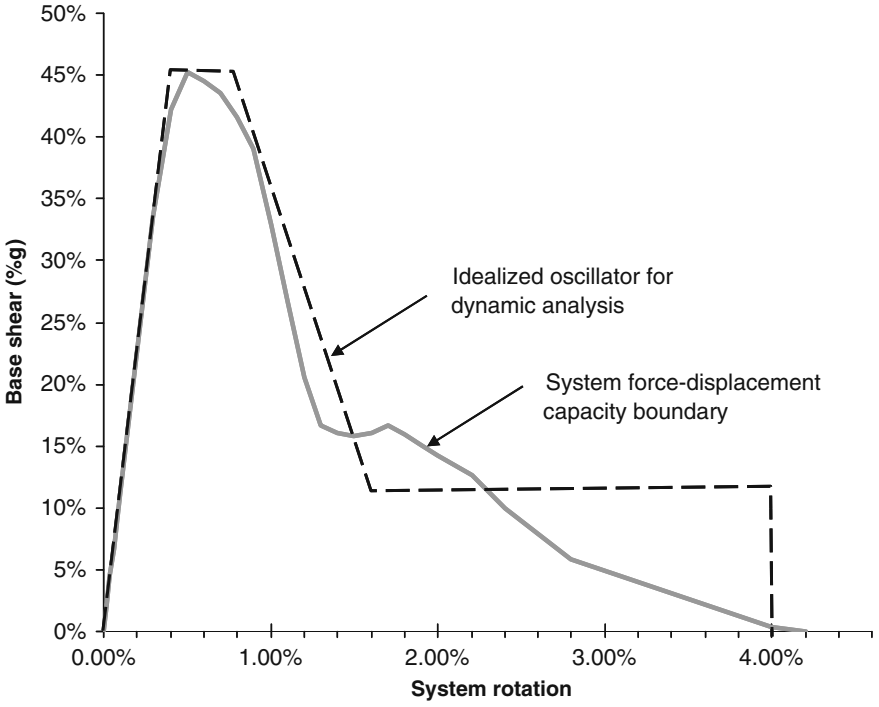

Fig. 16.12 Capacity boundary for example building model

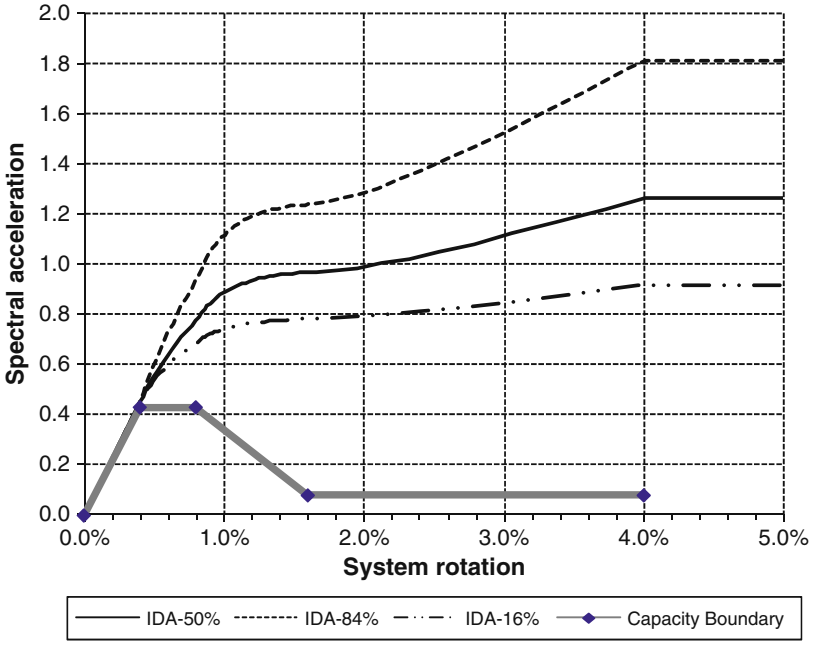

Fig. 16.13 Capacity boundary and incremental dynamic analysis results for example building model for a long residual strength plateau

The capacity boundary was used to represent a SDOF model of the building and subjected to an incremental dynamic analysis using a version of the software tool SPO2IDA [9]. The results are illustrated in Fig. 16.13. The capacity boundary is also shown in the figure.

As mentioned in the previous section the median values of each collapse mode demand can be used to estimate the associated risks. The intensities (R axis in Fig. 16.13) are converted to spectral acceleration at the period of the model, S_{aT}, by multiplying by the spectral acceleration at yield, S_{aYield}. These then are plotted on a seismic hazard curve for the site as shown in Fig. 16.14. This comparison indicates that supplemental vertical supports reduce the median risk of collapse in this example by a factor of about three.

This conclusion must be viewed cautiously as it is dependent upon some critical assumptions. The conclusions from ATC 62 include the observation that post-elastic characteristics of the capacity boundary control lateral dynamic instability. These parameters are:

1. the rate of degradation, $\alpha K_{initial}$,
2. the magnitude of the residual strength plateau,
3. the length of the plateau defining the point at which there is no lateral resistance, $max.\ \theta$.

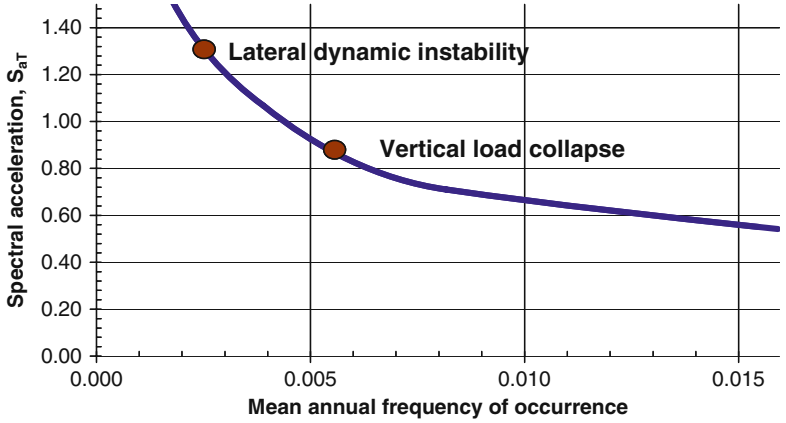

Fig. 16.14 Seismic hazard and annual frequency of vertical load collapse and dynamic instability

The rate of degradation is reasonably estimated from the capacity boundary. The magnitude and length of the residual strength plateau are relatively elusive. Buildings similar to the example retain some horizontal resistance at very high drifts even when discounted for P-delta effects. Supplemental vertical supports themselves do not contribute significantly to raising or extending the lower strength plateau. However, they might be augmented with beams or braces to do so. At present, there is no definitive process for estimating these parameters.

16.4 Summary and Conclusions

The use of supplemental vertical supports in building prone to loss of vertical load capacity caused by seismic distortion appears to an effective and economical retrofit strategy. They virtually eliminate preemptive vertical load collapse and reduce the risk of collapse to that associated with sidesway collapse due to lateral dynamic instability. The magnitude of risk reduction, and therefore the effectiveness of the retrofit, is dependent upon the risk of lateral dynamic instability. Improved information on the controlling post-elastic characteristics (i.e. rate of degradation, magnitude of residual strength plateau, length of residual strength plateau) are essential to more accurate assessment of lateral dynamic instability.

The use of supplemental vertical supports has the prospect of dramatically improving the safety of thousands of buildings in many areas of the world (e.g. Turkey, Central Asia, India, and Pakistan). Beyond the conceptual technical procedure presented here, realization of this goal requires the following:

1. The seismic hazard in regions where such buildings are prevalent needs to determined.
2. Prototype building models representing local and regional design and construction practice should be developed.

3. Parametric studies of the prototypes can be used to identify generalized behavior characteristics and to assess the cost effectiveness of supplemental vertical supports.
4. Simplified design guidelines addressing local and regional conditions can developed to facilitate implementation.
5. Coordinated local strategies for funding retrofit should be developed.

References

1. EERI (2008) World Housing Encyclopedia, www.world-housing.net
2. FEMA (2000) FEMA 356: Prestandard and commentary for the seismic rehabilitation of buildings, Report No. FEMA 356, prepared by Applied Technology Council, prepared for Federal Emergency Management Agency, Washington, DC
3. ASCE (2007) Seismic rehabilitation of existing buildings (ASCE 41-07), American Society of Civil Engineers, Reston, VA
4. EERI (2006) New information on the seismic performance of existing concrete buildings-, EERI Technical Seminar developed by PEER and funded by FEMA, video download @ www.eeri.org
5. Elwood KJ, Matamoros AB, Wallace JW, Lehman DE, Heintz JA, Mitchell AD, Moore MA, Valley MT, Lowes LN, Comartin CD, Moehle JP (2007) Update to ASCE/SEI 41 Concrete provisions, Spectra, Journal of the Earthquake Engineering Research Institute
6. ATC-62 (2008) The effects of degradation of stiffness and strength on the seismic response of structural systems, prepared for FEMA by the Applied Technology Council, Redwood City, California, in DRAFT
7. Vamvatsikos D, Cornell CA (2002) Incremental dynamic analysis, Earthquake Engineering and Structural Dynamics, 31(3):491–514
8. PEER (2005) Van Nuys hotel building testbed report:exercising seismic performance assessment. PEER Report 2005/11, Pacific Earthquake Engineering Research Center, College of Engineering, University of California, Berkeley
9. Vamvatsikos D, Cornell CA (2006) Direct estimation of the seismic demand and capacity of oscillators with multi-linear static pushovers through Incremental Dynamic Analysis. Earthquake Engineering and Structural Dynamics, 35(9):1097–1117

Chapter 17
How to Predict the Probability of Collapse of Non-Ductile Building Structures

Helmut Krawinkler and Dimitrios G. Lignos

Abstract This chapter attempts to cover the range from rigorous probabilistic collapse prediction of short period low-ductility buildings to simplified assessment of the collapse potential. The rigorous collapse predictions are based on modeling the deteriorating properties of structural elements with low ductility and predicting the collapse capacity for a given structural configuration and ground motion through incremental dynamic analysis. Consideration is given to the variation in collapse capacity due to randomness of the ground motion. A parameter study is summarized in which the effects of strength and deformation capacity on the collapse potential of frames with infill walls is evaluated. It is found that shear strength has the largest effect on the collapse capacity, and that deformation capacity and residual strength are of less importance.

17.1 Introduction

The large collapse potential of Istanbul's low-rise buildings in case of an earthquake is well documented and is acknowledged to be a major threat to the well-being of this great metropolis. The need exists to identify the most vulnerable buildings and to develop simple means and prescriptive rules for seismic upgrading of the vulnerable building stock.

Many of the vulnerable buildings have relatively poorly constructed concrete framing, which in part or fully is infilled with hollow clay or solid bricks. Configurations are often irregular, and the quality of construction is very variable. In many cases it is not clear how inertia forces find their way to the reinforced concrete (RC) framing and how the wall forces and moments are transferred into the soil. These are additional complications, but the basic concept remains that in most practical cases the infilled frames are the primary lateral load resisting elements that have to transfer lateral loads into the soil.

H. Krawinkler (✉)
Department of Civil and Environmental Engineering, Stanford University, Stanford, CA, USA
e-mail: krawinkler@stanford.edu

A. Ilki et al. (eds.), *Seismic Risk Assessment and Retrofitting*, Geotechnical, Geological, and Earthquake Engineering 10, DOI 10.1007/978-90-481-2681-1_17,

Thus, a basic challenge is to assess the strength and deformation capacity of these walls and to assess the collapse potential of buildings, given that the cyclic response characteristics of the lateral load resisting system are known. A rigorous assessment of collapse potential may sound like a fruitless effort, simply because of the huge uncertainty in the properties of the structural system. But the usefulness of such a collapse assessment is defended with two arguments. For one, setting aside the uncertainties in the properties of the lateral system and focusing on central values, the mean of collapse capacity, as a function of strength and deformation capacity, can serve as a basic measure for setting retrofit priorities. Perhaps more important is the question how much improvement in strength and deformation capacity is needed in order to achieve considerable (rather than incremental) improvement, and what are the structural parameters that most affect this improvement? It is the main theme of this chapter to address these questions so that informed decisions can be made in the seismic retrofit process.

In the following discussion assumptions will be made on the range of structural parameters representative for masonry infill walls, based on experimental observations. Given this range of parameters, so-called collapse fragility curves will be developed utilizing a set of representative ground motions. The median values of these collapse fragilities will be utilized to assess sensitivities of the collapse capacity to important structural parameters and to draw conclusions on effective retrofit strategies.

To rationalize this process, discussions are presented first on modeling of deterioration and the evaluation of the collapse capacity and collapse fragility curves given the properties of the structural system. It is postulated that modeling of deterioration in strength and stiffness is fundamental to understanding and quantifying behavior close to collapse. Development of a collapse fragility curve (probability of collapse given an appropriate ground motion intensity measure, such as spectral acceleration at the fundamental period of the structure) requires explicit modeling of deterioration and the execution of nonlinear response history analyses for a set of representative ground motions, whose intensity is increased until dynamic instability is observed in the predicted dynamic response.

17.2 Strength and Stiffness Deterioration

17.2.1 Modes of Deterioration Observed from Experiments

The need for analytical models that incorporate deterioration is evident from Fig. 17.1, which shows a monotonic load-displacement response and a superimposed quasi-static cyclic response of "identical" plywood shear wall panels reported in [4]. The response of an infill wall specimen does look similar]. The monotonic test result shows that strength is "capped" and is followed by a negative tangent stiffness. Thus, from a certain deformation on there is evident strength deterioration under monotonic loading. The cyclic hysteretic response indicates that cyclic

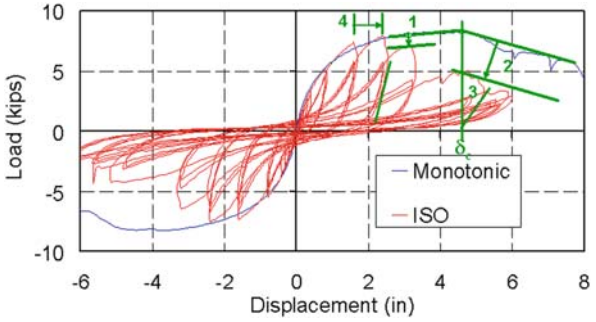

Fig. 17.1 Monotonic and cyclic experimental response of a plywood shear wall panel (data from [4])

loading causes additional modes of deterioration that may be classified as follows based on [6]:

Basic strength deterioration (1). The strength deteriorates with the number and amplitude of cycles, even if the displacement associated with the strength cap has not been reached. This is reflected in a translation of the pre-capping strength bound towards the origin.

Post-capping strength deterioration (2). The strength deteriorates further when a negative tangent stiffness is attained. This is reflected in a translation (and possibly rotation) of the post-capping strength bound towards the origin.

Unloading stiffness deterioration (3). The unloading stiffness deteriorates with the number and amplitude of cycles. This is reflected in a rotation of the unloading slope.

Accelerated reloading stiffness deterioration (4). For a given deformation amplitude the second cycle indicates a smaller peak strength than the first cycle; however, the resistance increases and the strength envelope is attained if the amplitude of the second cycle is increased. If the strength envelope is attained upon increasing the deformation amplitude, then this type of deterioration should not be referred to as strength deterioration but as accelerated reloading stiffness deterioration. It is reflected in a movement of the point at which the strength envelope is reached away from the origin.

The consequence of cyclic deterioration is that there rarely is stability in the load-deformation response of structural components. Also, the so-called "capping point" (the point at which maximum strength is attained) moves continuously as a function of the loading history. In most practical cases the capping point moves towards the origin under cyclic loading (i.e., the deformation at which the maximum strength is attained is smaller, and in some cases much smaller, than the deformation associated with maximum strength for monotonic loading). This is an important issue when assessing the deformation capacity of structural components, which in analytical models is often predicted from concepts that are based on monotonic loading.

The type of hysteretic behavior and the rate of deterioration depend strongly on the material, configuration, and details of structural components. At this time our

analytical tools are not adequate (and they never may be) to evaluate deterioration characteristics from principles of engineering mechanics. The best source of information from which to develop deterioration models is experimental data. Based on an evaluation of available and recently developed databases [11] it is concluded that the aforementioned four types of deterioration are rather generic and apply to component behavior regardless of material and configuration.

17.2.2 Analytical Modeling of Deterioration

Various models have been proposed in the literature to capture some or all of the aforementioned deterioration modes. The model used here is a modified version of the Ibarra-Krawinkler model, whose original version is described in detail in [6, 7]. This model has first been reported in a simplified form in [15] and has been refined and utilized extensively over the last ten years. The model is based on (a) a backbone curve, (b) a set of rules defining basic hysteretic behavior, and (c) a set of rules defining the rates of deterioration.

(a) Backbone curve. The shape of the backbone curve with associated definitions is provided in Fig. 17.2. The backbone curve defines the bounds within which the hysteretic response of the component is confined. It is close to the monotonic force-deformation response, but it contains compromises that need to be made in order to simplify response description. For instance, it accounts for an average effect of

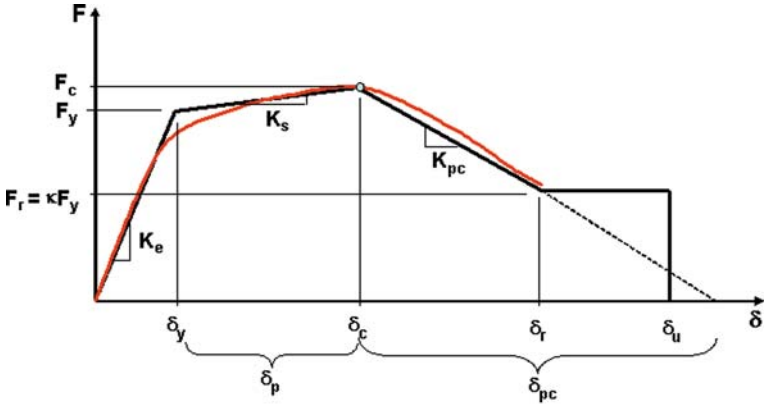

- Effective yield strength and deformation (F_y and δ_y)
- Effective elastic stiffness, $K_e = F_y/\delta_y$
- Capping strength and associated deformation for monotonic loading (F_c and δ_c)
- Plastic deformation capacity for monotonic loading, δ_p
- Effective post-yield tangent stiffness, $K_p = (F_c - F_y)/\delta_p$
- Post-capping deformation capacity, δ_{pc}
- Effective post-capping tangent stiffness, $K_{pc} = F_c/\delta_{pc}$
- Residual strength, $F_r = \kappa F_y$
- Ultimate deformation capacity, δ_u

Fig. 17.2 Backbone curve and associated definitions (taken from [2, 11])

cyclic hardening (which likely is small for RC components but may be significant for steel components). The quantities F and δ are generic force and deformation quantities. For plastic hinge regions $F = M$ and $\delta = \theta$. For the infill wall configurations used in this study, $F$is the story shear force and the deformation quantity $\delta$is the story drift ratio δ/h, denoted $\theta$from here on. The properties of the backbone curve may be different in the positive and negative directions.

Residual strength $F_r = \kappa F_y$ may or may not be present. The ultimate deformation capacity δ_u usually is associated with a sudden failure mode or with behavior that can no longer be relied upon. In general, seven parameters are needed to define the backbone curve comprehensively (F_y, δ_y, F_c, δ_c[or δ_p], δ_{pc}, F_r, and δ_u).

(b) Rules defining basic hysteretic characteristics. The model can be employed together with any of the basic linearized hysteretic models used widely in the literature, i.e., with a bilinear model, a peak-oriented model, or a pinching model.

(c) Rules for quantifying modes of deterioration. The cyclic deterioration rates are controlled by the rule developed by [15], which is based on the hysteretic energy dissipated when the component is subjected to cyclic loading. It is assumed that every component possesses an inherent reference hysteretic energy dissipation capacity, E_t, regardless of the loading history applied to the component. The cyclic deterioration in excursion $i$is defined by the parameter β_i, which is given by the following expression:

$$\beta_i = \left(\frac{E_i}{E_t - \sum_{j=1}^{i} E_j} \right)^c \tag{17.1}$$

where

β_i = parameter defining the deterioration in excursion i
E_i = hysteretic energy dissipated in excursion i
E_t = reference hysteretic energy dissipation capacity, expressed as a multiple of $F_y\delta_p$, i.e., $E_t = \lambda F_y \delta_p$
ΣE_j = hysteretic energy dissipated in all previous excursions
c = exponent defining the rate of deterioration (at this time all calibrations are based on a value of c of 1.0)

This deterioration parameter β can be applied to any of the four aforementioned deterioration modes, as discussed in [6]. For instance, its application to basic strength deterioration implies translating the strain hardening branch towards the origin by an amount equivalent to reducing the yield strength to

$$F_i = (1 - \beta_{s,i}) F_{i-1} \tag{17.2}$$

where

F_i = deteriorated yield strength after excursion i
$F_{i\text{-}1}$ = deteriorated yield strength before excursion i

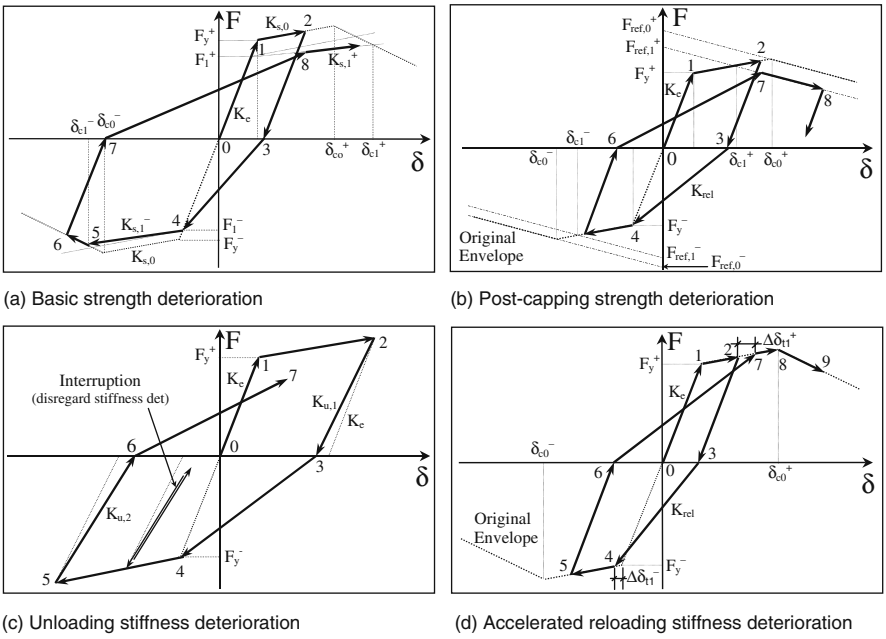

(a) Basic strength deterioration

(b) Post-capping strength deterioration

(c) Unloading stiffness deterioration

(d) Accelerated reloading stiffness deterioration

Fig. 17.3 Individual deterioration modes for Ibarra-Krawinkler model, illustrated on a peak-oriented model [6]

$\beta_{s,i}$ = deterioration parameter based on an appropriate λvalue for basic strengthdeterioration (obtained from calibration with experimental data)

Application of these rules for the four modes of deterioration is illustrated in Fig. 17.3.

Thus, the deterioration model has up to four deterioration parameters (appropriate λ values for each deterioration mode; see definition of λ in Eq. 17.1, i.e., $\lambda = E_t/F_y\delta_p$). It is found that the use of the same λ value for all four deterioration modes usually provides adequate description of each deterioration mode.

This model was tested previously on data obtained from experiments on steel, reinforced concrete, and wood components. Adequate simulations were obtained in all cases by tuning the model parameters to the experimental data. In the context of this study, the model is applied to simulation of the cyclic response of frames with infill walls.

17.3 Assessment of Collapse

Protection against collapse has always been a major objective of seismic design. Collapse refers to the loss of ability of a structural system, or any part thereof, to resist tributary gravity loads. Local collapse may occur, for instance, if a vertical

load carrying component fails in compression, or if shear transfer is lost between horizontal and vertical components (e.g., shear failure between a flat slab and a column). Such local collapse issues are not addressed in this chapter. Global (or at least story) collapse will occur if local collapses propagate (progressive collapse) or if an individual story displaces sufficiently so that the second order P-delta effects fully offset the first order story shear resistance and dynamic instability occurs (sidesway collapse). The latter collapse mode is the subject of this chapter.

Deterioration in strength and stiffness of individual components plays a critical role in the sidesway collapse mode. Therefore, assessment of collapse safety necessitates the capability to predict the dynamic response of deteriorating systems. Until recently the system collapse issue was seldom addressed because of the lack of hysteretic models capable of simulating deterioration behavior, and collapse was usually associated with an "acceptable" story drift or the attainment of a limit value of deformation in individual components of the structure. This approach does not permit a "redistribution" of damage and does not account for the ability of the system to sustain significantly larger deformations before collapse than those associated with first attainment of a limiting deformation in a component. These shortcomings are overcome in the collapse methodology utilized here.

17.3.1 Effect of Deterioration on Assessment of Collapse

Figure 17.4 shows two incremental dynamic analysis curves, IDAs, [16] for one specific structure (in this case an 8-story moment frame) and one specific ground motion. Plotted vertically is the spectral acceleration at the first mode period of the structure, $S_a(T_1)$, which identifies the intensity of the ground motion, and plotted horizontally is the computed maximum interstory drift ratio obtained from nonlinear response history analysis for various ground motion intensities.

The curve with solid dots is obtained from analysis with nondeteriorating structural component models (i.e., the hysteretic response is assumed to be bilinear and no monotonic or cyclic deterioration modes are considered). Since in this example the P-Delta effects are not large enough to overcome the strain-hardening effects inherent in the component models, the IDA curve continues to rise (not necessarily

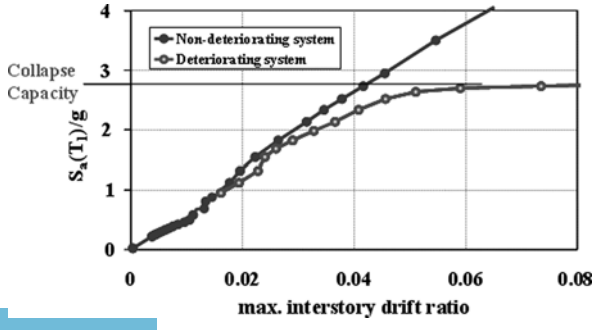

Fig. 17.4 IDA curves for a frame structure using non-deteriorating and deteriorating structural properties

as an almost straight line) to very (irrationally) large drifts of more than 20% (when the analysis was stopped).

The curve with open circles is obtained from analysis with deteriorating component properties. For relatively small drifts the responses are identical, but the curves deviate from one another once cumulative damage sets in. The differences in predicted drifts for a given ground motion intensity are relatively small until severe deterioration commences. From $S_a(T_1)$ of about 2.5 g on the slope of the second IDA curve decreases rapidly and approaches zero at 2.8 g. The implication of the latter is that that for a minute increase in intensity the increase in maximum story drift becomes very large, which indicates dynamic instability of the analytical model. Presuming that the model is accurate, this implies sidesway collapse of a single story or a series of stories. The ground motion intensity level associated with dynamic instability is denoted as the collapse capacity of the specific structure given the specific ground motion.

Performing this kind of analysis for a series of representative ground motions provides so-called collapse fragility curves, which, when combined with measures of modeling uncertainties can be utilized to evaluate the probability of collapse (or collapse margin) for the structure [1, 5, 7, 19, 20].

Unless deterioration is modeled in this process, collapse cannot be predicted for this structure or any other kind of structure. Clearly, the accuracy of collapse prediction depends strongly on the accuracy with which the deterioration characteristics of the structural components can be modeled. From a limited sensitivity study [7] it was found that the deformation at the capping point (δ_c) and the post-capping tangent stiffness have the largest effect on the collapse capacity (in addition to strength), followed by the rate of cyclic deterioration.

17.3.2 Methods for Assessing the Probability of Collapse

There are two approaches that recently have been developed to assess the probability of collapse of structures to extreme ground motions. The more conventional approach is to utilize an Load and Resistance Factor Design (LRFD) type demand/capacity format in which collapse is associated with a specific engineering demand parameter (*EDP)* demand (denoted as EDP_D) surpassing the *EDP* capacity (denoted as EDP_C). In its simplest form, collapse is associated with seismic demand exceeding a predefined deterministic deformation limit in the building's structural components (e.g., plastic hinge rotation). Such an approach ignores the ability of the structural system to redistribute seismic demands once an individual component passes the arbitrary deformation limit.

A refined form of the *EDP*-based approach estimates the probability of collapse using probability distribution functions of a more global seismic demand and capacity parameter (e.g., maximum interstory drift ratio). In this approach, which was employed by SAC [3], the probability of collapse at a given ground motion intensity (*IM*) level is defined as the probability that the structural demand parameter, EDP_D, exceeds the corresponding capacity, EDP_C, which requires the estimation

of $EDP_D|IM$ and EDP_C probability density functions. These can be obtained from IDAs under a variety of assumptions. This approach necessitates numerical integration at all *IM* hazard levels of interest, and relies on the somewhat arbitrary definition of the *EDP* capacity point for each IDA. It is not implemented in this study.

The alternative approach is to develop collapse fragility curves that can be employed directly for the evaluation of the probability of collapse at specific hazard levels or of a Mean Annual Frequency (MAF) of collapse. In this approach the collapse capacity for a given structure subjected to a given ground motion is defined as the ground motion intensity at which the structure experiences dynamic instability (i.e., the slope of the IDA curve approached zero), IM_c. [To obtain this collapse capacity value it is not necessary (but certainly helpful and educational) to execute a complete IDA, as only the last point on the IDA is sought.]

Collapse capacity values are computed for a sufficiently large number of ground motions so that a statistical evaluation of the collapse capacity values (IM_c) can be performed. Ordering these collapse capacity values and fitting an appropriate distribution function to the data provides a collapse fragility curve for the specific structure that accounts explicitly for the record-to-record (RTR) variability. For good reasons [7] a lognormal distribution is being used to represent the collapse fragility.

The process for obtaining the collapse capacity for an 8-story frame structure subjected to the set of 40 LMSR-N records is illustrated in Fig. 17.5 a. In this figure, each black curve shows an individual *IM-EDP* relation, using spectral acceleration at the first mode period [$S_a(T_1)$] as *IM*, and the maximum roof drift ratio (*RDR*) as *EDP*. The projection of the last point of each IDA curve (last stable solution) on the vertical axis, illustrated with a solid gray circle, shows the collapse capacity of this building for an individual record. The cumulative distribution function, assuming a lognormal distribution, of these spectral acceleration values that correspond to structural collapse is defined as the "collapse fragility curve" and is shown with a black line in Fig. 17.5a. A more conventional representation of the collapse fragility curve for this generic moment-resisting frame is shown in Fig. 17.5b with a solid black line along with the associated data points plotted with gray circles [19].

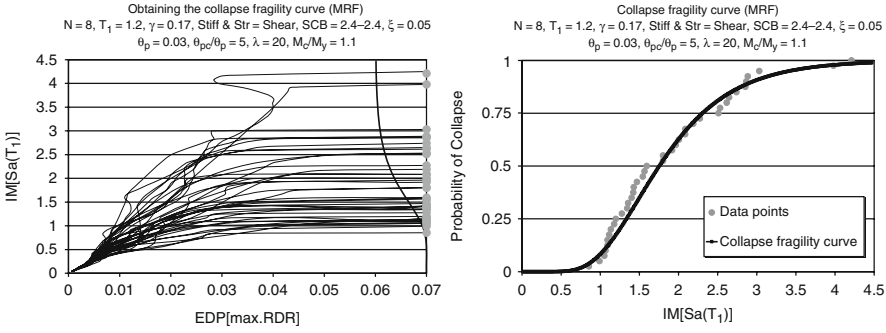

Fig. 17.5 Collapse fragilities; (**a**) determination of collapse capacity, (**b**) corresponding collapse fragility curve [19]

The fragility curve can be employed directly to evaluate the probability of collapse at specific hazard levels (*IM* values) or to evaluate the mean annual probability of collapse by integrating the fragility curve over the hazard curve. The assessment of probability of collapse and methods for incorporation of aleatory (RTR) and epistemic (modeling) uncertainties are discussed in [19, 20].

In the following sections such fragility curves are being developed and evaluated utilizing a range of load-deformation (base shear – story drift) relationships that are believed to be representative of typical infill wall configurations. This range of relationships is based on observations from experimental studies.

17.4 Experimental Observations – Frames with Infill Walls

Many cyclic experiments have been reported in the literature on reinforced concrete frames with infill masonry, using either hollow clay brick or solid brick without and with retrofit techniques (reinforced shotcrete, solid or banded FRPs, and more recently sprayed on engineered cementitious composites (ECCs), e.g., [8–10, 13, 14, 17, 18]. Almost all tests are in-plane, with load applied directly to the RC floor beams by means of actuators, and with the framing fixed to a rigid foundation. For the time being let us assume that such configurations represent actual buildings, i.e., the load – story drift responses of the test specimens do indeed represent the cyclic behavior of low-rise buildings (the issues of load transfer to the walls, out of-plane effects, and foundation effect are briefly addressed at the end of this chapter).

An evaluation of the cyclic load – story drift (story displacement over story height) relationships of many of these experiments resulted in the following general observations:

- Frames with infill walls are not brittle (except if the surrounding frame fails early in a brittle mode), i.e., the frame provides good confinement for the infill (conditioned that out-of-plane action is not important)
- Yield strength and elastic stiffness are ambiguous quantities that can only be estimated with judgment
- Envelopes of the cyclic response curves indicate that "yielding" is followed by strain hardening, a subsequent drop in strength, and strength stabilization at some residual value.
- Unfortunately, most tests stopped way short of full loss of strength, which means that little information exists on the actual ultimate drift at which the strength drops to a negligible value. But a drop of strength to very small values is rarely observed at story drifts of less than about 2%.

Support for these observations is provided in Fig. 17.6, which shows the cyclic response of two reduced-scale single-story infill wall specimens tested recently at Stanford University [10]. One specimen has a bare infill wall in which deterioration was caused primarily by bed joint sliding of the top brick course and the subsequent formation of a knee-braced mechanism, and the other specimen was retrofitted with

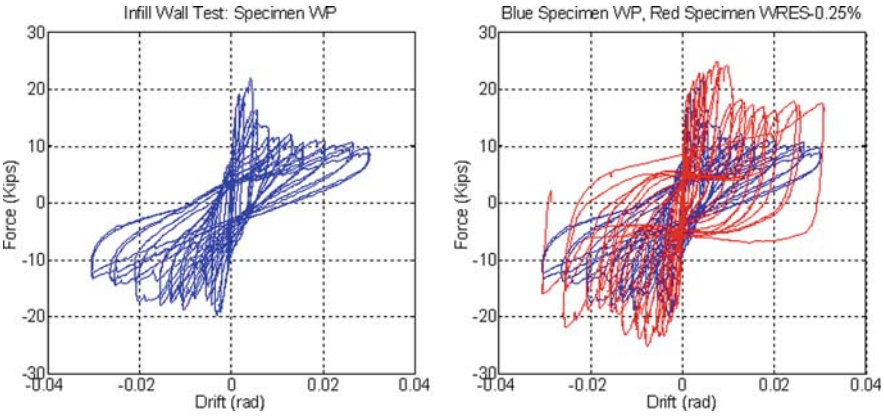

Fig. 17.6 Cyclic response of two reduced-scale infill wall specimens; (**a**) reference specimen without retrofit, (**b**) specimen with reinforced ECC layer superimposed on reference specimen [10] (See also Plate 23 in Color Plate Section on page 469)

Fig. 17.7 Failure modes of Stanford specimens; (**a**) reference specimen without retrofit, (**b**) specimen with ECC layer [10] (See also Plate 24 in Color Plate Section on page 469)

a layer of reinforced ECC, in which deterioration was caused by shear failure of the frame columns. ECC (engineered cementitious composite) is a mixture of Portland cement, fly ash, calcium aluminate cement, fine silica sand and 2% by volume of polyvinyl alcohol (PVA) fibers. In Fig. 17.6b the response of the second specimen is superimposed on that of the first one. Photos of the specimens after testing are shown in Fig. 17.7.

Further documentation of the aforementioned behavior patterns is provided in Fig. 17.8, which shows a series of monotonic test results from [13] with superimposed multi-linear backbone curves of the type used in the Ibarra-Krawinkler model (Fig. 17.2). Several calibrations were performed also of the cyclic response of test specimen responses, utilizing the parameters of the Ibarra-Krawinkler model. A typical example is shown in Fig. 17.9. The information shown here, and data from many other in-plane experiments have been used to define a range of structural parameters that is believed to be representative of the response characteristics of infill

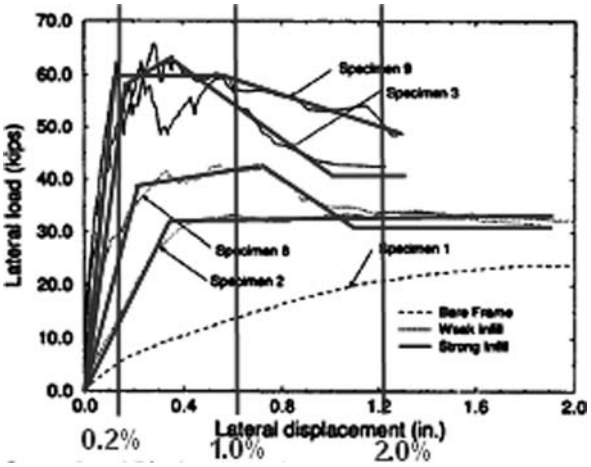

Fig. 17.8 Load-drift relationships of monotonically loaded infill wall specimens [13] with superimposed linearized relationships

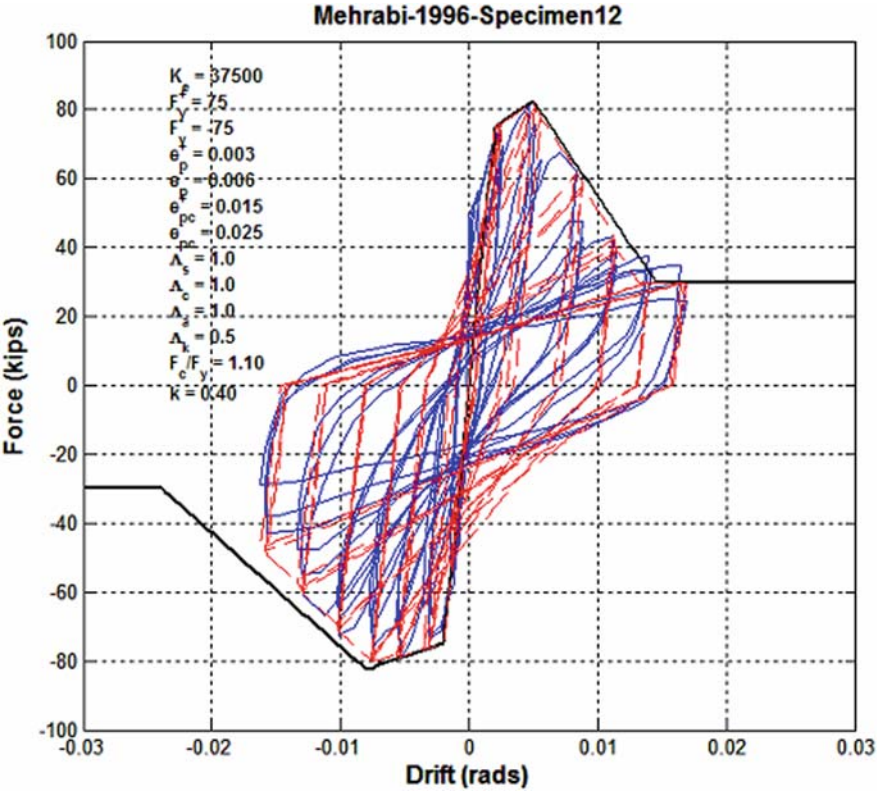

Fig. 17.9 Matching a cyclic response with the Ibarra-Krawinkler deterioration model (data from [14])

wall structures (provided that none of the previously mentioned other failure modes predominate).

17.5 Parameter Study Employing Deteriorating SDOF Systems

A parameter study was performed to assess the collapse potential of infill wall structural systems, using the aforementioned range of system parameters, in order to provide preliminary information on the probability of collapse of infill wall systems and on the effectiveness of retrofit techniques in reducing this probability. Perhaps most important, the questions are addressed how much can be gained by

1. increasing the strength of the infill walls
2. increasing the deformation capacity of the walls
3. increasing the residual strength capacity of the walls.

Only SDOF systems are used for this purpose; the assumption being that the primary concern is with low-rise construction in which higher mode effects are not very important and equivalent SDOF system can be used to represent dynamic behavior (this assumption eliminates structures with soft (weak) stories from consideration).

Based on the preceding discussions, answers to these questions necessitate the development of collapse fragility curves, which depend strongly on the backbone curve parameters illustrated in Fig. 17.2, on the cyclic deterioration parameter β, which in turn depends on the reference energy dissipation parameter λ, and on the set of ground motions selected for response history analysis.

17.5.1 Ground Motions

The Californian ground motion set LMSR-N (Large Magnitude Small Distance-New) was selected as representative of the frequency content of the ground motions. This set is discussed in detail in [12]. The records do not exhibit pulse-type near-fault characteristics and are recorded on stiff soil or soft rock, corresponding to soil type D (stiff soil). The source-to-site distance ranges from 13 to 40 km. and the moment magnitude from 6.5 to 6.9. The records are essentially ε-neutral, i.e., they may overestimate the collapse probability because they do not account for the effect of period elongation on the spectral shape.

17.5.2 Parameters of Structural Models

The generic backbone curve used to define the structural parameters is shown in Fig. 17.10. Both axes are normalized, i.e., the vertical axis shows the base shear coefficient $\theta = F/W$ (W is the seismically effective weight of the structure), and

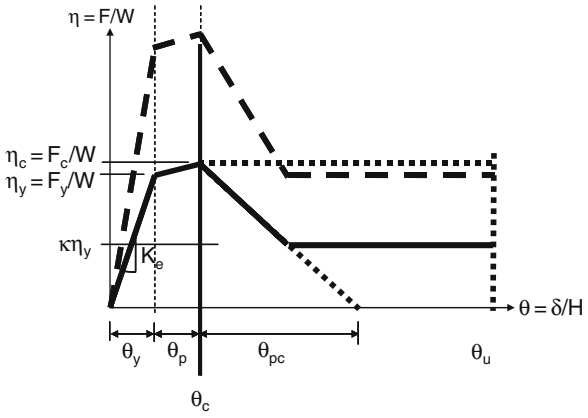

Fig. 17.10 Generic backbone curve for infill wall systems, with parameter variations

the horizontal axis shows the interstory drift ratio $\theta = \delta/H$. The backbone curve is defined by the following parameters:

- Yield strength $\theta_y = F_y/W$
- Cap strength $\theta_c = F_c/W$
- Residual strength $\theta_r = \kappa\theta_y$
- Yield drift θ_y
- Drift at capping $\theta_c = \theta_y + \theta_p$
- Post-capping drift θ_{pc}
- Ultimate drift θ_u

Two central cases were created, a "low ductility" central case and a "high ductility" central case as shown in Fig. 17.11. The central case parameters are circled and the variations around the central case values are partially illustrated in Fig. 17.11. The fundamental differences between "low" and "high" ductility are the θ_c and θ_{pc} values, which are doubled from low to high ductility. A strength variation implies that the backbone curve is stretched in the vertical direction as illustrated in Fig. 17.10 (dashed lines); it does not affect the deformation parameters. Somewhat arbitrary (because of the lack of information), but conceptually necessary, limits on the ultimate story drifts are set at 0.03 for the "low ductility" case and 0.04 for the "high ductility" case. In all cases the cyclic deterioration parameter λ is set at a constant value of 100 (based on calibrations of experimental results, and in order to eliminate one of the less important parameter variations). To assess the effect of residual strength, three cases are investigated; $\kappa = 0$ (no residual strength), $\kappa = 0.5$, and horizontal post-capping slope until θ_u is attained (i.e., $\theta_{pc} = \infty$).

- In summary the following parameters are utilized in the parameter study:
- Strength: $\theta_y = 0.15, 0.30, 0.45$
- Yield drift angle: $\theta_y = 0.001$, 0.002, and 0.003
- Elastic stiffness: $K_{eff} = \theta_y/\theta_y$

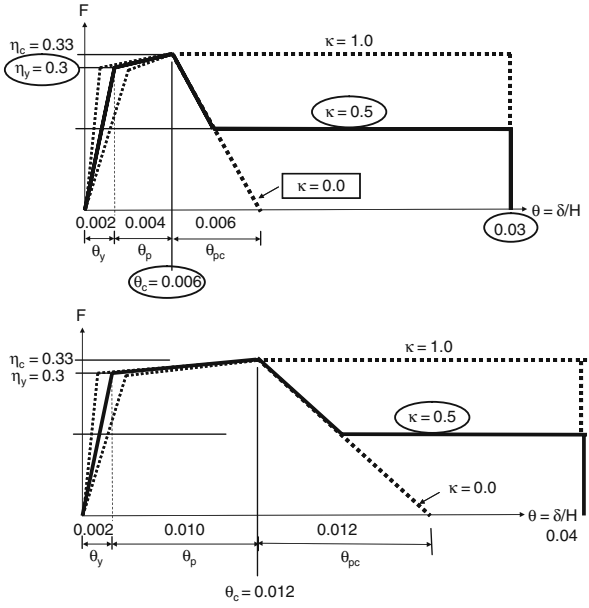

Fig. 17.11 "Low ductility" and "high ductility" central cases with parameter variations

- Fundamental period: $T_1 = 0.165 - 0.50$ s. for $h = 3$ m
- Drift angle at capping: $\theta_c = 0.006$ for "low ductility"
- $\theta_c = 0.012$ for "high ductility"
- Post-capping drift capacity: $\theta_{pc} = 0.006$ for "low ductility"
- $\theta_c = 0.012$ for "high ductility"
- Residual strength: $\kappa = 0.0$, 0.5, and $\theta_{pc} = \infty$ (approx. $\kappa = 1$)
- Cyclic deterioration param.: $\lambda = E_t/(F_y\theta_p) = 100$

17.5.3 Response – Examples

The importance of postulating an ultimate drift capacity, θ_u, is illustrated in Fig. 17.12 for the "high ductility" central case with no post-capping stiffness deterioration. This case is an unlikely one, but it illustrates that the collapse capacity can be strongly affected by the existence of an ultimate drift capacity beyond which no reliance can be placed on the resistance of the structural system. The figure shows IDA curves based on the assumption that no drift limit exists. Sooner or later (in the illustrated case around 7% drift) collapse will occur one way or another because of cyclic deterioration and P-Delta effect. But the ground motion intensity at which collapse occurs may depend strongly on the ultimate drift capacity, θ_u. If this capacity is only 3% (first vertical line), then the collapse capacity of the structural system is only about 2/3rd of that without a drift limit.

Typical hysteretic responses obtained from the response history analysis are presented in Fig. 17.13. The figure shows the responses close to collapse of a

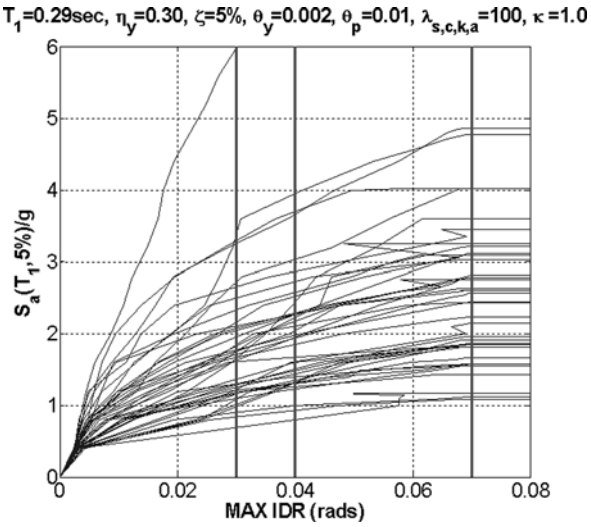

Fig. 17.12 Effect of ultimate drift limit on collapse capacity, horizontal post-capping slope

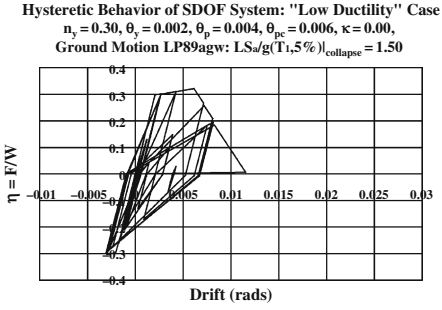

(a) no residual strength ($\kappa = 0.0$)

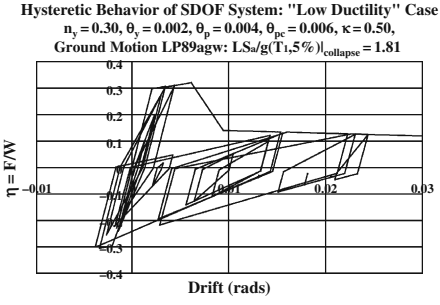

(b) 50% residual strength ($\kappa = 0.5$)

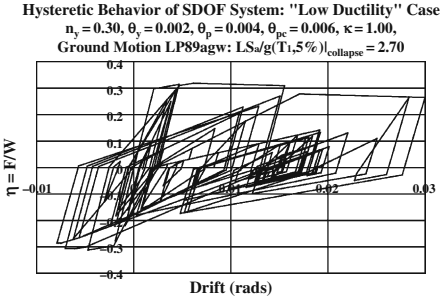

(c) horiz. post-capping slope till $\theta_u = 0.03$

Fig. 17.13 Hysteretic responses of "low ductility" central case to the LP89agw record, three cases of residual strength

"low ductility" central case system for the three cases of residual strength, using the LP89agw record (a 1989 Loma Prieta record). The responses are vastly different, but the collapse capacity (S_a/g at collapse) for $\kappa = 0.0$ and 0.5 are not much different (1.5 versus 1.81). Maintaining full strength (a desirable but unachievable objective) until $\theta_u = 0.03$ leads to a large increase in the collapse capacity ($S_a/g = 2.7$).

17.5.4 Collapse Fragility Curves

The bases for collapse assessment are the fragility curves derived from the response history analyses using the set of 40 ground motions. Typical collapse fragility curves obtained from the parameter study are presented in Fig. 17.14 for the low and high ductility central cases with 50% residual strength and the three values of base shear yield strength θ_y. Given that the mathematical model is correct and deterministic (as has been assumed so far) and that the ground motion frequency characteristics are representative for Istanbul conditions, the probability of collapse, as a function of base shear yield strength, can be read directly from these curves for a given value of spectral acceleration.

Postulating that the design spectral acceleration (at a 10/50 hazard level) for short period structures is about 1.0 g, it becomes evident that the collapse probability is high unless the base shear strength is very large. In concept this is not a surprise for short period structures since in the short period range the inelastic drift demand is known to be much larger than the elastic drift demand. But the quantification of this well known phenomenon in terms of the collapse probability is striking. For the low ductility central case the probability of collapse decreases from about 95% to about 8% by increasing the base shear yield strength from 0.15 W to 0.45 W, and for the high ductility case it decreases from about 80% to 3%. This shows that the effect of yield strength is larger than the effect of ductility, which again is not surprising for short period structures.

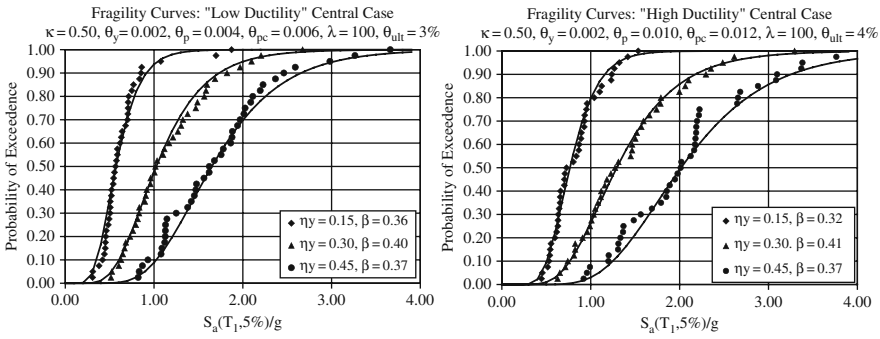

Fig. 17.14 Collapse fragility curves for low and high ductility central cases with 50% residual strength; variation in base shear yield strength θ_y

The intrinsic value of fragility curves is that they provide a perspective of the collapse probability for all values of spectral acceleration. Moreover, they can be utilized to assess the mean annual frequency (MAF) of collapse by integrating the fragility curve over the spectral acceleration hazard curve for a particular site. This exercise was performed using a typical short period hazard curve for the Los Angeles area, resulting in the following information:

For the high ductility cases the MAF of collapse is 0.0022, 0.00066, and 0.00014 for $\theta_y = 0.15$, 0.30, and 0.45, respectively. For the low ductility cases the corresponding values are 0.0047, 0.00125, and 0.00027, i.e., about twice as large as for the high ductility cases. This is the kind of information needed to make informed decisions about the type of retrofit that should be employed. Again, these numbers show that for these short period structures strength is a much more relevant parameter than ductility.

The hazard specific collapse probability and the MAF of collapse depend on aleatory and epistemic uncertainties. Most of the aleatory uncertainty comes from the record-to-record variability, which is accounted for in the fragility curves shown in Fig. 17.14 and is expressed by the β value (standard deviation of the log of the data) shown in the two graphs. The general observation is that the β value for aleatory uncertainties is on the order of 0.4 for all the cases investigated.

Not considered in this study is the dispersion due to epistemic modeling uncertainty. This uncertainty is large but it cannot be evaluated with any degree of confidence. If it were known, it could be incorporated in the collapse assessment by inflating the total dispersion [20] or by placing confidence levels on the collapse probability. In the simplified First-order second-moment (FOSM) approach advocated for general collapse assessment the epistemic uncertainty does not affect the median value of collapse capacity (the 50% probability of collapse value). For this reason the median collapse capacity is a stable parameter for assessing the effects of various structural parameters on the collapse potential of structural systems.

The following section attempts to assess the effect of basic structural parameters on the median collapse capacity.

17.5.5 Evaluation of Median (and 10-percentile) Collapse Capacity

The variations of collapse capacity of infill wall systems with various system parameters are illustrated in Figs. 17.15, 17.16, 17.17, and 17.18. In these figures a dotted horizontal line is drawn at $S_a(T_1)/g = 1.0$ in order to provide a perspective with respect to design spectral acceleration demands. From the presented graphs, and others not shown here, the following general observations can be made:

- Figure 17.15 shows that residual strength has some effect on the median collapse capacity, but this effect is considerable only if the base shear yield strength (θ_y) is large. It was hoped that the residual strength effect would be larger, but this did not materialize because of the necessary assumption that the drift capacity is limited (to a value of $\theta_u = 0.03$ for low ductility systems). If future experiments

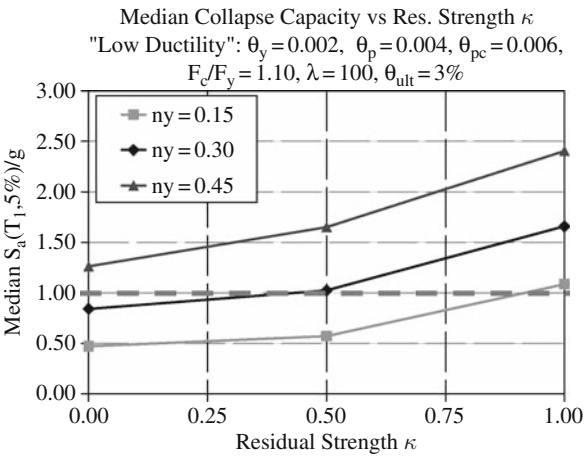

Fig. 17.15 Effect of residual strength (κ) on median collapse capacity, low ductility, θ_y = 0.15, 0.3, and 0.45

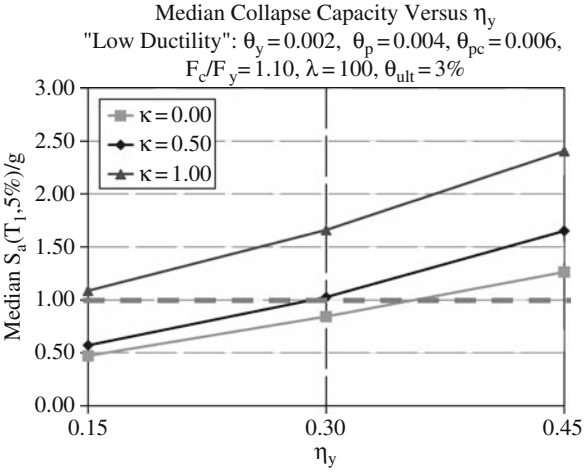

Fig. 17.16 Effect of yield strength (θ_y) on median collapse capacity, low ductility, κ = 0.0, 0.5, and 1.0

will show that the drift capacity is larger, more benefit can be given to the residual strength effect. The data for $\kappa = 1.0$ are given for reference but cannot be considered as realistic because a horizontal post-capping slope in the backbone curve is only wishful thinking.

- Figure 17.16 shows that yield strength has by far the largest effect on the median collapse capacity. Since a 50% probability of collapse at the design level should be unacceptable, the conclusion is that the provided base shear yield strength should be larger than 0.3 W, even if a 50% residual strength can be assured (the $\kappa = 1.0$ line is only for reference).
- Figures 17.17 and 17.18 present median and 10-percentile collapse capacities for low and high ductility systems, in a similar format as Figs. 17.15 and

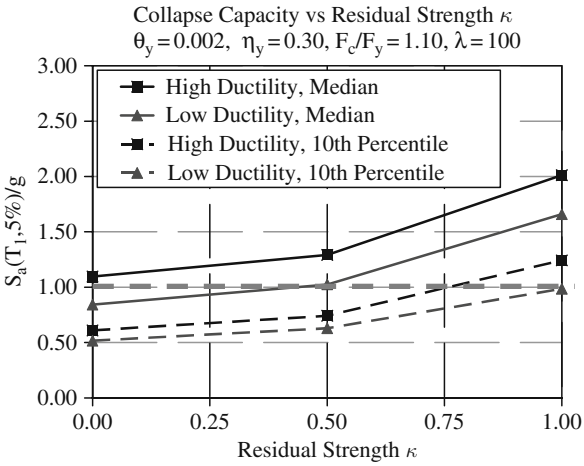

Fig. 17.17 Effect of residual strength (κ) on median and 10-percentile collapse capacity, low and high ductility, $\theta_y = 0.3$

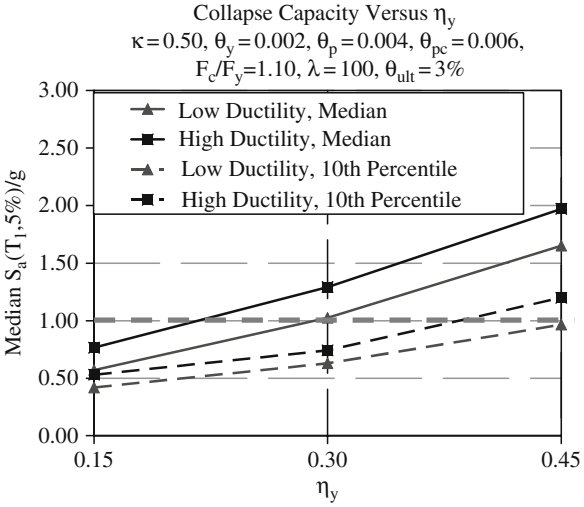

Fig. 17.18 Effect of yield strength (θ_y) on median and 10-percentile collapse capacity, low and high ductility, $\kappa = 0.5$

17.16. As said before, the effect of residual strength is not very important (except for $\kappa = 1.0$), and does not vary by much between low and high ductility systems, as seen from Fig. 17.17.

- Figure 17.18 illustrates the dominant effect of base shear yield strength. The differences between low and high ductility are not very large, indicating that for these short period systems ductility considerations are not dominant (this does not imply that no attention needs to be placed to ductility, as some ductility is necessary in all cases). The figure also shows that an effective base shear yield strength of about 0.45 W needs to be provided (together with 50% residual strength) if the probability of collapse in a design event ($S_a = 1g$) is to be held below 10%.

17.6 Concluding Remarks

This chapter summarizes a process for computing the collapse capacity of deteriorating structural systems. This process is implemented in a parameter study intended to provide global information on the collapse capacity of structural systems consisting of frames with infill walls. The structural systems are modeled as SDOF systems, using a range of structural parameters that is believed to be representative of in-plane cyclic behavior of frames with infill walls. The range of system parameters utilized in this study is based on observations from experimental data published in the literature. Almost all the tests available in the literature are concerned with in-plane behavior of walls only, and the loads are applied directly to the floor beams. Thus, no attention is paid to other failure modes that may invalidate the experimental data. The observations on collapse capacity made in the previous section must be understood in this context. But given that the experimental data indeed do represent reality, the following main conclusions are drawn from the parameter study:

- Base shear strength is the quantity that dominates the collapse capacity.
- Doubling the strength increases the median collapse capacity by about 60–100%
- Increasing the ductility capacity helps but does not save the day when a severe earthquake hits. Doubling the ductility capacity increases the median collapse capacity by about 15–25%.
- Residual strength helps but is not a dominant factor. P-Delta and other limitations (ultimate drift capacity) will take over once the drift demand exceeds the capping value θ_c.
- Low ductility systems ($\theta_c = 0.006$) without residual strength will collapse unless the strength is very large ($\theta_y > 0.6$ for probability of collapse less that 10% at $S_a = 1g$).
- Increasing the ultimate drift capacity (θ_u) helps for systems with residual strength, but the actual magnitude of θ_u is largely unknown because most tests stopped shot of replicating this event.

Caution must be exercised in the interpretation of the results presented here. The collapse capacity information can only be as good as the structural data on which the collapse predictions are based. Pure reliance of in-plane behavior of frame/wall elements cannot be justified in many cases for the following reasons:

- Infill walls are subjected to simultaneous in-plane and out-of-plane actions. The latter may reduce the in-plane shear capacity considerably unless out-of-plane confinement is provided (as is the case in most retrofit techniques.
- The major weakness may be anywhere in the load path from the floor slab to the soil, and a retrofit needs to address this major weakness so that a clear reduction of the risk of collapse is indeed achieved. It is possible that strengthening of one part of the structural system may create severe problems in another part, and may actually increase rather than decrease the risk of collapse.

- Floor slabs need to be capable of collecting the inertia forces and transferring them to the RC framing. This may require diaphragms that have to be much stronger than before the retrofit because the stiff infill walls may attract much higher shear forces (which before the retrofit may have been distributed to several frames).
- Infill strengthening may severely increase the shear demands in boundary columns. Do these columns have adequate strength to avoid brittle shear failure?
- The wall-foundation interface needs to be investigated.
- If the boundary columns are supported on basement walls then the walls act as fixed end cantilevers and the increased shear strength will lead to much larger overturning moments, which could trigger brittle compression or tension failure in the boundary columns (shoring of column will help).
- If the boundary columns are supported on spread footings then uplift may occur very early. This by itself is not believed to be a problem except if the uplift is large, which may trigger a vertical collapse of the slab because of shear failure in the slab system around the boundary columns. Also, uplift will limit the overturning moment capacity, which in turn will limit the shear transferred through the wall.
- Weak story mechanisms must be prevented.
- Wall retrofits should be applied in a manner that minimizes structural irregularities.

If all these issues are considered, then the addition of well confined infill walls (with various strengthening schemes as appropriate) is an effective retrofit technique for most building structures that have poorly reinforced concrete framing as the primary shear resisting system.

Acknowledgments The development of the collapse prediction methodology for deteriorating systems was supported by the Pacific Earthquake Engineering Research (PEER) Center and the NEESR research project CMS–0421551, both sponsored by the US National Science Foundation, and was carried out at Stanford University's John A. Blume Earthquake Engineering Center as part of a comprehensive effort to develop basic concepts for PBEE and supporting data on seismic demands and capacities Additional support was provided by the CUREE-Kajima Phase VI research program. The support of the sponsors is gratefully acknowledged. Any opinions, findings, and conclusions or recommendations expressed in this material are those of the authors and do not necessarily reflect the views of the National Science Foundation.

References

1. ATC-63 (2008) Recommended methodology for quantification of building system performance and response parameters; 90% draft, Applied Technology Council, Redwood City, CA, USA
2. ATC-72-1 (2008) Interim guidelines on modeling and acceptance criteria for seismic design and analysis of tall buildings, 90% draft, Applied Technology Council, Redwood City, CA, USA
3. Cornell CA, Jalayer F, Hamburger RO, Foutch DA (2002) Probabilistic basis for 2000 SAC/FEMA steel moment frame guidelines Journal of Structural Engineering, 128(4):526–533

4. Gatto KS, Uang CM (2002) Effects of loading protocol and rate of loading on woodframe shearwall response. Seventh U.S. National Conference on Earthquake Engineering, EERI, Oakland, CA
5. Ibarra L, Medina R and Krawinkler H (2002) Collapse assessment of deteriorating SDOF systems Proceedings of the 12th European Conference on Earthquake Engineering, London, Elsevier Science Ltd, paper # 665
6. Ibarra LF, Medina RA, Krawinkler H (2005) Hysteretic models that incorporate strength and stiffness deterioration. International Journal for Earthquake Engineering and Structural Dynamics, 34(12):1489–1511
7. Ibarra LF and Krawinkler H (2005) Global collapse of frame structures under seismic excitations John A. Blume Earthquake Engineering Center Report No. TR 152, Department of Civil Engineering, Stanford University and PEER Report 2005/06
8. Karadogan F (editor) (1998) Repair and strengthening of existing buildings. Proceedings of Second Japan-Turkey Workshop on Earthquake Engineering, Istanbul, February 1998
9. Kim YY, Fischer G, Lim YM, Li VC (2004) Mechanical performance of sprayed engineered cementitious composite (ECC) using wet-mix shotcreting process for repair applications. ACI Materials Journal, 101(1):42–49
10. Kyriakides MA, Billington SL (2008) Experimental investigations of engineered cementitious composites as a seismic retrofit for masonry infill walls. Proceedings of the 2008 IABSE Annual Meeting and Congress, Chicago
11. Lignos DG (2008) Sidesway collapse of deteriorating structural systems under seismic excitations. Ph.D. Dissertation, Department of Civil and Environmental Engineering, Stanford University, Stanford, CA
12. Medina R, Krawinkler H (2003) Seismic demands for nondeteriorating frame structures and their dependence on ground motions. PEER Technical Report #2003-15
13. Mehrabi AB, Shing PB, Schuller MP, Noland JL (1994) Performance of masonry-infilled R/C frames under in-plane lateral loads. Report No. CU/SR-94-6, Dept. of Civil, Environmental, and Architectural Engineering, University of Colorado, Boulder, CO
14. Mehrabi AB, Shing PB, Schuller MP, Noland JL (1996) Experimental evaluation of masonry-infilled RC frames. ASCE Journal of Structural Engineering, 122(3):228–237
15. Rahnama M, Krawinkler H (1993) Effects of soft soil and hysteresis model on seismic demands. John A. Blume Earthquake Engineering Center Report No. 108, Department of Civil Engineering, Stanford University
16. Vamvatsikos, D, Cornell, CA (2002) Incremental dynamic analysis. Earthquake Engineering and Structural Dynamics, 31(3):491–514
17. Wasti ST, Ozcebe G (editors) (2003) Seismic assessment and rehabilitation of existing buildings. NATO Science Series IV: Earth and Environmental Sciences – Vol. 29, Kluwer Academic Publishers
18. Wasti ST, Ozcebe G, (editors) (2006) Advances in earthquake engineering for urban risk reduction. NATO Science Series IV: Earth and Environmental Sciences – Vol. 66, Kluwer Academic Publishers
19. Zareian F (2006) Simplified performance-based earthquake engineering. Ph.D dissertation, Department of Civil and Environmental Engineering, Stanford University, Stanford CA
20. Zareian F, Krawinkler H (2007) Assessment of probability of collapse and design for collapse safety. Earthquake Engineering and Structural Dynamics, 36(13):1901–1914

Chapter 18
Strengthening of Brick Infilled Reinforced Concrete (RC) Frames with Carbon Fiber Reinforced Polymers (CFRP) Sheets

Emre Akin, Guney Ozcebe, and Ugur Ersoy

Abstract In Turkey, experimental research on seismic rehabilitation started at Middle East Technical University (METU) in 1969. Since then several research projects in this field leading to developing rehabilitation technologies have been carried out. Majority of these researches inquired the introduction of reinforced concrete infills to the selected bays of the frames. This method developed at METU was applied to a significant number of seismically deficient RC buildings and it was proven to be effective in the past earthquakes. Application of this method, however, necessitates evacuation of the building during construction. Urgent developments of new strengthening methodologies which do not require the evacuation of the building, therefore, become imperative. Subsequently, a research project was initiated at METU Structural Mechanics Laboratory in 2001, which aimed to strengthen the existing masonry infill walls by means of CFRP sheets, to convert these walls into structural elements forming a new lateral load resisting system. As a continuation of the former project, in this study eight 1/3 scaled 2-story 1-bay RC frames, having the common deficiencies of the structures in Turkey, were tested. In this chapter, the test results are revealed in terms of lateral strength, stiffness and energy dissipation characteristics of the specimens.

18.1 Introduction

The extensive structural damage caused by the recent earthquakes in Turkey revealed that majority of the structures in Turkey does not have satisfactory seismic performance. This observation impelled the researchers to intensify their work on developing effective pre-earthquake rehabilitation methods. Introduction of RC infills to the selected bays of the structure found wide acceptance among all other techniques, and was applied to a large number of buildings successfully [1, 7]. The performance of these buildings during the past earthquakes has proven the

U. Ersoy (✉)
Department of Civil Engineering, Bogazici University, Istanbul, Turkey
e-mail: ugur.ersoy@boun.edu.tr

A. Ilki et al. (eds.), *Seismic Risk Assessment and Retrofitting*, Geotechnical, Geological, and Earthquake Engineering 10, DOI 10.1007/978-90-481-2681-1_18,

effectiveness of the method. Application of RC infill walls, however, requires substantial amount of time and more importantly the evacuation of the building under rehabilitation. The evacuation of the buildings in this case turns out to be a significant problem when the huge building stock that needs urgent rehabilitation is concerned. Due to these limitations, development of new strengthening methodologies, which can be practically implemented without any major disruption to the occupants, is required [2–4, 9].

In early 2001, a research project was initiated at Middle East Technical University Structural Mechanics Laboratory for the development of such rehabilitation techniques. It was intended to improve the mechanical properties of the existing masonry walls by strengthening with CFRP sheets, integrating them with the existing structural system, and thereby constitute a new lateral load resisting system. In these studies, seven 1/3 scaled, two-story and one-bay deficient RC frames were tested. The main test parameters were the amount of CFRP sheet used, arrangement of the CFRP layers and the anchorage of the CFRP sheet to the wall and frame members. The test results indicated that the strength and energy dissipation increase due to the rehabilitation were significant. It was therefore, concluded that converting masonry infills into structural walls is possible by strengthening them with CFRP sheets connected both to the frame members and infill walls [5, 6]. In these studies, however, aspect ratio (height-to-width, h/w, ratio) of the infill walls was reported to be equal to one. In the current study, the possible effects of aspect ratio was investigated on the basis of the test results of eight 1/3 scaled RC frames. For this purpose two different aspect ratios were considered.

18.2 Test Program

18.2.1 Test Specimens and Materials

Eight one-bay, two-story RC frames were tested in two series with two different aspect ratios. All of the test specimens were designed and constructed such that they included the common structural deficiencies of the substandard RC buildings in Turkey. Due to the limitations of the existing test facility, the frames were designed to be a 1/3 scale model of a non-ductile frame having weak columns and strong beams. To be representative for most of the existing buildings in Turkey, plain bars were used for the reinforcement of the beams and columns. The ties were not closely spaced at the member ends and the free ends of the ties were anchored to the cover with 90° hooks, not into the core concrete. In addition, no ties were provided at the beam-column joints. Only the gravity loads were considered while detailing the beam reinforcement, therefore the anchorage of the beam bottom reinforcement was inadequate. In six of the test specimens, the column longitudinal bars were lapped at the first and second story floor levels over a length of $20d_b$ (d_b: bar diameter), which is half of the lap splice length required in Turkish Seismic Design Code [8] for plain bars, i.e. $40d_b$. The average compressive strength in the frame members was 17 MPa.

The cross-sectional dimensions of the columns and beams were 100 × 150 mm and 150 × 150 mm, respectively. Four 8-mm diameter bars constituted the

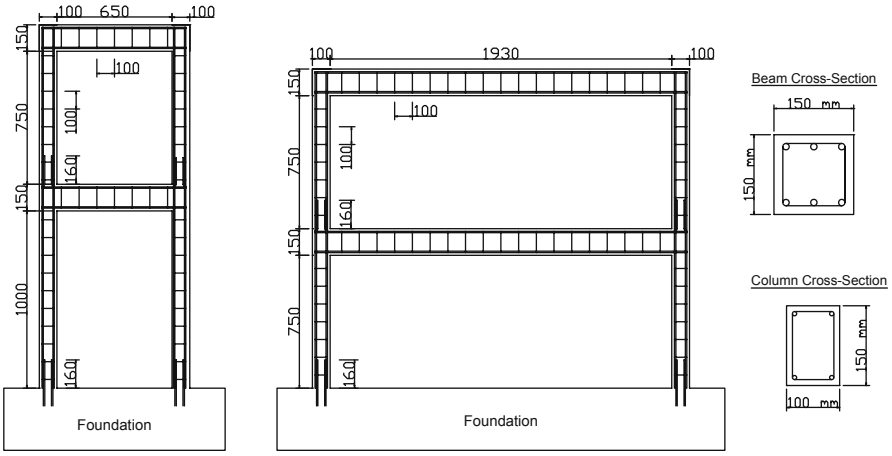

Fig. 18.1 Dimensions and reinforcement details of the test specimens

longitudinal reinforcement of the columns, whereas six bars of the same size were used for beams (3 top and 3 bottom). The lateral reinforcement for both members was fabricated by using 4-mm diameter plain bars and spaced at 100 mm. The geometry and reinforcement details of the test specimens are shown in Fig. 18.1. Specially produced 1/3 scale hollow clay tiles were used for the construction of masonry walls. The plaster with a thickness of 10 mm was applied on both faces of the infill. The construction of the wall and plaster was done by a professional mason following the curing period of the RC frames.

The tests were conducted in two series having two different aspect ratios *(h/w)*. The aspect ratios in Series N and L were 1.4 and 0.4, respectively. Four specimens were tested in each series. The first and second specimens in these series, which were bare and infill frames respectively, were regarded as reference specimens. The differences between the behaviors of these two reference frames will show the effect of infill walls on the bare frame response. The third and fourth specimens were strengthened by using the rapid and user friendly rehabilitation method which was developed in the previous studies carried out in METU [5, 6]. In each series, the longitudinal column bars of the two reference and one strengthened frames had lap splices at both story levels. The fourth specimens in both series, having continuous bars, were tested in order to conceive the possible changes in the behavior due to lap splices. The properties of the test specimens are given in Table 18.1.

Strengthening was carried out by fastening one-layered CFRP sheets along the main diagonals of infill walls using a special adhesive recommended by the manufacturer. The width of the diagonal sheets was adjusted to cover one-fifth of both height and width of the frame cells. The sheets were extended to the RC frame members. In order to prevent premature debonding, the CFRP sheets were anchored both to the infill walls and frame members by specially manufactured CFRP anchors, Fig. 18.2. Holes having a depth of 50 mm and a diameter of 10 mm were drilled into the frame members. These holes were cleaned out of dust. After placing the CFRP

Table 18.1 Properties and design details of the test specimens

Specimen	Type	Longitudinal reinforcement	Lap length (mm)	f_c' (MPa)	$f_m'^{**}$ (MPa)
LREF1	Bare	Lap Splice	$20d_b$	16.1	N/A
LREF2	Infilled	Lap Splice	$20d_b$	16.3	3.9
LSTR-L	Strengthened	Lap Splice	$20d_b$	16.7	3.9
LSTR-C	Strengthened	Continuous	N/A	21.0	4.0
NREF1	Bare	Lap Splice	$20d_b$	13.0	N/A
NREF2	Infilled	Lap Splice	$20d_b$	17.1	3.9
NREH	Rehabilitated	Welded*	$20d_b$	17.1	3.9
NSTR-L	Strengthened	Lap Splice	N/A	19.4	4.0
Material	Type	f_y(MPa)	f_u(MPa)	E (MPa)	
Steel	Stirrup	268	398	210,000	
	Longitudinal	405	605	205,000	
CFRP		N/A	3,430	230,000	
Epoxy		N/A	50	3,500	

*Only the two longitudinal bars at the outer faces of the first story columns were welded.
** f_m' is the compressive strength of the mortar and plaster.

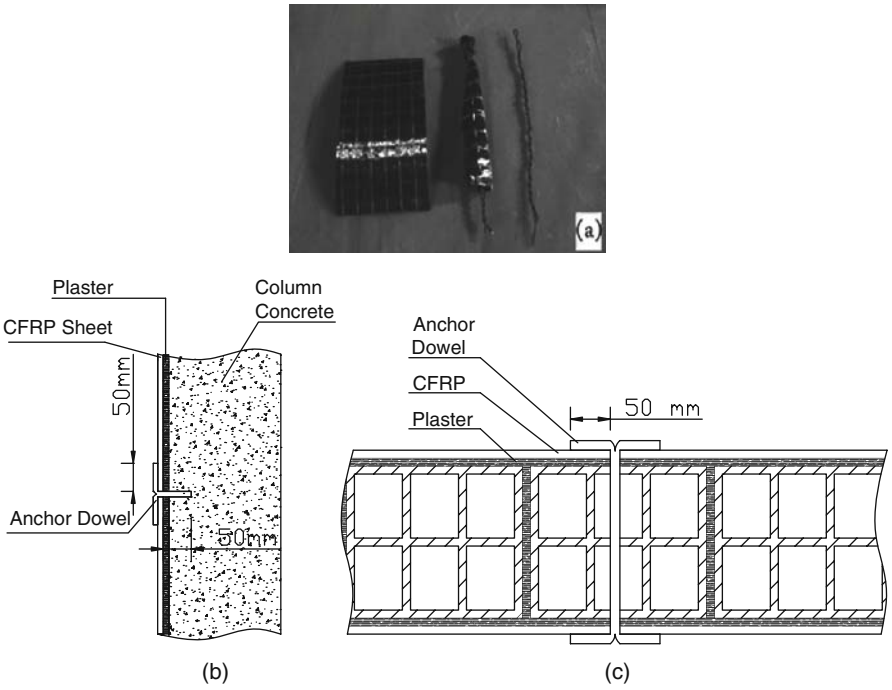

Fig. 18.2 (**a**) Made-up anchor dowels and application of the anchor dowels to (**b**) the frame members and (**c**) the masonry walls

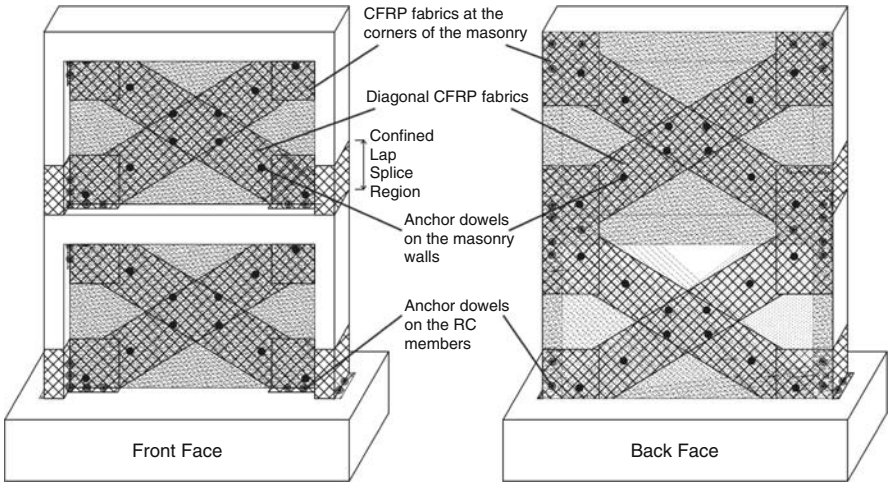

Fig. 18.3 The CFRP strengthening applied on the frame and location of the anchors

sheets on the specimen, the drilled holes were filled with epoxy and the anchor dowels were implanted in these holes by using the guide wires. The fibers of the anchors outside the holes (i.e. the free ends of the anchors) were then spread over the underlying CFRP sheets and were glued [5]. In order to confine the lap splice regions, the bottom ends of the columns were covered up with one-layer of CFRP over a height of 200 mm. These CFRP sheets were also beneficial to spread the struts forces over the column end regions more uniformly. Before applying carbon fiber at the lap splice regions, corners of columns were smoothened to prevent any possible rupture of CFRP. Finally, rectangular CFRP sheets (or gusset sheets) were bonded at the corners of the masonry walls where significant crushing of infill took place. Another function of gusset sheets was to distribute the load coming to the joints. The CFRP scheme of the strengthened specimens is given in Fig. 18.3.

18.2.2 Test Setup and Instrumentation

A strong floor was used in order to provide a base for the test specimens. The frames were tested under reversed cyclic lateral loading which was applied using a double acting hydraulic actuator fixed on a reaction wall. The capacity of the actuator was 600 kN in compression and 300 kN in tension. The lateral load was divided into two by a steel spreader beam and applied at both story levels, so that two thirds of the applied load goes to the upper story. A load-controlled loading scheme was adopted until the peak resistance was reached. The displacement-controlled loading scheme was applied after this point. Axial load was applied directly and equally to the columns by a vertical load distributing beam. The level of axial load was kept constant throughout the test at 10% of the nominal axial load capacity of each column, i.e. $P_{applied}=2\times30$ kN. A steel frame was used for restraining the out of plane

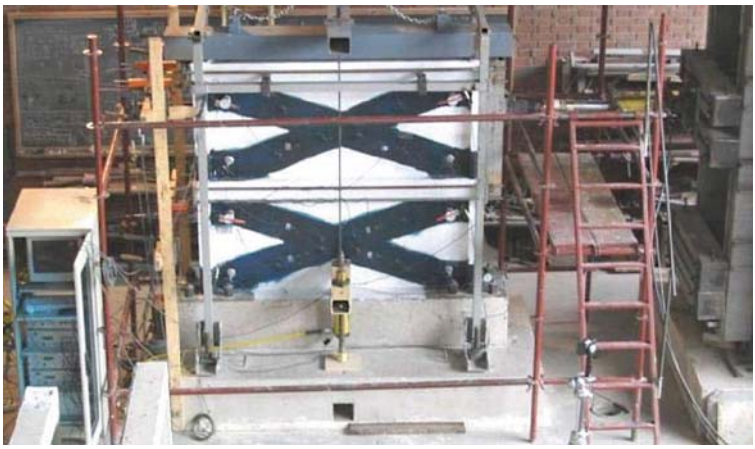

Fig. 18.4 The test setup and instrumentation (See also Plate 25 in Color Plate Section on page 470)

displacements. The measurement of the applied load level, in-plane displacements and strains was made by using an electronic data acquisition system with control feedback. Strain gage based linear variable differential transducers (LVDT's) were used to measure the lateral displacements. Two LVDT's were mounted at the second story level, so that the average measurements of these two devices were used to evaluate the top story displacements. The shear deformations on the masonry walls, horizontal base displacement and frame base slip of the infill specimens were also measured by LVDT's. The strain levels on the CFRP sheets of the strengthened specimens were measured by means of strain gauges attached to the cross overlays. The test setup and instrumentation are shown in Fig. 18.4.

18.2.3 Behavior of the Test Specimens

The observed behavior of the specimens at some critical stages during the test is summarized for the two series separately. The photos of the test specimens showing the failure pattern are given in Fig. 18.5.

18.2.3.1 Series-L Tests

The specimen LREF1 was a bare frame with no infill walls. It was regarded as the first reference specimen. The first observed crack was a flexural one on the lap-splice region of the first story column in the 2nd forward cycle. The lateral load was 8 kN when the this crack was detected. After two cycles, the specimen reached the ultimate load capacity at 13 kN. Beyond that point, the flexural cracks accumulated at the lap-splice region of the first story columns and shear cracks formed at the beam-column joints. When the applied load level decreased to 65% of the ultimate

Fig. 18.5 Failure pattern of the test specimens

LSTR-C

General view after the test

Rupturing of CFRP

Crushing of cover concrete

NREF1

General view after the test

Crushing of cover concrete

NREF2

General view after the test

Shear cracks at beam-column joints

Fig. 18.5 (continued)

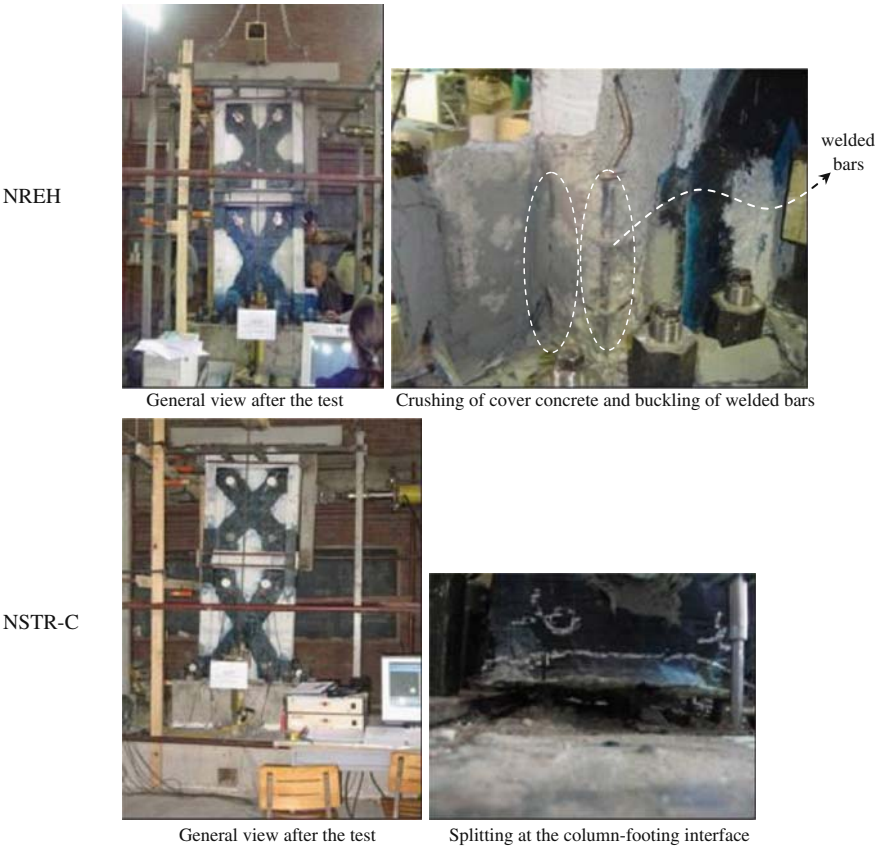

Fig. 18.5 (continued)

load, failure was observed with the crushing of the cover concrete in columns just above the foundation level and wide shear cracks at beam-column joints.

The second specimen was the non-strengthened infill frame, LREF2 which was tested to assess the effect of infill walls on the overall behavior. During the third cycle when the applied load was 40 kN, first flexural cracks were observed at the column-footing interface. Three cycles later, the specimen reached its lateral load resisting capacity at 70 kN. The infill wall acted as a diagonal strut beyond the ultimate load under increasing lateral deflections, accompanied by the separation of the infill on the opposite side. At 2.67% inter-story drift, the top-left hand corner of the infill crushed. After that stage, the response of the specimen deteriorated noticeably, and it rapidly approached the response displayed by the bare frame. It should be noted that the resistances of the specimen in the forward and backward loading directions were similar.

The third specimen in this series, LSTR-L, was strengthened by diagonal CFRP strips. These strips were actually used as tension ties and reduced the inter-story

deformation demands, similar to steel cross-bracing. The column longitudinal reinforcements of specimen LSTR-L were lapped at both story levels. The first crack was observed at a lateral load level of 70 kN in the 5th forward cycle at the intersection of the first story infill and the foundation. In the next forward cycle, at a lateral load of 80 kN, the first visible flexural crack developed just above the lap splice region that was wrapped with CFRP sheet. The majority of the cracks were observed on the masonry infill wall in the vicinity of the CFRP cross overlay sheets. However, the performance of the CFRP anchorages and cross overlay sheets was quite satisfactory until the ultimate load level of 120 kN was reached in the 10th cycle. The lateral drift ratio was 0.5% at that point. Beyond that stage, the diagonal CFRP sheets experiencing large compressive deformations started to debond at the corners of the first story infill walls. These CFRP sheets began to rupture during the consecutive half cycle under tension. Rupturing of both diagonal sheets on the first story infill terminated the beneficial contribution of the CFRP reinforcement to the frame response. Additionally, crushing of the column cover concrete inactivated the CFRP sheets which were used as lateral reinforcement at the lap splice region of the first story columns. At this point the lateral load level was nearly 30% of the ultimate load, and this event determined the end of the test.

The last frame tested in Series-L was specimen LSTR-C which was strengthened in the same manner as the previous frame, LSTR-L. The only difference between the reinforcement details of the strengthened specimens in this series was that LSRT-C had continuous column longitudinal reinforcement. The first visible cracks were flexural hairline cracks which were detected at a relatively low load level, 40 kN. These cracks were observed on the column at two different locations, just above the lateral CFRP sheet and at the mid-height of the column. An ultimate lateral load of 160 kN was reached in the 13th positive loading cycle where the lateral drift ratio was 0.5%. The use of continuous column reinforcement resulted in over 30% increase in the lateral load capacity, The performances of the CFRP anchorage and cross overlay sheets were similar to those of the previous specimen. The diagonal CFRP sheets, which started to debond under high compressive deformations, ruptured suddenly in the following half cycles. This was followed by rupturing of the CFRP sheets used as lateral reinforcement on the columns and crushing of cover concrete at these locations. The test was terminated when the load level was 40% of the ultimate lateral load.

18.2.3.2 Series-N Tests

The bare frame, NREF1 was the first reference specimen in this series. Initially, hairline flexural cracks formed at the bottom of the column at a lateral load of 6 kN in the 2nd forward half cycle. Flexural cracks spread on the first story column and shear cracks formed at the beam-column joints in the consecutive loading cycles. The frame reached its ultimate load capacity during the 4th cycle at a lateral load of 10 kN. The flexural cracks widened considerably towards the end of the test.

Specimen NREF2 was the non-strengthened infill frame which served as the second reference specimen. The initial flexural cracks were observed above the lap splice region of the first story columns at a load of 19 kN in the 2nd loading cycle. In the following cycles, the flexural cracks spread over the first story columns and diagonal cracks formed on the masonry wall. After the frame reached its ultimate lateral load capacity at 26 kN, the lateral stiffness started to decrease rapidly. The contribution of the masonry infill walls to the system behavior continued until significant separation of the infill walls from the neighboring frame members took place. After this stage, the flexural cracks on the first story column widened significantly and shear cracks were observed at the beam-column joints. Eventually, the system response approached the bare frame response.

A premature failure was observed in testing of the first strengthened specimen of this series (NSTR). Due to the bond-slip of the lapped column longitudinal bars at the footing level during the early phases of the loading, it was not possible to increase the load when the specimen started to rock on its base. This indicated that the CFRP wrap provided at the column end for better confinement of the lapped spliced region apparently did not provided the required confinement effect. This was mainly due to the type of bars used as longitudinal reinforcement. As mentioned in previous paragraphs, plain bars were used in the fabrication of all specimens. This observation indicated that CFRP wrapings are not effective for the confinement of lap splice regions where plain bars are lapped.

As there was no visible damage, the test was stopped at this stage and the specimen was rehabilitated by removing the cover concrete and welding the lapped longitudinal reinforcements at the exterior corners of both columns. This region was then filled up with repair mortar and wrapped by one-layer CFRP, over a height of 200 mm. This specimen was renamed as NREH. During the test of this specimen, first visible cracks were the diagonal crack on the masonry infill and flexural crack on the columns. These cracks were formed simultaneously at a lateral load of 40 kN. The ultimate load capacity of the frame was reached in the following cycle when the lateral load was 50 kN at a lateral drift ratio of 0.5%. After a drift ratio of 1.2%, the cracks which formed at the base of the first story columns widened considerably and the diagonal CFRP sheets started to debond. Finally, the lateral CFRP reinforcement at the bottom of the first story columns rupture at lateral drift ratio of 2.7%. This event triggered crushing of the cover concrete and buckling of the welded longitudinal reinforcements at this region.

The frame, NSTR-L was the last specimen in Series-N which had lapped splices at both stories. The first flexural cracks were detected at the mid-height of the first story columns at a lateral load of 30 kN. Further flexural cracks were observed on the first story columns in the next cycle when the specimen reached its ultimate lateral load capacity at 36 kN. The lateral drift ratio of the frame was 0.4% at this stage. Beyond a drift level of 1%, the lateral CFRP reinforcement at the base of the first story columns detached from the foundation and the damage concentrated at the infill wall -foundation and column-foundation interfaces. The test was terminated when the crack width reached 30 mm at the column-foundation interface. At this stage the lateral drift ratio was 3%.

18.3 Discussion of Test Results

The strength, stiffness, drift and energy dissipation characteristics of the test specimens were compared for the two series. In Table 18.2, the experimental results are shown in terms of initial stiffness, cracking load, lateral load and top story displacements at yield and peak points, and displacements at 85% of the peak load. These results were estimated from the idealized bi-linear curves which were fitted

Table 18.2 Comparison of test results

Spec.	P_{cr} (kN)	P_y (kN)	P_{max} (kN)	Δ_y (mm)	Δ_m (mm)	Δ_{85} (mm)	K^+ (kN/mm)	Δ_{85}/Δ_y (%)	Failure Mechanism
LREF1	4.8	12.0	12.8	13.1	38.2	59.5	0.92	4.54	FF
LREF2	29.2	66.0	70.0	1.4	2.2	11.1	49.5	7.93	CIC
LSTR-L	70.0	110.3	122.0	2.1	8.6	15.6	52.5	7.43	DDS, CIC
LSTR-C	90.0	142.7	160.0	2.8	8.5	12.1	142.7	12.1	DDS, CCC, CIC
NREF1	3.0	8.7	9.8	5.8	27.1	56.8	1.5	9.79	FF
NREF2	9.4	24.8	25.4	2.3	7.9	30.4	10.9	13.39	SIF, CIC
NREH	21.0	49.2	50.0	2.4	10	60.2	21	25.6	DDS, CCC
NSTR-L	23.0	35.2	36.0	2.0	7.3	9.3*	18	4.77*	SCFI

* For this specimen, the displacement at 85% of the ultimate load was relatively low because of the sudden decrease in lateral strength after the ultimate capacity. There was no sudden drop of the lateral load after this stage.

FF: flexural failure, CIC: crushing of infill corners, DDS: debonding of diagonal CFRP sheets, CCC: crushing of cover concrete of column, SIF: separation of infill and frame, SCFI: splitting at the column-footing interface

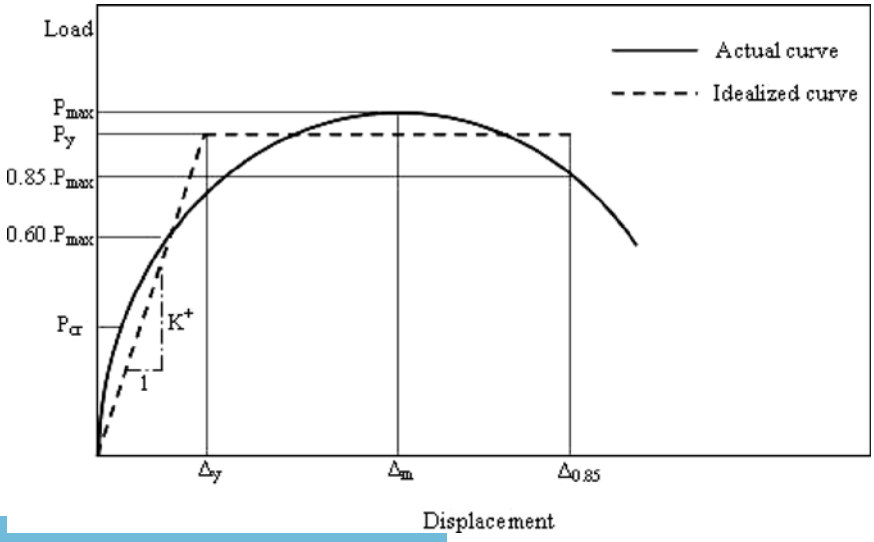

Fig. 18.6 Bi-linear approximation of envelope curves

to the forward cycle envelope curves using an iterative process based on equal area concept, Fig. 18.6.

The lateral load versus roof displacement hysteretic relationships of Series-L and Series-N specimens are shown in Figs. 18.7 and 18.8, respectively. For a better comparison of the test results, envelope curves were constructed by connecting the maximum points of the hysteretic relationships. These envelope curves are shown in Figs. 18.9 and 18.10, for Series-L and Series-N specimens, respectively.

When the ultimate lateral loads of the first and second reference specimens are compared in both series, it is observed that the addition of the plaster applied masonry infill walls increased the base shear capacity of the bare frames considerably. The increase was 5.5 folds in the case of Series-L and 2.6 folds in the case of Series-N specimens. CFRP application on the masonry walls of the specimens having lap splices resulted in further increases in the lateral load capacity of the test specimens in each series. The base shear capacity of the specimen LSTR-L was 1.74 times that of LREF2. In series-N, the ratio of the base shear capacity of specimen NSTR-L to that of NREF2 was 1.42. These observations indicated that, regardless of the aspect ratio of the infill walls, the proposed rehabilitation technique increases the base shear capacity of the frames considerably, although this was more notable in Series-L. The lap splices of the column bars had an unfavorable influence on the ultimate lateral load capacity of the specimens. The capacity increase due to the welding of lapped bars at the two exterior faces of the first story columns in specimen NREH was in the order of 40% when compared with specimen NSTR-L. On the other hand, the use of continuous column longitudinal bars in specimen LSTR-C of Series-L resulted in a capacity increase of 30% with respect to specimen LSTR-L.

The slope of the line, which connects the point corresponding to 60% of the ultimate load on the ascending part of the forward envelope curve to the origin, is assumed to represent the initial stiffness of the test specimens. The initial stiffness, K obtained in this way are given in Table 18.2. The addition of plastered masonry infill walls increased the initial stiffness of test specimens considerably in both series. This increase, however, was more prominent in Series-L than Series-N. Strengthening of the frame having lap splices in Series-L (specimen LSTR-L) did not change the stiffness of the system. This indicates that reinforcing squat masonry infill walls with CFRP does not affect the stiffness of the original structure, but do increases the base shear capacity. This further indicates that the proposed rehabilitation methodology applied on infill walls having low aspect ratio increases the base shear capacity of the system without increasing the seismic demand on the structure during a particular earthquake, as the stiffness characteristics of the building remain unchanged. A significant stiffness increase was observed due to the use of continuous column reinforcement in Series-L. The ratio of initial stiffness of specimen LSTR-C to that of specimen LSTR-L was nearly 2.7. In Series-N, the initial stiffness increased nearly 65% due to strengthening of the frame having lap splices. This increase was at a level of 92% in the case of NREH which was rehabilitated by welding the lapped longitudinal bars at the exterior faces of the first story columns, addition to the CFRP strengthening. The stiffness increases in specimens NREH and LSTR-C were mainly due to the elimination of the loss of lateral stiffness resulting from column bar slip deformations.

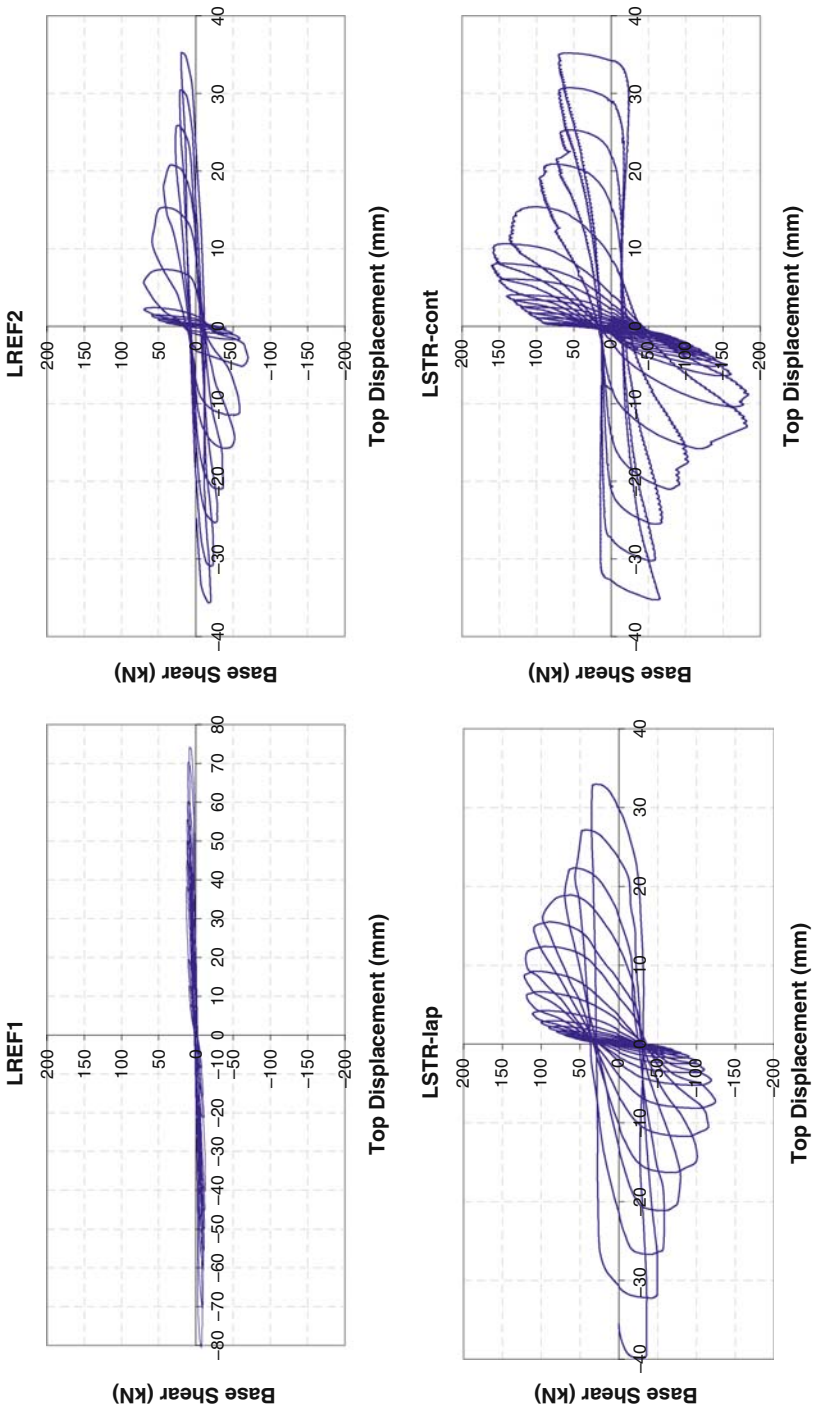

Fig. 18.7 Lateral Load-Roof Displacement hysteresis curves of Series-L specimens

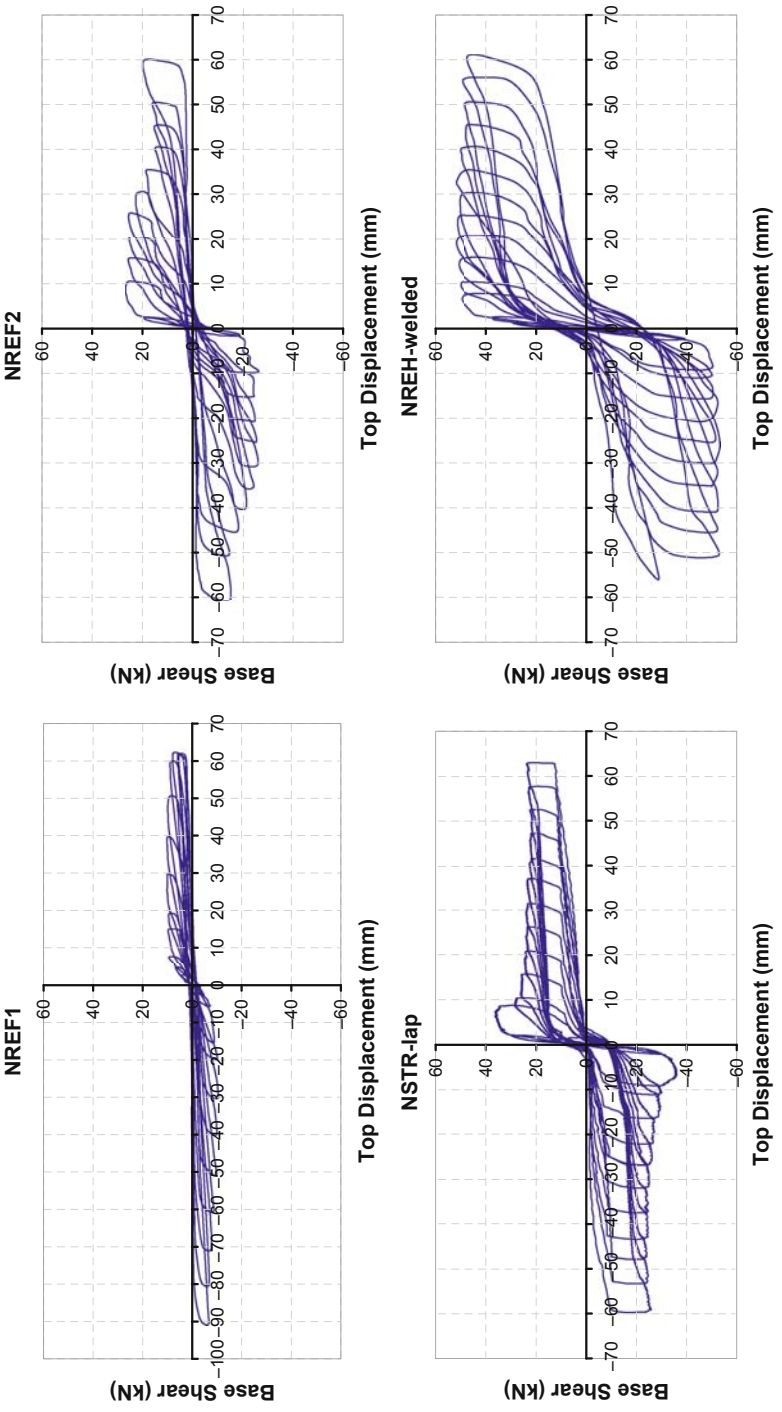

Fig. 18.8 Lateral load-roof displacement hysteresis curves of Series-N specimens

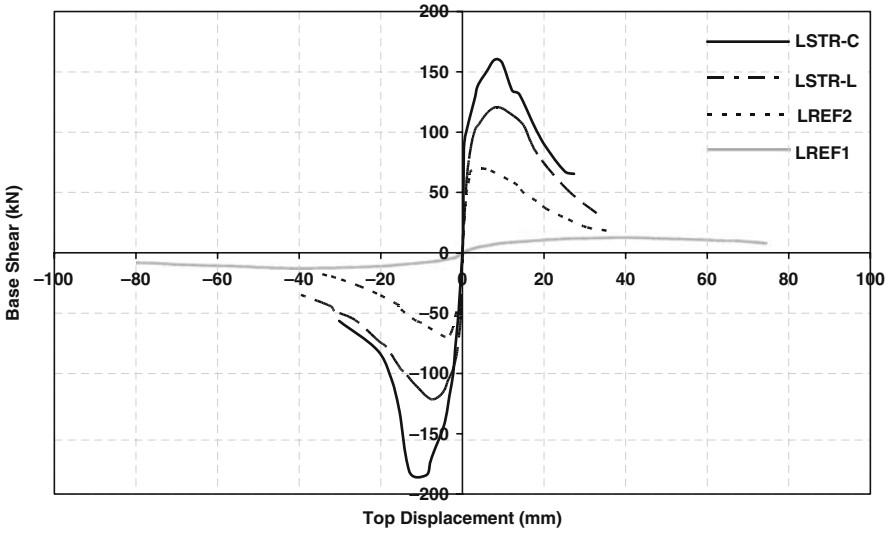

Fig. 18.9 Base shear-roof displacement envelope curves for Series-L specimens

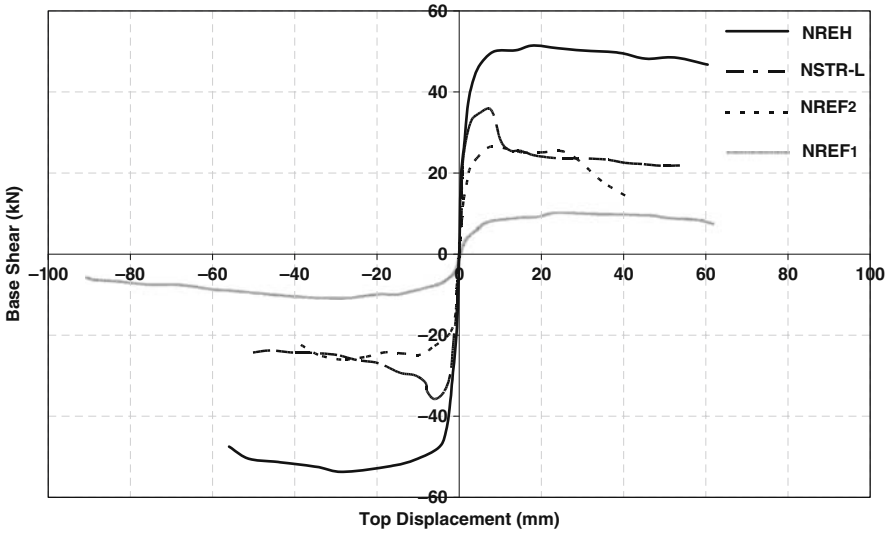

Fig. 18.10 Base shear-roof displacement envelope curves for Series-N specimens

The comparison of the envelope curves in Figs. 18.9 and 18.10 provided important information about the drift properties of the test specimens. Except specimens NSTR-L and NREH, the two strengthened frames in Series-N, all masonry infill frames displayed a behavior tending to a bare frame response at large displacement amplitudes. In specimen NSTR-L, after the ultimate capacity was reached, a sudden strength and stiffness decrease was observed, which may be an issue related

to the large bond-slip rotations at the base of the first story columns. However, at an approximately constant load level corresponding to 60% of the ultimate load, the specimen continued to undergo large displacements without a new sudden decrease in strength. Welding of the lapped reinforcement in specimen NREH prevented the formation of large bond-slip rotations and this specimen displayed the most ductile response among all specimens. The load-displacement hysteresis curves of NREH, however, displayed some pinching. This pinching may be due to partial welding of

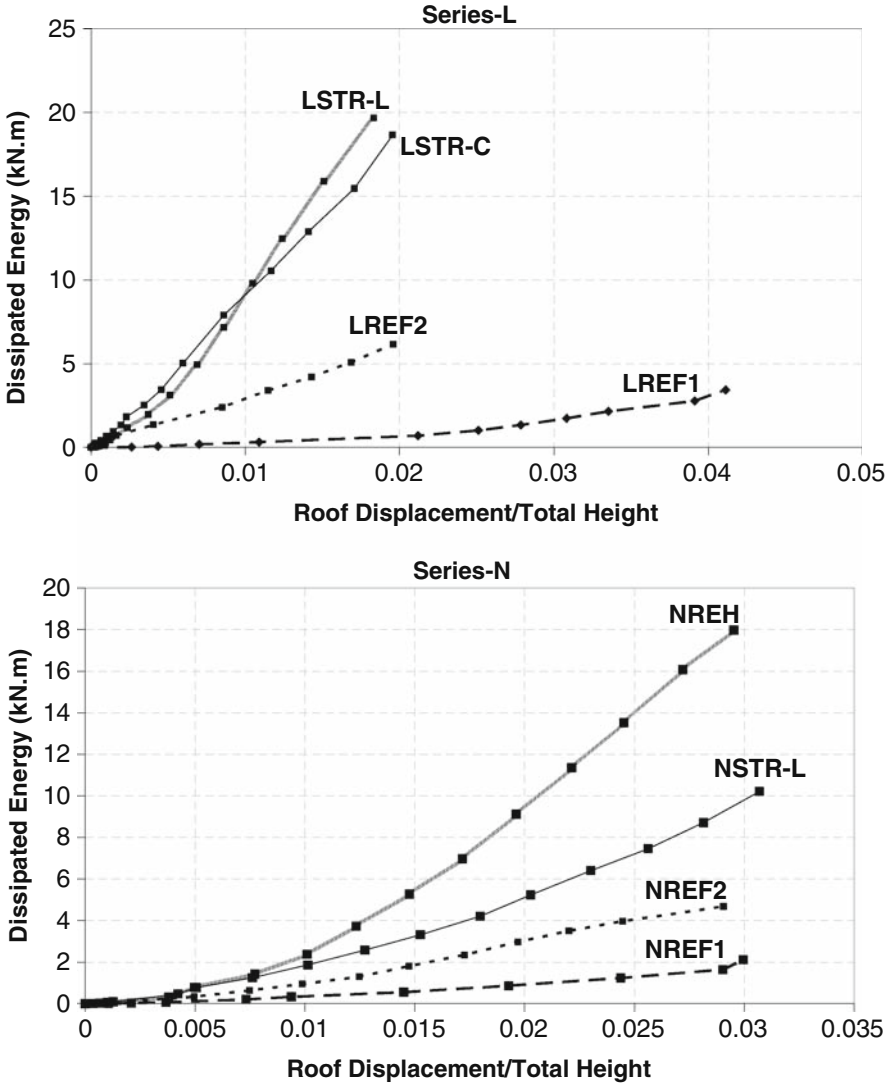

Fig. 18.11 Dissipated energy vs. roof drift ratio relationships for the test specimens

the lapped reinforcement. As mentioned before, only two of the four column lapped bars were welded.

In Table 18.2, top story displacements at yield, Δ_y and at a load level corresponding to 85% of the ultimate load on the descending branch, $\Delta_y$are given. The displacement ductility ratios, $\Delta_{0.85}\Delta_y$is also shown in the same table for each test specimen. In Series-L specimens, strengthening of the frames having lap splices with CFRP did not increase the system ductility significantly. In this series, however, the use of continuous column reinforcement in strengthened specimen, LSTR-C lead to a nearly 60% increase in the ductility ratio when compared with LREF2 and LSTR-L. On the other hand, in Series-N, ductility ratio of the strengthened specimen, NSTR-L was only 35% of specimen NREF2. However, the displacement value at 85% of the maximum capacity is relatively small because of the sudden drop of the lateral load after the ultimate point. After this drop in the load capacity, the frame response was quite ductile under increasing lateral displacements, Fig. 18.10. Besides, partial welding of the lapped bars at the first story columns in specimen NREH increased the system ductility nearly 100% when compared with specimen NREF2.

The energy dissipation characteristics of the test frames are shown in Fig. 18.11. Due to the addition of masonry infill walls, the second reference specimens dissipated more energy than the bare frames in both series. The CFRP intervention resulted in further increases in energy dissipation capacity of the frames.

18.4 Conclusions

Based on the test results of eight 1/3 scale RC frames, the following conclusions are summarized. These conclusions should not be generalized without due judgment. Further experimental studies on larger scale, multi-bay specimens are needed. Such a testing program is being carried out at METU Structural Mechanics Laboratory.

1. Tests have revealed that converting masonry infills into structural walls is possible by strengthening such non-structural members by CFRP sheets and strips connected to the frame members.
2. As the application of this technique does not require the evacuation of the building under consideration, it seems to be a feasible and economical solution.
3. After rehabilitation, the lateral strength of all specimens showed a significant increase under reversed cyclic loading. The strength increases in Series-L were about 75% and 120% for specimens LSTR-L and LSTR-C, respectively. In Series-N, the increases were at a level of 40% and 100% for NSTR-L and NREH, respectively.
4. The CFRP reinforcement did not noticeably change the system stiffness in Series-L. However, in Series-N, a 65% increase was observed in system stiffness due to strengthening.

5. Tests have indicated that the use of CFRP wraps for the confinement of lap splice regions where plain bars are lapped is not an effective measure of insuring proper stress transfer between the lapped bars.
6. The use of continuous/welded column reinforcement in strengthened specimens resulted in further increases in both strength and stiffness of the frames.
7. In specimen NSTR-L, due to the extreme bond slip deformations developing at the lap splice regions of the first story columns, a sudden decrease in strength took place after the ultimate capacity was reached. This shows the unfavorable influence of the lap splices on the flexural response of the frames subjected to lateral forces.
8. The drift characteristics of the test specimens improved considerably with strengthening.
9. It should be noted that welding should not be applied unless weldability of the reinforcement is assured.
10. The rehabilitation applied in Series-N by welding the lapped bars, however, led to further improvements in the drift characteristics. The system ductility of the unreinforced masonry infill frame was increased by nearly 100% by this implementation.
11. A comparison of the test results reported here with the test results on frames with reinforced concrete infills revealed that the behavior of frames with CFRP reinforced masonry infills is not as ductile as frames with reinforced concrete infills, [7].
12. In Series-L specimens, the CFRP sheets used as lateral reinforcement at the lap splice regions of the columns prevented serious local failures at these locations. This conclusion cannot be extended to Series-N specimens. To overcome this deficiency welding of lapped reinforcing bars is essential.
13. The comparison of the dissipated energy vs. roof drift ratio curves indicates that the CFRP strengthening increases the energy dissipation capacity of the test specimens significantly.

References

1. Canbay E, Ersoy U, Ozcebe G (2003) Contribution of reinforced concrete infills to the seismic behavior of structural systems. ACI Structural Journal, 100(5):637–643
2. Ersoy U, Ozcebe G, Tankut T, Akyuz U, Erduran E, Erdem I (2003) Strengthening of infilled walls with CFRP sheets. Proc. International Advanced Research Workshop, Seismic Assessment and Rehabilitation of Existing Buildings, Izmir
3. Erdem I, Akyuz U, Ersoy U, Ozcebe G (2006) An experimental study on two different strengthening techniques for RC frames. Engineering Structures, 28:1843–1851
4. Akguzel U (2003) Seismic retrofit of brick infilled R/C frames with lap splice problems in columns. MS Thesis, Graduate Program in Civil Engineering, Bogazici University, Istanbul
5. Ozcebe G, Ersoy U, Tankut T, Akyuz U, Erduran E (2004) Rehabilitation of existing reinforced concrete structures using CFRP fabrics. Proc. 13th Conference on Earthquake Engineering, Vancouver, BC
6. Ozcebe G, Binici B, Ersoy U, Tankut T, Ozden S, Karadogan F, Yuksel E, Ilki A (2006) Analysis of infilled reinforced concrete frames strengthened with FRP's. Retrofitting of Concrete Structures by Externally Bonded FRPs, fib, Technical Report

7. Sonuvar MO (2001) Hysteretic response of reinforced concrete frames repaired by means of reinforced concrete infills. PhD Thesis, Department of Civil Engineering, Middle East Technical University, Ankara
8. The Ministry of Public Works and Settlement (2006) Turkish code for buildings in seismic zones. Draft Version
9. Van Den Einde L, Zhao L, Seible F (2003) Use of FRP composites in civil structural applications. Construction and Building Materials, 17:389–403

Chapter 19
Improved Infill Walls and Rehabilitation of Existing Low-Rise Buildings

Faruk Karadogan, Sumru Pala, Alper Ilki, Ercan Yuksel, Waiel Mowrtage, Pinar Teymur, Gulseren Erol, Kivanc Taskin, and Rasit Comlek

Abstract Five to 10% of buildings in earthquake prone areas, with structural deficiencies and non-structural partitioning walls are expected to collapse totally during a severe earthquake. Relying on the encouraging early test results, transforming a selected number of non-structural partitioning walls to structural walls has been considered as one of the realistic preventive measures if sufficient reliability is achieved both experimentally and theoretically. The major part of the recent experimental and theoretical works of *The Structural and Earthquake Engineering Laboratory of Istanbul Technical University (ITU)* has been devoted to achieve better understanding of the seismic behavior of brittle partitioning walls which are generally ignored in the design, rehabilitation design or evaluation stages of ordinary *low-cost, low-rise*, reinforced concrete relatively old buildings. In this chapter the complementary tests and analytical works carried out for this purpose are summarized to come up with a cost-effective prescriptive solution to prevent the total collapse of buildings. The proposed retrofitting technique is exemplified through the mathematical models of strengthened buildings offered by codes which are reviewed as well. The experimentally developed data such as the modulus of elasticity of clay brick walls, damping ratios, shear strength of improved partitioning walls and earthquake load reduction factors are referred in the analyses.

19.1 Introduction

It is estimated that there are approximately 700,000 low-rise vulnerable buildings just in Istanbul where an earthquake with the magnitude of seven or more has a $41 \pm 14\%$ probability of occurrence within the next 30 years [1]. From the structural engineering point of view, this means that, some realistic procedures should be developed as quickly as possible for retrofitting the existing buildings. Most of these buildings are structurally irregular and weakly constructed low-rise reinforced concrete buildings altered in time partly because of the rapid industrialization and

F. Karadogan (✉)
Istanbul Technical University (ITU), Istanbul, Turkey
e-mail: karadogan@itu.edu.tr

A. Ilki et al. (eds.), *Seismic Risk Assessment and Retrofitting*, Geotechnical, Geological, and Earthquake Engineering 10, DOI 10.1007/978-90-481-2681-1_19,

urbanization at that particular period of time in Istanbul. Starting with the 1992 Erzincan Earthquake, universities and governmental offices have accelerated the organized and systematic investigations, not only on the sites but also in the laboratories. If the documents and experiences collected and accumulated after the 1995 Dinar Earthquake, 1998 Adana-Ceyhan Earthquake and 1999 Kocaeli Earthquakes are put together, some important statistical results may be achieved from which realistic approaches can be generated to retrofit the existing *low-cost, low-rise* buildings before another catastrophy hits the population with all aspects. The building stocks, the expected financial burdens of retrofitting, seismicity of the regions (Fig. 19.1), peak ground acceleration (PGA) map of Istanbul for 10% probability of exceedance in 50 years [2] (Fig. 19.2), structural deficiencies observed, properties of concrete and steel used in constructions, are all known statistically. Therefore prescriptive solutions for retrofitting such structurally unimportant buildings can be proposed so that even heavy damages are foreseen for those buildings, collapse prevention level can be achieved in a cost effective way.

During seismic actions, brittle hollow clay brick infill walls, even if their compressive strengths are very low, can have a certain amount of contribution to the lateral and vertical load resistance of existing weak reinforced concrete frames, in terms of strength, stiffness and damping. Free vibration measurements carried out on three similar 12 story reinforced concrete buildings in different stages of construction show the controversial effects of partitioning walls on free vibrational characteristics which are essential quantities to estimate the earthquake design forces [3]. In many cases, they significantly control the mode of collapse. Nevertheless, generally they are not considered as load resisting elements of the building. On the other hand laboratory tests, as well as site observations of structural damages after earthquakes, have proven the significant contribution of infill walls to seismic resistance as long as they do not loose their stability in their own planes. It is clear that any measure that may enhance the weak tensile properties of the infill walls may further

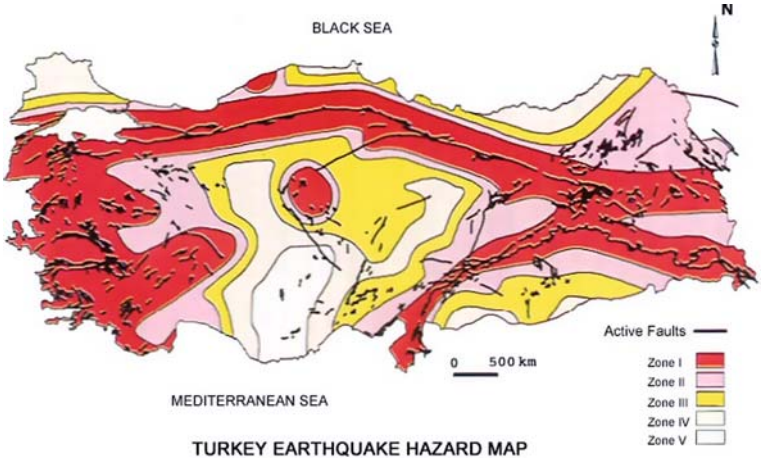

Fig. 19.1 Seismicity of Turkey (See also Plate 26 in Color Plate Section on page 470)

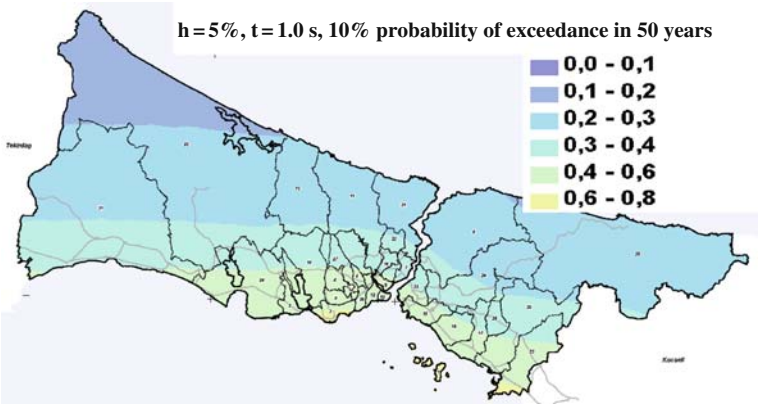

Fig. 19.2 PGA map of Istanbul (See also Plate 27 in Color Plate Section on page 471)

increase the contribution of infill walls to the overall seismic behavior of reinforced concrete frames. It is also clear that any kind of intervention in their plane of bare frames has the chance to modify the lateral strength and ductility features of it, if it is done properly. That is why research is going on and it will go on using new materials and new techniques.

The following paragraphs are devoted to the common structural deficiencies observed in local practices, common material properties, the early element level tests of brittle brick walls which were carried out essentially in the *Structural and Earthquake Engineering Laboratory of Istanbul Technical University* and elsewhere [4–7].

After having introduced the results of several groups of structural tests on stiffness, strength and damping properties of infill walls, in the preceding sections, several parametric works are added to exemplify the efficiency of the proposed prescriptive technique which is essentially based on improvement of some of the selected non-structural infill walls in the building to structural walls. Some bare frames in the building can be utilized for the same purpose if some new partitioning walls are allowed from architectural point of view.

19.2 Common Deficiencies and Material Characteristics

Depending on the statistical data obtained after the destructive 1999 Kocaeli Earthquake, it is strongly probable that 5–10% of existing *low-cost, low-rise* reinforced concrete buildings will totally collapse as it is seen in Fig. 19.3. Those are generally four to five story high buildings which have theoretically *moment resistant ductile reinforced concrete frame* skeletons. Unfortunately, most of those very flexible structures were not able to show the expected seismic behavior because of some common structural deficiencies and lack of proper application of related codes and standards. Most of the common deficiencies are summarized in a schematic

Fig. 19.3 Total collapse of low cost–low-rise reinforced concrete buildings (See also Plate 28 in Color Plate Section on page 471)

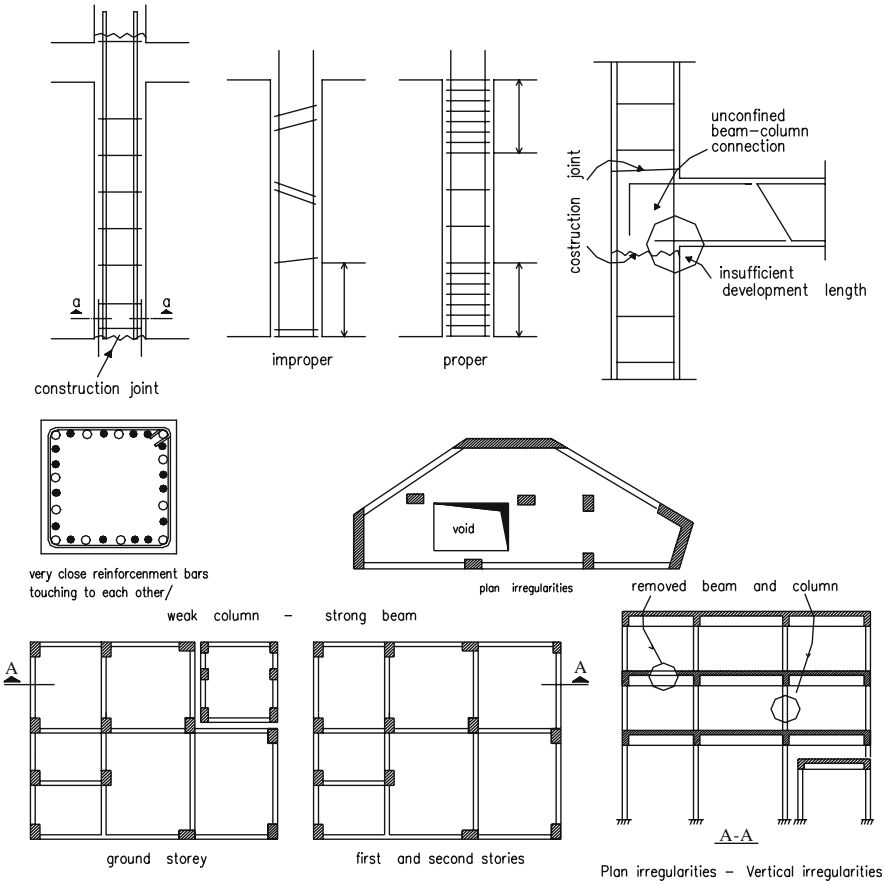

Fig. 19.4 Various structural deficiencies observed

way in Fig. 19.4. Among them one can list *poor detailing*, *lateral and vertical irregularities*, *non – engineered structural alterations* such as weakening and/or removing beams, columns, or illegally *added stories* etc. It has been observed on the sites that confinements especially in columns are not satisfying the minimum code requirements, which means that premature shear failures and lack of sectional ductilities are almost inevitable. Beam-column connections have not been prepared as it is required in codes, which means that shear forces developed either in beams or in upper columns can not be transmitted to lower columns properly. In other words, the integration of columns and beams is not good enough to resist the earthquake forces all together. Therefore disintegration of structural elements should strongly be expected at the early stages of seismic activities.

If the design forces defined by codes of those construction years are examined it would be seen that they are only around 3–4% of seismic weight of the structure, which means that even the buildings that have been properly constructed they would not be satisfactory anymore according to the recent design criterion. Even the building under investigation has practically none of the structural deficiencies exemplified above they are all very flexible structures with strong beams and weak columns. Hence, they will expose large story drifts during a severe earthquake especially when they are more transparent due to architectural demands in their first stories than the upper stories. When this is the case then the second order effects of axial forces start to become dominant in overall structural behavior quickening the total collapse of building.

An excessive research has been carried out on the concrete compressive strength achieved in many sites and after statistical evaluation it has been concluded that the concrete strength is around $f'_c = 10 \pm 2.8$ MPa which is lower than the minimum code requirement and it means that the expected shear resistance and bond of concrete is going to be low as well [7, 8]. One can also expect that this quality concrete used in most of the buildings can not be able to protect the reinforcements against corrosion, which means that in certain critical sections, contact no longer exists between the concrete and the remaining parts of non-corroded reinforcements.

19.3 Experimental Works

The complementary results achieved by means of different experiments within the framework of the general purpose of transforming the nonstructural infill walls to structural walls and new strengthening procedures, are being summarized in the following three sections.

19.3.1 First Stage Experiments

Some early experimental works in Istanbul Technical University goes back to nineteen sixties on *shear stress – axial stress relationships* of infill walls used widely in

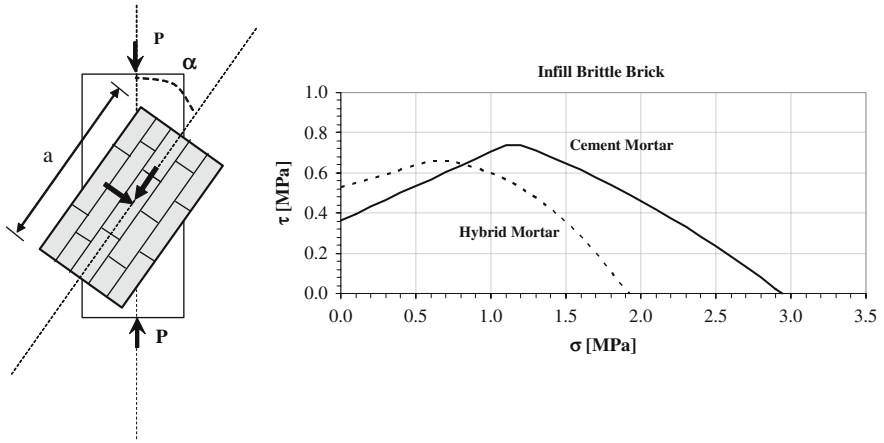

Fig. 19.5 Shear stress-axial stress interaction curves obtained for wall assemblies

the local housing practice [6]. This work was providing clear ideas about the shear strength of certain type solid brick walls under the gravity load effects, Fig. 19.5. Different kind of mortars had been used in those tests.

Tremendous amount of so-called *pure shear* or *diagonal tension* tests have been carried out using different type of bricks and strengthening techniques. The testing set-ups of *four brick shear tests* and *pure shear or diagonal tension tests* and the limited findings which were mainly pertinent to the carbon fiber reinforced polymer (CFRP) strengthened brittle brick walls specimens, are all presented in Figs. 19.6, 19.7 and 19.8, respectively.

If Figs. 19.5 and 19.6 are examined it will be seen that the lateral load resisting capacities of partitioning walls can not be neglected. Contrary to that they should be definitely utilized especially when the rehabilitation costs are not affordable. In other words there are some cases for which some of these walls can be modified to

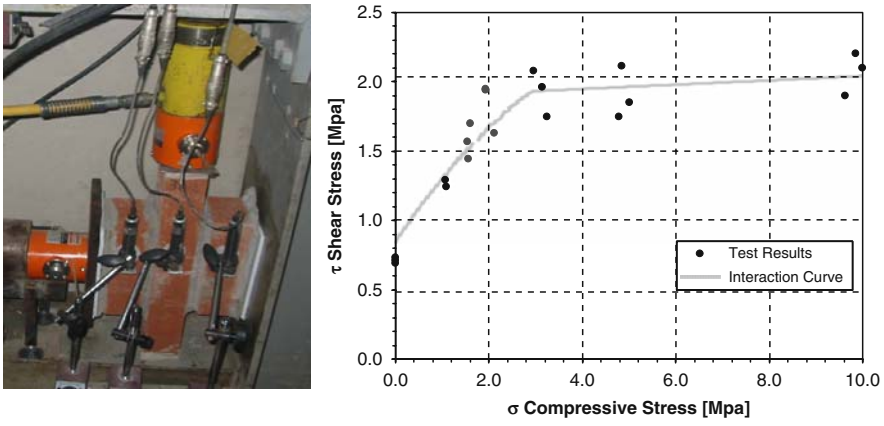

Fig. 19.6 Four brick shear tests

Fig. 19.7 Pure shear tests of brittle walls (See also Plate 29 in Color Plate Section on page 471)

structural walls depending on engineering decisions so that the building will survive of total collapse. The test results presented in Fig. 19.4 is related to the specimens made from solid ordinary bricks and indicates that even for zero axial stress which is increasing the shear strength up to certain level when exists, the shear strengths of walls build with ordinary mortar are between 0.4 MPa and 0.6 MPa and may go up near to 0.8 MPa when special mortar is used, see Fig. 19.5, [6]. Those are not negligible amounts especially if they are compared with the shear strength of low quality concrete which can be calculated as follows by Eq. 19.1, [9].

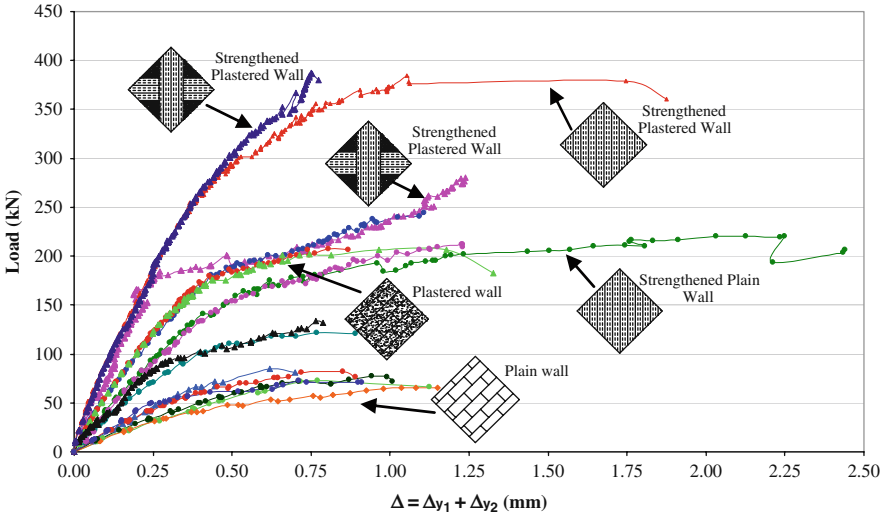

Fig. 19.8 Force-displacement curves (See also Plate 30 in Color Plate Section on page 472)

$$0.35\sqrt{f_c'} = 0.35\sqrt{10} = 1.1\ MPa \tag{19.1}$$

Four brick shear test results given in Fig. 19.6 which exposes the similar tendency observed in Fig. 19.5 are associated to the high strength brick wall tests with special mortar.

755×755 mm square specimens which are similar to ones defined in [10] have been skillfully fabricated using hollow clay bricks which were utilized widely in the region as non-structural partitioning walls. Those bricks have only 2.5 MPa compressive strength perpendicular to their holes. The two different clay bricks used had the dimensions of 135×190×190 and 85×190×190 mm. 10 mm thick continuous mortar layers had water:cement:lime:sand volumetric mixture proportion as 1:1:0.5:4.5. The 10 mm thick plaster had the volumetric mixture proportions as 1.25:1:0.5:4.5, [8]. Three different CFRP patterns were used for strengthening the plastered masonry panel specimens Fig. 19.7, [11]. The test results presented in Fig. 19.8 indicates that the shear carrying capacities of specimens are increasing by the help of CFRP. CFRP strips may become as effective as the CFRP which covers the whole wall, which is important from economical point of view. Force-deformation curves presented in Fig. 19.8 were converted to τ-γ *shear stress-shear strain diagrams* which can be utilized later in more rigorous finite element analyses [12–15].

From the initial slope of the force-deformation curves presented in Fig. 19.8, one can determine the equivalent modulus of elasticity of the brick wall, E_e, referring to the following simple equation, Eq. 19.2,

$$E_e = P/(F \times \Delta/L) \tag{19.2}$$

where $F = b \times t$ and $\Delta = \Delta_{y1} + \Delta_{y2}$. b and t indicate the average width of the fictitious bar loaded and the thickness of wall, respectively. b has been chosen as the width of the load transferring rigid element of testing set-up and this has been verified by the vertical cracks of the specimen during the tests. The results achieved for E_e which can be utilized when the walls are idealized by means of diagonal equivalent struts, are presented in Fig. 19.9. It indicates that plastering the clay brick walls has important contribution on the stiffness of the wall which can not be neglected especially in retrofitting stage of buildings under consideration. CFRP strips have important role on keeping the wall pieces stable. If their positive contribution on stiffness is neglected than an average value of 6000 MPa can be tried for E_e in rehabilitation design stage for all type of plastered walls. It is important to note that this value matches with the results given in [3] and more or less six times higher than the code suggested values. For plain walls E_e can be taken as 2000 MPa which is twice of the code suggested corresponding value.

Shotcreted special 3D wire-cages have been tested for the same purpose with the above mentioned group of tests and they have been used in 2D, and 3D structural tests, Fig. 19.10, [16]. A set of sophisticated analyses have been carried out using *the reduction factor R* extracted from the test shown in Fig. 19.10, [13], in the elasticity matrix of a finite element formulation of plane stress element, Fig. 19.10. It should

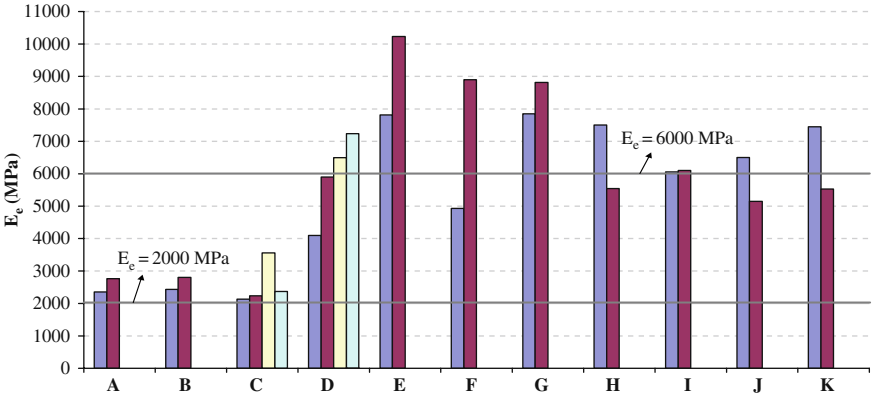

A:	Plain wall (t = 135 cm)	F:	CFRP covered plastered wall
B:	Plain wall (t = 85 cm)	G:	Plastered wall strengthened by 300 mm wide CFRP NO.1 stripes
C:	Plain wall – CFRP stripes in mortar layer	H:	Plastered wall strengthened by 300 mm wide CFRP NO.2 stripes
D:	Plastered wall (t = 135 cm)	I:	Plastered wall strengthened by 300 mm wide CFRP NO.3 stripes
E:	Plastered wall (t = 85 cm)	J:	Plastered wall strengthened by 150 mm wide CFRP NO.2 stripes
		K:	Plastered wall strengthened by 100 mm wide CFRP NO.2 stripes

CFRP Type	Fiber Type	Fiber Orientation	Weight (±10%) (g/m^2)	Fabric Design Thickness (mm)	Tensile Strength of Fibers (MPa)	Tensile E-Modulus of Fibers (MPa)	Strain at Break of Fibers (%)
CFRP No.1	Mid-strength carbon fibers	0^0 (unidirectional)	230	0.131	4300	238000	1.8
CFRP No.2			200	0.111	3900	230000	1.5
CFRP No.3			100	0.056	3900	230000	1.5

Fig. 19.9 Equivalent modulus of elasticity of the clay brick wall specimens, E_e

be noted that for having pure shear effects on the test panels special attention have been paid to distribute the shear forces along the sides of the specimens tensile forces utilized for testing. It has been observed that distributed tensile stresses over the entire specimen were dominant on the failure mode, see Fig. 19.10.

19.3.2 Second Stage Experiments

After having tested a typical one story-one bay bare reinforced concrete reference frame, Fig. 19.11, for certain displacement controlled load reversals, different type of interventions have been made into the similar frames and they have been tested for the same displacement reversals, given in Fig. 19.11, by the help of testing set-up shown in Fig. 19.12.

This group of tests started with the specimen shown in Fig. 19.13 which has been prepared so that full integration between the wall and frame has been achieved. In

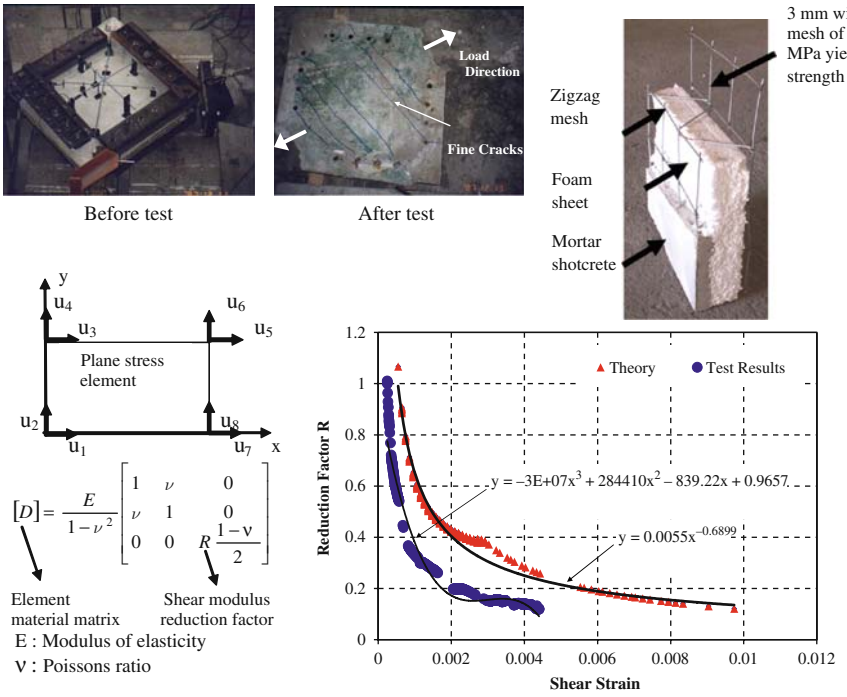

Fig. 19.10 Pure shear tests of 3D wire panels – reduction factor in plane stress element

order to reach full integration, wall has been constructed first with shear keys on three sides and the concrete of frame has been cast later on to penetrate into the wall as it is done in the rural areas of Turkey. One of the two specimens prepared in the same way has been strengthened by means of fine wire mesh and shotcreted on both sides of specimens, and CFRP strips were bonded on two faces of the wall without having any connection to the reinforced concrete members as a first time in Turkey, in year 2001 for strengthening purpose of brittle walls in the other one, Fig. 19.14. For more details, one can refer to [5, 17].

One of the typical specimens which have epoxy resin bonded shear keys made from short deformed reinforcement bars all around and a special wire cage in the middle is shown in Fig. 19.15. Wire-cage with a styrofoam sheet in middle plain has been shotcreted from both sides for having cost effective strengthening [18]. The reference frame used in this experiment was tested and repaired simply injecting epoxy into cracks before it was strengthened and it was tested again imposing the same displacement reversals.

After having inserted steel shear keys into the beams and columns of a bare frame, a wall made of high strength bricks have been constructed leaving gaps between the two adjacent columns and the beam. Later on, concrete has been cast all around the wall to provide contact between the wall and peripheral reinforced concrete elements, Fig. 19.16.

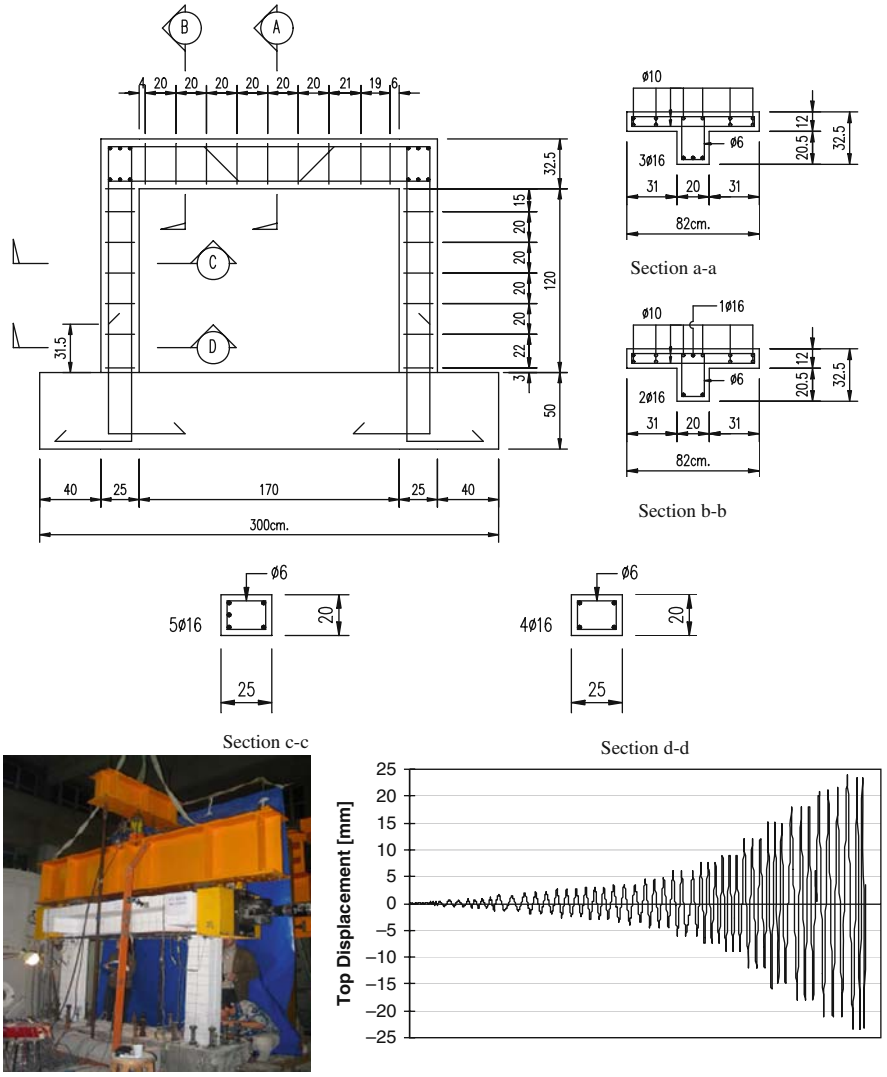

Fig. 19.11 Bare reference frame-testing setup-displacement pattern

The lateral load–top displacement hysteresis loops and their backbone curves, presented in Figs. 19.17, 19.18 and 19.19, have been obtained at the end of tests of those four specimens.

After examining the collapse failure modes of specimen presented in Fig. 19.14, three more specimens with different connection details of CFRP strips, in addition to infill wall made from clay brick, Fig. 19.20, have been prepared and tested in the same way and the results are given in Fig. 19.21 together with the one obtained for the reference bare frame. Specimen N2 has been prepared so that full bonding

Fig. 19.12 Testing set-up and integrated wall (See also Plate 31 in Color Plate Section on page 472)

Fig. 19.13 Integrated wall and strengthening by wire mesh (See also Plate 32 in Color Plate Section on page 473)

(a) Before testing (b) After testing

Fig. 19.14 Integrated wall and strengthening by CFRP strips (See also Plate 33 in Color Plate Section on page 473)

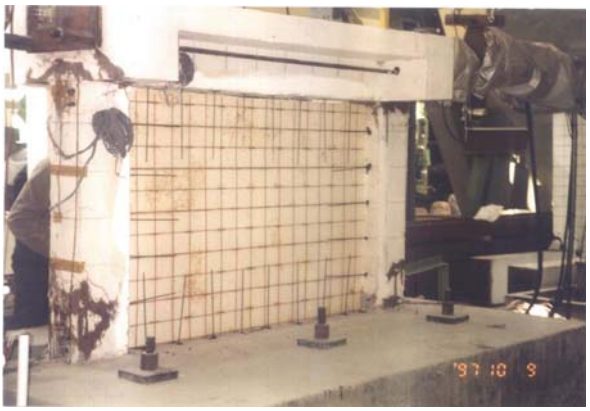

Fig. 19.15 Strengthening of an epoxy repaired and tested bare frame by 3D wire panel (See also Plate 34 in Color Plate Section on page 474)

Fig. 19.16 Strengthening of a bare frame by integrated high strength bricks (See also Plate 35 in Color Plate Section on page 474)

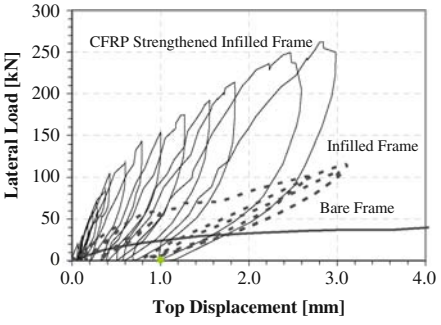

(a) Limited top disp. (Specimens in Fig. 19.14)

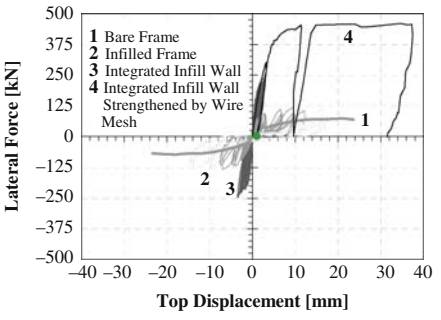

(b) Unlimited top disp. (Specimens in Fig. 19.13)

Fig. 19.17 Test results of frames with strengthened and integrated wall

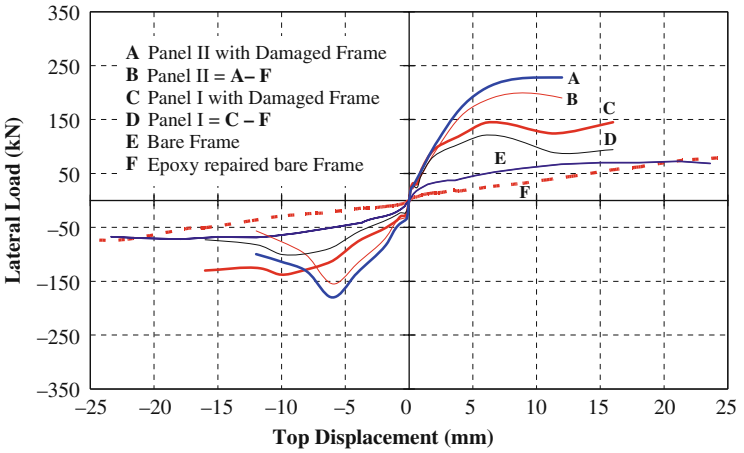

Fig. 19.18 3D wire – cage panel test results (Specimens in Fig. 19.15)

Fig. 19.19 Integrated high strength bricks test result (Specimens in Fig. 19.16)

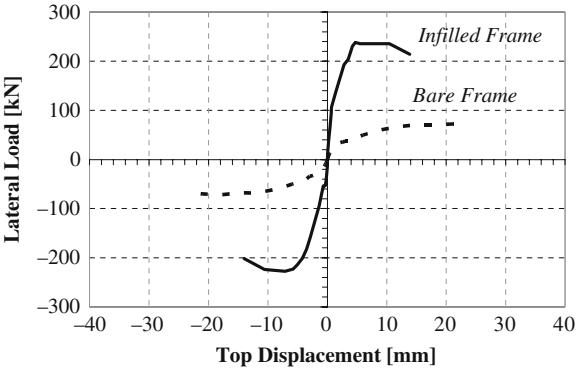

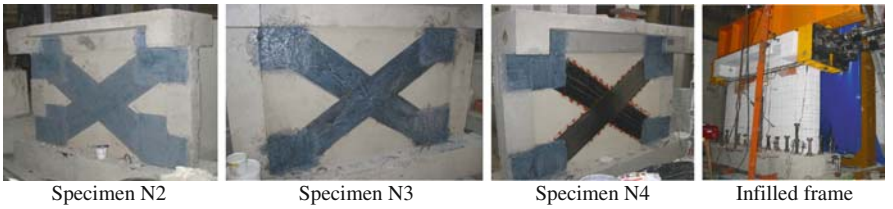

Fig. 19.20 Different CFRP applications and infilled frame specimen (See also Plate 36 in Color Plate Section on page 475)

of CFRP strips both on wall and reinforced concrete frame has been achieved on contrary to Specimen N4 where CFRP strips were not bonded on the wall except the corners. The reason of this is epoxy bonded CFRP strips becoming very brittle and losing their strength as soon as they are subjected to compression. In Specimen N3, same size CFRP anchorages with CFRP strips have been utilized to connect the diagonal CFRP strips to the reinforced concrete frame elements. In specimens N2

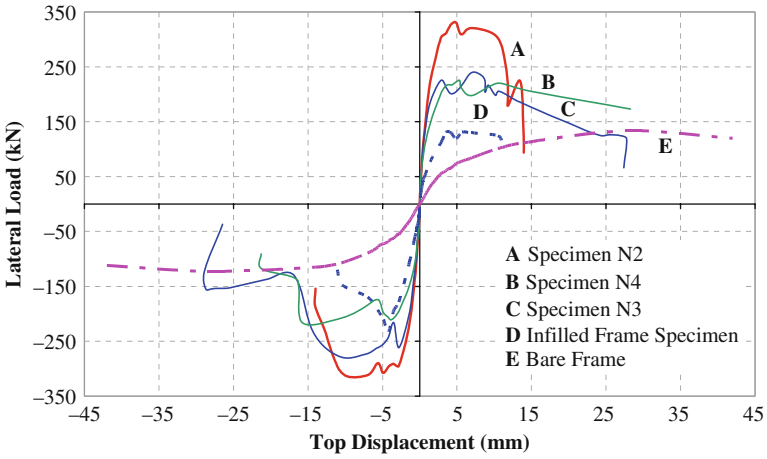

Fig. 19.21 Test results of three different CFRP applications (See also Plate 37 in Color Plate Section on page 475)

and N3 CFRP strips on both sides of the wall have been connected to each other by same size CFRP shear keys. It is obvious that those connecters will carry only tension after having small deformations. The efficiency of these connecters has been observed during the tests.

Another set of tests have been launched to see the possible effects of camber introduced to the beams on the shear wall which was produced as shotcrete panel. In order to create a certain amount of additional shear capacity in the wall and to release the axial forces of adjacent columns, pre-reverse deflection has been imposed to the existing beam before shotcreting the walls and it is released after the curing period of concrete. Three specimens have been fabricated for having a chance of full comparison; one of them was a bare frame similar to the one shown in Fig. 19.11. And the second one was an ordinary shear wall intervention. The third specimen was similar to the second one except the pre-reverse deflection imposed to the frame, Fig. 19.22. The test results achieved for the lateral load carrying capacities of the shotcreted two wall specimens and the reference bare frame are given together in Fig. 19.23. As it is observed in this figure, the lateral load carrying capacities of the specimens with and without pre-reverse deflection have increased by a factor of 2.2 and 2.8 when compared with the bare frame's, respectively in the expense of lower displacement ductility which can be improved by cambering the existing beams, [19].

As it is known the rotational ductilities of a section subjected to bending and axial force is mainly dependent on the amount of axial force and the ultimate concrete strain. If the axial load is less than 10% of the plastic axial load, the negative effect of axial force can be neglected [20].

On the other hand that much axial force will have positive effect on the increment of shear strength of concrete, Fig. 19.5. If the concrete compressive strength is relatively small as it is expected in the *low-cost low-rise* reinforced concrete buildings than sectional ductility will be relatively high. Because of these three reasons

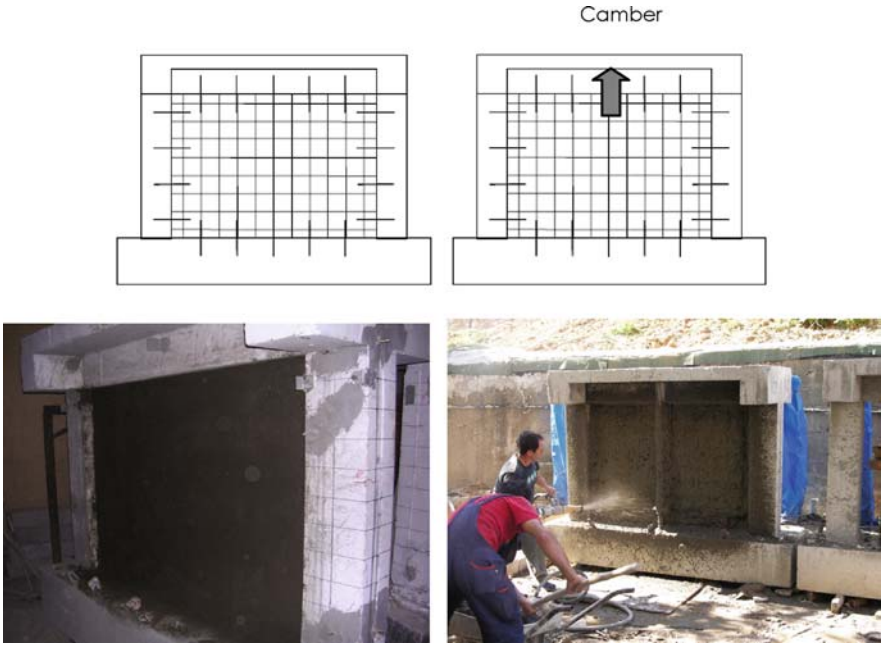

Fig. 19.22 Strengthening by shotcreted 2D wire mesh (See also Plate 38 in Color Plate Section on page 476)

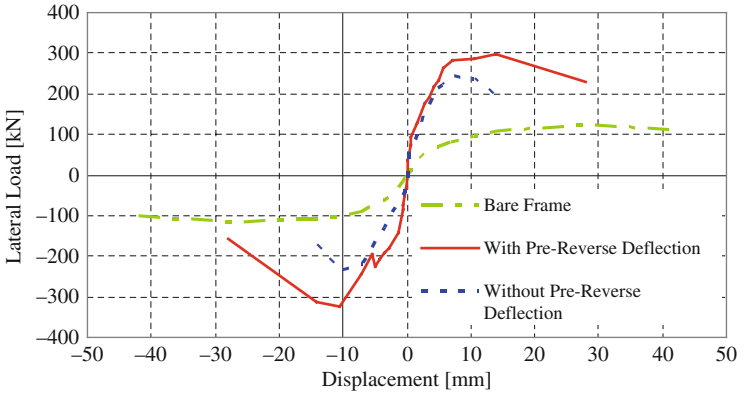

Fig. 19.23 Test results of strengthening by shotcreted 2D wire mesh (See also Plate 39 in Color Plate Section on page 476)

it would be interesting to create a certain amount of axial stress on the newly added shear walls through cambering the existing beam on the wall first and releasing it afterwards.

In order to have more simplification in retrofitting process and to focus on more energy dissipation and story drift limitation, another kind of attempt has been done using ordinary steel pipe bracing diagonal systems shown in Fig. 19.24. The special diagonal system which was introduced in Fig. 19.24a aims essentially to enforce

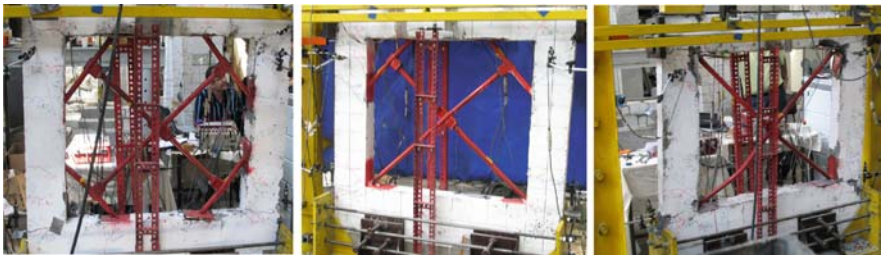

(a) Four knee braced RC frame (FKNEE) (b) Two knee braced RC frame (DKNEE) (c) Concentrically braced RC frame (CONBRACE)

(Diameter of the braces is 26.9 mm and thickness is 3 mm)

Fig. 19.24 Energy dissipating simple bracing systems (See also Plate 40 in Color Plate Section on page 477)

the reinforced concrete sections which are not stressed very much neither by vertical nor lateral loads and the beam-column connections which are already known as the weak zones of building. It is obvious that the bigger and/or thicker circular sections for bracing bars will provide higher shear resistance to the frames to

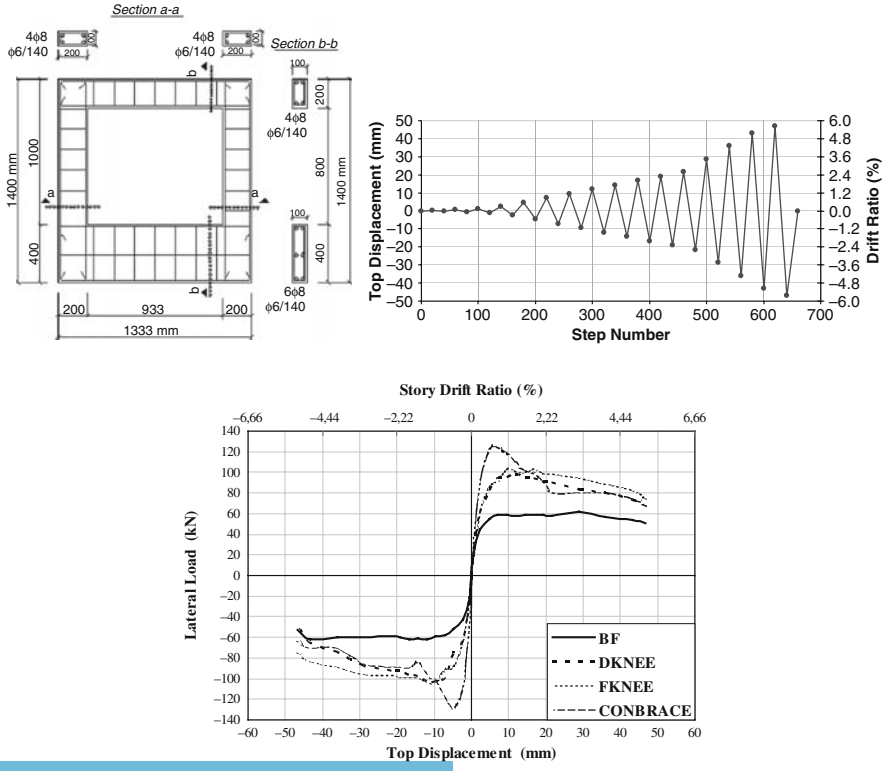

Fig. 19.25 Testing of energy dissipating simple bracing systems

satisfy the targeted rehabilitation design requirements. Testing set-up, reference frame, displacement pattern and the test results are presented in Fig. 19.25.

If the backbone curves presented in Fig. 19.25 is examined it will be seen that the overall displacement ductility is getting smaller from four knee braced specimen to concentrically braced specimen, and the shear capacities are much bigger than the shear capacity of bare frame in all three cases as it is expected. It should also be noted that the orientation of the same size braces are effective either on shear strength or an energy dissipation capacities. Since most of the existing reinforced concrete buildings have weak beam column zones it should be preferred to have a solution not enforcing these critical zones.

19.3.3 Third Stage Experiments

Several two story-one bay reinforced concrete specimens Fig. 19.26a have been fabricated in the laboratory within the framework of a cooperative complementary study supported by NATO [21, 22]. The bare frame specimens were chosen to represent *weak column/strong beam type structures* that were very common in Turkey, especially for the buildings constructed before the current earthquake code, [24]. The specimens had non-seismic details such as large spacing of confinements, no lateral reinforcements in beam-column connection region and no use of 135° seismic hooks. *Bare frame, plastered infilled frame, plastered and CFRP strengthened infilled frame specimens* (see Figs. 19.26a, 19.27) have been tested by the help of testing set-up shown in Fig. 19.26b with the displacement reversals given in Fig. 19.26c.

Diagonal CFRP on both sides of infill were connected to each other by means of anchors made of same size CFRP sheets and CFRP diagonals helped the infill wall to be intact even after a considerable damage. Therefore dissipating significant amount of energy, the infill walls may provide an excellent damping effect against the seismic actions.

The results achieved are given in Fig. 19.28 as the experimentally obtained base shear-top displacement relationships. Even the frame with infill walls without any retrofit performs better than the bare frame due to significantly increased lateral strength. Introduction of CFRP diagonals further increases the lateral strength as well as providing a less steep descending branch in the lateral load – displacement relationship. The observed damages are shown in Fig. 19.29.

19.3.4 Experimentally Obtained Damping Ratios and Earthquake Load Reduction Factors

19.3.4.1 Damping Ratios

Hysteretic damping, $\xi_{hysteretic}$, has been determined for most of the specimens used in the second and third stages of this investigation through the hysteresis lateral load-top displacement curves. Paying attention on the stabilized loops, some aver-

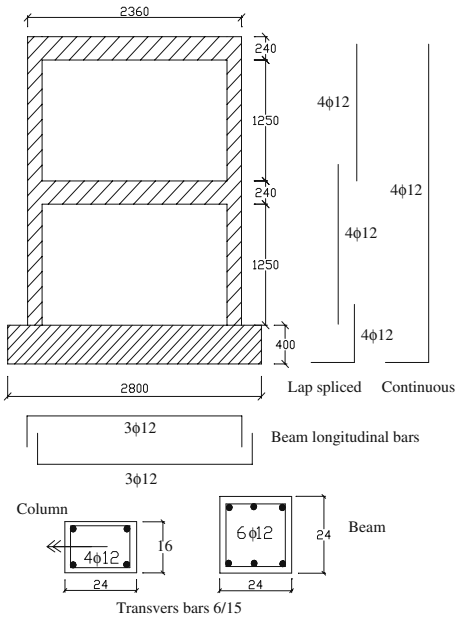

(a) Specimen's details

(b) Testing set-up

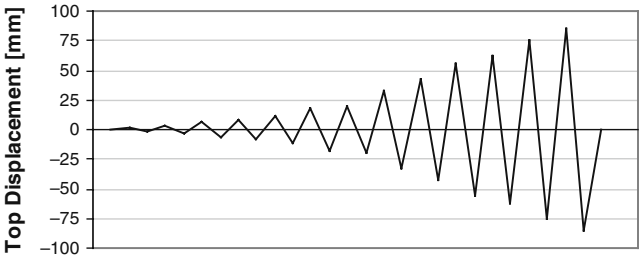

(c) Loading protocol

Fig. 19.26 Two story – one bay specimens

age equivalent viscous damping ratios which can be used in the rehabilitation design stage of low-cost, low-rise ordinary buildings were obtained. It was concluded that the damping ratio can definitely be taken as higher than 5% of critical damping which is being suggested by current codes [23, 24]. The suggested equivalent viscous damping for rehabilitation design stage is between 8% and 15% of critical damping depending on the type of modification.

The lower and upper limits suggested above have been calculated through the formula which is given in Eq. 19.3.

$$\xi_{eq} = 0.05 + \beta\xi_{hysteretic} = 0.05 + \beta \times \left(\frac{W_D}{4\pi W_S}\right) \tag{19.3}$$

Infilled RC frame *Strengthening by CFRP strips on the infill wall*

Fig. 19.27 Strengthening two story – one bay specimens (See also Plate 41 in Color Plate Section on page 477)

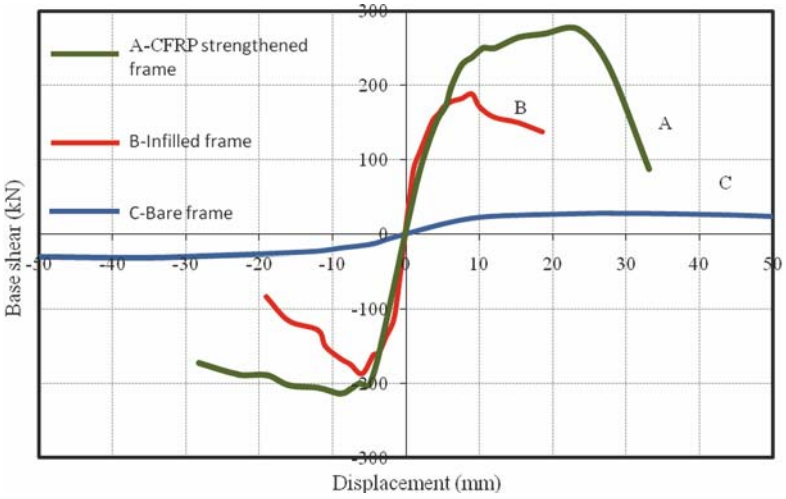

Fig. 19.28 Lateral load – top displacement envelopes (See also Plate 42 in Color Plate Section on page 478)

where β is a coefficient between 0.33 and 1.0 [25] and W_D and W_S are indicating the energy dissipated in one cycle of preferably stabilized displacement and the strain energy at the corresponding displacement, Fig. 19.30, [26–28].

The constant value of 0.05 in Eq. 19.3 represents the viscous damping of reinforced concrete building inherently exist in the structure and $\xi_{hysteretic}$ can be taken approximately as 10% of critical damping depending on the tests results summarized in Section 19.3.2 and the diagrams that are given in Fig. 19.31. One can easily find by the corresponding factors for these damping ratios to define the redesign

Fig. 19.29 Some of the observed damages (See also Plate 43 in Color Plate Section on page 478)

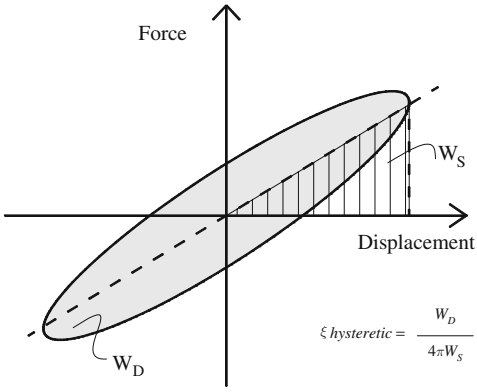

Fig. 19.30 Dissipated and strain energy

demand curves referring the standard one, which may have some minor differences from source to source [25, 29]. In this work the demand spectrum curve based on 10% of equivalent damping ratio has been chosen as *a Suggested Demand Spectrum*, SDS, see Fig. 19.37.

19.3.4.2 Earthquake Load Reduction Factors

The experimental works carried out indicate that the defined *Lateral Load Reduction Factors*, *R*, by codes need not be reduced after having any kind of intervention to the structure for preventive retrofitting against total collapse. In contrary to that, even bigger *R* values can be used in retrofitting design. However some additional tests are needed to give more refined values for the *R* factor. The following definitions and tabulated results can be reviewed for that purpose.

The *equal displacements assumption* which is based on the similarity of linear and nonlinear responses of buildings under consideration has been assumed valid for this part of the research just for the sake of simplicity. In fact, the fundamental free vibration periods determined for this purpose justifies this assumption since they are calculated as longer than 0.5 s. for the buildings dealt with (see Section 19.4 and Fig. 19.37). Therefore one can take the *Structural Ductility Ratios* as the *Earthquake Load Reduction Factors* which were experimentally obtained to be higher than the existing code proposals, [24].

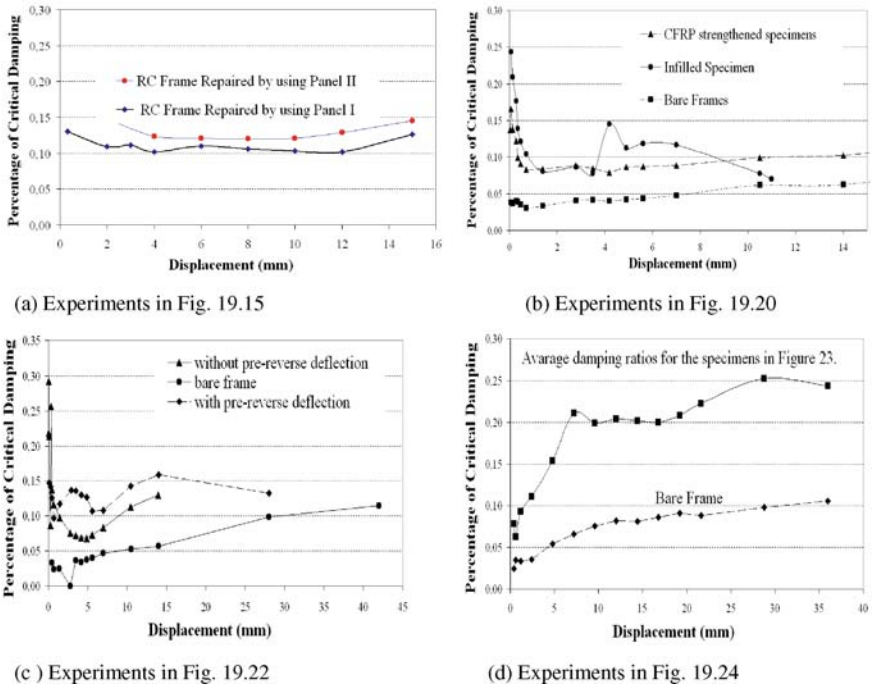

Fig. 19.31 Equivalent damping for various tests

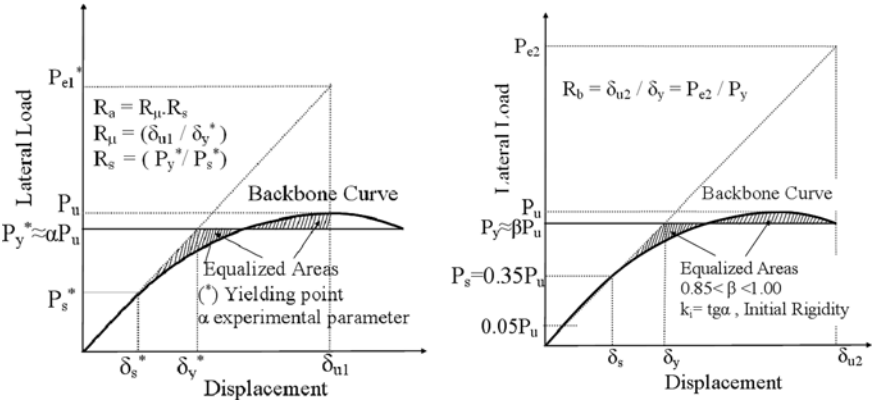

Fig. 19.32 Bilinearization, initial rigidity and ductility ratio

Depending on the backbone curves of the hysteresis loops obtained experimentally, two slightly different approaches which are schematically summarized in Fig. 19.32a,b have been followed up to define, *R*.

In the first approach, Fig. 19.32a, *Earthquake Load Reduction Factor*, R_a, is defined as the multiplication of two factors R_μ and R_s [30, 31] as follows;

Table 19.1 For specimens shown in Fig. 19.20

Specimen	δ_y*	δ_{u1}	P_{e1}*	R_μ	R_s	**R_a**	P_u	δ_y	δ_{u2}	**R_b**
Bare frame	4.8	27.9	530	5	2.1	**9.6**	133	4.8	42	**8.8**
Infilled frame	1.2	5.7	432	4	2.2	**9.1**	131	1.2	11	**9.2**
N2	1.3	4.9	1027	4	2.2	**8.2**	330	1.3	10	**8.0**
N3	1.0	7.0	1257	6	1.7	**10.5**	239	1.0	11	**11.0**
N4	1.2	10.5	1251	7	1.9	**12.6**	225	1.2	14	**12.0**

Table 19.2 For specimens shown in Fig. 19.26

Specimen	δ_y*	δ_{u1}	P_{e1}*	R_μ	R_s	**R_a**	P_u	δ_y	δ_{u2}	**R_b**
Infilled frame CFRP strength	5.2	23.5	928	4	2.3	**8.4**	275	3.5	28	**7.9**
Frame	2.2	9.0	576	3	1.7	**6.0**	188	1.8	11	**6.1**

Table 19.3 For specimens shown in Fig. 19.22

Specimen	δ_y*	δ_{u1}	P_{e1}*	R_μ	R_s	**R_a**	P_u	δ_y	δ_{u2}	**R_b**
With pre-reverse deflection	1.5	14.0	1380	6	1.9	**10.7**	297	2.1	23	**10.9**
Without pre-reverse deflection	1.8	7.0	679	3	2.1	**7.1**	243	1.8	13	**7.2**

Table 19.4 For specimens shown in Fig. 19.24

Specimen	δ_y*	δ_{u1}	P_{e1}*	R_μ	R_s	**R_a**	P_u	δ_y	δ_{u2}	**R_b**
Bare frame	1.6	9.6	338	6	1.6	**9.6**	61	2.1	22	**10.5**
DKNEE	2.4	12	432	5	2.2	**10.4**	103	2.7	26	**9.7**
FKNEE	2.2	17.5	494	5	2.5	**13.2**	104	3.0	36	**12.0**
CONBRACE	1.5	6.2	384	3	2.0	**6.9**	129	2.0	12	**6.0**

$$R_a = R_\mu R_s \tag{19.4}$$

According to the second approach, *Earthquake Load Reduction Factor*, R_b, values which are simply based on the bilinearization technique given in Fig. 19.32b were determined for four groups of experiments and presented in Tables 19.1, 19.2, 19.3 and 19.4, respectively for wall specimens strengthened by CFRP given in Figs. 19.20 and 19.26, shotcreted panels given in Fig. 19.22 and the knee bracings given in Fig. 19.24, together with R_a values.

In Fig. 19.32a P_s* and corresponding δ_s* are indicating the initiation of plastic deformations observed during the experiments, which may be slightly different than the approximate value of $P_s = 0.35\ P_u$. And the initial stiffness used Fig. 19.32b has been has been defined as the slope of the line took place between the points of $0.05\ P_u$ and $0.35\ P_u$ where P_u is the ultimate load.

It is interesting to note that both R_a and R_b values which are based on different approaches are close to each other and as *Lateral Load Reduction Factors* they are

found bigger than the expected and code suggested values. Therefore, in redesign stage, there is no important reason to use lower R values for the stiffened buildings by interventions than the code recommendations.

19.4 Hypothetical Building

The five story hypothetical building which has 20 cm thick brittle clay brick partitioning walls in its all spans, Fig. 19.33, has been designed satisfying most of the requirements of Turkish Earthquake Code of 1975, [32, 33]. Dead loads and 30% of live loads of building is used to define the earthquake design loads of the building according to that code which gives the base shear coefficient as 6.4% for the type of ductile moment resistant frames chosen. Undeformed reinforcement bars which were very common three decades ago with 220 MPa ultimate tensile stress was used in design. Dimensions of columns are given in Table 19.5 and the longitudinal reinforcement ratios of columns are taken as 1%. The dimensions of all beam sections are 20/50/10 cm and they have 0.5% longitudinal reinforcement bars. Then it has been assumed that the compressive strength of concrete which was proposed originally as, 225 kg/cm^2 is only 10 MPa as it is widely found on site investigations. Material coefficient for concrete and steel has taken as unity at the rehabilitation design stage.

It has been assumed that the four external partitioning walls shown in Fig. 19.34 a have been improved to structural walls in all stories. Any one of the brittle brick

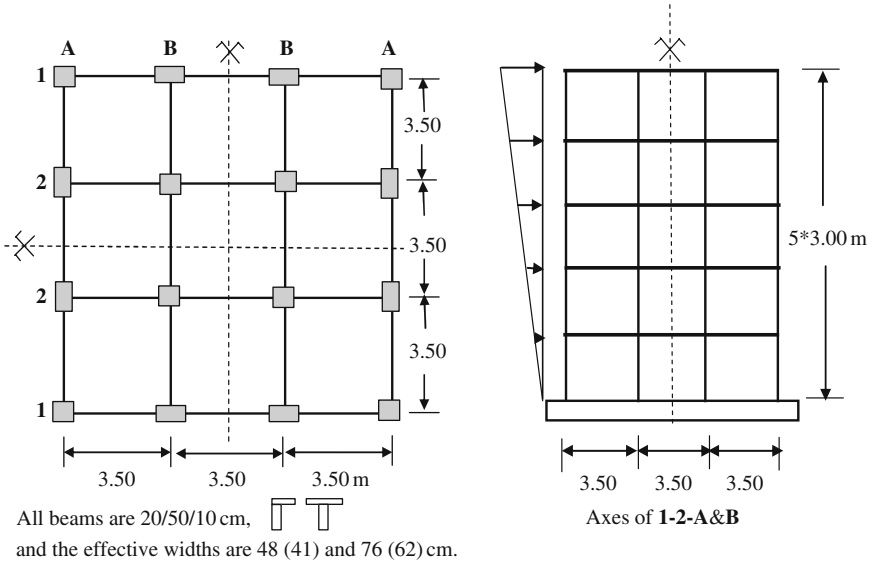

Fig. 19.33 Typical plan and elevation of hypothetical building

Table 19.5 Column sectional dimensions (all dimensions are in cm)

	Axe 1		Axe 2		Axe A		Axe B	
Storey	Axe A	Axe B	Axe A	Axe B	Axe 1	Axe 2	Axe 1	Axe 2
1–2	25×25	25×35	35×25	40×40	25×25	35×25	25×35	40×40
3–4	25×25	25×30	30×25	35×35	25×25	30×25	25×30	35×35
5	25×25	25×25	25×25	30×30	25×25	25×25	25×25	30×30

wall modification techniques which are integrating the walls and peripheral reinforced concrete elements presented in previous paragraphs, could be selected for that purpose. In this example plastered clay brick wall with and without CFRP has been selected. The modulus of elasticity for ordinary clay bricks are suggested as $E_{\text{wall}} = 1000\,\text{MPa}$ in the code [24]. On the other hand the experimentally found modulus of elasticity is suggested here and elsewhere [3] as $E_{\text{wall}} = 6000\,\text{MPa}$ see Fig. 19.6. Both values are referred in the following comparative examples.

3D pushover analyses have been carried out for both original and strengthened structures using essentially the mathematical models, Figs. 19.33 and 19.34b, which have been prepared according to the present codes [24] by the help of software [34]. The diagonal pairs in the model are indicating the equivalent compressive and tensile struts representing the modified walls, see Appendix.

Some of the features of the mathematical models and the assumptions done for this purpose are listed below;

1. Building is a skeleton type structure which consists of beam and column elements.
2. The contribution of slabs to the flexural characteristics of beams is limited with the effective widths of slabs. Hence beams may develop perfect plastic hinges with limited rotational capacities.
3. Infill walls have no contribution to the lateral stiffness and strength of the structure. They are simply considered as a part of the mass of the structure.
4. Brick infill walls, reinforced concrete ordinary shear walls, infill walls strengthened by carbon fibers integrated or disintegrated to the columns, or any kind of intervention between columns can be represented by a pair of diagonal struts.
5. Even the column and beams integrated to the strengthened walls can be handled as original bare elements.
6. Column foundations are fixed for all cases. Beam-column connections are perfectly rigid and very well prepared.

Although all these assumptions need to be reviewed and be discussed in detail this is beyond the scope of this work. However limited amount of discussion and justification is inevitable. Several critics on the listed assumptions and counter measures to modify the mathematical model are as follows;

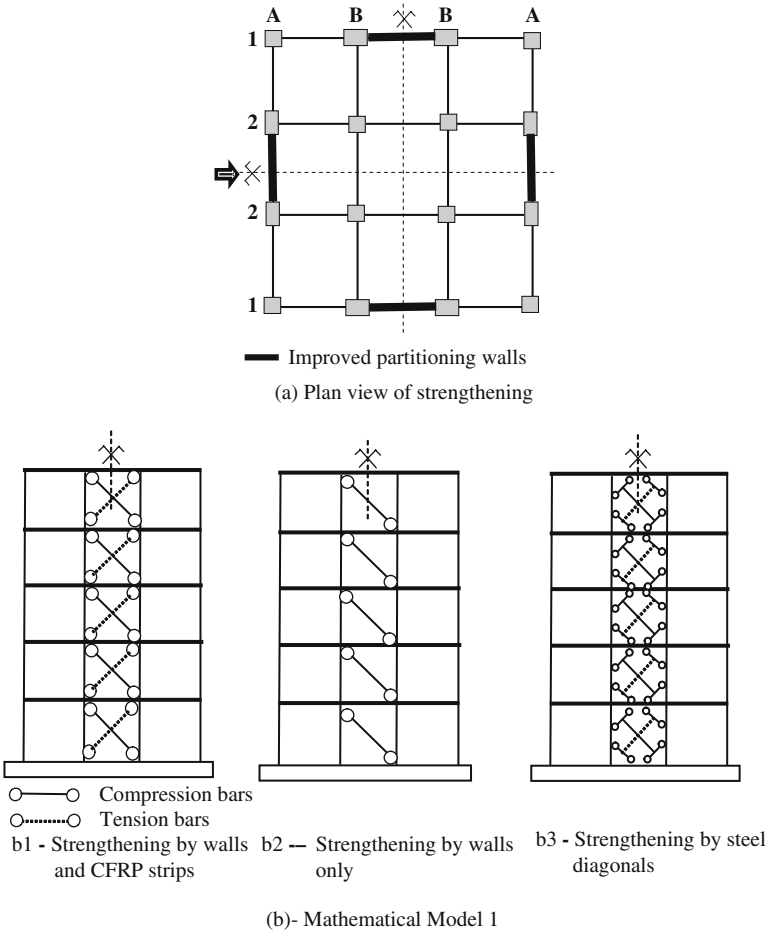

Fig. 19.34 Different type of strengthening for hypothetical building

1. The inspection of heavily damaged and collapsed buildings indicated that almost no plastic hinging occurs in the beams if they are cast monolithically with slabs which are the common local practice. Therefore rotational ductilities may be taken fictitiously as infinite to match the response of hypothetical building and the reality.
2. Columns and beams which are integrated to the walls are not acting alone anymore. Fictitiously their ductilities should be taken infinite as well. And the axial force to be calculated for columns is not going to be realistic. Actually integrated beams and columns will be no longer individual flexural elements. Therefore flexural rigidities calculated on the base of cracked section concept are going to be no longer valid for these particular elements.

3. Foundations of columns are never absolutely fixed. It is better to have a more realistic mathematical model considering the limited rotational stiffness of foundations.

Taking into considerations all these critics and expectations, the mathematical models shown in Fig. 19.35a,b which are roughly equivalent to each other are proposed instead. In these models it is assumed that the *simple beam theory* is valid and there exist no interaction between moment and shear capacities of wall sections. The shear walls in that model should have the flexural rigidity, *EI*, bending moment capacity, M_u, and shear capacity, V_u, as described schematically in Fig. 19.35c, respectively. In addition to that all the peripheral elements integrated to these walls should have fictitiously infinite ductility in order to have realistic results. The advantage of the model given in Fig. 19.35b to the one given in Fig. 19.35a is that it needs only minor modifications of the input introduced to computer for original structure given in Fig. 19.33. The detailed discussions on the mathematical model are not considered in the scope of this chapter. On the other hand, the results of 3D push-over analyses based on different assumptions are presented in Fig. 19.36 for five story original and strengthened hypothetical buildings.

The push-over curves BF1 and BF2 corresponds to the bare frame models with limited and unlimited rotational capacities of existing beam elements, respectively. In fact, all the push over analyses presented have been carried out with unlimited rotational ductility of beams as well. Curves SF1-6000, SF2-6000 and SF1-1000, SF2-1000 correspond to the push-over analyses carried out for the mathematical 3D models of strengthened building given in Figs. 19.34a,b1. The axial fictitious strength and rigidities of diagonal struts are given at the end of Appendix both for $E = 6000$ MPa and $E = 1000$ MPa and push-over curves were designated accordingly. Base shear force defined by the codes [32, 23] for bare and strengthened buildings are 240 kN, 610 kN, 300 kN, 790 kN respectively. The ductility coefficient, *k*, and lateral load reduction factor, *R*, have been chosen as 0.8 and 4

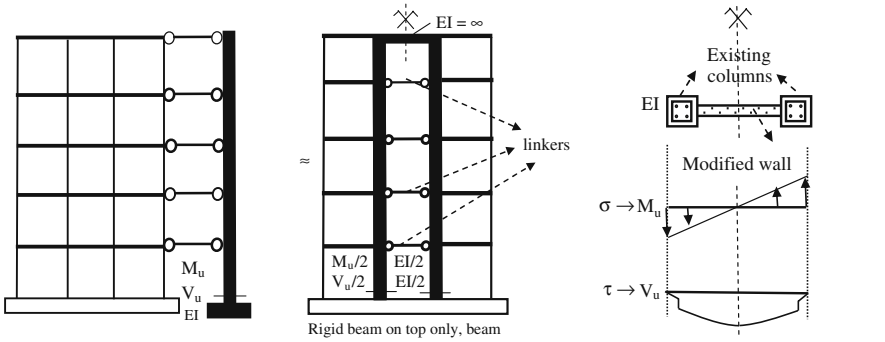

(a) Mathematical Model 2 (b) Mathematical Model 3 (c) Cross section of integrated wall

Fig. 19.35 Possible other mathematical models of strengthened hypothetical building

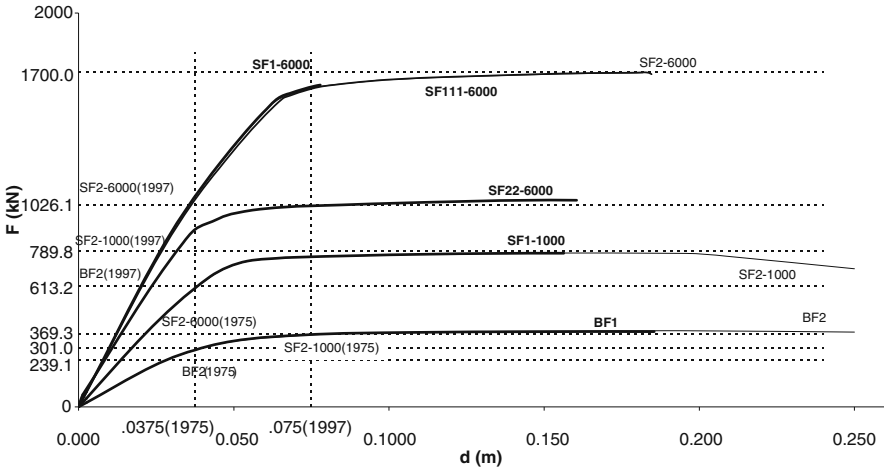

Fig. 19.36 Comparative results obtained through different mathematical models

respectively to determine base shear forces accordingly. And it has been assumed that building is located on a moderately firm type soil, *Z*2 [24]. The determined fundamental periods of the structure for these two cases are 1.18 and 0.62 s. All base shear force levels are indicated in Fig. 19.36 which corresponds to the modulus of elasticity of walls for both 1000 MPa and 6000 MPa.

If the push-over curves are examined the following conclusions can be extracted;

1. Almost no difference is observed between the ultimate lateral load carrying capacities of bare frames with limited and unlimited beam plastic rotations.
2. Modified infill walls provide very high lateral load carrying capacities to the building; see curves SF1-6000 and SF2-6000, SF1-1000 and SF2-1000. It should be kept in mind that the amount of strengthening namely the width of walls and/or the size of CFRP strips are all the parameters which will be specified by an engineer. The amounts used in this example are chosen by rule of thumb. In other words even higher lateral load capacities can be achieved by thicker walls and using more CFRP strips at the expense of lower global ductilities.
3. If only the partitioning walls integrated to the peripheral reinforced concrete elements were used without CFRP strips, Fig. 19.34b2 for this model, it would provide sufficient strength to building as well, see Fig. 19.36 curve SF22-6000.
4. If the fictitious rigidities of fifth story's wall and CFRP is taken half of the lower story's rigidities, the ultimate strength calculated is not affected very much, see curve SF111-6000 and as it is expected better structural behavior is achieved as far as the strain demands of upper column section are concerned. On the other hand if the strengthening in the fifth story is totally omitted than ultimate strength drops down 750 kN because of the premature failure of top story. This means that not only the amount of strengthening but also the configuration of it needs engineering decisions.

It should also be noted that the damping ratios of existing older buildings are higher than newly constructed buildings and the possibility of having the shocks of stronger earthquakes is smaller for old buildings in comparison to new buildings. These two reasons are good enough to justify the elastic demand spectrum shifted down. This shifted curves based on suggested damping ratios which can be chosen between 8% and 15% of critical damping should be referred to find out the performance point of strengthened old buildings. The fundamental period of vibration to be used for that purpose should be calculated taking the walls into consideration not only in terms of their masses, but their lateral rigidities also. The properly scaled push-over curves and elastic demand curves are all indicated in Fig. 19.37, to obtain the corresponding performance points, [35]. After having had the actual top displacements depending on the performance points all the push-over analyses have been carried out again for the possible concrete and steel strain demands which are presented in Table 19.6. The sectional ductility demands of the critical sections which are essentially the uppermost and the lower down column's sections after having had the shear wall intervention are bigger than the requested values at least for the cases SF1-6000, SF2-6000, Table 19.6. Of course it is possible to find some other additional better solutions depending on engineering decisions such as changing the thickness of the wall, the concrete quality, the quality of wall, the size of CFRP strips and choosing proper damping ratios and considering the bigger strain limits proposed for Collapse Limit, *CL*, stage, etc.

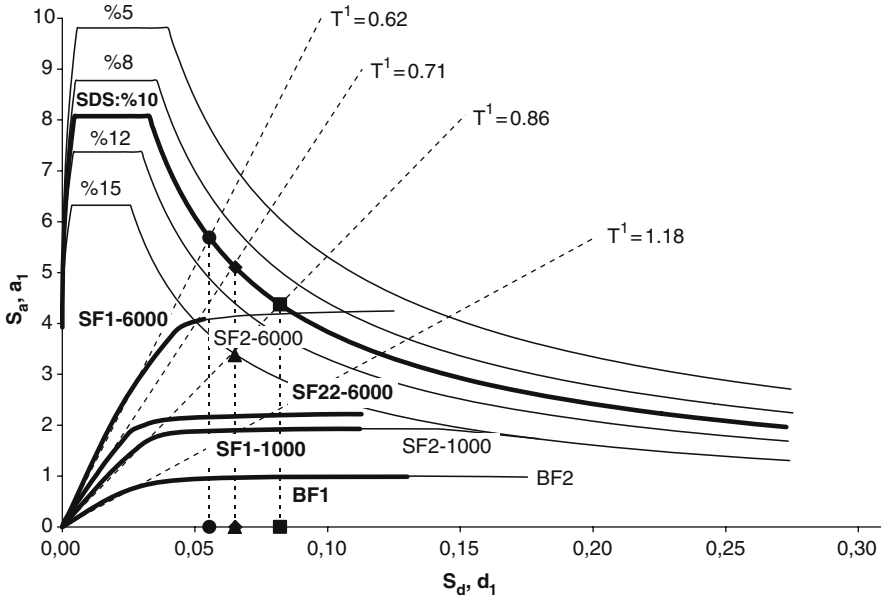

Fig. 19.37 Performance points

Table 19.6 Maximum strains obtained in the critical column sections

	Stories			First St.			Second St.			Third St.			Forth St.		Fifth St.	
	Columns [cmxcm]			A1	A2	B2	A1	A2	B2	A1	A2	B2	A1 25×25 B2	A2	A1	A2 25×25 B2
Model	N	ξ	$\epsilon \times 10^3$	25×25	35×25	40×40	25×25	35×25	40×40	25×25	30×25	35×25	35×25	30×25	25×25	30×30
BF	1	0.05	ϵ_c	7.55	>10	>10	–	1.00	–	>10	6.40	5.05	–	1.60	–	–
			ϵ_s	13.60	>10	>12	–	0.90	–	>44	17.43	9.52	–	2.20	–	–
	2	0.10	ϵ_c	4.25	6.65	6.45	–	–	–	1.30	–	–	–	–	–	–
SF2			ϵ_s	6.80	6.80	7.40	–	–	–	1.90	–	–	–	–	–	–
1000	3	0.15	ϵ_c	2.45	4.05	4.05	–	–	–	0.85	–	–	–	–	–	–
			ϵ_s	3.10	4.50	4.50	–	–	–	0.78	–	–	–	–	–	–
SF22	4	0.10	ϵ_c	2.90	4.60	4.65	–	–	–	–	–	–	–	–	–	–
6000			ϵ_s	4.00	4.60	5.30	–	–	–	–	–	–	–	–	–	–
SF2	5	0.10	ϵ_c	1.15	2.15	2.30	–	–	–	–	–	–	–	–	1.35	–
6000			ϵ_s	0.86	1.70	2.20	–	–	–	–	–	–	–	–	4.20	–

19.5 The Proposed Rehabilitation Technique

It is almost inevitable to increase the lateral stiffness and strength of the ordinary *low-cost, low-rise* reinforced concrete millions of buildings in order to rehabilitate them against the expected destructive earthquake. Intervention to the structure for this purpose could be a newly constructed shear walls or improved partitioning walls by means of any techniques tested and mentioned above. The positive contributions of shear walls to the overall structural behavior can be summarized as below, [36];

1. Storey drifts will be reduced,
2. The possibility of having story mechanisms will be diminished,
3. Short column effects will be omitted,
4. The efficiency of moment-resistant frames will be reduced, hence the weaknesses if exist, in beam-column connections will not be dominant in controlling the lateral load response of the structure,
5. The additional shear wall can be oriented so that some of the irregularities in plan and in elevation can be eliminated,
6. Since the biggest portion of the lateral load will be attracted by additive shear walls, the existing lateral load carrying elements will be a kind of back-up elements with their reserve strengths.

It has been demonstrated through the hypothetical example presented in details above that simple prescriptive solutions for rehabilitation of ordinary buildings are possible. The proposed rehabilitation technique is essentially based on the following administrative, economical and technical realistic assumptions;

1. Either from administrative and/or economical point of view it is not reasonable to expect the rehabilitation of millions of vulnerable low story reinforced concrete buildings to be completed in relatively short time before the expected destructive earthquake hit those buildings, so that *Immediate Occupation* becomes possible for the code defined earthquake loads. *Collapse Prevention* should be better targeted for those ordinary buildings instead, letting the building experience more plastic deformations without having total collapse for properly defined rehabilitation design loads.
2. There is no need to waste time and financial sources for different levels of assessment based on *screening procedures* for those ordinary buildings. It can simply be assumed that those buildings have no lateral load resisting capacity or their existing capacities can preferably be considered as reserve strength since the proposed technique for gaining additional strength and stiffness, is relatively cheap and easily applicable way for rehabilitation.
3. Statistically evaluated data for materials already used in those buildings and the data collected for structural deficiencies are at the satisfactory level to predict the possible earthquake behavior of those simple buildings.
4. It is assumed that at least the structural drawings of critical story are available for the building under consideration. Unfortunately it is known that this

is not a realistic assumption simply because of very bad documentation habits and archive classifications. Therefore realistic approaches should be developed for having the drawings of critical stories and municipalities, local and military authorities should pay enough attention to this subject. Because this is what the design engineers need first for all type of rehabilitation techniques to be adopted.
5. Site seismicity and soil conditions are roughly known.
6. The existing relatively old buildings have higher damping capacities than the new buildings, and for those buildings the probability of expectance of a design earthquake is smaller than the new buildings. Because of these two reasons elastic demand spectrums can be lowered down using equivalent effective damping ratios for rehabilitation works of buildings which are not classified as important buildings, [24].

The major steps of the proposed rehabilitation technique which is essentially based on two shear walls in two directions are as follows:

1. The orientation of two walls in two directions are chosen by the designer so that
   - walls can be constructed in the same locations in all stories without restricting the architectural demands,
   - walls modify the torsional characteristics of the building if it is needed,
   - walls lessen the negative effects of irregularities and structural deficiencies.
2. Either newly constructed walls or modified existing partitioning wall should
   - have at least effective shear area not less than 1.5% of total floor area in one of the two design directions,
   - be fully integrated to the peripheral reinforced concrete elements,
   - be kept in their own plane during the whole course of earthquake,
   - not be expanded beyond the necessary stories and not be set totally free at the foundation level. In both cases the controversy effects of shear walls may overload the existing column elements of upper and lower stories respectively. Therefore reasonably fixed foundations for shear walls which permit rocking and lessened shear wall sections on top stories, better be preferred.

Although it is preferable to have four walls placed to the periphery to strengthen the building, theoretically it is also possible to put the two walls together only in one direction to keep the torsional resistance provided by the new walls. Namely three walls instead of four which are not passing through the same point in the plan are enough for the application of this technique. Trained specialists at the rehabilitation design and construction stages are needed.

The quick hand calculation exemplified below can be utilized at least as a preliminary design stage before any sophisticated analyses is employed for a final stage of rehabilitation design.

19.6 Hypothetical Example

An example has been prepared to justify the validity of the proposed prescriptive technique by means of simplified hand calculations which can be utilized in preliminary design stage as well, before having sophisticated analyses. For that purpose a five story old building with plan dimensions of 10.5×10.5 m square which has 10 kN/m^2 distributed uniform self weight has been chosen, Fig. 19.38. And it has been assumed that this building has all kind of deficiencies listed in previous sections and the concrete compressive strength is only around 10 MPa and the building is constructed on firm soil. Although the base shear coefficient defined by 1975 and 1997 codes is 6.4 and 15% of seismic weight, respectively, it has been assumed also that base shear coefficient is around 15% just to be on the safe side for the whole building.

The total base shear $V = ((10.5\times10.5\times1)\times5)\times0.15 = 827$ kN. The overturning moment $M = (827\times15\times2/3) = 8270$ kNm. Roughly it can be assumed that the 30% of overturning moments will be resisted by individual columns and 70% of it by the additional axial force couples in columns. The resultants of those axial forces, F, are shown in Fig. 19.38b. And one can easily calculate as $F = (8270\times0.70)/7 = 827$ kN. Just for being on safe side once again it can be assumed that the axial forces due to the overturning moment will be resisted by only the two exterior frames with new shear walls because of their relatively high lateral shear rigidity. Then if this is the case the additional axial forces of single exterior columns will be; $N_1 = (827/10.5) \times (10.5/2) = 414$ kN. If the axial force due to gravity which is around; $N_2 = (((3.5/2) \times (3.5/2) \times 1) \times 50 = 153$ kN and then the total axial force for the critical corner column becomes $N = N_1 + N_2 = 567$ kN. The approximate axial load capacity of this corner column is roughly $(25 \times 25) \times 1000 = 625$ kN which is bigger than the expected axial load during a severe design earthquake. 625 > 567, Fig. 19.38c. If the minimum value for shear capacity shown in Fig. 19.5 is used then

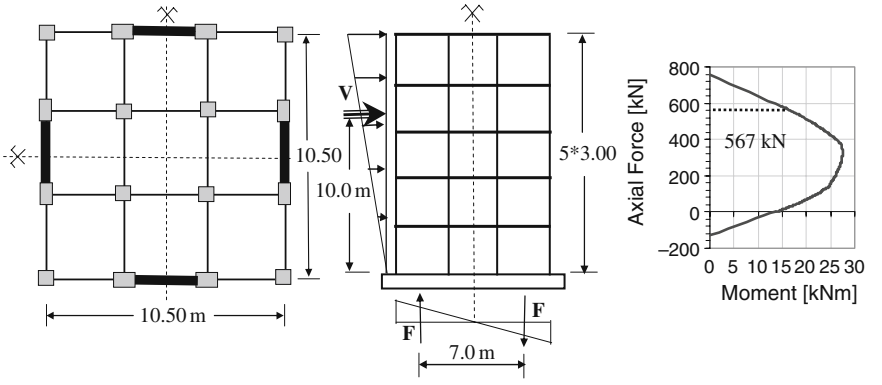

(a) Typical story plan (b) Typical frame (c) Column interaction curve

Fig. 19.38 Hypothetical example

one can calculate the shear resistance of two new shear walls integrated to existing columns as $V_u = (((350 + 35) \times 20) \times 60) \times 2 = 924$ kN. This amount of shear capacity is very close to the determined shear demand, $924 > 827$.

The rigorous inelastic analyses carried out for hypothetical building which is very similar to the hypothetical example indicates that all the changes in structural behavior due to shear wall intervention can be encountered easily by engineering decisions. Most of the common minor changes observed are negligible in comparison to the expected uncertainties inherently exist in seismic events. Special attention should be paid to the individual first and top story columns.

19.7 Conclusions

Additional lateral load resisting new elements can be created by simply improving the non-structural infill walls to structural walls for the buildings that are successfully bearing the gravity loads. Most of the vulnerable existing *low-cost, low-rise* un-engineered buildings in the earthquake prone areas can be considered in this group of buildings. The lateral load resisting capacities they possess are neglected for being on the safe side in the procedure presented herein. It has already been proven that *three* or *four* properly chosen improved infill walls will be enough to resist the realistically defined rehabilitation design earthquake forces. One of the cost-effective techniques for having improved infill walls tested and presented in this chapter can be chosen for that purpose. The general conclusions are as follows:

1. The lateral strength and stiffness of the infilled specimens are significantly higher than bare frame specimens. While bending cracks were spread along the columns for all the improved infilled specimens, the damage observed, was accumulated in the vicinity of the beam-column joints and lower parts of the first story columns at bare frame specimens. This damage formation indicates that bare frame specimens' *frame type behavior* changed into *shear wall type behavior* by the intervention of infill walls integrated to the peripheral reinforced concrete elements. The only exception of this is the knee braced specimens.
2. Sufficient reliability has already been achieved in the following issues either experimentally and/or theoretically:
   - Damping ratios selected for rehabilitation design stage should be above 5% of critical damping. The suggested value of the effective damping ratio can be selected between 8% and 15% of critical damping depending on the retrofitting techniques submitted in this chapter.
   - Based on the experimentally achieved results it can be concluded that there is no need to make a drastic change for the *Lateral Load Reduction Factor, R*, at the rehabilitation design stage of the strengthened buildings which are stiffened by improved infill walls acting as shear walls for preventing the ordinary buildings against total collapse.

- The additional strength requirement which is the most important parameter for the rehabilitation design stage can be obtained easily by means of any one of the techniques tested and shown in this chapter. These techniques are not only providing enough strength but also enough lateral rigidity to save the building from secondary harmful affects. Either totally new walls integrated to the building can be introduced or the existing nonstructural infill walls can be improved to structural walls utilizing the techniques proven by sufficient amount of laboratory tests.
- The ultimate lateral load resisting capacity of the building is controlled by the bending strength of the columns where energy dissipating knee bracings are connected, Fig. 19.34b3. Therefore the size of diagonal pipe sections are not dominant on the earthquake behavior of the system and they are easily becoming enough to increase the lateral load capacity to the required level in the rehabilitation design stage. The buckled diagonals are reactivated when they are subjected to tension. Care should be paid to the connection details of diagonal steel bars to reinforced concrete elements where heavy damage observed during the tests. It should be noted that the hysteretic damping in this retrofitting technique is the highest among the others. In stabilized loops it is about 20% of critical damping, Fig. 19.31.
- The parameters such as the thickness of the wall, the shear strength of the wall, the length of the wall, can be easily changed and the required level of shear resistance can be achieved. Since the total shear is being carried by new walls, the rest of the structure will mostly be affected by gravity loads only and the structure will have a certain amount of *reserve lateral strength* as much as the original structure possesses.
- One should not worry about the rotational ductility demands of beam sections adjacent to the new shear walls. Slabs will have extra contributions if additional rotational capacities are required from beams, to reach the newly provided shear strength. Catastrophic damages have not been observed in beams casted simultaneously with slabs. These types of slabs are capable enough to collect the inertia forces and transfer them to the lateral load resisting elements due to their high in-plane rigidities and shear capacities. Because of the newly added or created lateral stiffness by shear walls, story drifts which may cause substantial amount of cracks in brittle partitioning walls will be restricted and these shear walls will minimize the probability of developing story mechanisms, the second order effects of axial forces and the negative effects of other deficiencies such as bad beam-column connection, poor workmanship etc.

3. Experimental works indicate that the fictitious modulus of elasticity for walls can be taken higher than code recommended values for preventive rehabilitation design against total collapse.
4. There is neither the need to perform material test for all ordinary buildings under consideration nor the need to do structural assessment other than the drawing of critical stories.
5. It has been proven by the set of analyses of chosen five storey hypothetical structures that all the expected positive and negative changes in structural behavior

of the building due to the intervention of newly proposed shear walls can either be utilized or handled respectively. The proposed four walls should have a shear resisting cross sectional area not smaller than 1.5% of the total gross floor area in each design direction for a five story building. The orientation of proposed four walls which is supposed to the based on an engineering decision in this solution need to be properly chosen so that the vulnerability against torsion should be minimized. These walls will be placed on top of each other all the way up to the top of the building with a foundation to resist only limited amount of moment.

6. Retrofitting the specimens by CFRP, prevented corner crushing and diagonal cracks spread over the whole infill. Although the infill walls were severely damaged at the end of the tests, total collapse of infill walls was not observed. As it is expected, increment in the lateral load capacities and lateral stiffnesses are observed. The sudden load drops observed at base shear versus top displacement curves due to CFRP rupture showed that the contributions of diagonal CFRP on overall behavior is substantial. It should also be noted that even when all the diagonal CFRP sheets were broken, the specimens continued carrying lateral load and the base shear versus top displacement curves moved closer to curves of bare frame specimens.
7. For more rigorous analyses based on finite elements the *shear-stress, shear-strain* diagrams obtained experimentally for the different type of walls can be utilized. The proposed mathematical models in the codes should be refined. More experimental works for both proposed techniques and newly developed materials and simplified analytical tools are needed.

All in all, it should be kept in mind that it is time to make use of all the valuable data collected in-situ such as the seismicity and soil characteristics of the regions, and the results achieved through experimental and analytical works if one intends to have more resilient cities and societies as quickly as possible. Awareness of the people, preparedness of the community should be increased, cost-effective techniques should be employed and all *administrative measures* should be taken for that purpose without vesting time.

19.8 Appendix: Mathematical Model of the Retrofitted Infill Wall

The general application style of the CFRP on brittle infill wall is shown in Fig. 19.39, [24]. Both sides of the infilled frame were covered partly by CFRP and connected each other by anchor bolds made from CFRP. The retrofitted infill was modeled by a compression and a tension diagonal, Fig. 19.39.

(a) Compression Member: The thickness of the equivalent compression member can be calculated using Eq. 19.5 in which a_{wall} stands for the thickness of the wall. h_k represents the height of columns, r_{wall} is the diagonal wall dimension from center to center of beam-column connections. All dimensions are in mm. λ_{wall} can be calculated by Eq. 19.6.

$$a_{wall} = 0.175\,(\lambda_{wall}\,h_k)^{-0.4}\,r_{wall} \tag{19.5}$$

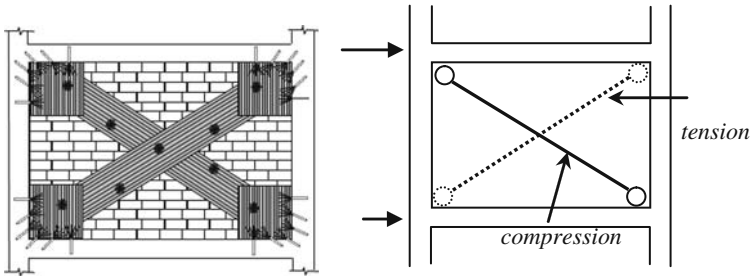

Fig. 19.39 Application and modeling of CFRP retrofitted infill wall

$$\lambda_{\text{wall}} = \left[\frac{E_{\text{wall}} t_{\text{wall}} \sin 2\theta}{4 E_{\text{c}} I_{\text{k}} h_{\text{wall}}}\right]^{\frac{1}{4}} \tag{19.6}$$

In Eq. 19.6 E_{wall} ve E_{c} are modulus of elasticity for infill wall and reinforced concrete, respectively. t_{wall} ve h_{wall} are thickness and height of the infill wall. I_{k} is second moment of inertia of the column, θ is the inclination angle of the diagonal.

Axial stiffness of the compression member, k_{wall}, is calculated using Eq. 19.7.

$$k_{\text{wall}} = \frac{a_{\text{wall}} t_{\text{wall}} E_{\text{wall}}}{r_{\text{wall}}} \tag{19.7}$$

The shear strength of the retrofitted infill wall, V_{wall}, is computed as the lateral component of the axial force capacity of the compression member, see Eq. 19.8. A_{wall}, f_{wall} and τ_{wall} are cross sectional area of infill wall, compression and shear strengths of the infill wall, respectively.

$$V_{\text{wall}} = A_{\text{wall}} \tau_{\text{wall}} \leq 0.22 A_{\text{wall}} f_{\text{wall}} \tag{19.8}$$

The code specified strengths for various types of infill walls are given in Table 19.7.

(b) Tension Member: The tension strength of the equivalent tension member is given in Eq. 19.9.

$$T_{\text{f}} = 0.003\, E_{\text{f}}\, w_{\text{f}}\, t_{\text{f}} \tag{19.9}$$

Table 19.7 Strengths of various types of infill walls

Type	E_{wall} [MPa]	f_{wall} [MPa]	τ_{wall} [MPa]
Perforated Brick	1000	1.0	0.15
Solid Brick	1000	2.0	0.25
Aerated concrete	1000	1.5	0.20

Table 19.8 Parameters used for modeling improved infill walls

Parameter	Unit	Math. Model 1	Math. Model 1	Parameter	Unit	Math. Model 1	Math. Model 1
r_{wall}	mm	3982.5	3982.5	A_{wall}	mm^2	620000	620000
h_k	mm	3000	3000	f_{wall}	MPa	1.00	3.00
E_{wall}	MPa	1000	6000	τ_{wall}	MPa	0.15	0.50
E_c	MPa	15811	15811	V_{wall}	kN	93.0	310.0
t_{wall}	mm	200	200	P_{wall}	kN	119.5	398.2
h_{wall}	mm	2500	2500	E_f	MPa	210000	210000
I_k	mm^4	$400\times400^3/12$	$400\times400^3/12$	w_f	mm	474.3	396.5
θ	°	38.88	38.88	t_f	mm	0.5	0.5
λ_{wall}		8.72E-4	1.37E-3	T_f	kN	149.4	125.9
a_{wall}	mm	474.3	396.5	k_t*	N/mm	12505	10453
k_{wall}	N/mm	23819	119469	A_{wall}	mm^2	620000	620000

* k_{wall} stiffness was used in the analytical work instead of k_t

The shear strength of the tension member is computed as the lateral component of the tension force capacity.

Axial stiffness of the tension member, k_t, is calculated using Eq. 19.10.

$$k_t = \frac{w_f\, t_f\, E_f}{r_{wall}} \tag{19.10}$$

E_f, w_f and t_f are the modulus of elasticity, width and thickness of CFRP retrofitted strip, r_{wall} is the diagonal length of the retrofitted infill wall.

The parameters used in the analytical works have been summarized in Table 19.8.

Acknowledgments The assistance of staff and students of Istanbul Technical University (ITU) Structural and Earthquake Engineering Laboratory are acknowledged. Some part of the study is financially supported by NATO (977231), TUBITAK (ICTAG-I 575) and TUBITAK (104M562, 106M045, 106M050, 106M075) research projects. The support of Kilsan, Isıklar, Zenon, Sika and Balkar Eng. companies are also gratefully acknowledged.

References

1. Parsons T (2004) Recalculated probability of M>=7 earthquakes beneath the Sea of Marmara, Turkey. J. Geophysical Res. Solid Earth109 (B5): Art. No. B05304
2. Istanbul Metropolitan Municipality, http://www.ibb.gov.tr/enUS/SubSites/IstanbulEarthquake/Pages/EarthquakeRiskMaps.aspx
3. Ersin UD, Yuksel E, Kocak A, Hayashi M, Karadogan HF (1998) System identification by means of micro tremor measurements. Proc. Second Japan-Turkey Workshop on Earthquake Engineering, 663–648 Istanbul
4. Yuksel E (1998) Nonlinear analysis of 3D large structures with certain irregularities. Ph.D. Thesis submitted to Graduate School of Istanbul Technical University (ITU) Istanbul in Turkish)
5. Karadogan HF, Yuksel E (2001) Some experimental work carried on infilled reinforced concrete frames. A National Symposium Seismic Strengthening of Existing Buildings and Problems of Buildings with Set-Back. 104–124 Istanbul (in Turkish)

6. Yorulmaz M, Atan Y (1971) The structural behavior of different type of walls subjected to bi-directional loading. Istanbul Technical University (ITU) Istanbul (in Turkish)
7. Uyan M, Akyuz S, Yildirim H (1999) A statistical evaluation on concretes produced in Istanbul and around. J Turkish Ready Mixed Concrete Association 6
8. Igarashi S (1999) Recommendations on minimizing earthquake damage in big cities in Turkey. Proc., Int. Conf. on the Kocaeli Earthquake, 271–286 Istanbul
9. TS 500 (2000) Requirements for design and construction of reinforced concrete structures. TSE Turkish Standard
10. ASTM C 1391-81 (1981) Standard test method for diagonal tension (shear) in masonry assemblages. USA
11. Erol G, Karadogan HF, Cili F (2008) Seismic strengthening of infilled RC frames by CFRP. The 14th World Conference on Earthquake Engineering: PN12-03-041 Beijing
12. Karadogan F, Yuksel E, Erol G, Saruhan H (2005) Low strength brick infill walls strengthened by CFRP fabric. Interim Report – II, Istanbul Technical University (ITU) Istanbul
13. Mowrtage W (2000) Use of shotcreted panels for strengthening and construction of low-rise buildings. Ph.D. Thesis submitted to Graduate School of Istanbul Technical University (ITU) Istanbul
14. Erol G, Yuksel E, Saruhan H, Sagbas G, Teymur TP, Karadogan F (2004) A complementary experimental work on brittle partitioning walls and strengthening by carbon fibers. Proc. The 13th World Conference on Earthquake Engineering, 979, Vancouver
15. Erol G, Demir C, Ilki A, Yuksel E, Karadogan F (2006) Effective strengthening RC with and without lap splice problems. Proc. 8th National Conference on Earthquake Engineering, 288 San Francisco
16. Mowrtage W, Karadogan F (2009) Behavior of single-story lightweight panel building under lateral loads. Journal of Earthquake Engineering, 13:100–107
17. Karadogan HF, Yuksel E (2001) A discussion on earthquake retrofitting and code. Proc. Turkish Civil Engineering 16th Technical Congress Ankara (in Turkish)
18. Mowrtage W, Yuksel E, Ilki A, Karadogan F (1998) Strengthening and/or upgrading the RC frames by means of special shotcreted diaphragms. Proc. SecondJapan-Turkey Workshop on Earthquake Engineering, 1:318–326 Istanbul
19. Cili F, Pala S, Yuksel E, Teymur P (2008) Retrofitting of low ductile reinforced concrete frames with shotcrete Walls. TUBITAK Engineering Research Grant Group Project 106M075 Istanbul (In Turkish)
20. Cakiroglu A, Karadogan HF (1997) Plastic hinge capacities, curvature and structural ductilities of reinforced concrete structures. Proc. First Japan-Turkey Workshop on Earthquake Engineering, Ductility and Strength Concepts in Reinforced Concrete Structures, 1:23–40, Istanbul
21. Yuksel E, Ilki A, Erol G, Demir C, Karadogan F (2006) Seismic retrofit of infilled reinforced concrete frames with CFRP composites. Proc. NATO Workshop Advances in Earthquake Engineering for Urban Risk Reduction: 977231 Istanbul
22. Binici B, Ozcebe G (2006) Analysis of infilled reinforced concrete frames strengthened with FRPs. Advances in Earthquake Engineering for Urban Risk Reduction Istanbul
23. Turkish code for earthquake resistant design (1997), Ministry of Public Works and Settlement Ankara
24. Turkish code for earthquake resistant design (2007), Ministry of Public Works and Settlement Ankara
25. FEMA 273 (1997) NEHRP guidelines for the seismic rehabilitation of buildings. Federal Emergency Management Agency, Washington, DC
26. Chopra AK (2007) Dynamics of structures, theory and application of earthquake engineering. Third Edition, Pearson Education, Inc., USA
27. Priestley MJN, Calvi GM, Kowalsky MJ (2007) Displacement-based seismic design of structures. IUSS press Pavia
28. Mosalam KM, White RN, Ayala G (1998) Response of infill frames using psedo-dynamic experimentation. Earthquake Engineering and Structural Dynamics, 27: 589–608

29. NEHRP national earthquake hazard reduction program (2000) NEHRP recommended provisions for seismic regulations for new buildings and other structures. Federal Emergency Management Agency Washington, DC
30. Maheri MR, Kousari R, Razazan M (2003) Pushover tests on steel X-braced and knee-braced RC frames. Engineering Structures 25:1697–1705
31. Mwafy AM, Elnashai AS (2002) Calibration of force reduction factors of RC buildings. Journal of Earthquake Engineering, 6:239–273
32. Turkish code for earthquake resistant design (1975) Ministry of Public Works and Settlement, Ankara
33. Comlek R (2008) The prevention of total collapse of low-rise existing reinforced concrete structures. M.Sc. Thesis Submitted to Graduate School of Istanbul Technical University (ITU) Istanbul (in Turkish)
34. SAP2000 (2007) Static and dynamic finite element analysis of structures, ver. 11. Computer and Structures, Inc. California
35. ATC 40 (1996) Seismic evaluation and retrofit of concrete buildings. Applied Technology Council ATC 40 1 California Seismic Safety Commission, USA
36. Cakiroglu A, Karadogan H F, Ozer E (1998) Upgrading and strengthening philosophy of reinforced concrete low-rise buildings. Proc. Second Japan-Turkey Workshop on Earthquake Engineering, 1:1–10, Istanbul

Chapter 20
How to Simulate Column Collapse and Removal in As-built and Retrofitted Building Structures?

Mohamed M. Talaat and Khalid M. Mosalam

Abstract This chapter first presents a direct element removal procedure for use in finite element (FE) applications. The procedure accounts for the sudden removal of a structural member during an ongoing FE simulation, based on dynamic equilibrium and the resulting transient change in system kinematics, by applying imposed accelerations instead of external forces at a node where an element was once connected. The algorithm is implemented into an open-source FE code, numerically tested using a demonstration structural system with simplified element removal criteria, and shown able to capture the effect of uncertainty in member capacity. Subsequently, the chapter presents a number of material and cross-section constitutive models and uses them to develop realistic criteria for the collapse and removal of as-built and retrofitted reinforced concrete (RC) columns. Finally, a progressive collapse analysis of a RC structure with unreinforced masonry infill wall is presented as a demonstration for the developed procedure and material models.

20.1 Introduction

Progressive collapse assessment using nonlinear time-history finite element (FE) simulation is becoming popular with the increased access to advanced computing resources and the ability via simulation to account for uncertainty in the modeling process. There is limited literature on experimental measurements applicable to this field since few investigations have been conducted on reinforced concrete (RC) frames that are redundant enough to experience progressive collapse, e.g. [1– 3]. Experimental data from these studies are intended to establish the behavior of RC systems after the collapse of one or more deficient columns designed to lose axial load capacity. However, observed collapse modes are difficult to generalize to cases involving disconnection and subsequent collision by collapsed elements.

K.M. Mosalam (✉)
Department of Civil & Environmental Engineering, University of California, Berkeley, CA, USA
e-mail: mosalam@ce.berkeley.edu

A. Ilki et al. (eds.), *Seismic Risk Assessment and Retrofitting*, Geotechnical, Geological, and Earthquake Engineering 10, DOI 10.1007/978-90-481-2681-1_20,

A recent analytical study in [4] uses post-yield strength and stiffness degradation to conduct quasi-static progressive failure analysis. Another study in [5] defines a macro-level damage index to predict collapse of yielding beam-column elements based on maximum deformations and accumulated plastic energy. The released internal forces from the removed elements are re-imposed as external nodal forces using a step function for the duration of the subsequent load step. This approach is sensitive to the choice of time step size during dynamic simulations and may not represent the energy released into the damaged structure. In [6], the rigid-body downward motion of the collapsed element is tracked using a condensation method without redefining degrees of freedom (DOFs) and splitting one node into two. This is extended in [5] to include a simplified account for impact on the structure by a collapsed element.

The effect of locally released internal energy on exciting transient vibrations in the damaged structure was presented in [7] using an energy balance approach, which concludes that a quasi-static equilibrium-based progressive failure analysis is not conservative, and confirms this with both experiments and computations on a single degree-of-freedom (SDOF) wheel structure. Another study on a multiple degree-of-freedom (MDOF) truss structure in [8] demonstrates similar conclusions. An analytical formulation was developed in [9] which uses an energy balance method to amplify the displacement demands on a structural system following the removal of a gravity load-carrying column. It conservatively ignores the energy dissipated by viscous damping in the system due to the short duration involved, and characterizes the kinetics of the damaged system at the onset of column collapse using nodal displacements only. Two studies in [10, 11] include the effect of uncertainty on simulated progressive collapse assessment of MDOF building systems. These studies assume ductile details and adopt for the definition of collapse a sideway mechanism of columns within an entire floor, not explicitly conducting any removal of elements during the simulation.

To capture the progression of collapse, one must model the behavior of structural components under extreme loading and identify the criteria for their removal. In this chapter, two modes of RC column collapse, namely shear-axial and flexure-axial, are investigated. Shear-axial collapse was recently investigated in a number of experimental and analytical studies reviewed in [3]. The shear friction-based model developed in [12] is introduced and used to establish limit-states for shear-axial collapse. The damage indices developed in [13] for fiber-discretized cross-sections are introduced and used for flexure-axial collapse. These indices are material model-dependent and reflect the damage accumulation at individual fibers. For non-ductile and retrofitted – using fiber-reinforced polymers (FRP) – column behavior, new models are introduced from [14] for confined fiber-discretized cross-section and confinement-sensitive concrete material behavior, and from [13] for confinement-sensitive bar buckling and lap-splice behavior. The inclusion of confinement sensitivity in the uniaxial material constitutive model enables the use of efficient beam-column elements while accounting for external retrofit using FRP overlays. Computational implementation was carried out in OpenSees [15].

20.2 Direct Element Removal

The node illustrated in Fig. 20.1a is in dynamic equilibrium. At time t, beams *B1* and *B2* and columns *C1* and *C2* are attached to the node. For clarity, externally applied or damping-induced nodal forces are not shown. In Fig. 20.1, F and M refer respectively to internal resisting forces (shear and axial) and bending moments. The node has a lumped translational mass m and a rotational mass moment of inertia I. Equilibrium is satisfied by the nodal inertia forces ma_x, ma_y, and $I\alpha$, where a_x and a_y are translational accelerations in the respective x and y directions and α is a rotational acceleration in the x-y plane.

At time t, column element *C1* reaches its collapse limit-state, and is removed from the computational model at time $t' = t + \Delta t$, where Δt is the numerical integration time step, with the resulting free body diagram illustrated in Fig. 20.1b. The nodal masses and accelerations are updated to m', I', a'_x, a'_y and α', respectively. Practically, the majority of the lumped nodal masses are derived from the floor system, and the updated masses due to column collapse may not be significantly different from the original ones. The dynamic equilibrium of the node under resisting and inertia forces can be expressed by

$$\vec{P}_{ex} + \sum \begin{Bmatrix} F_x \\ F_y \\ M \end{Bmatrix} - \begin{Bmatrix} ma_x \\ ma_y \\ I\alpha \end{Bmatrix} = \vec{P}'_{ex} + \sum \begin{Bmatrix} F'_x \\ F'_y \\ M' \end{Bmatrix} - \begin{Bmatrix} m'a'_x \\ m'a'_y \\ I'\alpha' \end{Bmatrix} \tag{20.1}$$

where $\vec{P}_{ex}$ is the vector of externally applied nodal loads, if any, assumed independent of the element connectivity and not affected by element removal but may change with time to $\vec{P}'_{ex}$. The summation is for the elements connected to the node. Upon abrupt element removal, this dynamic equilibrium is disturbed by the sudden release of internal forces from element *C1* and must be restored before the solution

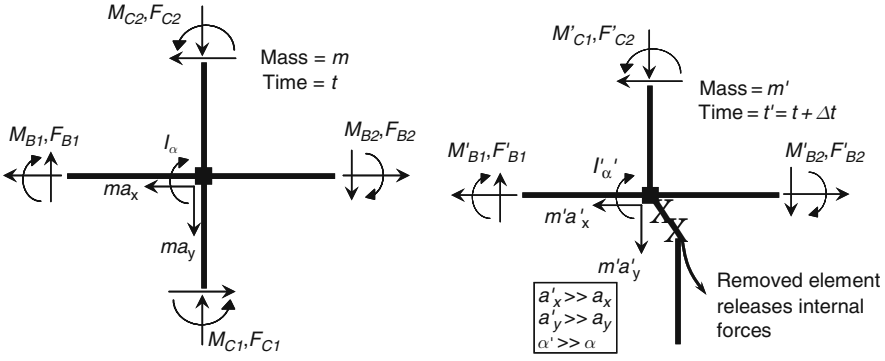

(a) Before element removal (b) After element removal

Fig. 20.1 Dynamic equilibrium of a node connected to a collapsed element

continues. The resisting forces in the connected elements (F' and M') can only change as a result of updated element deformations, and hence changes in relative displacements (and possibly velocities) between individual elements' end-nodes. These changes require updated nodal velocities and accelerations and will not happen instantaneously. The inertia forces are directly related to nodal accelerations a'_x, a'_y, and α', which can change abruptly to satisfy dynamic equilibrium at time t'. This abrupt change is first localized at the shared node at time t' since the connected elements' end-nodes other than their shared node are under dynamic equilibrium.

In the following time steps, the resulting changes in nodal kinetics lead to an updated set of resisting (and inertia) forces that propagate outward through the connected elements into neighboring nodes. This process continues to propagate in the damaged system through element connectivity until updated nodal configurations corresponding to a new equilibrium state are reached. The nodal velocities will result in overshooting the corresponding displacements, amplifying deformation demand in the structural elements. In the hypothetical absence of external excitation, and assuming that the increased deformation demands do not result in the collapse of additional elements, free vibration of the system follows a brief transient state after which it oscillates about the new equilibrium state. If additional collapse takes place, a second transient phase is excited, and this process continues until the system either (a) reaches an equilibrium state about which it can safely oscillate and the progression of collapse is arrested; (b) experiences overall gravity load collapse; or (c) experiences partial collapse which is nevertheless compartmentalized while the rest of it survives. In case (c), the structure may need to be ultimately demolished, but life safety is maintained compared to case (b).

In seismic simulations, the input ground motion is treated as equivalent external loads. The integration time step may need to be reduced immediately after element removal to capture the transient effects involving local axial vibrations in stiff structural elements with significantly short natural periods. An adaptive time stepping scheme can be used for computational efficiency. The advantages of explicitly removing elements instead of assigning them low stiffness are: (a) to avoid numerical problems associated with ill-conditioned stiffness matrices; (b) to compute and use the complete system kinetics (i.e. displacements, velocities, and accelerations) at the time of element collapse in determining whether it can successfully survive to a new equilibrium state; and (c) to enable the tracking of relative motion between removed element and damaged system and estimate the time and kinetics at subsequent collision. If collision is detected, a soft-impact analysis can characterize the resulting duration, forces, and redistribution of masses [16].

An algorithm is designed and implemented for automated removal of collapsed elements during an ongoing simulation. The element removal subroutine is called by the main analysis program after each converged load step, and checks each element for possible violation of its prescribed removal criteria. A violation of any criterion triggers the activation of the element removal procedure on the violating element before returning to the main analysis program. The algorithm is split into two main sets of procedures. The first set includes updating nodal masses, checking if the removal of the collapsed element results in leaving behind dangling nodes or floating elements (Fig. 20.2) which must be removed as well, and removing all

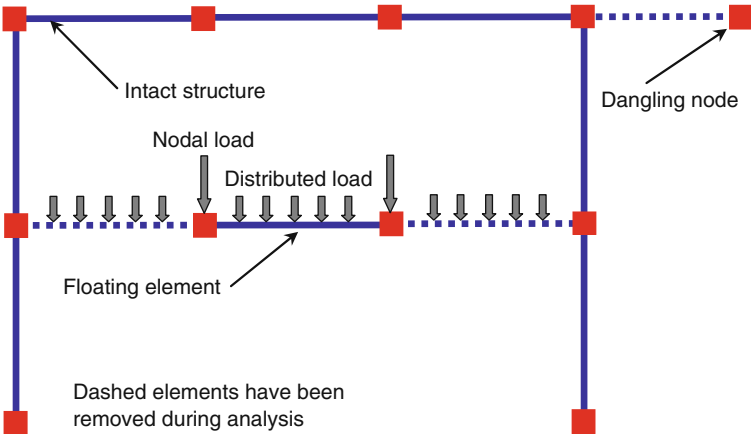

Fig. 20.2 Automatic element removal algorithm (See also Plate 44 in Color Plate Section on page 479)

associated element and nodal forces, imposed displacements, and constraints. The second set is optional and involves the tracking of the removed element motion for possible collision. The kinetics of the separated end-node(s) at the time of separation are identified from the last converged state of the system, representing the initial conditions for the free falling or rotating motion of the collapsed element. This motion is tracked using the assumption of rigid body motion of the element under effects of its own weight, and compared to the position of the damaged system to determine if and when collision takes place. At the time of collision, the relative impact velocity is computed and used to determine the impact duration and the magnitude and temporal variation of impact force to be superposed on the damaged system during the subsequent time steps.

After completing both sets of procedures, the algorithm updates the state of the system to the new masses, geometry and impact forces. The assumption of Rayleigh viscous damping (mass and/or stiffness proportional) is implicitly affected. Since numerical convergence may face difficulties following such extreme events, especially in softening structural systems, the solution parameters may need to be updated. This can be conducted by iteratively switching solver type, convergence criteria, and other analysis options, e.g. time step, so that an ultimate failure to converge would likely take place only if the damaged structural system experiences global instability. A complete discussion of the element removal algorithm can be found in [13].

The algorithm implementation is numerically tested using a demonstration problem of an idealized structural system consisting of two trussed cantilever beam canopies. The structural model element formulation uses the co-rotational geometric transformation to account for large deformations associated with collapse [17]. Further discussion on this benchmark problem and the considered cases of different element properties for different collapse scenarios can be found in [13]. All simulations were successfully conducted without numerical convergence problems. Cases 1 and 2 corresponded to no element removal or collapse in either upper or lower canopies

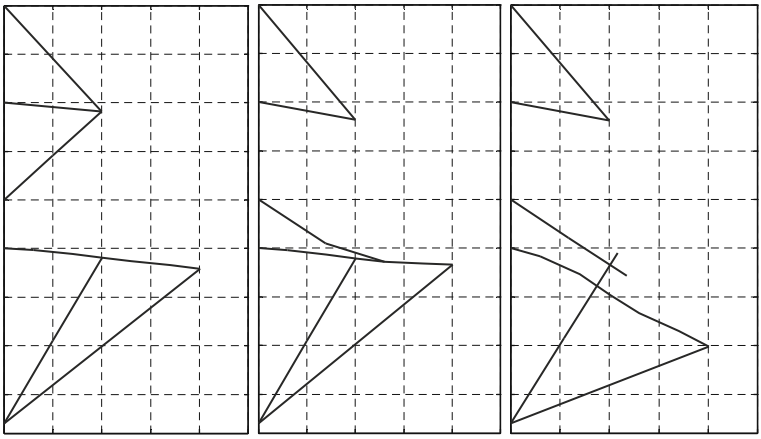

Fig. 20.3 Snapshots of benchmark structural model deformation without any magnification

(Fig. 20.3a). Case 3 corresponded to element removal from the upper canopy and then collision with the lower canopy but without further element removal (Fig. 20.3b). Finally, Case 4 is similar to Case 3 but with subsequent element removal in the lower canopy followed by complete collapse (Fig. 20.3c). It is concluded that the simulation results differed from case to case because of path dependency and sensitivity to uncertainty in the structural model parameters. Hence, there is an obvious need to conduct simulation-based progressive collapse assessment within a probabilistic framework.

20.3 Element Removal Criteria

Three element removal criteria are defined for two different modes of failure in seismically deficient and retrofitted RC beam-columns and for truss members. These criteria are presented in the following sub-sections.

20.3.1 RC Columns in Flexure-Axial Collapse

A set of material damage indices, $0 \leq D_{fiber} \leq 1$, presented in the next section, were calibrated in [13] to represent the damage at individual locations in fiber-discretized cross-sections. These material-level damage indices define two aggregated cross-section damage indices, D_A and D_M, to reflect the loss of a cross-section's capacity to resist axial loads and bending moments, respectively,

$$D_A = 1 - \mathrm{I}_{\mathrm{conf}} \left(1 - \sum_{\text{fibers}} \left(D_{\text{fiber}} A_{\text{fiber}} / A_{\text{cross-section}} \right) \right) \tag{20.2}$$

$$D_M = 1 - \mathrm{I}_{\mathrm{conf}} \left(1 - \sum_{\mathrm{fibers}} \left(D_{\mathrm{fiber}} A_{\mathrm{fiber}} h_{\mathrm{fiber}}^2 \Big/ I_{\mathrm{cross-section}} \right) \right) \tag{20.3}$$

where A and I refer to transformed area and moment of inertia, and h to the distance between the fiber's center and the uncracked section centroid. I_{conf} is an indicator for the loss of confinement whose value is 0 if the confining medium (e.g. transverse ties or FRP jacket) fracture is detected and 1 otherwise. These damage indices are suitable for use with deficient and FRP-retrofitted RC columns. When the value of D_A reaches a threshold value, the associated column cross-section loses its axial load capacity and the element removal algorithm is invoked on the associated element. The threshold value is defined as $D_A = 1$ in this chapter. A future extension may explicitly reflect the axial load level in the column. An analogous approach can be defined for D_M, but is not of interest in this chapter.

20.3.2 RC Columns in Shear-Axial Collapse

This element removal criterion corresponds to violating the drift capacity model developed in [12], where shear-axial coupled springs are connected in series to a beam-column element. When the lateral drift-axial load limit is reached, the corresponding spring is removed from the structural model, and the connectivity between the associated beam-column element and the structure is severed at one end. The model defines a shear-friction-based expression for the drift at axial failure.

$$\frac{\Delta_a}{L} = \frac{4}{100} \frac{1 + \tan^2 \theta}{\tan \theta + P(s / A_{st} f_{yt} d_c \tan \theta)} [\text{MPa units}] \tag{20.4}$$

where Δ is the lateral displacement of a column of length L, subscript a refers to values at the axial limit state, P is the applied axial load, A_{st} and f_{st}, respectively, are the area and yield stress of transverse reinforcement, d_c is the core depth from centerline to centerline of transverse reinforcement, and $\theta = 65°$ is assumed to be the orientation of the shear failure plane.

20.3.3 Truss Elements

This element removal criterion corresponds to violating maximum (positive) or minimum (negative) axial deformation values defined by the analyst. The choice of such values enables modeling both brittle and ductile behavior as was the case for the benchmark problem discussed in the previous section.

20.4 Deficient and Retrofitted Component Models

One model for the confining stress distribution within RC cross-sections and three confinement-sensitive uniaxial material constitutive models for core and cover concrete, buckling-prone steel bars, and lap-spliced steel bars are presented from [13]. These are used to model the deteriorating flexural behavior of deficient and FRP-retrofitted RC columns, and quantify damage for element removal criteria.

20.4.1 Confined RC Cross-Section Model

Consider a circular RC cross-section with radius R, wrapped with an FRP jacket, and subjected to the combined effect of axial force and uniaxial bending moment (Fig. 20.4). Assuming (1) a linear axial strain distribution for the cross-section, (2) FRP and adhesive are thin compared to the RC cross-section and carry only axial and shear stresses, respectively, and (3) elastic bond model governs the bond-slip relationship between the jacket and the RC cross-section, the non-uniform confining stress distribution can be estimated as follows [13]

$$\sigma_3 = \sigma_{3,max} \sinh(A\theta) \big/ \sinh(A\theta_c) \tag{20.5}$$

where σ_3 is the FRP stress, A is a bond stress parameter defined according to $A^2 = (R^2 G_a)/(E_f t_f t_a)$, t_f and E_f are the FRP thickness and modulus of elasticity, respectively, t_a and G_a are the adhesive thickness and shear modulus, respectively, and θ and θ_c are defined in Fig. 20.4. Once the maximum jacket stress $\sigma_{3,max}$ is known, the confining stress at any location in the compression zone can be computed using Eq. 20.5. This approach can be extended to non-circular cross-sections by introducing shape efficiency factors [18]. For typical column retrofits, estimated values for the parameter A typically fall within the range 1–5. For this range,the

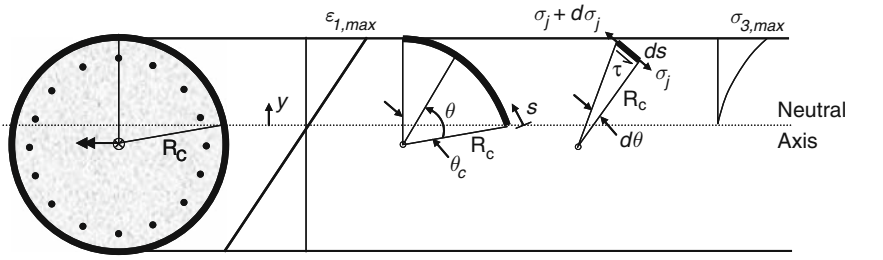

Fig. 20.4 Confining stress distribution on a RC circular cross-section

confining stress distribution resembles a power function of the vertical distance from the neutral axis, and can be approximated by

$$\sigma_3 / \sigma_{3,max} \approx \left(y / R_c \right)^{p_s} \tag{20.6}$$

The confined RC cross-section model was verified using an experimental program [13]. The experiments were designed specifically for the purpose of assessing the model validity and calibrating the exponent p_s in Eq. 20.6. The experimental program was conducted at the Middle East Technical University, Turkey. Four reduced-scale RC columns with identical dimensions and steel reinforcement were subjected to combined axial loads and bending moments. One of the columns is investigated in its as-built condition under constant axial load and monotonically-increasing eccentricity, while the other three columns are strengthened by one layer of Carbon FRP (CFRP) laminate and subjected to monotonically-increasing axial load at three different eccentricity levels including no eccentricity. Details of the experimental study are discussed in [13], while only the results pertaining to the strain distribution in the confining jacket are presented here. CFRP jacket circumferential strains were measured and recorded during the experiments using electronic strain-gauges surface-mounted at four different locations around the cross-sections at the mid-heights of the tested columns. The circumferential stresses in the jacket and the resulting confining stresses in the cross-section are directly proportional to the measured strains since the CFRP jacket used in the experiments exhibited a linear-elastic response until rupture.

Figure 20.5 illustrates the confining ratio computed at each of the four gauge locations using the circumferential strains measured at successive load increments for specimen 3, plotted against the relative distance from the cross-section centroid (normalized by the cross-section radius). This data is reduced in Fig. 20.6 which illustrates the confining stress normalized by the maximum confining stress computed from the strain measurements at Gauge 4. Superimposed on the experimental relationships is the estimated confining stress distribution according to Eq. 20.5, using a bond parameter $A = 5$, as well as power-function approximations of Eq. 20.6 using the 2nd and 4th orders. In the modeling applications discussed in [13], the cross-section moment capacity showed moderate (10–15%) sensitivity to the changing the value of p_s in an assumed range of 0.5–4, while the curvature capacity showed lower sensitivity. Both quantities were negatively affected by increasing the order of the power function.

The confining stress distribution is observed to have a nonlinear profile which exhibits a close agreement with the analytical confined cross-section model. Furthermore, the comparison suggests that the confining stress distribution can be well represented using a 4th order power function for the present cross-section geometry. The normalized strain values suggest that the neutral axis position lies above that of the cross-section centroid throughout most of the experiments (note the negative normalized circumferential strains at the location of Gauge 1 in Fig. 20.5). Hence, a closer agreement between the analytical and experimental results can be achieved using a more accurate determination of the neutral axis position.

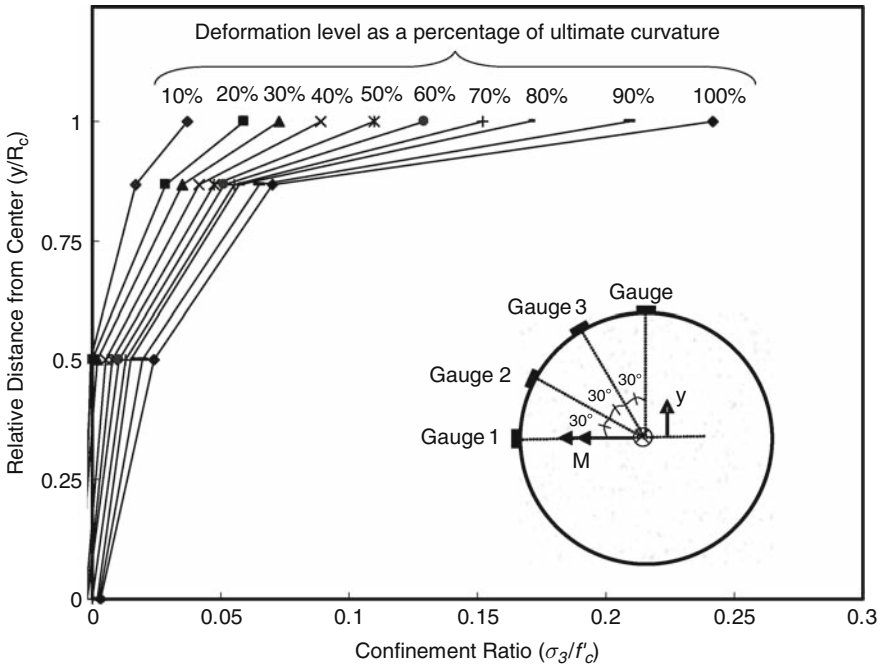

Fig. 20.5 Experimental results of confinement ratios at gauge locations on the CFRP jacket

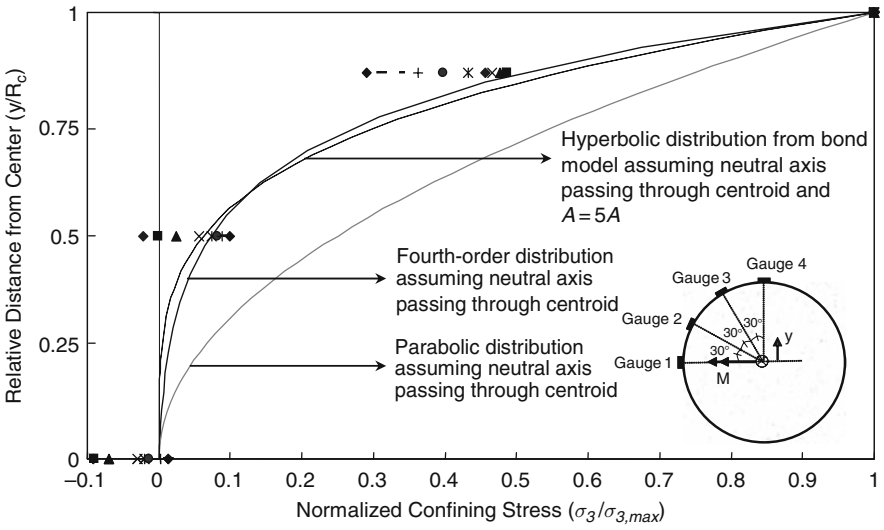

Fig. 20.6 Normalized confinement ratios compared to model predictions

20.4.2 Confined Concrete Material Model

20.4.2.1 Behavior in Compression

The confined concrete model (Fig. 20.7) is a combination of a variable-confinement material envelope and hysteretic rules modified to account for variable confinement. The envelope model was first developed in [19]. It describes the axial stress-strain behavior of confined concrete using three continuous Popovics-type functions [20] for the ascending and descending branches, and incorporates a Leon-Pramono failure criterion [21] and the confinement ratio $\phi = \sigma_3/f'_c$, where f'_c is the 28-day concrete uniaxial compressive strength of the standard cylinder. Moreover, it enforces a constraint that the area under the softening region is equal to the compressive fracture energy – a material property obtained from uniaxial compression test – divided by a characteristic length of the specimen in the loading direction, G_{fc}/l_c. Hence, stresses and strains should be interpreted as average values over the localization length l_c. Deformations in the transverse direction are computed using the secant strain ratio $\upsilon_s = -\varepsilon_3/\varepsilon_1 = \upsilon_s(\varepsilon_1,\phi)$. This ratio is confinement-dependant, and follows a continuous function of ε_1, starting with Poisson's ratio of concrete in

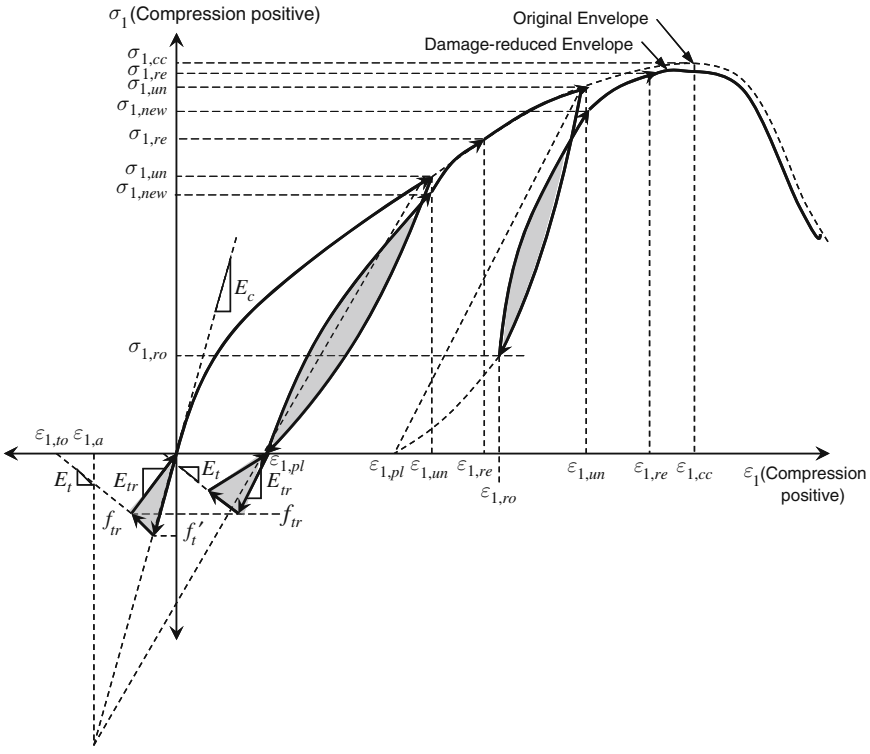

Fig. 20.7 Confined concrete model components

the elastic region ($\upsilon_s = \upsilon_o = 0.15 \sim 0.20$) up to a limiting value at large strains ($\upsilon_s = \upsilon_l = 0.5 + (\phi + 0.85)^{-4}$), satisfying the assumption of no volumetric strain at the ultimate compressive strength ($\upsilon_s = \upsilon_p = 0.50$).

For an imposed axial strain ε_1, strain compatibility is enforced in the lateral direction between the circumferential strains in the confining jacket and lateral strains in the neighboring concrete. The confinement provided by the jacket on the concrete cross-section and the jacket strain are computed by iteratively solving the nonlinear equation, $\varepsilon_1 \upsilon_s(\varepsilon_1, \phi) + \varepsilon_3(\sigma_3) = 0$, where $\varepsilon_3(\sigma_3)$ is the circumferential strain (compression positive) corresponding to the stress in the confining jacket according to the jacket's constitutive material model. This compatibility equation is enforced for the extreme concrete fiber in compression, and confinement is then computed at individual fibers within the compression zone using Eq. 20.6. The modeling approach described above incorporates the variation in the confinement distribution for the compression zone and is capable of monitoring evolution in jacket strain until it exceeds a pre-defined rupture strain limit.

The hysteretic material model for confined concrete was modified from [22]. It postulates that the relationship between stress and strain is invariant in the principal shear space. The key elements of the hysteretic model are graphically illustrated in Fig. 20.7 and its main constitutive equations are presented herein with further details in [13]. Upon unloading from the envelope, the axial stress response is defined by the unloading point ($\varepsilon_{un}, \sigma_{un}$) and the plastic strain ε_{pl} – computed through the surrogate point ε_a– as follows,

$$\varepsilon_{i,pl} = \varepsilon_{i,un} - \sigma_{i,un}\left(\varepsilon_{i,un} - \varepsilon_{i,a}\right) \Big/ \left(\sigma_{i,un} - E_c \varepsilon_{i,a}\right) \quad \text{for i} = 1, 3 \tag{20.7}$$

The problem is then transformed to the normalized principal shear space, where the principal shear stress $\tau = (\sigma_1 - \sigma_3)/2$ and strain $\gamma = (\varepsilon_1 - \varepsilon_3)/2$ are normalized as follows,

$$\begin{aligned} \bar{\gamma}_{un} &= \left(\gamma - \gamma_{pl}\right) \Big/ \left(\gamma_{un} - \gamma_{pl}\right) \\ \bar{\gamma}_{un} &= \left(\gamma - \gamma_{pl}\right) \Big/ \left(\gamma_{un} - \gamma_{pl}\right) \end{aligned} \tag{20.8}$$

where τ_{un} and γ_{un} correspond to $\sigma_{t,un}$ and $\varepsilon_{t,un}$, respectively, and τ_{pl} and γ_{pl} correspond to $\sigma_{t,pl}$ and $\varepsilon_{t,pl}$, respectively. It should be noted that $\sigma_{1,pl} = 0$ and $\sigma_{3,pl} = \sigma(\varepsilon_{3,pl}) \geq 0$ according to the constitutive model of the jacket. The unloading curve in the normalized principal shear space is then defined as follows,

$$\bar{\tau}_{un} = 0.43\left(e^{1.2\bar{\gamma}_{un}} - 1\right) \tag{20.9}$$

The best-fit unloading relationship between the normalized axial and lateral strains, similar to those in Eq. 20.8, is expressed as $\bar{\varepsilon}_{1,un} = \left(\bar{\varepsilon}_{3,un}\right)^{1/p}$ where $p = -0.0035 f'_c + 1.445$ [MPa units]. Moreover, the reloading curve follows a similar procedure and is defined by a reloading point ($\varepsilon_{ro}, \sigma_{ro}$) and a return point ($\varepsilon_{new} = \varepsilon_{un}, \sigma_{new}$) where

$$\sigma_{1,new} = \begin{cases} \sigma_{1,un} & \text{for } \varepsilon_{1,new} \leq \varepsilon_{1,el} \\ 0.92\sigma_{1,un} + 0.08\sigma_{1,ro} & \text{for } \varepsilon_{1,new} \geq \varepsilon_{1,cc} \end{cases} \tag{20.10}$$

with parabolic transition in between. In Eq. 20.10, $\varepsilon_{1,el}$ and $\varepsilon_{1,cc}$ are the axial strain values corresponding to the elastic limit of the confined concrete and its ultimate compressive strength, respectively, as defined by the envelope model. During reloading, the principal shear stresses and strains are normalized as follows,

$$\begin{aligned} \bar{\tau}_{re} &= (\tau - \tau_{ro}) \big/ (\tau_{new} - \tau_{ro}) \\ \bar{\gamma}_{re} &= (\gamma - \gamma_{ro}) \big/ (\gamma_{new} - \gamma_{ro}) \end{aligned} \tag{20.11}$$

where τ_{new} and γ_{new} correspond to $\sigma_{i,new}$ and $\varepsilon_{i,new}$, respectively, and τ_{ro} and γ_{ro} correspond to $\sigma_{i,ro}$ and $\varepsilon_{i,ro}$, respectively. The reloading curve in the normalized principal shear space is then defined as follows,

$$\bar{\tau}_{re} = \ln(\bar{\gamma}_{re} + 1) \big/ \ln(2) \tag{20.12}$$

The best-fit reloading relationship between normalized axial and lateral strains [22] is expressed as $\bar{\varepsilon}_{1,re} = \left(\bar{\varepsilon}_{3,re}\right)^{p}$. Finally, the material follows a parabolic transition curve to return back to the envelope. This transition curve is defined by the stress and tangent at the return point (ε_{new},σ_{new}), the ultimate compressive strength of the confined envelope $\sigma_{1,cc}$, and the envelope stress at the reentry point (ε_{re},σ_{re}) where $\sigma_{1,re} = \sigma\left(\varepsilon_{1,re}\right)$ according to the envelope model in [19] and $\varepsilon_{1,re}$ as defined in [22].

20.4.2.2 Stress Reduction, Damage Index, and Experimental Calibration

In order to account for hysteretic strength degradation in the concrete material, the stress response of the envelope model is reduced by a factor obtained from a hysteretic damage model. In [13], the following hysteretic energy-based reduction factor was formulated and calibrated to the experimental results reported in [22].

$$R_f(n) = \left(\sum_{i=1}^{n-1} (U_{re} - U_{un})_i \Big/ G_{fc} \right)^{\alpha_e} \tag{20.13}$$

where $(U_{re} - U_{un})_i$ is the energy dissipated during the ith unloading-reloading cycle (shaded in Fig. 20.7) and $\alpha_e = 1.175$ is a model calibration parameter. If cracking takes place during a tensile loading cycle, the energy dissipated therein is automatically included in Eq. 20.13, which results in a corresponding reduction of the monotonic envelope curve in compression. Consequently, previously-cracked concrete will exhibit lower peak strength in compression.

In addition to the stress reduction factor, the following maximum dilation-based damage index is defined

$$D_f = \left(\max\{\varepsilon_3\} \big/ \varepsilon_{3,\max}\right)^{\alpha_f} \tag{20.14}$$

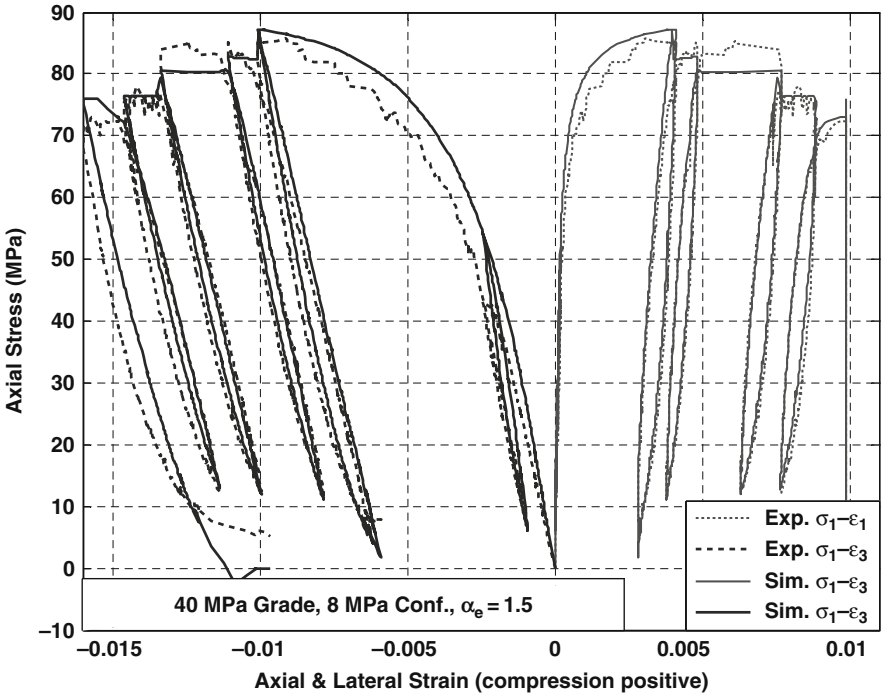

Fig. 20.8 Simulated experimental response from [22]

where $\varepsilon_{3,max}$ is the fracture or maximum estimated strain in the transverse reinforcement of the confining jacket before the loss of confinement and α_f is a model calibration parameter. Typically, $\alpha_f = 1$ is assumed if this damage index is solely used to determine whether complete disintegration has occurred. It may be calibrated to other values using experimental data if it is to correspond to intermediate visual characteristics of damage defined as milestones prior to that. In that regard, it represents the damage level in the confined concrete fibers by considering the amount of lateral expansion sustained in the material and comparing it to the expected maximum expansion allowed before disintegration takes place. Figure 20.8 shows sample reproduction of experimental results from [22], where accurate predictions of strength, level of hysteretic degradation, and lateral strain response can be observed. Finally, this hysteretic model is extended to variable confinement by computing σ_3 for each load step from strain compatibility with the jacket and its confining stress profile in Eq. 20.16.

20.4.2.3 Behavior in Tension

The behavior in tension is assumed independent of the lateral stress. Figure 20.7 illustrates the hysteretic model which the material response follows in uniaxial tension. If tensile stress is detected during unloading, the material follows a

linear-elastic response along the initial tangent modulus E_c up to the cracking stress f'_t. Subsequently, the material follows a linear tension softening modulus E_t towards a vanishing stress at a strain $\varepsilon_{1,to}$ (determined from the tensile fracture energy G_{ft}). Upon reloading to compression from tension, cracks are assumed to fully close following a linear secant modulus E_{tr} if a residual tensile stress f_{tr} is still maintained, and the reloading point in compression is relocated at the plastic strain. Subsequent tensile response of a cracked material follows the current secant modulus E_{tr} up to f_{tr} and then starts to soften with modulus E_t.

20.4.3 Buckling-Enabled Longitudinal Steel Material Model

20.4.3.1 Detecting the Onset of Buckling

This uniaxial material model assumes that buckling takes place over a buckling length L_b spanning more than one transverse tie spacing s_t, and that the restraining effect of the transverse ties can be modeled by uniformly distributed nonlinear springs of stiffness α_t [13]. This model is illustrated in Fig. 20.9 for a buckled bar at equilibrium in a deformed configuration with buckling-induced lateral displacement δ. A harmonic shape function $y = \sum \left(\delta_n/2\right)\left[1 - \cos\left(2\pi nx/L_b\right)\right]$, $n = 1,\ldots,\infty$ is assumed to describe the lateral displacement y at location x along the bar and satisfy the kinematic boundary conditions. The strain energy in the system from bar bending and springs stretching is equated to the external work increment,

$$\Delta U_e = \frac{EJ}{2}\int_0^{L_b}\left(\frac{\partial^2 y(x)}{\partial x^2}\right)^2 dx + \frac{1}{2}\int_0^{L_b}\beta\, y^2\,(x)\, dx = \sum_{n=1}^{\infty}\frac{EJ}{L_b^3}(n\pi^2)^2\delta_n^2 + \sum_{n=1}^{\infty}\frac{3\beta}{16}L_b\delta_n^2 \tag{20.15}$$

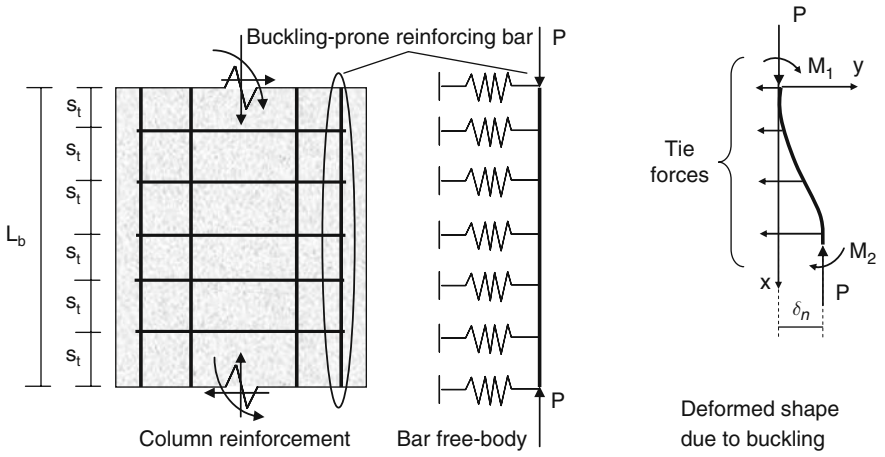

Fig. 20.9 Geometry and free-body diagram for buckling-enabled longitudinal steel model

$$\begin{aligned}\Delta W = P\Delta L = PL_b\left(\int_0^{L_b}\left(\sqrt{1+\left(dy/dx\right)^2}-1\right)dx\right)\\ \approx \left(-\sigma AL_b/2\right)\int_0^{L_b}\left(dy/dx\right)^2 dx = \left(-\sigma A/2\right)\sum_{n=1}^{\infty}\frac{1}{4L_b}\pi^2\delta_n^2\end{aligned} \tag{20.16}$$

where $\beta = \alpha_t/s_t$ is the uniform equivalent of the tie stiffness, E is the elastic modulus of the bar material, A and J are area and moment of inertia of the bar cross-section, respectively, and P and σ are the effective axial load and stress in the bar, respectively. For inelastic increments, E is replaced by the reduced modulus $E_r = 4EE_t\Big/\left(\sqrt{E}+\sqrt{E_t}\right)^2$ where E_t is the current tangent modulus of the bar material. Enforcing the equality and setting $n = 1$ lead to the critical load P_{cr} to be minimized for the critical length $L_{cr,min}$ and stress at onset of buckling $\sigma_{cr,min}$.

$$P_{cr} = \frac{4\pi^2 E_r J}{L_{cr}^2}\left(1+\frac{3\beta L_{cr}^4}{16\pi^4 E_r J}\right) \tag{20.17}$$

$$L_{cr,\min} = \left\{L_{cr}: \frac{\partial P_{cr}}{\partial L_{cr}} = \frac{-8\pi^2 E_r J}{L_{cr}^3}+\frac{3\beta L_{cr}}{2\pi^2} = 0\right\} = 2\pi\sqrt[4]{\frac{E_r J}{3\beta}} \geq s_t \tag{20.18}$$

$$\sigma_{cr,\min} = \begin{cases} -\dfrac{2\sqrt{3\gamma_{cr}}}{A_b} & \text{if} \quad L_{cr,\min} > s_t \\ -\dfrac{4\pi^2 E_r J}{A_b s_t^2} & \text{if} \quad L_{cr,\min} = s_t \end{cases} \tag{20.19}$$

where $\gamma_{cr} = E_r J\beta$ reflects the effect of bar and tie inelasticity on the critical buckling stress. The constraint $L_{cr,min} \geq s_t$ addresses widely spaced ties where buckling takes place between two ties and linearly uniform spring stiffness is not valid.

20.4.3.2 Monotonic Post-Buckling Behavior

First, consider the linear behavior of a classic axially loaded steel bar with time-invariant boundary conditions and buckling length L_{cr} corresponding to a critical stress σ_{cr}. An initial imperfection in the bar is assumed that results in an initial deviation from being fully straight by a quantity δ_i at mid-height. The initial lateral deflection profile along the bar is assumed to follow a harmonic shape. This initial imperfection results in an initial shortening from the full height corresponding to an initial stress-free strain ε_{fi}.

$$\varepsilon_{fi} = \frac{\Delta L_i}{L_{cr}} \approx \left(-\frac{1}{2L_{cr}}\right)\int_0^{L_{cr}}\left(dy/dx\right)^2 dx = -\frac{\pi^2\delta_i^2}{4L_{cr}^2} \tag{20.20}$$

Under an axial load P, the deflection profile $y(x)$ is the sum of the initial profile $y_t(x)$ and the second-order equilibrium solution of a beam with fixed ends $y_1(x)$. Define the ratio $\alpha_P = \sigma / \sigma_{cr} = P \Big/ \left(4\pi^2 EJ / L_{cr}^2\right)$ and differentiate to obtain

$$y(x) = \frac{\delta_i}{2}\left[1 - \cos\left(\frac{2\pi}{L_{cr}}x\right)\right]\frac{1}{(1-\alpha_P)} = \frac{y_i(x)}{(1-\alpha_P)} \tag{20.21}$$

$$\varepsilon_f = \frac{\varepsilon_{fi}}{(1-\alpha_P)^2} \tag{20.22}$$

Hence, the initial imperfection in the bar is amplified and so is the stress-free average strain ε_f resulting from it. The total strain observed in the bar is $\varepsilon_t = \varepsilon_s + \varepsilon_f$ with ε_s as the mechanical strain. The value of ε_f is insignificant prior to buckling or yielding in compression and can be neglected in estimating the linear response. However, yielding or buckling of the bar significantly changes the effective stiffness and alters the value of α_p. Hence, when the bar reaches either limit case, the problem can be redefined with the current configuration being set as initial condition. Consider loading the bar as in Eq. 20.21 after yielding; with initial conditions $\sigma_i^h(\varepsilon_i) = -\sigma_y$ and $\varepsilon_{fi}^h = -\varepsilon_y + \varepsilon_{fi} \big/ (1-\alpha_P)^2 \approx -\varepsilon_y$, where superscript h refers to the hardening phase. The strain decomposition becomes

$$\begin{aligned} \varepsilon_t^h &= \left(\varepsilon_s^h - \varepsilon_{fi}^h\right) + \varepsilon_f^h \\ \varepsilon_f^h &= \frac{\varepsilon_{fi}^h}{(1-\alpha_{\Delta P})^2} \\ \alpha_{\Delta P} &= \frac{\sigma\left(\varepsilon_s^h\right) - \sigma_i^h}{\sigma_{cr}^h - \sigma_i^h} \geq 0 \end{aligned} \tag{20.23}$$

Equation 20.23 can be satisfied using an iterative solver. Note that ${\varepsilon_t}^h$ and ${\varepsilon_s}^h$ are not affected by the hardening regime and can be simply replaced by ε_t and ε_s. If the updated critical stress ${\sigma_{cr}}^h$ (calculated by Eq. 20.19 using the reduced tangent modulus E_r) is less than the yield stress, the material effectively unloads; while the observed strain increases due to the amplification factor in Eq. 20.23. This approach is equivalent to a parallel material model, where a suitable constitutive material model for steel bars can be used at the choice of the analyst, as long as it renders accurate prediction of the tangent modulus E_t during loading.

Finally, consider the case of a general material law for a steel bar encased in concrete with nonlinear transition from linear to hardening behavior and nonlinear transverse tie stiffness. Once buckling is detected, define σ_b and ε_b, the compressive stress at the onset of buckling and the corresponding compressive strain, respectively; as given by Eq. 20.24. Then a system similar to Eq. 20.23 can be defined, with its initial condition parameters given by Eq. 20.25.

$$\begin{aligned} \sigma_b &= \max_{\varepsilon_s}\left\{\sigma(\varepsilon_s) \,|\, \sigma(\varepsilon_s) \leq \sigma_{cr,\min}\right\} \\ \varepsilon_b &= \sigma^{-1}(\sigma_b) - \sigma^{-1}(0) \end{aligned} \tag{20.24}$$

$$\begin{aligned} \varepsilon_{fi}^{h} &= \varepsilon_b \\ \sigma_i^{h} &= \sigma_b \\ \sigma_{cr}^{h} = \sigma_{cr|\infty} = \sigma_{cr,\min} &\left(-\varepsilon_s >> \varepsilon_y, \gamma_{cr} = \min_{\varepsilon_s}\{\gamma_{cr}\}\right) \end{aligned} \tag{20.25}$$

where $\sigma_{cr|\infty}$ is the critical equilibrium stress of the buckled bar at large deformations; corresponding to asymptotic material tangent moduli (or rupture, if applicable) in the bar and transverse ties. Details of this material model are given in [13].

20.4.3.3 Hysteretic Post-Buckling Behavior

Following a loading half-cycle during which buckling was detected, experimental results reported in the literature show that bars exhibit reduced axial stiffness, the buckling-induced shortening decreases, and the bar straightens out. This behavior can be modeled consistently using strain decomposition. The recovered buckling-induced shortening is expressed in terms of a positive stress-free strain increment $\Delta\varepsilon_f$. Hence, the bar material temporarily follows its constitutive law with a reduced mechanical strain increment $\Delta\varepsilon_s = \Delta\varepsilon_t - \Delta\varepsilon_f$. This results in a reduced overall unloading stiffness $E^{un} = \partial\sigma(\varepsilon_s)/\partial\varepsilon_t$ up to the point when $\varepsilon_f = 0$ and $\Delta\varepsilon_s = \Delta\varepsilon_t$. Afterwards, the relationship $\varepsilon_t = \varepsilon_s$ is restored and the bar material follows its pre-buckling constitutive law until subsequent buckling is detected.

The relationship governing the distribution of strain increments is formulated as

$$\Delta\varepsilon_f = \eta_f \frac{\varepsilon_f}{\varepsilon_f^{un}} \Delta\varepsilon_t \le \Delta\varepsilon_t \quad \text{where } 0 \le \eta_f \le 1 \tag{20.26}$$

where ε_f and $\varepsilon_f{}^{un}$ are the stress-free strains corresponding to the current and unloading stress-states, respectively. Moreover, for numerical stability, the resulting change in bar stiffness is gradual and continuous along the regime in which the stress-free strain varies from $\varepsilon_{f=}\varepsilon_f{}^{un}$ to $\varepsilon_f = 0$, allowing a smooth transition to the constitutive material law. The choice of θ_f is such that bars suffering from severe buckling exhibit lower axial stiffness $E_i{}^{un}$ at the beginning of the compression unloading half-cycle. A study in [23] suggests that $E_i{}^{un}$ can be expressed by

$$E_i^{un} = E_s \left(\sigma^{un} / \sigma\left(\varepsilon_t^{un}\right)\right)^2 \tag{20.27}$$

where $\sigma(\varepsilon_t{}^{un})$ is the stress in the bar corresponding to the unloading strain without considering the effects of buckling. Note that the effective bar stiffness is given by

$$E^{un} = \frac{d\sigma}{d\varepsilon_t} = \frac{d\sigma}{d\varepsilon_s}\frac{d\varepsilon_s}{d\varepsilon_t} = E_s \frac{d\varepsilon_s}{d\varepsilon_t} \tag{20.28}$$

During a compression unloading half-cycle, the derivative in the last term is expressed using Eq. 20.26 as follows,

$$\frac{d\varepsilon_s}{d\varepsilon_t} = \frac{d}{d\varepsilon_t}\left(1 - \eta_f \frac{\varepsilon_f}{\varepsilon_f^{un}}\right)\varepsilon_t = 1 - \eta_f \frac{\varepsilon_f}{\varepsilon_f^{un}} + O\left(\eta_f^2\right) \approx 1 - \eta_f \frac{\varepsilon_f}{\varepsilon_f^{un}} \tag{20.29}$$

where $O(\theta^2{}_f)$ follows the usual asymptotic notation. Substituting Eq. 20.29 in 20.28 and equating to 20.27 when $\varepsilon_f = \varepsilon_f{}^{un}$ yields

$$\eta_f = 1 - \left(\sigma^{un} / \sigma\left(\varepsilon_t^{un}\right)\right)^2 \tag{20.30}$$

20.4.3.4 Stress Reduction, Damage Index, and Experimental Calibration

The Coffin-Manson fatigue model was employed as described in [24] to model the hysteretic degradation of reinforcing steel bars and subsequent fracture. This model is based on the accumulation of plastic strain. It defines a cumulative damage index calculated at the end of each loading half-cycle according to

$$D_s = \sum_{half\ cycles} \left(\frac{\varepsilon_p}{2M_f}\right)^{1/\alpha_{cm}} \leq 1 \tag{20.31}$$

where α_p is the plastic strain accumulated between strain reversals. It is assumed equal to the strain amplitude after subtracting an elastic strain value; equal to the stress amplitude ($\sigma_s{}^{max} - \sigma_s{}^{min}$) divided by the elastic stiffness modulus E_s. M_f is the strain corresponding to fracture in monotonic tension, and α_{cm} is a model calibration parameter (typically 0.5–0.7 for metals). The damage index calculated after each loading half-cycle is used to compute a hysteretic stress reduction factor for subsequent loading half-cycles as follows,

$$R_s = (1 - D_s)^{\alpha_s} \tag{20.32}$$

where α_s is another model calibration parameter. When the damage index value reaches unity, the stress reduction factor becomes zero and the bar becomes inactive. For reinforcing steel bars, calibration values are suggested for $M_f = 0.130$ and $\alpha_{cm} = 0.506$ in [24] and for $\alpha_s = 0.1$ and 0.3 for two different sets of bars in [13].

Figure 20.10 illustrates the comparison between the model prediction and the cyclic loading tests in [25] for steel bars with slenderness ratios of 8 and 11. The simulation is successful in estimating the cycles where buckling is observed and the subsequent softening in stress. The simulation is also successful in estimating the reduced stiffness moduli of the buckled bars upon unloading from compression and in reproducing the subsequent hysteretic behavior in tension. The simulation exhibits less energy dissipation than experiment upon unloading from a tensile stress.

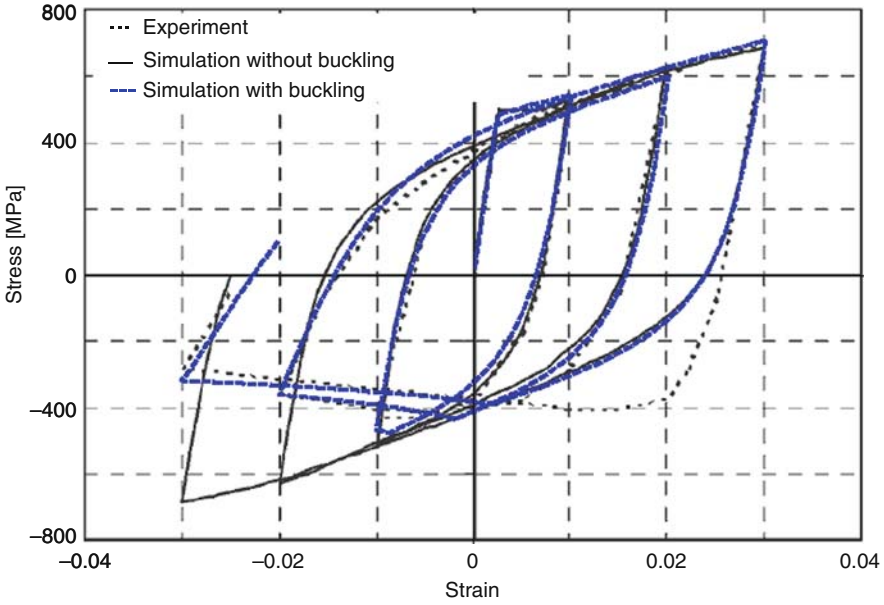

Fig. 20.10 Model simulations of bar-buckling experiments in [25] for length/diameter ratio = 11 (See also Plate 45 in Color Plate Section on page 479)

20.4.4 Deficient Lap Splice Material Model

A strain decomposition approach is used to model the confinement-sensitive behavior of the longitudinal steel bar lap splices in the plastic hinge region [26]. At any location along a splice length, according to the integration point distribution for a fiber element discretization, the total steel strain ε_{st} is dictated by the strain profile of the cross-section. This total strain is decomposed into slip strain $\varepsilon_{ss} = u_s/L_s$ and elongation strain driving the stress response in the bar ε_{se}, i.e. $\varepsilon_{st} = \varepsilon_{ss} + \varepsilon_{se,}$ where u_s is the slip deformation along the splice length L_s. The strain components ε_{ss} and ε_{se} are computed iteratively such that equilibrium along the splice length is satisfied. For any location along a spliced or starter bar, the equilibrium equations of the bars can be shown to be as follows,

$$\tau_i \ (\pi d_b \, l_i)/2 \ = \ \sigma_{si} \left(\pi d_b^2 \Big/ 4\right) \text{ for i} = 1, 2 \tag{20.33}$$

where τ_i is the shear resistance between the bar and concrete, l_1 is the distance to the stress-free end of the bar, d_b is the spliced bar diameter, and σ_{si} is the steel stress at the considered location. It is assumed that the distributions of τ for the two bars are similar and follow a linear variation given by $\tau_i = \tau_m l_i/L_s$ where τ_m is the maximum shear resistance along the splice length L_s, and $i = 1,2$ is the bar indicator. The proposed shear stress distribution satisfies the zero stress condition at the free end of the bar. Adding Eq. 20.33 for $i = 1,2$ and $l_2 = L_s - l_1$, the equilibrium

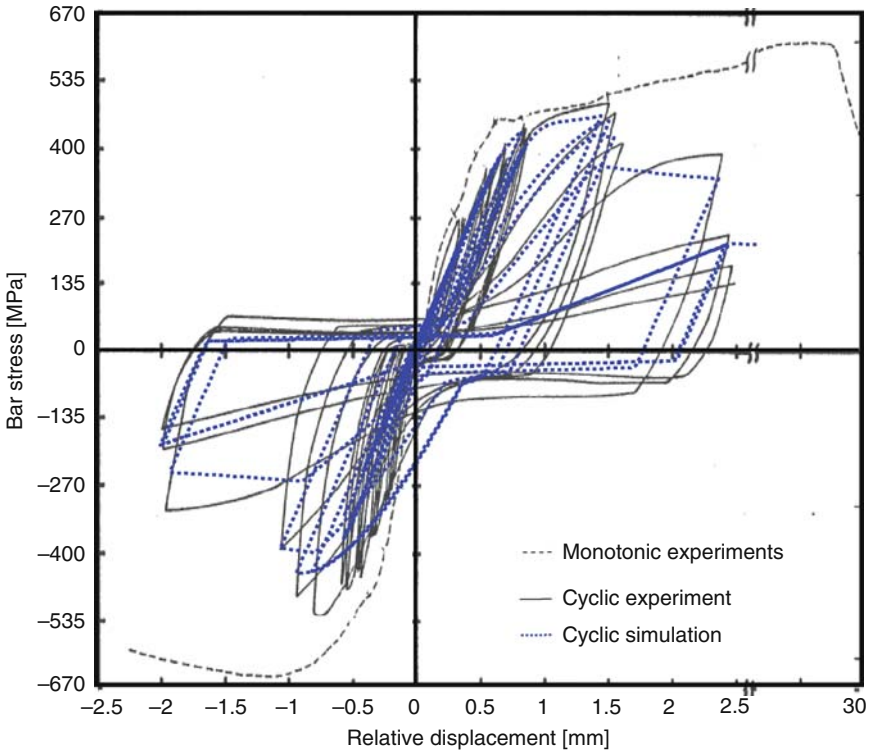

Fig. 20.11 Theoretical and calibrated stress-strain response of lap-spliced bars (See also Plate 46 in Color Plate Section on page 480)

equation for the splice becomes,

$$\tau_m = \sigma_s \, d_b \Big/ \left[2 \left(l_1^2 + (L_s - l_1)^2 \right) \Big/ L_s \right] \tag{20.34}$$

where the effective steel stress $\sigma_s = \sigma_{s1} + \sigma_{s2} = \sigma(\varepsilon_{se})$ is the sum of the two reinforcing bar stresses and satisfies the bar material's constitutive law. The following monotonic bond stress-slip relationship proposed in [27] is used to characterize the monotonic lap-splice behavior.

$$\tau_m = \tau_{\max} r \left(u / u_{\max} \right) \Big/ \left[r - 1 + \left(u_s / u_{s,\max} \right)^r \right] \tag{20.35}$$

where $\tau_{\max} = \tau' + 1.4\sigma_3$, $\tau' = 20\sqrt{f_c'}/d_b$ [N, mm units], $r = r_o - 13\sigma_3/f_c' \geq 1.1$, r_o is 2 for Grade 60 and 1.5 for Grade 40 steel, $u_{s,\max} = 0.25\left(1 + 75\sigma_3/f_c'\right)$[mm units]. The confining stress σ_3 is computed from the confined cross-section model, corresponding to a maximum concrete dilation strain, $\varepsilon_{dl} \approx 0.0010$ to 0.0015, after which confinement is experimentally observed to have insignificant effect on clamping the splices, refer to [27].

20.4.4.1 Stress Reduction, Damage Index, and Experimental Calibration

In [13], a hysteretic behavior rule is developed and calibrated for the monotonic bond-slip model (Fig. 20.11) using experimental results of bar pullout tests from [28]. Upon unloading after slip has taken place, the maximum slip reached is $u_s{}^{un}$ and the corresponding bond stress $\tau_m{}^{un}$. These values, in each direction of loading, characterize and control the hysteretic behavior rules, which can be reviewed in [13]. The hysteretic slip behavior has the following characteristics: (a) linear unloading with reduced stiffness; (b) linear pinching; (c) linear hardening back to the bond-slip envelope; and (d) hysteretic reduction of the envelope. The strain decomposition approach effectively creates a parallel material that represent the slip behavior alongside the bar mechanical stress-strain behavior. Hence, any constitutive material for steel bar stress-strain behavior can be used at the choice of the analyst using this approach for modeling lap-spliced bars. Upon summing the responses of both components of the material, the resultant may be nonlinear even though the hysteretic loading-unloading rules of the bond-slip model are linear.

The following maximum slip displacement-based damage index is proposed for the hysteretic degradation accumulated in the lap splice region due to bond-slip

$$D_p = \max\left\{\left|u_s^{un}\right|\right\} / u_{s,ult} \tag{20.36}$$

where $u_{s,ult}$ is the slip displacement corresponding to the loss of bond stiffness and can be determined experimentally or estimated as a multiple of $u_{s,max}$ depending on confinement and bar surface conditions [13].

20.5 Applications of Damage and Collapse Identification

Two one-third scale RC bridge column tests reported in [29] were modeled using the component models described in Section 20.4. The columns had a diameter of 610 mm and a length of 2440 mm, were subjected to reversible lateral loads under two levels of axial load (415P = 20% of nominal capacity, 415S = 10% of nominal capacity), and experienced ductile axial-flexure failure. Bar buckling was experimentally observed during the 5% lateral drift cycle, and tie fracture during the 7% cycle. Figure 20.12 illustrates the axial damage index D_A as simulated in [13], with and without modeling of bar buckling. The damage index is consistently higher for specimen 415P which is subjected to a higher axial load. When bar buckling is modeled, the resulting increased dilation strain demand on the spiral reinforcement causes it to fracture leading to a damage index of 1.0.

Figure 20.13a shows a shaking table specimen tested at the University of California, Berkeley [30]. The structural system consisted of three seismically detailed RC frames connected by RC beams and slabs at the top level. The middle frame is infilled with an unreinforced masonry (URM) wall. The FE model in Fig. 20.13b was constructed using equivalent truss elements for the URM wall and RC slab, and

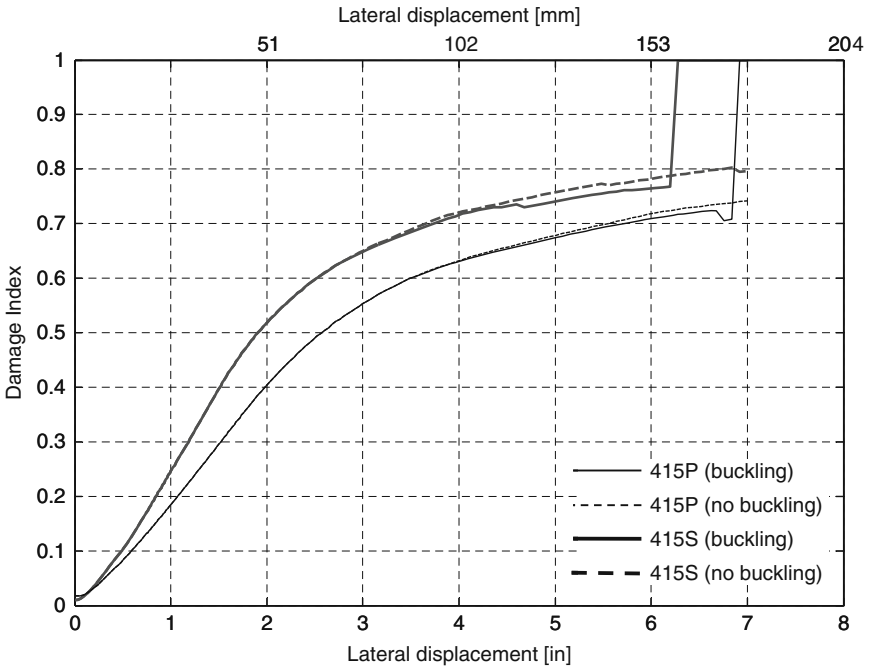

Fig. 20.12 Theoretical and calibrated stress-strain response of lap-spliced bars

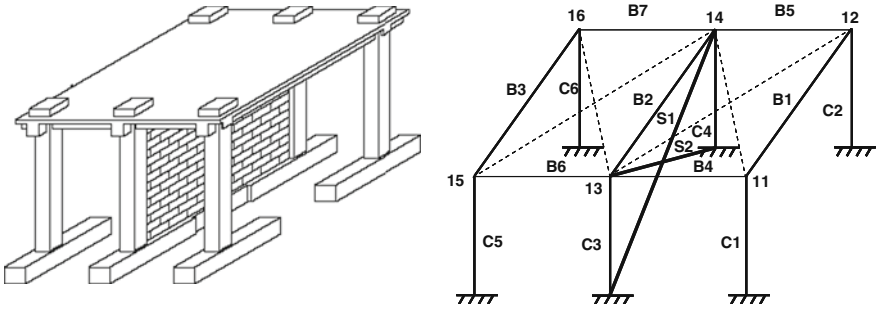

(a) Test specimen (b) FE model

Fig. 20.13 Shaking table test specimen and FE model of tests conducted in [30]

calibrated to the test specimen. It was then intentionally weakened by introducing lap splices at the footing base of columns C5 and C6, and increasing the transverse tie spacing to render shear-critical columns C3 and C4 in the infilled frame and bar buckling-prone columns C1 and C2. The deficient component models and removal criteria described in Sections 20.3 and 20.4 were used to model the structural components of this structural system [13].

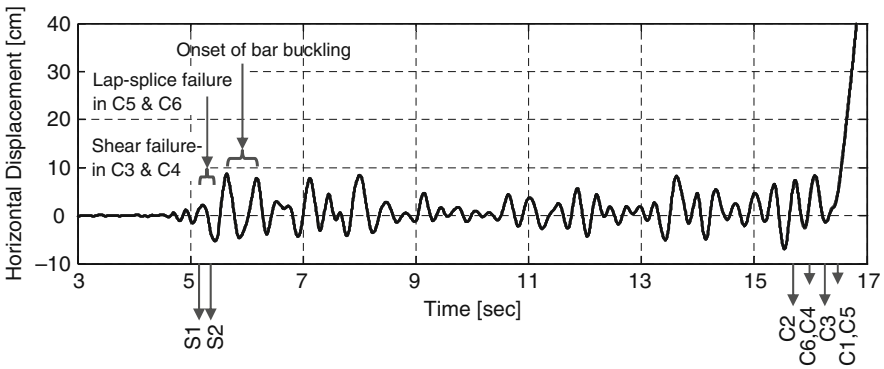

Fig. 20.14 Roof displacement response history for the FE model [13]

Figure 20.14 shows the roof displacement history of the FE model in response to a damaging earthquake which causes it ultimately to collapse, and identifies the progression of damage in each structural component. The sequence and times of element removal are indicated along the horizontal axis until complete collapse. The system was subjected to ground acceleration record from Düzce (1999) earthquake, scaled to a first-mode 5%-damped elastic spectral acceleration of 3.39 g, which corresponds to a return period of 2500 years for an assumed building site in Los Angeles County, USA.

20.6 Concluding Remarks

This chapter describes a FE procedure for simulating progressive collapse in structural systems using direct removal of collapsed elements. The element removal analytical formulation is based on the dynamic equilibrium of forces. It accounts for the dynamic redistribution of internal forces from a collapsed elements and its propagation into the structure. The procedure was implemented as a computational algorithm and tested using a demonstration problem of simplified geometry, material properties, and element removal criteria. The demonstration problem resulted in numerically stable solutions and successfully simulated the collapse sequence of the structural system. Four alternate case studies demonstrated the sensitivity of the element removal algorithm to uncertainty in material properties and element removal criteria and its ability to account for the effect of random input. It is therefore considered most suitable for simulation-based progressive collapse assessment within a probabilistic framework.

The element removal procedure is complemented by the introduction of criteria of element removal for RC columns collapsing due to flexure-axial interaction and shear-axial interaction, as well as truss elements. Flexure-axial dominated columns are removed based on cross-section damage indices aggregated on the material level.

The following component models were introduced for modeling as-built and FRP-retrofitted RC columns:

- A confined cross-section model for fiber-discretized elements.
- A constitutive model and hysteretic damage index for confined concrete.
- A uniaxial constitutive model and hysteretic damage index for confinement-sensitive buckling-enabled longitudinal steel bars.
- A uniaxial constitutive model and hysteretic damage index for confinement-sensitive lap-splices in longitudinal steel bars.

An application of damage identification in flexure-axial RC column collapse was demonstrated using the proposed damage index. Finally, the element removal procedure, component models, and damage indices were combined to simulate the sequence of seismic deterioration and eventual collapse of a RC frame with URM infill wall. The system was calibrated using results from a previous shaking table experiments then modified to introduce seismically deficient details.

Acknowledgments This study was supported by the Earthquake Engineering Research Centers Program of the NSF under Award No. EEC-9701568 to PEER at UC Berkeley. Financial support from the research sponsor is gratefully acknowledged. Opinions and findings presented are those of the authors and not necessarily the sponsors.

References

1. Kim Y, Kabeyasawa T (2004) Dynamic test and analysis of an eccentric reinforced concrete frame to collapse. 13th World Conference on Earthquake Engineering, Vancouver, Canada
2. Wu C-L, Loh C-H, Yang Y-S (2006) Shake table tests on gravity load collapse of low-ductility RC frames under near-fault earthquake excitation. Advances in Experimental Structural Engineering, Itoh and Aoki, Eds: 725–732
3. Ghannoum W (2007) Experimental and analytical dynamic collapse study of a reinforced concrete frame with light transverse reinforcements. PhD Dissertation, University of California, Berkeley
4. Grierson DE, Xu L, Liu Y (2005) Progressive-failure analysis of buildings subjected to abnormal loading. Computer-Aided Civil and Infrastructure Engineering, 20(3):155–171
5. Kaewkulchai G, Williamson EB (2006) Modeling the impact of failed members for progressive collapse analysis of frame structures. Journal of Performance of Constructed Facilities, 20(4):375–383
6. Kaewkulchai G, Williamson EB (2004) Beam element formulation and solution procedure for dynamic progressive collapse analysis. Computers and Structures, 82(7–8):639–651
7. Pretlove AJ, Ramsden M, Atkins AG (1991) Dynamic effects in progressive failure of structures. International Journal of Impact Engineering, 11(4):539–546
8. Ramsden M (1987) Dynamic effects in the progressive failure of lattice structures. PhD Dissertation, University of Reading, UK
9. Powell G (2005) Progressive collapse: case studies using nonlinear analysis. Structures Congress and Forensic Engineering Symposium, New York, 2185–2198
10. Haselton CB, Deierlein GG (2005) Benchmarking seismic performance of reinforced concrete frame buildings. Structures Congress and Forensic Engineering Symposium, New York, 1891–1902

11. Zareian F, Krawinkler H (2007) Assessment of probability of collapse and design for collapse safety. Earthquake Engineering & Structural Dynamics, 36(16):1901–1914
12. Elwood KJ, Moehle JP (2005) Axial capacity model for shear-damaged columns. ACI Structural Journal, 102(4):578–587
13. Talaat M, Mosalam KM (2008) Computational modeling of progressive collapse in reinforced concrete frame structures. PEER Technical Report 2007/10
14. Mosalam KM, Talaat M, Binici B (2007) A computational model for reinforced concrete members confined with fiber reinforced polymer lamina: implementation and experimental validation. Composites Part B: Engineering, 38(5–6):598–613
15. Mazzoni S, et al. (2004). Opensees User's Manual. www.opensees.berkeley.edu
16. Zineddin M, Krauthammer T (2007) Dynamic response and behavior of reinforced concrete slabs under impact loading. International Journal of Impact Engineering, 34(9):1517–1534
17. Crisfield MA, Moita GF (1996) Unified co-rotational framework for solids, shells and beams. International Journal of Solids and Structures, 33(20–22):2969–2992
18. Mander JB, Priestley M, Park R (1988) Theoretical stress-strain model for confined concrete. ASCE Journal of Structural Engineering, 114(8):1804–1826
19. Binici B (2003) An analytical model for stress-strain behavior of confined concrete. Eng. Structures, 27(7):1040–1051
20. Popovics S (1973) A numerical approach to the complete stress–strain curves for concrete. Cement and Concrete Research, 3(5):583–590
21. Pramono E and Willam K (1985) Fracture-energy based plasticity formulation of plain concrete. ASCE Journal of Engineering Mechanics, 115(8):1183–1204
22. Lokuge W, Sanjayan J and Setunge S (2004) Constitutive model for confined high strength concrete subjected to cyclic loading. ASCE Journal of Materials in Civil Engineering, 16(4):297–305
23. Dhakal R, Maekawa K (2000) Modeling for post-yield buckling of reinforcement. ASCE Journal of Structural Engineering, 128(9):1139–1147
24. Brown J, Kunnath S (2000) Low cycle fatigue behavior of longitudinal reinforcement in reinforced concrete bridge columns. Report No MCEER-00-0007
25. Monti G and Nuti C (1992) Nonlinear cyclic behavior of reinforcing bars including buckling. ASCE Journal of Structural Engineering, 118(12):3268–3284
26. Binici B, Mosalam KM (2007) Analysis of reinforced concrete columns retrofitted with fiber-reinforced polymer lamina. Composites B: Engineering, 38(2):265–276
27. Xiao Y, Ma R (1997) Seismic retrofit of RC circular columns using prefabricated composite jacketing. ASCE Journal of Structural Engineering, 123(10):1357–1364
28. Viwathanatepa S (1979) Bond deterioration of reinforcing bars embedded in confined concrete blocks. PhD Dissertation, University of California, Berkeley
29. Henry L (1998) Study of Buckling of Longitudinal Bars in Reinforced Concrete Bridge Columns. MS Thesis, University of California, Berkeley
30. Hashemi A, Mosalam KM (2007) Seismic evaluation of reinforced concrete buildings including effects of masonry infill walls. PEER Technical Report 2007/100

Color Plates

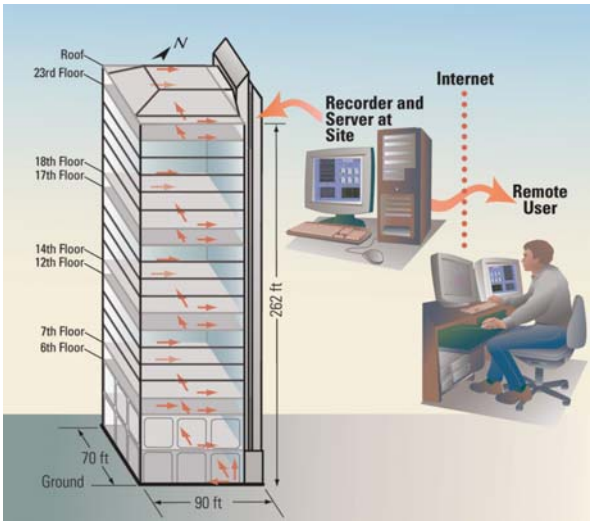

Plate 1 Schematic of real-time seismic monitoring of the building (see also Fig. 1.7 on page 8)

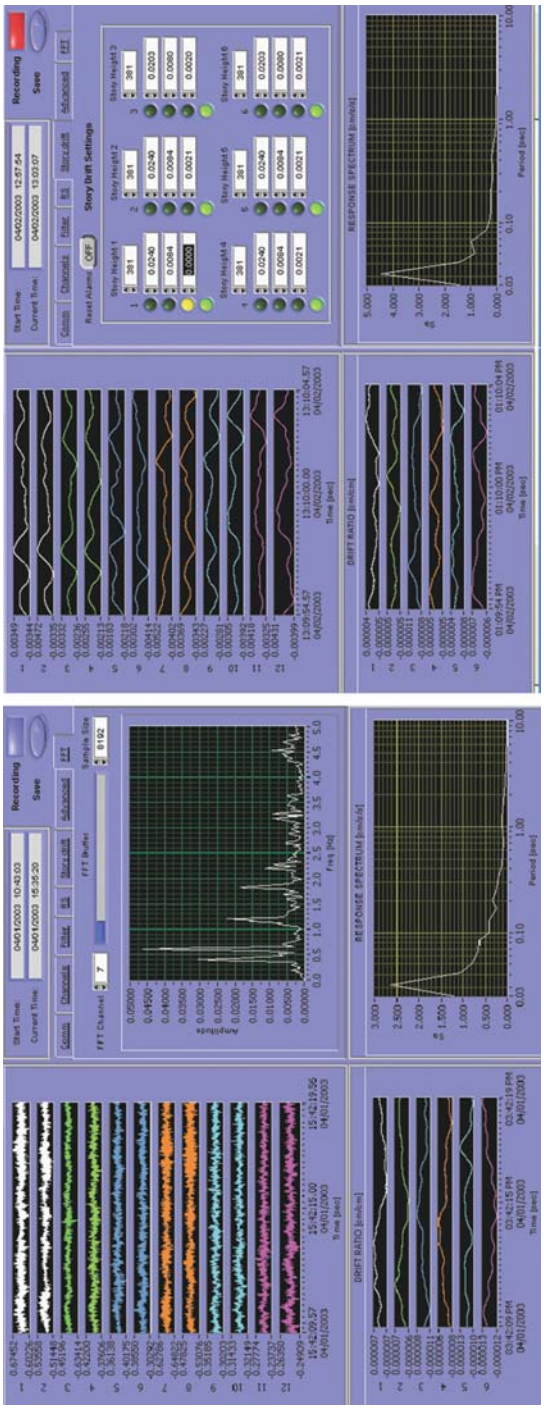

Plate 2 Screen snapshots of sample client software displays: (*left*) acceleration streams and computed amplitude and response spectra, and (*right*) displacement and corresponding drift ratios and alarm systems corresponding to thresholds (see also Fig. 1.8 on page 9)

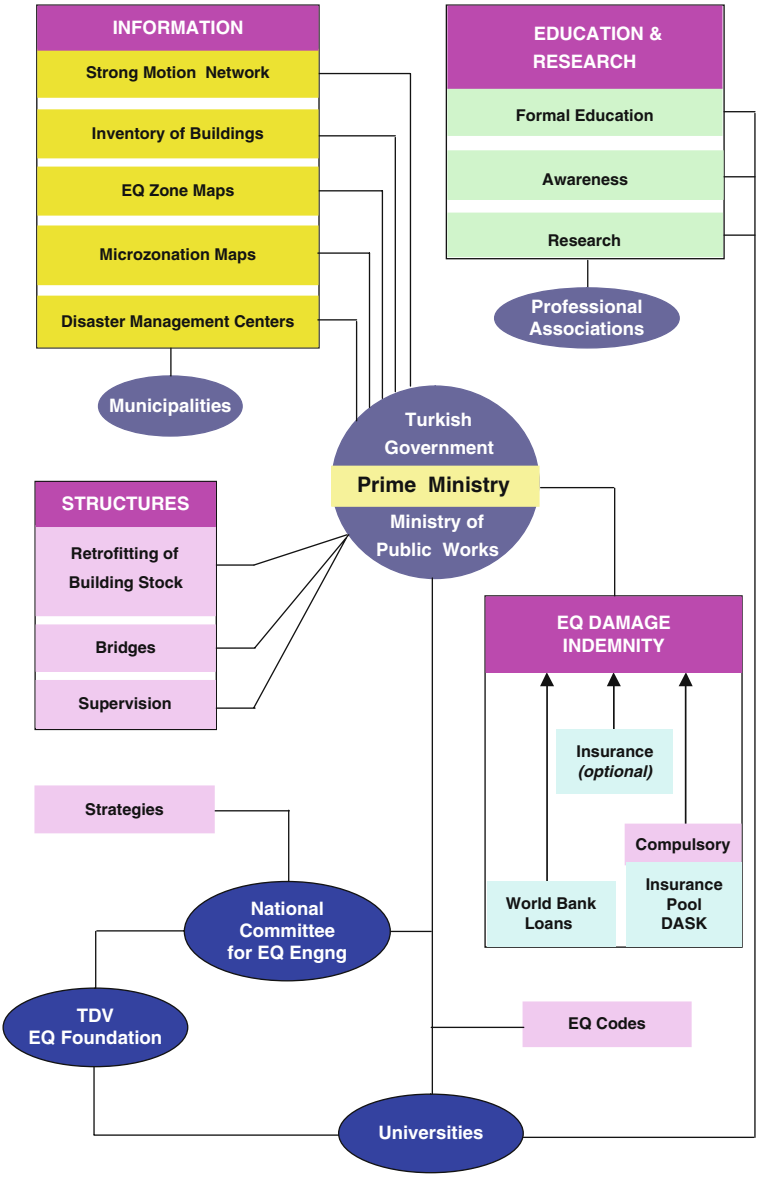

Plate 3 Basic institutions and activities related to earthquake risk management in turkiye (see also Fig. 4.1 on page 73)

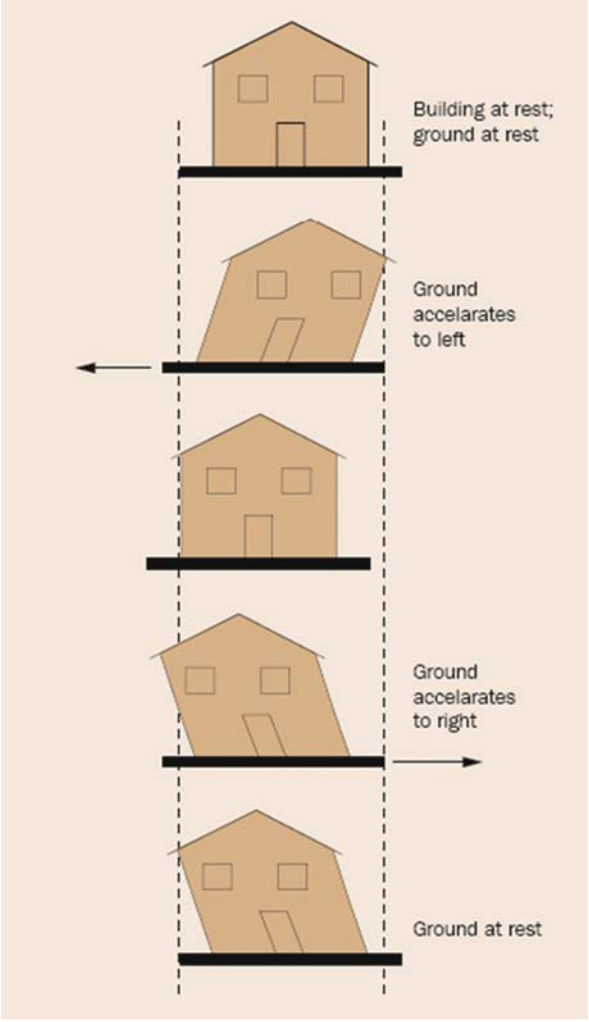

Plate 4 What happens to a building in an earthquake? (see also Fig. 6.1 on page 112)

Plate 5 Shear failure of column (see also Fig. 6.2 on page 114)

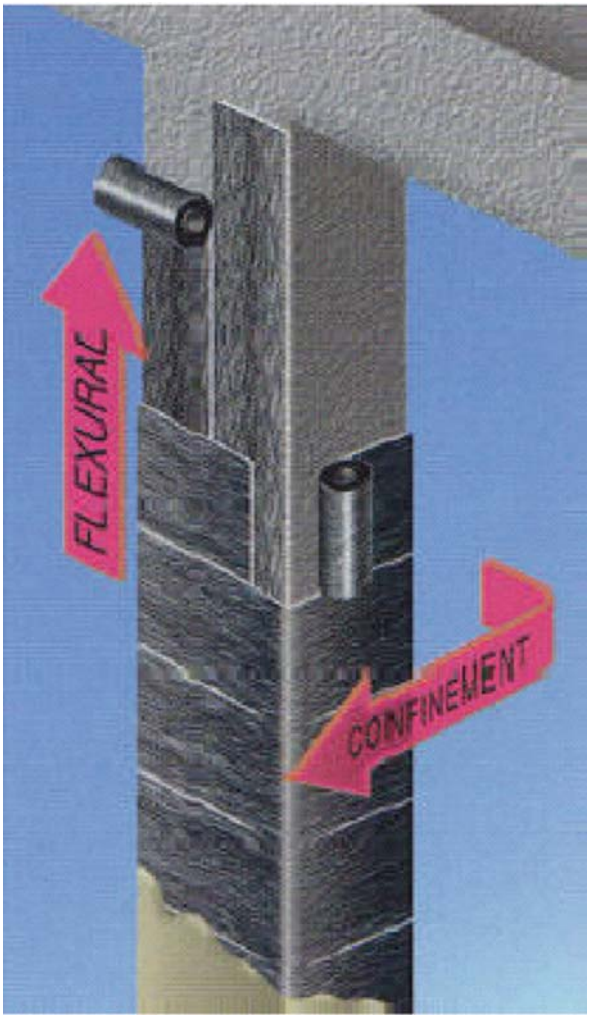

Plate 6 Retrofitting a column with FRP for seismic performance (see also Fig. 6.4 on page 116)

Plate 7 Method of pre-stressing (see also Fig. 6.5 on page 117)

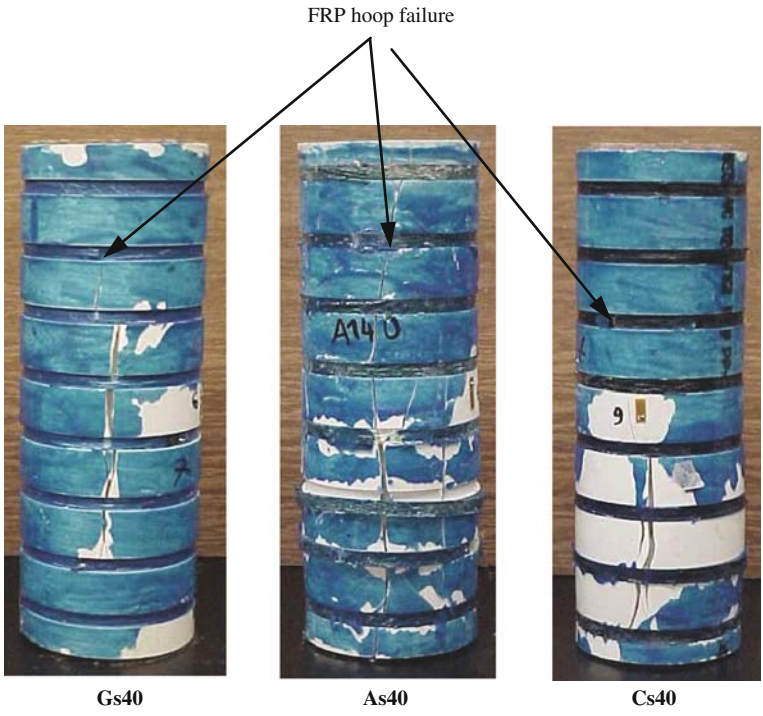

Plate 8 Typical failure mode of PVC-FRP confined concrete specimens (see also Fig. 6.8 on page 119)

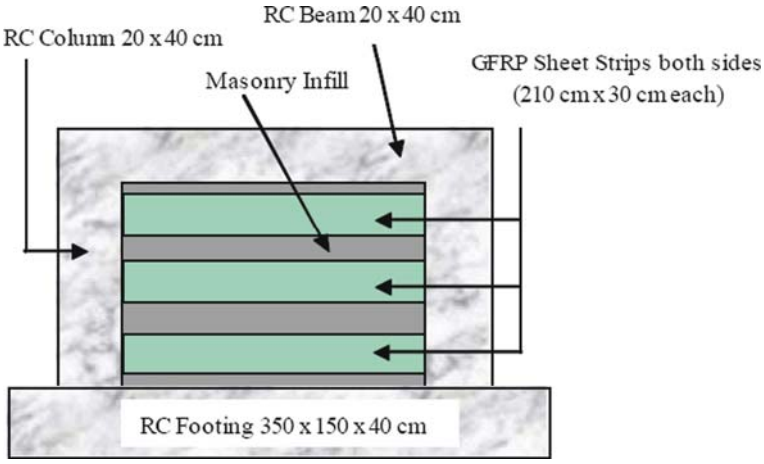

Plate 9 GFRP strips applied to masonry infill wall (see also Fig. 6.9 on page 120)

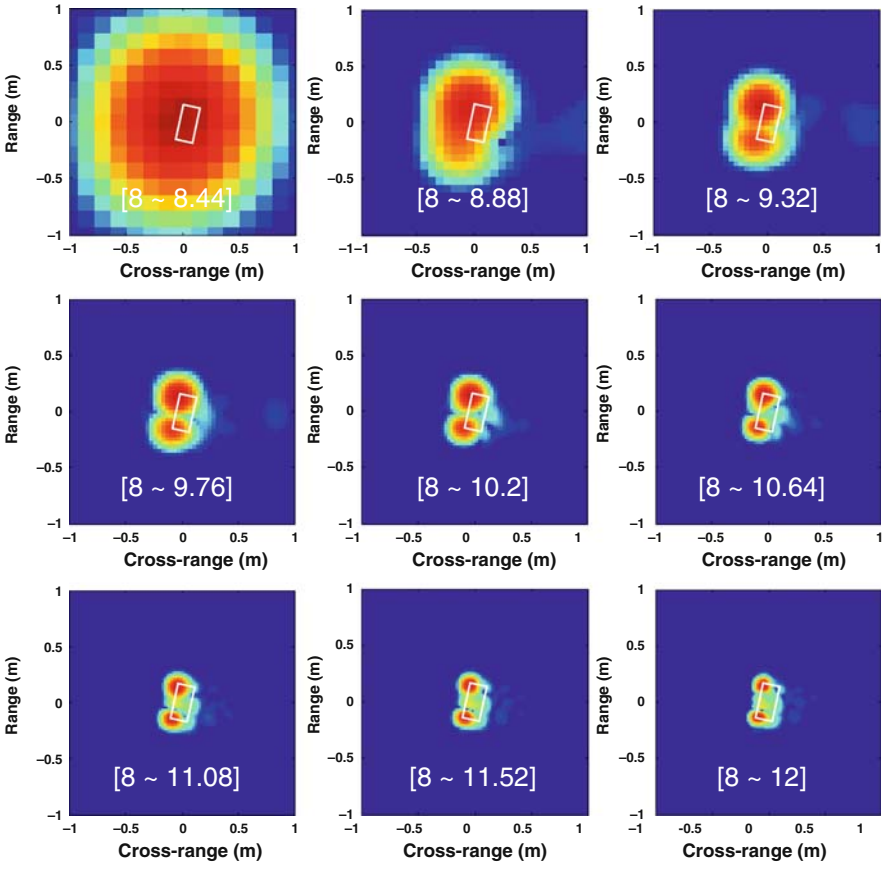

Plate 10 Processed images of the intact specimen with various bandwidths (see also Fig. 7.5 on page 136)

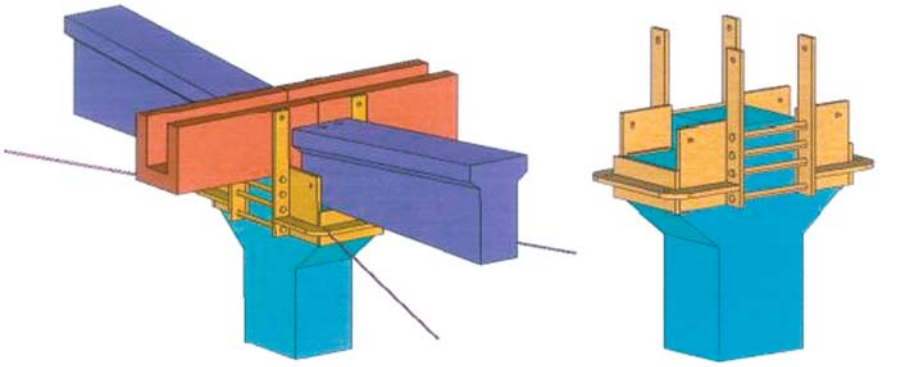

(a) With Roof Girders and Gutter Beams (b) Column and Clamping Device

Plate 11 Details of strengthening scheme for interior connections (see also Fig. 9.20 on page 183)

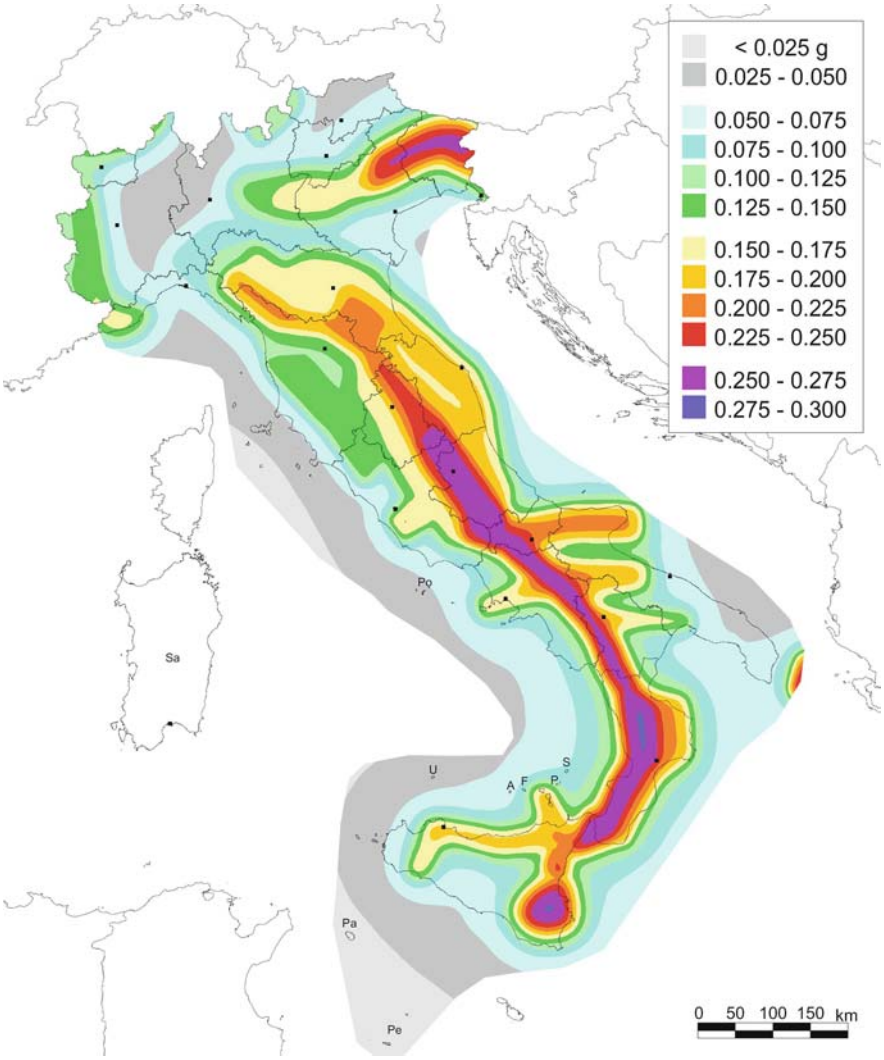

Plate 12 Italian seismic hazard map taken from INGV website (see also Fig. 10.1 on page 190)

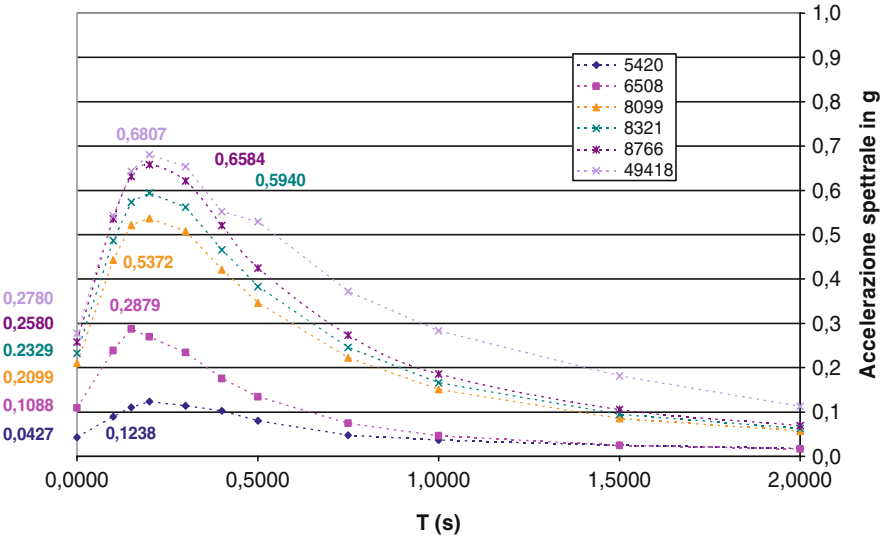

Plate 13 Sample of five response spectra computed for different locations in Italy (see also Fig. 10.2 on page 191)

Plate 14 Damages of soft-first-story buildings during Kobe earthquake (see also Fig. 11.1 on page 212)

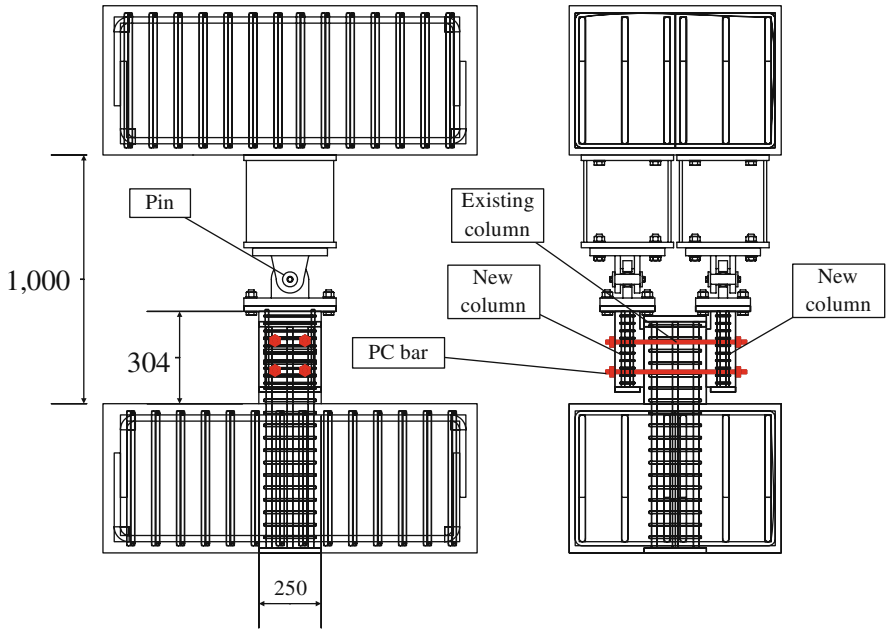

Plate 15 Specimens (see also Fig. 11.20 on page 227)

Plate 16 Resistance contribution of connectors on pushover curve (1st 3rd and 6th floor) (see also Fig. 12.25 on page 263)

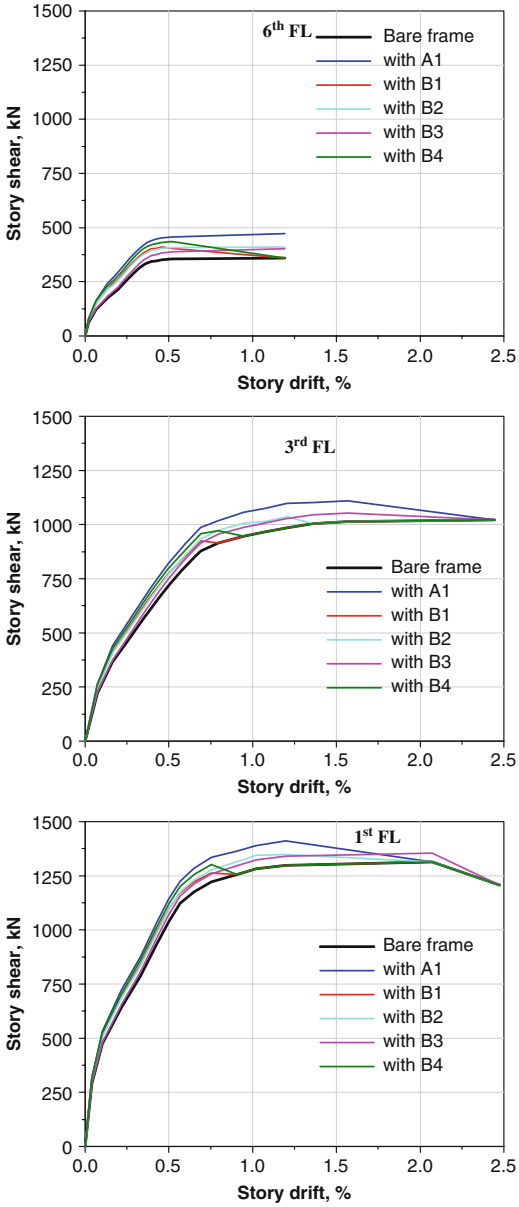

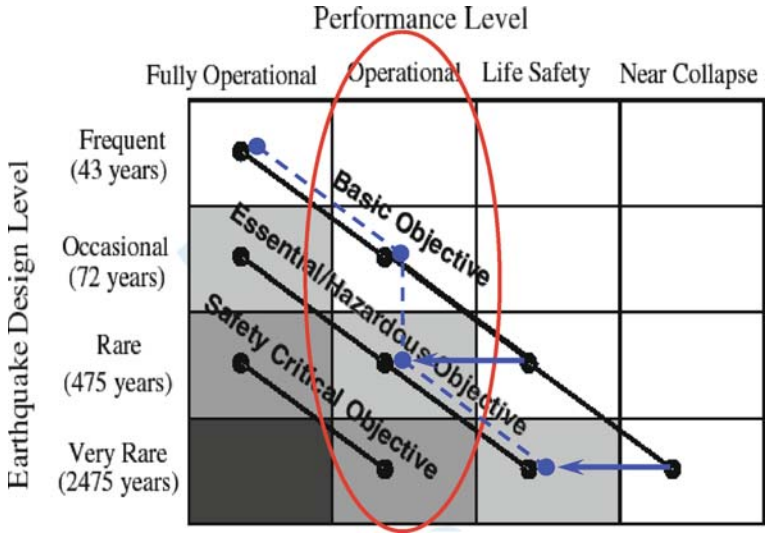

Plate 17 Seismic performance design objective matrix as defined by SEAOC Vision 2000 PBSE Guidelines [6] and proposed modification of the basic-objective curve towards a damage-control (*dashed blue line*) (see also Fig. 13.1 on page 270)

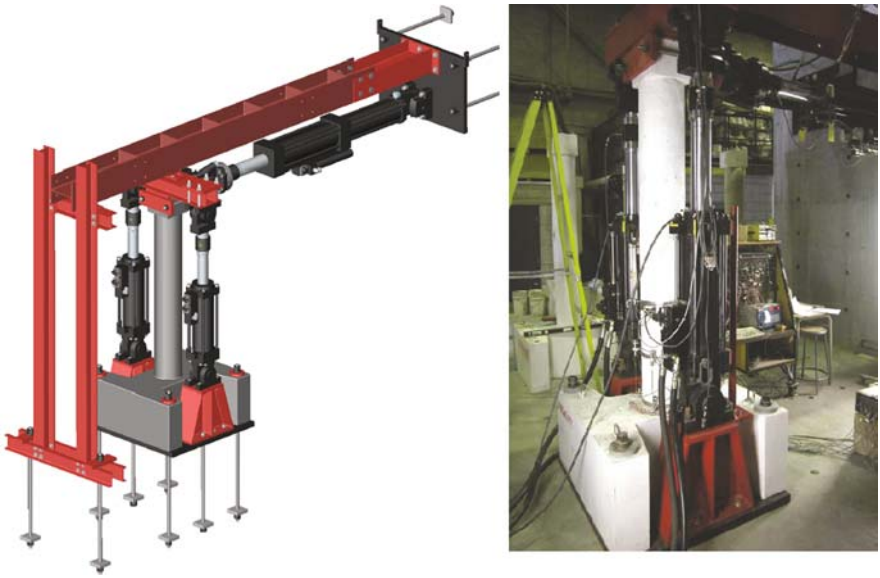

Plate 18 Test setup (see also Fig. 14.1 on page 298)

Plate 19 Story collapse vertically downward without significant lateral movement (note vertical alignment with adjacent uncollapsed wing) (see also Fig. 16.1 on page 330)

Plate 20 Side sway mechanism with incipient collapse (see also Fig. 16.2 on page 330)

Plate 21 Steel column "pre-shoring" examples from Stanford University and University of California, Berkeley (see also Fig. 16.3 on page 331)

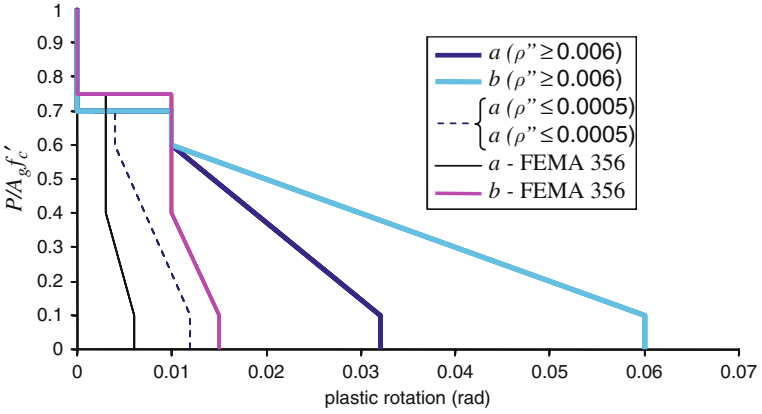

Plate 22 Comparison of modeling parameters for Condition ii and previous *FEMA 356* parameters for columns "controlled by flexure" with nonconforming transverse reinforcement and $v \leq (f_c')^{1/3}$ (see also Fig. 16.5 on page 334)

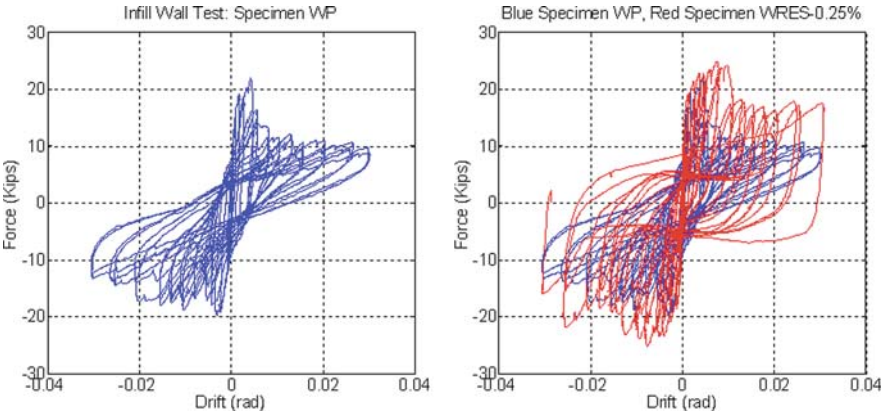

Plate 23 Cyclic response of two reduced-scale infill wall specimens; (**a**) reference specimen without retrofit, (**b**) specimen with reinforced ECC layer superimposed on reference specimen [10] (see also Fig. 17.6 on page 353)

Plate 24 Failure modes of Stanford specimens; (**a**) reference specimen without retrofit, (**b**) specimen with ECC layer [10] (see also Fig. 17.7 on page 353)

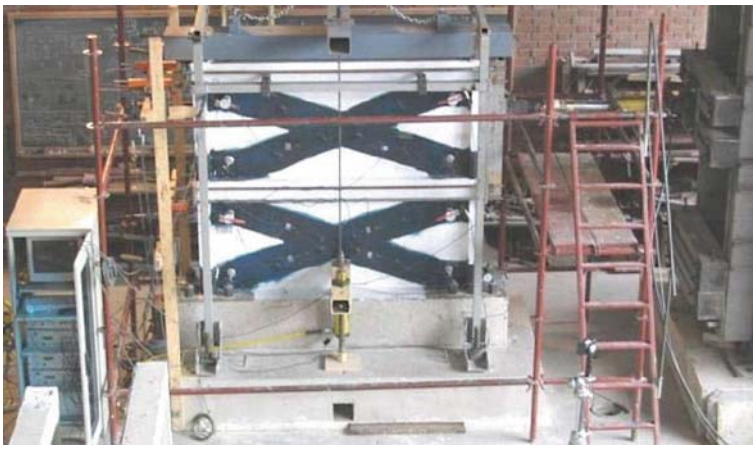

Plate 25 The test setup and instrumentation (see also Fig. 18.4 on page 372)

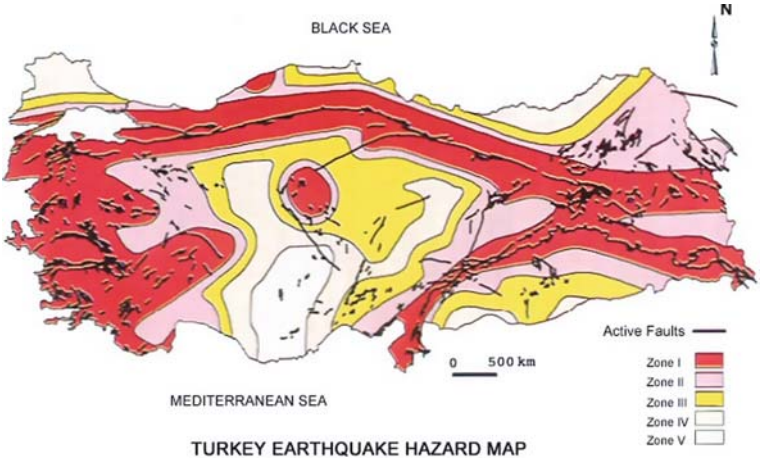

Plate 26 Seismicity of Turkey (see also Fig. 19.1 on page 388)

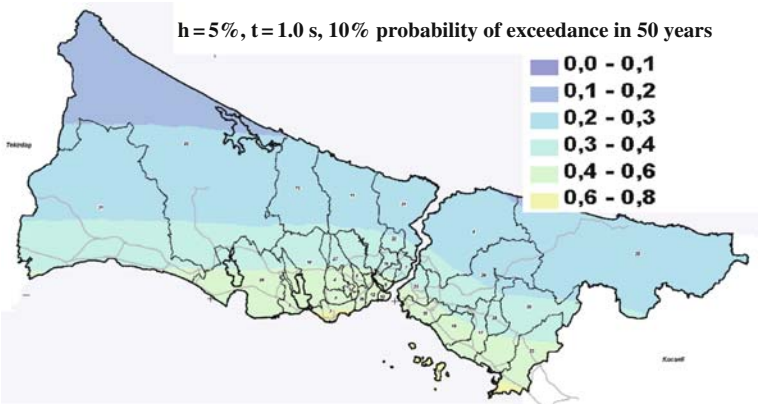

Plate 27 PGA map of Istanbul (see also Fig. 19.2 on page 389)

Plate 28 Total collapse of low cost–low-rise reinforced concrete buildings (see also Fig. 19.3 on page 390)

Plate 29 Pure shear tests of brittle walls (see also Fig. 19.7 on page 393)

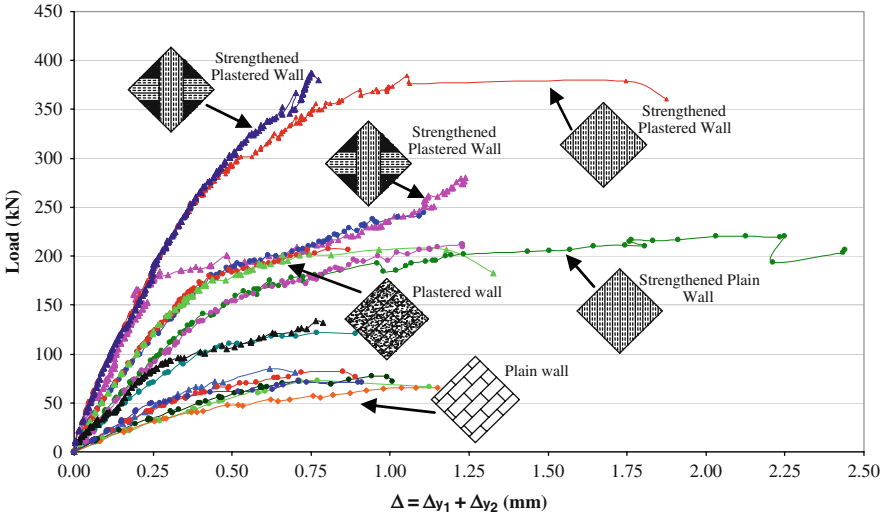

Plate 30 Force-displacement curves (see also Fig. 19.8 on page 393)

Plate 31 Testing set-up and integrated wall (see also Fig. 19.12 on page 398)

Plate 32 Integrated wall and strengthening by wire mesh (see also Fig. 19.13 on page 398)

(a) Before testing (b) After testing

Plate 33 Integrated wall and strengthening by CFRP strips (see also Fig. 19.14 on page 398)

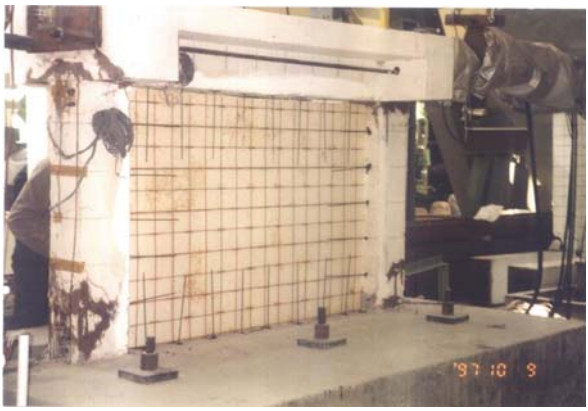

Plate 34 Strengthening of an epoxy repaired and tested bare frame by 3D wire panel (see also Fig. 19.15 on page 399)

Plate 35 Strengthening of a bare frame by integrated high strength bricks (see also Fig. 19.16 on page 399)

Plate 36 Different CFRP applications and infilled frame specimen (see also Fig. 19.20 on page 400)

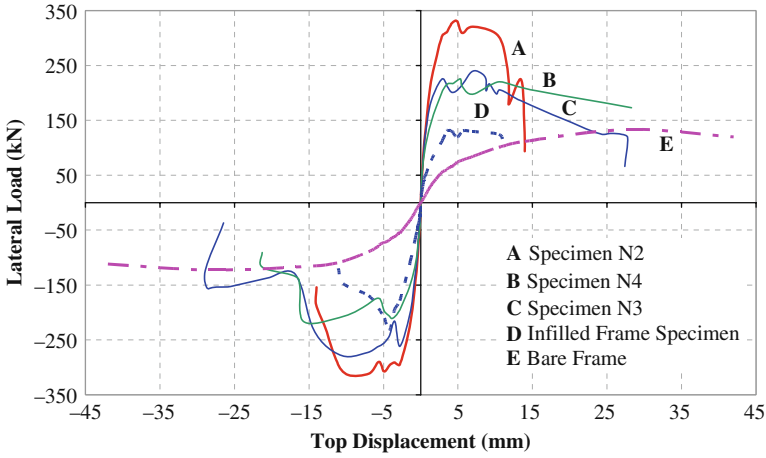

Plate 37 Test results of three different CFRP applications (see also Fig. 19.21 on page 401)

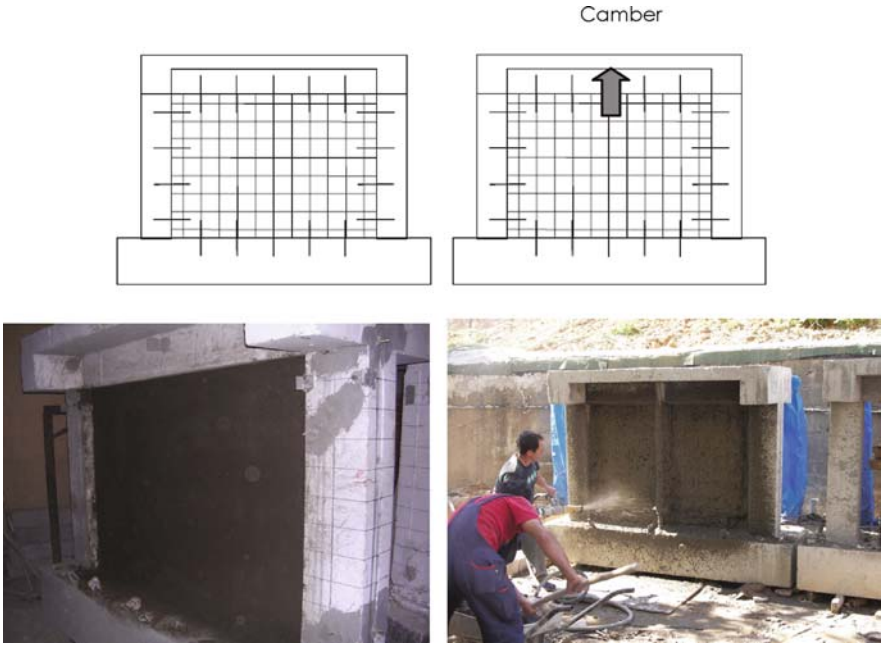

Plate 38 Strengthening by shotcreted 2D wire mesh (see also Fig. 19.22 on page 402)

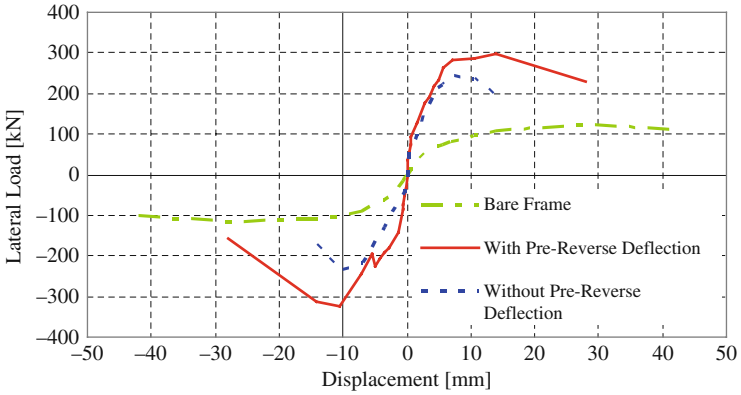

Plate 39 Test results of strengthening by shotcreted 2D wire mesh (see also Fig. 19.23 on page 402)

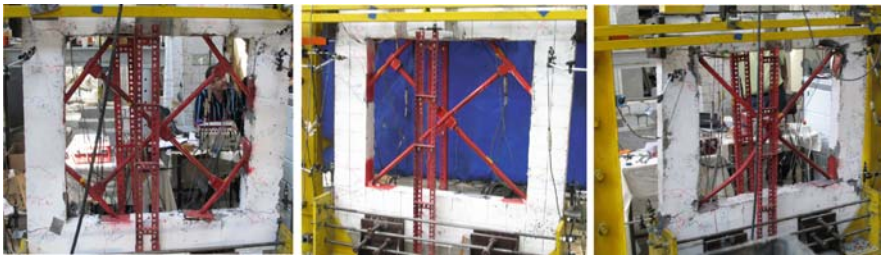

(a) Four knee braced RC frame (FKNEE) (b) Two knee braced RC frame (DKNEE) (c) Concentrically braced RC frame (CONBRACE)

(Diameter of the braces is 26.9 mm and thickness is 3 mm)

Plate 40 Energy dissipating simple bracing systems (see also Fig. 19.24 on page 403)

Infilled RC frame *Strengthening by CFRP strips on the infill wall*

Plate 41 Strengthening two story – one bay specimens (see also Fig. 19.27 on page 406)

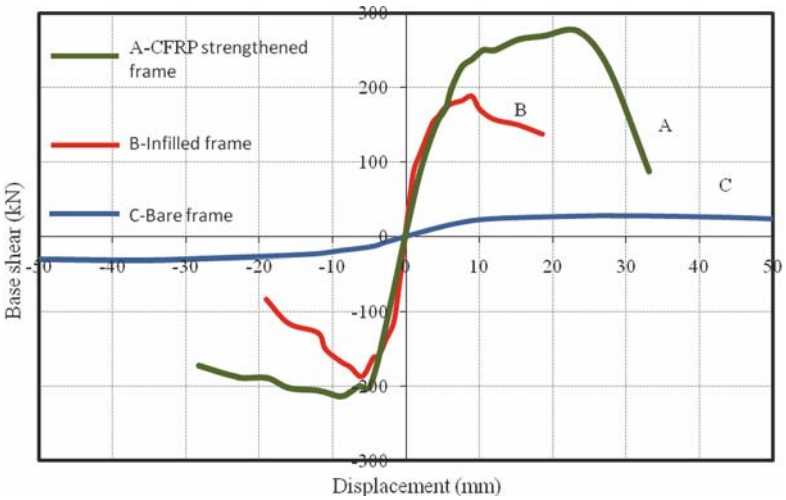

Plate 42 Lateral load – top displacement envelopes (see also Fig. 19.28 on page 406)

Plate 43 Some of the observed damages (see also Fig. 19.29 on page 407)

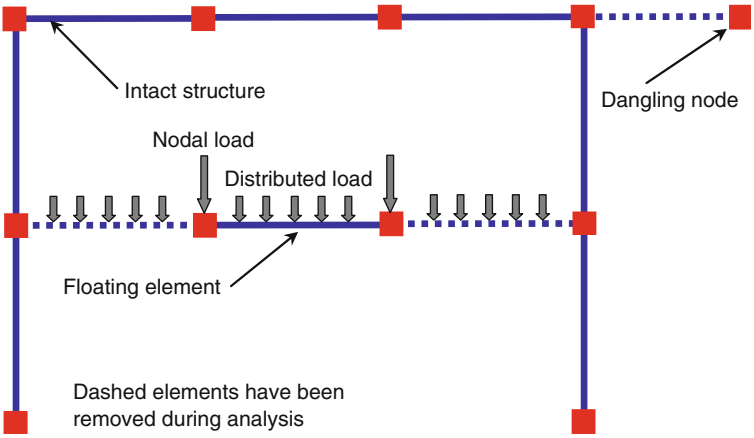

Plate 44 Automatic element removal algorithm (see also Fig. 20.2 on page 431)

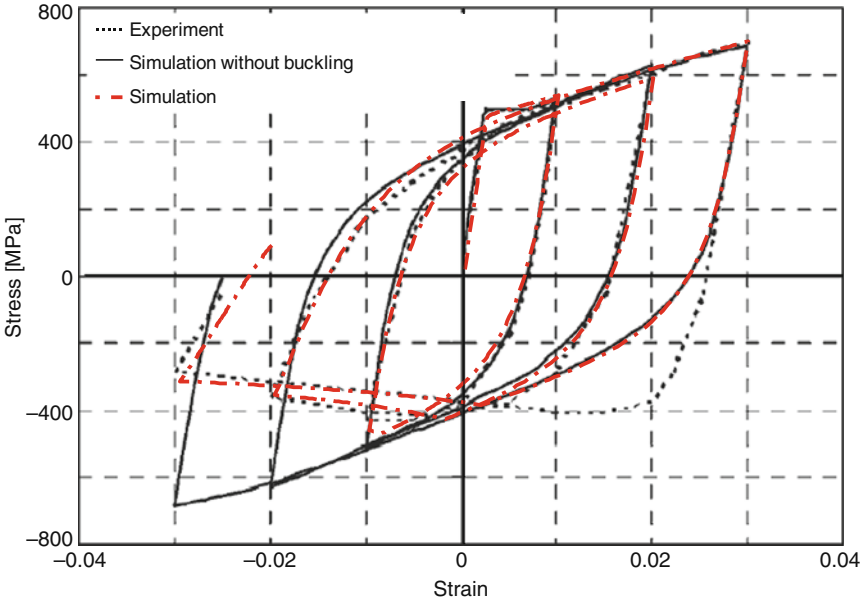

Plate 45 Model simulations of bar-buckling experiments in [25] for length/diameter ratio = 11 (see also Fig. 20.10 on page 446)

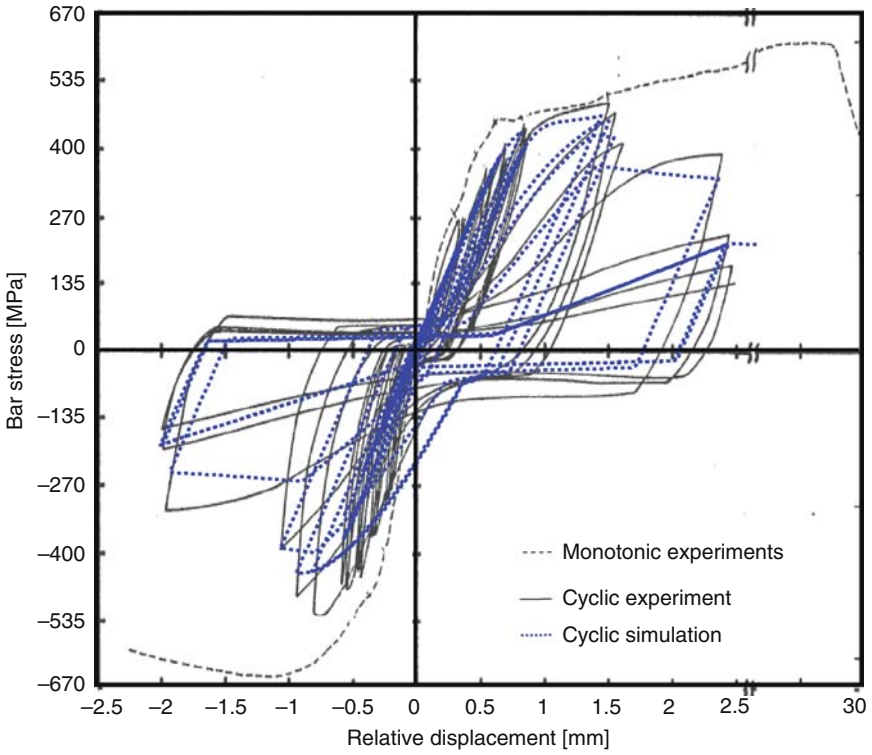

Plate 46 Theoretical and calibrated stress-strain response of lap-spliced bars (see also Fig. 20.11 on page 447)

Index